University of Coimbra
Faculty of Science and Technology
Department of Chemistry

Reactivity in Cryogenic Matrices: Case Studies including Thermal, Photochemical, IR-Induced and Tunneling Processes

Susy Branco Lopes

Coimbra
2011

University of Coimbra
Faculty of Science and Technology
Department of Chemistry

Reactivity in Cryogenic Matrices: Case Studies including Thermal, Photochemical, IR-Induced and Tunneling Processes

Susy Branco Lopes

Academic Dissertation to be presented for public criticism in order to obtain the PhD in Chemistry.

Coimbra
2011

Acknowledgements

To Professor Rui Fausto, group leader and my first supervisor, I owe special thanks for giving me the opportunity to work at the Laboratory for Molecular Cryospectroscopy and Biospectroscopy (LMCB) of the Department of Chemistry, University of Coimbra in Portugal, as an undergraduate student up to the research project undertaken in this Thesis. I thank him for his guidance throughout the different stages of this work and well as encouragement and support in many ways.

I would also like to thank the members of the LMCB of the Department of Chemistry, University of Coimbra in Portugal, present and past, Dr. Igor Reva, Dr. Andrea Gómez-Zavaglia, Susana Jarmelo, Ana Borba, Susana Breda, Archna Sharma, Michela Giuliano, Luis Duarte, Alcides Simão and Bruno Almeida for being there and cheering me up when I needed.

To Dr. Teresa Pinho e Melo of the Organic Chemistry Group of the Department of Chemistry of the University of Coimbra and specially to Cláudio Manaia Nunes for his availability to carry out all the necessary syntheses of the compounds studied in this work.

I thank Dr. Mário Rosado for his willingness to help my computational doubts and questions while working with Gamess.

To my second supervisor Professor Markku Räsänen for the warm welcome at the Laboratory of Physical Chemistry of the Department of Chemistry of the University of Helsinki in Finland. In particular, to Dr. Leonid Khriachtchev, for his patience and incredible work capability in the laboratory.

To the other members of the Laboratory of Physical Chemistry, Ksenyia, Sasha and Timur for making my stay in Helsinki an experience I wish to repeat.

The Portuguese Foundation for Science and Technology is thanked for the grant that allowed the accomplishment of this research (SFRH/BD/29698/2006).

To the Photochemistry and Molecular Spectroscopy group of the Department of Chemistry of the University of Coimbra, and the Department of Chemistry of the University of Helsinki, in particular the Laboratory of Physical Chemistry, for providing the necessary research facilities used in this work.

To my parents for unconditional support and understanding throughout the course of this dissertation.

Contents

Abstract

In the first part of this Thesis, the detailed characterization of the molecular structure, photochemistry and spectroscopic properties of a series of heterocyclic molecules containing nitrogen or/and their precursors and photoproducts was undertaken by matrix isolation infrared spectroscopy and high-level quantum chemical calculations.

The characterization of the low energy conformers was made by undertaking a systematic investigation of the DFT(B3LYP)/6-311++G(d,p) potential energy surface of the molecules. In the case of the azide representative (methyl (Z)-2-azido-3-chloro-3-benzoylpropenoate, MACBP) and its photoproducts, systematic preliminary explorations of the potential energy surfaces were performed using the semi-empirical PM3 method.

The studied five-membered ring derivatives (methyl 4-chloro-5-phenyl-1,3-oxazole-2-carboxylate and methyl 4-chloro-5-phenylisoxazole-3-carboxylate) and MACBP represent interesting systems where conformational cooling takes place during deposition of the matrices and partial conversion of higher energy isomers into the more stable forms during matrix annealing were found to be relevant.

The photochemical transformations resulting from *in situ* irradiation of the matrix-isolated compounds were studied using broadband ultraviolet light (UV) for all compounds, and narrowband UV laser irradiation for methyl aziridine-2-carboxylate.

In the second part of this Thesis, formic and acetic acids were studied in solid nitrogen. The low-energy *trans* and high-energy *cis* conformers of monomeric forms of formic and acetic acids, have been identified and their IR spectra assigned. The higher-energy *cis* conformers of these molecules were produced by vibrational excitation of the more stable *trans* conformers. The decay of the *cis* forms into the *trans* forms was observed and explained by tunneling of hydrogen atom through the *cis*–to–*trans* torsional barrier, similarly to what has been previously observed for these species in rare-gas matrices.

Three *trans-trans* and two *trans-cis* dimers of acetic acid were produced in solid nitrogen and structurally and vibrationally characterized. One *trans-trans* dimer and both observed *trans-cis* dimers were reported for the first time.

On the whole, the studies reported in this Thesis address some of the most important chemical phenomena and processes taking place for criteriously chosen molecules isolated in matrices: thermally induced reactions (conformational cooling; thermally induced-conformational isomerization upon annealing of the matrices; thermal mobilization of monomers to produce dimers); photochemical reactions (UV-induced conformational isomerizations, tautomerizations and other rearrangements, including complex bond breaking – bond forming processes); infrared-induced conformational conversions; and reactions occurring by tunneling mechanism.

Resumo

Na primeira parte desta Tese, a caracterização detalhada da estrutura molecular, fotoquímica e propriedades espectroscópicas numa série de moléculas heterocíclicas contendo um átomo de nitrogénio e/ou seus precursores e seus fotoprodutos foi efectuado através da espectroscopia de infravermelho com isolamento em matrizes e recorrendo a métodos teóricos de química quântica.

A caracterização dos confórmeros de menor energia foi realizado através de um varrimento da superfície de energia potencial das diferentes moléculas ao nível DFT(B3LYP)/6-311++G(d,p). No caso do representante da azida ((Z)-2-azido-3-cloro-3-benzoilpropenoato de metilo, "MACBP") e dos seus fotoprodutos, foi realizado um varrimento do espaço conformacional preliminar usando o método semi-empírico PM3.

Os derivados com anéis de cinco membros (4-cloro-5-fenil-1,3-oxazole-2-carboxilato de metilo e 4-cloro-5-fenil-isoxazole-2-carboxilato de metilo) e "MACBP" representam casos de sistemas interessantes em que ocorre arrefecimento conformacional durante a deposição das matrizes e conversão parcial dos isómeros mais energéticos nas formas mais estáveis em experiências de variação de temperatura da matriz ("annealing").

As transformações fotoquímicas resultantes da irradiação *in situ* dos monómeros das moléculas isoladas em matrizes de árgon e xénon foram estudadas usando irradiação na região do ultravioleta (UV) de banda larga, e com irradiação na região do ultravioleta (UV) de banda estreita no caso da aziridina-2-carboxilato de metilo.

Na segunda parte desta Tese, os ácidos fórmico e acético foram estudados em matrizes de nitrogénio. O confórmero menos energético *trans* e o mais energético *cis* das formas monoméricas dos ácidos fórmico e acético, foram identificados e os espectros vibracionais atribuídos. Os confórmeros mais energéticos *cis* destas moléculas foram produzidos por excitação vibracional dos confórmeros mais estáveis *trans*. O decaimento das formas *cis* nas formas *trans* foi observado e explicado recorrendo ao mecanismo do efeito de túnel do átomo de hidrogénio através da

barreira torsional *cis* → *trans*, que ocorre de um modo similar ao observado anteriormente para estas espécies em outras matrizes criogénicas.

Três dimeros *trans-trans* e dois dimeros *trans-cis* do ácido acético, foram produzidos em nitrogénio sólido e estrutural e vibracionalmente caracterizados. Um dos dímeros *trans-trans* e ambos os dímeros *trans-cis* foram observados pela primeira vez.

No seu todo, os estudos referidos nesta Tese relatam alguns dos fenómenos e processos químicos mais importantes que ocorrem para moléculas criteriosamente escolhidas isoladas em matrizes: reacções termicamente induzidas (arrefecimento conformacional; isomerizações conformacionais termicamente induzidas; mobilização térmica dos monómeros para produzir dímeros); reacções fotoquímicas (isomerizações conformacionais induzidas por radiação UV, tautomerizações, e outros rearranjos, incluindo processos complexos envolvendo quebra de ligações – formação de novas ligações); conversões conformacionais induzidas por radiação na região do infravermelho e reacções que ocorrem através do mecanismo do efeito de túnel.

List of original publications

Partial results of this thesis have already been published in the following publications:

1- "Low temperature IR spectroscopy and photochemistry of matrix-isolated α-pyridil", S. Lopes, A. Gómez-Zavaglia and Rui Fausto, *J. Photochem. Photobiol. A: Chemistry*, **2008**, *200*, 169-180.

2- "4-Halo-1,3-Oxazoles: Unambiguous Structural Assignment of 2-halo-2-benzoyl-2*H*-azirine-3-carboxylates thermal ring expansion products", S. Lopes, C. M. Nunes, R. Fausto and T.M.V.D. Pinho e Melo, *J. Mol. Struct.*, **2009**, *919*, 47-53.

3- "Conformational Space and Vibrational Spectra of Methyl 4-Chloro-5-phenyl-1,3-oxazole-2-carboxylate", S. Lopes, C. M. Nunes, A. Gómez-Zavaglia, T.M.V.D. Pinho e Melo and R. Fausto, *J. Phys. Chem. A*, **2010**, *114*, 9074-9082.

4- "Formic and Acetic Acids in a Nitrogen Matrix: Enhanced Stability of the Higher Energy Conformer", S. Lopes, A. Domanskaya, R. Fausto, M. Räsänen and L. Khriachtchev, *J. Chem. Phys.*, **2010**, *133*, 144507-7.

5- "Photochemistry and Vibrational Spectra of Matrix-Isolated Methyl 4-Chloro-5-phenylisoxazole-3-carboxylate", S. Lopes, C. M. Nunes, A. Gómez-Zavaglia, T. M.V.D. Pinho e Melo and R. Fausto, *J. Phys. Chem. A*, **2011**, *115*, 1199-1209.

6- "3-Azido-Acrylophonones as Photochemical Precursors of Oxazoles: A Matrix Isolation Infrared Spectroscopy Study", S. Lopes, C. M. Nunes, A. Gómez-Zavaglia, T. M.V.D. Pinho e Melo and R. Fausto, *Tetrahedron* (**2011) -** submitted.

7- "Acetic Acid Dimers in a Solid Nitrogen Matrix", S. Lopes, A. Domanskaya, R. Fausto, M. Räsänen and L. Khriachtchev (*to be submitted*).

8- "UV-Induced Photochemistry of Methyl Aziridine-2-Carboxylate Isolated in Low Temperature Inert Matrices", S. Lopes, I. Reva and R. Fausto (*to be submitted*).

General organization of the Thesis

This Thesis consists of five chapters. In the first chapter, a general introduction is presented, with emphasis on the relevance of the systems studied, and methods applied. A brief introduction to the matrix isolation infrared spectroscopy technique as well as to thermally and infrared induced conformational isomerizations, photochemical transformations and tunneling in cryomatrices is presented, in addition to a short overview of the theoretical methods used in this work. In chapter 2, the experimental and computational details relevant for the general description of the research strategies and approaches used in this study are provided. Chapters 3 and 4 contain the case studies. Chapter 3 includes the work concerning the nitrogen containing heterocycles here investigated; Chapter 4 the studies on formic and acetic acids. In chapter 5 a general conclusion is presented and perspectives for the future development of this research project are presented. Finally, the supporting information related to the reproduced papers (Chapters 3 and 4) is provided at the end of this Thesis.

1 Introduction

The work presented in this Thesis was carried out in the Laboratory for Molecular Cryospectroscopy and Biospectroscopy (LMCB) of the Department of Chemistry, University of Coimbra in Portugal, and of the Laboratory of Physical Chemistry of the Department of Chemistry of the University of Helsinki in Finland.

This work contains examples of thermally induced conformational isomerizations, and ultraviolet (UV) induced photochemical changes of a series of selected heterocyclic ring molecules containing nitrogen isolated in low-temperature matrices. The heterocyclic compounds include six-, five- and three-membered rings [(α-pyridil, methyl 4-chloro-5-phenyl-1,3-oxazole-2-carboxylate (MCPOC), methyl 4-chloro-5-phenylisoxazole-3-carboxylate (MCPIC), methyl (Z)-2-azido-3-chloro-3-benzoylpropenoate, (MACBP) and methyl aziridine-2-carboxylate (MA2C)]. All the molecules, except α-pyridil contain an ester carboxylic group, which can exist in *cis* and *trans* configurations.

For the thermally induced processes, conformational cooling during deposition and partial conversion of higher energy isomers into lower energy ones was observed for MCPOC, MCPIC and its precursor MACBP. Furthermore, unimolecular photoprocesses were observed upon broadband UV irradiation ($\lambda > 235$ nm) for MCPIC and MACBP, and narrowband tunable laser light irradiation ($\lambda = 235$ nm) for MA2C, followed by identification and assignment of the resulting photoproducts. In the case of α-pyridil, isomerizations of the pyridine rings to their valence Dewar or Hückel (aza-benzvalene) isomers were found to be the preferred photochemical pathways.

The second series of studies described in this Thesis focus on light induced conformational changes induced by infrared (IR) radiation. In particular, selective vibrational excitation of the lower-energy *trans* forms of two carboxylic acids, formic acid (HCOOH, FA) and acetic acid (CH_3COOH, AA), allowed to produce *in situ* the higher-energy *cis* conformers of these compounds, and study their stability in the cryogenic matrices. Combined with thermal mobilization of matrix-isolated molecules, vibrational pumping of the *trans* conformers of formic and acetic acids allows us to produce also novel dimers of these substances, determine their stability

and characterize them spectroscopically. When let in the dark, the *cis* carboxylic acid forms were found to spontaneously convert into the lower-energy *trans* conformers *via* dissipative proton tunneling through the torsional barrier. Their stabilities were also studied as a function of temperature, host and isotopic composition.

Extensive theoretical calculations carried out at the DFT(B3LYP)/6-311++G(d,p) and MP2 levels of approximation, using the 6-311++G(d,p) and the 6-311++G(2d,2p) basis sets, were used to aid the conformational and vibrational analysis as well as the structural characterization of each of the studied molecules, and their photoproducts.

1.1 The relevance of the systems studied

Heterocycles such as **isoxazoles** and **oxazoles** are important classes of organic compounds that have a remarkable number of applications, from building blocks in organic synthesis, to drug design.[1-4] As a result, the knowledge of their properties, structural characterization and chemical behavior is crucial for understanding their reactivity patterns. The most interesting aspect of the reactivity of isoxazoles (**1,** in **Scheme 1**) is their capability to be converted into other heterocylic compounds through a ring-opening reaction and subsequent re-cyclization. The first step of this type of chemical transformation is the cleavage of the labile N–O single bond, which can be either thermally[5-10] or photochemically induced.[10-15] The generation of vinyl nitrene intermediates (**2**) has been proposed,[7-9,11,14] which rearrange into the corresponding *2H*-azirines (**3**). The ***2H*-azirines** can then undergo ring cleavage to nitrile-ylides (**4**) followed by recyclization to give oxazoles (**5**) as the final products (see **Scheme 1**).[7,13-15] Other possible reaction pathways may, however, be conceived. Photochemical processes involving cleavage of the C–N bond have also been observed for substituted azirines bearing electron-withdrawing substituents in the ring.[16-22] In the work by Inui and Murata,[16-19] upon photolysis of 3-methyl-2-(1-naphthyl)-2*H*-azirines both C–C and C–N bonds were found to be cleaved in the matrices depending on the excitation wavelength used. They concluded that the tendency toward the C–N bond cleavage of the azirine ring increases with the electron-withdrawing ability of the ring substituents (*e.g.* introduction of an electron-

withdrawing nitro group into the naphthyl ring). This was the first observation of the C–N bond cleavage in the photochemistry of 2*H*-azirines. Similar conclusions were obtained from the study of the photolysis of two 3-methyl-*2H*-azirines bearing electron-withdrawing substituents at C2, methyl 3-methyl-*2H*-azirine-2-carboxylate (MMAC) and methyl 2-chloro-3-methyl-*2H*-azirine-2-carboxylate (MCMAC), isolated in rare gas matrices carried out in our laboratory.[20-22]

The relevance of the vinyl nitrene has also raised controversy.[23-28] Padwa and co-workers,[23,24] reported the thermal and photochemical ring expansion reactions of 2-vinyl-substituted *2H*-azirines (2-formyl-3-phenyl-2H-azirine-N-allylimine and 3-phenyl-2-styryl-*2H*-azirine). Both azirines underwent thermal rearrangement by rupture of the C–N single bond to give a butadienyl nitrene which subsequently underwent cyclization. Isomura *et al.*,[25] demonstrated that a vinyl nitrene is the intermediate in the thermal rearrangement of 3-methyl-2-phenyl-*2H*-azirine into 2-methylindole by rupture of the C–N single bond. On the other hand, Wendling and Bergman[26,27] studied the thermal decomposition of several *2H*-azirines (2-phenyl-3-methyl-*2H*-azirine, 2-methyl-3-phenyl-*2H*-azirine, 2-ethyl-3-phenyl-*2H*-azirine, 2,2-dimethyl-3-phenyl-*2H*-azirine) by the less common thermal cleavage of the C–C bond, which led initially to iminocarbene intermediates and not the vinyl nitrene intermediate was evidenced by the formation of the products observed. An *ab intio* MO study on thermal rearrangements on the C_2H_3N potential energy hypersurface, has disregarded vinyl nitrene structure as an intermediate due to its absence as an energy minimum on the potential energy surface.[28]

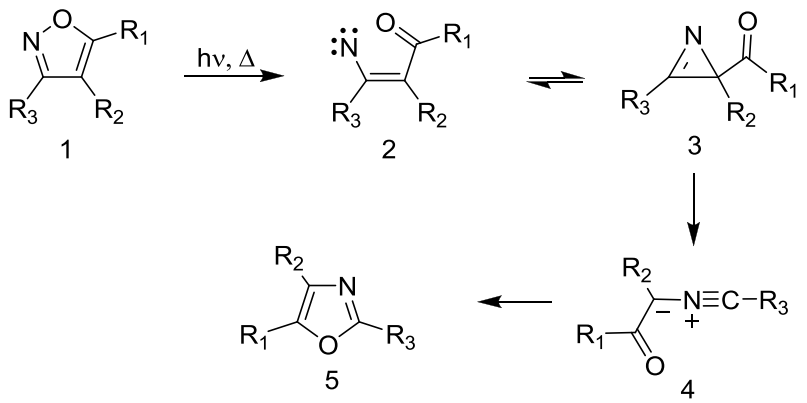

Scheme 1.

In this work, the monomeric forms of methyl 4-chloro-5-phenylisoxazole-3-carboxylate (MCPIC; **1a** in **Scheme 2**) and its oxazole counterpart, methyl 4-chloro-5-phenyl-1,3-oxazole-2-carboxylate (MCPOC; **5a**) were studied. The analysis of matrix-isolated MCPIC and MCPOC FTIR spectra allowed a detailed vibrational and structural characterization of these molecules. It was also shown that the methyl 2-benzoyl-2-halo-2*H*-azirine-3-carboxylates (*e.g.*, **3a**) undergo thermal ring expansion to give 4-halo-5-phenyl-1,4-oxazole-2-carboxylates (*e.g.*, MCPOC, **5a**) and not the isoxazole counterpart, (*e.g.*, MCPIC), as previously suggested.[29] In the studied processes, the precursor of the azirine was its related **azide** (**6**) and all intermediate species converting the azide into the corresponding isoxazole could be experimentally identified. The observations seem to indicate that in the case of the compounds studied, formation of the vinyl nitrene from the azide and, with all probability also from the azirine does not take place. The observed photostability of the studied oxazole (**1a**) seems also to point to the irrelevance vinyl nitrene (**2a**) to the reactivity of oxazoles substituted with electron withdrawing groups.

Indeed, our studies showed that that the thermolysis of the azide precursor (**6**) produces the azirine (**3a**) in a concerted manner, instead of *via* vinyl nitrene intermediate (**2a**). This conclusion was extracted taking into account the fact that the final product was the oxazole (**5a**) instead of the isoxazole (**1a**), which would be the expected product if the nitrene were formed along the process, either directly from the azide or from the azirine initially formed. In fact, the formation of the oxazole was initially not expected,[29] since it is generally accepted that 2*H*-azirines react preferentially upon thermal excitation through cleavage of the C–N bond, the required route to the nitrene species,[23-25,30-32] whereas thermal cleavage of the C–C bond is considered to be less common.[26,27] In a recent study carried out in our laboratory, the photochemistry of matrix-isolated unsubstituted isoxazole ring in an argon matrix was found to lead to the corresponding azirine but not to the oxazole.

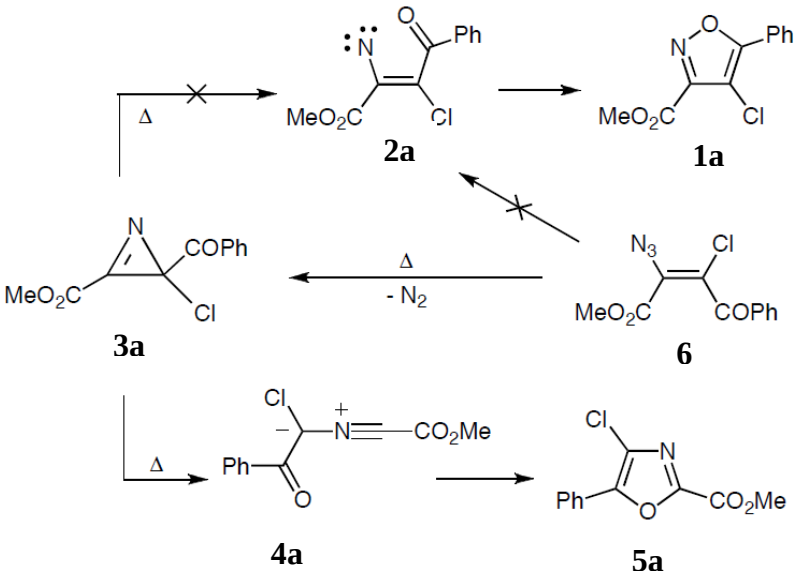

Scheme 2.

The **aziridine** ring can be found in natural products such as mitomycins, carzinophilin and azinomycins, which display strong antibiotic and antitumor properties.[33-36] Aziridines are extremely versatile compounds used in the synthesis of molecules such as amino acids, nitrogen-containing larger-ring heterocycles, pharmaceutical intermediates, etc.[30,37-45] In particular, aziridine-2-carboxylates and their derivatives have been used as intermediates in the syntheses of α- and β-amino acids, both natural and non-natural, by stereospecific ring-opening reactions of the heterocyclic ring with nucleophiles, including organometallic reagents.[46-50]

Like *2H*-azirines, aziridines, (**7**, in **Scheme 3**) are reactive three-membered heterocycles containing one nitrogen atom that can undergo C–N or C–C bond cleavages. They owe their ring strain their high reactivity.[37,51,52] Also like in the case of *2H*-azirines the nature of the substituents and their position in the aziridine ring, in particular the nature of the substituent at the N-atom, play a crucial role in determining the preferred reactive pathways in these molecules.[37,39,42,43,51,52] It is well known that upon irradiation (disrotatorial) or on thermal activation (conrotatorial), aziridines undergo ring-opening (through C–C bond cleavage) to the corresponding azomethine ylides. The occurrence of a hydrogen atom shift leads to the formation of new species.

For example, in the work by Gaebert *et al.*,[53] the matrix isolation technique was applied to the identification and characterization of azomethine ylides resulting from the photochemical C–C bond cleavage of phenyl-substituted aziridines in freon

matrices at 77 K. However, cleavage of the C−N bonds may also take place, leading to different final products. In total six potential photoproducts can be realized (**Scheme 3**). The understanding of how different substituents in the aziridine ring influence the preference for the carbon-nitrogen or the carbon-carbon bond cleavage reactions, is, however, still an open question.[54,55]

In the present work, the photochemistry of methyl aziridine-2-carboxylate (MA2C) was found to follow the classical pattern, being dominated by the C−C bond cleavage. The primary photoproduct was identified as methyl 2-(methyleneamino)-acetate (MMAA), which is formed after subsequent migration of one hydrogen atom of the azomethine ylide. The use of narrowband tunable laser light irradiation allowed the observation of the two most stable isomers of MMAA. Subsequent photodecomposition photoprocesses, were also observed leading to formation of carbon monoxide and other still unidentified products.

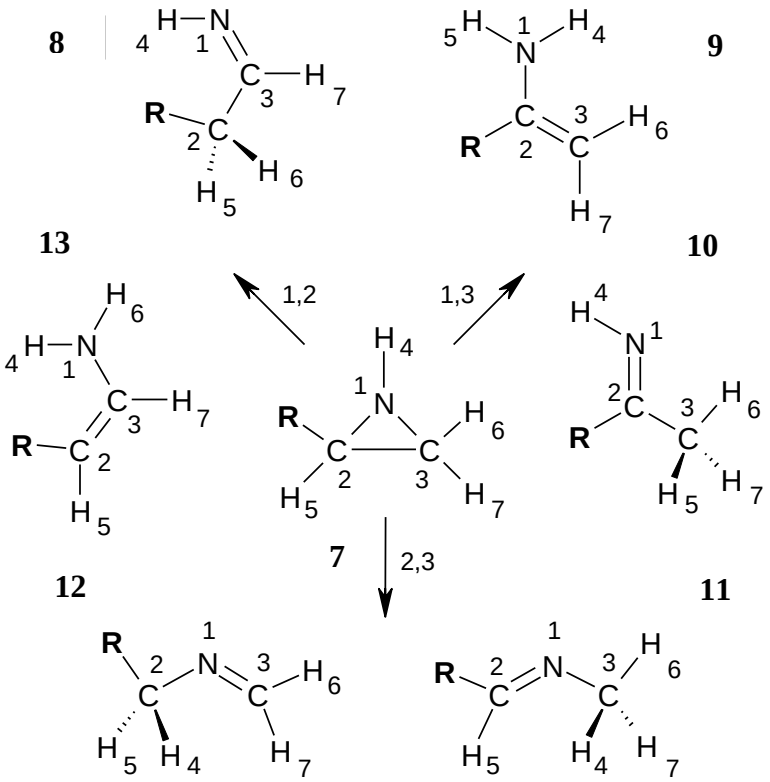

Scheme 3. Possible products resulting from different ring-opening reactions of 2-substituted aziridine. Pairs of numbers next to the arrows specify the atom numbers where the bond cleavage occurs.

The unsubstituted pyridine ring has been widely studied, both experimentally and theoretically. Specifically, the infrared spectrum of matrix isolated pyridine has been studied in different cryomatrices (*e.g.*, argon, nitrogen or xenon), and the results from its UV photolysis were discussed.[56-59] The experimental observation and identification of high-energy isomers of pyridine, like the Dewar isomer (where two tautomers can be considered) and azaprismane, has been reported.[56,59] Other valence isomers of pyridine (aza-benzvalenes, Hückel, prismane and bicyclopropenyls) were also considered theoretically.[60-62]

α–Pyridil consists of two pyridine rings connected to the central dicarbonyl fragment. Derivatives of α–pyridil are main components of many pesticides, herbicides and fungicides[63-65] and have been used as reagents in the production of several compounds with pharmaceutical interest.[66-69] α–Pyridils have also found important applications in the preparation of transition metal complexes[70-72] and as organic inhibitors for mild steel corrosion in hydrochloric acid.[73]

In the present study, the structure of α–pyridil (**Scheme 4**) was investigated and its photochemistry analysed. The molecule was found to adopt a skewed structure in which the pyridyl rings are twisted. UV irradiation $\lambda > 235$ nm of the matrix-isolated compound showed that the compound prefers to isomerize into unusual molecular species bearing Hückel-type pyridine (aza-benzvalene) rings, contrary to what was observed for benzil (the similar dicarbonyl compound with two benzene rings), where irradiation has the effect of increasing the average O=C–C=O dihedral angle by relaxation in the excited electronic states, (S_1 and T_1), which contrarily to the ground state have planar configurations with the O=C–C=O dihedral angle equal to 180º,[74] or diacetyl ($CH_3C(=O)C(=O)CH_3$) and 1-phenyl-1,2-propanedione ($CH_3C(=O)C(=O)C_6H_5$) which were found to undergo photocleavage of the central C–C bond leading to production of carbon monoxide and acetone or acetophenone, respectively.[75,76]

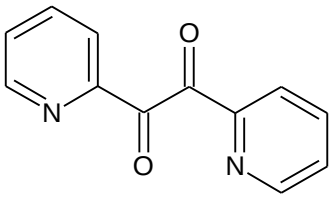

Scheme 4. Schematic representation of α–pyridil.

On the whole, the studies preformed on the nitrogen containing heterocycles allowed achieving considerable advances on the understanding of the reactivity of these compounds, specially the three-membered rings, and demonstrated its richness and versatility: from valence isomerizations to complex bond-breaking/bond-forming multi steps processes.

The other type of systems investigated in this study, though appearing to be very simple, revealed themselves also extremely challenging to investigation. Formic and acetic acids are indeed quite simple molecules, but their intramolecular dynamics and aggregation processes were found to be very interesting and complex.

FA and AA have attracted a great deal of interest for a number of reasons. They are the simplest carboxylic acids, and therefore serve as model compounds for understanding the reactivity of more complex biologically relevant molecular systems containing the carboxylic moiety. Acetic acid is of particular importance due to its structural proximity to glycine, the simplest amino acid. Both carboxylic acids have been identified in the interstellar medium.[77,78]

FA and AA have only two conformers (*trans* and *cis*, in **Scheme 5**) which can interconvert in one another through internal rotation around the C-O bond. The *cis* form is higher in energy than the *trans* form. Detailed infrared spectroscopic data for *trans* and *cis* conformers of these acids and some of their isotopomers have been reported in rare-gas matrices.[79-87] Narrowband vibrational excitation of the lower energy form (*trans*) was used to produce the higher energy *cis* conformer. The *cis* form subsequently converts to the lower energy conformer *via* dissipative proton tunneling through the torsional barrier, which limits its lifetime. Detailed studies of this type of processes for other compounds in noble gas matrices have also been reported.[88-100]

In the present study, the *trans* and *cis* forms of monomeric forms of FA and AA were investigated in nitrogen matrices. As in previous studies,[79-87] the higher energy *cis* conformer of these molecules was produced by vibrational excitation of the more stable *trans* conformer. It was found that for both molecules the tunneling is considerably slower in a nitrogen matrix than in rare-gas matrices (for example, the *cis*–to–*trans* conversion of HCOOH slows down in a nitrogen matrix by four orders of magnitude compared to a neon matrix) and a mechanism explaining this observation was proposed.

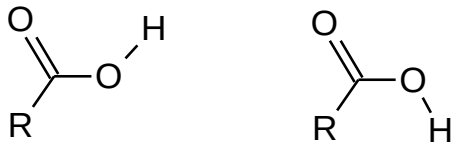

Scheme 5. *Trans* (most stable) and *cis* (higher energy) conformers of formic acid (R= H) and acetic acid (R= CH_3).

In addition to the monomeric forms of AA (*trans* and *cis*), in the present study AA dimers were also studied in a nitrogen matrix. Dimerization (and aggregation in general) in carboxylic acid systems is of fundamental importance in many areas of research, in particular materials science and biologically oriented subjects. The infrared spectra of three *trans-trans* and two *trans-cis* acetic acid dimers (Figure 1.1) were reported and analyzed. Both *trans-cis* dimers observed as well one of the trans-trans dimers were identified experimentally for the first time. One of the *trans-cis* AA dimers bearing an eight-membered ring with one C–H···O= and one OH···O= intermolecular H–bond, was produced by selective vibrational excitation of a structurally related *trans-trans* dimer; the other with a single OH···O= intermolecular hydrogen bond and the two monomeric units in a nearly perpendicular position, was obtained by thermal mobilization of a mixture of *trans* and *cis* monomers of AA, the latter being produced in an initial step by vibrational excitation of the *trans* monomer.

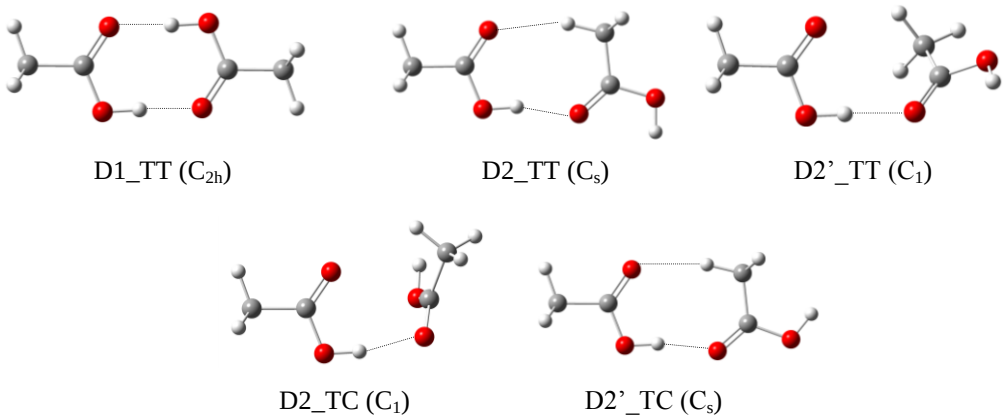

Figure 1.1 - Calculated structures for AA dimers (*trans-trans* and *trans-cis*) observed in solid nitrogen.

1.2. Experimental Methods

Matrix isolation spectroscopy

The term matrix isolation was first introduced by Pimentel, Whittle and Dows,[101] in 1954, to describe the technique of trapping molecules or atoms (guests) in solidified inert (or occasionally reactive) gases (hosts).[102-105] The principle of the matrix isolation method is to simulate the gas phase for the species by surrounding it with an inert and transparent solid (often rare gas solids such as Ar, Kr, Xe, or cryogenic solids *e.g.*, N_2, O_2, CO, methane) so that the interactions between the molecules of the trapped species are negligible as are the case of molecules in the gas phase at low pressures.

The extremely low working temperatures allow species which are normally short-lived, such as reactive intermediates and other unstable species resulting from chemical processes (*e.g.*, nitrenes and carbenes), to be preserved and studied with leisure. A variety of spectroscopic methods can then be applied to the detection and characterization of the trapped species, *e.g.*, infrared, ultraviolet/visible, nuclear magnetic resonance (NMR) and Raman spectroscopies. Among these methods, infrared spectroscopy is the most effective technique to determine the structure of the molecules isolated in low-temperature matrices. The low concentration of the trapped species makes negligible the interactions between guest molecules, while the usual chemical matrix of the host minimizes host-guest interactions. This leads to a decrease in dispersion of the vibrational levels, facilitating the comparison of the experimental spectra with the theoretical results (quantum chemical calculations or molecular mechanics), which normally treats the molecule like an isolated species in vacuum. In matrix isolation studies, the assignment of bands in IR spectra of intermediates was based primarily on the registry of the characteristic absorption bands, whenever possible with use of the isotopic substitution, reactions of primary intermediates, etc. Nowadays, the interpretation of experimental IR spectra is greatly simplified due to the development of accurate theoretical methods for their calculation, such as Density Functional Theory (DFT) based methods or up-tp-date perturbational approaches (*e.g.*, Møller-Plesset methods).[106]

The rigidity of the matrix inhibits diffusion of the molecules and minimizes aggregation, also contributing to increase the spectral resolution. Furthermore, if for instance the trapped molecules are made to react by *in situ* irradiation with UV light, in general the fragments resulting from the precursor species are unable to escape from the matrix cage where they were formed, precluding cross recombination reactions between fragments originated in different molecules. Such feature strongly simplifies the possible chemistry, thus making this method a very useful one to study reaction mechanisms.

Significant sharpening of the bands and increase in the peak intensities are observed in matrix isolation when compared to spectra obtained in most of current experimental conditions, where bands due to different vibrations are frequently overlapped, not allowing their separation. Another general finding for all matrix-isolation spectra is that the bands positions are weakly usually shifted when compared with gas phase spectra. However, care should still be taken in the band assignment, since, for example, it is frequent that in matrix isolation spectral bands show splittings caused by matrix (or site) anisotropy. Thus, the nature of the observed splittings can be due to different chemical species (different conformers) or to the same species in different trapping sites. Changing the matrix host is the most common method for distinguishing between these two possibilities. This procedure usually does not have a significant effect on the bands due to different chemical species but produces a drastic change in the profile of the signals due to distinct trapping sites. Another effective method to distinguish between bands originated by different chemical species and due to matrix interactions is to change the temperature of the gaseous mixture before deposition: this way, the relative gas phase populations of the different species may be altered, leading to a corresponding change in the intensity of the bands in the matrix whereas in principle the site splittings are insensitive to this procedure.

A matrix isolated sample can be prepared by deposition of a pre-mixed gaseous mixture or by co-deposition of the species to be studied (or a suitable precursor) and the host gas. In both situations, the gas mixture is directed towards a cold window kept typically in the 4-60 K temperature range and at very low pressure (10^{-8}–10^{-10} atm) inside a cryostat. A rapid cooling of the sample mixed with the inert matrix allows an efficient trapping of the populations of the different conformational

species, once the energy barriers separating them are large enough. Hence, the method is particularly suitable in the study of conformational isomerism.

Matrix isolation is also a quite powerful technique to investigate aggregation and H–bonding, since control of temperature of a pre-deposited matrix (or of the substrate, during deposition) can allow to efficiently control the levels of aggregation in a sample. The technique is then suitable for study of dimers and small aggregation.[107-118]

Thermally induced conformational isomerizations in cryomatrices

Matrix isolation infrared spectroscopy has been employed in numerous studies of conformational or tautomeric isomerization reactions, in the high or low temperature ranges (deposition temperature *vs.* "annealing").[119-125] In the high temperature range, as the temperature of the sample mixture is increased prior to deposition, the equilibrium among conformers is shifted in favour of the less stable conformers (or tautomers), *i.e.*, the more energetic forms. Assuming that no isomerization occurs during deposition, it is possible to determine the relative population of the conformers which should correspond to the equilibrium existing in the gas phase prior to deposition. However, for systems with low energy barriers (of a few kJ mol^{-1}) conversion of higher energy forms into lower energy forms can take place, being exceptions to this rule. In such systems the low temperature matrix distribution may differ considerably from that of the equilibrium gas phase due to ***conformational cooling*** during deposition of the matrix.[119-125] On the other hand, temperature variation studies by annealing of the matrices to higher temperatures, may also lead to loss of the less stable forms.[119-125] In practical terms, all these changes should be observed regarding the intensity of the bands assigned to the different conformers and not reflect in the appearance of new bands, which would indicate different species than those molecules present in the deposited matrix. Annealing of the matrices can be attained to 35, 45 and 60 K, for argon, krypton and xenon matrices, so that in some cases observation of isomerization can only be observed in the heavier atom matrix gases, depending on the energy required for the conversion.[119]

1,2-Butanediol[122] represents an extreme case of conformational cooling. The molecule has three conformationally relevant rotational axes, which can result in 81

possible conformations. In this molecule, as a result of massive conformational cooling occurring upon matrix deposition, only five conformers of 1,2-butanediol were retained in the samples deposited at 10 K. The theoretically predicted energy barriers are high enough to allow these five minima to be trapped in the matrices at this temperature. On the other hand, annealing of the matrices up to 50 K, resulted in the conversion of all higher energy forms into the most stable single conformer.

Cyanoacetic acid (CAA) and methyl cyanoacetate (MCA) are two related systems, which differ from each other by replacing the acid hydrogen atom by a methyl group.[123] *Ab initio* calculations predicted that both systems have two isoenergetic conformers (*gauche* and *syn*) separated by similar low energy barriers (*ca.*3 kJ mol^{-1}). The relative populations of the two conformational states trapped in the matrices however, were found to strongly depend on the temperature of the optical substrate during deposition. When CAA was deposited in a xenon matrix at 20 K, only bands due to one conformer (more stable) was observed, contrarily to what could be expected, since calculations predicted that both conformers should co-exist in the gas phase. By decreasing the substrate temperature to 10 K, the second conformer could, however, been trapped in the matrix, because at that temperature the barrier for interconversion is high enough to prevent conformational cooling to take place during deposition. In the case of MCA, both argon and xenon matrices have been studied and both *syn* and *gauche* isomers were observed. During annealing of the matrices the *gauche* form was converted into the *syn*, as well as in the series of experiments in which matrices were deposited at increased substrate temperature. The different behaviour shown by these two similar structures indicates that necessary care must be taken in transferring the gas phase potential energy landscape to matrices. Indeed, in some cases, interaction with the matrix results in considerable change in the PES and direct comparison with gas phase is no more possible. In general, more polar and more planar conformers are favoured in matrices relatively to the gas phase.[121,123] The three most stable conformers of dimethyl sulphite (GG, GG' and GT) could be isolated and characterized in argon matrices.[124,125] Annealing of the matrix allows the conversion of the GG' into GT form, which in turn yields the most stable GG form. The two observed processes were found to occur at two temperatures in consonance with the relative values of the predicted energy barriers: GG′→GT, 1.90 kJ mol^{-1}; GT→GG, 9.64 kJ mol^{-1}; and GG′→GG, 19.46 kJ mol^{-1}.

The knowledge of the energy barriers for interconversion between the conformers is, as stated above, of extreme importance in the interpretation of the experimental results. It will be shown in Chapter 3 that, in the case of MCPIC and MACBP molecules studied in this project the energy barrier between conformers **III** and **II,** being extremely low, lead conformer **III** to relax into conformer **II** during matrix deposition, thus precluding its experimental observation in both argon and xenon matrices. Also, the moderately low barrier for the **II**→**I** isomerization (*ca.* 4 kJ mol^{-1}) in MCPIC resulted in partial conversion of **II** into **I** during matrix deposition. On the other hand, in the case of MCPOC, the predicted barrier for the **II**→**I** isomerization (20.5 kJ mol^{-1}) is high enough to prevent this reaction to take place during matrix deposition. With an energy barrier this high, a considerable wider range of temperatures should be used to allow for conformational relaxation. Indeed, annealing of the xenon matrices up to *ca.* 60 K allowed observation of a redistribution of the intensities of the bands due to monomers, indicating conversion of form **II** into conformer **I**.

Photochemistry in matrices

Besides the low working temperature and chemical inertia of a noble gas cryomatrix, which helps stabilizing less stable chemical species, the relative rigidity of the matrix cage is particularly relevant for photochemical studies of matrix isolated species. These conditions facilitate the study of photochemical reactions in general, as the processes are restricted to a specific matrix cage. Due to the general inhibition of molecular diffusion, the observed processes do not involve more than one reactant molecule, and, in secondary steps, more than the products formed from a unique initial reactant molecule. Photochemical excitation by ultraviolet irradiation of the matrix-isolated molecules can promote conformational and/or other types of isomerization reactions, of the trapped species can undergo other photochemical transformations such as photodegradations or rearrangement reactions through bond cleavage (or bond cleavage/bond forming) originating new products.

Irradiation *in situ* of the matrix with ultraviolet light allows observation of processes with high energy barriers, since it may allow providing the molecule with a

large amount of energy. However, in some cases, subsequent reactions to photoexcitations can be quite exothermic, resulting in significant increase of local temperature. This can lead to subsequent reaction steps and also partial diffusion of the species still present in the matrix.

Conformational changes leading to an increase in population of one or more high energy conformers can be achieved upon irradiation of the matrices with ultraviolet light. Nishino and Nakata[126,127] studied the photoreaction mechanism for halogen substituted carboxylic acids. The rotational isomerism of 2-choloropropionic acid (2CPA)[126] in a low temperature argon matrix was investigated. The photoisomerization from *syn* to *anti* forms around the C–O bond and around the central C–C bond of 2CPA was observed upon irradiation at $\lambda > 240$ nm. In an earlier study, 2-chlorobenzoic acid (2CBA)[127] was investigated. The spectra of the two most stable isomers, SC and ST, were observed after deposition in argon and xenon matrices. Upon UV irradiation, two less stable isomers, AT and AC, were formed.

Several types of photoinduced tautomerization reactions are known (*e.g.*, keto-enol,[128,129] amino-imino[130-132] and oxo-hydroxy[133,134]) and have been extensively studied in matrices. One of the simplest models for keto-enol tautomerism is the 2-hydroxypyridine/2(1H)-pyridinone system.[129] The amino-imino tautomerization in several amino pyridine derivatives, such as 2-aminopyridine, 2-amino-5-methylpyridine and 2-(methylamino)pyridine, was investigated by Akai *et al.*[130-132] In the case of 2-amino-5-methylpyridine,[131] the amino tautomer is more stable and changes into the imino tautomer (5-methyl-2(1H)-pyridinimine) upon UV irradiation ($370 > \lambda \geq 340$ nm), while the reverse change occurs by longer wavelength ($420 > \lambda \geq 340$ nm) irradiation. The two most stable forms of hypoxanthine,[133] oxo-N(9)-H and oxo-N(7)-H, as well as a very small amount of the minor hydroxy-N(9)-H tautomer were observed in argon matrices directly after their deposition. UV irradiation of the matrices induced conversion of the oxo tautomers of the compound into the hydroxy-N(9)-H and hydroxy-N(7)-H forms, respectively. According to the reports of Maier and Enders[135] and of Duvernay *et al.*,[136] an analogous oxo $\rightarrow$ hydroxy phototautomerism occurs also for the simple molecule of formamide.

UV irradiation can also promote photodissociation reactions of matrix-isolated species. As mentioned above, the processes are restricted to a specific matrix cage,

thus preventing the formation of many of the photoproducts expected to be formed in gas phase or solution.

The photochemistry of matrix-isolated 1-phenyl-1,2-propanedione in solid xenon was studied by Lopes *et al.*[76] Irradiation of the matrix with UV light (λ > 235 nm) led to decarbonylation of the compound, with generation of acetophenone and carbon monoxide, with an almost complete consumption of the reagent after 20 hours of irradiation. The reaction proceeds with formation of radicals but no signs of the putative products resulting from cross-reactions including different molecules could be detected in the spectra of the photolyzed matrix.

Two 3-methyl-*2H*-azirines bearing electron-withdrawing substituents at C2, clearly related to some of the compounds studied in the present work, methyl 3-methyl-*2H*-azirine-2-carboxylate and methyl 2-chloro-3-methyl-*2H*-azirine-2-carboxylate, were studied by Gómez-Zavaglia *et al.*[20-22] *In situ* broadband UV (λ > 235 nm) excitation led to the observation of two primary photoprocesses: C–C bond cleavage with production of nitrile ylides and C–N bond cleavage with formation of methylated ketenimines.

For the oxazole representative described in this thesis (methyl 4-chloro-5-phenyl-1,3-oxazole-2-carboxylate; MCPOC), no photodecomposition of the oxazole ring was observed upon broadband UV irradiation. The situation for the isoxazole counterpart (MCPIC) was the opposite. Irradiation of the matrix-isolated compound lead to formation of MCPOC as final photoproduct. In agreement with the mechanism for the isoxazole→oxazole photoisomerization previously proposed,[7,8,13-15] the expected azirine and nitrile-ylide intermediates could be identified spectroscopically in the photolyzed matrices in the present study.

In turn, methyl (Z)-2-azido-3-chloro-3-benzoyl-propenoate (MACBP) was also found to be transformed into MCPOC in a reaction where the azirine and nitrile ylide also work as intermediates. This reaction was found to be accompanied by a second one, leading to formation of the ketenimine *C*-chloro-*C*-benzoyl-*N*-methoxycarbonylketenimine (CBMK). The non-observation of the corresponding isoxazole suggests the concerted nature of the different steps leading to the observed final products. This also supports the idea that in the studied system the putative vinyl

nitrene intermediate is not involved in the conversion of the azide into the azirine, as well as in the subsequent reactions of this latter.

The photochemistry of methyl aziridine-2-carboxylate (MA2C) was also addressed in the present study. The primary photoproduct was found to be methyl 2-(methyleneamino)-acetate (MMAA) obtained from the 1,2 hydrogen atom shift from the azomethine ylide resulting from ring-opening through cleavage of the aziridine C–C bond. Irradiation at λ = 290 nm using narrowband tunable laser light led to the decrease of bands due to of the most stable form of MMAA and formation of other photoproducts derived from the latter. Subsequent photodecomposition photoprocesses were also observed leading to formation of carbon monoxide and other unidentified products.

In the case of matrix-isolated α-pyridil, as mentioned before, contrarily to other α-dicarbonyl compounds (*e.g.*, diacetyl, 1-phenyl-1,2-propanedione),[75,76] which undergo cleavage of the intercarbonyl group followed by decarbonylation from one of the radicals initially formed and recombination of the two resulting radicals to form, as final product, the ketone, α-pyridil was found to prefer to isomerize into unusual molecular species bearing Hückel-type pyridine (aza-benzvalene) rings upon irradiation at $\lambda > 235$ nm.

Infrared induced conformational isomerization and tunneling in cryomatices

Infrared irradiation, in particular, irradiation in the near infrared region using a narrowband tunable light source recently became of practical use to induce conformational isomerizations in low-temperature matrices.[79-100,107-111] This approach allows the selective excitation of a specific vibrational mode of a given species and convert this species into other forms. The effect of near-infrared irradiation was first observed by Pimentel and his co-workers for the *cis-trans* isomerization in nitrous acid (HONO),[93,94] which is the smallest stable molecule exhibiting rotational isomerism. Isomerization rates for HONO[95,96] were reported to depend strongly on the host matrix. By using infrared band pass filters, Hall and Pimentel[94] demonstrated that both *cis* $\rightarrow$ *trans* and the reverse *trans* $\rightarrow$ *cis* interconversions took place simultaneously, but at different rates. Khriachtchev *et al.*[97] showed that *trans-cis*

isomerization of HONO in a krypton matrix takes place when either the OH stretching or N=O first overtone modes are excited. Very interestingly, the isomerization process is found to be selective with respect to matrix sites, demonstrating the stability of the host cage under the resonant IR irradiation. Narrowband near-infrared irradiation was also used to produce the higher energy conformer of hydroxyacetone.[91]

The high energy *cis* forms of several carboxylic acids, (formic, acetic, propionic and propiolic acid) and their isotopomers could be prepared from the lower energy corresponding *trans* forms by this method and studied in different cryogenic matrices.[79-88,90] The *cis* form subsequently converts to the lower energy *trans* conformer *via* dissipative proton tunneling through the torsional barrier, which limits their lifetime.

Cis-CH_3COOH has a shorter lifetime in rare-gas matrices than *cis*-HCOOH (*ca.* 50 s[85] *versus* 8 min[86] in solid argon at 8 K). Deuteration of the OH group influences greatly the tunneling process, slowing it down by about four orders of magnitude. The conversion process of *cis*-CH_3COOD and *cis*-HCOOD to the *trans* forms in an argon matrix at 8 K takes about 15 days.[85,87] On the other hand, the tunneling rates in formic[86] and acetic acids[85] increase upon deuteration of CH or CH_3 groups. This secondary isotopic effect is very interesting but was not yet explained.

The tunneling rates in these species are strongly dependent on the matrix material. The *cis*-HCOOH decay rates increase with the matrix polarizability as $k_{Xe} < k_{Kr} < k_{Ar} < k_{Ne}$.[86] However, the decay of *cis*-HCOOD follows almost the opposite trend: $k_{Xe} \approx k_{Kr} > k_{Ar} \approx k_{Ne}$.[87] With respect to the reaction barrier height, which increases in more polarizable hosts, the order of the rate constants in HCOOD is anomalous.[86,107] Similar "anomalous" behavior was also reported for AA ($k_{Xe} \geq k_{Ar} > k_{Kr}$).[85] Clearly, in addition to the barrier change upon solvation in polarizable media, other factors can also influence the *cis*-to-*trans* conversion.[86,87,107]

In the present study, both HCOOH and CH_3COOH were studied in nitrogen matrices. It was shown that the *cis* conformers of these compounds are stabilized in N_2 matrix by factors of 55 and 600 (compared to argon matrix) due to interactions of $OH^{\cdots}N_2$ type. The IR spectra of the *cis* and *trans* conformers of both acids were assigned.

Exciting new research has been opened with the preparation by vibrational excitation of the *trans–trans* dimeric forms of FA in neon and argon matrices, yielding

trans–cis dimers.[108-111] It was found that tunneling decay of *cis* formic acid is substantially slower in the dimeric form compared to monomer, especially in solid neon.[109] This stabilization effect was explained by a complexation-induced increase of the reaction barrier, which was confirmed computationally.[108]

In this thesis, data for dimers of FA and AA in N_2 matrices are presented. Three new acetic acid dimers were produced *in situ*, characterized structurally and spectroscopically and evaluated from the point of view of stability (for *cis* containing dimers).

1.3 Computational Methods

The use of computational methods can simplify significantly the interpretation of results obtained from experimental studies. It is in general possible nowadays to find a suitable method with a level of calculation adequate to the study of the desired systems or properties. These methods include Molecular Mechanics (MM), semi-empirical, *ab initio* and density functional methods.[137-141] In a simple view, MM can be considered to be based on a model where a molecule is described as a collection of atoms represented as balls whose mass depends on the elements connected by chemical bonds that are treated as springs whose stiffness depends on which elements are bound together, and whether the bond is single, double or triple. If the normal spring lengths and the angles between them are known, and how much energy it takes to stretch and bend the springs, then the energy of a particular set of balls and springs, *i.e.*, of a given molecule, can be calculated; changing the geometry until the lowest energy is found enables us to do a geometry optimization, *i.e.*, to calculate a stable geometry for the molecule.[138,140]

Semi-empirical methods are based on approximate solutions of the Schrödinger equation, using appropriate parameters derived from experimental data in order to simplify the calculation and achieve a faster solution (using less computational resources). The large majority of semi-empirical methods use only s- and p- functions, and the basis functions are Slater type orbitals (STO). Therefore, the computational cost is reduced by reducing the number of integrals which are required

to be calculated. Semi-empirical calculations are slower than MM, but much faster than *ab initio* calculations.[138,140]

Ab initio calculations are also based on the Schrödinger equation, however, no experimental parameters are used in the calculations. Their computations are based only on the laws of quantum mechanics and on the values of a small number of physical constants (the speed of light, the masses and charges of electrons and nuclei, Planck's constant). Both the semi-empirical and the *ab initio* approaches calculate a molecular wave function and molecular orbital energies and thus represent wave function methods.[137-140]

Density Functional Theory (DFT) calculations define the energy of an electronic system in terms of its electronic probability density function, $\rho(\vec{r})$, and not in terms of a wave function. In addition, they include the effects of electron correlation within a single configuration representation of the ground electronic state of atoms and molecules.[137-141] They are in general more efficient then *ab initio* methods in terms of computational efforts and have been widely used in structural chemistry and theoretical spectroscopy during the last two decades.

Semi-empirical methods

Semi-empirical methods are simplified versions of Hartree-Fock theory using empirical (derived from experimental data) corrections in order to improve performance. The first step in reducing the computational problem to solve, is to consider the valence electrons, ignoring core (non-valence) electrons and making major theoretical assumptions. Furthermore, only a minimum basis set is used for the valence electrons. These methods allow the user a way to study larger molecules, however, it is not possible to compute all molecules using these methods. Semi-empirical methods do not behave well with hydrogen bonding, transition sates, or molecules with non-parameterized atoms.[138,140]

The most frequently used methods include the Modified Neglect of Differential Overlap (MNDO),[142] Austin Method 1 (AM1)[143] and Parameterization Method 3 (PM3).[144-146] All of them are based on the Neglect of Differential Diatomic Overlap (NDDO) integral approximation, while older methods use simpler integral

schemes such as Complete Neglect of Differential Overlap (CNDO) and Intermediate Neglect of Differential Overlap (INDO). All three approaches belong to the class of Zero Differential Overlap (ZDO) methods, in which all two-electron integrals involving two-center charge distributions are neglected. Of the various methods, PM3 is the most commonly cited in computational chemistry literature. This was the selected semi-empirical method to be used in this study, whenever required.

The PM3 method was developed by J. P. Stewart in the late 1980s.[144-146] The name derives from the fact that this was the third NDDO method (following MNDO and AM1). PM3 is considered a variation of AM1, as PM3 contains many of the parameters as does AM1, differing mainly in how the parametrization is done. PM3 uses two Gaussian functions per atom, instead of the variable number used by AM1 (which uses between one and four Gaussians per element). The increase in the numerical values of the parameters permitted an efficient search of the parameter space compared to AM1. As compared to MNDO, the parameters are quite different, but the accuracy of the calculation is close to the same. With the publication of the 44 sets of parameters in 2004,[147] the mapping of the more important elements of the main group is completed for the semi-empirical methods MNDO, AM1, and PM3.

Ab initio calculations

The general objective of *ab initio* quantum chemical methods is the solution of the time-independent Schrödinger equation[148]

$$\hat{H}\Psi(r,R) = E(R)\Psi(r,R) \tag{1.3.1}$$

where $\hat{H}$ is the Hamiltonian operator, E is the molecular energy and $\Psi(r,R)$ is the molecular wave function that depends on the coordinates of the electrons and nuclei.

The Hamiltonian operator for a molecule with N nuclei and n electrons can be expressed (in atomic units) as:

$$\hat{H} = -\sum_{i=1}^{n}\frac{1}{2}\nabla_i^2 - \sum_{A=1}^{N}\frac{\nabla_A^2}{2M_A} - \sum_{i=1}^{n}\sum_{A=1}^{N}\frac{Z_A}{r_{iA}} + \sum_{i<j}^{n}\sum_{j=1}^{n}\frac{1}{r_{ij}} + \sum_{A<B}^{N}\sum_{B=1}^{N}\frac{Z_A Z_B}{R_{AB}} \tag{1.3.2}$$

where *i* and *j* are electron indices, *A* and *B* are nuclei indices, *r* is the distance between electrons or electron-nuclei and *R* is the distance between nuclei, *e* is the electron charge, *Z* is the atomic number, M_A is the mass of nucleus *A*, and finally, ∇_i^2 and ∇_A^2 represent the Laplace operators associated to electrons and nuclei, respectively.

The first and second term represent the electronic and nuclear kinetic energy operators, respectively, which depend on the mass and coordinates of the particles. The third to fifth terms represent the potential energy operators, nuclear-electronic attraction, electronic-electronic repulsion and the nuclear-nuclear repulsion, respectively.

Since the above equation does not have an analytical solution, a few approximations were set up. The Born-Oppenheimer approximation[149] was introduced to separate the nuclear and the electronic motion. Within this approximation, the wave function is separated into electronic and nuclear parts. One can consider the electrons in a molecule to be moving in the field of fixed nuclei. Consequently, the kinetic energy of the nuclei can be neglected and the repulsion between the nuclei can be considered to be constant. The Hamiltonian operator can then be separated into two equations, the electronic (1.3.3) and nuclear Hamiltonians (1.3.4):

$$\hat{H}^{elec} = \hat{T}^{elec}(r) + \hat{V}^{elec-nuc}(r,R) + \hat{V}^{elec-elec}(R) \qquad (1.3.3)$$

where the first term represents the electronic kinetic energy operator, the second and third terms correspond to the nuclear-electronic attraction and electronic-electronic repulsion potential energy operators;

$$\hat{H}^{nuc} = \hat{T}^{nuc}(R) + E^{eff}(R) \qquad (1.3.4)$$

where $\hat{T}^{nuc}$ is the nuclear kinetic energy operator and E^{eff} is the nuclear effective potential. The introduction of this nuclear effective potential means that each electron is subjected to a field that models the effect of the other electrons in the system (this is a reasonable first approximation to the way that electrons interact with each other).

The Hartree-Fock Theory

A first approximation in solving the Schrödinger equation for *n* electrons systems, is treating the electron-electron repulsion that one electron experiences from another electron as a mean field repulsion (Hartree-Fock procedure). The wave function is taken as a single product of *n* one-electron functions (molecular orbitals, MOs), which is known as a Hartree product

$$\Psi = \prod_i \phi_i = \phi_1(x_1)\phi_2(x_2)...\phi_n(x_n) \tag{1.3.5}$$

However, the wave function must be antisymmetric with respect to the exchange of the positions (and spin) of any two electrons, *i.e.*, the Pauli Exclusion Principle must be followed. Since the Hartree product fails to satisfy the antisymmetry principle, to ensure that an approximate wave function meets these criteria, it may be written as a determinant of spin orbitals (Slater determinant):[150]

$$\Psi(x_1, x_2, ..., x_n) = \frac{1}{\sqrt{n!}} \begin{vmatrix} \phi_1(x_1) & \phi_2(x_1) & \dots & \phi_n(x_1) \\ \phi_1(x_2) & \phi_2(x_2) & \dots & \phi_n(x_2) \\ \dots & \dots & \dots & \dots \\ \phi_1(x_n) & \phi_2(x_n) & \dots & \phi_n(x_n) \end{vmatrix} \tag{1.3.6}$$

By minimizing the energy of the spin-orbital wave function, through the variational principle, the Hartree-Fock equations are obtained[151,152]

$$\hat{f}\phi_i = \varepsilon_i \phi_i \tag{1.3.7}$$

where $\hat{f}$ is an effective one-electron operator or Fock operator, ε_i is the energy of orbital *i*, and ϕ_i represents the spin orbital. The Fock operator is given by

$$f(i) = -\frac{1}{2}\nabla_i^2 - \sum_{A=1}^{N} \frac{Z_A}{r_{iA}} + v^{HF}(i) \tag{1.3.8}$$

where $v^{HF}(i)$ is the average potential experienced by the *i*th electron due to the presence of the other electrons. From a practical point, the treatment of the equations is iterative, also called as self-consistent (*Self-Consistent Field*, SCF). The method searches until the orbitals and the average potential no longer change.

Unfortunately, the Hartree-Fock equations cannot be solved for systems larger than atoms or molecules with small number of electrons. Each MO can then be expressed as a linear combination of atomic orbitals (AO) called *basis sets*

$$\phi_i = \sum_{\nu=1}^{M} c_{\nu i}\chi_\nu \tag{1.3.9}$$

where $c_{\nu i}$ are the expansion coefficients of the molecular orbital ϕ_i in the basis functions, χ_ν, usually called as atomic orbitals (AO). The Hartree-Fock-Roothan[153] equations can be written in matrix form as

$$\sum_{\nu}^{M} F_{\mu\nu}c_{\nu i} = \varepsilon_i \sum_{\nu}^{M} S_{\mu\nu}c_{\nu i} \qquad i=1,2,...,M \tag{1.3.10}$$

or even more simply as

$$FC = SC\varepsilon \tag{1.3.11}$$

where $F_{\mu\nu}$ are elements of the Fock matrix, *F*, $S_{\mu\nu}$ are elements of the overlap matrix *S*, and ε_i is the orbital energy of the molecular orbital ϕ_i.

The Hartree-Fock method produces an energy that is higher than the actual value (a consequence of the Variational Principle) due to the approximation of the wave function. Furthermore, the Schrödinger equation is not actually separable, and so the nuclear orbital approximation introduces inaccuracy in this respect. Moreover, it also treats the Coulombic repulsion between electrons in an average way only, whereas the instantaneous interaction between electrons must be considered for a more accurate counter. The motion of the electrons is said to be correlated and it is the

instantaneous electronic interaction (not just an average repulsion) that is referred to as electron correlation. The correlation energy (E_{corr}) is the difference between the exact non-relativistic energy of the system (ε) and the Hartree-Fock energy (E_{HF})

$$E_{corr} = \varepsilon - E_{HF} \tag{1.3.12}$$

Because the Hartree-Fock energy is an upper bound to the exact energy, the correlation energy is negative.

Basis sets

Most methods require a specific basis set. As mentioned, basis set is a mathematical description of the molecular orbitals within a system, expanded as linear combinations used to approximate the electronic wave function. *Slater Type Orbitals* (STO) are commonly used as basis functions in molecular calculations, however the two-electron integrals require excessive computer time. Nowadays, Gaussian type atomic functions, *i.e.*, *Gaussian Type Orbitals* (GTO), are currently used as basis functions in electronic structure calculations. GTOs can be written in terms of polar or Cartesian coordinates

$$\chi_{\zeta nlm}(r,\theta,\varphi) = NY_{lm}(\theta,\varphi)r^{n-1}e^{-\zeta r^2}$$
$$\chi_{\zeta nlm}(x,y,z) = Nx^{l_x}y^{l_y}z^{l_z}e^{-\zeta r^2} \tag{1.3.13}$$

where *N* is a normalization constant and the sum l_x, l_y and l_z determines the type of orbital. If $l_x + l_y + l_z = 0$, the GTO is a *s*-type; if the sum is equal to 1 or 2, the GTO is a *p*-type or *d*-type, respectively. However, individual Gaussian functions do not represent the electronic distribution as well as the STO, requiring the use of a linear combination that allows a better representation of the STO. Linear combinations of primitive Gaussians which are used to form the basis function are designated as *Contracted Gaussian Functions* (CGF) according to

$$\chi_r = \sum_a^M d_{ar} \chi_a \tag{1.3.14}$$

where M is the number of primitive gaussians used in the linear combination, the contraction coefficients d_{ar} do not vary independently but are held fixed within each linear combination.

A minimal basis set consists of the smallest number of functions. For instance, STO-3G[154] basis set is a minimal basis set which combines three contracted gaussians functions for each AO. The double zeta (DZ, $double-\zeta$) and triple zeta (TZ, $triple-\zeta$) type basis are included in the split valence basis set which uses two or more STO for each inner-shell. A DZ basis set contains two times as many functions as the minimal basis set, each atomic orbital is represented by two STO basis functions. The letter (ζ) is the exponent of the STO basis functions. The basis sets 3-21G, 4-31G, 6-31G and 6-311G[155-159] are a few examples of split valence basis sets.

This type of basis set can incorporate polarization functions, *e.g.*, 6-31G* or 6-31G(d), include *d*-type orbitals to describe the heavy atoms, while 6-311G** or 6-311G(d,p) also include *p*-type orbitals to describe the hydrogen atoms in addition to the *d*-type orbitals to describe the heavy atoms.[160] In addition, diffuse functions can also be added, denoted by + or ++, that consist of *s*-type and *p*-type orbitals to portray the heavy atoms and the hydrogen atoms.[161] Diffuse functions are necessary for correct description of anions and weak bonds and are frequently used for calculations of such properties as dipole moments, polarizabilities, hydrogen bonds, etc.

Two basis sets were used in this work, 6-311++G(d,p)[159] for the heterocyclic compounds and 6-311++G(2d,2p)[159,160] for formic and acetic acids. Both basis set include polarization and diffuse functions. In both basis sets, 6-311 can be explained as 6 Gaussian functions for the inner shells, 5 Gaussian functions to describe the valence orbitals, composed of three, one and one contracted Gaussians, representing triple zeta basis set. On the other hand, the basis set 6-311++G(2d,2p), adds 2 *d*-type and 2 *p*-type orbitals on heavy atoms and hydrogen atoms. These basis sets constitute appropriate choices for the systems studied, enabling a good comparison between the quality of the results and the computational effort.

Møller-Plesset Perturbation Theory

A relatively simple treatment of electron correlation is the Perturbation Theory described by Møller-Plesset in 1934.[162] According to the Perturbation Theory the Hamiltonian $\hat{H}$ is divided into two parts, described as the sum of the unperturbed Hamiltonian $\hat{H}^0$ and a perturbation applied to $\hat{H}^0$, $\hat{H}'$:

$$\hat{H} = \hat{H}^0 + \lambda\hat{H}' \tag{1.3.15}$$

λ is an arbitrary real parameter that satisfies the relation $0 \leq \lambda \leq 1$.

In order to obtain the exact solution to the Schrödinger equation, one must start from the solutions of the unperturbed system. Therefore, the unperturbed wave function, $\psi^{(0)}$ is the HF wave function and the HF energy is the sum of the zeroth order correction (λ=0), $E^{(0)}$, and the first order one (λ=1), $E^{(1)}$:

$$E_{HF} = E^{(0)} + E^{(1)} \tag{1.3.16}$$

The first correction to the electronic ground state energy is given by the second order perturbation (MP2):

$$E^{(2)} = -\sum_{J\neq 0} \frac{\left|\left\langle \psi^{(0)} \middle| H' \middle| \psi_J \right\rangle\right|^2}{E_J - E^{(0)}} = -\sum_{J\neq 0} \frac{\left|\left\langle \psi^{(0)} \middle| H' \middle| \psi_J \right\rangle\right|^2}{\varepsilon_i + \varepsilon_j - \varepsilon_a - \varepsilon_b} \tag{1.3.17}$$

where *J* concerns the degree of substitution of the wave function (in this case, two electrons are promoted from the occupied orbitals *i* and *j* to virtual orbitals *a* and *b*, with energies ε_i, ε_j, ε_a e ε_b, respectively).

Thus,

$$E_{MP2} = E_{HF} + E^{(2)} \tag{1.3.18}$$

where the knowledge of the Hartree-Fock orbitals (ϕ) and its respective energies (ε) is required.

To improve further the Hartree-Fock energy, higher order energy corrections should be calculated, $E^{(3)}, E^{(4)}$, etc. MP calculations are designated by MP2, MP3, MP4, according to their order of energy correction $E^{(2)}, E^{(3)}$ or $E^{(4)}$, respectively.

Some of the advantages of the MP theory include the size-consistency, interpretability in terms of correlations between specific number of electrons, and the ability to describe van der Waals attractive forces. Furthermore, the MP theory always provides improved geometries and relative energies for the stationary points on the potential energy surface compared to HF theory. However, for some molecules convergence problems might occur when the molecule is far from the equilibrium geometry or when the fundamental ground state is not sufficiently displaced from the lowest excited state. In practical terms, it could become more advantageous to use a higher basis set with a MP2 calculation than use a smaller basis set with a MP3 or MP4 level calculation. In the present study MP2 calculations were selected,[163] with the 6-311++G(d,p) and 6-311++G(2d,2p) basis sets. The use of MP2 calculations was found to be particularly relevant in the studies of dimeric structures (Chapter 4). The optimized geometries of the minima of MA2C were also calculated at the MP2 level using the 6-311++G(d,p) basis set.

Density Functional Theory

Density Functional Theory (DFT) methods are nowadays the most widespread methods used in computational science and solid state physics, due to its high computational efficiency and very good accuracy compared to HF or MP methods.[137-141] Its foundations emerged for the first time in the late 1920s, with the work developed by Thomas and Fermi,[164,165] based on the uniform electron gas. The main advantage of DFT is that the energy of an electronic system can be defined in terms of its electronic probability density, $\rho(\vec{r})$. For a system with *n* electrons, $\rho(\vec{r})$ represents the total electron density at a particular point in space *r*. The electronic energy *E* is regarded as a functional of the electron density, $E[\rho]$.

The Hohenberg-Kohn theorems[166] were able to relate the energy and other properties of the system with the electron density. The first theorem (*Existence Theorem*) demonstrates that all the properties of a molecule in the ground electronic state are uniquely defined by its electron density. Although, the first theorem confirms the existence of a functional relating the electron density and the energy of a system, it does not tell us the form of such functional. The second theorem (*Variational Theorem*) states that the functional that delivers the ground state energy of the system delivers the lowest energy if and only if the input density is the true ground state density.

Nowadays, DFT calculations are based on the Kohn and Sham approach,[167] which allowed to overcome the difficulty related to the kinetic energy functional of the system. The basic idea in the Kohn e Sham formalism is splitting the kinetic energy functional into two parts, one part that can be calculated exactly, which considers non-interacting electrons, and a small correction term accounting for electron-electron interaction. In the non-interacting case, $E[\rho]$ has a kinetic contribution and a contribution from the external potential:

$$E(\rho) = E^T(\rho) + E^V(\rho) + E^J(\rho) + E^{XC}(\rho) \tag{1.3.19}$$

where E^T is the electronic kinetic energy term, E^V is the potential energy of the nuclear-electronic attraction term, E^J, is the classic Coulomb repulsion between electrons, the finally, E^{XC}, is the exchange correlation-energy term.

There are a large number of approximations that attempt to calculate the electron exchange-correlation energy functional. The Local Density Approximation (LDA) constitutes the simplest approach to represent this functional. At the center of this model is the concept of a uniform electron gas. In short, LDA assumes that the density is uniform throughout the molecule. The LDA exchange-correlation energy functional can be written as

$$E_{XC}^{LDA}[\rho] = \int \rho(\vec{r}) \varepsilon_{XC}(\rho(\vec{r})) d\vec{r} \tag{1.3.20}$$

In this equation, $\varepsilon_{XC}\left(\rho(\vec{r})\right)$ is the exchange-correlation energy per particle of uniform electron gas of density $\rho(\vec{r})$. The exchange-correlation energy, ε_{XC}, can be further split into two separate parts, the exchange energy, ε_X, and the correlation energy, ε_C.[164,165,168]

The Local Spin Density Approximation (LSDA) represents a more general application of LDA, which introduces spin dependence into the functionals and has been gradually replacing LDA for open shell systems. Within the LSDA approach, the total electronic density is equal to the sum of the α spin density and the β spin density.

Although LDA and LSDA produce good results for certain systems, this is not the case for other molecules. For many molecules, the electron density is not uniform, therefore, functionals that combine electron density and are gradient corrected were created. Generalized Gradient Approximation (GGA) methods also referred to as non-local methods take into account this effect. The GGA exchange-correlation energy functional can be written as

$$E_{XC}^{GGA}\left[\rho^{\alpha},\rho^{\beta}\right]=\int f\left(\rho^{\alpha}(\vec{r}),\rho^{\beta}(\vec{r}),\nabla\rho^{\alpha}(\vec{r}),\nabla\rho^{\beta}(\vec{r})\right)d\vec{r} \qquad (1.3.21)$$

where *f* is any given function of the spin densities and their corrected gradients. The GGA exchange-correlation energy, E_{XC}^{GGA}, can also be divided into two parts, exchange energy and correlation energy.[137-141]

There are also bybrid methods that combine functionals from other methods with pieces of a Hartree-Fock calculation, usually the exchange integrals. Among the most popular hybrid functionals, the exchange functional developed by Becke in 1988 (B or B88),[169] Perdew-Wang in 1986 (PW86),[170] modified to Perdew-Wang in 1991 (PW91),[171] the correlation functionals of Lee, Yang and Parr (LYP),[172,173] Perdew in 1986 (P86)[174] and, Vosko, Wilk and Nusair (VWN) in 1980,[175] are now in wide use. The B3LYP hybrid functional one of the most popular functional used in theoretical calculations today. The B3LYP functional is given as[169,172,173,175]

$$E_{XC}^{B3LYP}=(1-a)E_X^{LSDA}+aE_X^{HF}+b\Delta E_X^{B}+(1-c)E_C^{VWN}+cE_C^{LYP} \qquad (1.3.22)$$

In this equation, the exchange energy E_X^{HF}, is sometimes denoted as HF exact exchange energy functional, E_X^{exact}. The parameters *a*, *b* and *c* have the same values as those attributed by Becke for the B3PW91 functional (0.2, 0.72 and 0.81, respectively). The exchange functional developed by Becke in 1988 is:

$$E_X^B = E_X^{LSDA} - b\sum_{\sigma=\alpha,\beta}\int \frac{(\rho^\sigma)^{\frac{4}{3}}\chi_\sigma^2}{1+6b\chi_\sigma \sinh^{-1}\chi_\sigma} d\vec{r} \qquad (1.3.23)$$

where $\chi_\sigma \equiv \left|\nabla_\rho\right| / (\rho^\sigma)^{4/3}$ and *b* is an empirical parameter (normally 0.042 atomic units). The correlation functional of Lee, Yang and Parr (LYP) is

$$E_C^{LYP} = -a\int \frac{\rho + b\rho^{-\frac{2}{3}}\left[t_{HF} - 2t_W\right]e^{c\rho^{-\frac{1}{3}}}}{1+d\rho^{-\frac{1}{3}}} \qquad (1.3.23)$$

where the constants a=0.049, b=0.132, c=0.2533 and d=0.349, while t_{HF} and t_W are the kinetic energy density of Hartree-Fock and Weizsacker, respectively.

In this study, the B3LYP was the most frequently used functional.

Normal Coordinate Analysis

Normal coordinate analysis was undertaken in the internal coordinate space, as described by Schachtschneider and Mortimer[176] using the BALGA program.[177] For each molecule, the potential energy distribution (PED) associated with each normal mode was obtained.

The vibrational potential, *V*, can be given in terms of the normal coordinates, Q_k by the following expression:

$$V = \frac{1}{2}\sum_k Q_k^2 \sum_i \sum_j L_{jk} L_{ik} F_{ij} \qquad (1.3.24)$$

where *F* denotes the potential energy matrix and *L* is the transformation matrix between internal (or symmetry) coordinates and normal coordinates; *i* is the number of coordinates and *j, k, l* are the numbers of internal coordinates.

Instead of computing the $L_{jk}L_{ik}F_{ij}$ terms, a single potential energy distribution matrix, PED, is usually applied, whose elements are given by[178,179]

$$\left[PED\right]_{kj} = \sum_{i} L_{jk}L_{ik}F_{ij} \tag{1.3.25}$$

By normalizing the matrix elements with respect to the calculated eigenvalues, λ_k , the equation be written as

$$\left[PED\right]^{\lambda}_{kj} = \sum_{i} L_{jk}L_{ik}F_{ij}/\lambda_k \tag{1.3.26}$$

By rearranging equation (1.3.26), into a matrix product, a simpler PED is obtained

$$\left[PED\right]^{\lambda}_{kj} = L_{jk}\sum_{i} L_{ik}F_{ij}/\lambda_k = L_{jk}\left[FL\Lambda^{-1}\right]_{jk} = \tilde{L}_{kj}\left[\Lambda^{-1}\tilde{LF}\right]_{kj} \tag{1.3.27}$$

where *L* represents the transpose of L.

On the basis of the vibrational eigenvalue equation it can be proved that

$$\Lambda^{-1}\tilde{L}F = L^{-1} \tag{1.3.28}$$

The substitution of this expression in equation (1.3.26) renders

$$\left[PED\right]^{\lambda}_{kj} = \tilde{L}_{kj}\left[L^{-1}\right]_{kj} \tag{1.3.29}$$

However, this expression does not contain potential energy matrix elements or eigenvalues, on its own the L matrix includes all the information characteristic of the normalized potential energy distribution.

If the elements belonging to a given row or column of the PED matrix are summed, the expression obtained is equivalent to an element of a product matrix

$$\sum_j \left[PED\right]_{kj}^{\lambda} = \sum_j \tilde{L}_{kj} L_{kj}^{-1} = \sum_j L_{kj}^{-1} L_{kj} = \left[L^{-1}L\right]_{kk} \tag{1.3.30}$$

$$\sum_k \left[PED\right]_{kj}^{\lambda} = \sum_k \tilde{L}_{kj} L_{kj}^{-1} = \sum_k L_{jk} L_{kj}^{-1} = \left[LL^{-1}\right]_{jj} \tag{1.3.31}$$

Since $LL^{-1} = E$ are equal to one, the discussed property has been proved.

1.4 References

[1] Lang Jr., S. A.; Lin, Y.-L. in: Katritzky, A. R.; Rees, C. W.; Potts, K. T. (Eds.), *Comprehensive Heterocyclic Chemistry*, vol. 6, Pergamon, Oxford, **1984**, (Chapters 4.16 and 4.18).

[2] Ponnuswamy, M. N.; Gromiha, M. M.; Sony, S. M. M.; Saraboji, K. *Top Heterocyl. Chem.*, **2006**, *4*, 81-147.

[3] Pinho e Melo, T. M. V. D. *Curr. Org. Chem.*, **2005**, *9*, 925-958.

[4] Yeh, V. S. C. *Tetrahedron*, **2004**, *60*, 11995-12042.

[5] Lifshitz, A.; Wohlfeilert, D. *J. Phys. Chem.*, **1992**, *96*, 4505-4515.

[6] Higgins, J.; Zhou, X. Liu, R. *J. Phys. Chem. A*, **1997**, *101*, 7231-7235.

[7] Pérez, J. D.; Yranzo, G. I.; Wunderlin, D. A. *J. Org. Chem.*, **1982**, *47*, 982-984.

[8] Nishiwaki, T.; Saito, T.; Onomura, S.; Kondo, K. *J. Chem. Soc. C*, **1971**, 2644-2647.

[9] Pérez, J. D.; Wunderlin, D. A. *J. Org. Chem.*, **1987**, *52*, 3637-3640.

[10] Padwa, A.; Chen, E. Ku, A. *J. Am. Chem. Soc.*, **1975**, *97*, 6484-6491.

[11] Singh, B.; Ullman, E. F. *J. Am. Chem. Soc.*, **1967**, *89*, 6911-6916.

[12] Darlage, L. J.; Kinstle, T. H.; McIntosh, C. L. *J. Org. Chem.*, **1971**, *36*, 1088-1093.

[13] Sauers, R. R.; Hadel, L. M.; Scimone, A. A.; Stevenson, T. A. *J. Org. Chem.*, **1990**, *55*, 4011-4019.

[14] Ferris, J. P.; Trimmer, R. W. *J. Org. Chem.*, **1976**, *42*, 13-19.

[15] Tanaka, H.; Matsushita, T.; Osamura, Y.; Nishimoto, K. *Int. J. Quant. Chem.*, **1980**, *18*, 463-468.

[16] Inui, H.; Murata, S. *J. Am. Chem. Soc.*, **2005**, *127*, 2628-2636.

[17] Inui, H.; Murata, S. *Chem. Lett.*, **2001**, *30*, 832-833.

[18] Inui, H.; Murata, S. *Chem. Comm.*, **2001**, 1036-1037.

[19] Inui, H.; Murata, S. *Chem. Phys. Lett.*, **2002**, *359*, 267-272.

[20] Kaczor, A.; Gómez-Zavaglia, A.; Cardoso, A. L.; Pinho e Melo, T. M. V. D.; Fausto, R. *J. Phys. Chem. A*, **2006**, *110*, 10742-10749.

[21] Gómez-Zavaglia, A.; Kaczor, A.; Cardoso, A. L.; Pinho e Melo, T. M. V. D.; Fausto, R. *J. Phys. Chem. A*, **2006**, *110*, 8081-8092.

[22] Gómez-Zavaglia, A.; Kaczor, A.; Cardoso, A. L.; Pinho e Melo, T. M. V. D.; Fausto, R. J. Mol. Struct. **2007**, *834-836*, 262-269.

[23] Padwa, A.; Smolanoff, J.; Temper, A. *J. Org. Chem.*, **1976**, *41*, 543-549.

[24] Padwa, A.; Smolanoff, J.; Temper, A. *J. Am. Chem. Soc.*, **1975**, *97*, 4682-4691.

[25] Isomura, K.; Ayabe, G.-I.; Hatano, S.; Taniguchi, H. *J. Chem. Soc. Chem. Comm.*, **1980**, 1252-1253.

[26] Wendling, L. A.; Bergman, R. G. *J. Am. Chem. Soc.*, **1974**, *96*, 309-309.

[27] Wendling, L. A.; Bergman, R. G. *J. Org. Chem.*, **1976**, *41*, 831-836.

[28] Lohr, L. L.; Hanamura, H.; Morokuma, K. *J. Am. Chem. Soc.*, **1983**, *105*, 5541-5547.

[29] Pinho e Melo, T. M. V. D.; Lopes, C. S. J.; d'A Rocha Gonslaves, A. M.; Storr, R. C. *Synthesis*, **2002**, *5*, 605-608.

[30] Padwa, A. in: Katritzky, A.; Ramsden, S.; Scriven, E.; Taylor, R. (Eds.) *Comprehensive Heterocyclic Chemistry III*, **2008**, Chapter 1.01 - *Aziridines and Azirines: Monocyclic*, 1-104.

[31] Singh, B.; Zweig, A.; Gallivan, J. B. *J. Am. Chem. Soc.*, **1972**, *94*, 1199-1206.

[32] Orton, E.; Collins, S. T.; Pimentel, G. C. *J. Phys. Chem.*, **1986**, *90*, 6139-6143.

[33] Patrick, J. B.; Williams, R. P.; Meyer, W. E.; Fulmor, W.; Cosulich, D. B.; Broschard, R. W.; Webb, J. S. *J. Am. Chem. Soc.*, **1964**, *86*, 1889-1890.

[34] Coleman, R. S.; Kong, J.-S.; Richardson**,** T. E. *J. Am. Chem. Soc.*, **1999**, *121*, 9088-9095.

[35] Vedejs, E.; Naidu, B. N.; Klapars, A.; Warner, D. L.; Li, V.-S.; Na, Y.; Kohn, H. *J. Am. Chem. Soc.*, **2003**, *125*, 15796-15806.

[36] Hashimoto, M.; Matsumoto, M.; Yamada, K.; Terashima, S. *Tetrahedron*, **2003**, *59*, 3089-3097.

[37] Yudin, A. K. (Ed.), *Aziridines and Epoxides in Organic Chemistry*, WILEY-VCH Verlag GmbH & Co. KGaA, Weinheim, **2006**.

[38] Osborn, H. M. I.; Sweeney, J. *Tetrahedron: Asymmetry*, **1997**, *8*, 1693-1715.

[39] McCoull, W.; Davis, F. A. Synthesis, **2000**, *10*, 1347-1365.

[40] Beresford, K. J. M.; Church, N. J.; Young, D. W. *Org. Biomol. Chem.*, **2006**, *4*, 2888-2897.

[41] Wang, J.-Y.; Hu, Y.; Wang, De-X.; Pan, J.; Huang, Z.-T.; Wang, M.-X. *Chem. Commun.*, **2009**, 422-424.

[42] Concellón, J. M.; Bernad, P. L.; Suárez, J. R.; García-Granada, S.; Díaz, M. R. *J. Org. Chem.*, **2005**, *70*, 9411-9416.

[43] Stanković, S.; D'hooghe, M.; De Kimpe, N. *Org. Biomol. Chem.*, **2010**, *8*, 4266-4273.

[44] Dahanukar, V.H.; Zavialov, L.A. *Curr. Opin. Dug Discov. Devel.*, **2002**, *5*, 918-927.

[45] Hu, X. E. *Tetrahedron*, **2004**, *60*, 2701-2743.

[46] Cardillo, G; Gentilucci, L.; Tolomelli, A. *Aldrichim. Acta*, **2003**, *36*, 39-50.

[47] Zwanenburg, B.; ten Holte, P. *Top. Curr. Chem.*, **2001**, *216*, 93-124.

[48] Dodd, R. H. *Molecules*, **2000**, *5*, 293-298.

[49] Shtrumfs, B.; Hermane, J.; Kalvinsh, I.; Trapencieris, P. *Chem. Heterocycl. Compd.*, **2007**, *43*, 169-174.

[50] Baldwin, J. E.; Adlington, R. M.; O'Neil, I. A.; Schofield, C.; Spivey, A. C.; Sweeney, J. B. *J. Chem. Soc., Chem. Comm.*, **1989**, 1852-1854.

[51] Cremer, D.; Kraka, E. *J. Am. Chem. Soc.*,**1985**, *107*, 3800-3810.

[52] Sweeney, J. B. *Chem. Soc. Rev.*, **2002**, *21*, 247-258.

[53] Gaebert, C.; Mattay, J.; Toubartz, M.; Steenken, S.; Müllen, B.; Bally, T. *Chem. Eur. J.*, **2005**, *11*, 1294-1304.

[54] Paasche, A.; Arnone, M.; Flink, R. F.; Schirmeister, T.; Engels, B. *J. Org. Chem.*, **2009**, *74*, 5244-5249.

[55] Bigot, B.; Devaquet, A.; Sevin, A. *J. Org. Chem.*, **1980**, *45*, 97-105.

[56] Wilzbach, K. E.; Rausch, D. J. *J. Am. Chem. Soc.*, **1970**, *92*, 2178-2179.

[57] Chapman, O. L.; McIntosh, C. L.; Pacansky, J. *J. Am. Chem. Soc.*, **1973**, *95*, 614-617.

[58] Johnstone, D.E.; Sodeau, J. R. *J. Phys.Chem.*, **1991**, *95*, 165-169.

[59] Kudoh, S. ; Takayanagi., M.; Nakata, M. *J. Photochem. Photobiol. A*, **1999**, *123*, 25-30.

[60] Yavari, I.; Moradi, S.; Fard. H. K.; Nourmohammadian, F.; Tahmassebi, D. *J. Mol. Struct. (Theochem)*, **2002**, *578*, 249-253.

[61] Priyakumar, U. D.; Dinadayalane, T. C.; Sastry, G. N. *Chem. Phys. Lett.*, **2001**, *337*, 361-367.

[62] Priyakumar, U. D.; Dinadayalane, T. C.; Sastry, G. N. *New J. Chem.*, **2002**, *26*, 347-353.

[63] Garcia, A. M.; Benavides, F. G.; Fletcher, T.; Orts, E. *Scand. J. Environ. Health*, **1998**, *24*, 445-447.

[64] Ellwood, C. W.; Tikhonov, A. Ya. Rhone Poulenc Agriculture (GB) and Novosib of Organic Chemistry (RU), Patent WO9803479, **1998**.

[65] Robson, M. J.; Worthington, P. A. ICI PLC (GB), Patent WO9208714, **1992**.

[66] Brodney, M. A. Pfizer Prod Inc. (US), Patent WO2006106416, **2006**.

[67] Schnettler, R. A.; Jones Jr., W. D.; Claxton, G. P. Merrell Dow Pharma (US), Patent KR900000369B, **1990**.

[68] Fevig, J.; Cacciola, J.; Clark, C. G.; Patrick, Y.-S. L.; Donald, J. P. P.; Pruitt, J. R.; Rossi, K. A.; Han, Qi.; Quan, M. DU PONT Pharm CO (US), Patent EA4515, **2004**.

[69] Cheshire, D.; Cladingboel, D.; Hardern, D.; Stocks, M. Astra Pharma Prod (GB), Patent HU9900143, **1999**.

[70] Slater, J. W.; D'Alessandro, D. M.; Keene, F. R.; Steel, P.J. *Dalton Trans.*, **2006**, 1954-1962.

[71] López, R.; Boys, D.; Loeb, B.; Zuloaga, F. *J. Chem. Soc. Perkin Trans. 2*, **1998**, 877-884.

[72] Colton, D. F.; Geary, W. J. *J. Chem. Soc. Dalton Trans.*, **1972**, *4*, 547-551.

[73] Ita, B. I.; Offiong, O. E. *Mat. Chem. Phys.*, **1997**, *51*, 203-208.

[74] Lopes, S.; Gómez-Zavaglia, A.; Lapinski, L.; Chattopadhyay, N.; Fausto, R. *J. Phys. Chem. A*, **2004**, *108*, 8256-8263.

[75] Gómez-Zavaglia, A.; Fausto, R. *J. Mol. Struct.*, **2003**, *661*, 195-208.

[76] Lopes, S. ; Gómez-Zavaglia, A.; Lapinski, L.; Fausto, R. *J. Phys. Chem. A.*, *J. Phys. Chem. A.*, **2005**, *109*, 5560-5570.

[77] Zuckerman, B.; Ball, J. A.; Gottlieb, C. A. *Astrophys. J.*, **1971**, *163*, L41-L45.

[78] Mehringer, D. M.; Snyder, L. E.; Miao, Y.; Lovas, F. J. *Astrophys. J.*, **1997**, *480*, L71-L74.

[79] Pettersson, M.; Maçôas, E. M. S.; Khriachtchev, L.; Fausto, R.; Räsänen, M. *J. Am. Chem. Soc.*, **2003**, *125*, 4058-4059.

[80] Pettersson, M.; Lundell, J.; Khriachtchev, L.; Räsänen, M. *J. Am. Chem. Soc.*, **1997**, *119*, 11715-11716.

[81] Maçôas, E. M. S.; Lundell, J.; Pettersson, M.; Khriachtchev, L.; Fausto, R.; Räsänen, M. *J. Mol. Spectrosc.*, **2003**, *219*, 70-80.

[82] Marushkevich, K.; Khriachtchev, L.; Lundell, J.; Domanskaya, A. V.; Räsänen, M. *J. Mol. Spectrosc.*, **2010**, *259*, 105-110.

[83] Maçôas, E. M. S.; Khriachtchev, L.; Pettersson, M.; Fausto, R.; Räsänen, M. *J. Am. Chem. Soc.*, **2003**, *125*, 16188-16189.

[84] Maçôas, E. M. S.; Khriachtchev, L.; Fausto, R.; Räsänen, M. *J. Phys. Chem. A*, **2004**, *108*, 3380-3389.

[85] Maçôas, E. M. S.; Khriachtchev, L.; Pettersson, M.; Fausto, R.; Räsänen, M. *J. Chem. Phys.*, **2004**, *121*, 1331-1338.

[86] Pettersson, M.; Maçôas, E. M. S.; Khriachtchev, L.; Lundell, J.; Fausto, R.; Räsänen, M. *J. Chem. Phys.*, **2002**, *117*, 9095-9098.

[87] Domanskaya, A.; Marushkevich, K.; Khriachtchev, L.; Räsänen, M. *J. Chem. Phys.*, **2009**, *130*, 154509-5.

[88] Maçôas, E. M. S.; Khriachtchev, L.; Pettersson, M.; Fausto, R.; and Räsänen, M. *J. Phys. Chem. A*, **2005**, *109*, 3617-3624.

[89] Maçôas, E. M. S.; Fausto, R.; Pettersson, M.; Khriachtchev, L.; Räsänen, M. *J. Phys. Chem. A*, **2000**, *104*, 6956-6961.

[90] Isoniemi, E.; Khriachtchev, L.; Makkonen, M.; Räsänen, M. *J. Phys. Chem. A*, **2006**, *110*, 11479-11487.

[91] Sharma, A.; Reva, I. ; Fausto, R., *J. Am. Chem. Soc.*, **2009**, *131*. 8752-8753.

[92] Lapinski, L.; Reva, I.; Nowak, M. J. ; Fausto, R. *Phys. Chem. Chem. Phys.*, **2011**, *13*, 9676-9684.

[93] Baldeschwieler, J. D.; Pimentel, G. C. *J. Chem. Phys.*, **1960**, *33*, 1008-1015.

[94] Hall, R.T.; Pimentel, G. C. *J. Chem. Phys.*, **1963**, *38*, 1889-1897.

[95] McDonald, P. A., Shirk, J. S. *J. Chem. Phys.*, **1982**, *77*, 2355-2364.

[96] Shirk, A. E., Shirk, J. S. *Chem. Phys. Lett.*, **1983**, *97*, 549-552.

[97] Khriachtchev, L.; Lundell, J.; Isoniemi, E. Räsänen, M., *J. Chem. Phys.*, **2000**, *113*, 4265-4273.

[98] Amiri, S.; Reisenauer, H. P.; Schreiner, P. R. *J. Am. Chem. Soc.*, **2010**, *132*, 15902-15904.

[99] Akai, N.; Kudoh, S.; Takayanagi, M.; Nakata, N. *Chem. Phys. Lett.*, **2002**, *356*, 133-139.

[100] Akai, N.; Kudoh, S.; Takayanagi, M.; Nakata, M. *J. Phys. Chem. A*, **2002**, *106*, 11029-11033.

[101] Whittle, E.; Dows, D. A.; Pimentel, G. C. *J. Chem. Phys.*, **1954**, *22*, 1943-1944.

[102] Downs, A. J.; Hawkins, M. *Advances in Infrared and Raman Spectroscopy*, Vol. *10*, Chapter 1. 1, page 1.

[103] Fausto, R. *Low Temperature Molecular Spectroscopy*, NATO-ASI Series, Vol. *483*, Fausto, R. (Ed.) Kluwer, Dordrecht, NL, page 125, **1995**.

[104] Dunkin, I. R. *Matrix-Isolation Techniques: A Practical Approach*, Harwood, L. M.; Moody, C. J. (Eds.), Oxford University Press Inc., New York, **1998**.

[105] Durig, J. R. *Vibrational Spectra and Structure*, Durig, J. R. (Ed.) Elsevier Science Publishers B.V., Amsterdam, NL, **1983**, Vol. *12*.

[106] Meier, R. *Vibrational Spectrosc.*, **2007**, *43*, 26-37.

[107] Khriachtchev, L. *J. Mol. Struct.*, **2008**, *880*, 14-22.

[108] Marushkevich, K.; Khriachtchev, L.; Lundell, J.; Räsänen, M. *J. Am. Chem. Soc.*, **2006**, *128*, 12060-12061.

[109] Marushkevich, K.; Khriachtchev, L.; Räsänen, M. *J. Chem. Phys.*, **2007**, *126*, 241102-4.

[110] Marushkevich, K.; Khriachtchev, L.; Lundell, J.; Domanskaya, A.; Räsänen, M. *J. Phys. Chem. A*, **2010**, *114*, 3495-3502.

[111] Marushkevich, K.; Siltanen, M.; Räsänen, M.; Halonen, L.; Khriachtchev, L. *J. Phys. Chem. Lett.*, **2011**, *2*, 695-699.

[112] Gómez-Zavaglia, A.; Fausto, R. *J. Phys. Chem. A*, **2004**, *108*, 6953-6967.

[113] Mardyukov, A.; Sanchez-Garcia, E.; Rodziewicz, P.; Doltsinis, N. L.; Sander, W. *J. Phys. Chem. A*, **2007**, *111*, 10552-10561.

[114] Sanchez-Garcia, E.; Mardyukov, A.; Adem, A.; Crespo-Otero, R.; Montero, L. A.; Sander, W.; Jansen, G. *Chem. Phys.*, **2008**, *343*, 168-185.

[115] Olbert-Majkut, A.; Meilke., Z.; Tokhadze, K. G. *Chem. Phys.*, **2002**, *280*, 211-227.

[116] Engdahl, A.; Nelander, B.; Karlstrom, G. *J. Phys. Chem. A*, **2001**, *105*, 8393-8398.

[117] Sundararajan, K.; Viswanathan, K. S.; Kulkarni, A. D.; Gadre, S. R. *J. Mol. Struct.*, **2002**, *613*, 209-222.

[118] Tanskanen, H.; Johansson, S.; Lignell, A.; Khriachtchev, L.; Räsänen, M. J. Chem. Phys., **2007**, *127*, 154313-7.

[119] Barnes, A. J. *J. Mol. Struct.* **1984**, *113*, 161-174.

[120] Stepanian, S. G.; Reva, I. D.; Radchenko, R. D.; Rosado, M. T. S.; Duarte, M. L. T. S.; Fausto, R.; Adamowicz, L. *J. Phys. Chem. A* **1998**, *102*, 1041-1054.

[121] Reva, I.; Simão, A.; Fausto, R. R. *Chem. Phys. Lett.*, **2005**, *406*, 126-136.

[122] Rosado, M. T. S.; Lopes de Jesus, A. J.; Reva, I. D.; Fausto, R.; Redinha, J. S.; *J. Phys. Chem. A* **2009**, *133*, 7499-7507.

[123] Reva, I. D.; Stepanian, S. G.; Adamowicz, L.; Fausto, R. *Chem.Phys.Lett.*, **2003**, *374*, 631-638.

[124] Borba, A.; Gómez-Zavaglia, A.; Simões, P. N. N. L.; Fausto, R. *J. Phys. Chem. A*, **2005**, *109*, 3578-3586.

[125] Borba, A.; Gómez-Zavaglia, A.; Fausto, R. *J. Mol. Struct.*, **2006**, *794*, 196-203.

[126] Nishino, S.; Nakata, M. *J. Mol. Struct.*, **2008**, *875*, 520-526.

[127] Nishino, S.; Nakata, M. *J. Phys. Chem. A*, **2007**, *111*, 7041-7047.

[128] Nagashima, N.; Kudoh, S.; Takayanagi, M.; Nakata, M. *J. Phys. Chem. A*, **2001**, *105*, 10832-10838.

[129] Nowak, M. J.; Lapinski, L.; Fulara, J.; Les, A.; Adamowicz, L. *J. Phys. Chem.*, **1992**, *96*, 1562-1569.

[130] Akai, N.; Ohno, K.; Aida, M. *Chem. Phys. Lett.*, **2005**, *413*, 306-310.

[131] Akai, N.; Harada, H.; Shin-ya, K.; Ohno, K.; Aida, M. *J. Phys. Chem. A*, **2006**, *110*, 6016-6022.

[132] Akai, N.; Ohno, K.; Aida, M. *J. Photochem. Photobiol. A*, **2007**, *187*, 113-118.

[133] Gerega, A.; Lapinski, L.; Nowak, M. J.; Rostowska, H. *J. Phys. Chem. A*, **2006**, *110*, 10236-10244.

[134] Chmura, B.; Rode, M. F.; Sobolewski, A. L.; Lapinski, L.; Nowak, M. J. *J. Phys. Chem. A*, **2008**, 112, 13655-13661.

[135] Maier, G.; Endres, J. *Eur. J. Org. Chem.*, **2000**, 1061-1063.

[136] Duvernay, F.; Trivella, A.; Borget, F.; Coussan, S.; Aycard, J.-P.; Chiavassa, T. *J. Phys. Chem. A*, **2005**, *109*, 11155-11162.

[137] Szabo, A.; Ostlund, N. S. *Modern Quantum Chemistry. Introduction to Advanced Electronic Structure Theory*, Dover Publications Inc., Mineola, New York, **1996**.

[138] Jensen, F. *Introduction to Computational Chemistry*, John Wiley & Sons, Chichester, England, **1999**.

[139] Foresman, J. B.; Frisch, *Æ. Exploring Chemistry with Electronic Structure Methods*, Gaussian Inc., Pittsburgh, PA, **1996**.

[140] Lewars, E. *Computational Chemistry – Introduction to the Theory and Applications of Molecular and Quantum Mechanics*, Kluwer Academic Publishers, Dordrecht, **2004**.

[141] Parr, R. G.; Yang, W. *Density-Functional Theory of Atoms and Molecules*, Oxford University Press, Oxford, **1989**.

[142] Dewar, M. J. S.; Thiel, W. *J. Am. Chem. Soc.*, **1977**, *99*, 4899-4907.

[143] Dewar, M. J. S.; Zoebisch, E. G.; Healy, E. F.; Stewart, J. J. P. *J. Am. Chem. Soc.*, **1985**, *107*, 3902-3909.

[144] Stewart, J. J. P. *J. Comput. Chem.* **1989**, *10*, 209-220.

[145] Stewart, J. J. P. *J. Comput. Chem.*, **1989**, *10*, 221-264.

[146] Stewart, J. J. P. *J. Comput. Chem.*, **1991**, *12*, 320-341.

[147] Stewart, J. J. P. *J. Mol. Model.*, **2004,** *10*, 155-164.

[148] Schrödinger, E. *Ann. Physik*, **1926**, *79***,** 361-361.

[149] Born, M.; Oppenheimer, J. R. *Ann. Phys.*, **1927**, *84*, 457-484.

[150] Slater, J. C. *Phys. Rev.*, **1930**, *35*, 509-529.

[151] Hartree, D. R. *Proc. Cambridge Philos. Soc.*, **1928**, *24*, 89-110.

[152] Fock, V. A. *Z. Phys.*, **1930**, *61*, 126-135.

[153] Roothaan, C. C. J. *Rev. Mod. Phys.*, **1951**, *23*, 69-89; **1960**, *32*, 179-185.

[154] Hehre, W. J.; Stewart, R. F.; Pople, J. A. *J. Chem. Phys.*, **1969**, *51*, 2657-2664.

[155] Binkley, J. S.; Pople, J. A.; Hehre, W. J. *J. Am. Chem. Soc.*, **1980**, *102*, 939-947.

[156] Gordon, M. S.; Binkley, J. S.; Pople, J. A.; Pietro, W. J.; Hehre, W. J. *J. Am. Chem. Soc*, **1982**, *104*, 2797-2803.

[157] Ditchfield, R.; Hehre, W. J.; Pople, J. A. *J. Chem. Phys.*, **1971**, *54*, 724-728.

[158] Hehre, W. J.; Ditchfield, R.; Pople, J. A. *J. Chem. Phys.*, **1972**, *56*, 2257-2261.

[159] McLean, A. D.; Chandler, G. S. *J. Chem. Phys.*, **1980**, *72*, 5639-5648.

[160] Frisch, M. J.; Pople, J. A.; Binkley, J. S.; *J. Chem. Phys.*, **1984**, *80*, 3265-3269.

[161] Clark, T.; Chandrasekhar, J.; Spitznagel, G. W.; Schleyer, P. v. R. *J. Comp. Chem.*,**1983**, *4*, 294-301.

[162] Møller, C.; Plesset, M. S. *Phys. Rev.*, **1934**, *46*, 618-622.

[163] Frisch, M.; Head-Gordon, M.; Pople, J. A. *Chem. Phys. Lett.*, **1990**, *166*, 281-289.

[164] Thomas, L. H. *Proc. Chambridge Philos. Soc.*, **1927**, *23*, 542-548.

[165] Fermi, E. *Rend. Accad. Lincei*, **1927**, *6*, 602-607.

[166] Kohn, W.; Hohenberg, P. *Phys. Rev. B*, **1964**, *136*, 864-871.

[167] Kohn, W.; Sham, L. J. *Phys. Rev. A*, **1965**, *140*, 1133-1138.

[168] Dirac, P. A. M. *Proc. Cambridge Phil. Roy. Soc.*, **1930**, *26*, 376-385.

[169] Becke, A. D. *Phys. Rev. A* **1988**, *38*, 3098-3100.

[170] Perdew, J. D.; Wang, Y. *Phys. Rev. B*, **1986**, *33*, 8800-8802.

[171] Perdew, J. D.; Wang, Y. *Phys. Rev. B*, **1992**, *45*, 13244-13249.

[172] Lee, C. T.; Yang, W. T.; Parr, R. G. *Phys. Rev. B* **1988**, *37*, 785-789.

[173] Meihlich, B.; Savin, A.; Stoll, H.; Preuss, H. *Chem. Phys. Lett.*, **1989**, *157*, 200-206.

[174] Perdew, J. D. *Phys. Rev. B*, **1986**, *33*, 8822-8824; **1986**, *34*, 7406-7406.

[175] Vosko, S. H.; Wilk, L.; Nusair, M. *Can. J. Phys.*, **1980**, *58***,** 1200-1211.

[176] Schachtschneider, J. H.; Mortimer, F. S. *Vibrational Analysis of Polyatomic Molecules*. VI. FORTRAN IV Programs for Solving the Vibrational Secular Equation and for the Least-Squares Refinement of Force Constants. Report Nº.

31450. Structural Interpretation of Spectra, Technical Report nº 57-650, Shell Development Co. Emeryville, CA, **1969**.

[177] Keresztury, G.; Jalkovszky, G. *J. Mol. Struct.*, **1971**, *10*, 304-305.

[178] Orville-Thomas, W. J. *J. Chem. Phys.*, **1951**, *19*, 1162-1166.

[179] Morino, Y.; Kuchitsu, K. *J. Chem. Phys.*, **1952**, *20*, 1809-1810.

2 Experimental and Computational Details

2.1 *Samples sources*

*Synthesis of methyl 4-chloro-5-phenyl-1,3-oxazole-3-carboxylate (**MCPOC**)*

The 2-halo-2*H*-azirine[1] (2.81 mmol) was dissolved in toluene (10 mL) and the reaction mixture was heated at reflux for 5 h. The solvent was evaporated giving the 1,3-oxazole as a solid. **MCPOC** was obtained as a solid (96%), mp 71-72 °C. IR (KBr) 1529, 1738, 2959 cm^{-1}; ^{1}H NMR 4.04 (3H, s), 7.47-7.51 (3H, m, Ar-H), 7.98-8.01 (2H, m, Ar-H); ^{13}C NMR 53.5, 125.6, 125.9, 126.6, 129.0, 130.2, 147.8, 148.7, 155.3; MS (EI) *m/z* 239 [M(^{37}Cl)$^{+}$] (34), 237 [M(^{35}Cl)$^{+}$] (100), 177 (17), 128 (8), 105 (55), 77 (59). Anal. Calcd. for $C_{11}H_8NO_3Cl$: C, 55.60; H, 3.39; N, 5.89. Found: C, 55.66; H, 3.32; N, 5.92%.

*Synthesis of methyl 4-chloro-5-phenylisoxazole-3-carboxylate (**MCPIC**)*

A solution of methyl 5-phenylisoxazole-3-carboxylate (70 mg, 0.345 mmol) and NCS (85 mg, 0.64 mmol) in 2.3 mL of 7% fuming nitric acid in acetic acid was irradiated for 40 min in the microwave reactor (CEM Focused Synthesis System, Discover S-Class) with the temperature set to 160 ºC. After cooling to room temperature, water (15 mL) was added and the mixture extracted with CH_2Cl_2 (2x15 mL). The organic phase was dried ($MgSO_4$) and evaporated off. The crude product was purified by flash chromatography [ethyl acetate–hexane (1:5)] to give **MCPIC** as a white solid (59%). mp 62-63 °C. IR (KBr) 1221, 1441, 1738, 2957 cm^{-1}; ^{1}H NMR 4.03 (3H, s), 7.52-7.55 (3H, m), 8.03-8.06 (2H, m);^{13}C NMR 53.1, 106.0, 125.6, 126.6, 129.0, 131.2, 153.3, 159.1, 165.8; MS (EI) *m/z* 237 (M^{+}, 99), 206 (14), 105 (100), 77 (68), 59 (78); HRMS (CI) *m/z* 237.0200 ($C_{11}H_8NO_3Cl$ [M^{+}], 237.0193).

*Synthesis of methyl (Z)-2-azido-3-chloro-3-benzoylpropenoate (**MACBP**)*

(Z)-3-azido-(E)-3-methylcarboxylate-2-chloro-acrylophenone (or methyl (Z)-2-azido-3-chloro-3-benzoylpropenoate, **MACBP 1**) was prepared using a known synthetic method procedure (**Scheme 1**).[1] The 2-

(triphenylphosphoranylidene)acetophenone **4**, obtained by reaction of 2-bromoacetophenone **3** and triphenylphosphine **2**, was added to a solution of triethylamine in dry toluene and treated with the appropriated acid chloride to give the methyl 2,4-dioxo-4-phenyl-3-triphenylphosphoranylidenebutanoate **5** almost in a quantitative yield. This ylide **5** reacts with azidotrimethylsilane and N-chlorosuccinimide in dichloromethane to give the crystalline methyl (Z)-2-azido-3-chloro-3-benzoylpropenoate **1** after the purification by column chromatography and crystallization.

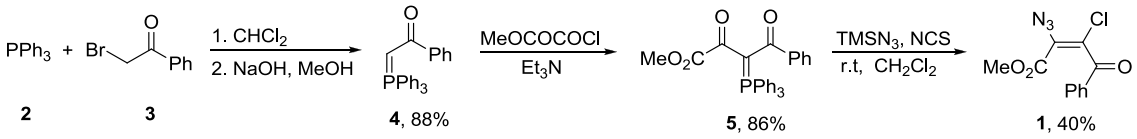

2 **3** **4**, 88% **5**, 86% **1**, 40%

Scheme 1.

Other compounds:

The commercially available compounds were methyl aziridine-2-carboxylate (**MA2C**), α-pyridil, formic and acetic acids.

MA2C (97% purity) was purchased from TCI Europe. Prior to usage, MA2C was additionally purified by using the standard freeze-pump-thaw technique.

The sample of α-pyridil (97 % purity) was obtained from Aldrich and used without any further purification.

Formic acid (FA) and acetic acid (AA) were supplied by KEBO LAB, both with 99% purity. The acids were also purified by a few freezing-pumping cycles.

2.2 *Matrices preparation and other sampling procedures*

The molecules studied at the Laboratory for Molecular Cryospectroscopy and Biospectroscopy (LMCB), Department of Chemistry (University of Coimbra) were MCPOC, MCPIC, MACBP, α-pyridil and MA2C. A similar procedure was followed regarding the deposition of the solid compounds studied in this work (MCPOC,

MCPIC, MACBP and α-pyridil). Matrices were prepared by co-deposition of sample vapors coming out from a specially designed thermoelectrically heatable mini-furnace (Figure 2.1), assembled inside the cryostat (APD Cryogenics closed-cycle helium refrigeration system) with a DE-202A expander, and large excess of the matrix gas (argon, N60; xenon, N48, both obtained from Air Liquide) onto the CsI substrate cooled to ~10 K (for argon matrices) and ~20 K (for xenon matrices). The average matrix deposition time was two hours. Care was taken to ensure that the matrices were not too thick, in order to avoid undesired scattering of the spectral beam.

In the case of the liquid (at room temperature) MA2C compound, the MA2C vapors were premixed with argon and xenon (N60 and N48, respectively, both supplied by Air Liquid) at a ratio of 1:1000 in a 3 L Pyrex glass reservoir to a pressure of 800 mbar, using the standard manometric procedure. During the experiments, the flux of the mixture was controlled by reading the drop pressure in the reservoir with a capacitance manometer. The pulsed valve controller allows different operating modes to define the sample introduction rate. In a typical experiment, the valve operated with an opening time of 5 ms and pulse frequency of 12 Hz during 1000 to 3000 seconds. In this case, the deposition temperatures were 15 K (Ar) and 30 K (Xe).

The low temperature solid amorphous layers of α–pyridil and MCPOC were prepared in the same way as matrices but with the flux of matrix gas cut off. The layers were then allowed to anneal at slowly increasing temperature up to 300 K and 280 K, for α–pyridil and MCPOC, respectively. After recording of the infrared spectrum of the obtained crystal, the sample was cooled back again to 10 K and a new spectrum of the crystalline phase was collected.

KBr pellets and nujol mulls containing MCPOC were prepared by standard procedures. Their IR spectra were collected at room temperature using a BOMEM (MB40) spectrometer, with a Zn/Se beam splitter and a DTGS detector, with 4 cm^{-1} spectral resolution. The Raman spectrum of solid MCPOC in the 3380–100 cm^{-1} range, was acquired at room temperature using a dispersive Raman instrument, model DXR SmartRaman^{TM}, from Thermo Fisher Scientific, equipped with a low-power, externally stabilized diode laser (λ= 780 nm), with a maximum power at output of laser head of 14 mW and a 3.0 mm beam diameter. The data were collected with an exposure time to laser radiation of 99 s, 100 sample exposures and a slit aperture of 25 μm.

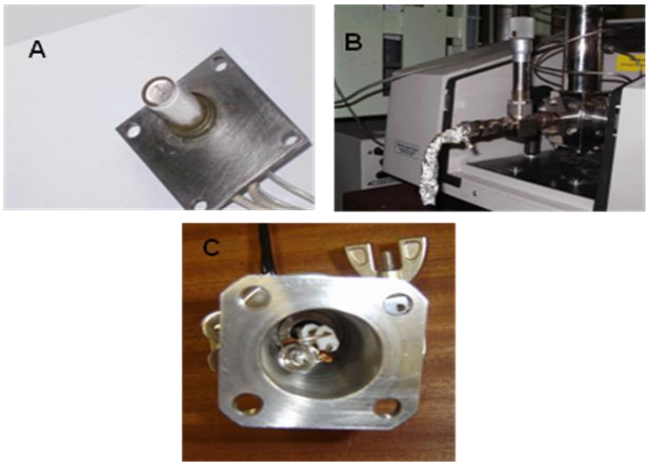

Figure 2.1 – Special devices for gas-inlet and sample deposition developed in the Laboratory for Molecular Cryospectroscopy and Biospectroscopy (LMCB) – Coimbra. A: internal mini-furnace, for deposition of non-volatile solid substances, B: doubly thermostattable Knudsen cell, with shut-off capability, for separate controlling of the temperature of the compound to be deposited and of the vapor immediately prior to deposition, C: internal mini-furnace used nowadays, for deposition of non-volatile solid substances.

Formic (FA) and acetic acid (AA) were studied at The Laboratory of Physical Chemistry, Department of Chemistry (University of Helsinki). Gaseous mixtures of FA and AA with nitrogen were prepared with a typical ratio of 1:1200 (monomers) and 1:1500 (acetic acid dimers). The acids were purified by a few freezing-pumping cycles (Figure 2.2). Nitrogen was used as supplied. HCOOD molecules were produced by an H/D exchange with deuterated surfaces in the deposition line.

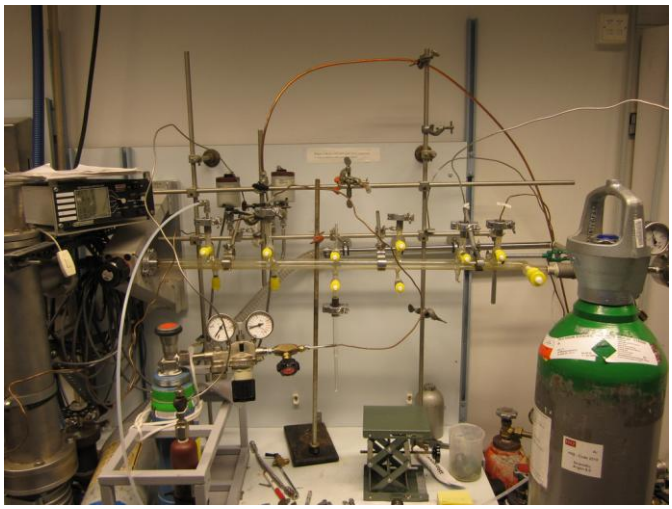

Figure 2.2 – Vacuum line used in the freezing-pumping cycles for FA and AA at the Laboratory of Physical Chemistry, Department of Chemistry (University of Helsinki).

2.3 *IR absorption measurements*

At the LMCB: the IR spectra were recorded with 0.5 cm^{-1} spectral resolution in the spectral range 4000-400 cm^{-1} using a Mattson (Infinity 60AR Series) (Figure 2.3-A) or a Nicolet 6700 Fourier Transform infrared spectrometers (Figure 2.3-B), equipped with a deuterated triglycine sulphate (DTGS) detector and a Ge/KBr beam splitter. The spectra were acquired after accumulating interferograms from 256 and 128 scans, for the Mattson (Infinity 60AR Series) and Nicolet 6700 Fourier Transform infrared spectrometers, respectively.

Necessary modifications of the sample compartment of the spectrometer were done in order to accommodate the cryostat head and allow purging of the instrument by a stream of dry nitrogen, to remove water vapors and CO_2.

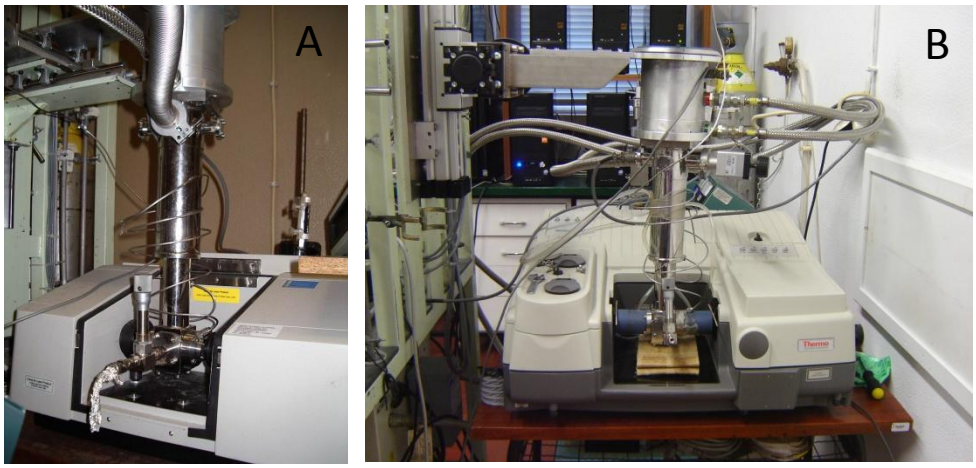

Figure 2.3 – A: Mattson (Infinity 60AR Series) Fourier Transform infrared spectrometer, and B: Nicolet 6700 Fourier Transform infrared spectrometer (Department of Chemistry – University of Coimbra).

At the Helsinki Laboratory of Physical Chemistry: the gaseous mixtures of FA and AA were deposited onto a CsI window at *ca.* 8.5 K in a close–cycle helium cryostat (APD, DE 202A). The spectra were recorded with a Nicolet 60SX FTIR instrument by co–adding 200 interferograms with 1 cm^{-1} spectral resolution (Figure 2.4).

Figure 2.4 – Nicolet 60SX Fourier Transform infrared spectrometer at the Laboratory of Physical Chemistry (Department of Chemistry – University of Helsinki).

2.4 *Narrow band selective IR and UV irradiations*

Irradiation of the matrices of all compounds was carried out with unfiltered light from a 500 W Hg(Xe) lamp (Newport, Oriel Instruments), with output power set to 200 W shown in Figure 2.5-A, through the outer KBr (λ > 235 nm) and quartz (λ > 215 nm) windows of the cryostat. A series of longpass optical filters were also used: λ > 397, 367, 328, 313 and 288 nm. However, either no photochemical changes were observed or the changes were very limited. The time of the irradiation of the matrix depended on the studied molecule, which varied between minutes to several hours (without longpass filters).

For MA2C, matrices were also irradiated with the frequency doubled signal beam of the Quanta-Ray MOPO-SL pulsed (10 ns) optical parametric oscillator (FWHM ~0.2 cm^{-1}, repetition rate 10 Hz, pulse energy E 1.0 mJ) pumped with a pulsed Nd:YAG laser (Figure 2.5-B). Irradiation of the matrices was undertaken using narrowband tunable UV irradiation by different wavelengths (λ = 235 and 290 nm).

Figure 2.5 – Irradiation sources used in the Laboratory for Molecular Cryospectroscopy and Biospectroscopy (LMCB) – Coimbra: A: 500 W Hg(Xe) lamp (Newport, Oriel Instruments), B: Quanta-Ray MOPO-SL pulsed (10 ns) optical parametric oscillator (FWHM ~0.2 cm^{-1}, repetition rate 10 Hz, pulse energy E 1.0 mJ) pumped with a pulsed Nd:YAG laser.

For FA and AA, vibrational excitation was carried out with tunable pulsed IR radiation provided by an optical parametric oscillator (Continuum, OPO Sunlite with IR extension, operated by Dr. Leonid Khriachtchev, see Figure 2.6). The pulse duration was ~5 ns, the spectral linewidth ~ 0.1 cm^{-1} and the repetition rate 10 Hz. The pulse energy of the OPO was measured at the sample position with a pulse energy meter (Molectron) to be ~ 0.1 mJ in the 3000-3700 cm^{-1} and ~ 0.4-0.6 mJ in the 4000-7000 cm^{-1} spectral region. The OPO radiation frequency was measured with a Burleigh WA-4500 wavemeter providing an absolute accuracy better than 1 cm^{-1} for the IR pumping radiation.

During the decay kinetic studies of the high energy species (*cis*-FA, *cis*-AA and *trans*-*cis* dimers of AA) a long–pass optical filter (>1500 cm^{-1}) was inserted between the sample and the Globar source in order to suppress high frequency light components which could accelerate the *cis*–to–*trans* conversion process. The Globar light was blocked between the measurements.

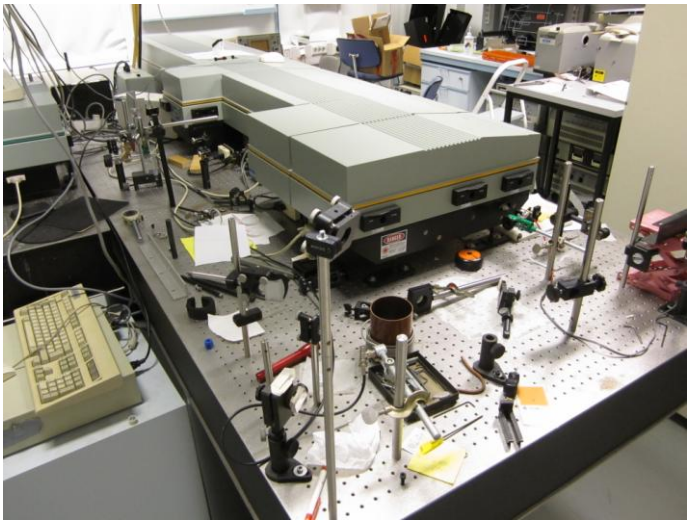

Figure 2.6 – OPO-based system (Continuum) providing 5-ns light pulses tunable in the 225 nm to 4 um range (the pulse duration was ~5 ns, the spectral linewidth ~ 0.1 cm^{-1} and the repetition rate 10 Hz) used in the Laboratory of Physical Chemistry, Department of Chemistry (University of Helsinki).

2. 5 *Computational Details*

The quantum chemical calculations were performed with Gaussian 03[2] at the DFT level of theory, using the split valence triple-ζ 6-311++G(d,p) basis set[3] and the three-parameter B3LYP density functional, which includes Becke's gradient exchange correction[4] and the Lee, Yang and Parr correlation functional,[5] for all the heterocyclic derivative molecules studied in this work. For the MA2C molecule, calculations were also carried out at the MP2 level of theory.

Geometrical parameters of the different conformations were optimized using the Geometry Direct Inversion of the Invariant Subspace (GDIIS) method.[6,7] Transition states were located using the synchronous transit-guided quasi-Newton (STQN) method.[8] In order to assist the analysis of the experimental spectra, vibrational frequencies and IR intensities were also calculated at the same level of approximation. The nature of stationary points on the potential energy surface was checked through the analysis of the corresponding Hessian matrix.

The computed harmonic frequencies were scaled down by a single factor (0.978 for α-pyridil, MACBP, MA2C and their corresponding photoproducts), which was chosen to correct them for the effects of basis set limitations, neglected part of electron correlation and anharmonicity effects. For MCPOC, the scaling factor was 0.9835, obtained from linear fitting of the calculated to experimental wavenumbers

(measured in xenon matrix), whereas, for MCPIC this factor (0.9817) was determined by simple linear fitting (with intercept fixed at zero) of the calculated wavenumbers to the experimental ones.

In addition, for MCPOC, Raman scattering activities (S^R) were also calculated at the same level of approximation. Theoretical Raman intensities (I^R) were obtained from the calculated Raman scattering activities according to the expression $I^R(i) = 10^{-12} (\nu_0-\nu_i)^4 \nu_i^{-1} S^R(i)$, where ν_0 is the excitation wavenumber and ν_i is the calculated wavenumber of the normal mode *i*.[9]

The potential energy surface of all the molecules studied in this thesis was undertaken at the DFT(B3LYP)/6-311++G(d,p) level of theory in order to determine all the minima. Taking into account the high flexibility of the MACBP molecule, with four conformationally relevant rotational axes, a systematic preliminary conformational exploration of the MACBP potential energy surface (PES) was initially carried out at the semi-empirical PM3 method[10,11] using the HyperChem Conformational Search module (CyberChem, Inc. © 2004).[12] These calculations provided a quick assessment of the main features of the conformational space of the molecule, which were later on taken into account in the subsequent analysis performed at the DFT(B3LYP)/6-311++G(d,p) level of theory.

For FA and AA, the quantum chemical calculations were performed using Gamess, version R1 (24-Mar-2007)[13] and version R2 (24-Mar-2010)[14] at the MP2 level of theory[15] using the 6-311++G(2d,2p) basis set.[16,17] The optimization criteria parameter OPTTOL was set to 0.00001 and 0.0001 hartree/bohr. This parameter corresponds to the maximum value allowed to the energy gradient and also controls the maximum allowed value of the root mean square gradient, which is given by 1/3 of OPTTOL. The optimized structures of all FA**…**N_2 and AA**…**N_2 complexes (0.00001 hartree/bohr) and the *trans-trans* and *trans-cis* dimers of AA (0.0001 hartree/bohr) were confirmed to correspond to the true energy minima on the potential energy surfaces by inspection of the Hessian matrices. The vibrational spectra were computed at the same level of theory. No scaling factor was used to scale the computed harmonic frequencies at this level of calculation.

Normal coordinate analysis was undertaken in the internal coordinates space, as described by Schachtschneider and Mortimer[18] using the BALGA program.[19] For

each molecule, the potential energy distribution (PED) associated with each normal mode was obtained.

The internal coordinates used in this analysis were defined following the recommendations of Pulay *et al.*[20]

2.6 *References*

[1] Pinho e Melo, T. M. V. D.; Lopes, C. S. J.; Cardoso, A. L.; d'A. Rocha Gonsalves, A. M. *Tetrahedron*, 2001, 57, 6203-6208.

[2] Frisch, M. J.; Trucks, G. W.; Schlegel, H. B.; Scuseria, G. E.; Robb, M. A.; Cheeseman, J. R.; Montgomery, J. A., Jr.; Vreven, T.; Kudin, K. N.; Burant, J. C.; Millam, J. M.; Iyengar, S. S.; Tomasi, J.; Barone, V.; Mennucci, B.; Cossi, M.; Scalmani, G.; Rega, N.; Petersson, G. A.; Nakatsuji, H.; Hada, M.; Ehara, M.; Toyota, K.; Fukuda, R.; Hasegawa, J.; Ishida, M.; Nakajima, T.; Honda, Y.; Kitao, O.; Nakai, H.; Klene, M.; Li,X.; Knox, J. E.; Hratchian, H. P.; Cross, J. B.; Bakken, V.; Adamo, C.; Jaramillo, J.; Gomperts, R.; Stratmann, R. E.; Yazyev, O.; Austin, A. J.; Cammi, R.; Pomelli, C.; Ochterski, J. W.; Ayala, P. Y.; Morokuma, K.; Voth, G. A.; Salvador, P.; Dannenberg, J. J.; Zakrzewski, V. G.; Dapprich, S.; Daniels, A. D.; Strain, M. C.; Farkas, O.; Malick, D. K.; Rabuck, A. D.; Raghavachari, K.; Foresman, J. B.; Ortiz, J. V.; Cui, Q.; Baboul, A. G.; Clifford, S.; Cioslowski, J.; Stefanov, B. B.; Liu, G.; Liashenko, A.; Piskorz, P.; Komaromi, I.; Martin, R. L.; Fox, D. J.; Keith, T.; Al-Laham, M. A.; Peng, C. Y.; Nanayakkara, A.; Challacombe, M.; Gill, P. M. W.; Johnson, B.; Chen, W.; Wong, M. W.; Gonzalez, C.; Pople, J. A. Gaussian 03, revision C.02; Gaussian, Inc. Wallingford, CT, 2004.

[3] Frisch, M.; Head-Gordon, M. Pople, J. A. *Chem. Phys. Lett.* **1990**, *166*, 281-289.

[4] Becke, A. D. *Phys. Rev. A* **1988**, *38*, 3098-3100.

[5] Lee, C. T.; Yang, W. T.; Parr, R. G. *Phys. Rev. B* **1988**, *37*, 785-789.

[6] Császár, P.; Pulay, P. *J. Mol. Struct.* **1984**, *114*, 31-34.

[7] Farkas, Ö.; Schlegel, H. B. *J. Chem. Phys*. **1999**, *111*, 10806-10814.

[8] Peng, C.; Schlegel, H. B. *Isr. J. Chem.* **1994**, *33*, 449-454.

[9] Michalska, D.; Wysokinski, R. *Chem. Phys. Lett.*, **2005**, *403*, 211-217.

[10] Stewart, J. J. P. *J. Comput. Chem.* **1989**, *10*, 209-220.

[11] Stewart, J. J. P. *J. Comput. Chem.*, **1989**, *10*, 221-264.

[12] HyperChem Conformational Search module (**2002**) *Tools for Molecular Modeling. Hypercube*, Inc., 1115 NW 4th St., Gainesville, FL 32608 (USA).

[13] GAMESS, version R1 (24-Mar-2007), Schmidt, M. W.; Baldridge, K. K.; Boatz, J. A.; Elbert, S. T.; Gordon, M. S.; Jensen, J. H.; Koseki, S.; Matsunaga, N.; Nguyen, K. A.; Su, S. J.; Windus, T. L.; Dupuis, M.; Montgomery, J. A. *J. Comput. Chem.*, **1993**, *14*, 1347-1363.

[14] GAMESS, version R2 (25-Mar-2010), Schmidt, M. W.; Baldridge, K. K.; Boatz, J. A.; Elbert, S. T.; Gordon, M. S.; Jensen, J. H.; Koseki, S.; Matsunaga, N.; Nguyen, K. A.; Su, S. J.; Windus, T. L.; Dupuis, M.; Montgomery, J. A. *J. Comput. Chem.*, **1993**, ***14***, 1347-1363.

[15] Møller, C.; Plesset, M. S. *Phys. Rev.*, **1934**, *46*, 618-622.

[16] McLean, A. D.; Chandler, G. S. *J. Chem. Phys.*, **1980**, *72*, 5639-5648.

[17] Frisch, M. J.; Pople, J. A.; Binkley, J. S.; *J. Chem. Phys.*, **1984**, *80*, 3265-3269.

[18] Schachtschneider, J. H.; Mortimer, F. S. *Vibrational Analysis of Polyatomic Molecules*. VI. FORTRAN IV Programs for Solving the Vibrational Secular Equation and for the Least-Squares Refinement of Force Constants. Report Nº. 31450. Structural Interpretation of Spectra, Technical Report nº 57-650, Shell Development Co. Emeryville, CA, **1969**.

[19] Keresztury, G.; Jalkovszky, G. *J. Mol. Struct.*, **1971**, *10*, 304-305.

[20] Pulay, P.; Fogarasi, G.; Pang, F. Boggs, J. E. *J. Am. Chem. Soc.* **1979**, *110*, 2550-2560.

3 Case Studies

The studies carried out in this project on the molecular structure, spectroscopy and reactivity of a series of selected heterocyclic ring compounds containing nitrogen (MCPOC, MCPIC, MACBP, MA2C and α-pyridil) were presented in this Chapter, which comprehends the following articles:

4-Halo-1,3-Oxazoles: Unambiguous Structural Assignment of 2-halo-2-benzoyl-2*H*-azirine-3-carboxylates thermal ring expansion products, S. Lopes, C. M. Nunes, R. Fausto and T.M.V.D. Pinho e Melo, *J. Mol. Struct.*, **2009**, *919*, 47-53.

Conformational Space and Vibrational Spectra of Methyl 4-Chloro-5-phenyl-1,3-oxazole-2-carboxylate, S. Lopes, C. M. Nunes, A. Gómez-Zavaglia, T.M.V.D. Pinho e Melo and R. Fausto, *J. Phys. Chem. A*, **2010**, *114*, 9074-9082.

Photochemistry and Vibrational Spectra of Matrix-Isolated Methyl 4-Chloro-5-phenylisoxazole-3-carboxylate, S. Lopes, C. M. Nunes, A. Gómez-Zavaglia, T. M.V.D. Pinho e Melo and R. Fausto, *J. Phys. Chem. A*, **2011**, *115*, 1199-1209.

3-Azido-Acrylophonones as Photochemical Precursors of Oxazoles: A Matrix Isolation Infrared Spectroscopy Study, Lopes, C. M. Nunes, A. Gómez-Zavaglia, T. M.V.D. Pinho e Melo and R. Fausto, *Tetrahedron* (**2011) -** submitted.

UV-Induced Photochemical Study of Methyl Aziridine-2-Carboxylate Isolated in Low Temperature Inert Matrices, S. Lopes, I. Reva and R. Fausto (*to be submitted*)

Low Temperature IR Spectroscopy and Photochemistry of Matrix-Isolated α-Pyridil, S. Lopes, A. Gómez-Zavaglia and Rui Fausto, *J. Photochem. Photobiol. A: Chemistry*, **2008**, *200*, 169-180.

Journal of Molecular Structure, **2009**, *919*, 47-53.

4-Halo-1,3-Oxazoles: Unambiguous Structural Assignment of 2-halo-2-benzoyl-2*H*-azirine-3-carboxylates thermal ring expansion products

Susy Lopes, Cláudio M. Nunes, Rui Fausto and Teresa M.V.D. Pinho e Melo

Department of Chemistry, University of Coimbra, P-3004-535 Coimbra, Portugal

ABSTRACT

IR spectroscopy in cryogenic argon matrix of methyl 4-chloro-5-phenyl-1,3-oxazole-2-carboxylate and methyl 4-chloro-5-phenylisoxazole-3-carboxylate was applied for the structural assignment of these isomeric heterocycles. It was demonstrated that methyl 2-benzoyl-2-halo-2*H*-azirine-3-carboxylates undergo thermal ring expansion to give 4-halo-5-phenyl-1,3-oxazole-2-carboxylates and not the isomeric isoxazoles.

1. Introduction

Oxazoles and isoxazoles are isomeric heterocyclic compounds having a remarkable number of applications and have been demonstrated to be very versatile building blocks in organic synthesis.[1] The wide range of biological activities of isoxazoles and oxazoles includes pharmacological properties such as hypoglycemic, analgesic, anti-inflammatory, anti-bacterial, anti-tumoral and HIV-inhibitory activity. Some isoxazole derivatives display agrochemical properties, namely herbicidal and soil fungicidal activity, and have applications as pesticides and insecticides. Isoxazoles have also been used as dyes, electric insulating oils, high temperature lubricants and polyisoxazoles have applications as semicondutors. The oxazole ring occurs naturally and the total synthesis of natural products with a wide variety of

biological activities containing oxazole moiety is an area of intense research. Other applications of oxazole derivatives include the use as pesticides, fluorescent whitening agents, lubricants, dyes and pigments. Therefore, there is considerable interest of having available efficient routes to these heterocycles and to better understand their reactivity.

In relation with our ongoing research on the synthesis and reactivity of 2-halo-2*H*-azirines[2] we reported the thermolysis of 2-halo-2-acyl-2*H*-azirines **(**Scheme 1).[2g] 2-Benzoyl-2-halo-2*H*-azirine-3-carboxylates (**1**) underwent ring expansion giving products in high yield which were identified as being 4-haloisoxazoles **3**. The same products were also obtained in high yield from the thermolysis of haloazidoalkenes **4** *via* intermediate 2-benzoyl-2-halo-2*H*-azirines **1**.

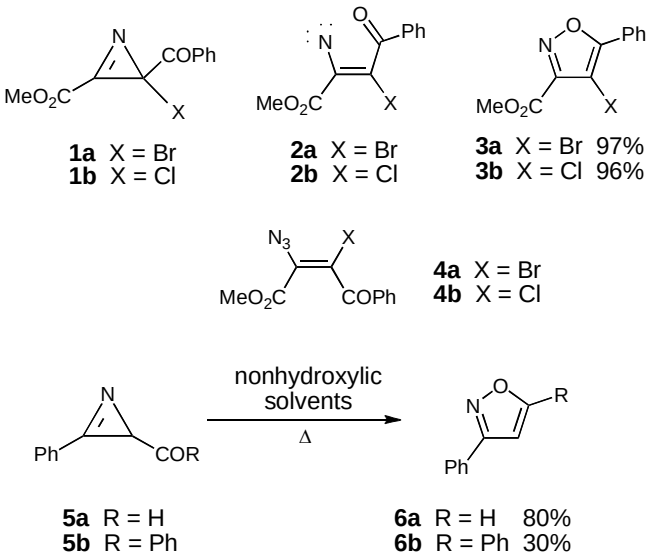

Scheme 1.

The thermolysis of 2*H*-azirines usually results in cleavage of the N-C2 single bond giving a transient vinylnitrene, the reverse of the cyclization of vinylnitrenes used to prepare *2H*-azirines.[3] Evidence for the existence of this intermediate comes from the thermal ring opening of 2,3-diaryl-2-cyano-2*H*-azirine where the vinylnitrene was trapped with phosphanes.[4] On the other hand, it was known that heating a solution of 3-phenyl-2*H*-azirine-2-carboxaldehyde (**5a**) at 200 °C leads to 3-phenylisoxazole (**6a**) in high yield.[5a] The same isoxazole can also be obtained in 90% yield by treatment of 3-phenyl-2*H*-azirine-2-carboxaldehyde at 25 ºC with Grubbs' catalyst.[5b] Furthermore, 2-benzoyl-3-phenyl-2*H*-azirine (**5b**) affords the corresponding isoxazole

6b upon heating in nonhydroxylic solvents.[5c] These observations led us to rationalize the thermal reaction of 2-benzoyl-2-halo-2*H*-azirine-3-carboxylates (**1**) as being the conversion into isoxazoles **3** via vinyl nitrenes **2** (Scheme 1).

Isoxazoles have also been obtained from (*Z*)-β-azido-α,β-unsaturated ketones and esters (**7** and **9a**) (Scheme 2).[5d,5e] Hassner *et al.* also observed that *meso*-1,2-benzoylethylene dibromide **12** reacts with two equivalents of sodium azide to give 3-benzoyl-5-phenylisoxazole **13** via a vinyl azide intermediate.[5f] However, the thermal induced reaction of (*E*)-β-azido-α,β-unsaturated ketone **9b** gives the corresponding 1,3-oxazole **11**.[5e] The different outcome of the thermolysis of the (*Z*)- and (*E*)-β-azido-α,β-unsaturated ketones led the authors to propose a concerted mechanism for the synthesis of isoxazoles starting from (*Z*)-β-azido-α,β-unsaturated ketones. In the case of the (*E*)-β-azido-α,β-unsaturated ketones the concerted mechanism would not

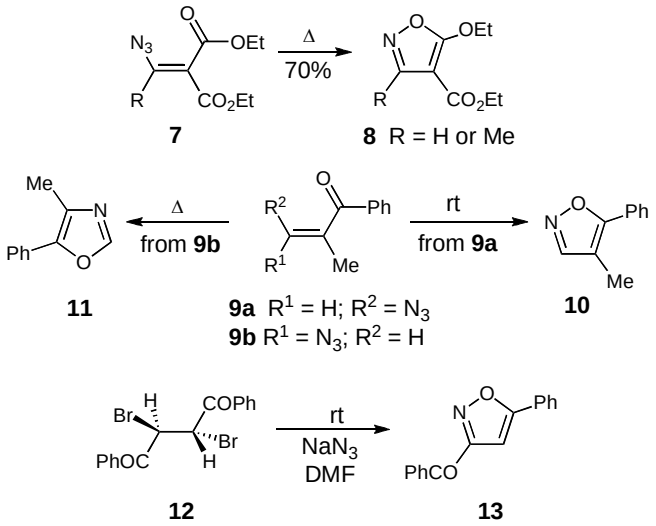

Scheme 2.

be possible due to the configuration of the alkene. Therefore, the formation of 2*H*-azirine intermediates was postulated followed by ring expansion reaction to oxazole, which would require a C2-C3 bond cleavage. These observations could lead to the conclusion that starting from 2-acyl-2*H*-azirines only oxazoles could be obtained. Nevertheless, this does not account for the fact that the thermolyses of both 3-phenyl-2*H*-azirine-2-carboxaldehyde (**5a**) and 2-benzoyl-3-phenyl-2*H*-azirine (**5b**) afford the corresponding isoxazoles (Scheme 1).[5a,5c] In fact, the reactivity pattern of 2*H*-azirine

derivatives has been shown to be more difficult to establish a piori then initially supposed, since it is significantly dependent on the nature of the substituents.

In fact, under thermal conditions the reactivity expected for 2*H*-azirines is the cleavage of the N-C2 single bond giving a transient vinylnitrene whereas the photolysis should lead to the cleavage of the C2-C3 bond giving nitrile ylide intermediates.[1,3] However, we have previously studied the UV induced photochemical reactions of two aliphatic 2*H*-azirines – methyl 2-chloro-3-methyl-2*H*-azirine-2-carboxylate and methyl 3-methyl-2*H*-azirine-2-carboxylate – isolated in argon matrices.[6a-6c] For both compounds, irradiation with $\lambda > 235$ nm led to the observation of two primary photoprocesses: the expected C2-C3 bond cleavage, with production of nitrile ylides, but also the N-C2 bond cleavage, with production of methylated ketene imines. Inui and Murata also demonstrated that both C2-C3 and N-C2 bonds can be cleaved upon photolysis of matrix-isolated 2*H*-azirines bearing an aromatic substituent at C2.[6d-6f] They concluded that the tendency toward the N-C2 bond cleavage increases with the electron-withdrawing ability of the ring substituents.

Thermally induced ring expansion reactions of 2-acyl-2*H*-azirines leading to oxazoles have also been reported, although these transformations required a base- or Lewis acid-catalysis or the use of organometallic catalysts.[5c,7]

Matrix isolation infrared spectroscopy is extremely powerful to undertake detailed structural and photochemical studies. Once the substance under investigation is isolated in a cryogenic inert matrix, *in situ* irradiation can be undertaken and the progress of the reaction probed spectroscopically. The use of criteriously chosen irradiation conditions can selectively induce a given reaction path, enabling a detailed characterization of the related intermediates. Thus, we decided to use matrix isolation infrared spectroscopy to carry out the structural and vibrational characterization as well as the study of the photochemistry of 4-haloisoxazoles.

The chloro compound obtained from the thermolysis of methyl 2-benzoyl-2-chloro-2*H*-azirine-3-carboxylate (**1b**) was selected for our study. The monomeric structure isolated in low temperature argon matrix was studied by FT-IR spectroscopy, supported by theoretical calculations undertaken at the DFT(B3LYP)/6-311++G(d,p) level of theory. For our surprise the theoretically predicted spectrum for isoxazole **3b** did not match the experimental IR spectrum. Indeed, the results described below will demonstrate that the studied compound cannot be methyl 4-chloro-5-phenylisoxazole-

3-carboxylate (**3b**) but instead we are in the presence of methyl 4-chloro-5-phenyl-1,3-oxazole-2-carboxylate (**15**) (MCPOC).

2. Experimental

^{1}H NMR spectra were recorded on a Bruker Avance 300 instrument operating at 300 MHz. ^{13}C spectra were recorded on a Bruker Avance 300 instrument operating at 75.5 MHz. The solvent is deuteriochloroform except where indicated otherwise. IR spectra were recorded on a Perkin Elmer 1720X FTIR spectrometer. Mass spectra were recorded on a HP GC 6890/MSD5973 instrument under electron impact (EI) except where indicated otherwise. Microanalyses were performed using an EA 1108-HNS-O Fisons instrument. Mp were recorded on a Reichert hot stage and are uncorrected. Flash column chromatography was performed with Merck 9385 silica as the stationary phase.

2.2. General procedure for the synthesis of 1,3-oxazoles 15 and 18 from 2-halo-2*H*-azirines.

The 2-halo-2*H*-azirine[2b] (2.81 mmol) was dissolved in toluene (10 ml) and the reaction mixture was heated at reflux for 5 h. The solvent was evaporated giving the 1,3-oxazole as a solid.

2.2.1. Methyl 4-chloro-5-phenyl-1,3-oxazole-2-carboxylate 15.[8] Compound **15** was obtained as a solid (96%), mp 71-72 °C. IR (KBr) 1529, 1738, 2959 cm^{-1}; ^{1}H NMR 4.04 (3H, s), 7.47-7.51 (3H, m, Ar-H), 7.98-8.01 (2H, m, Ar-H); ^{13}C NMR 53.5, 125.6, 125.9, 126.6, 129.0, 130.2, 147.8, 148.7, 155.3; MS (EI) *m/z* 239 [M(^{37}Cl)$^{+}$] (34), 237 [M(^{35}Cl)$^{+}$] (100), 177 (17), 128 (8), 105 (55), 77 (59). Anal. Calcd. for $C_{11}H_8NO_3Cl$: C, 55.60; H, 3.39; N, 5.89. Found: C, 55.66; H, 3.32; N, 5.92%.

2.2.2. Methyl 4-bromo-5-phenyl-1,3-oxazole-2-carboxylate 18. Compound **18** was obtained as a solid (97%), mp 66-68 °C. IR (KBr) 1737, 2958 cm^{-1}; ^{1}H NMR 4.04 (3H, s), 7.48-7.51 (3H, m, Ar-H), 8.03-8.06 (2H, m, Ar-H); ^{13}C NMR 4.04 (3H, s), 7.48-7.51 (3H, m, Ar-H), 8.03-8.06 (2H, m, Ar-H); MS (EI) *m/z* 283 [M(^{81}Br)$^{+}$]

(100), 281 [M(^{79}Br)$^+$] (100), 223 (18), 221 (18), 105 (55), 77 (89). Anal. Calcd. for $C_{11}H_8NO_3Br$: C, 46.84; H, 2.86; N, 4.97. Found: C, 47.24; H, 3.12; N, 5.29%.

2.3. General procedure for the synthesis of 1,3-oxazoles from haloazidoalkenes.

The azidoalkene[2b] (1 mmol) was dissolved in toluene (10 ml) and the reaction mixture was heated under reflux for 7 h. The solvent was evaporated and the residue was washed with cooled ethyl ether giving the 1,3-oxazole as a solid.

2.3.1. Methyl 4-chloro-5-phenyl-1,3-oxazole-2-carboxylate 15 (98%). Identified by comparison with the specimen isolated earlier.

2.3.2. Methyl 4-bromo-5-phenyl-1,3-oxazole-2-carboxylate 18 (95%). Identified by comparison with the specimen isolated earlier.

2.4. Methyl 4-chloro-5-phenylisoxazole-3-carboxylate 3b. A solution of methyl 5-phenylisoxazole-3-carboxylate **17**[9] (70 mg, 0.345 mmol) and NCS (85 mg, 0.64 mmol) in 2.3 mL of 7% fuming nitric acid in acetic acid was irradiated for 40 min in the microwave reactor (CEM Focused Synthesis System, Discover S-Class) with the temperature set to 160 ºC. After cooling to room temperature, water (15 mL) was added and the mixture extracted with CH_2Cl_2 (2x15 mL). The organic phase was dried ($MgSO_4$) and evaporated off. The crude product was purified by flash chromatography [ethyl acetate–hexane (1:5)] to give **3b** as a white solid (59%). mp 62-63 °C. IR (KBr) 1221, 1441, 1738, 2957 cm^{-1}; ^{1}H NMR 4.03 (3H, s), 7.52-7.55 (3H, m), 8.03-8.06 (2H, m);^{13}C NMR 53.1, 106.0, 125.6, 126.6, 129.0, 131.2, 153.3, 159.1, 165.8; MS (EI) *m/z* 237 (M$^+$, 99), 206 (14), 105 (100), 77 (68), 59 (78); HRMS (CI) *m/z* 237.0200 ($C_{11}H_8NO_3Cl$ [M$^+$], 237.0193).

2.4. Infrared spectroscopy

Matrix isolation of 1,3-oxazole **15** (MCPOC) and isoxazole **3b** (MCPIC): The IR spectra were collected, with 0.5 cm^{-1} spectra resolution, using a Mattson (Infinity 60AR series) or a Nicolet 6700 Fourier transform infrared spectrometer, equipped with a deuterated triglycine sulphate (DTGS) detector and a Ge/KBr beamsplitter.

To avoid interference from atmospheric H_2O and CO_2, a stream of dry nitrogen continuously purged the optical path of the spectrometers. All experiments were performed using an APD Cryogenics closed-cycle helium refrigeration system with a DE-202A expander.

To deposit the matrices, the compound to be studied was sublimated (T = 323 K) using a specially designed mini-furnace thermoelectrically heatable placed inside the cryostat and co-deposited with a large excess of the matrix gas (argon N60 obtained from Air Liquide) onto the CsI optical substrate of the cryostat cooled to 10 K.

2.5 Computational methodology

The quantum chemical calculations were performed with Gaussian 03 (Revision B.01) program[10] at the DFT level of theory, using the split valence triple-ζ 6-311++G(d,p) basis set and the three-parameter B3LYP density functional, which includes Becke's gradient exchange correction[11] and the Lee, Yang and Parr correlation functional.[12]

Geometrical parameters of the relevant conformations were optimized using the Geometry Direct Inversion of the Invariant Subspace (GDIIS) method.[13] In order to assist the analysis of the experimental spectra, vibrational frequencies and IR intensities were also calculated at the same level of approximation. The computed harmonic frequencies were scaled down by two factors (0.9894 for MCPOC and 0.9817 for MCPIC) to correct them for the effects of basis set limitations, neglected part of electron correlation and anharmonicity effects. The optimized structures of all conformers described in this study were confirmed to correspond to true minimum energy conformations on the potential energy surface investigated.

3. Results and Discussion

Two low energy conformers of MCPOC were predicted to exist by the calculations (Figure 1). The IR spectrum of matrix-isolated 1,3-oxazole **15** is presented in Figures 2 and 3 along with the calculated spectra for the two most stable conformers. The comparison of the IR spectrum of the product of the thermolysis of

methyl 2-benzoyl-2-chloro-2*H*-azirine-3-carboxylate (**1b**) with the theoretically predicted spectrum of MCPOC allow us to unambiguously establish the structure as being methyl 4-chloro-5-phenyl-1,3-oxazole-2-carboxylate (**15**).

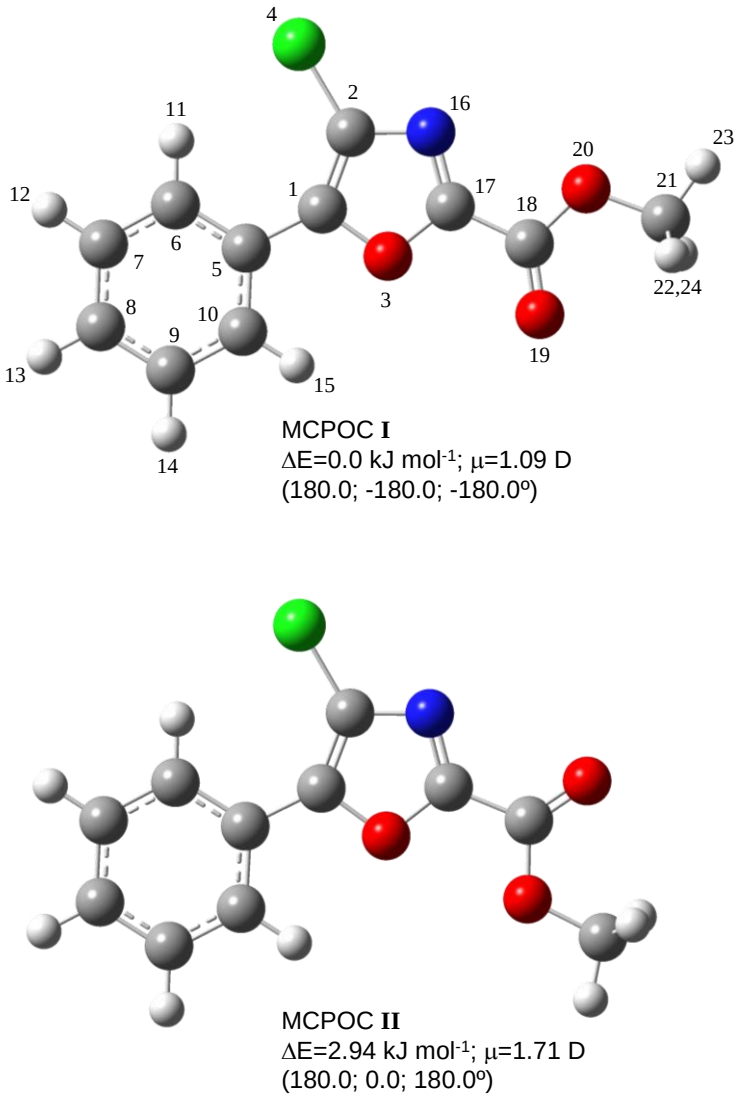

Figure 1. Conformers of methyl 4-chloro-5-phenyl-1,3-oxazole-2-carboxylate (**15**) (MCPOC) with atom numbering. Relative energies and dipole moments are also provided, as well as the C_6-C_5-C_1-O_3, N_{16}=C_{17}-C_{18}=O_{19} and C_{17}-C_{18}-O_{20}-C_{21} dihedral angles.

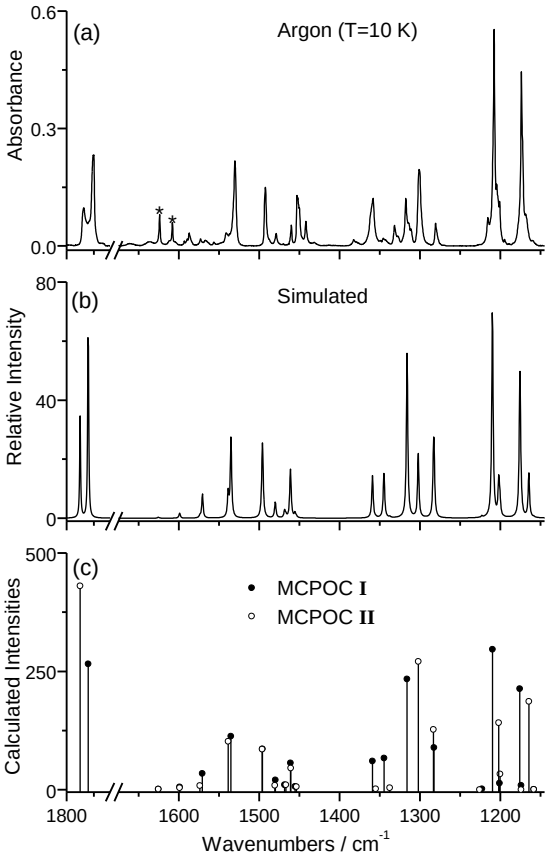

Figure 2. Infrared spectra of MCPOC (**15**) (1800-1145 cm^{-1} region): (a) spectrum of MCPOC isolated in an argon matrix (sublimation temperature: 323 K; substrate temperature: 10 K), (b) simulated population-weighted (at 323 K) spectrum of MCPOC using Lorentzian functions with 2 cm^{-1} half bandwidth and centred at the DFT(B3LYP)6-311++G(d,p) calculated wavenumbers for the two relevant conformers of MCPOC; and (c) theoretical spectra for the two conformers of MCPOC. Calculated wavenumbers were scaled by 0.9894. Bands marked with an asterisk are due to monomeric water impurity.

In the present case, the formation of oxazole **15** from 2*H*-azirine **1b** can be explained considering the thermal cleavage of the C2-C3 to give nitrile ylide **14** followed by recyclization giving oxazole **15** as the final product (Scheme 3). Since the oxazole is obtained in high yield (98%) we can conclude that only the reaction pathway **B** is observed.

Another relevant conclusion can be drawn from this study. In fact, the mechanism of formation of the 2*H*-azirine ring from the haloazidoalkene **4b** must be a concerted process since the formation of a vinylnitrene intermediate should lead to the competitive formation of the isoxazole **3b**.

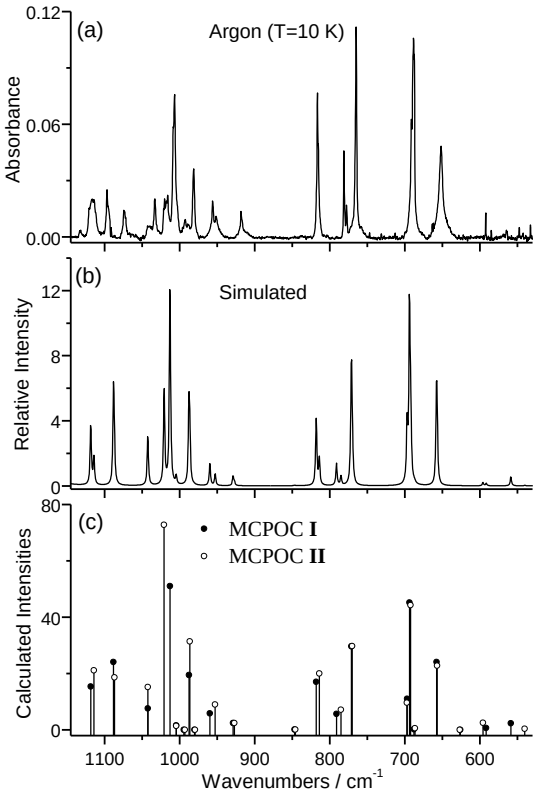

Figure 3. Infrared spectra of MCPOC (**15**) (1145-530 cm^{-1} region): (a) spectrum of MCPOC isolated in an argon matrix (sublimation temperature: 323 K; substrate temperature: 10 K), (b) simulated population-weighted (at 323 K) spectrum of MCPOC using Lorentzian functions with 2 cm^{-1} half bandwidth and centred at the DFT(B3LYP)6-311++G(d,p) calculated wavenumbers for the two relevante conformers of MCPOC; and (c) theoretical spectra for the two conformers of MCPOC. Calculated wavenumbers were scaled by 0.9894.

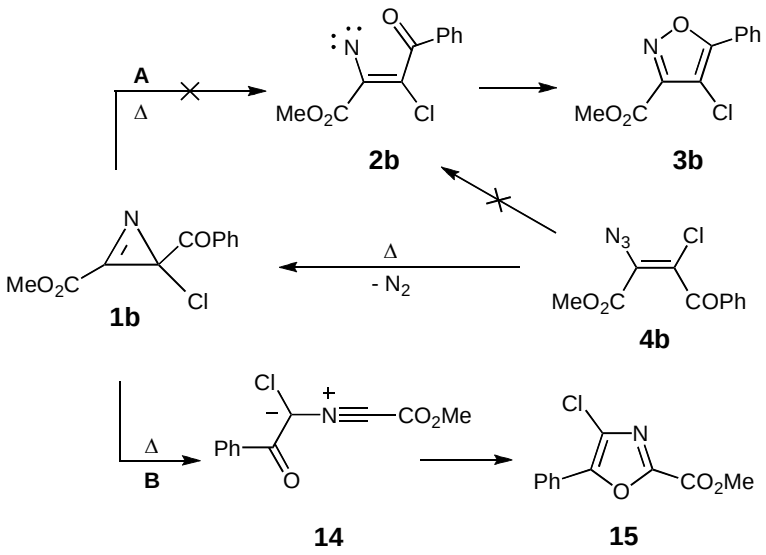

Scheme 3.

Recently, Li *et al.* reported the bromination of isoxazoles with *N*-bromosuccinimide in acid solvents using microwave irradiation.[14] The work included the synthesis of methyl 4-bromo-5-phenylisoxazole-3-carboxylate (**3a**). The authors observed that the ^{13}C NMR spectrum of this compound did not match the NMR data previously reported by us for the product of the thermolysis of 2-benzoyl-2-bromo-2*H*-azirine-3-carboxylate **1a**.[2g] This led the authors to confirm the structure of 4-bromo-5-phenylisoxazole-3-carboxylate **3a** by single crystal X-ray crystallography. This was another evidence that indicates that the thermolysis of 2-benzoyl-2-halo-2*H*-azirine-3-carboxylates **1** leads to oxazoles and not to isoxazoles.

In order to get further support to the structural assignment we decided to prepare 4-chloro-5-phenylisoxazole-3-carboxylate **3b** to study the compound by matrix-isolation FTIR. The synthesis of isoxazole **3b** is outlined in Scheme 4. The starting methyl 5-phenylisoxazole-3- carboxylate (**17**) was prepared by cyclization of 2,4-dioxo-4-phenylbutanoate (**16**) with hydroxylamine hydrochloride.[9] We applied the general procedure described by Li *et al.*[14] for the synthesis of 4-chloro-5-phenylisoxazole-3-carboxylate **3b** but using NCS instead of NBS. Using 5% fuming nitric acid in acetic acid as solvent the solution of isoxazole **17** was irradiated in the microwave reactor with the temperature set to 150 ºC for 25 minutes giving the desired product in 45% yield. However, the yield could be improved to 59% carrying out the microwave irradiation at 160 ºC for 40 minutes.

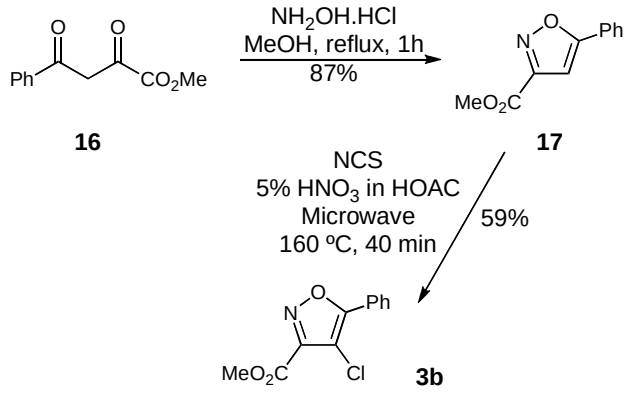

Scheme 4.

Three different low energy conformers of 4-chloro-5-phenylisoxazole-3-carboxylate **3b** (MCPIC) were predicted to exist by the calculations (Figure 4). The IR

spectrum of matrix-isolated 4-chloro-5-phenylisoxazole-3-carboxylate **3b** (MCPIC) is shown in Figures 5 and 6. The assignment of the observed bands was carried out by comparison with the theoretically predicted simulated spectrum, which nicely fits the observed spectrum (see Figures 5 and 6). This spectrum of MCPIC is significantly distinct from that of the product resulting from the thermolysis of **1b** (which, as already shown, corresponds to the 1,3-oxazole **15**).

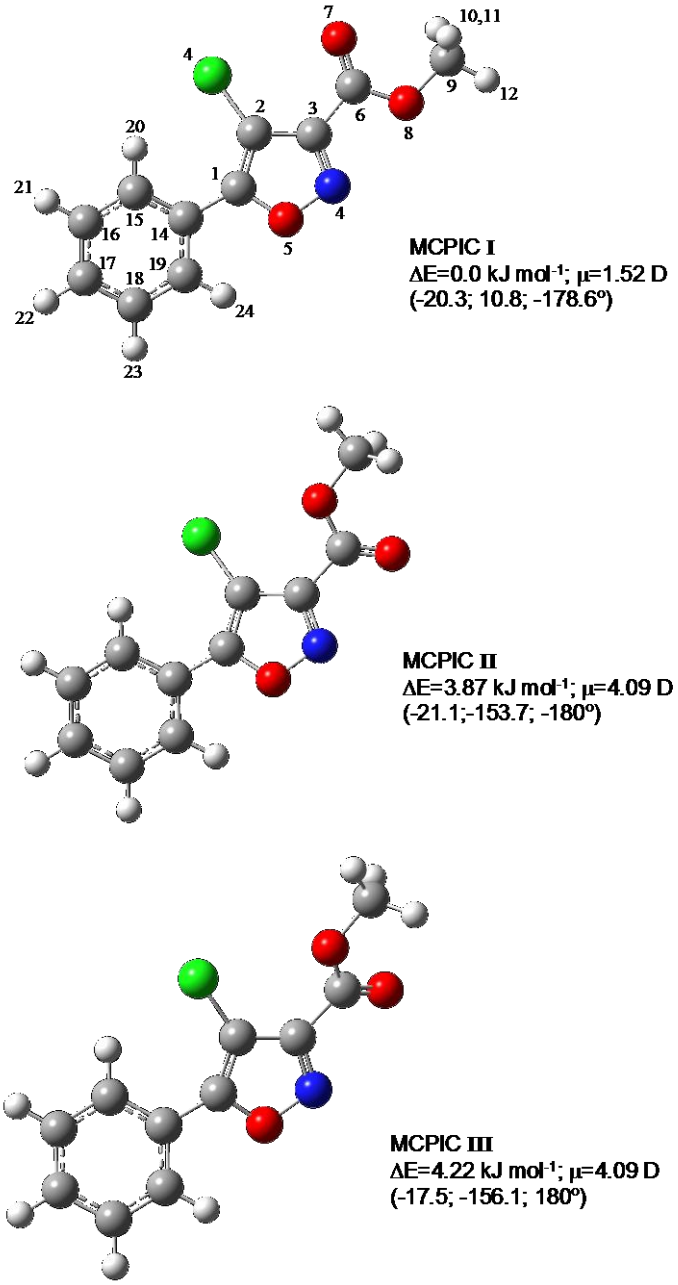

Figure 4. Conformers of methyl 4-chloro-5-phenylisoxazole-3-carboxylate (**3b**) (MCPIC) with atom numbering. Relative energies and dipole moments are also provided, as well as the C_{15}-C_{14}-C_1-C_2, O_7=C_6-C_3-C_2 and C_9-O_8-C_6-C_3 dihedral angles.

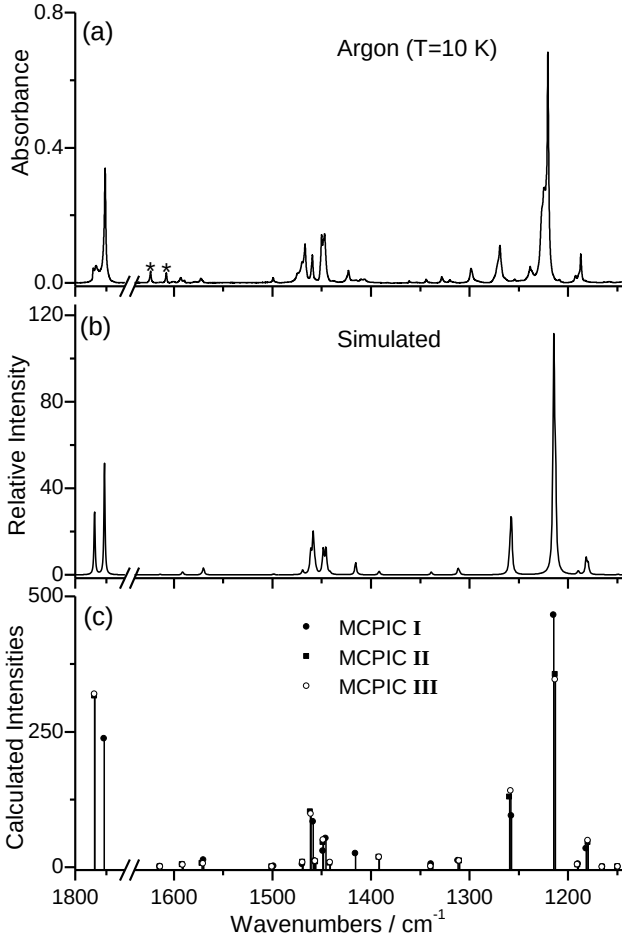

Figure 5. Infrared spectra of MCPIC (**3b**) (1800-1145 cm^{-1} region): (a) spectrum of MCPIC isolated in an argon matrix (sublimation temperature: 323 K; substrate temperature: 10 K), (b) simulated population-weighted (at 323 K) spectrum of MCPIC using Lorentzian functions with 2 cm^{-1} half bandwidth and centred at the DFT(B3LYP)6-311++G(d,p) calculated wavenumbers for the three relevant conformers of MCPIC; and (c) theoretical spectra of the three conformers of MCPIC. Calculated wavenumbers were scaled by 0.9817. Bands marked with an asterisk are due to monomeric water impurity.

In order to give further insight into the unusual thermolysis process of the studied 2-benzoyl-2*H*-azirine, we now also examined the possibility of occurrence of initial formation of the isoxazole, followed by isomerization to the oxazole ring, since the thermal rearrangement of 4-acylisoxazoles to 4-acyloxazoles is known.[15] In reference 15, the synthesis of the oxazoles from the corresponding isoxazoles was rationalized considering ring contraction reaction to give a 2*H*-azirine intermediate, followed by a ring expansion process via C2-C3 bond cleavage and cyclization.

Therefore, the thermolysis of 2-benzoyl-2-chloro-2*H*-azirine-3-carboxylate **1b** could also involve the formation of isoxazole **3b** followed by the rearrangement to oxazole **15**. However, this possibility was rolled out, since upon heating at reflux for 5 hours a solution of isoxazole **3b** in toluene no reaction was observed.

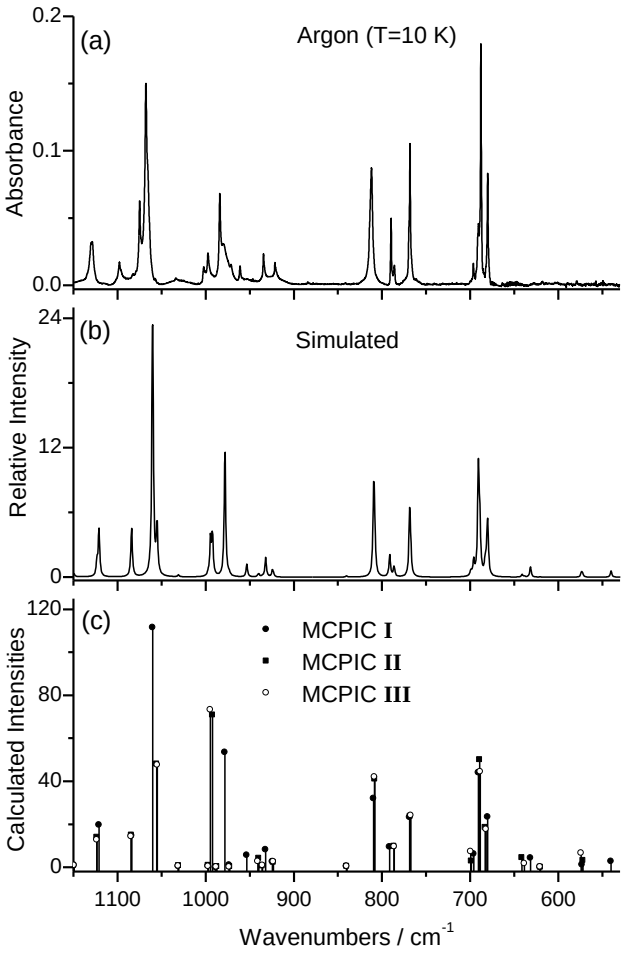

Figure 6. Infrared spectra of MCPIC (**3b**) (1145-530 cm^{-1} region): (a) spectrum of MCPIC isolated in an argon matrix (sublimation temperature: 323 K; substrate temperature: 10 K), (b) simulated population-weighted (at 323 K) spectrum of MCPIC using Lorentzian functions with 2 cm^{-1} half bandwidth and centred at the DFT(B3LYP)6-311++G(d,p) calculated wavenumbers of the three relevant conformers of MCPIC; and (c) theoretical spectra of the three conformers of MCPIC. Calculated wavenumbers were scaled by 0.9817.

4. Conclusion

It is clear from the analysis of the matrix-isolated 4-chloro-5-phenyl-1,3-oxazole-2-carboxylate **15** and methyl 4-chloro-5-phenylisoxazole-3-carboxylate **3b** FTIR spectra that this technique allows to distinguish easily these isomeric heterocycles. Therefore, it has been demonstrated that methyl 2-benzoyl-2-halo-2*H*-azirine-3-carboxylates **1** undergo thermal ring expansion to give 4-halo-5-phenyl-1,3-oxazole-2-carboxylates (**15** and **18**) in high yield. These 1,3-oxazoles can also be obtained in high yield from haloazidoalkenes **4** (Scheme 5).

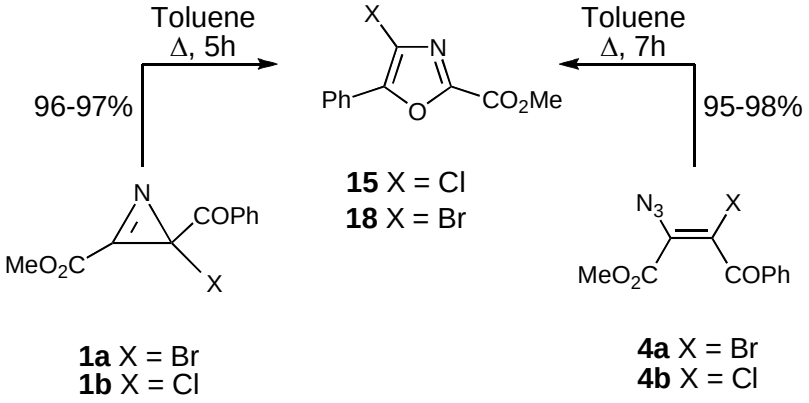

Scheme 5.

Acknowledgements

S. Lopes and C. M. Nunes acknowledge FCT for the Ph.D. grants (SFRH/BD/29698/2006 and SFRH/BD/28844/2006).

References:

[1] (a) Lang Jr, S. A.; Lin, Y.-I in A. R. Katritzky and C. W. Rees (series Eds), K. T. Potts (Ed.) *Comprehensive Heterocyclic Chemistry*, Vol. 6, Pergamon, Oxford, 1984, Chapter 4.16 and Chapter 4.18. (b) T. M. V. D. Pinho e Melo, Curr. Org.

Chem., 9 (2005) 925. (c) V. S. C. Yeh, Tetrahedron, 60 (**2004**) 11995. (d) Y. Hamada, T. Shioiri, *Chem. Rev.*, 105 (2005) 4441. (e) Wipf, P. *Chem. Rev.* **1995**, *95*, 2115.

[2] (a) T. M. V. D. Pinho e Melo, C. S. J. Lopes, A. M. d'A. Rocha Gonsalves, Tetrahedron Lett., 41 (2000) 7217. (b) T. M. V. D. Pinho e Melo, C. S. J. Lopes, A. L. Cardoso, A. M. d'A. Rocha Gonsalves, Tetrahedron, 57 (2001) 6203. (c) T. M. V. D. Pinho e Melo, C. S. J. Lopes, A. M. d'A. Rocha Gonsalves, A. M. Beja, J. A. Paixão, M. R. Silva, L. A. Veiga, J. Org. Chem., 67 (2002) 66. (d) T. M. V. D. Pinho e Melo, A. L. Cardoso, C. S. B. Gomes, A. M. d'A. Rocha Gonsalves, Tetrahedron, 59 (2003**)** 2345. (e) T. M. V. D. Pinho e Melo, Cardoso, A. L. Cardoso, C. S. B. Gomes, A. M. d'A. Rocha Gonsalves, Tetrahedron Lett., 44 (2003) 6313. (f) Pinho e Melo, T. M. V. D.; Rocha Gonsalves, A. M. d'A. *Curr. Org. Synth* **2004**, 1, 275. (g) T. M. V. D. Pinho e Melo, C. S. J. Lopes, A. M. d'A. Rocha Gonsalves, R. C. Storr, Synthesis, (2002) 605. (h) S. M. Fonseca, H. D. Burrows, C. M. Nunes, T. M. V. D. Pinho e Melo, A. M. d'A. Rocha Gonsalves, Chem. Phys. Lett., 414 (2005) 98.

[3] F. Palacios, A. M. O. Retana, E. M. Marigorta, J. M. Santos, Eur. J. Org. Chem., (2001) 2401.

[4] T. Nishiwaki, J. Chem. Soc. Chem. Comm., (1972) 565.

[5] (a) A. Padwa, J. Smolanoff, A. Tremper, J. Am. Chem. Soc., 97 (1975) 4682. (b) A. Padwa, T. Stengel, Tetrahedron Lett., 45 (2004) 5991. (c) B. Singh, E. F. Ullman, J. Am. Chem. Soc., 89 (1967) 6911. (d) G. L'abbé, Angew. Chem. Inter. Ed., 14 (1975) 775. (e) K. Friedrich, H. K. Thieme, Chem. Ber., 103 (1970) 1982. (f) A. Hassner, G. L'abbé, M. J. Miller, J. Am. Chem. Soc., 93 (1971) 981.

[6] (a) A. Gómez-Zavaglia, A. Kaczor, A. L. Cardoso, T. M. V. D. Pinho e Melo, R. Fausto, J. Phys. Chem. A, 110 (2006) 8081. (b) A. Kaczor, A. Gómez-Zavaglia, A. L. Cardoso, T. M. V. D. Pinho e Melo, R. Fausto, J. Phys. Chem. A, 110 (2006) 10742. (c) A. Gómez-Zavaglia, A. Kaczor, A. L. Cardoso, T. M. V. D. Pinho e Melo, R. Fausto, J. Mol. Struct., 834-835 (2007) 262. (d) H. Inui, S. Murata, *Chem. Phys. Lett.*, 359 (2002) 267; (e) H. Inui, S. Murata, J. Am. Chem. Soc., 127 (2005) 2628.

[7] (a) K. Isomura, Y. Hirose, H. Shuyama, S. Abe, G. Ayabe, H. Taniguchi, Heterocycles, 9 (1978) 1207. (b) S. Brahma, J. K. Ray, J. Heterocycl. Chem., 45 (2008**)** 311.

[8] R. Wingen, D. Guenther, J. Lignau, Ger. Offen. DE 3.706,881; Chem. Abstract., 110 (1989) 125315.

[9] (a) C. Maurion, F. Bailly, P. Cotelle, Tetrahedron, 60 (2004) 6479. (b) A. K. Roy, S. Batra, Synthesis, 15 (2003) 2325.

[10] M. J. Frisch, G. W. Trucks, H. B. Schlegel, G. E. Scuseria, M. A. Robb, J. R. Cheeseman, J. A. Montgomery Jr., T. Vreven, K. N. Kudin, J. C. Burant, J. M. Millam, S. S. Iyengar, J. Tomasi, V. Barone, B. Mennucci, M. Cossi, G. Scalmani, N. Rega, G. A. Petersson, H. Nakatsuji, M. Hada, M. Ehara, K. Toyota, R. Fukuda, J. Hasegawa, M. Ishida, T. Nakajima, Y. Honda, O. Kitao, H. Nakai, M. Klene, X. Li, J. E. Knox, H. P. Hratchian, J. B. Cross, V. Bakken, C. Adamo, J. Jaramillo, R. Gomperts, R. E. Stratmann, O. Yazyev, A. J. Austin, R. Cammi, C. Pomelli, J. W. Ochterski, P. Y. Ayala, K. Morokuma, G. A. Voth, P. Salvador, J. J. Dannenberg, V. G. Zakrzewski, S. Dapprich, A. D. Daniels, M. C. Strain, O. Farkas, D. K. Malick, A. D. Rabuck, K. Raghavachari, J. B. Foresman, J. V. Ortiz, Q. Cui, A. G. Baboul, S. Clifford, J. Cioslowski, B. B. Stefanov, G. Liu, A. Liashenko, P. Piskorz, I. Komaromi, R. L. Martin, D. J. Fox, T. Keith, M. A. Al-Laham, C. Y. Peng, A. Nanayakkara, M. Challacombe, P. M. W. Gill, B. Johnson, W. Chen, M. W. Wong, C. Gonzalez, J. A. Pople, Gaussian 03, revision B.01; Gaussian, Inc.: Wallingford, CT, (2004).

[11] A. D. Becke, Phys. Rev. A, 38 (1988) 3098.

[12] C. T. Lee, W. T. Yang, R. G. Parr, Phys. Review B, 37 (1988) 785.

[13] P. Csaszar, P. Pulay, J. Mol. Struct. (Theochem.), 114 (1984) 31.

[14] G. Li, R. Kakarla, S. W. Gerritz, Tetrahedron Lett., 48 (2007) 4595.

[15] (a) A. Padwa, E. Chen, J. Org. Chem., 39 (1974) 1976. (b) A. Padwa, E. Chen, A. Ku, J. Am. Chem. Soc., 97 (1975) 6484.

J. Phys. Chem. A, **2010**, *114*, 9074-9082.

Conformational Space and Vibrational Spectra of Methyl 4-Chloro-5-phenyl-1,3-oxazole-2-carboxylate

Susy Lopes,[a] Cláudio M. Nunes,[a] Andrea Gómez-Zavaglia,[a,b]

Teresa M.V.D. Pinho e Melo[a] and Rui Fausto[a]

[a] *Department of Chemistry, University of Coimbra, P-3004-535 Coimbra, Portugal*
[b] *Centro de Investigación y Desarrollo en Criotecnología de Alimentos (Conicet La Plata, UNLP) RA-1900, La Plata, Argentina*

ABSTRACT

Methyl 4-chloro-5-phenyl-1,3-oxazole-2-carboxylate (MCPOC) has been synthesized and isolated in cryogenic matrices (argon and xenon). FTIR spectroscopy studies on the matrix isolated compound, supported by DFT(B3LYP)/6-311++G(d,p) calculations, allow for the identification of two low energy conformers (**I** and **II**) of the molecule, which differ from each other in the orientation of the ester group relatively to the oxazole ring. In both these conformers, the ester moiety is in the *s-cis* configuration (O=C-O-CH_3 dihedral: 0º). Conformer **II** is *ca.* 3.0 kJ mol^{-1} higher in energy than form **I** in gas phase. Two additional higher energy conformers, **III** and **IV**, with relative energies of *ca.* 30 and 45 kJ mol^{-1}, respectively, were predicted to exist by the calculations, corresponding to structures where the ester group is in an approximately *s-trans* arrangement. Annealing of the compound isolated in xenon at 60 K led to aggregation and simultaneous reduction of the population of **I** compared to that of the more polar conformer **II**. These results suggest the inversion of the order of stability of the two conformers in that matrix, eventually accompanied by a higher trend of conformer **I** to aggregate. Full assignment of the observed infrared bands to the two experimentally accessible conformers was carried out for the matrix isolated monomeric species. In addition, the infrared spectra of the neat compound in the low temperature (10 K) amorphous and crystalline phases, as well as the infrared and Raman spectra of the crystal at room temperature were also obtained and assigned.

Introduction

Oxazole is a five-membered heterocyclic compound that contains the N=C–O moiety. The oxazole ring occurs naturally in numerous living systems, such as marine organisms, plants (*e.g.*, coffee, peanuts) and mushrooms.[1-9] In recent years, an increasing number of studies have been developed dealing with the total synthesis of natural products bearing oxazole moieties with interesting biological activities. In particular, oxazole containing molecules isolated from marine organisms constitute an ever-growing number of natural products that have been receiving different pharmacological uses (as anti-inflammatory, anti-bacterial, antibiotic, antiviral, analgesic and anti-tumor drugs).[3,4,10-26] Some oxazoles display scintillator properties[27,28] and are used as fluorescent whitening agents[29,30] and in dyes and pigments.[31] The practical uses of oxazoles extend to other industrial applications such as pesticides, in the production of electrophotographic materials, as additives to detergents, and in hydraulic fluids and lubricants.[32]

Because of their known multiple practical uses, aryl- and alkyloxazoles have been extensively studied both experimentally and theoretically.[33-43] On the other hand, halogen-substituted oxazoles are a relatively new family of compounds which, in spite of its relevance as synthetic intermediates in carbon-carbon bond making reactions,[44,45] have been paid little attention. In a previous publication,[46] we described the first structural assignment of methyl 4-chloro-5-phenyl-1,3-oxazole-2-carboxylate (MCPOC) in an argon matrix. In such study, we were able to confirm that the thermolysis product of methyl 2-benzoyl-2-choro-2*H*-azirine-3-carboxylate was MCPOC and not the isoxazole 4-choro-5-phenylisoxazole-3-carboxylate as previously suggested.[47]

In the present study, the conformational space of MCPOC was investigated in detail by a concerted matrix-isolation infrared spectroscopy (in both argon and xenon matrices) and quantum chemical theoretical [DFT(B3LYP)/6-311++G(d,p)] approach. As it will be described in detail in the next sections, from these studies it was possible to conclude on the existence of two significantly populated conformers of MCPOC in the gas-phase and in the cryogenic matrices (argon, xenon), and of two higher energy forms. The two experimentally relevant low-energy conformers were successfully characterized and the obtained experimental spectra interpreted. The infrared spectra of the neat compound in the low temperature (10 K) amorphous and crystalline

phases, as well as the infrared and Raman spectra of the crystal at room temperature were also obtained and assigned.

Experimental and Computational Methods

The procedure for the synthesis of methyl 4-chloro-5-phenyl-1,3-oxazole-2 carboxylate (MCPOC) has been reported elsewhere.[46]

Matrices were prepared by co-deposition of MCPOC vapors coming out from a specially designed thermoelectrically heatable mini-furnace, assembled inside the cryostat (APD Cryogenics, model DE-202A) chamber, and large excess of the matrix gas (argon, N60; xenon, N48, both obtained from Air Liquide) onto the CsI substrate cooled to 10 K (for argon matrices) and 20 K (for xenon matrices). The IR spectra were recorded with 0.5 cm^{-1} spectral resolution in a Mattson (Infinity 60AR Series) Fourier Transform infrared spectrometer, equipped with a deuterated triglycine sulphate (DTGS) detector and a Ge/KBr beam splitter. Necessary modifications of the sample compartment of the spectrometer were done in order to accommodate the cryostat head and allow purging of the instrument by a stream of dry nitrogen, to remove water vapors and CO_2.

The low temperature solid amorphous layer was prepared in the same way as matrices but with the flux of matrix gas cut off. The layer was then allowed to anneal at slowly increasing temperature up to 280 K and crystallization of the amorphous layer occurred. After recording of the infrared spectrum of the obtained crystal, the sample was cooled back again to 10 K and a new spectrum of the crystalline phase was collected.

KBr pellets and nujol mulls containing MCPOC were prepared by standard procedures. Their IR spectra were collected at room temperature using a BOMEM (MB40) spectrometer, with a Zn/Se beam splitter and a DTGS detector, with 4 cm^{-1} spectral resolution. The Raman spectrum of solid MCPOC in the 3380–100 cm^{-1} range, was acquired at room temperature using a dispersive Raman instrument, model DXR SmartRaman^{TM}, from Thermo Fisher Scientific, equipped with a low-power, externally stabilized diode laser (λ= 780 nm), with a maximum power at output of laser head of 14 mW and a 3.0 mm beam diameter. The data were collected with an

exposure time to laser radiation of 99 s, 100 sample exposures and a slit aperture of 25 μm.

The quantum chemical calculations were performed with Gaussian 03[48] at the DFT level of theory, using the split valence triple-ζ 6-311++G(d,p) basis set[49] and the three-parameter B3LYP density functional, which includes Becke's gradient exchange correction[50] and the Lee, Yang and Parr correlation functional.[51]

Geometrical parameters of the different conformations were optimized using the Geometry Direct Inversion of the Invariant Subspace (GDIIS) method[52,53] and the synchronous transit-guided quasi-Newton (STQN) method[54] was used to locate the transition states for conformational isomerization. In order to assist the analysis of the experimental vibrational spectra, wavenumbers and IR intensities and Raman scattering activities (S^R) were also calculated at the same level of approximation. Theoretical Raman intensities (I^R) were obtained from the calculated Raman scattering activities according to the expression $I^R(i)= 10^{-12} (\nu_0-\nu_i)^4 \nu_i^{-1} S^R(i)$, where ν_0 is the excitation wavenumber and ν_i is the calculated wavenumber of the normal mode *i*.[55] The computed harmonic frequencies were scaled down by a single factor, 0.9835, obtained from linear fitting of the calculated to experimental wavenumbers (measured in xenon matrix), to correct them for the effects of basis set limitations, neglected part of electron correlation and anharmonicity effects. The nature of stationary points on the potential energy surface was checked through the analysis of the corresponding Hessian matrix.

Normal coordinate analysis was undertaken in the internal coordinates space, as described by Schachtschneider[56] and the optimized geometries and harmonic force constants resulting from the DFT(B3LYP)/6-311++G(d,p) calculations. The internal coordinates used in this analysis were defined following the recommendations of Pulay *et al.*[57]

Results and Discussion

Potential Energy Landscape. The MCPOC molecule bears 4 conformationally relevant internal rotation axes, corresponding to rotations about the C_1–C_5, C_{17}–C_{18}, C_{18}–O_{20} and O_{20}–C_{21} bonds. In order to characterize structurally in detail the molecule, a systematic investigation of its potential energy surface was

undertaken at the DFT(B3LYP)/6-311++G(d,p) level of approximation, where these 4 internal degrees of freedom were taken into account. These calculations showed that in all minimum energy conformations (Figure 1) the geometry around the C_1–C_5 and O_{20}–C_{21} bonds, *i.e.*, the configurations assumed by the phenyl group in relation to the oxazole ring and that of the methyl group, respectively, are the same: *(i)* the phenyl group and the oxazole ring are co-planar (or nearly co-planar), as it could be expected considering the relevance of the π-electron delocalization between the two rings and the favorable interactions between H_{11} and the chlorine atom for this arrangement; *(ii)* the methyl group has one of its hydrogen atoms in the *anti*-periplanar position relatively to the carbonyl group and the other two hydrogen atoms symmetrically placed out of the molecular plane and forming H-C-O-C(=O) angles of *ca.* ±60º, as it happens usually in non sterically hindered methyl esters.[58-60]

Rotations about the C_{17}–C_{18} and C_{18}–O_{20} bonds led to existence of 6 minima on the potential energy surface of the molecule. Two of these minima are unique and belong to the C_s point group. They correspond to the two most stable conformers of MCPOC, **I** and **II** (see Figure 1). In these conformers, the configuration about the ester C_{18}–O_{20} bond is *s-cis* (O_{19}–C_{18}–O_{20}–C_{21} dihedral of 0º), whereas the N_{16}=C_{17}–C_{18}=O_{19} dihedral is 180º in the most stable conformer **I**, and 0º in conformer **II**, which is *ca.* 3.0 kJ mol^{-1} higher in energy than form **I**. The calculated barrier for the **II**→**I** isomerization reaction is 20.5 kJ mol^{-1} (Figure 2). The other 4 minima correspond to two symmetry-equivalent pairs and are related with the higher energy conformers **III** and **IV** represented in Figure 1. Conformer **IV** is the highest energy form (relative energy of 45.5 kJ mol^{-1}). It exists as a doubly-degenerated-by-symmetry form with C_6–C_5–C_1–O_3, N_{16}=C_{17}–C_{18}=O_{19} and O_{19}–C_{18}–O_{20}–C_{21} dihedral angles of 12.5º, 33.7º and –161.0º (or –12.5º, –33.7º and 161.0º). The two equivalent-by-symmetry forms **IV** are separated by an energy barrier of 3.6 kJ mol^{-1}, the transition state structure corresponding to the C_s symmetry structure where the C_6–C_5–C_1–O_3, N_{16}=C_{17}–C_{18}=O_{19} and O_{19}–C_{18}–O_{20}–C_{21} dihedral angles are 0º, 0º and 180º, respectively (see Figure 2). They are separated from conformer **II** by an energy barrier of 8.6 kJ mol^{-1} (Figure 2). In the case of the two symmetry-equivalent minima related with conformer **III** the situation is different because they are separated by an energy barrier that is below the zero point vibrational level associated with the

interconversion between them, making the transition state C_s symmetry structure to be the most probable structure defining a unique conformational state.

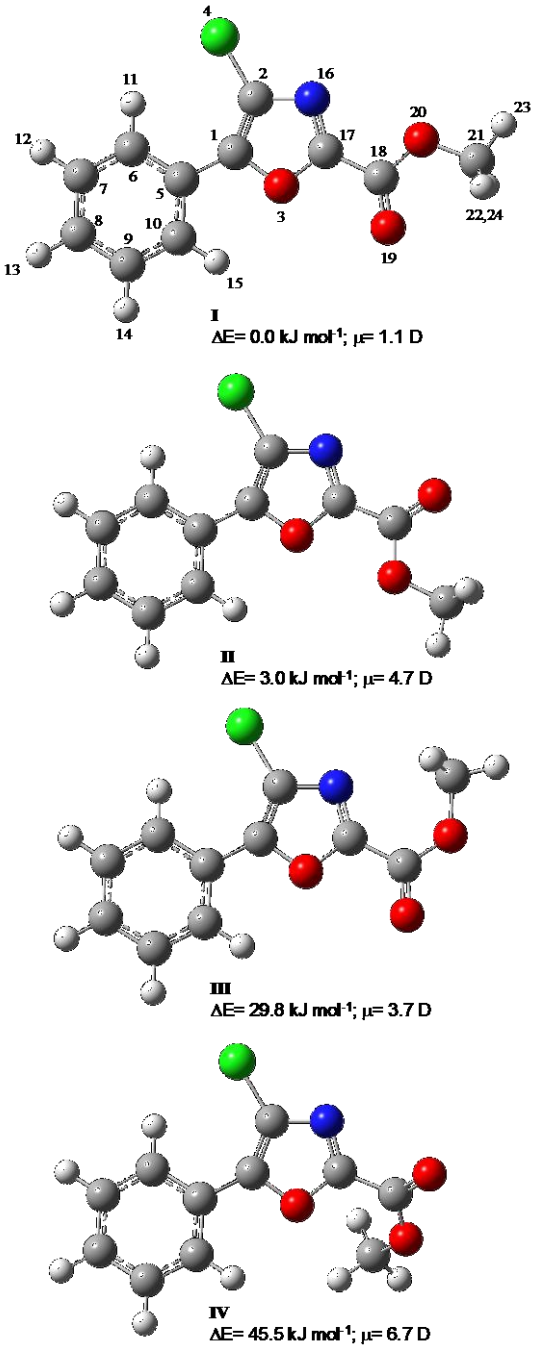

Figure 1. Minimum energy structures on the potential energy surface of MCPOC, with atom numbering. Relative energies, including zero-point energy corrections (ΔE/ kJ mol^{-1}) and dipole moments (μ/ D; 1 D= 3.33564 x 10^{-30} C m) are also provided. **III** and **IV** correspond to pairs of symmetry-equivalent minima with C_6–C_5–C_1–O_3, N_{16}=C_{17}–C_{18}=O_{19} and O_{19}–C_{18}–O_{20}–C_{21} dihedral angles (º) of 177.2, –172.5 and –175.5 (or -177.2, 172.5, 175.5) and 12.5, 33.7 and –161.0 (or –12.5, –33.7 and 161.0), respectively. However, because the transition state structure separating the two minima **III** lies below their zero point vibrational level, only conformer **IV** is doubly-degenerated-by-symmetry, while **III** is an unique conformer with most probable geometry at the geometry of the C_s symmetry structure separating the two minima. Note that the dipole moment value for conformer **II** indicated in [46] was misprinted (1.71 D, instead of the right value, 4.71).

The two minima have C_6–C_5–C_1–O_3, N_{16}=C_{17}–C_{18}=O_{19} and O_{19}=C_{18}–O_{20}–C_{21} dihedral angles equal to 177.2º, –172.5º and –175.5º, and –177.2º, 172.5º and 175.5º, respectively, and in the most probable C_s structure separating them these angles are 180º, 180º and 180º. Conformer **III** is 28.9 kJ mol^{-1} higher in energy than the most stable form and has energy barriers separating it from **I** and **IV** equal to 14.5 and 19.3 kJ mol^{-1}, respectively (see Figure 2).

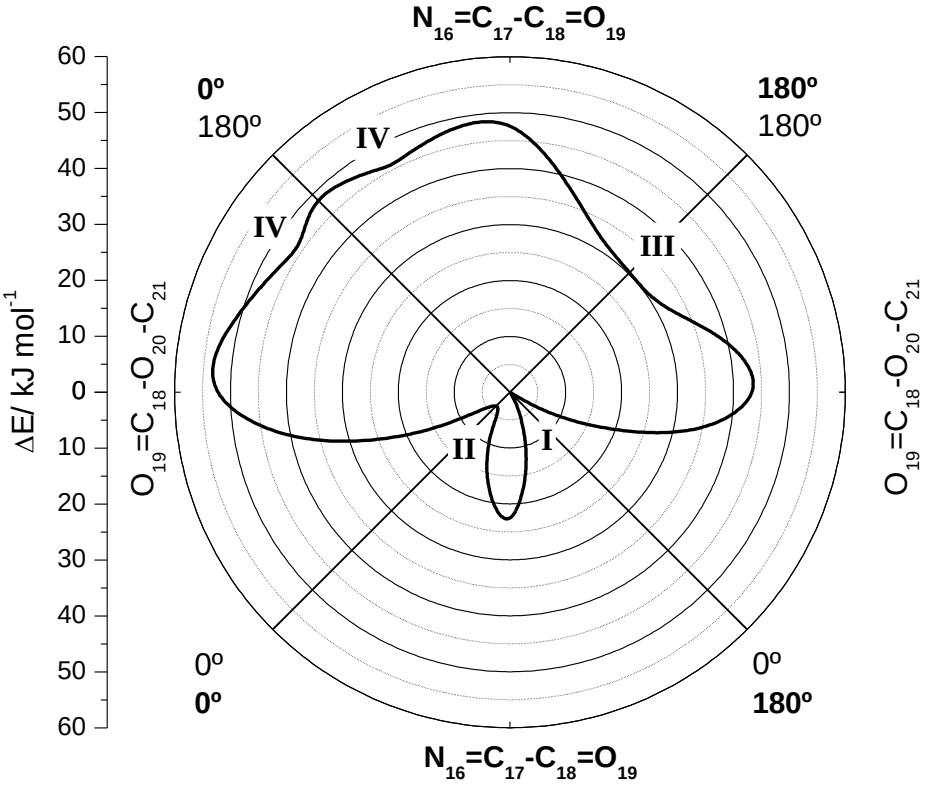

Figure 2. DFT(B3LYP)/6-311++G(d,p) calculated potential energy profiles for internal rotation around the C_{17}–C_{18} and C_{18}–O_{20} bonds. The curves were obtained by performing a relaxed scan on the potential energy surface of the molecule along the two relevant coordinates (N_{16}=C_{17}–C_{18}=O_{19} and O_{19}=C_{18}–O_{20}–C_{21} dihedral angles) in steps of 30º.

The reasons for the relative stability of the MCPOC conformers can be easily correlated with their structure. The large energy of conformer **III** relatively to form **I** and **II** results essentially from the fact that in the first form the arrangement of the ester group is the well-known less stable *s-trans* geometry,[61-65] whereas in the latter this group is in the *s-cis* geometry. The difference in energy between **III** and **I** is indeed similar to those between the *s-trans* and *s-cis* conformers of methyl formate,

acetate and chloroacetate, for example, all of them of *ca.* 32 kJ mol^{-1}.[61-63] Conformer **IV** has also the ester group in the *s-trans* arrangement, but its energy is even larger than that of conformer **III** due to the unfavorable strong repulsive steric interaction between the methyl ester group and the oxazole ring. This interaction (directly and through the reduction in the π-delocalization within the ester fragment and between this fragment and the oxazole ring it imposes by forcing the ester group to be considerably skewed and out of the plane of the oxazole ring) accounts for the additional *ca.* 15 kJ mol^{-1} energy of conformer **IV** relatively to **III**.

The relative energy of **I** and **II** is determined by the arrangement around the C_{17}–C_{18} bond, mostly by the relative importance of the repulsive interactions between the two oxygen atoms of the ester group and the N and O atoms of the oxazole ring. All these 4 atoms are negatively charged, but it is clear from Figure 3, where the charges calculated from the atomic polar tensors (APT charges) for these four atoms and the distances between them in **I** and **II** are depicted, that the most important repulsive interaction occurs conformer **II**, between the most negatively charged atom of each interacting fragment (the O_3 atom of the oxazole ring and the O_{20} ester atom), which are also those separated by the shortest distance.

The calculated geometrical parameters for conformers **I** and **II** are provided in Table S1 (Supporting Information). Optimized geometries for all MCPOC conformers, in Cartesian coordinates, are given in Table S2.

Taking into account the calculated relative energies for the different MCPOC conformers, their populations can be estimated according to the Boltzmann statistics. At room temperature (298 K) the **I** : **II** population ratio is 0.770 : 0.230, whereas the total population of conformers **III** and **IV** is smaller than $5x10^{-4}$. At 323 K, the temperature used to sublimate the compound in the matrix isolation spectroscopic experiments, the **I** : **II** population ratio slightly changes to 0.753 : 0.246, with the population of **III** being equal to 0.001 and that of **IV** less than 10^{-5}. These results mean that only conformers **I** and **II** are experimentally accessible as isolated species. Moreover, at the temperature of the cold substrate of the cryostat (10-20 K), only the lowest energy conformer would subsist if the system could reach the thermodynamic equilibrium. However, the predicted barrier for the **II**→**I** isomerization reaction is high enough (20.5 kJ mol^{-1}; see Figure 2) to be significantly overcome during deposition at these temperatures and it can then be expected that the populations of the two most stable conformers existing in the vapor of the compound prior to deposition

are efficiently trapped in the matrices, *i.e.*, a **I** : **II** population ration of *ca.* 3:1 are expected to be observed in the as-deposited matrices.

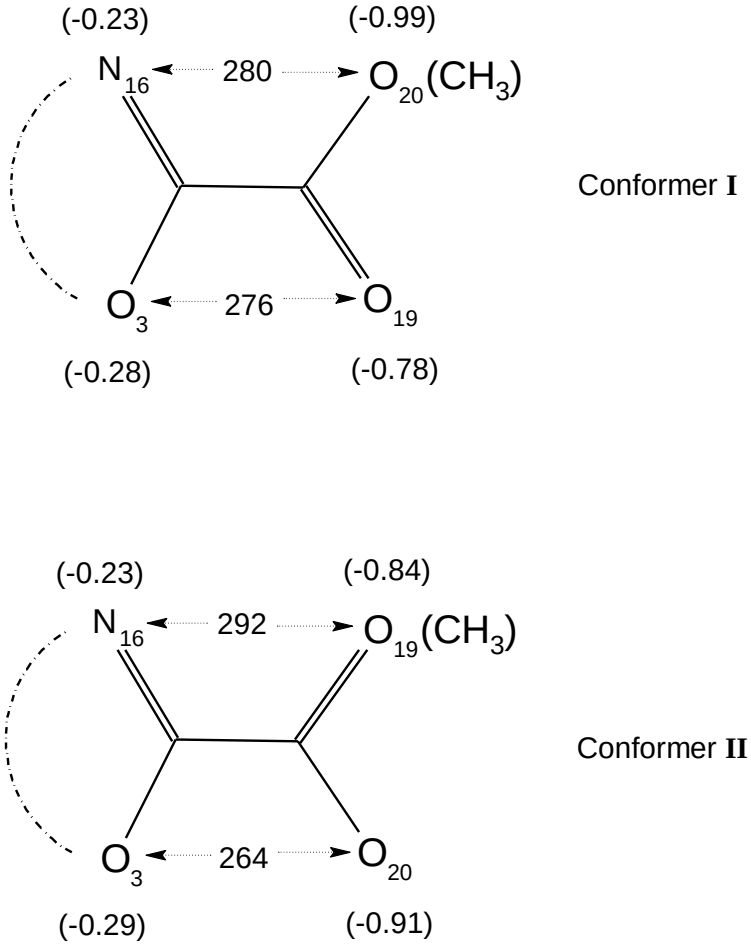

Figure 3. Calculated APT charges (units of electron; 1 *e* = 1.602176487 x 10^{-19} C) on selected atoms and distances (pm) between these atoms in the two most stable MCPOC conformers.

Matrix Isolation FTIR Results. The mid-infrared spectra of MCPOC isolated in both argon and xenon matrices were obtained in the 4000-400 cm^{-1} range. The temperature of the vapor immediately prior to the deposition of the matrices was 323 K, and the substrate temperature 10 K and 20 K, for argon and xenon matrices, respectively. The spectrum obtained in argon matrix and the simulated spectrum obtained by summing the DFT(B3LYP)/6-311++G(d,p) predicted spectra of the experimentally relevant conformers **I** and **II** weighted by their expected populations (0.75 : 0.25) is provided in the Supporting Information as Figure S1. In the simulated

spectrum, bands were represented by Lorentzian functions centered at the calculated wavenumbers scaled by 0.9835 and with fwhm (full width at half maximum) equal to 2 cm^{-1}. The simulated spectrum reproduces very well the experimental spectrum, providing a strong evidence for the presence in the matrices of the two low energy MCPOC conformers in the expected population ratio. The as-deposited spectrum obtained in xenon matrix is qualitatively identical to that obtained in argon. Results obtained in xenon were particularly useful for band assignment and conformers identification and will be discussed in detail later on.

Both experimentally relevant conformers of MCPOC belong to the C_s symmetry point group, with their 66 fundamental vibrations spanning the irreducible representations 44A´ and 22A´´, all being active in infrared. Results of normal coordinates analysis based on the DFT(B3LYP)/6-311++G(d,p) calculated data are provided in Tables S3-S5 (Supporting Information). The definitions of the adopted internal coordinates are given in Table S3 and the calculated wavenumbers, infrared and Raman intensities, and potential energy distributions resulting from the normal mode analysis carried out for **I** and **II** are presented in Tables S4 and S5, respectively.

As mentioned before, the predicted barrier for the **II**→**I** isomerization (20.5 kJ mol^{-1}) is high enough to prevent this reaction to take place during deposition of the matrices. Annealing of argon matrix up to the maximum possible work temperature (*ca.* 40 K; above this temperature the matrix starts to evaporate and loses its optical properties) did not allow for observation of any conformational isomerization as well. However, xenon matrices can be used in a considerably wider range of temperatures and, when MCPOC monomers isolated in this kind of matrix were annealed to *ca.* 60 K, besides aggregation one could observe a redistribution of the intensities of the bands due to the monomers, indicating that their relative populations changed. According to the Barnes' relationship,[66] this temperature is still significantly below that fitting the expectations for the temperature at which an isomerization reaction should start being observed for a process with an activation barrier of the order of that predicted for the **II**→**I** gas phase isomerization. Indeed, the Barnes' relationship implies that such temperature is about 70-75 K.[66] Such evidence indicates that the potential energy landscape for the matrix-isolated compound is considerably different of that corresponding to gas phase. Since the dipole moments of conformers **I** and **II** are significantly different (1.1 and 4.7 Debye, respectively), a different stabilization of the two conformers upon deposition in a matrix can be devised, in particular in the

case of the highly polarizable xenon matrix, where conformer **II** can be expected to be considerably stabilized relatively to form **I**. According to the experimental observations, the height of the energy barrier separating the two conformers seems also to be smaller than in the gas phase.

Figure 4 shows two selected spectral regions (1800-1725 cm^{-1} and 1180-700 cm^{-1}) of the infrared spectrum of the as-deposited xenon matrix of MCPOC (temperature of the vapor, 323 K; substrate temperature 20 K) and of the spectrum collected after annealing of the matrix at 60 K. At this temperature, aggregation has already started and all bands due to the monomers decrease. However, two groups of bands could be easily identified in the spectra, with one group of bands reducing considerably more of intensity than the other one. The two experimental spectra shown in Figure 4 were normalized by the bands which reduce less of intensity and bands due to aggregates were subtracted (the position of these bands was established doubtlessly by further annealing the matrix at higher temperature, where aggregates are by far the dominant species). Figure 4 also shows the DFT(B3LYP)/6-311++G(d,p) calculated infrared spectra of MCPOC conformers **I** and **II** (stick spectra) and the simulated spectrum obtained by summing the calculated spectra of **I** and **II**, weighted by their expected populations in the gas phase prior to deposition (0.75 : 0.25). Two main conclusions result from the comparison of these spectra with the experimental ones: (1) the simulated spectrum fits very well the as-deposited spectrum of the compound in xenon matrix, demonstrating that no significant isomerization took place during deposition of the matrix and the gas phase equilibrium populations could be efficiently trapped in the matrix; (2) the bands that decreased more of intensity upon annealing fit nicely the spectrum of conformer **I**, whereas those decreasing in small extent can be doubtlessly ascribed to conformer **II**.

The different behaviour of the bands due to each conformer upon annealing of the xenon matrix facilitated the assignment of the spectrum obtained in this matrix to the individual conformers. Comparison of the spectra obtained in xenon matrix with that registered in argon then led to a prompt assignment of this latter. The proposed assignments are presented in Table 1.

The striking fact resulting from the temperature variation experiments carried out in the xenon matrix was the observation that it was conformer **I** the species that reduces faster its population upon annealing.

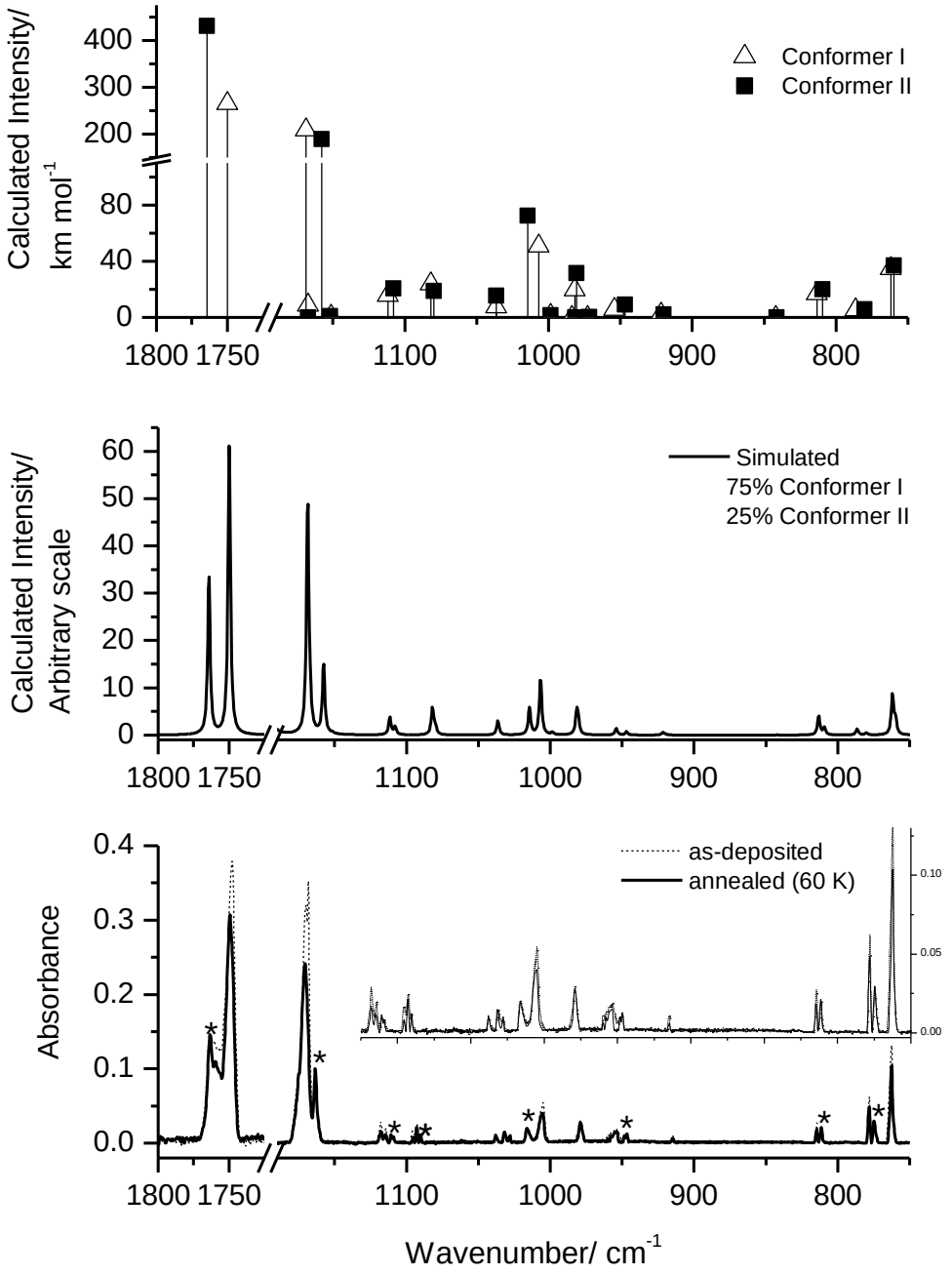

Figure 4. ***Top:*** Selected spectral regions (1800-1725 cm^{-1} and 1180-700 cm^{-1}) of the DFT(B3LYP)/6-311++G(d,p) calculated infrared spectra of MCPOC conformers **I** and **II** (stick spectra). ***Middle:*** The same spectral regions of the simulated spectrum obtained by summing the calculated spectra of **I** and **II**, weighted by their expected populations in the gas phase prior to deposition (0.75 : 0.25). In the simulated spectrum, bands were represented by Lorentzian functions centered at the calculated wavenumbers scaled by 0.9835 and with fwhm (full width at half maximum) equal to 2 cm^{-1}. ***Bottom:*** The same spectral regions of the infrared spectrum of MCPOC isolated in xenon matrix. *Dashed line*: spectrum of the as-deposited matrix (temperature of the vapor, 323 K; substrate temperature 20 K); *solid line*: spectrum of the annealed sample at 60 K. The experimental spectra were normalized to the bands ascribed to conformer **II** (marked with asterisks) and bands due to aggregates were subtracted.

Table 1 – Experimental (matrix-isolation) and DFT(B3LYP)/6-311++G(d,p) calculated infrared data for MCPOC and vibrational assignments based on the results of normal coordinate analysis.[a]

Experimental		Calculated					
Ar matrix	Xe matrix	Conformer **I**		Conformer **II**			Approximate description
ν	ν	ν[b]	I[c]	ν[b]	I[c]		
n.obs.	3090	3168	1.4	1369	0.4	A´	ν(C-H1)
n.obs.	3075	3153	1.9	3153	0.7	A´	ν(C-H5)
3084	3063	3138	13.2	3138	4.3	A´	ν(C-H2)
3073	3055	3137	8.1	3136	2.6	A´	ν(C-H3)
3039	3034	3117	0.2	3116	0.1	A´	ν(C-H4)
3013	2998	3113	8.7	3112	2.5	A´	νCH_3 as´
2963	~2953	3075	12.2	3077	3.8	A´´	νCH_3 as´´
2970	2948	3003	27.0	3004	8.4	A´	νCH_3 s
2854	2849						$2\delta CH_3$´
1751/1750 (**I**); 1769/1763 (**II**)	1748 (**I**); 1763/1759 (**II**)	1750	199.4	1764	106.6	A´	ν(C=O)
1612	n.obs.	1616	0.8	1616	0.3	A´	νPh3
1586	1585	1589	4.3	1589	1.1	A´	νPh4
1567	1567	1561	25.5	1564	2.2	A´	νOx3
1530 (**I**); 1541 (**II**)	1532 (**I**); 1535/1529 (**II**)	1526	84.6	1529	25.1	A´	νOx1
1492/1487	1489	1487	65.5	1487	21.5	A´	δ(C-H2)
1479	1474 (**I**); 1478 (**II**)	1471	15.4	1472	2.3	A´	δCH_3 as´
1460	1455	1459	7.8	1459	2.5	A´´	δCH_3 as´´
1453/1452/1451/1450	1450/1444	1452	43.3	1452	11.5	A´	δ(C-H3)
1442	1439/1436	1447	5.0	1446	1.2	A´	δCH_3 s
1360/1358 (**I**)	1361 (**I**)	1351	46.2	1347	0.5	A´	δ(C-H1)
1346 (**I**)	1341 (**I**)	1337	49.5	1329	1.1	A´	νPh2
1332/1327/1318/1313/1311[d] (**I**); 1301/1300 (**II**)	1330/1318/1309[d] (**I**); 1302 (**II**)	1308	175.9	1294	67.2	A´	νOx2; $\nu(C\text{-}C_\alpha)$
1281/1277	1280/1277	1275	66.6	1276	31.5	A´	νOx4
1215 (**I**)	1213 (**I**)	1215	1.4	1219	0.1	A´	$\nu(C\text{-}C_{IR})$
1208/1207 (**I**); 1204/1202 (**II**)	1209/1204 (**I**); 1197 (**II**)	1203	225.3	1196	38.9	A´	ν(C-O); γCH_3´
1194	1193	1194	11.4	1193	3.6	A´	δ(C-H4)
1174/1172 (**I**); 1168/1166 (**II**)	1174/1170/1168 (**I**); 1163 (**II**)	1169	157.2	1158	46.8	A´	γCH_3´; ν(C-O)
n.obs.	n.obs.	1167	6.6	1167	<0.1	A´	δ(C-H5)
n.obs.	n.obs.	1151	0.8	1152	0.9	A´´	γCH_3´´
1117	1118/1114 (**I**); 1110/1109 (**II**)	1112	11.8	1108	5.1	A´	νOx5
1096 (**I**); 1094 (**II**)	1095/1092 (**I**); 1090 (**II**)	1082	17.9	1080	4.6	A´	νPh6
1041/1033	1038/1031/1027	1036	5.7	1036	3.8	A´	νPh5
1008/1006 (**I**); 1020/1016 (**II**)	1007/1005 (**I**); 1016 (**II**)	1007	38.2	1014	17.9	A´	δOx1
993	989	999	1.2	999	0.4	A´	δPh1
n.obs.	n.obs.	984	<0.1	981	<0.1	A´´	γ(C-H5)
981	980	982	14.7	981	7.8	A´	νPh1
n.obs.	n.obs.	973	0.1	972	<0.1	A´´	γ(C-H4)
956 (**I**); 951 (**II**)	954 (**I**); 947 (**II**)	954	4.4	947	2.3	A´	$\nu(O\text{-}CH_3)$
918 (**I**); 917 (**II**)	914	922	1.7	920	0.5	A´´	γ(C-H3)
n.obs.	n.obs.	842	<0.1	841	<0.1	A´´	γ(C-H2)
817 (**I**); 815 (**II**)	815 (**I**); 812 (**II**)	813	12.9	809	4.9	A´	δ(OCO)
781 (**I**); 778 (**II**)	778 (**I**); 775 (**II**)	786	4.1	780	1.5	A´´	γ(C=O)
765	762	762	26.1	760	9.1	A´´	γ(C-H1)
691	690	693	8.4	693	2.4	A´	δPh3
689/688/687	686	685	26.0	683	6.9	A´´	τOx1
		682	26.0	681	2.9	A´´	τPh1
652	650/648	654	17.6	653	5.5	A´´	τOx2

[a] Wavenumbers in cm^{-1}, calculated intensities in km mol^{-1}, ν, bond stretching, δ, bending, γ, rocking, w, wagging, τ, torsion, s, symmetric, as, asymmetric, IR, inter-ring, Ox, oxazole ring, Ph, phenyl ring. n.obs., not observed. See Table S3 (Supplementary Material) for definition of internal coordinates and Tables S4 and S5 for potential energy distributions. [b] Scaled wavenumbers (0.9835). Intensities weighted by their expected populations: 0.75 (**I**) and 0.25 (**II**). [d] Fermi resonance with 2τOx1.

There are two possible mechanisms which can explain the observations, which may opperate separately or simultaneously. The first implies that aggregation is facilitated in conformer **I**, relatively to conformer **II**. Conformer selective aggregation was found for some matrix-isolated compounds, like dimethyl glycine,[67] dimethyl sulfite[68] and 5-methyl-1*H*,3*H*-pyrrolo[1,2-c][1,3]thiazole-6,7-dicarboxylate 2,2-dioxide.[69] Though this mechanism alone can explain the observations, it is known that the more polar or smaller conformers are those which are more prone to exhibit a preferential aggregation.[67-69] In MCPOC, however, it is conformer **II** that is simultaneously more polar (μ= 4.7 Debye *vs.* 1.1 Debye in **I**) and smaller (the calculated spatial extent of **I** and **II** is 4967 and 4821 a.u., respectively). The second mechanism, which we favour on the basis of the obtained experimental data and accumulated knowledge,[67-71] would require that an inversion in the order of stability of the two conformers took place in the matrix media. Then, conformer **I** (most stable in the gas phase) would relax to form **II** upon annealing of the xenon matrix, where this latter form would be the most stable species. The necessary general conditions that need to be satisfied to make possible experimental observation of this inversion of the relative stability of conformers are *(i)* close energies of the conformers in the gas phase (with the less polar form being the most stable), *(ii)* significant differences in the dipole moments of the conformers, and *(iii)* accessible energy barriers for conformational isomerization. Both first and second conditions above are fulfilled in the case of the relevant conformers of MCPOC, and it seems also possible that the energy barrier reduces in the matrix media to allow for conformational isomerization (**I**$\rightarrow$**II**) to take place. Examples of inversion of the relative order of stability of conformers upon deposition of a compound in a matrix can be found in recent literature, *e.g.*, for dimethyl glycine methyl ester,[70] methyl cyanoacetate[71] and 5-methyl-1*H*,3*H*-pyrrolo[1,2-c][1,3]thiazole-6,7-dicarboxy-late 2,2-dioxide.[69] The latter compound is in fact a case where both selective aggregation and inversion of the order of stability of conformers were found to take place simultaneously.

Spectroscopic Studies in the Neat Condensed Phases. The results discussed in the previous section indicated that the more polar conformer **II** of MCPOC is stabilized relatively to form **I** upon deposition in matrices. In order to get additional information regarding the relative importance of the two conformers in more polar media, spectroscopic studies were also undertaken for the compound in neat condensed

phases. Figure 5 presents a selected spectral range of the infrared spectra of MCPOC *(i)* in the amorphous layer resulting from fast deposition of the vapor of the compound at 343 K onto the cold substrate (10 K) of the cryostat, *(ii)* in the room temperature crystalline phase, both as a KBr pellet and a nujol mull, and *(iii)* in the crystalline phase resulting from warming the amorphous layer to 280 K, subsequently cooled down to 10 K. These spectra are compared with the DFT(B3LYP)/6-311++G(d,p) calculated infrared spectra of conformers **I** and **II**. Full range spectra are presented in Figure S2 (Supplementary Material), where the spectrum of the crystalline phase recorded immediately after its formation from the amorphous state at 280 K is also presented.

As it could be anticipated, the spectrum of the amorphous phase has characteristically broad bands due to both presence of the two conformers and significant disorder. The bands at 1361, 1330 and 1318 cm^{-1} can be assigned mainly to conformer **I** (compare the experimental spectrum with those calculated for the two conformers; Figure 5), whereas that observed at 1302 cm^{-1} is a band mark of conformer **II**. All the other bands shall contain contributions from both conformers. Upon crystallization of the amorphous phase (at *ca.* 280 K), the spectrum changes considerably (see Figure S2). Re-cooling of the sample to 10 K did not lead to further changes, except some further band narrowing. The 10 K spectrum of the crystalline phase obtained from the amorphous film (Figure 5) clearly reveals bands due to both conformers (see Table 2 for assignments). For example, besides the bands at 1348, 1330 and 1318 cm^{-1}, which relates to those observed and 1361, 1330 and 1318 cm^{-1} in the spectrum of the amorphous phase, other bands ascribable to conformer **I** are also observed at 1225, 1205, 1182, 1073 and 1009/1007 cm^{-1}, while bands due to conformer **II** are observed at 1302, 1221, 1201, 1172/1168, 1070 and 1012 cm^{-1}. From the intensity of the bands at 1318 cm^{-1} (**I**) and 1302 cm^{-1} (**II**), which are well separated and intense bands in the spectrum of the crystalline phase, a rough estimation of the relative population of molecules with conformation **I** and **II** in that phase could be obtained. The results indicate that the two conformations are essentially equally populated (**I**:**II** population ratio: 0.92±0.1), *i.e.*, they are compatible with a crystalline phase where both conformers exist in a 1:1 ratio. The spectra of the crystal at room temperature (both in KBr pellet and in nujol) are qualitatively identical to that of the crystal at low temperature, though, as expected, exhibiting bands considerably broader.

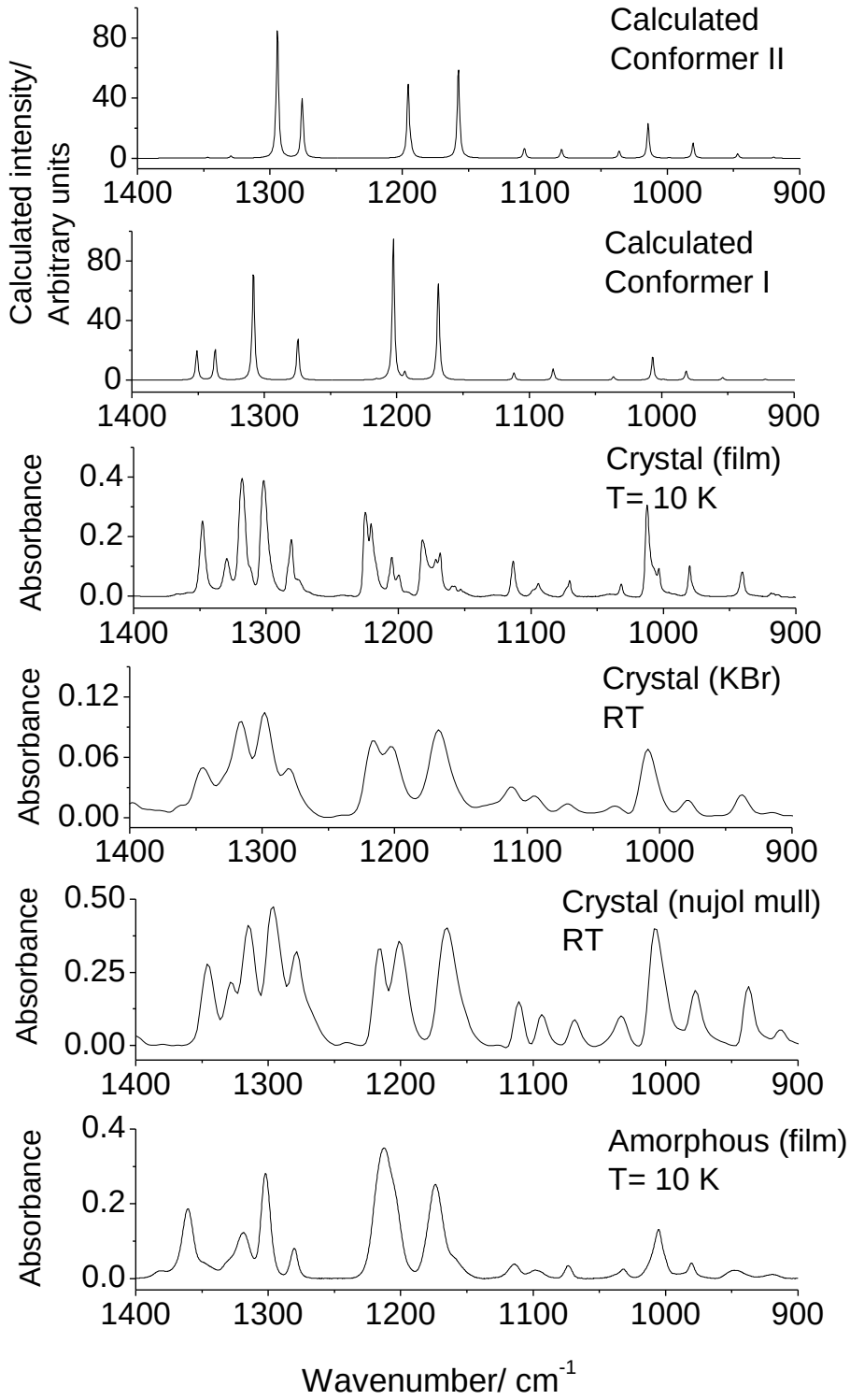

Figure 5. ***From bottom to top:*** 1400-900 cm^{-1} spectral range of the infrared spectra of MCPOC *(i)* in the amorphous layer resulting from fast deposition of the vapor of the compound at 343 K onto the cold substrate (10 K) of the cryostat; *(ii)* in the room temperature crystalline phase, as a nujol mull; *(iii)* in the room temperature crystalline phase, as a KBr pellet; *(iv)* in the crystalline phase resulting from warming the amorphous layer to 280 K, subsequently cooled down to 10 K; *(v)* and *(vi)* DFT(B3LYP)/6-311++G(d,p) calculated infrared spectra of conformers **I** and **II**, respectively. In the calculated spectra, bands were represented by Lorentzian functions centered at the calculated wavenumbers scaled by 0.9835 and with fwhm (full width at half maximum) equal to 2 cm^{-1}.

Table 2 – Assignment of the vibrational spectra of MCPOC in the neat condensed phases.[a]

Approximate Description	IR Glass (10 K)	IR Crystal (RT; KBr)	IR Crystal (10 K)	Raman Crystal (RT)
ν(C-H1)	3067	3066	3098	3077
ν(C-H5)			3093	
ν(C-H2)			3079	
ν(C-H3)			3069	
ν(C-H4)			3057	3056
νCH_3 as´	3037	3034	3034	3035
νCH_3 as´´	3005	3014	3013	3013
νCH_3 s	2956	2956	2957	2958
$2\delta CH_3$´	2849	2849	2849	2849
ν(C=O)	1743	1738	1736 (**I**); 1740 (**II**)	1740
νPh3	1608	1607	1607	1606
νPh4	1585	1577	1585	1585
νOx3	1566	1558	1553 (**I**); 1567 (**II**)	1566
νOx1	1530	1530 (**I**); 1542 (**II**)	1532 (**I**); 1541 (**II**)	1531
δ(C-H2)	1490	1510	1485	1499
δCH_3 as´	1484	1484	n.obs.	1484
δCH_3 as´´	1459	1458	1459/1455	1458
δ(C-H3)	1450	1449	1448/1447	1449
δCH_3 s	1438	1437	1438	1439
δ(C-H1)	1361 (**I**)	1362 (**I**)	1361 (**I**)	1369
νPh2	1348 (**I**)	1345 (**I**)	1348 (**I**)	1347
νOx2; $\nu(C\text{-}C_\alpha)$	1330/1319 (**I**); 1302 (**II**)	1330/1316 (**I**); 1298 (**II**)	1330/1318/1312 (**I**); 1302 (**II**)	1316 (**I**) 1299 (**II**)
νOx4	1281	1280	1283/1280	1280
$\nu(C\text{-}C_{IR})$	1212	1216	1225 (**I**); 1221 (**II**)	1215
ν(C-O); γCH_3´	1204	1203	1205 (**I**); 1201 (**II**)	1202
δ(C-H4)	n.obs.	n.obs.	n.obs.	n.obs.
γCH_3´; ν(C-O)	1174	1174	1182 (**I**); 1172/1168 (**II**)	1182 1168
δ(C-H5)	1158	1158	1158	1160
γCH_3´´	n.obs.	n.obs.	1152	n.obs.
νOx5	1114	1111	1114	1112
νPh6	1098	1094	1099 (**I**); 1095 (**II**)	1095
2ν(C-Cl)	1074	1070	1073/1070	1071
νPh5	1032	1034	1032	1034
δOx1	1005	1008	1007/1003 (**I**); 1012 (**II**)	1004
δPh1	n.obs.	n.obs.	n.obs.	
γ(C-H5)	n.obs.	n.obs.	n.obs.	n.obs.
νPh1	980	979	980	979
γ(C-H4)	n.obs.	n.obs.	n.obs.	n.obs.
$\nu(O\text{-}CH_3)$	948	937	940	938
γ(C-H3)	919	915	918/913	n.obs.
γ(C-H2)	844	834	840	841
δ(OCO)	817	813	815	813
γ(C=O)	778	774	778/776	n.obs.
γ(C-H1)	766	766	770	769
δPh3	691	687	692	687
τOx1			686	
τPh1			682	
τOx2	650	646	645	646
δPh2	619	622	617	619
w(Ox-Ph)	590	603	595	595

ν(C-Cl)	562		544	542
γ(Ph-Ox)	494	n.i.	494	495
δ(CC=O)	434		454	455
τPh3	n.i.	n.i.	n.i.	357
δOx2				314
γ(C–Cl)				293
δ(C–O–CH_3)				249
ν(C–C_α) [b]				233
w(C–Cl) (**I**)/ τPh2 (**II**)				162
τPh2 (**I**)/ w(C–Cl) (**II**)				145
τ(C–O)				106

[a] Wavenumbers in cm^{-1}. ν, bond stretching, δ, bending, γ rocking, τ torsion, w, wagging, s, symmetric, as, asymmetric, n.obs., not observed, n.i., not investigated. See Table S3 for definition of coordinates. [b] Combined with w(Ph–Ox) in **I** and with δ(C–O–CH_3) in **II** (see Tables S4 and S5).

Comparison of the Raman spectrum of the crystal at room temperature with those calculated for **I** and **II** (Figure S3; Supplementary Material), is also in agreement with the presence of the two conformers in the crystalline phase of MCPOC (see also Table 2), though the greater similarity of the Raman spectra of the individual conformers (the most conformationally characteristic Raman bands have very low intensities) makes these spectra less informative than the infrared spectra regarding this question.

On the whole, the results obtained for the neat condensed phases of MCPOC agree with the information obtained from the matrix-isolation studies regarding the stabilization of conformer **II** in more polar environments compared to gas phase.

Conclusion

The conformational preferences and spectroscopic properties of methyl 4-chloro-5-phenyl-1,3-oxazole-2-carboxylate (MCPOC) have been studied by FTIR spectroscopy for the compound isolated in cryogenic matrices (argon; xenon) and in neat condensed phases. The experimental studies were complemented with DFT(B3LYP)/6-311++G(d,p) calculations. Two experimentally relevant low-energy conformers (**I** and **II**) of the molecule were identified. These conformers differ from each other in the orientation of the ester group relatively to the oxazole ring. In both conformers, the ester moiety was found to be in the *s-cis* configuration (O=C-O-CH_3 dihedral: 0º). In gas phase, conformer **I** is *ca.* 3.0 kJ mol^{-1} more stable than form **II**, corresponding to a room temperature **I**:**II** relative population of *ca.* 3. Two additional

higher energy conformers, **III** and **IV**, of no experimental relevance, with relative energies of *ca.* 30 and 45 kJ mol^{-1}, respectively, were also predicted to exist by the calculations, corresponding to structures where the ester group is in an approximately *s-trans* arrangement.

Annealing of the compound isolated in xenon at 60 K led to aggregation and simultaneous reduction of the population of **I** compared to that of the more polar conformer **II**. These results suggest the inversion of the order of stability of the two conformers in that matrix, eventually accompanied by a higher trend of conformer **I** to aggregate. In agreement with these results, in the crystalline phase of the compound, presence of both conformers in a 1:1 population ratio was testified by both infrared and Raman spectroscopy. Full assignment of the observed infrared bands to the two experimentally accessible conformers was carried out for the matrix isolated monomeric species. In addition, the infrared spectra of the neat compound in the low temperature (10 K) amorphous and crystalline phases, as well as the infrared and Raman spectra of the crystal at room temperature were also assigned.

Acknowledgements

This work has been funded by the Portuguese Science Foundation (FCT, Lisbon) under research project PTDC/QUI/71203/2006. S. L. and C. M. N. also thank FCT for the Ph.D. Grants #SFRH/BD/29698/2006 and #SFRH/BD/28844/2006. A. G.-Z., thanks also to ANCPCyT (Project PICT(2006)/00068) and CYTED (Network 108RT0362) for partial financial support. AGZ is member of the Research Career Conicet, Argentina.

Supplementary Information Available:

Figure S1, infrared spectrum of MCPOC isolated in an argon matrix and simulated spectra calculated based on the theoretically obtained spectra of conformers **I** and **II**. Figure S2, room temperature infrared spectra of neat crystalline MCPOC (KBr pellet), low temperature amorphous and crystalline phase, and B3LYP/6-311++G(d,p) calculated infrared spectra for conformers **I** and **II**; Figure S3, room temperature Raman spectrum of neat crystalline MCPOC and B3LYP/6-311++G(d,p)

calculated Raman spectra for conformers **I** and **II**; Table S1, geometry of the two MCPOC most stable conformers calculated at the B3LYP/6-311++G(d,p) level of theory; Table S2, Cartesian coordinates for optimized minimum energy structures of MCPOC; Table S3, definition of internal coordinates used in the normal mode analysis of MCPOC; Tables S4 and S5, B3LYP/6-311++G(d,p) calculated spectroscopic data and results of normal coordinate analysis for the two most stable, experimentally relevant conformers of MCPOC (forms **I** and **II**). This material is available free of charge via the Internet at http://pubs.acs.org.

References:

[1] N. Fusetani and S. Matsunaga, *Chem. Rev.*, **93** (1993) 1793.

[2] M. Adamczeski, E. Quinoà and P. Crews, *J. Am. Chem. Soc.*, **110** (1988) 1598.

[3] M. B. Purvis, D. G. I. Kingston, N. Fujii and H. G. Floss, *J. Chem. Soc. Chem. Commun.*, (1987) 302.

[4] Y. Kato, N. Fusetani, S. Matsunaga, K. Hashimoto, S. Fujita and T. Furuya, *J. Am. Chem. Soc.*, **108** (1986) 2780.

[5] C. Sanz, D. Ansorena, J. Bello and C. Cid, *J. Agric. Food Chem.*, **49** (2001) 1364.

[6] M.-H. Lee, Ch.-Tang Ho and S. S. Chang, *J. Agric. Food Chem.*, **29** (1981) 686.

[7] Z. Jin, *Nat. Prod. Rep.*, **20** (2003) 584.

[8] J. R. Lewis, *Nat. Prod. Rep.*, **19** (2002) 223.

[9] J. A. Maga, *J. Agric. Food Chem.*, **26** (1978) 1049.

[10] V. S.C. Yeh, *Tetrahedron*, **60** (2004) 11995.

[11] Y. Hamada and T. Shioiri, *Chem. Rev.*, **105** (2005) 4441.

[12] P. Wipf, *Chem. Rev.*, **95**, (1995) 2115.

[13] A. B. Williams and R. S. Jacobs, *Cancer Lett.*, **71** (1993) 97.

[14] A. Bertram and G. Pattenden, *Nat. Prod. Rep.*, **24** (2007) 18.

[15] A. Bertram, N. Maulucci, O. M. New, S. M. M. Nor and G. Pattenden, *Org. Biomol. Chem.*, **5** (2007) 1541.

[16] T. Ichino, H. Arimoto and D. Uemura, *Chem. Comm.*, (2006) 1742.

[17] J. A. Bull, E. P. Balskus, R. A. J. Horan, M. Langner and S. V. Ley, *Angew. Chem. Int. Ed.*, **45** (2006) 6714.

[18] F. Yokokawa, T. Asano and T. Shioiri, *Org. Lett.*, **2** (2000) 4169.

[19] P. C. Unangst, D. T. Connor, W. A. Cetenko, R. J. Sorenson, C. R. Kostlan, J. C. Sircar, C. D. Wright, D. J. Schrier, R. D. Dyer, *J. Med. Chem.*, **37** (1994) 322.

[20] X.-Ping Zhou, M.-Xin Zhang, W. Sun, X.-Hong. Yang, G.-Shu Wang, Da-Yuan Sui, X.-Feng Yu and S.-Chun Qu, *Biol. Pharm. Bull.*, **32** (2009) 1986.

[21] P. Brown, D. T. Davis, P. O'Hanlon and J. M. Wilson, *J. Med. Chem.*, **39** (1996) 446.

[22] J. C. Milne, A. C. Eliot, N. L. Kelleher and C. T. Walsh, *Biochemistry*, **37** (1998) 13250.

[23] I. G. Stankova, G. I. Videnov, E. V. Golovinsky and G. Jung, *J. Peptide Sci.*, **5** (1999) 392.

[24] A. P. Kozikowski and N. Hasan, *J. Org. Chem.*, **42** (1977) 2039.

[25] S.-Li You and J. W. Kelly, *J. Org. Chem.*, **68** (2003) 9506.

[26] A. Gursöy, Ş. Demirayak, G. Çapan, K. Erol and K. Vural, *Eur. J. Med. Chem.*, **35** (2000) 359.

[27] Á. Vincze, J. Solymosi, I. Kása and Á. Safrany, *Rad. Phys. Chem.*, **76** (2007) 1395.

[28] S. Sodaye, Y. M. Scindia, A. K. Pandey and A. V. R. Reddy, *Sensors and Actuators B*, **123** (2007) 50.

[29] J. S. Tang and J. G. Verkade, *J. Org. Chem.*, **61** (1996) 8750.

[30] R. Kikkeri, H. Traboulsi, N. Humbert, E. Gumienna-Kontecka, R. Arad-Yellin, G. Melman, M. Elhabiri, A.-M. Albrecht-Gary and A. Shanzer, *Inorg. Chem.*, **46** (2007) 2485.

[31] R. M. A. El-Aal, *Dyes and Pigments*, **61** (2004) 251.

[32] I. J. Turchi and M. J. S. Dewar, *Chem. Rev.*, **75** (1975) 389.

[33] I. Schiketanz, A. Racoveanuschiketanz, M. D. Gheorghiu and A. T. Balaban, *Rev. Roum. Chim.*, **37** (1992) 1315.

[34] L. I. Belenkii, V. S. Bogdanov, I. A. Abronin, G. P. Gromova, M. A. Cheskis and R. Z. Zakharyan, *Chem. Scripta*, **25** (1985) 266.

[35] J. Jwazwinski, B. Kamienski, O. Staszewska-Krajewska. G. A. Webb, *J. Mol. Struct.*, **646** (2003) 1.

[36] M. H. Palmer, *J. Mol. Struct.*, **834-836** (2007) 113.

[37] M. Muniz-Miranda, *Vibrat. Spectrosc.*, **18** (1999) 227.

[38] A. A. Elazhary, A.A. Ghoneim, M. E. Elshakre, *J. Chem. Res.*, **9** (1995) 354.

[39] A. A. Shaffer and S. G. Wiershchke, *J. Comput. Chem.*, **14** (1993) 75.

[40] F. W. Heinemann, W. Dolling, T. Gildenast and H. Hartung, *J. Chem. Crystal.*, **25** (1995) 237.

[41] D. Kaiser, G. Videnov, C. Maihle-Mossmer, J. Strahle and G. Jung, *J. Chem Soc., Perkin Trans. 2*, **5** (2000) 1081.

[42] J. C. Lee, J. W. Seo and J. K. Baek, *Synthetic Comm.*, **37** (2007) 2159.

[43] V. V. Dabholkar and S. K. J. Mishra, *Heterocyclic Comm.*, **12** (2006) 241.

[44] B Li, R. A. Buzon and Z. Zhang, *Org. Proc. Res. Develop.*, **11** (2007) 951.

[45] M. Lachia and C. J. Moody, *Nat. Prod. Rep.*, **25** (2008) 227.

[46] S. Lopes, C. M. Nunes, R. Fausto and T. M. V. D. Pinho e Melo, *J. Mol. Struct.*, **919** (2009) 47.

[47] T. M. V. D. Pinho e Melo, C. S. Lopes, A. M. d'A. Rocha Gonsalves and R. C. Storr, *Synthesis.*, (2002) 605

[48] M. J. Frisch, G. W. Trucks, H. B. Schlegel, G. E. Scuseria, M. A. Robb, J. R. Cheeseman, J. A. Montgomery, Jr., T. Vreven, K. N. Kudin, J. C. Burant, J. M. Millam, S. S. Iyengar, J. Tomasi, V. Barone, B. Mennucci, M. Cossi, G. Scalmani, N. Rega, G. A. Petersson, H. Nakatsuji, M. Hada, M. Ehara, K. Toyota, R. Fukuda, J. Hasegawa, M. Ishida, T. Nakajima, Y. Honda, O. Kitao, H. Nakai, M. Klene, X. Li, J. E. Knox, H. P. Hratchian, J. B. Cross, V. Bakken, C. Adamo, J. Jaramillo, R. Gomperts, R. E. Stratmann, O. Yazyev, A. J. Austin, R. Cammi, C. Pomelli, J. W. Ochterski, P. Y. Ayala, K. Morokuma, G. A. Voth, P. Salvador, J. J. Dannenberg, V. G. Zakrzewski, S. Dapprich, A. D. Daniels, M. C. Strain, O. Farkas, D. K. Malick, A. D. Rabuck, K. Raghavachari, J. B. Foresman, J. V. Ortiz, Q. Cui, A. G. Baboul, S. Clifford, J. Cioslowski, B. B. Stefanov, G. Liu, A. Liashenko, P. Piskorz, I. Komaromi, R. L. Martin, D. J. Fox, T. Keith, M. A. Al-Laham, C. Y. Peng, A. Nanayakkara, M. Challacombe, P. M. W. Gill, B. Johnson, W. Chen, M. W. Wong, C. Gonzalez, J. A. Pople, Gaussian 03, Revision C.02 ed., Gaussian, Inc., Wallingford, CT, 2004.

[49] M. Frisch, M. Head-Gordon, Pople, *J. Chem. Phys. Lett.*, **166** (1990) 281.

[50] A. D. Becke, *Phys. Rev. A.*, **38** (1988) 3098.

[51] C. T. Lee, W. T. Yang and R. G. Parr, *Phys. Review B*, **37** (1988) 785.

[52] P. Csaszar and P. Pulay, *J. Mol. Struct. (Theochem.)*, **114** (1984) 31.

[53] Ö. Farkas and H. B. Schlegel, *J. Chem Phys* . **111**, 10806 (1999).

[54] C. Peng and H. B. Schlegel, *Isr. J. Chem.*, **33** (1994) 449.

[55] D. Michalska and R. Wysokinski, *Chem. Phys. Lett.*, **403** (2005) 211.

[56] J. H. Schachtschneider, *Technical Report*, Shell Development Co. Emeryville, CA, 1969.

[57] P. Pulay, G. Fogarasi, F. Pang, J. E. Boggs, *J. Am. Chem. Soc.*, **110** (1979) 2550.

[58] A. Gómez-Zavaglia, A. Kaczor, A.L. Cardoso, T.M.V.D. Pinho e Melo, R. Fausto, *J. Phys. Chem. A*, **110** (2006) 10742.

[59] A. Gómez-Zavaglia, A. Kaczor, A.L. Cardoso, T.M.V.D. Pinho e Melo, R. Fausto, *J.Phys. Chem. A*, **110** (2006) 8081.

[60] S. Jarmelo and R. Fausto, *J. Mol. Struct.*, **509** (1999) 183.

[61] R. Fausto and J. J. C. Teixeira-Dias, *J. Mol. Struct.*, **150** (1987) 381.

[62] R. Fausto and J. J. C. Teixeira-Dias, *J. Mol. Struct.*, **144** (1986) 215.

[63] R. Fausto and J. J. C. Teixeira-Dias, *J. Mol. Struct.*, **144** (1986) 225.

[64] J. J. C. Teixeira-Dias and R. Fausto, *J. Mol. Struct. (THEOCHEM)*, **282** (1993) 123.

[65] J. M. F. Neta and R. Fausto, *J. Mol. Struct.*, **443** (1998) 41.

[66] A. J. Barnes, *J. Mol. Struct.*, **113** (1984) 161.

[67] A. Gómez-Zavaglia, I. D. Reva and R. Fausto, *Phys. Chem. Chem. Phys.*, **5** (2003) 41.

[68] A. Borba, A. Gómez-Zavaglia and R. Fausto, *J. Mol. Struct.*, **794** (2006) 196.

[69] A. Kaczor, T. M. V. D. Pinho e Melo, M. I. Soares and R. Fausto, *J. Phys. Chem. A*, **110** (2006) 6531.

[70] A. Gómez-Zavaglia and R. Fausto, *Phys. Chem. Chem. Phys.*, **5** (2003) 52.

[71] I. D. Reva, S. G. Stepanian, L. Adamowicz, and R. Fausto, *Chem. Phys. Lett.*, **374** (2003) 631.

J. Phys. Chem. A, **2011**, *115*, 1199-1209.

Photochemistry and Vibrational Spectra of Matrix-Isolated Methyl 4-Chloro-5-phenylisoxazole-3-carboxylate

Susy Lopes,[a] Cláudio M. Nunes,[a] Andrea Gómez-Zavaglia,[a,b]
Teresa M.V.D. Pinho e Melo[a] and Rui Fausto[a]

[a] *Department of Chemistry, University of Coimbra, P-3004-535 Coimbra, Portugal*
[b] *Centro de Investigación y Desarrollo en Criotecnología de Alimentos (Conicet La Plata, UNLP) RA-1900, Argentina*

ABSTRACT

Methyl 4-chloro-5-phenylisoxazole-3-carboxylate (MCPIC) has been synthesized, isolated in low temperature argon and xenon matrices and studied by FTIR spectroscopy. The characterization of the low energy conformers of MCPIC was made by undertaking a systematic investigation of the DFT(B3LYP)/6-311++G(d,p) potential energy surface of the molecule. The theoretical calculations predicted the existence of three low energy conformers. Two of them (**I** and **II**) were observed experimentally in the cryogenic matrices. The third one (**III**) was found to be converted into conformer **II** during deposition of the matrices, a result that is in agreement with the predicted low **III**→**II** energy barrier (< 0.3 kJ mol^{-1}) . *In situ* UV irradiation (λ > 235 nm) of matrix-isolated MCPIC yielded as final photoproduct the corresponding oxazole (methyl 4-chloro-5-phenyl-1,3-oxazole-2-carboxylate). Identification of the azirine and nitrile-ylide intermediates in the spectra of the irradiated matrices confirmed their mechanistic relevance in the isoxazole→oxazole photoisomerization.

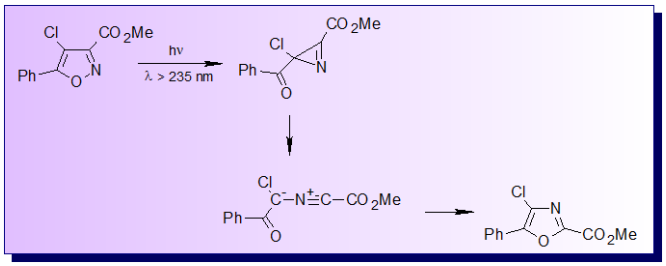

Introduction

Isoxazole and its derivatives are important building blocks of many compounds of biological interest. These heterocycles are reactants or intermediates in the synthesis of compounds that have been receiving pharmaceutical and medicinal applications.[1-12] In particular, several phenylisoxazoles with halogen or multiple halogen substituents have been reported as anthelmintics or possessing antiparasitic activity.[13,14] The agricultural uses of isoxazole derivatives include herbicidal, insecticidal and soil fungicidal activities.[15-18] Isoxazoles have also been used as semiconductors, as corrosion inhibitors in fuels and lubrificants, and in the production of photographic and liquid crystalline materials.[19-25]

Isoxazoles (**1**, in Scheme 1), including the unsubstituted compound, have been the subject of many studies by different well-known techniques, such as infrared (IR), Raman, NMR and microwave spectroscopies, mass spectrometry, and X-ray diffraction.[6,9,10,26-29] Many studies combined experimental techniques and theoretical methods at various levels of approximation, such as DFT and MP2.[30-34] One of the most interesting features of the reactivity of isoxazoles is their capability to be converted into other heterocylic compounds through a ring-opening reaction and subsequent re-cyclization. The first step of this type of chemical transformation is the cleavage of the labile N-O single bond, which can be either thermally [35-40] or photochemically induced.[40-45] The generation of vinyl nitrene intermediates (**2**) have been proposed,[37,39-41,44] which rearrange into the corresponding *2H*-azirines (**3**). The *2H*-azirines can then undergo ring cleavage to nitrile-ylides (**4**) followed by recyclization to give oxazoles (**5**) as the final products (see Scheme 1).[37,38,43-45] Although the detection of the *2H*-azirine is not always possible, their presence has been inferred in the isoxazole-oxazole rearrangement. The nature of the substituents and their position in the isoxazole ring are also important factors in determining the preferred reactive pathway and details of the chemical reactivity of isoxazoles.[46-48]

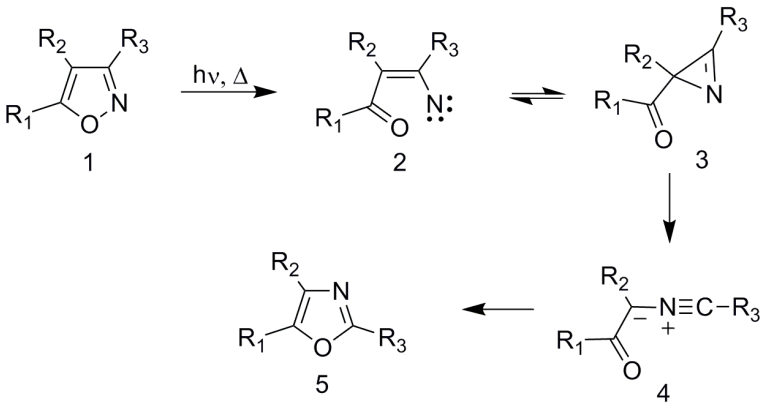

Scheme 1.

In a previous publication,[49] the monomeric forms of methyl 4-chloro-5-phenylisoxazole-3-carboxylate (MCPIC; **1a** in Chart 1) and its oxazole counterpart, methyl 4-chloro-5-phenyl-1,3-oxazole-2-carboxylate (MCPOC; **5a**) were studied using matrix-isolation infrared spectroscopy (argon matrix) and quantum chemical calculations. That study confirmed unambiguously the vibrational signature of both heterocycles through direct comparison of the experimental spectra of both compounds with the corresponding calculated spectra. The conformational space of MCPOC was subsequently investigated in detail both experimentally and theoretically,[50] the compound representing an interesting case where an inversion of the order of stability of the two most stable conformers occurs upon going from the gas phase to a xenon matrix.

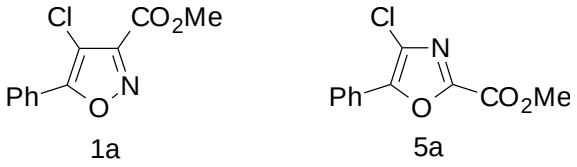

Chart 1.

In the present study, details of the vibrational spectra of matrix-isolated MPCIC (both in argon and xenon matrices) and its photochemistry were investigated using matrix-isolation infrared spectroscopy and DFT calculations. As it will be shown in detail below, the present study allowed us to conclude that, among the three low energy forms of MPCIC present in significant amount in the gas phase room temperature equilibrium, only two of them could be trapped in the matrices. On the

other hand, the third conformer converts into one of the observed forms during deposition of the matrices. These results could be explained taking into account the calculated energy barriers separating the different MPCIC conformers. UV irradiation ($\lambda > 235$ nm) of matrix-isolated MCPIC led to its conversion to the corresponding oxazole, with the azirine and nitrile-ylide intermediates being experimentally detected, thus confirming the previously proposed mechanism for the isoxazole→oxazole photoisomerization.[40-45]

Experimental Procedures

The procedure for the synthesis of MCPIC has been reported elsewhere.[49] Briefly, a solution of methyl 5-phenylisoxazole-3-carboxylate and N-chlorosuccinimide in 7% fuming nitric acid in acetic acid was irradiated with microwaves at 160 ºC during about 40 min. After cooling to room temperature, water was added and the mixture extracted with CH_2Cl_2, the organic phase was dried ($MgSO_4$) and evaporated off. The crude product was purified by flash chromatography [ethyl acetate–hexane (1:5)], to give MCPIC as a white solid (59%) [mp: 62–63 ºC; IR (KBr): 1221, 1441, 1738, 2957 cm^{-1}; ^1H NMR: 4.03 (3H, s), 7.52–7.55 (3H, m), 8.03–8.06 (2H, m); ^{13}C NMR: 53.1, 106.0, 125.6, 126.6, 129.0, 131.2, 153.3, 159.1, 165.8; MS (EI): m/z 237 (M^+, 99), 206 (14), 105 (100), 77 (68), 59 (78); HRMS (CI): m/z 237.0200 ($C_{11}H_8NO_3Cl$ [M^+], 237.0193).

Matrices were prepared by co-deposition of MCPIC vapors coming out from a specially designed thermoelectrically heatable mini-furnace, assembled inside the cryostat (APD Cryogenics, model DE-202A) chamber, and large excess of the matrix gas (argon, N60; xenon, N48, both obtained from Air Liquide) onto a CsI substrate cooled to 10 K (for argon matrices) and 20 K (for xenon matrices). The IR spectra were recorded with 0.5 cm^{-1} spectral resolution in a Mattson (Infinity 60AR Series) Fourier transform infrared spectrometer, equipped with a deuterated triglycine sulphate (DTGS) detector and a Ge/KBr beam splitter. Necessary modifications of the sample compartment of the spectrometer were done in order to accommodate the cryostat head and allow purging of the instrument by a stream of dry nitrogen, to remove water vapors and CO_2.

Irradiation of the matrices was carried out with unfiltered light from a 500 W Hg(Xe) lamp (Newport, Oriel Instruments), with output power set to 200 W, through the outer KBr windows of the cryostat ($\lambda > 235$ nm).

Computational Methods

The quantum chemical calculations were performed with Gaussian 03[51] at the DFT level of theory, using the split valence triple-ζ 6-311++G(d,p) basis set[52] and the three-parameter B3LYP density functional, which includes Becke's gradient exchange correction[53] and the Lee, Yang and Parr correlation functional.[54]

Geometrical parameters of the different conformations were optimized using the Geometry Direct Inversion of the Invariant Subspace (GDIIS) method.[55,56] Transition states were located using the synchronous transit-guided quasi-Newton (STQN) method.[57] In order to assist the analysis of the experimental spectra, vibrational frequencies and IR intensities were also calculated at the same level of approximation. The computed harmonic frequencies were scaled down by a single factor (0.9817) to correct them for the effects of basis set limitations, neglected part of electron correlation and anharmonicity effects. This factor was determined by simple linear fitting (with intercept fixed at zero) of the calculated wavenumbers to the experimental ones. The scaling procedure used was chosen mostly to achieve two goals: (1) respect the potential energy distribution (*i.e.*, mode composition) obtained directly from the MO calculations before scaling; this justifies the use of a single scale factor, and (2) provide the best possible comparison with the experimental data; this justifies the choice for a fitting procedure instead of using a more standard scale factor extracted from general literature.

Normal coordinate analyses were undertaken in the internal coordinates space, as described by Schachtschneider and Mortimer,[58] using the optimized geometries and harmonic force constants resulting from the DFT(B3LYP)/6-311++G(d,p) calculations. The internal coordinates used in these analyses were defined according to the recommendations of Pulay *et al.*[59]

Results and Discussion

Conformational Space of MCPIC. MCPIC is characterized by three conformationally relevant internal rotation axes defined around the C_{14}–C_1, C_3–C_6 and C_6–O_8 bonds (Figure 1). As in other carboxylic ester molecules,[60-65] internal rotation around the C_6–O_8 bond gives rise to *s-cis* and *s-trans* structures, with the *s-cis* species (C–C–O–C dihedral equal to 0º) being more stable than the *s-trans* forms by *ca.* 30 kJ mol^{-1}.[63-65] The latter species are then of no practical importance. On the other hand, internal rotations around the C_{14}–C_1 and C_3–C_6 bonds lead to different low energy conformers. A systematic investigation of the potential energy surface (PES) of the molecule was then undertaken by varying the C_{15}–C_{14}–C_1–O_5 and C_2–C_3–C_6–O_8 dihedral angles in steps of 30º and optimizing all remaining geometric parameters at each point.

Figure 2 presents the contour map of the DFT(B3LYP)/6-311++G(d,p) PES calculated as described above. Three sets of symmetry-equivalent energy minima were found on the PES, corresponding to three different conformers (**I**, **II** and **III**, see Figure 1). According to calculations, conformers **II** and **III** are 3.9 and 4.2 kJ mol^{-1} higher in energy than the most stable form (calculated values including zero-point energy corrections; the corresponding relative energies from the bottom of the potential wells are 4.0 and 4.4 kJ mol^{-1}).

The calculated optimized geometries for the three conformers are given in Table S1 (Supporting Information). In all these conformers, the position of the phenyl group in relation to the isoxazole ring is nearly the same, the angle between the planes of the two rings being *ca.* 20º (more precisely, 18.5, 19.0 and 15.6º in **I**, **II** and **III**, respectively; see Table S1). In the most stable conformer (**I**) the methyl ester group and the chlorine substituent of the isoxazole ring exhibit a nearly *trans* orientation, while in conformers **II** and **III** these groups exhibit a nearly *cis* arrangement: in conformer **I** the C_2–C_3–C_6–O_8 dihedral angle is ~170º, while in conformers **II** and **III** this angle is *ca.* –25º and 25º, respectively.[a]

[a] Here we are considering the minima where the C_{15}–C_{14}–C_1–O_5 dihedral angle is *ca.* 20º, *i.e.*, the minima corresponding to conformers **I** and **III** located in the 1st quadrant of the PES map shown in Figure 2, and that corresponding to conformer **II** located in the 4th quadrant. Other forms related to these by symmetry.

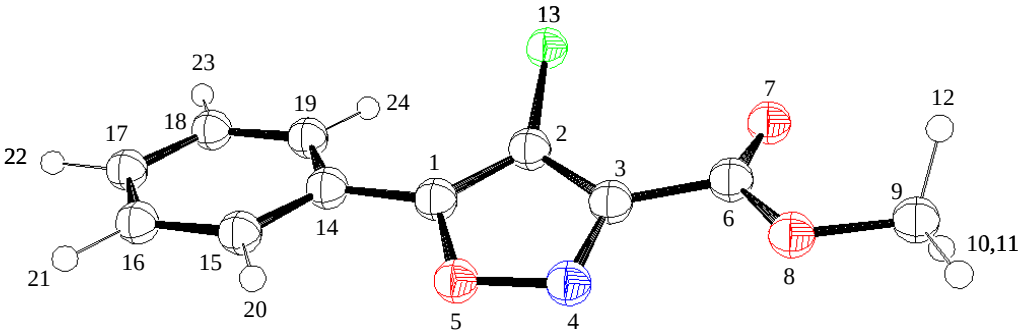

I (0.0)

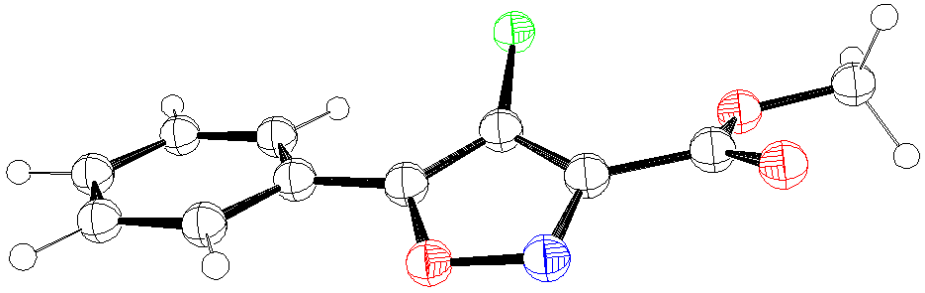

II (3.87)

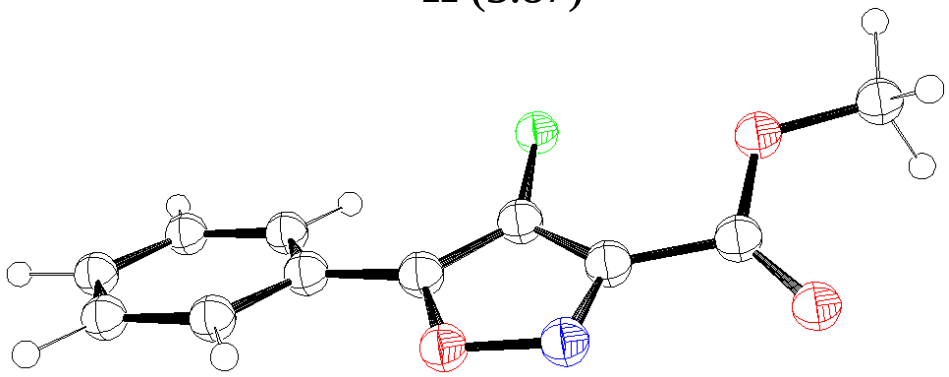

III (4.22)

Figure 1. Low energy conformers of MCPIC, optimized at the DFT(B3LYP)/6-311++G(d,p) level of theory, with atom numbering. Relative energies, including zero point corrections (ΔE^o/ kJ mol^{-1}) are given in parenthesis. The values of dipole moments (μ) for these conformers are: 1.52, 4.09 and 4.09 D (1 D= 3.33564 x 10^{-30} C m), respectively. Each conformer corresponds to four symmetry-related minima in the molecules' potential energy surface (see Figure 2). The complete calculated optimized geometries for the three conformers are given in Table S1 (Supporting Information). The picture was made using the Ortep-3 for Windows program (Farrugia, L. J. *J. Appl. Cryst*. 1997, **30**, 565). Atoms color code: carbon, hydrogen: black; nitrogen: blue; chlorine: green; oxygen: red.

The most stable conformer of MCPIC is similar to that determined by X-ray diffraction to be present in the crystal of the analogous bromo-substituted compound, 4-bromo-5-phenylisoxazole-3-carboxylate.[66] In that molecule, the angle between the phenyl and isoxazole ring was found to be 20.8º (compared to 18.5º now calculated for conformer **I** of MCPIC) and the C_2–C_3–C_6–O_8 dihedral angle 169.8º (compared to 169.3º for MCPIC).

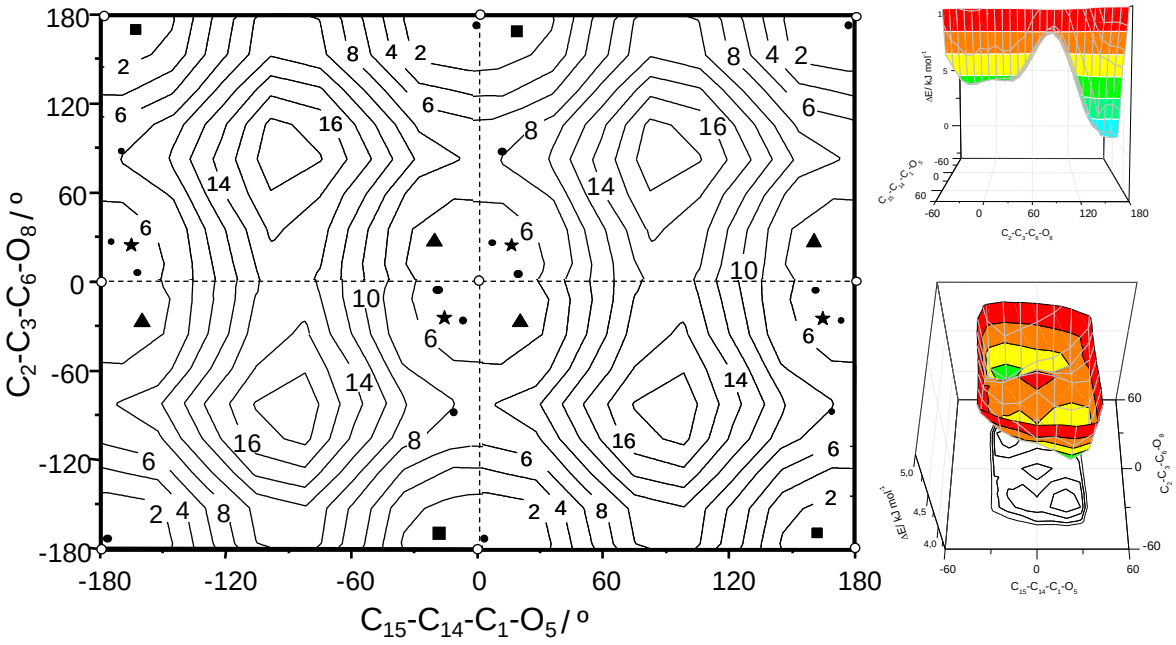

Left: B3LYP/6-311++G(d,p) potential energy map showing the position of the three low energy conformers of MCPIC. Each conformer correspond to four equivalent-by-symmetry minima; they are represented by squares (■, conformer **I**), triangles (▲, **II**) and stars (★, **III**). 1st order transition states interconnecting the conformers are represented by black circles (●), and the C_s symmetry structures, corresponding to 2nd order transition states, by open circles (○). The isoenergy contour lines (kJ mol^{-1}) were obtained by fitting a grid of energy values with increment in the two scanned dihedral angles of 30º, interpolated according to the Renka-Cline method. All remaining geometric parameters were optimized at each point. See Figure 1 for conformers structures and atom numbering. *Right-top:* PES profile along the C_2–C_3–C_6–C_8 coordinate, showing a possible pathway for interconversion between the three conformers. *Right-bottom:* expanded energy scale view of the PES in the vicinity of conformers **II** and **III**. In the two last panels, colors were used only for better visualization of the data.

In relation to the higher energy forms exhibiting an *s-trans* configuration about the C_6–O_8 bond, the calculations predicted the existence of only two conformers (forms **IV** and **V**; see Figure S1, Supporting Information). These conformers can be obtained from conformer **I** by rotation around the C_6–O_8 bond, and, as already mentioned, are *ca.* 30 kJ mol^{-1} higher in energy than the most stable conformer. The

conformationally relevant C_{15}–C_{14}–C_1–O_5, C_2–C_3–C_6–O_8 and O_7=C_6–O_8–C_9 dihedral angles in these high energy conformers were calculated as (14.9º, 137.0º, 173.1º) and (13.5º, –137.8º, –172.9º), for forms **IV** and **V**, respectively. No high energy conformers were found that could be obtained from rotation around the C_6-O_8 bond of forms **II** and **III**, *i.e.* exhibiting a C_2–C_3–C_6–O_8 dihedral angle in the ±25º region.

The main factors determining the relative stability of conformers **I**, **II** and **III** can be guessed based on the fact that the conformers do not have the phenyl and isoxazole rings and the heavy atoms of the ester group in the same plane. This is a clear indication that repulsive interactions between both the phenyl and ester fragments and the chlorine substituent of the isoxazole ring are the key interactions determining the precise geometry of the conformers and their relative energies. The interaction between the phenyl group and the chlorine atom involves the closest phenyl hydrogen atom (H_{24}) and must be of steric nature, since electrostatic interactions would, in this case, favor the coplanarity of the two rings (phenyl and isoxazole). This interaction is of equal importance in conformers **I** and **II** and slightly more important in conformer **III**, as implied by the relative values for the dihedral angle between the planes of the two rings in the three conformers (18.5, 19.0 and 15.6º, for **I**, **II** and **III**, respectively; see Figure 2 and Table S1), as well as H···Cl distances, which amount to 269.1 (**I**), 269.9 (**II**) and 265.9 (**III**) pm
(sum of H and Cl van der Waals radii is ~295 pm). The slightly higher energy of **III** compared with **II** is then partially accounted by this interaction.

On the other hand, the interactions between the ester group and the chlorine atom are different in the three conformers and, besides determining the non planarity of the ester and isoxazole fragments (as measured by the C_2–C_3–C_6–O_8 dihedral angle; see Figure 2 and Table S1), must be responsible for their relative energies. In conformer **I**, it is the carbonyl oxygen (O_7) which interacts with the chlorine atom, whereas in conformers **II** and **III** the interaction involves O_8. These interactions are both steric and electrostatic. The calculated atomic polar tensor (APT) charges[67] for the three conformers are shown in Table 1. From this table, it can be noticed that O_8 is more negative than O_7, so that the Cl···O_8 electrostatic repulsion in **II** and **III** is more important than the Cl···O_7 electrostatic repulsion in **I**. This difference seems to be the main factor justifying the lower energy of **I** compared to **II** and **III**. In addition, the Cl···$O_{7/8}$ contact distances decrease in the order **I** (316.1 pm) > **II** (312.0 pm) > **III** (309.6 pm) (sum of O and Cl van der Waals radii is ~327 pm), also contributing to

make the $Cl^{\cdots}O$ repulsive electrostatic interaction more important in the order **III** > **II** > **I**, and leading the $Cl^{\cdots}O$ steric interaction to follow also the same trend.

On the whole, the $H_{24}{}^{\cdots}Cl$ steric interactions and the $Cl^{\cdots}O_{7/8}$ electrostatic and steric interactions fully explain the relative energy of the three low energy conformers of MCPIC. It shall be noticed that in both conformers **I** and **II** the chlorine atom can move simultaneously apart from both H_{24} and $O_{7/8}$, since H_{24} and $O_{7/8}$ stay the same side of the isoxazole ring (see Figure 1). On the other hand, in conformer **III**, the situation is different, since H_{24} and O_8 stay in opposite sides of the isoxazole ring, thus restricting in some amount the flexibility of the molecule to release energy by rotation about the C_{14}–C_1 and C_3–C_6 bonds. This is consistent with the smaller dihedral angles between the two rings and about the C_3–C_6 bond in conformer **III**.

The pathways for interconversion between the three low energy conformers of MCPIC were also evaluated in this study. Two preliminary observations must be stressed. *(i)* The first one is that it is clear from Figure 2 that, for each conformer, two symmetry-equivalent minima exist in two different valleys on the PES. These two valleys are defined by values of the C_{15}–C_{14}–C_1–O_5 dihedral angle in the ranges (–30º,30º) and (150º,–150º) and extend the full range of the C_2–C_3–C_6–O_8 dihedral angle, being symmetrically equivalent. The two valleys are separated by barriers larger than 10 kJ mol^{-1}. *(ii)* The second preliminary observation is that the possible C_s symmetry structures, where the two rings and the heavy atoms of the ester fragment of MCPIC are in the same plane, correspond to second order transition states.

Within the same valley [let us consider that depicted in the central part of Figure 2, corresponding to C_{15}–C_{14}–C_1–O_5 in the (–60º,60º) range and shown in an extended energy scale in a separate graph in Figure 2], we found that the two equivalent-by-symmetry structures corresponding to conformer **I** can be interconverted directly to each other by crossing a barrier of 0.3 kJ mol^{-1} (0.2 kJ mol^{-1} if zero-point corrections are taken into account), following two symmetry equivalent pathways whose transition states have the C_{15}–C_{14}–C_1–O_5 and C_2–C_3–C_6–O_8 dihedral angles equal to –0.8º and 172.8º or 0.8º and –172.8º. These two first order transition states are symmetrically located in relation to the planar second order transition state with C_{15}–C_{14}–C_1–O_5 and C_2–C_3–C_6–O_8 dihedral angles equal to 0º and 180º (see Figure 2).

Table 1 – DFT(B3LYP)/6-311++G(d,p) calculated atomic polar tensor (APT) charges on atoms for conformers **I**, **II** and **III** of MCPIC.[a]

	APT charges/ *e*		
Atom	**I**	**II**	**III**
C_1	0.402	0.412	0.408
C_2	0.049	0.046	0.048
C_3	0.070	0.075	0.070
N_4	–0.150	–0.157	–0.157
O_5	–0.433	–0.421	–0.420
C_6	1.354	1.336	1.342
O_7	–0.739	–0.763	–0.766
O_8	–0.932	–0.890	–0.891
C_9	0.518	0.505	0.505
H_{10}	–0.019	–0.015	–0.017
H_{11}	–0.018	–0.017	–0.015
H_{12}	0.009	0.012	0.012
Cl_{13}	–0.157	–0.167	–0.167
C_{14}	0.015	0.010	0.017
C_{15}	–0.061	–0.060	–0.064
C_{16}	–0.040	–0.041	–0.041
C_{17}	–0.035	–0.035	–0.036
C_{18}	–0.041	–0.039	–0.038
C_{19}	–0.045	–0.044	–0.047
H_{20}	0.074	0.071	0.074
H_{21}	0.035	0.034	0.034
H_{22}	0.039	0.039	0.039
H_{23}	0.034	0.034	0.034
H_{24}	0.075	0.075	0.077

[a] See Figure 1 for atom numbering. $1e = 1.60217646 \times 10^{-19}$ C.

On the other hand, the symmetry-equivalent forms of both conformers **II** and **III** cannot be converted directly to each other, since no first order transition states exist between those forms. Direct conversion would imply simultaneous rotation about the C_{14}–C_1 and C_3–C_6 bonds, passing the second order transition state defined by C_{15}–C_{14}–C_1–O_5 and C_2–C_3–C_6–O_8 dihedral angles equal to 0º (see Figure 2). Conformers **II** and **III** can, alternatively, be easily converted into each other either by rotation around the C_{14}–C_1 or C_3–C_6 bonds. Though the barriers associated with these two pathways are both very small, the one implying a rotation around the C_3–C_6 bond is predicted to be slightly lower than that associated with the rotation around the C_{14}–C_1 bond: zero-point corrected values, $\Delta E_o^{\#}{}_{(\mathbf{III}\rightarrow\mathbf{II})}$= 0.1 kJ mol^{-1} *vs.* 0.2 kJ mol^{-1}

(0.4 *vs.* 0.6 kJ mol^{-1} in the opposite direction); values without zero-point corrections, $\Delta E^{\#}_{(\mathbf{III}\rightarrow\mathbf{II})}$= 0.1 kJ mol^{-1} *vs.* 0.3 kJ mol^{-1} (0.4 *vs.* 0.6 kJ mol^{-1} in the opposite direction).

Finally, both conformers **II** and **III** can also be converted into the most stable form. Interestingly, the two conversion pathways were found to include a common first order transition state (see Figure 2), which leads to **II**→**I** and **III**→**I** energy barriers of 3.9 and 3.6 kJ mol^{-1}, respectively (7.8 kJ mol^{-1} in the reverse direction) (zero point corrected values; non-corrected values are: 4.3 kJ mol^{-1} (**II**→**I**), 4.0 kJ mol^{-1} (**III**→**I**) and 8.3 kJ mol^{-1} (**I**→**II/III**).

Matrix Isolation IR Spectra of MCPIC (As-Deposited Matrices). All conformers of MCPIC belong to the C_1 symmetry point group, possessing 66 fundamental vibrations, all of them active in the infrared. In order to interpret the experimental spectra of the compound, the B3LYP/6-311++G(d,p) IR spectra of its experimentally relevant low energy conformers were obtained and normal coordinate analysis calculations were performed. The definition of the internal coordinates used in the vibrational analysis is provided in Table S2 (Supporting Information). The complete list of calculated wavenumbers, IR intensities and potential energy distributions resulting from the normal mode analyses are presented in Tables S3 and S4 (Supporting Information).

As discussed in detail in the previous section, the three low energy conformers of MCPIC have relative energies of 0.0 (**I**), 3.9 (**II**) and 4.2 (**III**) kJ mol^{-1}. At the sublimation temperature used to deposit the matrices (50 ºC), the estimated Boltzmann populations of these conformers are 69.2%, 16.4% and 14.4%, respectively. However, the energy barriers associated with the **III**→**II** conformational isomerization are very low (< 0.3 kJ mol^{-1}). Energy barriers of this magnitude are known[68-72] to be easily overcome during deposition of matrices under the experimental conditions used in this study. The gas being deposited is hot and the energy dissipated and made available during the landing of the molecules onto the cold substrate is enough to allow the barrier to be surpassed. In the present case, this can be expected to lead to relaxation of the higher energy conformer **III** into the lower energy conformer **II**. Hence, we can expect exclusive observation of conformers **I** and **II** in the as-deposited matrices of MCPIC. If no conversion from **II** to **I** takes place during deposition, the population of

conformer **II** in the matrices should correspond to the sum of those of conformers **II** and **III** in the vapor being deposited, *i.e.*, 30.8%.

Figure 3 shows the infrared spectra of MCPIC isolated in both argon and xenon matrices (sublimation temperature, 50 ºC; substrate temperature during deposition: argon, 10 K, xenon, 20 K). The B3LYP)/6-311++G(d,p) theoretically predicted spectra of conformers **I** and **II** are also presented in this figure (in format of stick spectra), as well as the simulated spectra of the expected conformational mixture at 50 ºC, built up by adding the calculated spectrum of conformers **I** and **II** with intensities scaled by their predicted populations (69% for conformer **I** and 31% for conformer **II**; see text).

The experimental spectra are well reproduced by the simulated spectrum, though it is clear that the population of conformer **II** is smaller than expected taking into account its predicted population in the vapor of the compound at 50 ºC. It can also be noticed that the population of **II** is smaller in the xenon than in the argon matrix. Indeed, the relative populations of the conformers present in the matrices were estimated from the observed integral bands intensities in the carbonyl stretching region (normalized by the calculated intensities of the conformers). According to this estimation, conformer **I** accounts for 86.1% of the total population in argon matrix and conformer **II** for the remaining 13.9%, whereas in the xenon matrix these values change to 90.4% (**I**) and 9.6% (**II**). All these results are consistent with the occurrence of two isomerization processes during deposition of the matrices: *(i)* conformer **III** is fully converted to form **II**, as expected taking into account the very low energy barriers for the **III**→**II** isomerization (<0.3 kJ mol^{-1}), and it is not present neither in the argon nor in the xenon matrix; *(ii)* conformer **II** is partially converted to the most stable conformer **I**. As discussed above, the last process has a predicted gas phase barrier of *ca.* 4 kJ mol^{-1}, which is still low enough to be accessible during deposition of the matrices, in particular in the case of the xenon matrix, where the temperature of the substrate during deposition was higher. A higher temperature of the substrate during deposition facilitates the conformational cooling.[68-72] Moreover, xenon has also been shown to facilitate conformational cooling in relation to argon.[69,70]

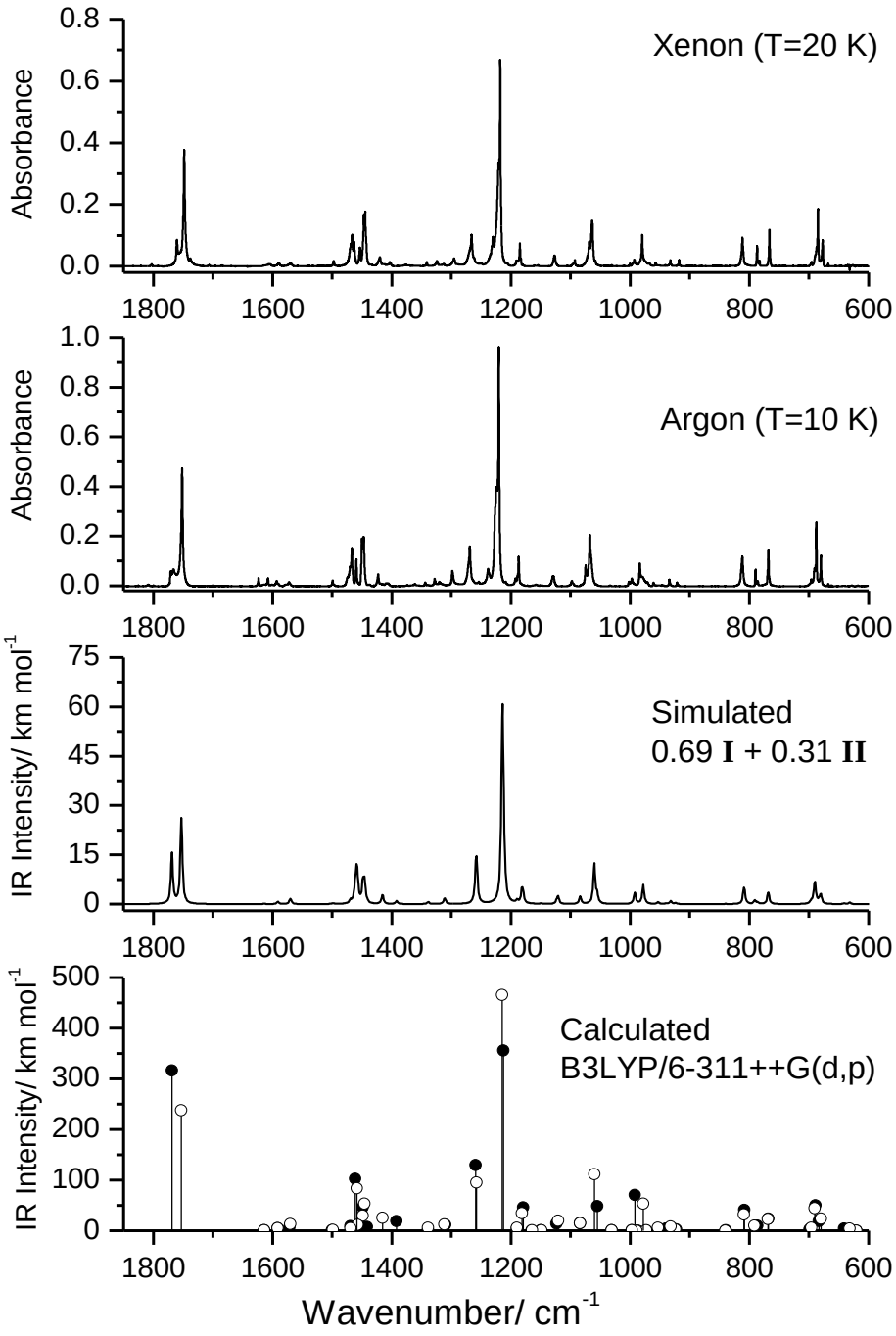

Figure 3. *Top* (two panels): Infrared spectra of MCPIC isolated in solid argon and xenon (as-deposited matrices; temperature of the deposited vapor: 50 ºC; substrate temperature during deposition: argon, 10 K, xenon, 20 K); *Bottom:* DFT(B3LYP)/6-311++G(d,p) calculated infrared spectra of MCPIC conformers **I** (open circles, ○) and **II** (black circles, ●) shown as stick spectra (wavenumbers scaled by 0.9817); *Middle:* simulated spectra of the expected conformational mixture at 50 ºC, built by adding the calculated spectrum of conformers **I** and **II** with intensities scaled by their predicted populations (69% for conformer **I** and 31% for conformer **II**; see text). In the simulated spectra, bands were represented by Lorentzian functions centered at the calculated wavenumbers (scaled by 0.9817) and with fwhm (full width at half maximum) equal to 4 cm^{-1}.

Annealing of the matrices to higher temperatures was also undertaken, in order to check the possibility of conformer **II** to be converted in conformer **I** after the matrix is formed. However, no significant changes could be observed in the spectra that could be unequivocally ascribed to the **II**→**I** conversion in the accessible range of temperatures (at *ca.* 30 K, the argon matrix started to deteriorate and aggregation of the compound started to be important; the same happened in the case of the xenon matrix at *ca.* 60 K). If we take into account the Barnes relationship between the temperature and the conversion barriers,[68] the non-observation of the **II**→**I** conversion till *ca.* 60 K indicates that the isomerization barrier for this process in the matrices must considerably increase to *ca.* 14-17 kJ mol^{-1}. Since this isomerization implies rotation of a voluminous fragment (the $COOCH_3$ moiety), such increase in the barrier to internal rotation in going from the gas phase to the solid state matrix could indeed be anticipated. In a matrix, this process would require extensive rearrangement of the matrix host, which is an energetically demanding process contributing to the increase of the effective barrier and, in the present case, precluding observation of the isomerization reaction.

The assignment of the bands in the experimental spectra was strongly aided by the excellent agreement between the experimental and the calculated data. The observed bands are mostly due to the most abundant conformer **I**, though in most of the cases they shall also contain a minor contribution from the less abundant conformer **II**, since the spectra of the two forms are quite similar (see Figure 3, bottom panel). The proposed assignments are presented in Table 2. A few bands (or prominent shoulders) could be tentatively ascribed to conformer **II**, besides those originated in the carbonyl stretching mode of this conformer, appearing at 1771/1767 cm^{-1} in argon, and 1760 cm^{-1} in xenon, whose assignment is unequivocal. Such bands appear at: 1472/1470 (δC-H1, νIsox1), 1410/1407 (νIsox4), 1272 (shoulder; νIsox2), 1239/1227/1224 (νC–O), 1129 (νIsox5, νIsox1), 1066/1063 (δIsox2) and 1002/1000/997/992 (νIsox5) cm^{-1} in argon and, correspondingly, at 1470/1469, 1404/1401, 1269 (shoulder), 1234/1232/1230/1221, 1124, 1064/1058 and 1002/1000/996/993 cm^{-1} in xenon (see Table S2 in the Supporting Information for designation of the vibrational modes and also Table S4).

~

Table 2 – Experimental (matrix-isolation) and calculated vibrational data for MCPIC with vibrational assignments based on the results of normal coordinate analysis.[a]

Experimental		Calculated		
Ar matrix	Xe matrix	Conformer **I**		Approximate description
ν	ν	ν	I	
3120	3114	3159	1.7	ν(C-H1)
3105	3096	3146	3.0	ν(C-H5)
3090/3081	3084	3132	16.9	ν(C-H2)
3070	3065/3060	3121	9.9	ν(C-H3)
3046/3035/3030	3040	3107	11.0	νCH_3 as´
3014	3027	3070	16.3	νCH_3 as´´
2964	2994	2998	34.3	νCH_3 s
1755/1752	1754/1748/1738	1753	237.5	νC=O
1601	n.obs.	1614	1.0	νPh3
1593	1590/1586	1591	4.8	νPh4
1573	1570	1570	13.1	νIsox3
1499	1497	1499	1.8	δ(C-H4)
n.obs.	1482	1469	5.2	δCH_3 as´
1467	1466/1463	1459	83.7	δ(C-H1), νIsox1
1459	1453	1457	11.6	δCH_3 as´´
1450	1445	1448	29.7	δCH_3 s
1448/1447	1445/1443(sh)	1446	53.1	νIsox2
1423	1423(sh)/1420	1416	25.5	νIsox4
1344/1340	1344(sh)/1341	1339	5.6	δ(C-H2)
1328/1320/1318/1315	1324/1315/1313	1312	12.1	νPh2
1269/1299 [b]	1297/1275/1266/1262 [b]	1258	94.7	$\nu(C\text{-}C_{IR})$
1221	1218	1215	465.5	νC-O
1192	1191/1189	1190	5.8	δ(C-H3)
1189(sh)/1187/1182	1185/1183/1180	1182	34.2	γCH_3´
1164	1161	1165	0.5	δ(C-H5)
1159	1155	1149	0.9	γCH_3´´
1130	1127	1121	19.6	νIsox1
1098/1096(sh)	1096(sh)/1093	1084	14.7	νPh6
1082/1079/1075/1073(sh)	1071/1069	1060	111.5	δIsox2
1034	1031	1031	0.5	νPh5
984/980/971	985(sh)/980/973/967	978	53.5	νIsox5
n.obs.	n.obs.	973	1.0	γ(C-H4)
961/957	957	953	5.5	$\nu(O\text{-}CH_3)$
934	933/931	932	8.1	$\nu(O\text{-}CH_3)$
921/920(sh)/919(sh)	920/918	924	2.6	γ(C-H5), γ(C-H1)
841	839	840	0.4	γ(C-H1)
814(sh)/812	812	809	31.9	δ(OCO)
790/788(sh)/786	787/784	791	9.5	γ(C=O)
769(sh)/768	766	769	23.2	γ(C-H3)
696/692(sh)/691	695/691/689/687	696	6.1	δPh3
688/684	685/681	691	44.0	τPh1
680	677	680	23.4	τIsox1
579	575	573	1.1	w(Isox-E), w(Isox-Ph), w(C-Cl)
486/485/477	484/482	485	2.7	γ(Ph-Isox)

[a] Wavenumbers (cm^{-1}, scaled by 0.9817), calculated intensities (km mol^{-1}), ν, bond stretching, δ, bending, γ, rocking, w, wagging, τ, torsion, s, symmetric, as, antisymmetric, IR, inter–ring; Isox, isoxazole ring; Ph, phenyl ring; E, ester, sh, shoulder; n.obs., not observed; see Table S2 (Supporting Information) for definition of internal coordinates and Table S3 for potential energy distributions. [b] Fermi resonance with τPh1 + (w(Isox-E), w(Isox-Ph), w(C-Cl)).

Photolysis Experiments (In Situ UV-irradiation with λ > 235 nm). In situ UV irradiation experiments were carried out to study the photochemistry of MCPIC in argon and xenon matrices. Upon broadband UV irradiation (λ > 235 nm) of the matrix isolated compound, significant changes occurred in the infrared spectrum, with bands due to MCPIC decreasing of intensity while new bands due to photoproducts emerged (Figures 4 and 5). The obtained results were identical in both argon and xenon matrices, with the difference that the observed reactions were found to be considerably faster in the latter matrix, indicating that triplet states are involved in the photoprocesses,[71,73] as it has also been suggested before based on the relative quantum yields for isoxazole→oxazole conversion of the studied compound and its bromo-substituted analogue in solution,[74] and acetone-sentitized conversion of 3-acetyl-5-methylisoxazole into the corresponding oxazole in different solvents.[75] The involvement of triplet states in the photoisomerization of isoxazole to oxazole has also been predicted theoretically.[45,76] In a xenon matrix, after 90 min of irradiation *ca.* 90% of the initially deposited MCPIC was transformed into other species, while in argon matrix only *ca.* 50% of the reactant was consumed. Below, we will concentrate the discussion in the results obtained in the xenon matrix.

Figure 4 (middle panel) shows the difference infrared spectrum obtained by subtracting to the spectrum of the MCPIC xenon matrix irradiated during 90 min (λ> 235 nm) the spectrum of the as-deposited MCPIC xenon matrix. The negative bands shown in this spectrum correspond to the bands of the reactant whose IR spectrum in a freshly deposited xenon matrix is also shown in the Figure as reference (bottom panel). The spectrum shown in the top panel of Figure 4 is the infrared spectrum of methyl 4-chloro-5-phenyl-1,3-oxazole-2-carboxylate (MCPOC) deposited in xenon matrix at 20 K in a different experiment. It is clear from the data shown in that Figure that the main product from the photolysis (λ> 235 nm) of matrix isolated MCPIC is its isomeric oxazole, MCPOC.

It is also clear from Figure 4 that, in addition to the bands due to MCPOC, other bands appear in the spectrum of the photolyzed matrix (positive bands in the difference spectrum shown in Figure 4; *e.g.*, in the 1800-1650 cm^{-1} region, and at 1601, 1584, 1256, 1240 and *ca.* 705 cm^{-1}), which must be assigned to different photoproducts. In order to allow for a clear examination of these bands, the spectrum of MCPOC was subtracted (multiplied by an appropriated intensity factor) from the

difference spectrum presented in Figure 4. The obtained new difference spectrum is shown in Figure 5. In this Figure, the presented spectral region corresponds to that where the strongest and most characteristic bands of other than the oxazole photoproduct are observed.

The identification of the photoproducts contributing to the positive bands shown in Figure 5 was done both by calculating the IR spectra of a series of possible photoproducts at the DFT(B3LYP)/6-311++G(d,p) level of theory and, whenever available, by comparing the position of the bands with characteristic bands of similar molecules.

According to the previously proposed mechanism for the photochemical isoxazole-oxazole rearrangement[46-48] the primary photoproduct, resulting from cleavage of the weakest bond in isoxazole, the N–O bond, should be the vinyl nitrene (**2**, in Scheme 1, where for the present molecule R_1 is a phenyl group, R_2 a chlorine substituent and R_3 the methyl ester fragment). Such species has never been experimentally detected and it is supposed to rearrange very easily to the closed ring 2*H*-azirine (**3**, in Scheme 1). Hence, the first molecule here considered as a possible contributing species to the spectrum of the photolyzed matrix (besides MCPOC) was the azirine methyl 2-benzoyl-2-chloro-2*H*-azirine-3-carboxylate (MBCAC). Substituted 2*H*-azirines with a methyl ester group have characteristic intense bands around 1780, 1750 and 1250 cm^{-1}, corresponding to the symmetric and antisymmetric combination of the νC=N and νC=O coordinates, and the νC–O stretching mode, respectively.[41,73,77] The spectrum calculated in this study for the most stable conformer of MBCAC is presented (in the form of stick spectrum) in Figure 5 and accounts for most of the positive bands of the difference spectrum shown in this Figure, allowing for unequivocal identification of MBCAC in the spectrum of the photolyzed matrix.

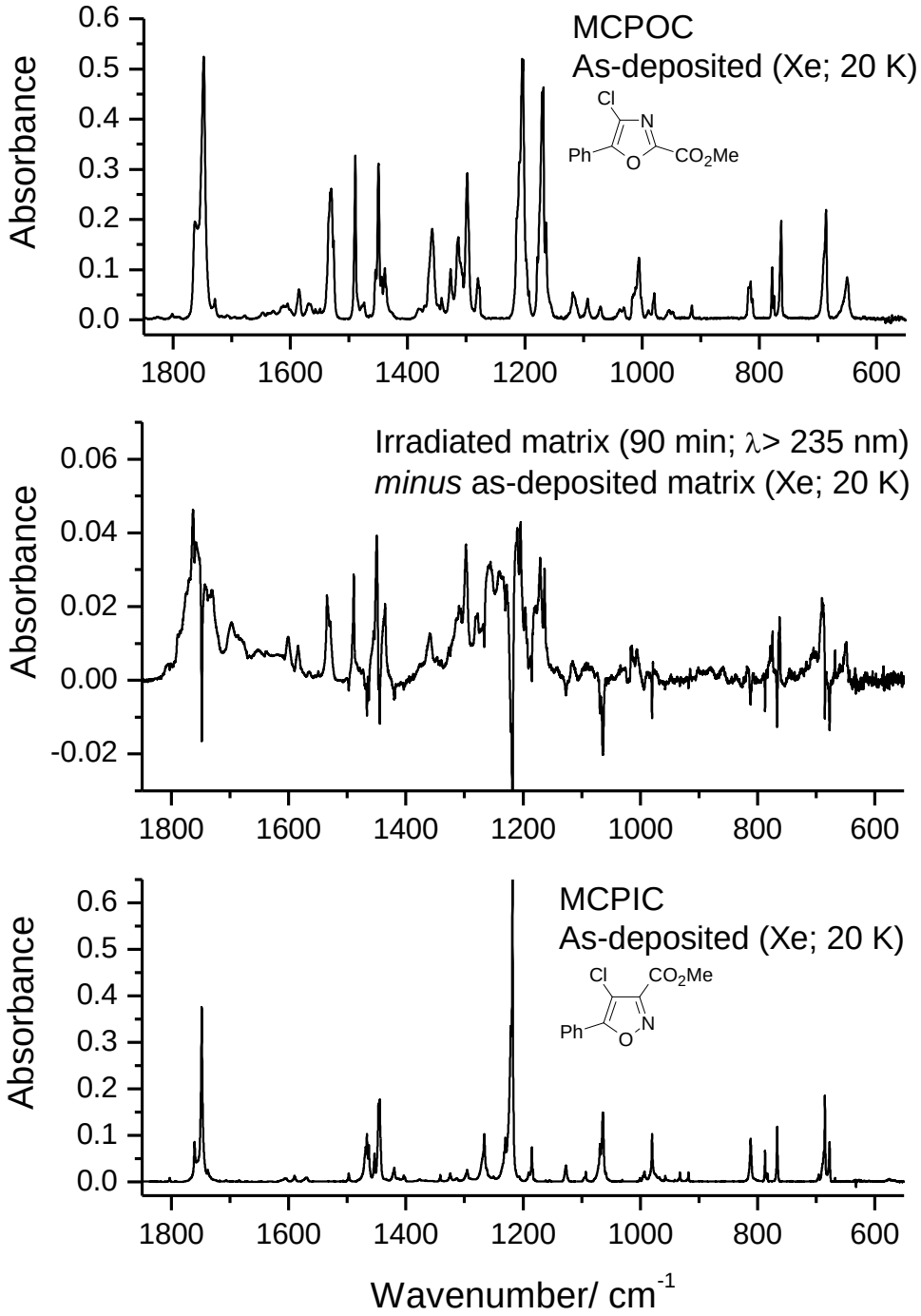

Figure 4. *Bottom*: IR spectrum (1850-550 cm^{-1} range) of MCPIC in a xenon matrix (as deposited; 20 K); *Middle*: IR difference spectrum (λ> 235 nm irradiated xenon matrix during 90 min *minus* as-deposited matrix); *Top*: IR spectrum of MCPOC in a xenon matrix (as-deposited; 20 K).

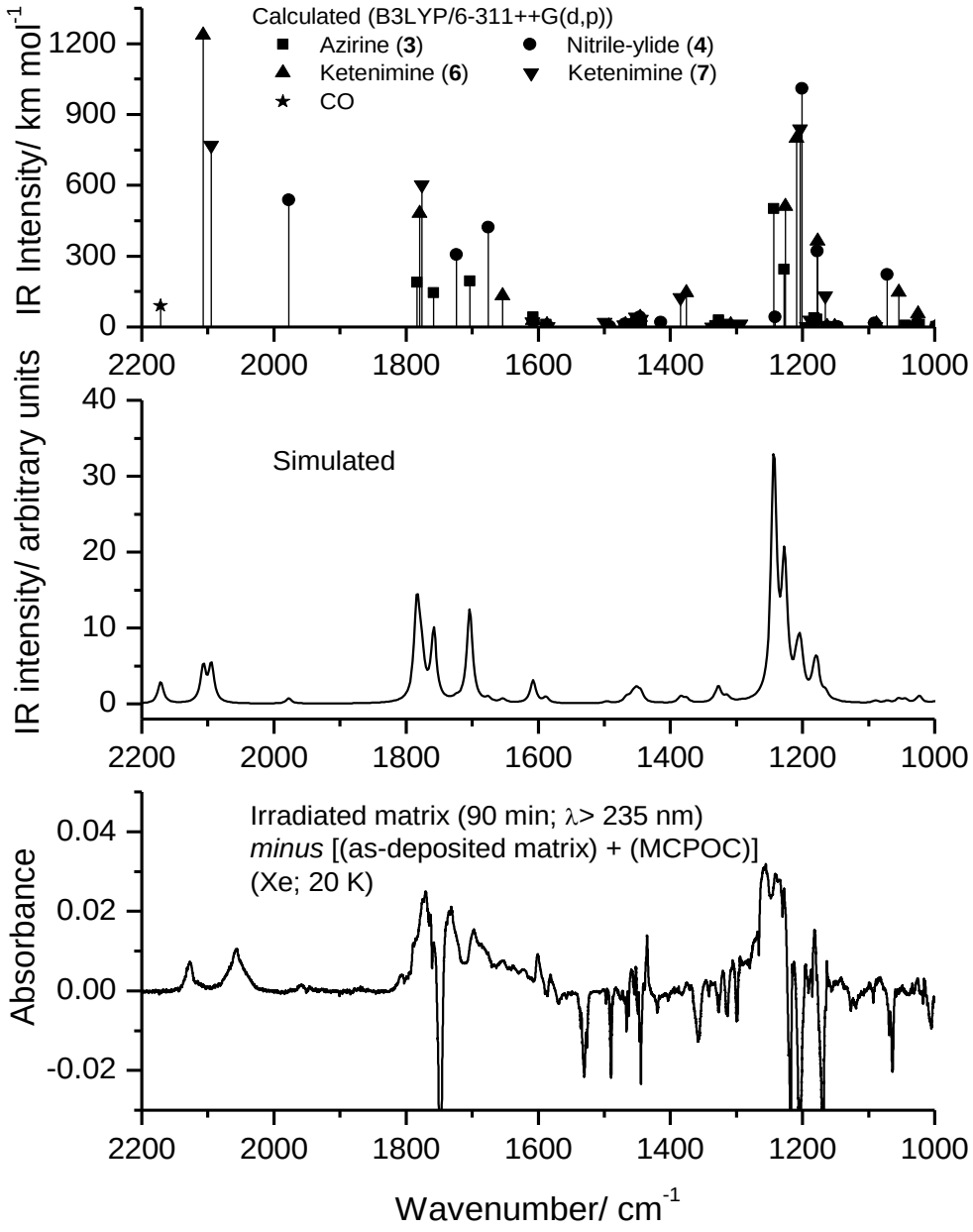

Figure 5. *Top*: B3LYP/6-311++G(d,p) calculated IR stick spectra for other than MCPOC observed photoproducts of MCPIC (wavenumbers scaled by 0.9817); *Middle*: Simulated IR spectrum built from the B3LYP/6-311++G(d,p) calculated spectra shown in the top panel (intensities of the different species were arbitrarily scaled in order to obtain the best match with the experimental data; bands were simulated by Lorentzian functions centered at the calculated frequencies and with FWHM equal to 10 cm^{-1}); *Bottom*: IR difference spectrum (2300-1000 cm^{-1} range) obtained by subtracting to the difference spectrum shown in Figure 4 (λ> 235 nm irradiated xenon matrix during 90 min *minus* as-deposited matrix) the spectrum of MCPOC in a xenon matrix (as-deposited; 20 K) multiplied by an appropriated intensity factor. The bands pointing down in this spectrum correspond to both MCPIC and MCPOC.

The identification of the remaining photoproducts was mainly made on the basis of the bands appearing in the 2300-1900 cm^{-1} spectral region, which is a clean region in the spectra of MCPIC, MCPOC and MBCAC.

The first band in this region is observed at 1955 cm^{-1} and appears at the characteristic wavenumber of the antisymmetric stretching of the CNC fragment of a nitrile-ylide.[77,78] The intensity of this band is low and all other bands predicted by the calculations to be intense for the nitrile-ylide resulting from MCPIC (**4** in Scheme 1) are expected to appear in regions where either MCPOC or MBCAC also absorb. Hence, this corresponds to the sole band unequivocally ascribable to the nitrile-ylide. However, its very characteristic wavenumber[77,78] ensures certainty in the identification of this species. Together with the observation of the azirine MBCAC, the observation of the nitrile-ylide in the spectrum of the matrix resulting from the photolysis of MCPIC (see also Figure 5), confirms the previously proposed mechanism for the photochemical isoxazole→oxazole rearrangement.[46-48]

The other bands found in the 2300-1900 cm^{-1} spectral region of the spectrum of the photolyzed matrix result from species photoproduced from the vinyl nitrene and/or the azirine in alternative competing photochemical pathways (see Scheme 2).

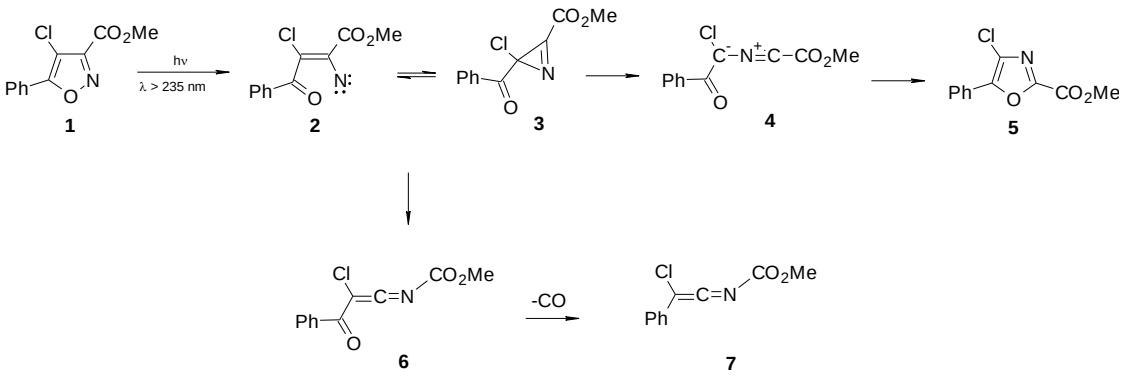

Scheme 2.

The band observed at 2057 cm^{-1} is characteristic of the ketenimine νC=C=N antisymmetric stretching mode,[77-79] and can then be ascribed to the ketenimine **6** (Scheme 2), which can result both from rearrangements of the azirine and vinyl nitrene intermediates. In Figure 5 it can be seen that the calculated wavenumber for

the ketenimine **6** νC=C=N antisymmetric stretching mode fits nicely that of the experimentally observed band here ascribed to this mode. Contrarily to nitrile-ylides, which result from the usually preferred photochemical breakage of the C–C bond of the azirine ring, ketenimines result from cleavage of the C–N bond. Nevertheless, the photochemical formation of ketenimines from 2*H*-azirines (in particular those substituted by a methyl ester group in the position 3 of the ring) has been observed.[71,73-80] The subsequent decarbonylation of the ketenimine **6** can account for the observation of the characteristic band of CO in the photolyzed MCPIC matrices. This band is observed at in the 2139-2119 cm^{-1} range, with maximum at 2127 cm^{-1}. Monomeric CO isolated in a xenon matrix gives rise to a band at 2133 cm^{-1}.[81,82] The product formed together with CO, which is also a ketenimine (**7**, in Scheme 2), shall also contribute to the band at 2057 cm^{-1} (see Figure 5). Decarbonylation of conjugated ketenimines like **6** has also been previously described.[71,73]

Conclusions

Methyl 4-chloro-5-phenylisoxazole-3-carboxylate was isolated in cryogenic matrices of noble gases (argon, xenon), and the preferred conformations assumed by the monomer of the compound probed by infrared spectroscopy, supported by theoretical calculations undertaken at the DFT(B3LYP)/6-311++G(d,p) level of approximation. The theoretical potential energy surface revealed the existence of three low energy conformers, the most stable form, **I**, being characterized by C_{15}–C_{14}–C_1–O_5, C_2–C_3–C_6–O_8 and O_7=C_6–O_8–C_9 dihedral angles of 169.8º, 18.5º and –1.2º, being similar to the conformer present in the crystal of the analogous bromo-substituted compound, 4-bromo-5-phenylisoxazole-3-carboxylate.[66] Conformers **II** and **III** differ from **I** fundamentally in the orientation of the ester fragment, and are 3.9 and 4.2 kJ mol^{-1} higher in energy than the most stable conformer. The $H_{24}\cdots Cl$ steric interactions and $Cl\cdots O_{7/8}$ electrostatic and steric interactions were found to explain the relative energy of the three conformers.

Conformers **I** and **II** were observed in the matrix isolation experiments, whereas conformer **III** was found to be totally converted into conformer **II** during deposition of the matrices. These results are in consonance with the very low energy barrier associated with the **III**→**II** conversion (< 0.3 kJ mol^{-1}), which can be easily

overcome during deposition of the matrices. Moreover, partial conversion of **II** into **I** during matrix deposition was also observed, a result that is also consistent with the moderately low predicted isomerization barrier for the **II**→**I** conversion (*ca.* 4 kJ mol^{-1}). On the other hand, annealing of the matrices up to 60 K (in xenon) did not promote any conversion of **II** into **I**, which point to a much larger barrier for this process in the solid matrix environment.

The assignment of the bands observed in the IR spectra [3500-400 cm^{-1} range] of MCPIC in both argon and xenon matrices was undertaken, aided by the excellent agreement between the experimental and the calculated spectroscopic data.

Broadband UV (λ> 235 nm) irradiation of matrix-isolated MCPIC was found to lead to the corresponding oxazole, methyl 4-chloro-5-phenyl-1,3-oxazole-2-carboxylate, as final photoproduct. In agreement with the mechanism for the isoxazole→oxazole photoisomerization previously proposed,[40-45] the expected azirine and nitrile-ylide intermediates could be identified spectroscopically in the present study in the photolysed matrices.

Supporting Information Available: Figure S1, High energy conformers of MCPIC optimized at the B3LYP/6-311++G(d,p) level of theory; Table S1, the calculated geometries for MCPIC low energy conformers **I**, **II** and **III**; Table S2, definition of internal coordinates used in the normal-mode analysis of MCPIC. Tables S3 and S4, B3LYP/6-311++G(d,p) calculated spectroscopic data and results of normal coordinate analysis for the two most stable, experimentally relevant conformers of MCPIC (forms **I** and **II**). This material is available free of charge *via* the Internet at http://pubs.acs.org.

Acknowledgements

These studies were partially funded by the Portuguese Science Foundation (Project No. FCOMP-01-0124-FEDER-007458, cofunded by QREN-COMPETE-UE, and Grants No. SFRH/BD/29698/2006 and #SFRH/BD/28844/2006). The authors also thank Milipeia Computer Centre (research project "Computação Avançada em Espectroscopia Molecular"), MinCyt-FCT (bilateral grant PO/09/18) and the

Iberoamerican Program for the Development of Science and Technology, CYTED (Network 198RT0362). A.G.Z. is member of the Research Career CONICET, Argentina.

References:

[1] Sechi, M.; Sannia, L.; Carta, F., Palomba, M.; Dallocchio, R.; Dessì, A.; Derudas, M.; Zawahir, Z.; Neamati, N. *Antivir. Chem. Chemother*. **2005**, *16*, 41-61.

[2] Diana, G. D.; Cutcliffe, D.; Oglesby, R. C.; Otto, M. J.; Mallamo, J. P.; Akullian V.; McKinlay, M. A. *J. Med. Chem*. **1989**, *32*, 450-455.

[3] Youn, H. S.; Lee, E. J.; Lee, J. E.; Park, W.-K.; Baek, Du-J.; Cho, Y. S.; Koh, H. Y.; Choo H.; Pae, A. N. *Bull. Korean Chem. Soc.* **2009**, *30*, 1873-1876.

[4] Calí, P.; Nærum, L.; Mukhija S.; Hjelmencrantz, A. *Bioorg. Med. Chem. Lett.* **2004**, *14*, 5997-6000.

[5] Tatee, T.; Kurashige, S.; Shiozawa, A.; Narita, K.; Takei, M.; Ito, S.; Miyazaki, H.; Yamanaka, H.; Mizugaki, M.; Sakamoto, T.; Fukuda, H. *Chem. Pharm. Bull.* **1986**, *34*, 1634-1642.

[6] Habeeb, A. G.; Rao, P. N. P.; Knaus, E. E. *Drug Develop. Res.* 2000, 51, 273-286.

[7] Rapposelli, S.; Lapucci, A.; Minutolo, F.; Orlandini, E.; Ortore, G.; Pinza M.; Balsamo, A. *Il Farmaco* **2004**, 59, 25-31.

[8] Saunders, J. C.; Williamson, W. R. N. *J. Med. Chem.* **1979**, *22*, 1554-1558.

[9] Eddington, N. D.; Cox, D. S.; Roberts, R. R.; Butcher, R. J.; Edafiogho, I. O.; Stables, J. P.; Cooke, N.; Goodwin, A. M.; Smith, C. A.; Scott, K. R. *Eur. J. Med. Chem.* **2002**, *37*, 635-648.

[10] Al-Omran F.; El-Khair, A. A. *J. Heterocyclic Chem.* **2004**, *41*, 327-333.

[11] Simoni, D.; Roberti, M. Invidiata, F. P.; Rondanin, R.; Baruchello, R.; Malagutti, C.; Mazzali, A.; Rossi, M.; Grimaudo, S.; Capone, F.; Dusonchet, L.; Meli, M.; Raimondi, M. V.; Landino, M.; D'Alessandro, N.; Tolomeo, M.; Arindam, D.; Lu, S.; Benbrook, D. M. *J. Med. Chem.* **2001**, *44*, 2308-2318.

[12] Shin, K. D.; Lee, Mi-Y.; Shin, D.-S.; Lee, S.; Son, K.-H.; Koh, S.; Paik, Y.-Ki; Kwon, B.-M.; Han, D.C. *J. Biol. Chem.* **2005**, *280*, 41439-41448.

[13] Carr, J. B.; Durham, H. G.; Hass, D. K. *J. Med. Chem.* 1977, *20*, 934-939.

[14] Haugwitz, R. D.; Angel, R. G.; Jacobs, G. A.; Maurer, B. V.; Narayanan, V. L.; Cruthers, L. R.; Szanto, J. *J. Med. Chem.* **1982**, *25*, 969-974.

[15] Goulding, K. H.; Yung, K.-M.; Hall, A. M.; Cremlyn, R. J. W. *Pestic Sci.* **1983**, *14*, 158-166.

[16] Pallett, K. E.; Cramp, S. M.; Little, J. P.; Veerasekaran, P.; Crudace, A. J.; Slater, A. E. *Pest. Manag. Sci.* **2001**, *57*, 133-142.

[17] Baker, A. D.; Betteridge, D.; Kemp, N. R.; Kirby, R. E. *Anal. Chem.* **1970**, *42*, 1064-1073.

[18] Liu, Y.; Cui, Z.; Liu, B.; Cai, B.; Li, Y.; Wang, Q. *J. Agric. Food Chem.* **2010**, *58*, 2685-2689.

[19] Naka, K. Horii, E. Chujo, Y. *Polym. J.* **2000**, *32*, 73-74.

[20] Shang, Y.-J.; Wang, Y.-G. *Tetrahedron Lett.* **2002**, *43*, 2247-2249.

[21] Abdel-Hafiz, S. A.; El-Kholy, Y. M. *Pigm. Resin Technol.* **1995**, *24*, 13-16.

[22] Al-Abdallah, M. M.; Abu-Orabi, S. T. *Anti-Corros. Methods Mat*. **1989**, *36*, 4-6.

[23] Lang, Jr. S. A. Lin, Y.-I. in Katristzky, A. R. Rees, C. W. (Series Eds.), Potts, K. T. (Ed.), *Comprehensive Heterocyclic Chemistry*, Vol. **6**, Part 4B, Pergamon, Oxford, 1984 (Chapter 4.16) page 1-130.

[24] Silva, L.; Gallardo, H.; Magnago, R. F.; Begnini, I. M. *Mol. Cryst. Liq. Cryst.* **2005**, *432*, 1-13.

[25] Santos, D. R.; Oliveira, A. G. S.; Coelho, R. L.; Begnini, I. M.; Magnago, R. F.; Silva, L. *Arkivoc* **2008**, *17*, 157-166.

[26] Uno, T.; Machida, K. Hanai, K. *Chem. Pharm. Bull.* **1966**, *14*, 756-762.

[27] Takasuka, M. Nakai, H. *Vibrat. Spectrosc.* **2001**, *25*, 197-204.

[28] McGlone, S.; Bauder, A. *J. Chem. Phys.* **1998**, *103*, 5383-5392.

[29] Stiefvater, O. L. *J. Chem. Phys.* **1975**, *63*, 2560-5569.

[30] Jezierska, A.; Panek, J.; Ryng, S. *J. Mol. Struct. (Theochem)* **2003**, *636*, 203-214.

[31] Jezierska, A.; Panek, J.; Ryng, S.; Głowiak, T.; Koll, A. *J. Mol Model.* **2003**, *9*, 159-163.

[32] Robertson, E. G. *J. Mol. Spectrosc.* **2005**, *231*, 50-56.

[33] Palmer, M. H.; Larsen, R. W.; Hegelund, F. *J. Mol. Spectrosc.* **2008**, *252*, 60-71.

[34] Pace, A.; Pierro, P.; Buscemi, S.; Vivon, N.; Barone, G. *J. Org. Chem.* **2009**, *74*, 351-358.

[35] Lifshitz, A.; Wohlfeilert, D. *J. Phys. Chem.* **1992**, *96*, 4505-4515.

[36] Higgins, J.; Zhou, X. Liu, R. *J. Phys. Chem. A* **1997**, *101*, 7231-7235.

[37] Pérez, J. D.; Yranzo, G. I.; Wunderlin, D. A. *J. Org. Chem.* **1982**, *47*, 982-984.

[38] Nishiwaki, T.; Saito, T.; Onomura, S.; Kondo, K. *J. Chem. Soc. C* **1971**, 2644-2647.

[39] Pérez, J. D.; Wunderlin, D. A. *J. Org. Chem.* **1987**, *52*, 3637-3640.

[40] Padwa, A.; Chen, E. Ku, A. *J. Am. Chem. Soc.* **1975**, *97*, 6484-6491.

[41] Singh, B.; Ullman, E. F. *J. Am. Chem. Soc.* **1967**, *89*, 6911-6916.

[42] Darlage, L. J.; Kinstle, T. H.; McIntosh, C. L. *J. Org. Chem.* **1971**, *36*, 1088-1093.

[43] Sauers, R. R.; Hadel, L. M.; Scimone, A. A.; Stevenson, T. A. *J. Org. Chem.* **1990**, *55*, 4011-4019.

[44] Ferris, J. P.; Trimmer, R. W. *J. Org. Chem.* **1976**, *42*, 13-19.

[45] Tanaka, H.; Matsushita, T.; Osamura, Y.; Nishimoto, K. *Int. J. Quant. Chem.* **1980**, *18*, 463-468.

[46] De Munno, A.; Bertini, V.; Luchesini, F. *J. Chem. Soc., Perkin Trans. 2* **1977**, 1121-1124.

[47] Lee, C. K. Y.; Easton, C. J.; Gebara-Coghlan, M.; Radom, L.; Scott, A. P.; Simpson, G. W.; Wills, A. C. *J. Chem. Soc., Perkin Trans. 2* **2002**, 2031-2038.

[48] Pavlik, J. W.; St. Martin, H.; Lambert, K. A. Lowell, J. A. Tsefrikas, V. M. Eddins, C. K.; Kebede, N. *J. Heterocyclic Chem.* **2005**, *42*, 273-281.

[49] Lopes, S.; Nunes, C. M.; Fausto, R.; Pinho e Melo, T. M. V. D. *J. Mol. Struct.* **2009**, *919*, 47-53.

[50] Lopes, S.; Nunes, C. M.; Gómez-Zavaglia, A.; Pinho e Melo, T. M. V. D.; Fausto, R. *J. Phys. Chem. A* **2010**, *114*, 9074-9082.

[51] Frisch, M. J.; Trucks, G. W.; Schlegel, H. B.; Scuseria, G. E.; Robb, M. A.; Cheeseman, J. R.; Montgomery, J. A., Jr.; Vreven, T.; Kudin, K. N.; Burant, J. C.; Millam, J. M.; Iyengar, S. S.; Tomasi, J.; Barone, V.; Mennucci, B.; Cossi, M.; Scalmani, G.; Rega, N.; Petersson, G. A.; Nakatsuji, H.; Hada, M.; Ehara, M.; Toyota, K.; Fukuda, R.; Hasegawa, J.; Ishida, M.; Nakajima, T.; Honda, Y.; Kitao, O.; Nakai, H.; Klene, M.; Li,X.; Knox, J. E.; Hratchian, H. P.;

Cross, J. B.; Bakken, V.; Adamo, C.; Jaramillo, J.; Gomperts, R.; Stratmann, R. E.; Yazyev, O.; Austin, A. J.; Cammi, R.; Pomelli, C.; Ochterski, J. W.; Ayala, P. Y.; Morokuma, K.; Voth, G. A.; Salvador, P.; Dannenberg, J. J.; Zakrzewski, V. G.; Dapprich, S.; Daniels, A. D.; Strain, M. C.; Farkas, O.; Malick, D. K.; Rabuck, A. D.; Raghavachari, K.; Foresman, J. B.; Ortiz, J. V.; Cui, Q.; Baboul, A. G.; Clifford, S.; Cioslowski, J.; Stefanov, B. B.; Liu, G.; Liashenko, A.; Piskorz, P.; Komaromi, I.; Martin, R. L.; Fox, D. J.; Keith, T.; Al-Laham, M. A.; Peng, C. Y.; Nanayakkara, A.; Challacombe, M.; Gill, P. M. W.; Johnson, B.; Chen, W.; Wong, M. W.; Gonzalez, C.; Pople, J. A. Gaussian 03, revision C.02; Gaussian, Inc.: Wallingford, CT, 2004.

[52] Frisch, M.; Head-Gordon, M. Pople, J. A. *Chem. Phys. Lett.* **1990**, *166*, 281-289.

[53] Becke, A. D. *Phys. Rev. A* **1988**, *38*, 3098–3100.

[54] Lee, C. T.; Yang, W. T.; Parr, R. G. *Phys. Rev. B* **1988**, *37*, 785–789.

[55] Császár, P.; Pulay, P. *J. Mol. Struct.* **1984**, *114*, 31-34.

[56] Farkas, Ö.; Schlegel, H. B. *J. Chem. Phys*. **1999**, *111*, 10806-10814.

[57] Peng, C.; Schlegel, H. B. *Isr. J. Chem.* **1994**, *33*, 449-454.

[58] Schachtschneider, J. H.; Mortimer, F. S. Vibrational Analysis of Polyatomic Molecules. VI. FORTRAN IV Programs for Solving the Vibrational Secular Equation and for the Least-Squares Refinement of Force Constants. Report Nº. 31450. Structural Interpretation of Spectra, Technical Report nº 57-650, Shell Development Co. Emeryville, CA, 1969.

[59] Pulay, P.; Fogarasi, G.; Pang, F. Boggs, J. E. *J. Am. Chem. Soc.* **1979**, *110*, 2550-2560.

[60] Kulbida, A.; Ramos, M. N.; Räsänen, M.; Nieminen, J.; Schrems, O.; Fausto, R. *J. Chem. Soc., Faraday Trans* **1995**, *91*, 1571-1585.

[61] Reva, I. D.; Stepanian, S. G.; Adamowicz, L.; Fausto, R. *J. Phys. Chem. A* **2001**, *105*, 4773-4780.

[62] Wiberg, K. B. K. E.; Laidig, K. E. *J. Am. Chem. Soc.* **1987**, *109*, 5935-5943.

[63] Fausto, R.; Teixeira-Dias, J. J. C. *J. Mol. Struct.* **1986**, *144*, 215-223.

[64] Fausto, R.; Teixeira-Dias, J. J. C. *J. Mol. Struct.* **1987**, *150*, 381-389.

[65] Fausto, R.; Teixeira-Dias, J. J. C. *J. Mol. Struct. (Theochem.)* **1993**, *282*, 123-129.

[66] Li, G.; Kakarla, R. Gerritz, S. W. *Tetrahedron. Lett.* **2007**, *48*, 4595-4599.

[67] Cioslowski, J. *J. Am. Chem. Soc.* **1989**, *111*, 8333-8336.

[68] Barnes, A. J. *J. Mol. Struct.* **1984**, *113*, 161-174.

[69] Reva, I. D.; Stepanian, S. G.; Adamowicz, L.; Fausto, R. *Chem. Phys. Lett.* **2003**, *374*, 631-638.

[70] Gómez-Zavaglia, A.; Fausto, R. *J. Mol. Struct.* **2004**, *689*, 199-212.

[71] Gómez-Zavaglia, A.; Kaczor, A.; Cardoso, A. L.; Pinho e Melo, T. M. V. D.; Fausto, R. *J. Phys. Chem. A* **2006**, *110*, 8081-8092.

[72] Borba, A.; Gómez-Zavaglia, A.; Simões, P. N. N. L.; Fausto, R. *J. Phys. Chem. A* **2005**, *109*, 3578-3586.

[73] Kaczor, A.; Gómez-Zavaglia, A.; Cardoso, A. L.; Pinho e Melo, T. M. V. D.; Fausto, R. *J. Phys. Chem. A* **2006**, *110*, 10742-10749.

[74] Fonseca, S. M.; Burrows, H. D.; Nunes, C. M.; Pinho e Melo, T. M. V. D. *Chem. Phys. Lett.* **2009**, *474*, 84-87.

[75] Sauers, R. R.; Van Arnum, S. D. *Tetrahedron Lett.* **1987**, *28*, 5797-5800.

[76] Tanaka, H.; Osamura, Y.; Matsushita, T; Nishimoto, K. *Bull. Chem. Soc. Jpn.*, **1981**, *54*, 1293-1298.

[77] Orton, E.; Collins, S. T.; Pimentel, G. *J. Phys. Chem.* **1986**, *90*, 6139-6143.

[78] Inui, H.; Murata, S. *J. Am. Chem. Soc.* **2005**, *127*, 2628-2636.

[79] Kurtz, D. W.; Shechter, H. *Chem. Commun.* **1966**, *19*, 689-690.

[80] Yranzo, G. I.; Elguero, J. E.; Flammang, R.; Wentrup, C. *Eur. J. Org. Chem.* **2001**, 2209-2220.

[81] Charles, S. W.; Lee, K. O.; *Trans. Faraday Soc.* **1965**, *61*, 614-619.

[82] Abe, H.; Yamada, K. M. T. *Struct. Chem.* **2003**, *14*, 211-215.

Tetrahedron – Submitted (**2011**)

3-Azido-Acrylophonones as Photochemical Precursors of Oxazoles: A Matrix Isolation Infrared Spectroscopy Study

Susy Lopes,[†] Cláudio M. Nunes,[†] Andrea Gómez-Zavaglia,[†,‡]
Teresa M.V.D. Pinho e Melo[†] and Rui Fausto[†]

[†] *Department of Chemistry, University of Coimbra, P-3004-535 Coimbra, Portugal*
[‡] *Centro de Investigación y Desarrollo en Criotecnología de Alimentos (Conicet La Plata, UNLP) RA-1900, Argentina*

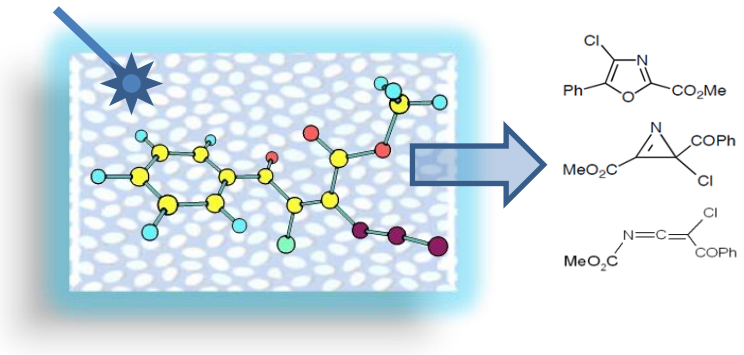

ABSTRACT

(Z)-3-azido-(E)-3-methylcarboxylate-2-chloro-acrylophenone (or methyl (Z)-2-azido-3-chloro-3-benzoylpropenoate; MACBP) has been synthesized, isolated in low temperature argon and xenon matrices and studied by FTIR spectroscopy, complemented by DFT(B3LYP)/6-311++G(d,p) calculations. The molecule was characterized both structurally and spectroscopically, and its photochemistry used to probe the mechanism of photo-induced conversion of 3-azido-acrylophenones into oxazoles. In situ UV irradiation ($\lambda > 235$ nm) of matrix-isolated MACBP yielded as primary photoproduct a 2H-azirine, which undergoes subsequent photoisomerization to the oxazole (methyl 4-chloro-5-phenyl-1,3-oxazole-2-carboxylate). This reaction is accompanied by a second one leading to formation of a ketenimine. The non-

observation of the corresponding isoxazole points to the concerted nature of the different steps leading to the observed final products. This also supports the idea that in the studied system a vinyl nitrene intermediate is not involved in the conversion of the azide into the azirine, as well as in the subsequent reactions of this latter.

Introduction

Molecules containing the azido-moiety (-N_3) are energy-rich and flexible chemical systems that have enjoyed increased interest over the years. Organic azides constitute a versatile class of compounds used as building blocks in organic synthesis,[1-5] with particular relevance in peptide and bioorganic chemistry.[6-14] The copper(I)-catalyzed Huisgen azide-alkyne 1,3-dipolar cycloaddition forming triazoles,[7,10,11,14-20] known as the 'click reaction', is one of the most effective ways to make connections between structures that bear a wide variety of functional groups. This reaction has found applications in a wide variety of research areas, for example, in materials science and drug design.[10,11,14]

It is well known that azides are also explosive substances that decompose with the release of nitrogen through the slightest input of external energy.[4] However, in spite of their explosive properties, the industrial interest in organic azide compounds extends to a number of areas, as they have applications in polymer synthesis[9,13,16,17] and light-induced activation of polymer surfaces,[21,22] as photo resistors for lithography,[23,24] in photo affinity labeling biological methods,[25,26] or as energetic additives for solid propellants.[27,28]

The mechanisms for the decomposition of azides through thermal and/or photochemical treatment and the intermediates formed have been extensively investigated. Nevertheless, there are still many cases where general consensus in relation to the precise mechanism involved in these processes could not been obtained. For example, it is considered that, in general, the release of molecular nitrogen is accompanied by the formation of a nitrene intermediate, which then undergoes further reactions, including isomerization to ketenimines, cyclization to azirines, C-H bond insertion or C=C bond addition.[29-39] However, even in the case of the common synthetic approach for preparing *2H*-azirines from photolysis or thermolysis of vinyl azides the precise mechanism of the reaction has been questioned, in particular in

relation to the involvement of the nitrene intermediate in the process (*vs.* concerted rearrangement).[32-39]

Recently,[40] we proposed that the thermolysis of 3-azido-3-carboxylate-2-halo-acrylophenones (**1**, in Scheme 1) produces the corresponding 2-benzoyl-2-halo-2*H*-azirine-3-carboxylates (**2**) in a concerted manner, instead of *via* vinyl nitrene intermediate (**3**). This conclusion was extracted taking into account the fact that the final product was the oxazole species (**6**) instead of the isoxazole (**4**), which would be the expected product if the nitrene were formed along the process, either directly from the azide or from the azirine initially formed. The production of the oxazole was in fact initially not expected,[41] since it is generally accepted that 2*H*-azirines react preferentially upon thermal excitation through cleavage of the C-N bond, the required route to the nitrene species,[42-51] whereas thermal cleavage of the C-C bond is less common.[45]

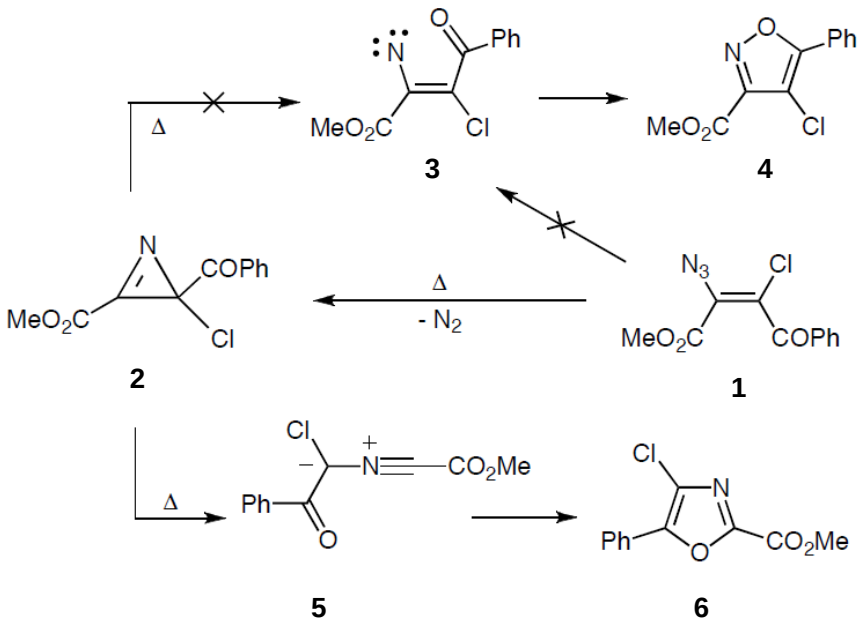

Scheme 1.

On the other hand, photochemical excitation of 2*H*-azirines leads most frequently to the C-C bond cleavage of the azirine ring, yielding the corresponding

nitrile ylides (**5**),[46-53] which are the expected intermediates to the oxazole production. However, photochemical processes involving cleavage of the C-N bond have also been observed upon photolysis of substituted azirines bearing electron- withdrawing substituents in the ring.[48-51,54,55]

In the present study, (Z)-3-azido-(E)-3-methylcarboxylate-2-chloro-acrylophenone (or methyl (Z)-2-azido-3-chloro-3-benzoylpropenoate, MACBP; Figure 1, see Experimental Section) has been chosen as target to further investigation of the mechanism of conversion of 3-azido-acrylophenones into oxazoles. The compound was synthesized and then isolated in cryogenic matrices (Ar, Xe), where its conformational preferences and UV-induced photochemistry were investigated by infrared spectroscopy, supported by DFT calculations. The matrix isolation technique was selected to carry out this study because in a matrix the reactions are cage-confined, since molecular diffusion is inhibited, and no reactions involving molecules initially located in different matrix sites can occur. Hence, only unimolecular reactions are expected to take place in relation with the molecule of the initial reactant, a characteristic that introduces a very useful simplification in the study of photochemical reactivity, in particular in the characterization of the associated reaction mechanisms.

As it will be shown in detail in this paper, upon photolysis ($\lambda > 235$ nm) matrix isolated MACBP evolves to the corresponding azirine (methyl 2-benzoyl-2-chloro-2*H*-azirine-3-carboxylate; MBCAC), which subsequently undergoes ring expansion to the oxazole (methyl 4-chloro-5-phenyl-1,3-oxazole-2-carboxylate; MCPOC). An additional photoproduct resulting from C-N ring cleavage of the initially formed azirine in a concerted Curtius type rearrangement was also observed (*C*-chloro-*C*-benzoyl-*N*-methoxycarbonylketenimine; CBMK). No formation of the isoxazole compound was observed upon photolysis, which supports the conclusion that the vinyl nitrene species is not involved in the conversion of the azide into the azirine, as well as in the subsequent reactions of this latter.

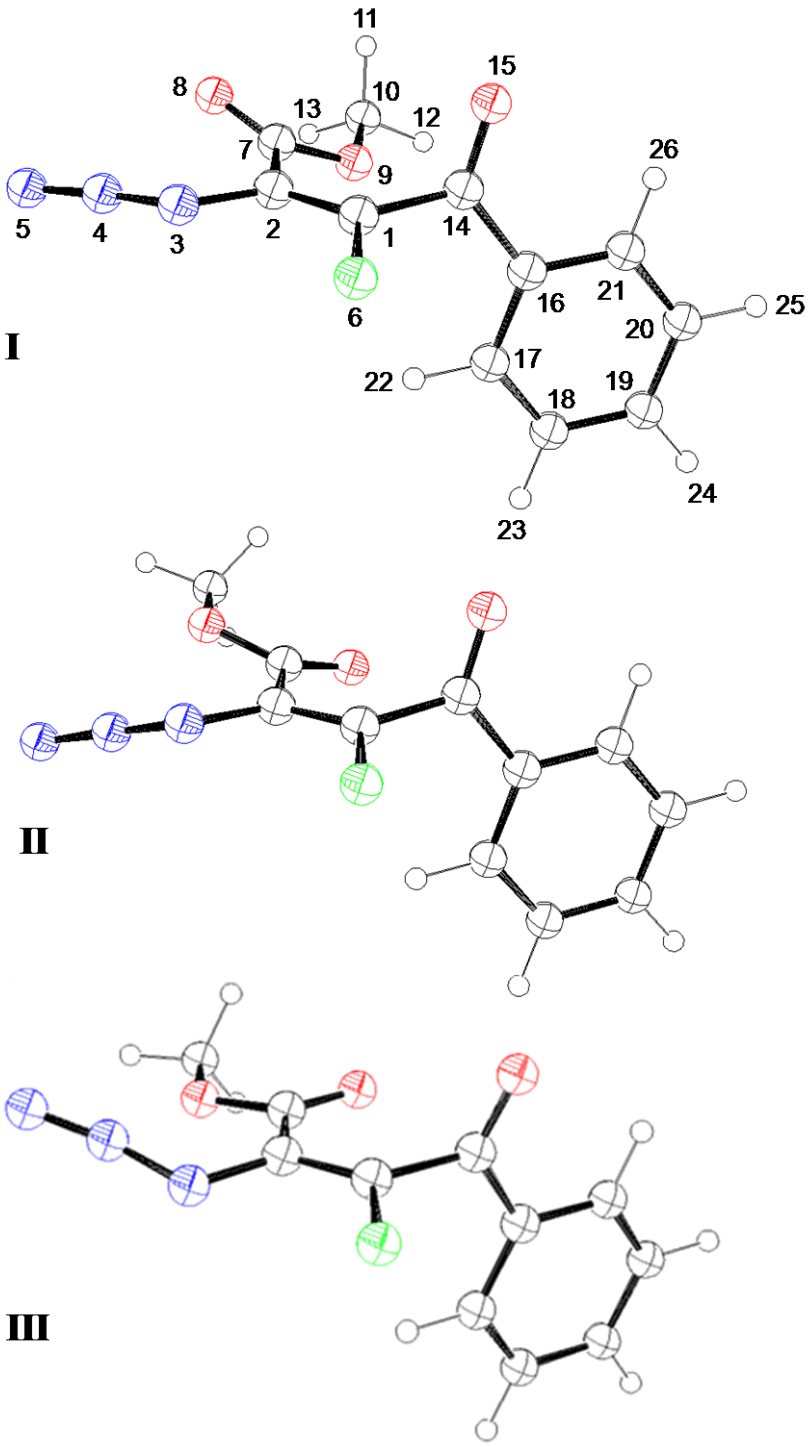

Figure 1. Low energy conformers of MACBP, optimized at the DFT(B3LYP)/6-311++G(d,p) level of theory, with atom numbering. The picture was made using the Ortep-3 for Windows program (Farrugia, L. J. *J. Appl. Cryst.* **1997**, *30*, 565). Atoms color code: carbon, hydrogen: black; nitrogen: blue; chlorine: green; oxygen, red.

Experimental Section

Synthesis of MACBP. (Z)-3-azido-(E)-3-methylcarboxylate-2-chloro-acrylophenone (or methyl (Z)-2-azido-3-chloro-3-benzoylpropenoate, MACBP **1**) was prepared using a known synthetic method procedure (Scheme 3).[39] The 2-(triphenylphosphoranylidene)acetophenone **12**, obtained by reaction of 2-bromoacetophenone **11** and triphenylphosphine **10**, was added to a solution of triethylamine in dry toluene and treated with the appropriated acid chloride to give the methyl 2,4-dioxo-4-phenyl-3-triphenylphosphoranylidenebutanoate **13** almost in a quantitative yield. This ylide **13** reacts with azidotrimethylsilane and N-chlorosuccinimide in dichloromethane to give the crystalline methyl (Z)-2-azido-3-chloro-3-benzoylpropenoate **1** after the purification by column chromatography and crystallization.

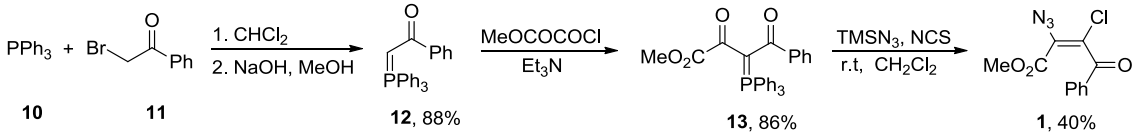

10 **11** **12**, 88% **13**, 86% **1**, 40%

Scheme 3. Synthesis of methyl (Z)-2-azido-3-chloro-3-benzoylpropenoate **1**.

Matrix Isolation Experiments. Matrices were prepared by co-deposition of MACBP vapors coming out from a specially designed thermoelectrically heatable mini-furnace, assembled inside the cryostat (APD Cryogenics, model DE-202A) chamber, and large excess of the matrix gas (argon, N60; xenon, N48, both obtained from Air Liquide) onto a CsI substrate cooled to 10 K (for argon matrices) and 20 K (for xenon matrices). The IR spectra were recorded with 0.5 cm^{-1} spectral resolution in a Mattson (Infinity 60AR Series) Fourier transform infrared spectrometer, equipped with a deuterated triglycine sulphate (DTGS) detector and a Ge/KBr beam splitter. Necessary modifications of the sample compartment of the spectrometer were done in order to accommodate the cryostat head and allow purging of the instrument by a stream of dry nitrogen, to remove water vapors and CO_2.

Irradiation of the matrices was carried out with unfiltered light from a 500 W Hg(Xe) lamp (Newport, Oriel Instruments), with output power set to 200 W, through the outer KBr windows of the cryostat ($\lambda > 235$ nm).

Computational Methods

A systematic preliminary conformational exploration of the MACBP potential energy surface (PES) was performed using the semi-empirical PM3 method[56,57] and the HyperChem Conformational Search module (CyberChem, Inc. © 2004).[58] These calculations provided a quick assessment of the main features of the conformational space of the molecule, which were later on taken into account in the subsequent analysis performed at higher level of theory. Taking into account the high flexibility of the MACBP molecule, a random search appeared as the most appropriate way to perform the conformational search.[59-61] The program generates starting conformations for energy minimization using a random variation of the conformationally relevant dihedral angles obtained for previously located minima.[60,61] The method searches on until no new minima are generated. The same approach was used in the structural studies performed for the conformationally flexible photoproducts of MACBP, specifically the azirine (MBCAC) and ketenimine (CBMK) photoproducts. For all three compounds 30000 initial structures were generated by varying the relevant dihedral angles, and the structures corresponding to the 25 (18 for CBMK) lowest energy unique minima were saved and used as input geometries for the subsequent higher level calculations undertaken with Gaussian 03[62] at the DFT level of theory, using the split valence triple-ζ 6-311++G(d,p) basis set[63] and the three-parameter B3LYP density functional.[64,65] Structures were optimized using the Geometry Direct Inversion of the Invariant Subspace (GDIIS) method.[66,67] Transition states for conformational interconversions were determined at the same level of approximation, with help of the synchronous transit-guided quasi-Newton (STQN) method.[68]

In order to assist the analysis of the experimental infrared (IR) spectra, vibrational frequencies and IR intensities were also calculated at the same level of theory. The computed harmonic frequencies were scaled down by a single factor (0.978) to correct them for the effects of basis set limitations, neglected part of electron correlation and

anharmonicity effects. The nature of stationary points on the potential energy surface was checked through the analysis of the corresponding Hessian matrix.

Normal coordinate analysis was undertaken in the internal coordinates space, as described by Schachtschneider and Mortimer[69] and the optimized geometries and harmonic force constants resulting from the DFT(B3LYP)/6-311++G(d,p) calculations. The internal coordinates used in this analysis were defined following the recommendations of Pulay *et al.*.[70]

Results and Discussion

Molecular structures and relative energies of MACBP conformers. MACBP has four conformationally relevant rotational axes defined by the N_4=N_3–C_2=C_1, O_8=C_7–C_2=C_1, C_{16}–C_{14}–C_1=C_2 and C_{17}–C_{16}–C_{14}–C_1 dihedral angles. The *s-cis* conformation of a methyl ester group (C_{10}–O_9–C_7=O_8 equal to ~0º) is well-known[71-73] to be considerably more stable than the *s-trans* one (C_{10}–O_9–C_7=O_8 equal to ~180º) and only structures with the first type of arrangement were taken into account (*s-trans* methyl ester minima can be expected to be at least 25 kJ mol^{-1} higher in energy than the *s-cis* forms[71-73]). After re-optimizing at the DFT(B3LYP)/6-311++G(d,p) level of theory the structures obtained from the preliminary semi-empirical random conformational search, fourteen different minima were found on the PES of the molecule with relative energies within 19 kJ mol^{-1}. These minima correspond to 7 pairs of equivalent-by-symmetry conformers, all of them belonging to the C_1 symmetry point group. Table 1 displays the predicted relative energies (including zero-point corrections) of these conformers.

According to the calculations, conformers **II** and **III** are 3.95 and 5.40 kJ mol^{-1} higher in energy than the most stable conformer **I** (Figure 1). The remaining forms (conformers **IV** to **VII**; Figure S1 in the Supporting Information) have calculated relative energies at least 12 kJ mol^{-1} higher than that of conformer **I**, and as a whole are predicted to constitute less than 1.0% of the total conformational population in gas phase at room temperature (see Table 1).

Table 1. DFT(B3LYP)/6-311++G(D,P) Calculated Relative Energies (ΔE_0/ Kj Mol^{-1}), Including Zero-Point Vibrational Contributions, and Predicted Relative Populations for the Conformers of MACBP.

Conformer [a]	ΔE_0	Population (%)	
		T= 298 K	T= 323 K
I	0.00	75.3	72.4
II	3.95	15.3	16.6
III	5.40	8.5	9.7
IV	12.73	0.4	0.6
V	14.07	0.3	0.4
VI	15.26	0.2	0.2
VII	18.71	~0.0	0.1

[a] See Figures 1 and S1 (Supporting Information) for structures of the conformers.

The calculated optimized geometries for the three most stable conformers are given in Table S1 (Supporting Information). In the description of the structures of the conformers, the position of the azide (-N=N≡N), carboxylic ester (-$COOCH_3$) and benzoyl (-C_6H_5C=O) groups will be considered in relation to the central C_1=C_2 double bond.

Rotation around the N_3–C_2 bond defines the relative orientation of the azide group in relation to the C_2=C_1 double bond. The calculations show that the orientation of the azide moiety allows us to divide the conformers into two groups: one where the azide is in an almost *trans* orientation, to which the three lower energy conformers belong (**I**, **II** and **III**, where the N_4=N_3–C_2=C_1 dihedral angle is −171.0º, −160.1 and +155º, respectively), and the other where the azide in an nearly *cis* orientation (N_4=N_3–C_2=C_1 dihedral angle of *ca.* ±40º), to which the higher energy conformers (**IV**-**VII**) belong. The higher energy of conformers **IV**-**VII** can then be associated with unfavorable interactions between the closely located azide and chlorine substituents in these forms.

The carboxylic ester group can be arranged in a *cis* (O_8=C_7–C_2=C_1 ~0º) or *trans* (O_8=C_7–C_2=C_1 ~180º) orientation towards the central double bond, while the benzoyl group exhibits a quasi-planar configuration and assumes a nearly perpendicular geometry in relation to the main molecular plane in all conformers. Among the three most stable conformers (see Figure 1), conformer **I** presents the unique arrangement of its carboxylic ester in the *trans* orientation relative to the C_2=C_1 bond, while in **II** and **III** this group adopts the *cis* arrangement. For the higher energy conformers, the

carboxylic ester group is *cis* in conformers **IV** and **VI** and *trans* in conformers **V** and **VII**.

According to calculations, repulsive interactions between the azide and carboxylic ester groups should be considered the main factor determining the relative stability of the three lower energy conformers of MACBP. In conformer **I**, it is the carbonyl oxygen (O_8) which interacts with the azide group, whereas in conformers **II** and **III** the interaction involves the methoxyl oxygen atom (O_9). The calculated atomic polar tensor (APT) charges[74] for the three conformers are shown in Table 2. From this table, it can be noticed that O_9 is more negatively charged than O_8, so that the $N_3 \cdots O_9$ electrostatic repulsion in **II** and **III** is more important than the $N_3 \cdots O_8$ electrostatic repulsion in **I**. In addition, the $N_3 \cdots O_{8/9}$ contact distances decrease in the order **I** (285.8 pm) > **II** (276.7 pm) > **III** (275.5 pm), also contributing to make the $N_3 \cdots O_{8/9}$ repulsive electrostatic interaction more important in the order **III** > **II** > **I**.

Table 2. DFT(B3LYP)/6–311++G(D,P) Calculated Atomic Polar Tensor (APT) Charges on Atoms (With Hydrogens Summed Into Heavy Atoms) for Conformers I, II and III of MACBP.[a]

	APT charges/ *e*		
Atom	**I**	**II**	**III**
C_1	0.117	0.182	0.218
C_2	0.249	0.205	0.176
N_3	–0.905	–0.883	–0.882
N_4	1.164	1.127	1.130
N_5	–0.618	–0.617	–0.616
Cl_6	–0.314	–0.304	–0.298
C_7	1.196	1.236	1.233
O_8	–0.746	–0.715	–0.729
O_9	–0.818	–0.911	–0.897
C_{10}	0.465	0.483	0.482
C_{14}	1.208	1.210	1.192
O_{15}	–0.789	–0.800	–0.798
C_{16}	–0.339	–0.342	–0.332
C_{17}	0.068	0.110	0.103
C_{18}	–0.051	–0.052	–0.046
C_{19}	0.061	0.061	0.058
C_{20}	–0.052	–0.055	–0.052
C_{21}	0.104	0.065	0.058

[a] See Figure 1 for atom numbering. $1e = 1.60217646 \times 10^{-19}$ C.

It is interesting to point out that the crystal structure determined by X-ray diffraction of the analogous bromo-substituted compound, methyl (Z)-2-azido-3-bromo-3-benzoyl-propenoate[41] bears great similarity to the second stable conformer (**II**) of MACBP. In the bromo-substituted molecule, the $N_4=N_3-C_2=C_1$, $O_8=C_7-C_2=C_1$ and $C_{16}-C_{14}-C_1=C_2$ dihedral angles were found to be −162.7(6)º, 14.4(10)º and −102.0(10)º, which can be compared with the values for the same dihedral angles calculated for conformer **II** of MACBP (−160.1º, 19.6º and −106.6º, respectively).

Matrix isolation infrared spectra of as-deposited matrices. As shown in the previous section, the calculations predicted three experimentally relevant conformers of MACBP in gas phase: conformers **I**, **II** and **III**, with estimated relative energies of 0.0, 3.95 and 5.40 kJ mol^{-1}, respectively. At the sublimation temperature used to prepare the cryogenic matrices (T= 323 K) the estimated gas phase equilibrium Boltzmann populations are 72.4%, 16.6% and 9.7% (see Table 1). The combined populations of the higher energy conformers (**IV**-**VII**) are 1.3 % and therefore these forms are of no practical interest for our study.

Another important piece of information for interpretation of the matrix-isolation experimental spectroscopic results described in this section is the knowledge of the energy barriers for interconversion between the conformers whose abundance in the gas phase prior to deposition is significant. This is because when a higher energy conformer is separated from a lower energy form by a small barrier (of a few kJ mol^{-1}) the higher energy form can be converted into the lower energy form during matrix deposition, since the thermal energy available in the gaseous beam might be enough to allow surpassing of the barrier during the landing of the molecules onto the cold substrate of the cryostat (conformational cooling effect[75-82]). The energy barrier between **III**→**II** was indeed found to be extremely low, amounting only to *ca.* 0.03 kJ mol^{-1} (1.4 kJ mol^{-1} in the opposite direction), indicating that conformer **III** shall relax into conformer **II** during matrix deposition. On the other hand, the energy barrier separating forms **I** and **II** is ~15 kJ mol^{-1} (for **II**→**I**; *ca.* 19 kJ mol^{-1} in the reverse direction). With an energy barrier of this magnitude, the **II**→**I** conversion cannot occur during deposition of the matrices at the deposition temperatures used (10-20 K)[75-82], so that we can expect experimental observation of both conformers **I** and **II** in the matrices, the latter with a population equal to the sum of the populations

of conformers **II** and **III** in the gas phase before deposition. The expected **I**:**II** population ratio in the matrices is then 72.4 : 26.3, *i.e.*, nearly 3:1.

Figure 2 shows the infrared spectra of MACBP isolated in both solid argon and xenon (as-deposited matrices; nozzle temperature 50 ºC, substrate temperature: argon, 10 K, xenon, 20 K), together with the calculated spectra for conformers **I** and **II** and the simulated spectrum of the predicted conformational mixture in the matrices assuming the relative abundances equal to 72.4 : 26.3. In the simulated spectra, bands were represented by Lorentzian functions centered at the calculated wavenumbers (scaled by 0.978) and with fwhm (full width at half maximum) equal to 2 cm^{-1} (see Experimental Section for methodology used in the matrix isolation experiments).

The spectra obtained in argon and xenon matrices look very similar and they are generally well reproduced by the simulated spectrum. The proposed assignments for the fundamental bands are given in Table 3. MACBP has 72 fundamental vibrations, all of them active in the infrared. The definition of the internal coordinates adopted in the performed vibrational analysis is provided in Table S2 (Supporting Information). The calculated wavenumbers, infrared intensities and potential energy distributions resulting from normal mode analysis carried out for the two experimentally relevant conformers are presented in Tables S3 and S4 (Supporting Information).

Due to the similarity of the spectra of the two conformers, secure assignment of bands to a unique conformer is not possible, except in the 1270-1230 cm^{-1} spectral range, where the calculations predict a different pattern for the spectral profile of the two forms (see Figure 2). Besides the azide anti-symmetric stretching band observed as an intense band at ~2130 cm^{-1} (both in argon and xenon), the bands in the 1270-1230 cm^{-1} range are the most intense of the spectra. These bands are due to the νC–O ester (also with some contribution from the stretching of the adjacent C–C bond; notated as $\nu C–C_{\alpha}$ E in Table 3) and $\nu C_{14}–C_{16}$ (designated as $\nu C–C_{Ph}$ in Table 3) stretching modes. The higher frequency band, observed in argon matrix at 1267/1261 cm^{-1} (1268/1262 cm^{-1} in xenon) is due to the ester νC–O stretching in conformer **I**, which is predicted to occur at 1251 cm^{-1} with an intensity of 324.0 km mol^{-1} by the calculations. The middle band observed in this region (1251 cm^{-1} in argon and 1249 cm^{-1} in xenon) is due to the same mode in conformer **II**, where it is predicted by the calculations to occur at 1238 cm^{-1} with an intensity of 595.2 km mol^{-1}. The lower

frequency band (1240 cm^{-1} in argon; 1237 cm^{-1} in xenon) results from the absorption of the νC_{14}–C_{16} stretching mode in the two conformers. This last vibration is predicted at 1231 cm^{-1} with an intensity of 413.1 km mol^{-1} in form **I**, and at 1230 cm^{-1} with an intensity of 141.9 km mol^{-1} in form **II**, so that the predominant contribution to the band is due to conformer **I**.

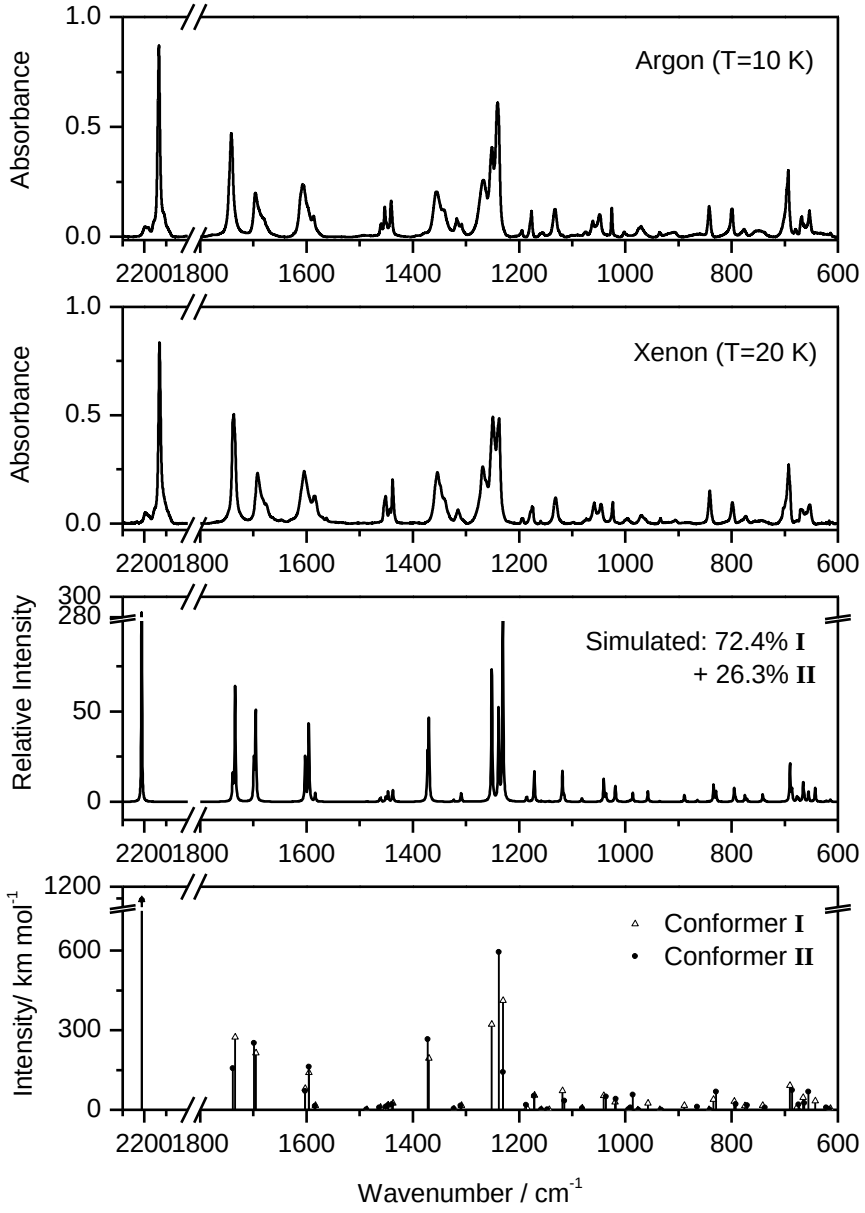

Figure 2. ***Top*** (two panels): Infrared spectra of MACBP isolated in solid argon and xenon (as-deposited matrices; temperature of the deposited vapor: 323 K; substrate temperature during deposition: argon, 10 K, xenon, 20 K); ***Bottom:*** DFT(B3LYP)/6-311++G(d,p) calculated infrared spectra of MACBP conformers shown as stick spectra (wavenumbers scaled by 0.978): **I** (open triangles, △) and **II** (black circles, ●); ***Middle:*** simulated spectrum of the expected gas phase equilibrium conformational mixture at 323 K, built by adding the calculated spectrum of conformers **I** and **II** with intensities scaled by their predicted populations (72.4% for conformer **I** and 26.3% for conformer **II**; see text). In the simulated spectra, bands were represented by Lorentzian functions centered at the calculated wavenumbers (scaled by 0.978) and with fwhm (full width at half maximum) equal to 2 cm^{-1}.

Table 3. Experimental (Matrix-Isolation) and Calculated Vibrational Data for MACBP with Vibrational Assignments Based on the Results of Normal Coordinate Analysis.[a]

Experimental		Calculated				
Ar matrix	Xe matrix	Conformer **I**		Conformer **II**		Approximate description[b]
ν	ν	ν	I_{IR}	ν	I_{IR}	
3109	3101	3129	7.8	3131	7.2	ν(C-H5); ν(C-H1)
3095/3093	3087	3124	7.4	3123	8.6	ν(C-H1); ν(C-H4)
3074/3068	3064	3115	15.5	3115	18.2	ν(C-H4); ν(C-H5)
3042	3037	3107	5.6	3107	5.5	ν(C-H2)
3038	3030	3100	6.9	3100	8.5	νCH_3 as´
		3097	0.1	3097	0.2	ν(C-H3)
3021/3012	3001	3067	10.0	3067	11.2	νCH_3 as´´
2967/2964	2951	2991	24.1	2991	25.2	νCH_3 s
2158/2134/2109	2153/2130	2213	981.7	2212	972.7	ν(N=N) as
1746 sh/1742/1740	1739/1737/1735 sh	1734	274.2	1739	156.0	ν(C=O) E
1697/1689/1679	1692/1684/1676	1696	214.9	1699	252.4	ν(C=O) Ph
1611/1607	1610	1603	81.2	1603	71.2	νPh3
1605/1597	1604	1596	140.3	1595	162.4	ν(C=C)
1589/1586	1585/1582	1583	16.5	1584	14.7	νPh4
1492	1491	1486	0.8	1487	0.9	δ(C-H2)
1461 (**II**); 1459 (**I**)	1455/1453 (**II**); 1451 (**I**)	1461	10.6	1463	8.7	δCH_3 as´
1453/1449	1443	1451	7.5	1451	10.8	δCH_3 as´´
		1447	18.3	1447	16.8	νPh6, δ(C-H3)
1442/1441/1439 sh	1438/1436 sh	1437	25.2	1439	21.5	δCH_3 s
1356/1341	1353/1348/1341	1370	194.6	1372	265.6	ν(N=N) s
1317/1315	1315	1323	3.5	1323	3.8	δ(C-H1)
1311/1307	1311	1309	17.2	1310	16.3	νPh2
1267/1261 (**I**); 1251 (**II**)	1268/1262 (**I**); 1249 (**II**)	1251	324.0	1238	595.2	ν(C-O), ν(C-C_α) E
1240	1237	1231	413.1	1230	141.9	ν(C-C_{Ph})
1194	1194/1192	1185	8.5	1186	18.9	γCH_3´
1180/1177	1178/1175/1174	1171	55.2	1172	52.4	δ(C-H4)
1158/1156/1155	1159	1159	1.5	1158	1.0	δ(C-H5)
.	.	1144	1.7	1147	0.9	γCH_3´´
1132	1131	1119	72.5	1115	33.5	ν(C-O), ν(O-CH_3)
1074	1073	1082	6.7	1082	5.5	νPh6
1061 (**I**); 1047 (**II**)	1059 (**I**); 1045 (**II**)	1041	53.7	1036	50.5	νPh5, ν(C-C)
1026	1023	1019	29.2	1018	40.6	νPh1
		994	1.1	994	1.1	δPh1
1002/998	1000/996	992	0.1	990	8.6	γ(C-H5)
		977	0.6	975	0.2	γ(C-H4)
		-	-	986	57.4	ν(O-CH_3)
975/971 (**I**)	969/962 (**I**)	958	26.1	-	-	ν(O-CH_3)
935	934	935	1.3	933	0.2	γ(C-H3)
918 (**I**); 906 (**II**)	910 (**I**); 906 (**II**)	889	16.5	865	12.1	ν(C-Cl)
842	841	843	0.8	841	0.5	γ(C-H2)
						δ(C=O), ν(C-N);
		834	40.1	829	67.7	ν(C-N)
799/798	798/796	795	33.1	792	20.7	γ(C=O)
783/776	780/773	775	15.4	771	17.6	γ(C=O) E
746	746	742	17.3	737	8.5	γ(C=O) E, δ(OCO); γ(C=O) E, ν(C-Cl)
702/697/693	702/692/689	690	91.9	686	74.4	γ(C-H1)
679	677	677	11.9	674	20.6	τPh1
668/665/663	670/666/662	665	46.3	664	25.4	δPh3; δ(NNN), δ(OCO)
659 (**II**)	660/659 (**II**)	-	-	655	68.6	δ(NNN)
653 (**I**)	653 (**I**)	643	33.7	-	-	δPh3
621	622	617	0.4	622	8.1	δPh2; δ(CCC_{Ph}), γ(C-Cl)
614/610	613/610	614	5.1	616	2.4	γ(C-Cl); δPh2
530	526	516	4.0	522	7.5	γ(NNN)

[a] Wavenumbers (cm^{-1}, scaled by 0.978), calculated intensities (km mol^{-1}). [b] In the approximate description, the symbol ";" separates the description for **I** and **II**, when they are different, while "," indicates that the approximate description for a given mode has more than one relevant contributing coordinate; ν, bond stretching, δ, bending, γ, rocking, τ, torsion, s, symmetric, as, asymmetric, Ph, phenyl ring, E, ester; sh, shoulder, n.obs., not observed. See Table S2 (Supplementary Information) for definition of internal coordinates and Tables S3 and S4 (Supplementary Information) for potential energy distributions.

Very interestingly, compared with the simulated spectrum, the intensity of the νC–O stretching band of form **II** appears larger in the experimental spectra in relation to both the νC–O stretching band of form **I** and that assigned to $\nu C_{14}–C_{16}$ stretching mode (which, as stated above, has also a predominant contribution of this latter conformer). Furthermore, the relative intensification of the band due to conformer **II** is greater in the spectrum obtained in xenon than in argon (see Figure 2). These observations cannot be interpreted as an indication of partial conversion of **I** into **II** during deposition of the matrices, since the calculated barrier is large enough to prevent this isomerization and, more importantly, if any isomerization between these two conformers could take place (*e.g.*, in case the isomerization barriers in the matrices were much smaller than in gas phase), this would have to occur exactly in the opposite direction, *i.e.*, the less stable conformer **II** would have to be converted into the most stable form **I**. Moreover, this hypothetical conversion would have to occur in larger extent during deposition of the xenon matrix than during deposition of the argon matrix, both because xenon is well-known to be a better matrix medium for conformational cooling to take place than argon, and because the temperature of the cold window of the cryostat was kept at a higher temperature in the xenon experiments than in the argon ones.[75-82] Experimental observations show exactly the opposite trend, thus requiring a different explanation.

According to the calculations, the C–O ester bond is highly polarized in both conformers (see Table 2). However, it is considerably more polarized in conformer **II**, since the positive charge in the C_7 is larger in this form and the charge in O_9 is also more negative in conformer **II** than in **I**. These results are in agreement with the calculated relative infrared intensities of the νC–O bands: intense bands are predicted for this mode in both conformers, but the intensity in conformer **II** (595.2 km mol^{-1}) is almost twice that in conformer **I** (324.0 km mol^{-1}). This means that the C–O ester bond in **II** is also more sensitive to the polarizability of the media than the same bond in conformer **I**, being additionally polarized in greater extent in more polarizable media. Consequently, the relative infrared intensities of the νC–O stretching modes in conformer **II** compared to form **I** can be expected to grow in the order: gas phase < argon matrix < xenon matrix, as observed experimentally.

Assignment of a few other less intense bands to a single conformer was also attempted and is presented in Table 3, but they must be considered as tentative, *e.g.*,

bands ascribed uniquely to the less stable conformer (**II**) at 1461 (δCH_3 as´), 1047 [phenyl ring stretching vibration (δPh5, as defined in Table S2) mixed with $\nu(C_1–C_{14})$], 906 [ν(C–Cl)] and 659 cm^{-1} [δ(NNN)] in argon, which in xenon appear at 1455/1453, 1045, 906 and 660/659 cm^{-1}, respectively.

Photochemistry of matrix-isolated MACBP. Upon *in situ* broadband UV irradiation (λ > 235 nm) of matrix-isolated monomeric MACBP, a significant decrease in the intensity of the bands of the compound was observed, while new bands due to photoproducts emerged. These changes were already clearly visible after 10 min of irradiation, whereas more than 90% of the original compound was consumed after 450 minutes of irradiation of both argon and xenon matrices (see Experimental Section for methodology used in the matrix isolation experiments). Analysis of the kinetical profiles of the bands appeared upon photolysis provided essentially two distinct patterns: a) a set of bands starting to grow in the early stages of irradiation and then decreasing of intensity, and b) the remaining bands starting to noticeably increase of intensity later on and in a continuous way. This behavior is shown in Figures 3, which presents the infrared difference spectrum of the irradiated Xe matrix of MACBP obtained subtracting the spectrum after 40 min of irradiation from that collected after 690 min of irradiation (before subtraction, residual bands due MACBP were subtracted from the spectra of the irradiated matrix). Bands pointing down in this spectrum correspond to the initially formed species, while those pointing up are due to photoproducts appearing at a later stage of irradiation. Results obtained upon irradiation of the argon matrix were qualitatively identical (see Figure S3 in the Supporting Information).

It can be seen in both Figures 3 and S3 that the spectrum of the initial photoproduct fits well that theoretically predicted for the postulated azirine, methyl 2-benzoyl-2-chloro-2*H*-azirine-3-carboxylate (MBCAC; **2**), while the set of bands corresponding to the species formed later on can be well reproduced by consideration of possible photoproducts of this latter compound, specifically, the oxazole derivative, methyl 4-chloro-5-phenyl-1,3-oxazole-2-carboxylate (MCPOC; **6**) and the ketenimine *C*-chloro-*C*-benzoyl-*N*-methoxycarbonylketenimine (CBMK; **7** in Scheme 2). No formation of the isoxazole derivative was observed upon photolysis, which supports

the conclusion[40] that the vinyl nitrene species is not involved in the generation of ketenimine **7**, which with all probability, is obtained from the starting azide *via* a Curtius type concerted rearrangement. Thus, the formation of 2*H*-azirine **2** and keteimine **7** are competitive processes, being the former a more favourable process, since with a short time of irradiation only the 2*H*-azirine is detected.

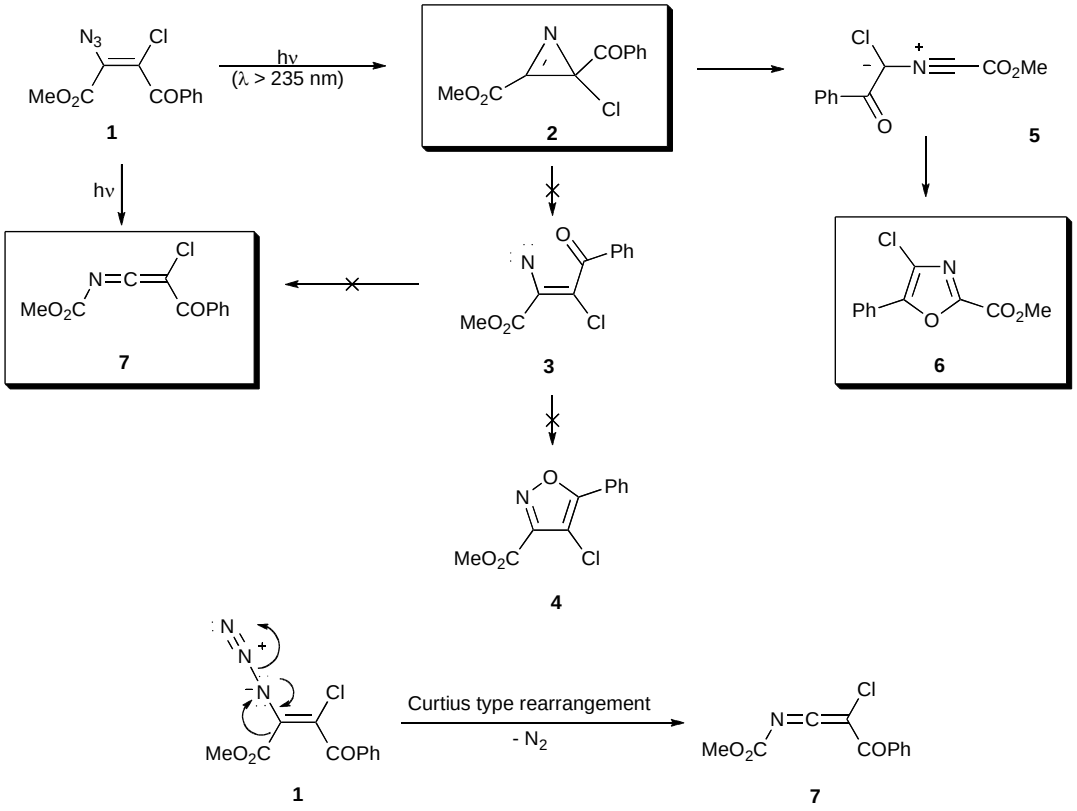

Scheme 2.

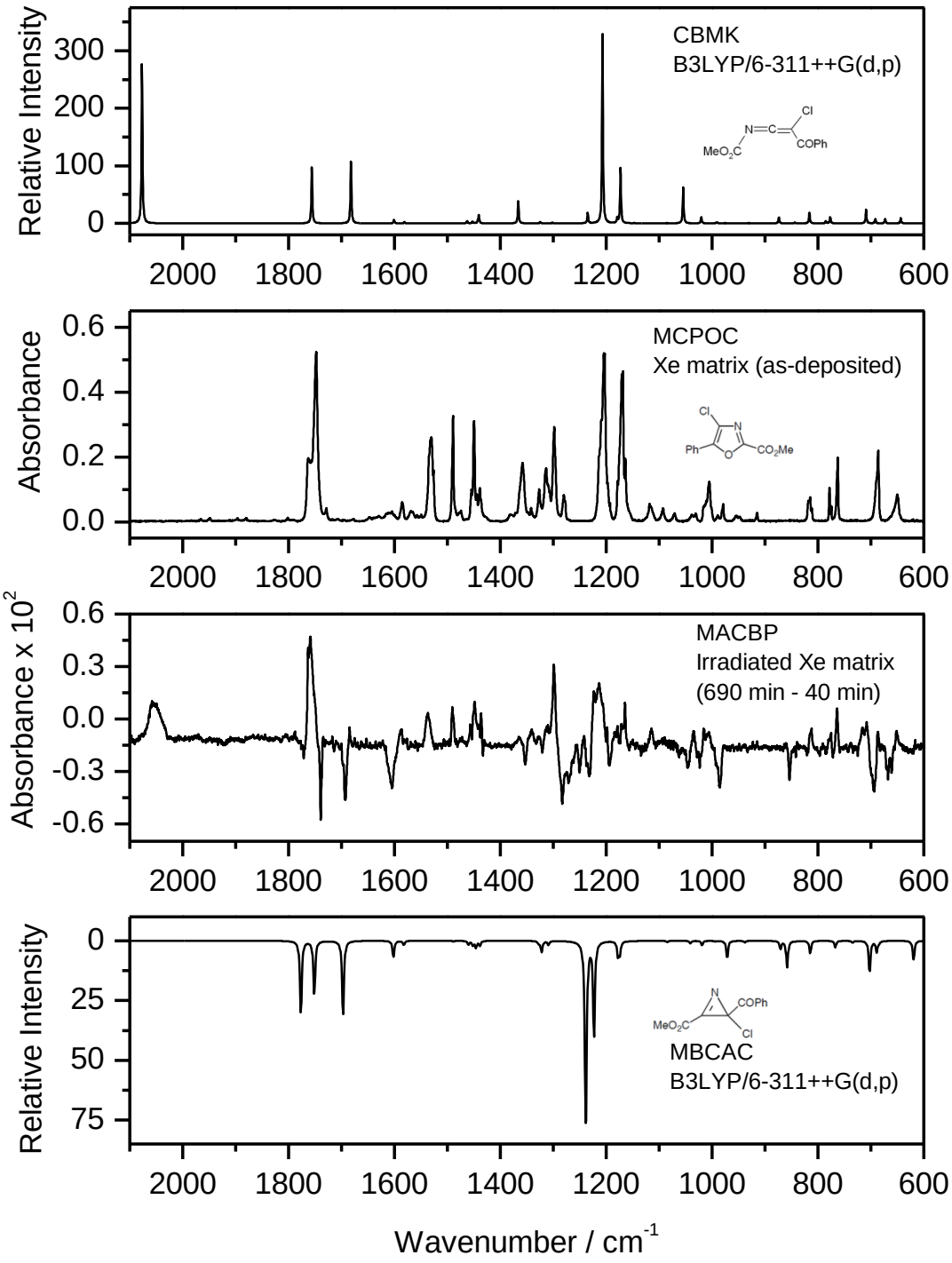

Figure 3. ***Top*****:** Simulated IR spectrum of CBMK (most stable conformer); ***Middle top:*** IR spectrum of MCPOC in xenon matrix (as deposited; 20 K); ***Middle bottom*****:** IR difference spectrum of irradiated Xe matrix of MACBP (λ> 235 nm irradiated matrix during 690 min *minus* λ> 235 nm irradiated matrix during 40 min; before subtraction, residual bands due MACBP were subtracted from the spectra of the irradiated matrix); ***Bottom:*** simulated IR spectrum of MBCAC (most stable conformer). In the simulated spectra, bands were represented by Lorenztian functions centered at the DFT(B3LYP)/6-311++G(d,p) calculated wavenumbers (scaled by 0.978) and with fwhm (full width at half maximum) equal to 2 cm^{-1} (in case of MBCAC, the spectrum was multiplied by –1).

Table 4 – Vibrational assignments of the bands observed in the UV irradiated matrices of MACBP.[a]

Irradiated MACBP Ar matrix	Irradiated MACBP Xe matrix				Approximate description[b]
MCPOC		Ar matrix		Xe matrix	
ν	ν	ν		ν	
1764/1760/1753	1763/1758/1751	1769/1763/1751/1750		1763/1759/1748	ν(C=O)
1541/1536/1530	1537	1541/1530		1535/1532/1529	νOx1
1492	1490/1488	1492/1487		1489	δ(C-H2)
1478/1472	1474	1479		1478/1474	δCH_3 as´
1456	1456	1460		1455	δCH_3 as´´
1450	1451/1448	1453/1452/1451/1450		1450/1444	δ(C-H3)
1447	1443	1442		1439/1436	δCH_3 s
1360/1358	1364/1340	1360/1358/1346		1361/1341	δ(C-H1); νPh2
1317/1313/1300	1313/1310/1298	1332-1300		1330-1302	νOx2; ν(C-C_α)
1226-1198	1223/1199	1215-1202		1213-1197	ν(C-C_{IR}); ν(C-O); γCH_3´
1173/1168	1171/1163	1174/1172/1168/1166		1174/1170/1168/1163	γCH_3´; ν(C-O)
1118	1114	1117		1118/1114/1110/1109	νOx5
1093/1085	1089	1096/1094		1095/1092/1090	νPh6
1034	1034	1041/1033		1038/1031/1027	νPh5
1018/1008	1015/1006	1020/1016/1008/1006		1016/1007/1005	δOx1
977	977	981		980	νPh1
814	813	817/815		815/512	δ(OCO)
778	776	781/778		778/775	γ(C=O)
765	762	765		762	γ(C-H1)
690		691		690	δPh3
688	686	689/688/687		686	τOx1
653	651	652		650/648	τOx2
MBCAC		Calculated			
ν	ν	ν[c]	I		
1776	1772	1777	188.4		ν(C=N) A
1742	1740	1752	144.7		ν(C=O) E
1706/1696	1694	1697	193.8		ν(C=O)
1608	1604	1602	42.6		νPh
	1584	1582	11.0		νPh
1464	1463	1460	9.5		δCH_3 as´´
1454	1454	1452	11.3		δCH_3 as´
1444	1442	1446	18.2		δ(C-H) Ph
1438	1432	1439	12.8		δCH_3 s
1322	1320	1322	29.8		ν(C-C) A
1285	1283/1270/1262	1239	501.6		ν(C-C_{Ph})
1254/1244/1234	1251/1236/1232	1223	244.3		ν(C-O)
1195	1194.	1178	38.2		δ(C-H) Ph
1181	1175	1174	32.8		γCH_3´
1047	1045	1041	7.3		ν(C-C(=O)); δ(C-H) Ph
1029/1025	1027/1021	1019	11.9		δPh
990	975	971	44.9		ν(O-CH_3)
862		871	20.3		ν(C-N) A
854	854	858	70.6		ν(C-Cl)
	819	815	33.0		δ(OCO)
785/773	784/771	767	17.7		γA-E
724	724	735	4.8		γ(C=O) E
702/694	694	702	81.1		γ(C-H) Ph
668/661	667/660	689	29.5		δPh
	623	619	51.1		δ(CC=O)
CBMK		Calculated			
ν	ν	ν[c]	I		
2059	2055	2077	875.3		νC=C=N as
1764	1763	1756	311.6		ν(C=O) E
1680	1685	1682	350.9		ν(C=O)
	1588	1601	19.5		νPh
1440	1440	1441	45.7		δCH_3 s
1378	1366	1366	123.2		νC=C=N s
1238	1242	1235	56.7		ν(C-C_{Ph})
[d]	[d]	1207	1042.2		ν(C-O)
1187	1184/1178	1173	304.8		γCH_3´
1067		1055	198.1		ν(C-C(=O)); δ(C-H) Ph
	823	816	60.3		ν(C-Cl)
718/711	715/708	709	76.9		γ(C-H) Ph
680	678	673	23.5		δPh
643	643	643	28.7		δ(CC=O); γ(C=C=N)

[a] Wavenumbers (ν) in cm^{-1}, calculated intensities (I) in km mol^{-1}, ν, bond stretching, δ, bending, γ, rocking, τ, torsion, s, symmetric, as, asymmetric, Ox, oxazole ring, Ph, phenyl ring, A, azirine ring; E, ester, IR, inter-rings. [b] Approximate descriptions for MCPOC as in ref 83. [c] Scaled wavenumbers (0.978). [d] buried within the profile due to MCPOC bands.

The assignments of the bands due to the photoproducts are presented in Table 4. It is worth mentioning that the spectrum of the photoproduced oxazole (MCPOC) in both argon and xenon matrices is well-known,[40,83] so that the identification of this compound in the irradiated MACBP matrices was doubtless and band assignment followed that presented before.[83] For example, bands at 1764/1760, 1753, 1541/1536/1530, 1492, 1300 and 1173/1168 cm^{-1}, in argon, with counterparts at 1763/1758, 1751, 1537, 1490/1488, 1298 and 1171/1163 cm^{-1}, in xenon, respectively, are intense characteristic bands of MCPOC.[83] On the other hand, for both the azirine and ketenimine species no experimental data for the matrix isolated compounds were reported hitherto, so that their identification and band assignments were based on the comparison with theoretically predicted spectra obtained at the DFT(B3LYP)/6-311++G(d,p) level of theory and on data for other molecules of the same families.[50,51,84-94] Moreover, these two compounds have conformationally flexible molecules and, according to the structural calculations performed on these species, several low energy conformers exist in both cases. For the azirine, the calculations predicted the existence of five different conformers with relative energies within 10 kJ mol^{-1}. In the case of the ketenimine, the calculations yielded seven conformers with relative energies within the same limit. Nevertheless, the calculated infrared spectra of all low-energy forms predicted theoretically for each molecule were found to be quite similar, thus facilitating their experimental identification and band assignments. Figure 3 (and Figure S3, in Supporting Information) show only the spectra corresponding to the most stable conformer of each molecule, MBCAC and CBMK (see Figure S2 for structures of these forms), while the calculated data for these molecules shown in Table 4 also belong only to their most stable forms.

Among the bands ascribed to MBCAC (see Table 4) the most intense ones were observed at 1776, 1742, 1706/1696, 1608, 1285, 702/694 and 668/661 cm^{-1} in argon (1772, 1740, 1694,1604, 1283/1270/1262, 694 and 667/660 cm^{-1} in xenon), corresponding to the ν(C=N) stretching of the azirine ring, ν(C=O) stretchings in ester and benzoyl fragments, the highest frequency stretching mode of the phenyl group, the stretching vibration of the C-C_{Ph} bond, and the all in phase rocking out-of-plane C-H deformation and a skeletal deformational mode of the phenyl group, which were predicted to occur at 1777, 1752, 1697, 1602, 1239, 702 and 689 cm^{-1}, respectively. The most characteristic band of CBMK was observed at 2059 cm^{-1} (argon) and 2055

(xenon) cm^{-1}, and is ascribed to the ketenimine νC=C=N antisymmetric stretching mode.[48-51,54,55]

In the present study, among the species predicted to take part in the azide→oxazole photochemical conversion (see Scheme 1), only the nitrile ylide **5** could not be doubtlessly observed, indicating that for the system under study this species is a quite unstable intermediate, which is promptly converted to the oxazole. The intrinsically strong band in infrared due to the antisymmetric stretching of the $CN^{+}C^{-}$ moiety of a nitrile-ylide appears usually at a characteristic frequency of about 1950 cm^{-1}.[48,49,54,55] In both the infrared spectra of the photolyzed argon and xenon matrices of MACBP, the presence of such band could not be confirmed.

Conclusions

The 3-azido-acrylophenone MACBP (or methyl (Z)-2-azido-3-chloro-3-benzoyl-propenoate) has been shown to be a photochemical precursor of the related oxazole, methyl 4-chloro-5-phenyl-1,3-oxazole-2-carboxylate (MCPOC), in a reaction where the azirine and nitrile ylide work as intermediates. This reaction is accompanied by a second one leading to formation of the ketenimine *C*-chloro-*C*-benzoyl-*N*-methoxycarbonylketenimine (CBMK). The non-observation of the corresponding isoxazole points to the concerted nature of the different steps leading to the observed final products. This also supports the idea that in the studied system the putative vinyl nitrene intermediate is not involved in the conversion of the azide into the azirine, as well as in the subsequent reactions of this latter.

MACBP was synthesized, isolated in low temperature argon and xenon matrices and structurally and vibrationally characterized by infrared spectroscopy and quantum chemical calculations before execution of the photochemical studies. Seven different low energy conformers were found on the DFT(B3LYP)/6-311++G(d,p) PES, with the 3 lower energy forms (which correspond to the conformers predicted to have significant populations in the gas phase equilibrium at the sublimation temperature required to produce the cryogenic matrices) showing an orientation of the azide group in a nearly *trans* orientation. In the matrix isolation experiments, however, only the two most stable conformers of the compound (**I** and **II**) were observed, whereas conformer **III** was found to be totally converted into conformer **II**

during deposition of the matrices, a result that is in consonance with the very low energy barrier associated with the **III**→**II** conversion (*ca.* 0.03 kJ mol^{-1}).

Acknowledgements

These studies were partially funded by the Portuguese Science Foundation (Project No. FCOMP-01-0124-FEDER-007458, cofunded by QREN-COMPETE-UE), CYTED Program (Iberoamerican Program for the Development of Science and Technology) [Network 108RT0362]. S. Lopes and C. M. Nunes acknowledge FCT for Grants No. SFRH/BD/29698/2006 and SFRH/BD/ 28844/2006. AGZ is member of the Research Career, Conicet (National Research Council, Argentina).

Supporting Information Available:

Additional figures with schematic representations of the four higher energy conformers of MACBP and the low energy conformers of MBCAC and CBMK; tables with optimized geometries, IR spectroscopic data of the or the two most stable, experimentally relevant conformers of MACBP (forms **I** and **II**). Cartesian coordinates and absolute energies for the relevant forms calculated and discussed. This material is available free of charge via the Internet at …

References:

[1] Bräse, S.; Baneet, K. (Eds.), *Organic Azides, Syntheses and Applications*, John Wiley & Sons Ltd, U.K., 2010.

[2] Patai, S. (Ed.), *The Chemistry of the Azido Group*, Wiley, New York, 1971.

[3] Scriven, E. F. V.; Turnbull, K. *Chem. Rev.* **1988**, *88*, 297.

[4] Bräse, S.; Gil, C.; Knepper, K.; Zimmerman, V. *Angew. Chem. Int. Ed.* **2005**, *44*, 5188.

[5] Fotsing, J. R.; Banert, K. *Synthesis* **2006**, *2*, 261.

[6] Maurus, R.; Bogumil, R.; Nguyen, N. T.; Mauk, A. G.; Brayer, G. *Biochem. J.* **1998**, *332*, 67.

[7] Canalle, L. A.; Löwik, D. W. P. M.; Hest, J. C. M. *Chem. Soc. Rev.* **2010**, 39, 329.

[8] Pathak, T. *Chem. Rev.* **2002**, *102*, 1623.

[9] Greenberg, W. A.; Priestley, E. S.; Sears, P. S.; Alper, P. B.; Rosenbohm, C.; Hendrix, M.; Hung, S.-C.; Wong, C.-H. *J. Am. Chem. Soc.* **1999**, *121*, 6527.

[10] Hein, C. D.; Liu, X.-M.; Wang, D. *Pharmaceut. Res.* **2008**, *25*, 2216.

[11] Colombo, M.; Peretto, I. *Drug Discov. Today* **2008**, *13*, 678.

[12] Reddy, N. N.; Mohan, Y. M.; Varaprasad, K.; Ravindra, S.; Vimala, K.; Raju, K. M. *J. Appl. Polym. Sci.* **2010**, *115*, 1589.

[13] Lakshmi, S.; Kumar, S. S.; Jayakrishnan, A. *J. Biomed. Mater. Res.*, **2002**, *61*, 26.

[14] Nájera, C.; Sansano, J. M. *Org. Biomol. Chem.* **2009**, *7*, 4567.

[15] Huisgen, R. *1,3-Dipolar Cycloaddition Chemistry*, (Ed.: A. Padwa), Wiley, New York, 1984, Vol. 1, p. 1–176.

[16] Lutz, J.-F. *Angew. Chem. Int. Ed.* **2007**, *46*, 1018.

[17] Binder, W. H.; Sachsenhofer, R. *Macromol. Rapid Commun.* **2008**, *29*, 952.

[18] Himo, F.; Lovell, T.; Hilgraf, R.; Rostovtsev, V. V.; Noodleman, L.; Sharpless, K. B.; Fokin, V. V. *J. Am. Chem. Soc.* **2005**, *127*, 210.

[19] Nulwala, H.; Burke, D. J.; Khan, A.; Serrano, A.; Hawker, C. J. *Macromolecules* **2010**, *43*, 5474.

[20] Dabbagh, A. H.; Mansoori, Y. *Dyes and Pigments* **2002**, *54*, 37.

[21] Yan, M.; Cai, S. X.; Wybourne, M. N.; Keana, J. F. W. *J. Am. Chem. Soc.* **1993**, *115*, 814.

[22] Nahar, P.; Wali, N. M.; Gandhi, R. P. *Anal. Biochem.* **2001**, *294*, 148.

[23] Cai, S. X.; Glenn, D. J.; Kanskar, M.; Wybourne, M. N.; Keana, J. F. W. *Chem. Mater.* **1994**, *6*, 1822.

[24] Tattersall, P. I.; Breslin, D.; Grayson, S. M.; Heath, W. H.; Lou, K.; McAdams, C. L.; McKean, D.; Rathsack, B. M.; Willson, C. G. *Chem. Mater.* **2004**, *16*, 1770.

[25] Fleming, S. A. *Tetrahedron* **1995**, *51*, 12479.

[26] Ballell, L.; Alink, K. J.; Slijper, M.; Versluis, C.; Liskamp, R. M. J.; Pieters, R. J. *ChemBioChem* **2005**, *6*, 291.

[27] Kubota, N. *J. Propul. Power* **1995**, *11*, 677.

[28] Badgujar, D. M.; Talawar, M. B.; Asthana, S. N.; Mahulikar, P. P. *J. Hazard. Mater.* **2008**, *151*, 289.

[29] L' Abbé, G. *Chem. Rev.* **1969**, *69*, 345.

[30] Hassner, A. *Azides and Nitrenes. Reactivity and Utility*; Scriven, E. F. V. (Ed.); Academic Press: Orlando, 1984.

[31] Platz, M. S. *Acc. Chem. Res.* **1995**, *28*, 487.

[32] Wentrup, C. *Topics Current Chem.* **1976**, 175.

[33] Hassner, A.; Fowler, F. W. *J. Am. Chem. Soc.* **1968**, *90*, 2869.

[34] Hassner, A.; Wiegand, N. H.; Gottlieb, H. E. *J. Org. Chem.* **1986**, *51*, 3176.

[35] Morawietz, J.; Sander, W. *J. Org. Chem.* **1996**, *61*, 4351.

[36] Dyke, J. M.; Levita, G.; Morris, A.; Ogden, J. S.; Dias, A. A.; Algarra, M.; Santos, J. P.; Costa, M. L.; Rodrigues, P.; Barros, M. T. *J. Phys. Chem. A* **2004**, *108*, 5299.

[37] Bock, H.; Damme1, R. *J. Am. Chem. Soc.* **1988**, *110*, 5261.

[38] Gritsan, N. P. *Russ. Chem. Rev.* **2007**, *76*, 1139.

[39] Pinho e Melo, T. M. V. D.; Lopes, C. S. J.; Cardoso, A. L.; d'A. Rocha Gonsalves, A. M.; *Tetrahedron* **2001**, *57*, 6203.

[40] Lopes, S.; Nunes, C. M.; Fausto, R.; Pinho e Melo, T. M. V. D.; *J. Mol. Struct.* 2009, *919*, 47.

[41] Pinho e Melo, T. M. V. D.; Lopes, C. S. J.; d'A Rocha Gonslaves, A. M.; Storr, R. C.; *Synthesis* **2002**, *5*, 605.

[42] Padwa, A.; Smolanoff, J.; Temper, A. *J. Org. Chem.* **1976**, *41*, 543.

[43] Padwa, A.; Smolanoff, J.; Temper, A. *J. Am. Chem. Soc.* **1975**, *97*, 1945.

[44] Isomura, K.; Ayabe, G.-I.; Hatano, S.; Taniguchi, H. *J. Chem. Soc. Chem. Comm.* **1980**, 1252.

[45] Wendling, L. A.; Bergman, R. G. *J. Org. Chem.* **1976**, *41*, 831.

[46] Singh, B.; Zweig, A.; Gallivant, J. B. *J. Am. Chem. Soc.* **1972**, *94*, 1199.

[47] Orton, E.; Collins, S. T.; Pimentel, G. C. *J. Phys. Chem.* **1986**, *90*, 6139.

[48] Inui, H.; Murata, S. *J. Am. Chem. Soc.* **2005**, *127*, 2628.

[49] Inui, H.; Murata, S. *Chem. Lett.* **2001**, *30*, 832.

[50] Kaczor, A.; Gómez-Zavaglia, A.; Cardoso, A. L.; Pinho e Melo, T. M. V. D.; Fausto, R. *J. Phys. Chem. A* **2006**, *110*, 10742.

[51] Gómez-Zavaglia, A.; Kaczor, A.; Cardoso, A. L.; Pinho e Melo, T. M. V. D.; Fausto, R. *J. Phys. Chem. A* **2006**, *110*, 8081.

[52] Bornemann, C.; Klessinger, M. *Chem. Phys.* **2000**, *259*, 263.

[53] Klessinger, M.; Bornemann, C. *J. Phys. Org. Chem.* **2002**, *15*, 514.

[54] Inui, H.; Murata, S. *Chem. Comm.* **2001**, 1036.

[55] Inui, H.; Murata, S. *Chem. Phys. Lett.* **2002**, *359*, 267.

[56] Stewart, J. J. P. *J. Comput. Chem.* **1989**, *10*, 209.

[57] Stewart, J. J. P. *J. Comput. Chem.*, **1989**, *10*, 221.

[58] HyperChem Conformational Search module (2002) Tools for Molecular Modeling. Hypercube, Inc., 1115 NW 4th St., Gainesville, FL 32608 (USA).

[59] Saunders, M. *J. Am. Chem. Soc.*, **1987**, *109*, 3150.

[60] Saunders, M.; Houk, K. N.; Wu, Y.-D.; Still, W. C.; Lipton, J. M.; Chang, G.; Guidal, W. C. *J. Am. Chem. Soc.* **1990**, *112*, 1419.

[61] Howard, A. E.; Kollman, P. A. *J. Med. Chem.* **1988**, *31*, 1669.

[62] Frisch, M. J.; Trucks, G. W.; Schlegel, H. B.; Scuseria, G. E.; Robb, M. A.; Cheeseman, J. R.; Montgomery, J. A., Jr.; Vreven, T.; Kudin, K. N.; Burant, J. C.; Millam, J. M.; Iyengar, S. S.; Tomasi, J.; Barone, V.; Mennucci, B.; Cossi, M.; Scalmani, G.; Rega, N.; Petersson, G. A.; Nakatsuji, H.; Hada, M.; Ehara, M.; Toyota, K.; Fukuda, R.; Hasegawa, J.; Ishida, M.; Nakajima, T.; Honda, Y.; Kitao, O.; Nakai, H.; Klene, M.; Li,X.; Knox, J. E.; Hratchian, H. P.; Cross, J. B.; Bakken, V.; Adamo, C.; Jaramillo, J.; Gomperts, R.; Stratmann, R. E.; Yazyev, O.; Austin, A. J.; Cammi, R.; Pomelli, C.; Ochterski, J. W.; Ayala, P. Y.; Morokuma, K.; Voth, G. A.; Salvador, P.; Dannenberg, J. J.; Zakrzewski, V. G.; Dapprich, S.; Daniels, A. D.; Strain, M. C.; Farkas, O.; Malick, D. K.; Rabuck, A. D.; Raghavachari, K.; Foresman, J. B.; Ortiz, J. V.; Cui, Q.; Baboul, A. G.; Clifford, S.; Cioslowski, J.; Stefanov, B. B.; Liu, G.; Liashenko, A.; Piskorz, P.; Komaromi, I.; Martin, R. L.; Fox, D. J.; Keith, T.; Al-Laham, M. A.; Peng, C. Y.; Nanayakkara, A.; Challacombe, M.; Gill, P. M. W.; Johnson, B.; Chen, W.; Wong, M. W.; Gonzalez, C.; Pople, J. A. Gaussian 03, revision C.02; Gaussian, Inc. Wallingford, CT, 2004.

[63] Frisch, M.; Head-Gordon, M. Pople, J. A. *Chem. Phys. Lett.* **1990**, *166*, 281.

[64] Becke, A. D. *Phys. Rev. A* **1988**, *38*, 3098.

[65] Lee, C. T.; Yang, W. T.; Parr, R. G. *Phys. Rev. B* **1988**, *37*, 785.

[66] Császár, P.; Pulay, P. *J. Mol. Struct.* **1984**, *114*, 31.

[67] Farkas, Ö.; Schlegel, H. B. *J. Chem. Phys*. **1999**, *111*, 10806.

[68] Peng, C.; Schlegel, H. B. *Isr. J. Chem.* **1994**, *33*, 449.

[69] Schachtschneider, J. H.; Mortimer, F. S. *Vibrational Analysis of Polyatomic Molecules*. VI. FORTRAN IV Programs for Solving the Vibrational Secular Equation and for the Least-Squares Refinement of Force Constants. Report Nº. 31450. Structural Interpretation of Spectra, Technical Report nº 57-650, Shell Development Co. Emeryville, CA, 1969.

[70] Pulay, P.; Fogarasi, G.; Pang, F. Boggs, J. E. *J. Am. Chem. Soc.* **1979**, *110*, 2550.

[71] Fausto, R.; Teixeira-Dias, J. J. C. *J. Mol. Struct.* **1986**, *144*, 215.

[72] Fausto, R.; Teixeira-Dias, J. J. C. *J. Mol. Struct.* **1986**, *144*, 225.

[73] Fausto, R.; Teixeira-Dias, J. J. C. *J. Mol. Struct.* **1986**, *144*, 241.

[74] Cioslowski, J. *J. Am. Chem. Soc.* **1989**, *111*, 8333.

[75] Barnes, A. J. *J. Mol. Struct.* **1984**, *113*, 161.

[76] Reva, I. D.; Stepanian, S. G.; Adamowicz, L.; Fausto, R. *Chem. Phys. Lett.* **2003**, *374*, 631.

[77] Gómez-Zavaglia, A.; Fausto, R. *J. Mol. Struct.* **2004**, *689*, 199.

[78] Gómez-Zavaglia, A.; Kaczor, A.; Cardoso, A. L.; Pinho e Melo, T. M. V. D.; Fausto, R. *J. Phys. Chem. A* **2006**, *110*, 8081.

[79] Borba, A.; Gómez-Zavaglia, A.; Simões, P. N. N. L.; Fausto, R. *J. Phys. Chem. A* **2005**, *109*, 3578.

[80] Rosado, M. T. S.; Lopes de Jesus, A. J.; Reva, I. D.; Fausto, R.; Redinha, J. S.; *J. Phys. Chem. A* 2009, *133*, 7499.

[81] Reva, I. D.; Lopes de Jesus, A. J.; Rosado, M. T. S.; Fausto, R.; Eusébio, M. E.; S. Redinha, J. S.; *Phys. Chem. Chem. Phys.* **2006**, *8*, 5339.

[82] Reva, I. D.; Stepanian, S.G.; Adamowicz, L.; Fausto, R.; *Chem. Phys. Lett.* **2003**, *374*, 631.

[83] Lopes, S.; Nunes, C. M.; Gómez-Zavaglia, A.; Pinho e Melo, T. M. V. D.; Fausto, R. *J. Phys. Chem. A* **2010**, *114*, 9074.

[84] Finnerty, J.; Mitschke, U.; Wentrup, C. *J. Org. Chem.* **2002**, *67*, 1084.

[85] Jacox, M. E.; Milligan, D. E. *J. Am. Chem. Soc.* **1963**, *85*, 278.

[86] Jacox, M. E. *Chem. Phys.* **1979**, *43*, 157.

[87] Guillemin, J.-C.; Denis, J.-M.; Lasne, M.-C.; Ripoll, J.-L. J. *Tetrahedron* **1988**, *44*, 4447.

[88] Ripoll, J.-L.; Thuillier, A. *Tetrahedron Lett.* **1978**, 463.

[89] De Corte, B.; Denis, J.-M.; De Kimpe, N. *J. Org. Chem.* **1987**, *52*, 1147.

[90] Amatatsu, Y.; Hamada, Y.; Tsuboi, M. *J. Mol. Spectrosc.* **1987**, *123*, 476.

[91] August, J.; Klemm, K.; Kroto, H. W.; Walton, D. R. M. *J. Chem. Soc., Perkin Trans. 2* **1989**, 1841.

[92] Winter, H.-W.; Wentrup, C. *Angew. Chem.* **1980**, *92*, 743.

[93] Winter, H.-W.; Wentrup, C. *Angew. Chem., Int. Ed. Engl.* **1980**, *19*, 720.

[94] Orton, E.; Collins, S. T.; Pimentel, G. C. *J. Phys. Chem.* **1986**, *90*, 6139.

(*to be submitted*)

UV-Induced Photochemistry of Methyl Aziridine-2-Carboxylate Isolated in Low Temperature Inert Matrices

Susy Lopes, Igor Reva, and Rui Fausto

Department of Chemistry, University of Coimbra, P-3004-535 Coimbra, Portugal

ABSTRACT

Methyl aziridine-2-carboxylate (MA2C) has been isolated in low temperature argon and xenon matrices and its structure and photochemistry were studied by FTIR spectroscopy. The reactant as well as the main photoproducts were characterized by comparison of their experimental IR spectra with the spectra calculated at the DFT(B3LYP)/6-311++G(d,p) level. The theoretical calculations predicted the existence of two low energy MA2C conformers differing by the orientation of the O=C−C−N dihedral angle. Both conformers were identified in the studied matrices. Upon broadband UV irradiation ($\lambda > 235$ nm) of matrix-isolated MA2C, the most common photoreaction was observed: cleavage of the C−C bond of the aziridine ring. The primary photoproduct of this reaction, azomethine ylide, undergoes a [1,2]-shift of hydrogen atom rearranging into methyl 2-(methyleneamino)-acetate (MMAA). The same phototransformation was observed using narrowband UV laser irradiation at 235 nm. Subsequent irradiation at 290 nm led to the observation of new bands resulting from further decomposition of the main photoproduct, MMAA. These bands fit well the spectrum of methyl formate. The spectra of the photolyzed matrices also show bands which result from non-identified photoproducts, possibly resulting from C−N cleavage of the aziridine.

Introduction

Aziridines are saturated three-membered heterocycles containing a nitrogen atom, which occur naturally and have innumerable applications.[1,2] The best known examples of natural products containing an aziridine ring include biologically active compounds such as mitomycins, carzinophilin and azinomycins, which possess strong antibiotic and antitumor properties.[3-6] Aziridines are also extremely versatile compounds used in the synthesis of molecules such as amino acids, nitrogen-containing larger-ring heterocycles and alkaloids, chiral ligands, natural products, pharmaceutical intermediates, etc, via ring opening and ring expansion reactions.[1-18] In particular, aziridine-2-carboxylates and their derivatives have been used as intermediates in the syntheses of α- and β-amino acids, both natural and non-natural, by stereospecific ring-opening reactions of the heterocyclic ring with nucleophiles, including organometallic reagents.[19-24]

The reactivity of aziridines toward ring opening (either by C−N or C−C bond cleavage) and expansion relates to their extremely high ring strain (above 110 kJ mol^{-1}).[1,25,26] The nature of the substituent at the N−atom plays a crucial role in the nucleophilic ring opening of aziridines through C−N bond cleavage, as aziridines are classified into two groups, "activated" and "nonactivated".[1,2,9,26] The first group includes electron-withdrawing substituents such as tosyl or acyl functional groups,[15,21] which can stabilize the negative charge of the nitrogen atom and increase the reactivity of aziridine rings towards nucleophiles. In the case of the nonactivated group, non-oxygenated substituents such as the hydrogen atom, alkyl or aryl functional groups, the aziridine ring is more stable and less reactive towards nucleophiles, thus a Lewis acid catalyst is frequently employed.[13,14,18]

Aziridines can also undergo ring opening involving carbon-carbon bond cleavage in a conrotatory (thermolysis) or disrotatory (photolysis) process yielding azomethine ylides (see Scheme 1). The latter can undergo 1,3-dipolar cycloadditions or, less frequently observed, addition to nucleophiles.[27-32] The matrix isolation technique was previously applied in the identification and characterization of azomethine ylides resulting from the photochemical C−C bond cleavage of phenyl-substituted aziridines in Freon matrices at 77 K.[33] However, it is not yet understood how different substituents in the aziridine ring influence the preference for the carbon-nitrogen or the carbon-carbon bond cleavage reactions.[34-36]

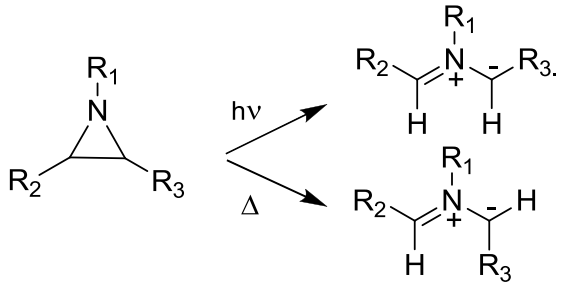

Scheme 1. The carbon-carbon bond cleavage in aziridine yields azomethine ylide. The ring-opening processes induced by thermolysis (bottom) and photolysis (top) are conrotatory and disrotatory, respectively.

In the present study, we report on the UV-induced photochemical behaviour of a compound that belongs to the class of non-activated aziridines (bearing hydrogen atoms at the ring nitrogen and one of the ring carbon atoms), having a carboxylate substituent at the aziridine ring. Monomers of methyl aziridine-2-carboxylate (MA2C) were isolated in inert cryogenic matrices and their unimolecular photochemistry was followed by the interpretation of the IR spectra of the starting compound and of the resulting photoproducts. In addition to ring-opening photoreactions, UV irradiation using laser light was found to lead to the observation of new products originating from a secondary photoreaction involving MMAA (the dominant photoproduct resulting from C−C bond cleavage). We also performed a detailed theoretical investigation of the potential energy surfaces of MA2C and of the possible photoproducts resulting from both C−C and C−N bond cleavage of the aziridine ring at the DFT(B3LYP)/6-311++G(d,p) level. To the best of our knowledge, no studies on matrix-isolated MA2C and its photochemistry have been reported hitherto.

Experimental and Computational Methods

Methyl aziridine-2-carboxylate (MA2C) (97% purity) was purchased from TCI Europe. Prior to usage, MA2C was additionally purified by the standard freeze-pump-thaw technique. The MA2C vapors were premixed with argon and xenon (N60 and N48, respectively, both supplied by Air Liquide) at a ratio of 1:1000 in a 3 L Pyrex glass reservoir to a pressure of 800 mbar, using the standard manometric procedure. During the experiments, the flux of the mixture was controlled by reading the drop pressure in the reservoir with a capacitance manometer. The pulsed valve controller

allows different operating modes to define the sample introduction rate. In a typical experiment, the valve operated with an opening time of 5 ms and pulse frequency of 12 Hz during 1000 to 3000 seconds. Matrices were prepared by deposition of the mixture onto a CsI substrate cooled to 15 K (Ar) and 30 K (Xe) assembled inside the cryostat (APD Cryogenics closed-cycle helium refrigeration system) with a DE-202A expander. The temperature of the (MA2C : inert gas) mixture prior to deposition was 297 K and this temperature defined the conformational composition of MA2C monomers.

The IR spectra, in the 4000-400 cm^{-1} range, were obtained using a Mattson (Infinity 60AR Series) or a Thermo Nicolet 6700 Fourier transform infrared spectrometers, equipped with a deuterated triglycine sulphate (DTGS) detector and a Ge/KBr beam splitter, with 0.5 cm^{-1} spectral resolutions. To avoid interference from atmospheric H_2O and CO_2, a stream of dry air was continuously purged through the optical path of the spectrometer.

Matrices were irradiated using two sources. The broadband irradiation was carried out with UV light from a 500 W Hg(Xe) lamp (Newport, Oriel Instruments), with output power set to 200 W, through the outer KBr window of the cryostat. A series of longpass optical filters, transmitting UV-light with λ > 397, 367, 328, 313 and 288 nm, was used. No change was observed in the spectra of MA2C upon irradiation under these conditions. Photochemical changes were observed only without longpass filters, *i.e.*, for λ > 235 nm (this value is defined by the absorbance edge of KBr in UV). Matrices were also irradiated with tunable UV light provided by the frequency doubled signal beam of the Quanta-Ray MOPO-SL pulsed (10 ns) optical parametric oscillator (FWHM ~0.2 cm^{-1}, repetition rate 10 Hz, pulse energy ~1.0 mJ) pumped with a pulsed Nd:YAG laser.

The quantum chemical calculations were performed using the Gaussian 03 program package[37] at the DFT level of theory, using the split valence triple-ζ 6-311++G(d,p) basis set[38] and the three-parameter B3LYP density functional, which includes Becke's gradient exchange correction[39] and the Lee, Yang and Parr correlation functional.[40] In the case of the MA2C, the structures of conformers, optimized at the DFT and MP2 levels, were confirmed to correspond to true minima on the potential energy surface, through the analysis of the corresponding Hessian matrices.

The calculated vibrational frequencies and IR intensities were also used to assist the analysis of the experimental spectra. The computed harmonic frequencies were scaled down by a single factor (0.978) to correct them for the effects of basis set limitations, neglected part of electron correlation and anharmonicity effects. The transition states structures and energy barriers were located using the synchronous transit-guided quasi-Newton (STQN) method.[41]

In addition, relaxed potential energy scans and two-dimensional potential energy maps were calculated to locate all the minima of the possible photoproducts resulting from ring-opening reactions (C−C and C−N bond cleavage) aiding in a more detailed characterization. All structures corresponding to the stationary points (both transition states and local minima) were optimized and the harmonic vibrational frequencies and infrared intensities were calculated at the DFT(B3LYP)/6-311++G(d,p) level.

Normal coordinate analysis was undertaken in the internal coordinates space, as described by Schachtschneider and Mortimer[42] using the optimized geometries and harmonic force constants resulting from the DFT(B3LYP)/6-311++G(d,p) calculations. The internal coordinates used in this analysis were defined following the recommendations of Pulay *et al.*[43]

Results and Discussion

Calculated structures

The MA2C molecule has one chiral center, carbon atom C3 (see Figure 1 for atom numbering). The geometric parameters of MA2C reported in this work refer to the S-enantiomer.

MA2C has three intramolecular degrees of freedom that lead to different conformers. These are: (i) rotation of the ester group around the exocyclic C_1−C_3 bond; (ii) rotation of the methoxy group around the C_1−O_{10} bond; (iii) pyramidality at the nitrogen atom. The three above listed coordinates can assume two minimum-energy orientations each. They correspond approximately to *cis* and *trans* orientations around the (i) O_2=C_1−C_3−N_4; (ii) O_2=C_1−O_{10}−C_{11}; and (iii) H_9−N_4−C_3−C_1 dihedral angles, respectively. The latter coordinate is related with the sp^3 hybridization of N4 that renders two possible orientations of the NH group with respect to the plane of the

aziridine ring. The combinations of all possible orientations produce eight unique minima for the MA2C monomer (the optimized structures of the higher energy conformers of MA2C are shown in Figure S1 in the Supporting Information). The relative calculated energies of the eight conformers are presented in Table 1, and the main conformational dihedral angles are presented in Table 2. The Cartesian coordinates for calculated optimized geometries of the eight conformers are given in Table S1 (Supporting Information).

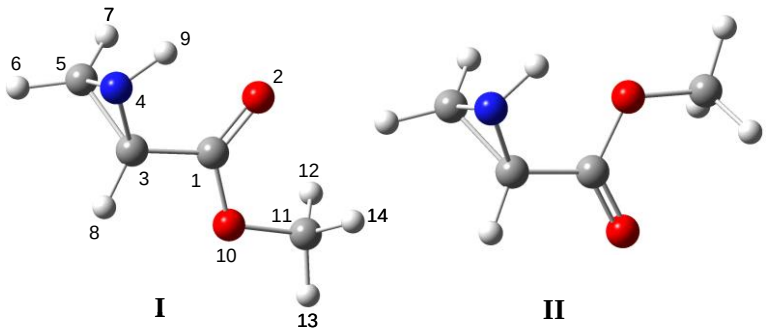

Figure 1. DFT(B3LYP)/6-311++G(d,p) optimized structures of the two most stable conformers of methyl aziridine-2-carboxylate (MA2C), with atom numbering adopted in this work. Color codes: carbon – grey, hydrogen – white, oxygen – red, nitrogen – blue.

The theoretical calculations carried out at the DFT(B3LYP)/6-311++G(d,p) level predicted the existence of two low-energy minima, both belonging to the C_1 symmetry point group (see Figure 1). In both conformers, the O=C−O−CH_3 group is in the *cis* orientation and the N−H bond is positioned in an *anti* orientation regarding the C_3−H_6 bond of the aziridine ring. Such orientation signifies that the NH and the ester groups are positioned on the same side of the aziridine ring and the NH group is in a close vicinity of one of the oxygen atoms. This fact results in a stabilizing interaction of the NH group with either the lone electron pairs of C=O group (in conformer **I)** or the lone electron pairs of C−O group (in conformer **II**). Higher energy structures were obtained when the ester group is in a *trans* orientation (O=C−O−CH_3 dihedral angle is about 180°) or the N−H bond is in a *cis* position regarding the C_3−H_6 bond of the aziridine ring (see Figure S1).

Table 1 – DFT(B3LYP)/6-311++G(d,p) and MP2/6-311++G(d,p) calculated relative energies (ΔE/ kJ mol^{-1}) including zero-point contributions and calculated relative Gibbs energy difference (ΔG/ kJ mol^{-1}) for the eight conformers of MA2C.

Conformer[a]	ΔE_{DFT}	ΔE_{MP2}	ΔG_{DFT}	ΔG_{MP2}
I	0.0	0.0	0.0	0.0
II	6.4	5.9	6.3	5.9
III	12.6	12.2	12.6	12.2
IV	14.6	13.6	13.4	13.6
V	33.1	33.6	33.4	33.6
VI	50.4	48.5	48.5	48.5
VII	54.8	56.3	52.2	56.3
VIII	73.5	73.1	73.1	–

[a] See Figure 1 and Figure S1 for optimized structures of the conformers of MA2C.

Table 2 – DFT(B3LYP)/6-311++G(d,p) and MP2/6-311++G(d,p) calculated values for the main conformational dihedral angles (º) of the eight conformers of MA2C.[a]

Conformer	$O_2=C_1–C_3–N_4$		$O_2=C_1–O_{10}–C_{11}$		$H_9–N_4–C_3–C_1$	
	DFT	MP2	DFT	MP2	DFT	MP2
I	–21.2	–22.4	–0.7	–0.6	3.6	4.1
II	158.3	157.5	1.4	1.8	4.8	5.1
III	–42.3	–40.3	0.2	0.3	–145.9	–147.6
IV	141.6	141.6	–2.3	–2.3	–143.0	–144.7
V	–12.5	–11.6	–175.3	–173.2	–145.9	2.8
VI	–100.6	–100.9	173.8	171.5	–146.3	–147.7
VII	173.8	166.5	–165.9	–160.6	–146.1	–147.5
VIII	140.9	–	147.8	–	12.1	–

[a] See Figure 1 for the optimized structures of the two most stable conformers of MA2C and for atom numbering; see Figure S1 for high-energy conformers of MA2C.

The energy (including the zero-point correction) of form **II** is higher by 6.4 kJ mol^{-1} (5.9 kJ mol^{-1} at MP2 level) than the most stable form. The relative Gibbs free energies are identical to the electronic energy (6.3 and 5.9 mol^{-1} at the DFT and MP2 levels, correspondingly). Considering the calculated relative stabilities of **I** and **II**, their expected populations in the equilibrium gas phase at room temperature (taking into account the relative Gibbs free energies) should be 92.7 and 7.3%, respectively. The calculated energy barrier between these two conformers is no less than *ca.* 20 kJ mol^{-1} in all directions. Figure 2 shows the potential energy profile associated with the internal rotation of the ester group around the exocyclic $C_1–C_3$ bond corresponding to the interconversion between the two most stable conformers. Therefore, the relatively high energy barriers prevent occurrence of the

conformational cooling during deposition of the matrices,[44-46] and the two conformers present in the gas phase are expected to be effectively trapped in the samples. Other MA2C conformers have calculated energies higher than 12 kJ mol^{-1} and are not experimentally relevant (see Table 1).

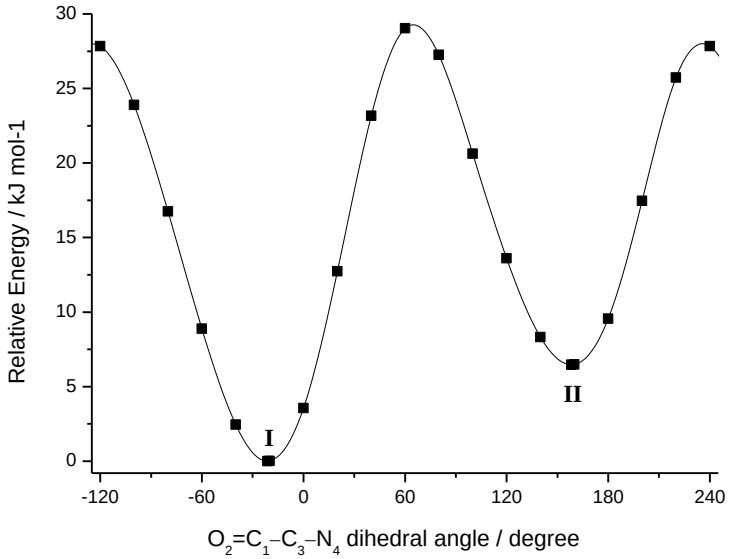

Figure 2. Calculated DFT(B3LYP)/6-311++G(d,p) potential energy profile for internal rotation of the ester group around the exocyclic C_1−C_3 bond corresponding to the interconversion between the two most stable conformers of MA2C.

Infrared spectroscopy: matrix isolation (as-deposited matrix)

The infrared spectra of MA2C monomers isolated in freshly deposited argon and xenon matrices are presented in Figure 3a and 3b. The theoretical spectra of the two most stable conformers calculated at the DFT(B3LYP)/6-311++G(d,p) level are also shown for comparison (Figure 3d). Intensities in the stick spectra were not scaled, however, in the simulated sum spectrum (Figure 3c) intensities were weighted by their expected populations (0.927 for conformer **I** and 0.073 for conformer **II**).

The good agreement between the experimental infrared spectra and the calculated spectra allowed an easy assignment of the fundamental bands (see Table 3). The definition of the internal symmetry coordinates adopted in the vibrational analysis for the two most stable conformers of MA2C is provided in Table S2 (Supplementary Information). The calculated wavenumbers, infrared intensities and potential energy distributions resulting from normal mode analysis, carried out for these conformers

are presented in Tables S3 and Table S4 (Supplementary Information). The MA2C molecule belongs to the C_1 symmetry point group with 36 fundamental vibrations, all of them active in the infrared.

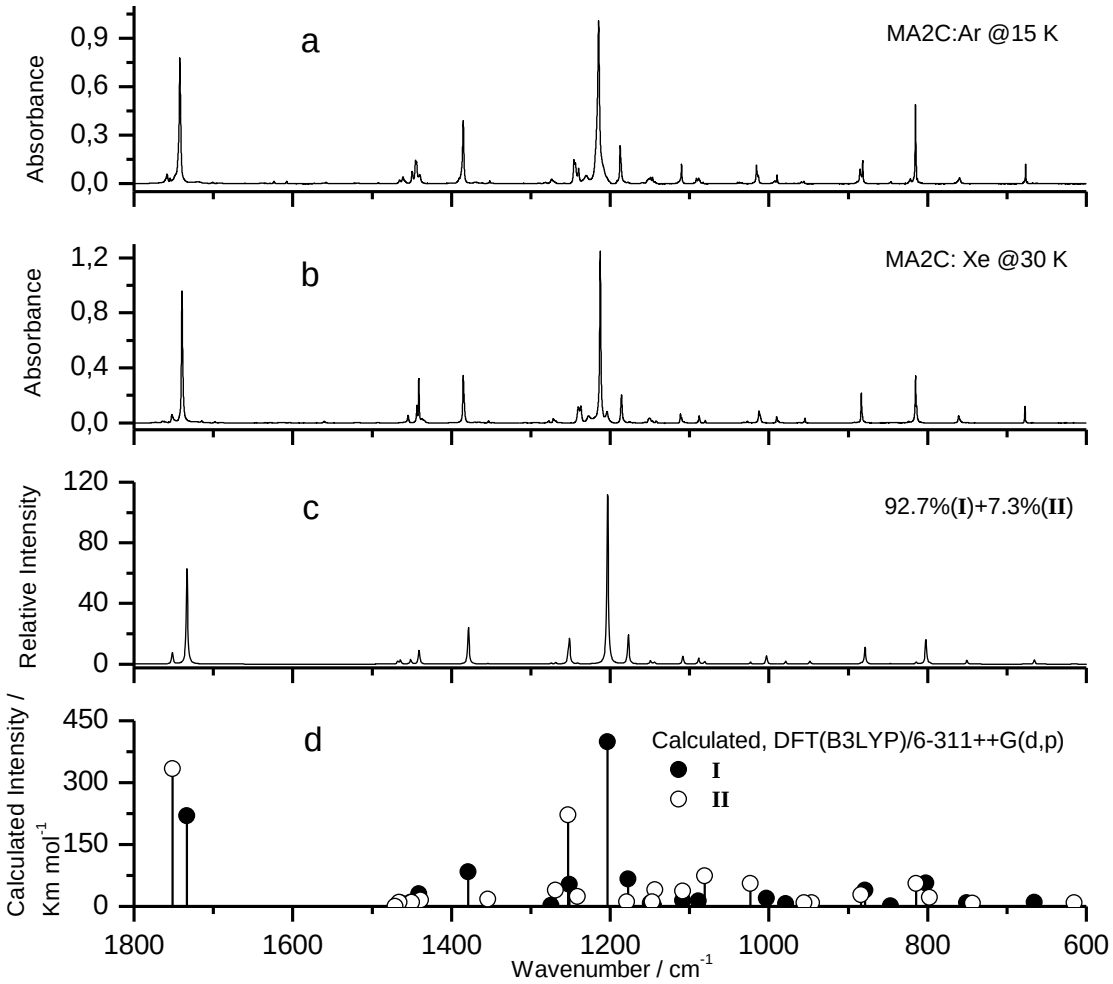

Figure 3. Experimental FTIR spectra of methyl aziridine-2-carboxylate (MA2C) isolated in an argon matrix at 13 K (a), and in a xenon matrix at 30 K (b), compared with the infrared spectrum simulated for the gas-phase equilibrium mixture of conformers **I** and **II** (c), theoretical infrared spectra of individual conformers (d) calculated at the DFT(B3LYP)/6-311++G(d,p) level. The sum spectrum (c) was simulated using Lorentzian functions (fwhm = 2 cm^{-1}) centered at the calculated wavenumbers (scaled by a single factor of 0.978). Calculated intensities of the bands due to individual conformers were weighted by their expected populations (0.927 for **I** and 0.073 for **II**), corresponding to the calculated relative Gibbs energy difference (6.3 kJ mol^{-1}) at room temperature. Intensities in the stick spectra (d) are not scaled.

Table 3 – Experimental (matrix-isolation) and DFT(B3LYP)/6-311++G(d,p) calculated infrared data for MA2C and vibrational assignments based on the results of normal coordinate analysis.[a]

Experimental		Calculated				
Ar matrix	Xe matrix	Conformer **I**		Conformer **II**		Approximate description
ν	ν	ν	I_{IR}	ν	I_{IR}	
3301/3298	3289/3286	3402.3	11.4	3434.6	10.9	ν(NH)
3084	3081/3069	3129.8	9.6	3129.2	10.9	$\nu_a(CH_2)$
3057/3050	n.obs.	3107.7	4.2	3108.0	11.1	ν(CH)
3040	3027	3091.4	12.6	3089.1	3.6	$\nu_a(CH_3)'$
3013	3000	3058.4	17.7	3058.3	11.8	$\nu_a(CH_3)''$
3005	2990	3039.6	17.8	3041.0	17.1	$\nu_s(CH_2)$
2966	2951sh/2947	2986.0	29.6	2985.6	17.9	$\nu_s(CH_3)$
1758/1755 (**II**)	1752 (**II**)	–	–	1751.7	333.4	ν(C=O)
1748/1742 (**I**)	1740 (**I**)	1733.3	220.1	–	–	ν(C=O)
1465/1461/1459sh	1465/1455	1467.7	5.7			$\delta(CH_2)$
		1464.2	8.8	1465.7	9.4	$\delta_2(CH_3)$
1449	n.obs.	1451.5	10.0	1450.0	9.6	$\delta_3(CH_3)$
1445/1444/1440	1443/1441	1440.9	30.4	1438.7	15.6	$\delta_1(CH_3)$
1390/1385 (**I**)	1385 (**I**)	1378.6	83.8	–	–	γ(CH8)
1352 (**II**)	1355/1353 (**II**)	–	–	1354.0	17.1	γ(CH8)
1290/1282sh/1274/1270sh /1264/1262/1258	1277/1272/1269/1263	1274.3	2.2	1268.6	39.4	γ(NH)
1245/1244/1240	1240/1237	1251.3	52.8	1252.9	222.1	δ(NH)
1230	1227	–	–	1241.1	23.5	ν(CO), ν(C1C3)
1215/1208sh	1220/1212/1204	1203.3	399.3	–	–	ν(CO)
1191/1187/1186sh/1178	1186/1176	1177.1	66.0	1179.2	10.6	$\delta_4(CH_3)$
1159/1151/1149/1147/ 1144	1156/1152sh/1150/1149sh /1147/1142/1141sh	1149.3	7.6	1146.9	11.0	γ(CH8), γ(NH); $\delta_5(CH_3)$
		1145.2	1.9	1143.7	39.8	wag(CH_2), δ(CH8)
1114/1112sh/1110	1111/1110/1107/1106	1108.4	14.4	1108.3	37.0	δ(CH8)
1094/1091/1088/1087 (**I**)	1089sh/1088 (**I**)	1088.6	13.4	–	–	wag(CH_2)
1083 (**II**)	1080 (**II**)	–	–	1080.9	73.5	wag(CH_2)
1039/1037 (**II**)	1031 (**II**)	–	–	1023.3	55.6	ν(O-CH_3)
1020/1016/1013/1010 (**I**)	1012/1011sh (**I**)	1003.0	19.0	–	–	ν(O-CH_3)
997/993/989	990/988	978.9	6.5	–	–	ν(O-CH_3), twist(CH_2)
959/956	956sh/955	948.4	6.9	955.8	9.1	rock(CH_2)
				946.0	9.0	twist(CH_2)
891/889/884sh/882	884/882sh	878.8	38.9	883.6	28.6	ν(NC)
846	839	846.6	1.2	–	–	ν(CN)
822 (**II**)	824 (**II**)	–	–	814.4	55.9	ν(CN)
815/813	815/814	802.2	56.8	797.3	21.2	ν(C3C5)
760	761	750.5	8.8	743.5	7.5	γ(C=O)
680/678/676/674	678sh/677	665.5	9.5	–	–	δ(CC=O),ν(C1C3)
n.i.	n.i.	–	–	615.3	9.2	γ(C1C3), ν(C1C3)
n.i.	n.i.	412.2	2.4	466.8	7.6	δ(OCC); δ(CC=O)
n.i.	n.i.	319.9	25.7	317.4	18.6	δ(C-O-CH_3)
n.i.	n.i.	293.6	13.2	291.7	11.3	δ(C1C3)
n.i.	n.i.	200.0	0.6	195.3	0.2	γ(C1C3); δ(OCC)
n.i.	n.i.	159.3	1.2	142.5	1.0	τ(CO)
n.i.	n.i.	123.8	0.4	119.6	1.0	τCH_3
n.i.	n.i.	75.7	2.8	85.7	1.1	τ(CC)

[a] Wavenumbers (cm^{-1}, scaled by 0.978), calculated intensities (km mol^{-1}), s = symmetric; a = antisymmetric; ν = stretching; δ = in-plane bending; γ = out-of-plane bending; τ = torsion; rock = rocking; wag = wagging; twist = twisting, n.obs. = not observed; n.i. = not investigated. See Table S2 for definition of symmetry coordinates and Tables S3 and S4 for potential energy distributions.

In agreement with prediction of relative energies, conformer **I** is the main species present in the matrices. On the whole, the experimental FTIR spectra of MA2C isolated in argon and xenon matrices are quite similar, nevertheless, it is possible to observe several bands which show unequivocally that conformer **II** is also present in the matrices. Figure 4 displays selected spectral regions of the infrared spectrum of MA2C isolated in a xenon matrix (T=30 K) compared with the theoretical calculated spectra of the two most stable conformers of MA2C. This Figure shows more precisely the position of the bands ascribed to the more energetic conformer. The bands observed at 1752, 1355/1353, 1080, 1031 and 824 cm^{-1} in a xenon matrix are ascribable to ν(C=O), γ(CH8), wag(CH_2), ν(CN), ν(O−CH_3) and ν(C3C5) vibrations of conformer **II** (See Table 3). These vibrations have strong predicted intensities in infrared and do not overlap with vibrations of conformer **I**. Their counterparts were also observed for MA2C monomers isolated in an argon matrix, and clearly show the presence of conformer **II** in the samples.

In the ν(C=O) stretching region, the two vibrations give rise to a doublet of bands at 1758/1755 and 1748/1742 cm^{-1} (Ar) assigned to conformers **II** and **I**, respectively, these bands are not the result of matrix-site effects which are known to occur frequently in an argon matrix. However, matrix-site effects are visible throughout both spectra, in particular in the argon matrix. In addition to the fundamentals, another interesting feature concerning the ν(C=O) vibration was the observation of the first overtone band at *ca.* 3468 cm^{-1} (Ar) and 3462 cm^{-1} (Xe) for this mode. Moreover, the triplet of bands at *ca*. 2910/2862/2821cm^{-1} (Ar) and their counterparts for the molecule isolated in a xenon matrix (2898/2854/2818 cm^{-1}) can be assigned as an overtone of the in-plane bending of the CH_3 group.

The ν(NH) vibration gives rise to bands of very weak intensity at 3301/3298 and 3289/3286 cm^{-1} for argon and xenon matrices, respectively. The calculations predict the ν(NH) mode at 3402.3 and 3434.6 cm^{-1}, for conformers **I** and **II**, correspondingly. Therefore, the position of the experimental bands is a clear indication of formation of intramolecular H−bonds, the bands shows a significant red-shift as they appear at much lower frequency compared to the predicted values. As mentioned above, the specific orientation of the NH and the ester groups, in particular, their position on the same side of the aziridine ring in the two most stable conformers, can originate different intramolecular H−bonds, strong N−H···O=C (2.4 Å) for

conformer **I** and weaker N−H···O−C (2.3 Å) for conformer **II**, is another factor of stabilization of conformer **I** regarding form **II**.

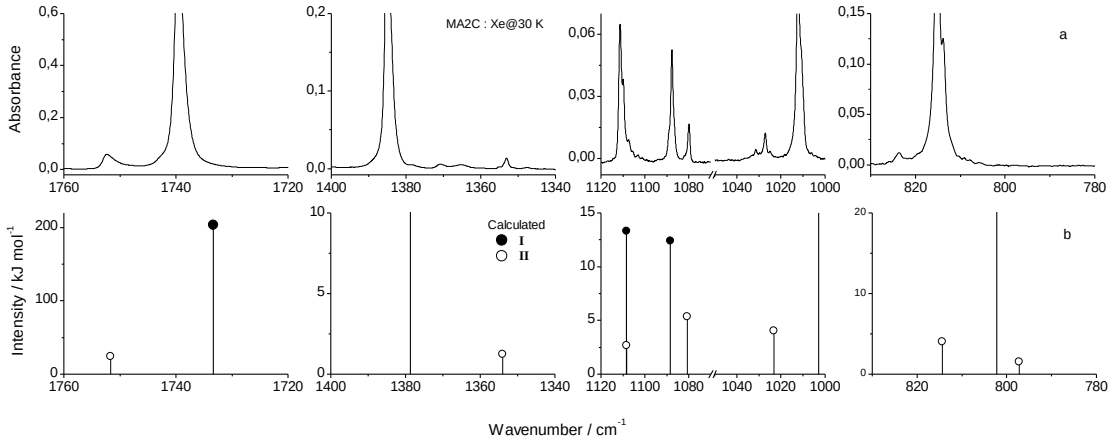

Figure 4. Selected regions of the experimental FTIR spectrum of methyl aziridine-2-carboxylate (MA2C) isolated in a xenon matrix at 30 K (a), compared with the theoretical infrared spectra of individual conformers **I** and **II** (b) calculated at the DFT(B3LYP)/6-311++G(d,p) level of theory. The calculated frequencies were scaled by a single factor (0.978). Calculated intensities were weighted by the expected populations of the individual conformers (0.927 for **I** and 0.073 for **II**) at room temperature. The ordinate scales are expanded to afford a better visibility of the bands due to the minor conformer **II** (thus the high intensity bands in the spectra of conformer **I** are truncated). Asterisk (in frame a) designates the band due to traces of matrix-isolated monomeric methanol impurity.

UV-Induced Photochemical Transformations – Ring Opening of the Aziridine ring

Upon broadband UV irradiation (λ > 235 nm) of matrix isolated monomeric MA2C, bands due to the initial compound decreased in intensity while new bands were formed. A detailed analysis of the infrared spectra after irradiation of the matrices shows that the appearance of these new bands is the result of both conformers being consumed (and also, that there is no photo-induced conformational isomerization). The appearance of new bands was discernible after just 1 minute of irradiation (total irradiation time was 240 min).

Upon UV-excitation in the gas phase, the unsubstituted aziridine yields primary products such as ethylene, ethane, methane, atomic and molecular hydrogen and nitrogen, ammonia, and methyl radicals.[47,48] As mentioned in the Introduction, two main reaction mechanisms regarding ring-opening of aziridines are possible (through C−C or C−N bond cleavage).

Figure 5 shows different possibilities of the ring-opening reaction for the 2-substituted aziridine system. The possible reaction paths are depicted by pairs of

numbers which specify where the bond cleavage occurs. Two reaction paths for the cleavage of the C–N bond are shown (1,2 and 1,3) and one for the C–C bond rupture (2,3). Atom numbering in Figure 5 differs from that adopted for MA2C, since Figure 5 has a more general character, and is proposed as a general complete set of possibilities for 2-substituted aziridines. The initially formed products undergo hydrogen atom shifts which lead to a total of six potential photoproducts, numbered as **1,2-A** and **1,2-B** and, **1,3-A** and **1,3-B** (in the case of C−N bond cleavage), and **2,3-A** and **2,3-B** (in the case of C−C bond cleavage). For MA2C, where R_1="ester group", only structures with the usually most stable *cis* orientation (O=C−O−CH_3 dihedral angle is about 0°) were considered. Furthermore, the general character of Figure 5 easily accounts for the possibilities of decarbonylation (R_2 equals $COCH_3$) or decarboxylation (R_3 equals CH_3) of MA2C and of the corresponding photoproducts (see Figure 5). Bigot *et al.*[48] performed an early theoretical study on the photochemical behaviour of the unsubstituted aziridine ring. Their analysis focused on the C–C and C–N bond ring-openings and rupture of the N–H bond. The main results are that in the gas phase the C–N bond ring-opening is favoured while in protic condensed media the C–C bond ring-opening competes with the C–N bond ring-opening.

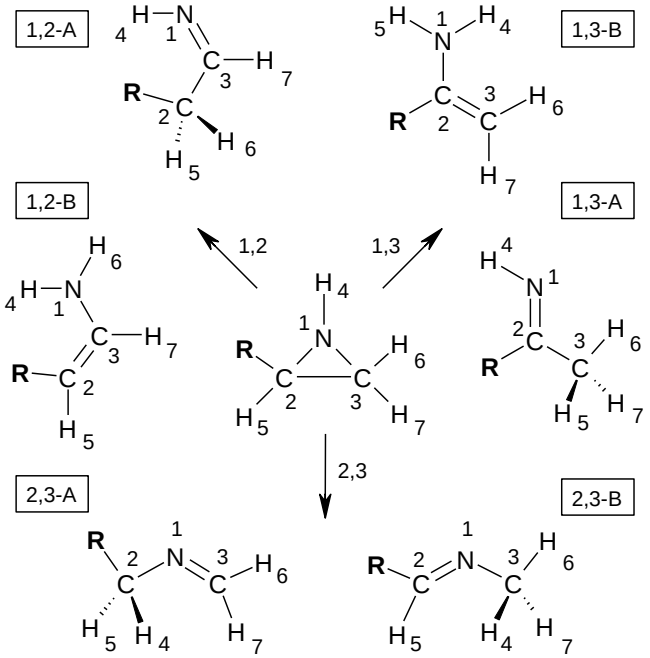

Figure 5. Possible structural rearrangements in 2-substituted aziridine resulting from different ring-opening reactions. Pairs of numbers next to the arrows specify the atom numbers where the bond cleavage occurs. R_1 equals to C(=O)OCH_3 for the non-reacted compound, R_2 equals to $COCH_3$ in the case of decarbonylation, R_3 equals to CH_3 in the case of decarboxylation.

C−C bond cleavage (2,3)

According to the literature,[36,48] the most likely photochemical reaction of MA2C corresponds to the C−C bond cleavage. The initial step in the cleavage of the C−C bond of the aziridine ring (2,3) results in the formation of the planar intermediate, azomethine ylide (AMY, see Scheme 1). Subsequently, a [1,2] hydrogen atom shift occurs and leads to the formation of two species: [**2,3-A** or methyl 2-(methyleneamino)-acetate, MMAA] and [**2,3-B** or methyl 2-(methylimino)-acetate, MMIA]. In channel (A) the hydrogen atom of the N−H bond migrates towards the C−H group, while in channel (B) this shift occurs in the opposite direction towards the CH_2 group rearranging into a methyl group.

For the MMAA product, internal rotation around C_1−C_3 and C_3−N_4 single bonds (according to the atom numbering adopted for this isomer, see Figure 6) may afford several conformers.

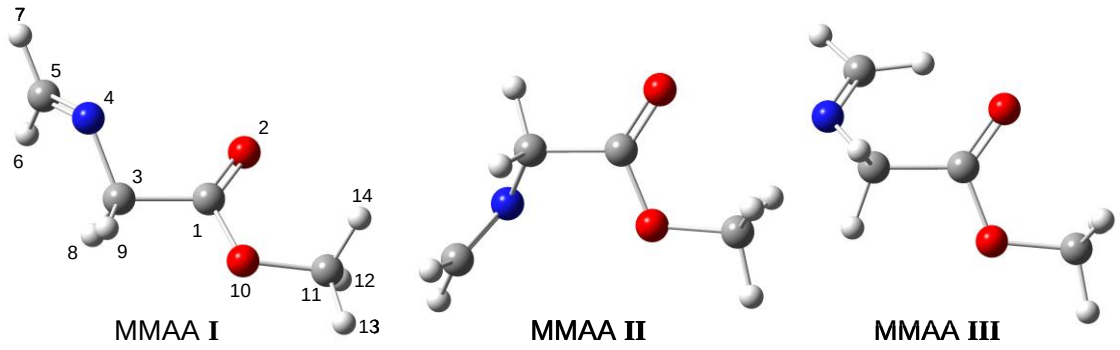

Figure 6. DFT(B3LYP)/6-311++G(d,p) optimized structures of the two most stable conformers of methyl 2-(methyleneamino)-acetate (MMAA), with atom numbering adopted in this work. Color codes: carbon – grey, hydrogen – white, oxygen – red, nitrogen – blue.

Three structures within the 0-7 kJ mol^{-1} energy range were located on the potential energy surface for this species (see Figure 7). Figure 7 presents the potential energy surface of MMAA calculated at the DFT(B3LYP)/6-311++G(d,p) level as a function of the CCN=C and O=CCN dihedral angles. These dihedral angles were incremented in steps of 20º and all remaining internal coordinates were optimized at each point. For the potential energy surface shown in Figure 7, the ester group was kept in a *cis* orientation (O=C−O−CH_3 dihedral angle is about 0°). Much higher energy structures were obtained when the ester group is in a *trans* orientation (O=C−O−CH_3 dihedral angle is about 180°). According to the calculations, MMAA

may adopt three different structures, with conformers MMAA **II** and MMAA **III** being 1.3 and 6.0 kJ mol^{-1} higher in energy than the most stable conformer **I** (see Figure 6 and Table S5), all of them belonging to the C_1 symmetry point group. The conformationally relevant dihedral angles O_2=C_1−C_3−N_4 and C_1−C_1−N_4=C_5 were calculated as (−35.2, 138.3 and 46.8º) and (111.5, 122.4, −0.9º) for conformers **I**, **II** and **III**, respectively, with mirror-like counterparts with O_2=C_1−C_3−N_4 and C_1−C_1−N_4=C_5 dihedral angles equal to (35.2, −138.3 and −46.8º) and (−111.5, −122.4, 0.9º), respectively (see Table S6). The orientation of the −CH_2−N=CH_2 group in relation to the C_1−C_3 single bond is a key factor that determines the stabilization between the conformers. The interaction between the nitrogen atom and the oxygen atoms (=O_2 and −O_{10}) of the ester group determines the non-planarity of this fragment. Completely planar structures were found to be transition states.

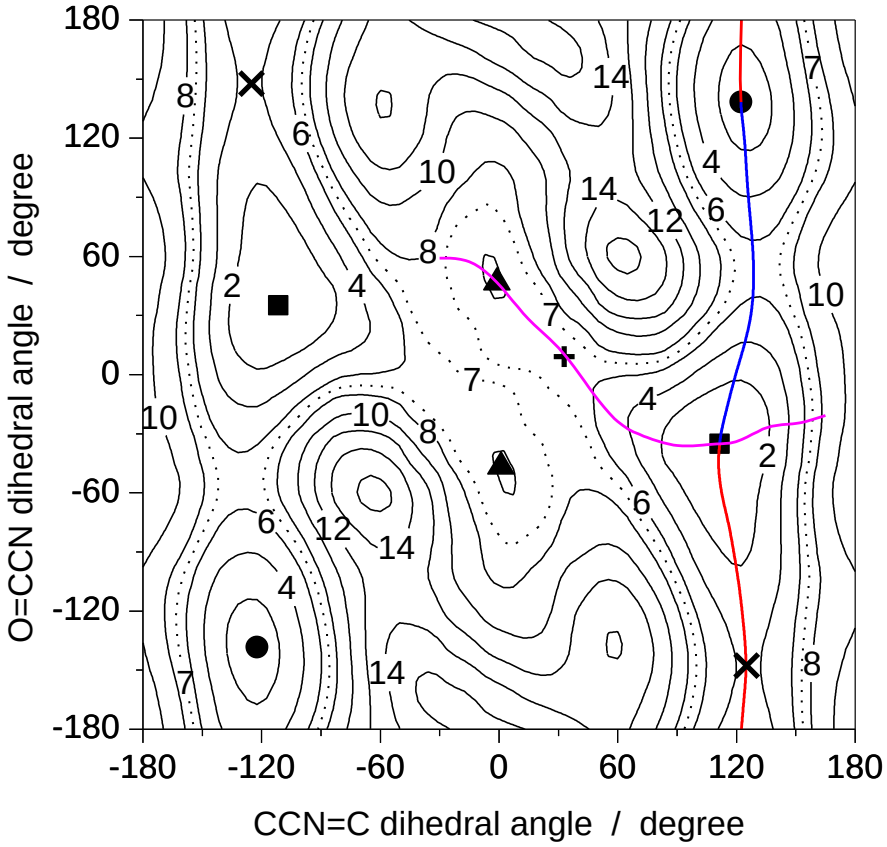

Figure 7. Potential energy map showing the position of the three low energy conformers of MMAA as a function of CCN=C and O=CCN dihedral angles. Calculations were carried out at the DFT/B3LYP/6-311++G(d,p) level. These dihedral angles were incremented in steps of 20º and all remaining internal coordinates were optimized at each point. Each conformer correspond to equivalent-by-symmetry minima and are represented by squares (■, conformer **I**), black circles (●, **II**) and triangles (▲, **III**). 1st order transition states interconnecting the conformers are represented by crosses (**x**). Energies are relative to the most stable conformer (**I**) and do not include zero-point vibrational corrections. The corresponding one-dimensional potential energy profiles are also shown. Isoenergy levels are spaced by 2 kJ mol^{-1}. See Figure 6 for conformer structures and atom numbering.

The energy barriers for interconversion of **II**→**I** and **III**→**I** were also calculated because the knowledge of the energy barriers for interconversion between the conformers is of extreme importance in the interpretation of the experimental results. A more detailed look at the possible pathway for interconversion between conformers is shown in Figure 8. Conversion between forms **I** and **II** imply internal rotation around the C_1-C_3 bond, with an energy barrier for **II**→**I** of 2.3 kJ mol^{-1} (3.5 kJ mol^{-1} in the reverse direction). In the case of interconversion between forms **I** and **III** the driving coordinate is the $C_1-C_1-N_4=C_5$ dihedral angle. The **III**→**I** energy barrier was found to be 0.3 kJ mol^{-1} only.

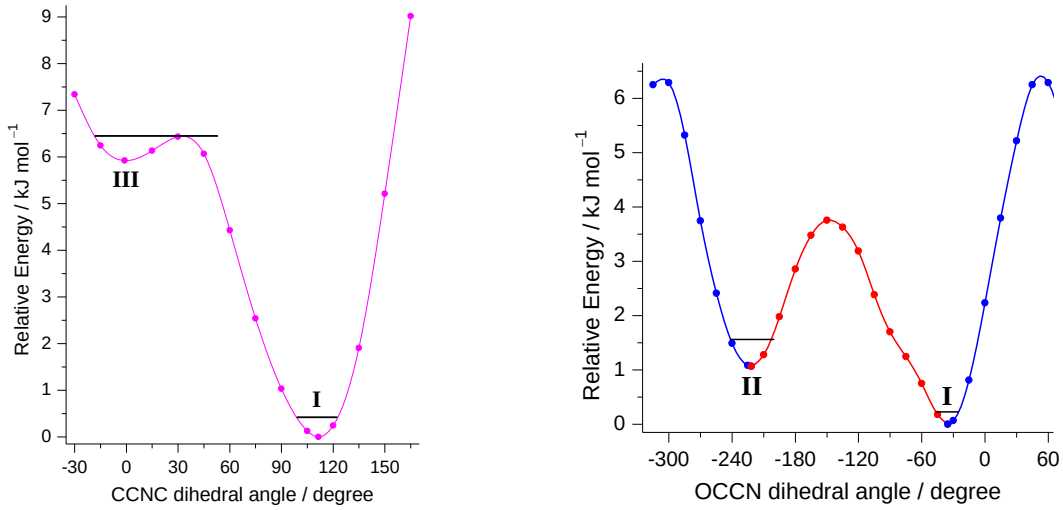

Figure 8. *Left:* PES profile along the CCNC coordinate, showing a possible pathway for interconversion between conformer **I** and **III**. *Right:* PES profile along the OCCN coordinate, showing a possible pathway for interconversion between conformer **I** and **II**.

The zero-point vibrational energy of structure **III**, for the coordinate transforming it to structure **I** (CCNC torsion), is equal to 0.3 kJ mol^{-1}, *i.e.*, exactly the same as the energy barrier in the **III**→**I** direction. Therefore, structure **III** cannot be treated as an independent conformation, but should be considered only as an excited vibrational state of conformer **I**. With respect to conformer **II**, the barrier separating it from the lower-energy conformer **I** is low enough to assume a possibility of conformational cooling[44,45] for this system in the matrix-isolation experiments. However, the height of the barrier is not the only factor responsible for stabilization, or non-stabilization, of this structure. The barriers were calculated for a monomer in

vacuum, however in the cryogenic matrix the bulky fragments of the guest molecule may be subjected to the confinement in a rigid environment (matrix cage). This will result in an additional increase of the torsional energy barrier, and a possible stabilization of the higher-energy conformer in the matrix. Such situation occurred, for example, in the pair of related molecules, cyanoacetic acid and methyl cyanoacetate, differing only by substitution of a hydrogen-atom by methyl group.[45] Therefore, the possibility of observation of the second MMAA conformer, must depend on the particular experimental conditions. As it will be shown in detail below, both low energy conformers of MMAA were indeed observed experimentally both in argon and xenon photolyzed matrices of MA2C.

On the other hand, there are four MMIA structures (**2,3-B**) resulting form [1,2] hydrogen atom shift of AMY below 18 kJ mol^{-1} (the optimized structures of the four most stable conformers of MMIA are shown in Figure S2 in the Supporting Information). These conformers can be divided into two groups relative to the position of the CH_3−N=C−C fragment. When the C_5–N_4=C_3–C_1 dihedral angle is 180º, *i.e.*, in a *trans* orientation, the group includes the lowest energy forms of MMIA (conformers **I** and **II**), while the other group, where the dihedral angle is in a *cis* orientation (C_5–N_4=C_3–C_1 dihedral angle ~0º), includes conformers **III** and **IV**. The interconversion energy barriers corresponding to the lowest energy pair of conformers, associated with the internal rotation around the central bond C_1−C_3, being the O_2=C_1−C_3−N_4 dihedral angle the driving coordinate) was also evaluated. The energy barriers separating these forms were calculated to be higher than *ca.* 10 kJ mol^{-1} in both directions.

An additional note should be mentioned regarding the two sets of putative products resulting from cleavage of the C−C bond of the aziridine ring. A comparison of the energies of MMAA and MMIA structures revealed that conformers belonging to MMIA have lower energies compared to the MMAA conformers, a fact that could be explained taking into consideration the hybridization of the nitrogen atom in both families. The sp^2 hybridization of the nitrogen atom in the MMIA molecule (**2,3-B**) compared to the sp^3 hybridization of the nitrogen atom in the MMAA molecule (**2,3-A**) adds to their enhanced stability. In consonance with this, the MMIA forms were not detected in the matrices after broadband UV irradiation or using laser light at any wavelength.

Broadband and Narrowband UV Irradiation

Figure 9 shows the effect of the subtraction resultant from the experimental spectrum recorded after UV irradiation at 235 nm during 80 min *minus* the spectrum recorded after deposition of MA2C in an argon matrix at 15 K (a); and the spectra theoretically simulated at the DFT(B3LYP)/6-31++G(d,p) level for two most stable conformers of MMAA (b). Irradiation of the xenon matrices using narrowband tunable UV irradiation gave essentially similar results. In fact, though irradiation using the two light sources (Hg(Xe) high-pressure lamp and laser light) led to the same main photoprocess, resulting from C−C bond cleavage of the aziridine ring, some additional bands belonging to other species not necessarily the same were observed in the spectra in both situations. The definition of the internal coordinates adopted in the vibrational analysis for the two most stable conformers of MMAA is provided in Table S7 (Supplementary Information). The calculated wavenumbers, infrared intensities and potential energy distributions resulting from normal mode analysis, carried out for these conformers are presented in Table S8 and Table S9 (Supplementary Information). The assignments of bands due to photoproducts are presented in Table 4 (laser light).

The most significant bands assigned to MMAA appear in the carbonyl region and in the 1200 cm^{-1} spectral region. The infrared spectra of the irradiated matrices reveal that two conformers of MMAA (**I** and **II**) can be assigned in agreement with calculated theoretical spectra. The most intense bands observed are due to the νC=O modes and are observed at 1772/1766 with a shoulder at 1768 cm^{-1} (**I**) and 1767/1762 cm^{-1} (**II**) in argon matrix (1757/1753 and 1751 cm^{-1}, for forms **I** and **II**, respectively in xenon). Bands at 1203, 1197/1196, 1183-1175 cm^{-1} (Ar) and 1201, 1197, 1182-1178 cm^{-1} (Xe) are ascribable to the wag($C5H_2$) and twist(CH_2), $\delta_4(CH_3)$ and wag($C5H_2$) vibrational modes (see Table 4 for details).

No photochemical reactions were noticed upon UV laser irradiation at $\lambda < 240$ nm. However, immediately after just 2 minutes of irradiation at $\lambda = 235$ nm new absorptions emerged throughout the spectrum, with emphasis in the carbonyl region (Figure 9) and around the 1200 cm^{-1} spectral region.

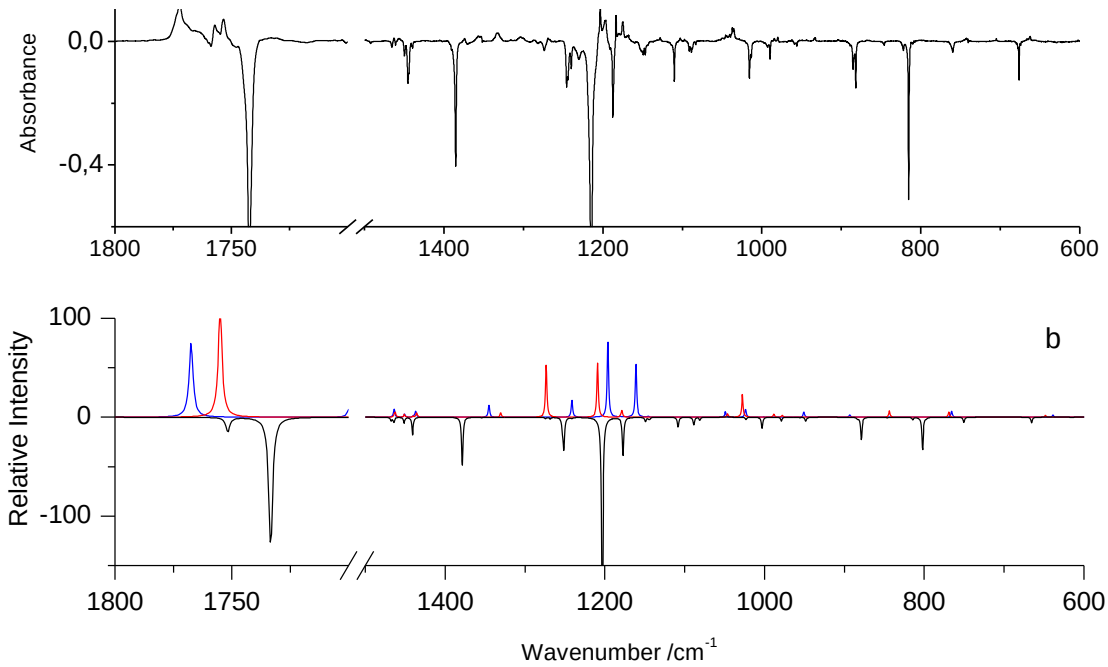

Figure 9. Experimental IR difference spectrum of irradiated Ar matrix of MA2C after UV irradiation at 235 nm during 80 minutes minus the spectrum of MA2C isolated in an argon matrix (a), compared with the infrared spectrum simulated for the gas-phase equilibrium mixture of conformers **I** and **II** of MA2C, together with the simulated spectra of the two most stable conformers of MMAA (b) calculated at the DFT(B3LYP)/6-311++G(d,p) level. The sum spectrum (most stable conformers of MA2C) was simulated using Lorentzian functions (fwhm = 2 cm^{-1}) centered at the calculated wavenumbers (scaled by a single factor of 0.978 and multiplied by –1). Calculated intensities of the bands due to individual conformers of MA2C were weighted by their expected populations (0.927 for **I** and 0.073 for **II**), corresponding to the calculated relative Gibbs energy difference (6.3 kJ mol^{-1}) at room temperature. Color codes: MA2C (sum spectrum) – black, MMAA **I** –dark blue and MMAA **II** – red. The strongest absorptions are truncated in both panels.

The carbonyl region proved to be an exceptional example providing a clear visualization of both generated forms of MMAA generated (see also Table 4). Figure 10 depicts the infrared spectra corresponding to the experimental spectrum of monomeric MA2C isolated in an argon matrix (15 K) and the spectrum resulting after UV irradiation at 235 nm during 80 minutes, as well as the subsequent irradiations at 290 nm (selected spectral regions). After 80 minutes irradiation, approximately 80% of the initially matrix-isolated compound had been consumed. The B3LYP)/6-311++G(d,p) theoretically predicted spectra of conformers **I** and **II** of MMAA and the most stable form of methyl formate and acetonitrile are also presented in this figure (panel b).

Table 4 – Experimental and DFT(B3LYP)/6-311++G(d,p) calculated infrared data and vibrational assignments of the observed photoproducts resulting from narrowband UV irradiation using laser light (λ = 235 nm) of MA2C in argon and xenon matrices.

Experimental		Calculated				
Ar matrix	Xe matrix	MMAA **I**		MMAA **II**		Approximate description
ν	ν	ν	I_{IR}	ν	I_{IR}	
1772/1768sh/1766 **(I)**	1767/1762 **(I)**	1767.4	235.9	–	–	ν(C=O)
1757/1753 **(II)**	1751 (**II**)	–	–	1755.0	339.5	ν(C=O)
1688	1700/1695	1699.7	27.5	1694.9	7.0	ν(N=C)
1457	1456	1464.3	8.4	1463.7	8.6	$\delta_2(CH_3)$
		1463.8	18.4	1462.4	13.4	$\delta(C5H_2)$
1442/1437	1438/1436	1439.3	2.9	1440.4	3.7	$\delta(CH_2)$
		1436.8	19.8	1435.6	14.0	$\delta_1(CH_3)$
1361/1356/1353 (**I**)	1356 (**I**)	1345.3	40.4	1330.3	14.7	$wag(CH_2)$
1316/1303; 1269 (**II**)	1300; 1275 (**II**)	–	–	1273.4	166.3	$twist(CH_2)$
1203 (**I**)	1201 (**I**)	1196.2	248.8	–	–	$wag(C5H_2)$
1197/1196 (**II**)	1197 (**II**)	–	–	1209.0	171.7	$wag(C5H_2)$, $twist(CH_2)$
1183(**I**) /1181/1179/ 1178/1175/1171/1169/ 1167	1182(**I**)/1181/1178/ 1166/1162/1159	1161.1	170.5	1178.5	21.4	$wag(C5H_2)$, $twist(CH_2)$
1148/1146	1149/1146	1145.5	2.6	1145.2	0.9	$\delta_5(CH_3)$
n.obs.	1077	–	–	–	–	γ(CH)
1050/1045/1043/ 1040/1037/1035	1049/1042/1035	1049.0	18.3	1046.3	10.9	γ(CH)
987/984/980	993	–	–	988.4	9.3	ν(CN)
962	962/961	–	–	–	–	$rock(CH_2)$
943	950	950.7	16.5	–	–	ν(CN)
–	926/924					ν(CN)
884	n.obs.	893.3	7.1	–	–	ν(CO)
748	740	–	–	–	–	δ(CC=O)

[a] Wavenumbers (cm^{-1}, scaled by 0.978), calculated intensities (km mol^{-1}), s = symmetric; a = antisymmetric; ν = stretching; δ = in-plane bending; γ = out-of-plane bending; τ = torsion; rock = rocking; wag = wagging; twist = twisting. See Table S7 for definition of internal coordinates and Table S8 and Table S9 for potential energy distributions.

Upon irradiation at λ = 290 nm, the band at 1772/1766 cm^{-1} assigned to the most stable form of MMAA (**I**) decreases in intensity while a significant increase in intensity of a new band at **1747** cm^{-1} is observed (the same effect occurred for the band at 1203 cm^{-1}, with appearance of a new band at **1205** cm^{-1}). On the other hand, the intensity of the doublet band at 1757/1753 cm^{-1} due to conformer **II** remains constant. According to previous publications,[49,50] these new bands are distinctive for methyl formate isolated in an argon matrix, attributed to νC=O and νC=O vibrations. These observations thus indicate that MMAA undergoes a secondary phototransformation into methyl formate and possibly acetonitrile, which can be in the origin of the band at 2234 cm^{-1}.

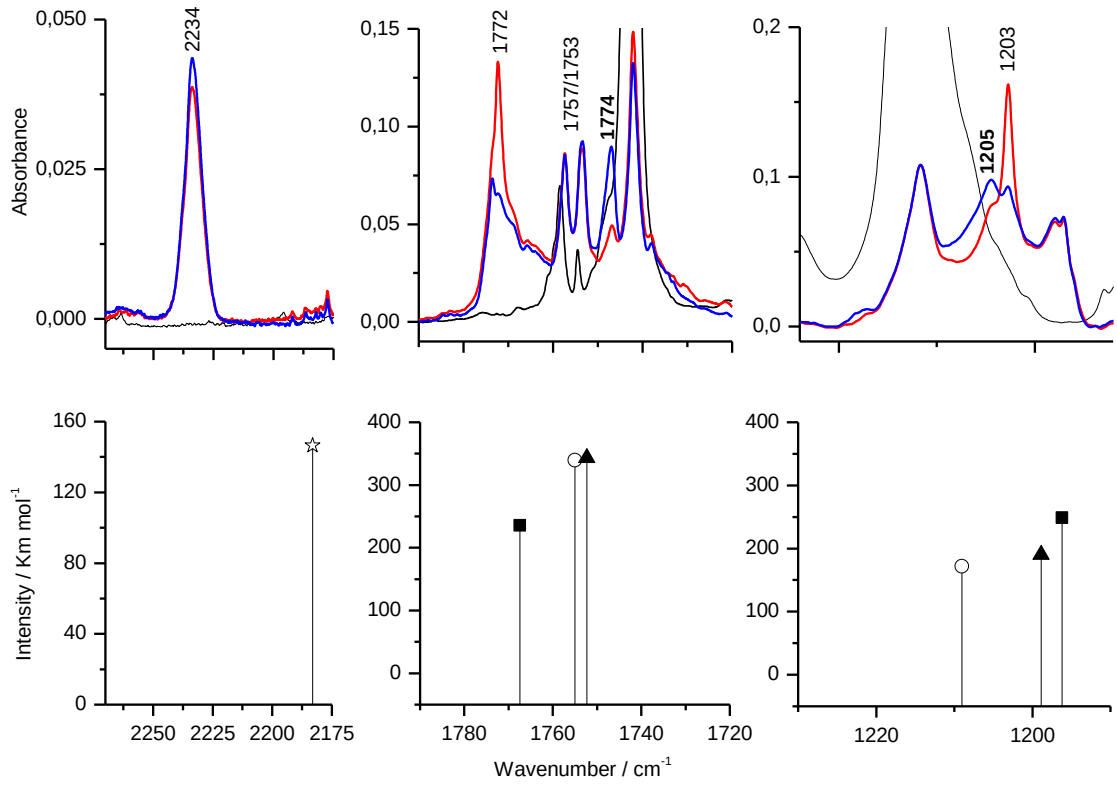

Figure 10. Selected spectral carbonyl stretching region (1790-1720 cm^{-1}) showing the phototransformation of MA2C into MMAA using UV irradiation at λ = 235 nm. *Panel a:* Fragments of the infrared spectrum of MA2C monomers isolated in an Ar matrix: (black) recorded after deposition of the matrix (15 K); after irradiation of the matrix with UV (λ = 235 nm) monochromatic laser (red); after irradiation of the matrix with UV (λ = 290 nm) monochromatic laser (blue). *Panel b:* In the theoretical spectra wavenumbers were scaled by 0.978, and intensities are not scaled: (■, MMAA **I**), open circles (○, MMAA **II**), triangles (▲, methyl formate) and stars (acetonitrile).

C–N bond cleavage (1,2) and (1,3)

The second photochemical process analysed is the cleavage of the C–N bond of the aziridine ring with two possible channels: 1,2 and 1,3 (see Figure 5). The simultaneous migration of the hydrogen atom (H6) towards the nitrogen and formation of the double C=N bond between C3 and N1 and the rupture of C-N bond (1,2) yields product **1,2-A** (methyl 3-iminopropanoate, M3IP). In this case, besides three internal degrees of freedom that can give to different conformers (the orientation of the ester group, the rotation around the single central C–C bond and around the C–C bond connected to the HN=CH fragment), the orientation of the HN=CH moiety itself can give rise to different isomers, as the HN=CH dihedral angle can be either *cis* or *trans*. Two independent potential energy scans were performed at the DFT(B3LYP)/6-31++G(d,p) level, taking into consideration the two possible

orientations of the HN=CH fragment. Figures S3 (Supporting Information) presents the two-dimensional potential energy surface of **1,2-A** with the HN=CH unit in a *cis* position as a function of N=CCC and O=CCC dihedral angles in steps of 20º and optimizing all remaining geometric parameters at each point. The PES of **1,2-A** (HN=CH *cis*) shows three different minima energies below 7 kJ mol^{-1}, as well as the interconversion pathways between the different minima and with the symmetry-equivalent structures (see Figure S4). The conformationally relevant N_4=C_5–C_3–C_1 and C_5–C_3–C_1=O_2 dihedral angles are (135.3, 123.8 and –1.9º) and (21.2, –137.4 and –95.5º), for conformers **I**–**III**, respectively (see Figure S4 for the exact location of these minima on the potential energy surface). The weak hydrogen bond formed between the carbonyl oxygen atoms and the hydrogen atom of the HN=CH fragment, closing an intramolecular five-membered ring H–C–C(H2)–C=O is the main factor responsible for the stabilization of the global minimum (**I**) with respect to conformers **II** and **III** (see Figure S4). It should be noticed that the interaction of the hydrogen atom with the lone pair of the carbonyl oxygen can be expected to be more important than with those of the methoxylic ester oxygen (as observed for conformer **II**), because in the first case the hybridization brings the maximum of electron density in the plane of the molecule and in the second case out of the plane. Rotation around the C–C central bond leads to conformer **II** and **III**.

On the other hand, the PES of **1,2-A** (HN=CH *trans*) exhibits four minima, all belonging to the C_1 symmetry point group, with energies between 0-4 kJ mol^{-1} (see Table S5), with symmetry-equivalent structures (see Figure 11).

The most striking result is the comparatively low energies between the three most stable forms, conformer **II** is less stable than **I** by only 0.1 kJ mol^{-1}, whereas for **III** the value is 0.4 kJ mol^{-1}. This closeness between the energies prompted us to undertake a two-dimensional potential energy surface to provide a better understanding of this particular group of conformers. As in the previous case, the two-dimensional potential energy surface of **1,2-A** where the HN=CH unit in a *trans* position was calculated as a function of N=CCC and O=CCC dihedral angles in steps of 20º and optimizing all remaining geometric parameters at each point is shown in Figure 12. The conformationally relevant N_4=C_5–C_3–C_1 and C_5–C_3–C_1=O_2 dihedral angles corresponding to conformer **I** are (16.0 and –41.2º), **II** (134.6 and 48.2º), **III** (120.4 and –119.4º) and **IV** (23.4 and 119.5º). For this set of structures, two weak hydrogen bonds can be formed between the carbonyl oxygen or methoxylic ester

oxygen atoms and the hydrogen atoms of the HN=CH fragment, closing into an intramolecular six-membered ring H=N–C–C(H2)–C(O) or a five-membered ring H–C–C(H2)–C(O) are the foremost important factors to consider in the stabilization of these minima. The six-membered ring is present in forms **I** and **IV**, where the =N–H···O distances are 2.2 and 2.3 Å, respectively. In conformers **II** and **III**, the =C–H···O distances are *ca.* 2.7 Å for the five-membered ring (see Figure 11). Figure 12 also depicts the interconversion barriers relating the four conformers with the corresponding transition states indicated by the letter T. The interconversion energy barriers between the different conformers were found to be low, with energies varying from 1–5 mol^{-1}.

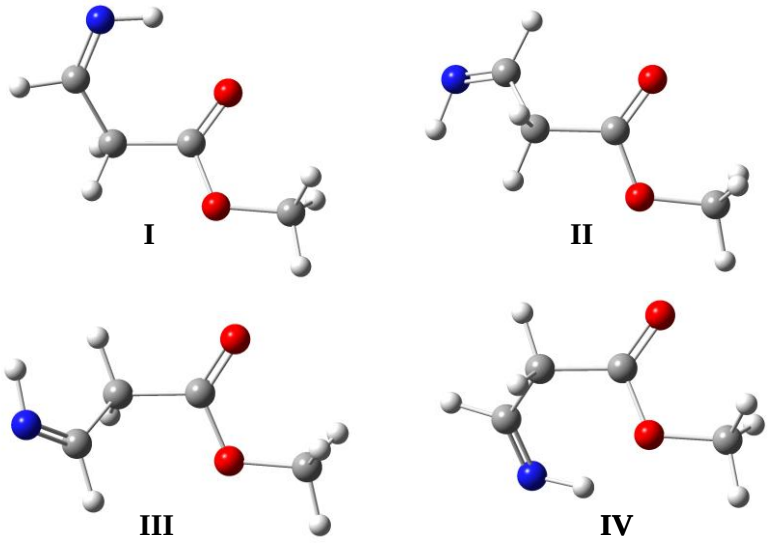

Figure 11. DFT(B3LYP)/6-311++G(d,p) optimized structures of the two most stable conformers of methyl 3-iminopropanoate (M3IP) with the HN=CH fragment in *trans* position. Color codes: carbon – grey, hydrogen – white, oxygen – red, nitrogen – blue.

Product **1,2-B** (methyl 3-aminoacrylate, M3AA) is obtained by cleavage of bond 1,2 followed by formation of a new double bond between carbon atoms 2 and 3. Four minima with higher energies that can be interconverted in each other by internal rotation around the central C–C bond were found with energies higher than the most stable form equal to 12.4, 14.7 and 19.1 kJ mol^{-1}, for conformers **II-IV**, respectively (see Table S5). The N_4=C_5–C_3–C_1 and C_5–C_3–C_1=O_2 dihedral angles are either 0º or 180.0º, however, only conformer **I** and **II** are indeed planar belonging to the C_s symmetry group (see Figure S5). Constraining conformers **III** and **IV** to planarity

yielded transition states. The main difference between the four minima lies in the arrangement of the NH_2 group. The nitrogen atom lies in the same plane as the C=C−(O=C−O−CH_3) group, with both hydrogen atoms arranged in an out of plane orientation towards the nitrogen atom.

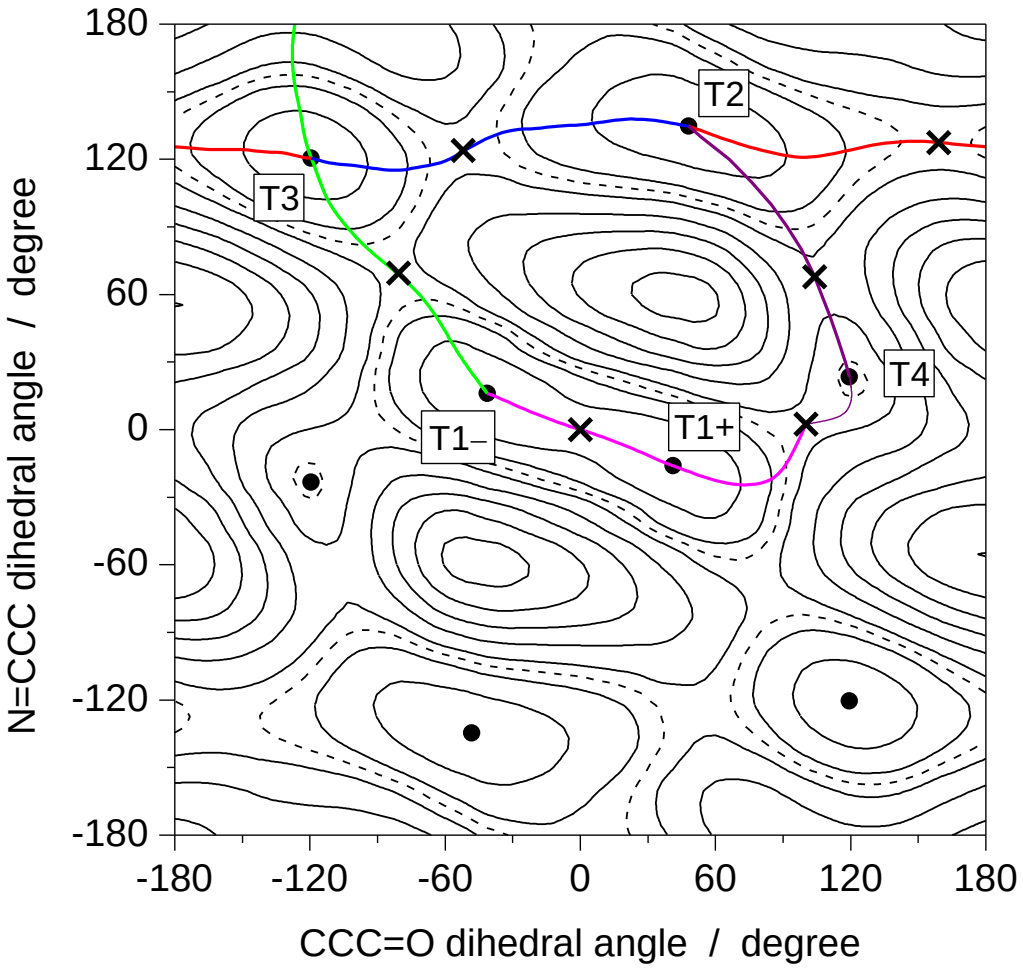

Figure 12. Potential energy map showing the position of the four low energy conformers of M3IP as a function of N=CCC and CCC=O dihedral angles. Calculations were carried out at the DFT/B3LYP/6-311++G(d,p) level. These dihedral angles were incremented in steps of 20º and all remaining internal coordinates were optimized at each point. Each conformer correspond to equivalent-by-symmetry minima and are represented by black circles (●) corresponding to conformer **I** (16.001 and –41.171º), **II** (134.641 and 48.218º), **III** (120.416 and –119.379º) and **IV** (23.397 and 119.463º). 1st order transition states interconnecting the conformers are represented by the letter T. The HN=CH fragment in *trans* position. Energies are relative to the most stable conformer (**I**) and do not include zero-point vibrational corrections. The corresponding one-dimensional potential energy profiles are shown in different colors (**III→II**, dark blue); (**I→I'**, pink); (**I→III**, green); (**II→III**, red) and (**II→IV**, purple). Isoenergy levels are spaced by 2 kJ mol^{-1}. See Figure 11 for conformer structures.

Finally, cleavage of the C–N ring bond (1,3) also yields two different products: **1,3-A** (methyl 2-iminopropanoate, M2IP) was formed after the concerted scission the C–N bond and the migration of the hydrogen atom (H5) from C_2 to C_3 with subsequent rearrangement into a methyl group of the initial $–CH_2$ group. **1,3-B** (methyl 2-aminoacrylate, M2AA) which resulted from the simultaneous migration of one the hydrogen atom from C_3 to N_1 due to the formation of a new C=C double bond between C_2 and C_3 (see Figures S6 and S7).

Two unique planar conformers (C_s symmetry) were theoretically calculated for the **1,3-A** product resulting from the rotation around the central C–C bond. The –N–H is orientated in a *cis* (most sable form) or *trans* position (second stable form) relative to the carbonyl double bond of the ester group. Once again, the predominance of a weak intramolecular five-membered ring formed between the hydrogen atom of the $H–N=C–CH_3$ component and the carbonyl oxygen or methoxylic ester oxygen atoms is the key factor determining the relative stability of these two forms. The energy barriers associated with the interconversion between these two forms are 15.4 for **II**→**I**, and 17.0 kJ mol^{-1} for **I**→**II**.

Methyl 2-aminoacrylate (**1,3-B**) molecule bears only one conformationally relevant internal rotation axis, corresponding to the rotation around the central C–C bond (non-planar structures). Completely planar structures were also theoretically calculated, however, they were found to be first order transition states. The calculated interconversion barrier between these two forms is very high in both directions (above 25 kJ mol^{-1}).

Broadband and Narrowband UV Irradiation

The presence of characteristics bands due to carbon monoxide (CO) in the 2170-2100 cm^{-1} spectral region and carbon dioxide (CO_2) in the 2370-2310 cm^{-1} spectral region were identified in both matrices after irradiation with broadband UV unfiltered light ($\lambda > 235$ nm) and narrowband tunable UV laser light. These observations indicate the possibility that in a secondary process, decarbonylation or decarboxylation can occur. The carbon monoxide band has a broad profile in both irradiation experiments; in argon, bands at 2149.3, 2138.5, 2134.6, 2132.0, 2127.5 and 2120.2 cm^{-1} from broadband irradiation, a doublet at 2162.6/2160.1 cm^{-1} and a

complex multiplet group of bands located at 2150-2130 cm^{-1} with UV laser light were observed, while in the xenon matrix the most intense bands appear at 2141.3, 2134.4, 2132.5, 2127.6 and 2122.5 cm^{-1} (broadband irradiation) and bands at 2161.5/2157.5 cm^{-1} and 2136.7, 2134.4, 2132.4 and 2127.5 cm^{-1} are the most intense from UV laser light irradiation. Monomeric CO isolated in an argon matrix gives rise to a band at 2138.5 cm^{-1} and the band at 2149.3 cm^{-1} has been assigned to the CO:H_2O complex (2133.2 and 2141.1 cm^{-1} in xenon, respectively).[51,52] The other bands observed must be due to CO complexed with other photoproducts.

Besides the bands assigned to the primary photoproduct, MMAA, resulting from cleavage of the C–C ring bond, the most outstanding spectral feature observed after broadband UV irradiation (λ = 235 nm) is the appearance of a band at *ca.* 2234 cm^{-1} in the argon matrix (*ca.* 2232 cm^{-1} in xenon). The appearance of this band in the 2100-2300 cm^{-1} spectral region, is characteristic for nitrile (C≡N stretching vibrational mode). This band can be partially due to acetonitrile formed in the secondary reaction of MMAA which simultaneously produces methyl formate. However, it probably also results from other still non-identified photoproducts. These are, with all probability result of cleavage of the C–N bond of aziridine. Note also that other bands (*e.g.*, 1374, 1333/1331, 1131/1130/1128, 1102, 1001, 1097, 962, 934/932 and 704 cm^{-1}) ascribable to unidentified photoproducts were also observed. Positive identification of these additional photoproducts is underway.

Conclusions

Quantum chemical calculations on MA2C carried out at the DFT/(B3LYP)/6-311++G(d,p) level predicted the existence of two low-energy minima. The energy barrier separating these two forms is above *ca.* 20 kJ mol^{-1} in both directions. These two low energy forms were found to be present in the as-deposited matrices (argon, xenon) of the compound and their spectra were fully assigned in both matrices. The photochemistry of MA2C has also been investigated, using broadband UV irradiation (λ > 235 nm) and narrowband tunable laser light irradiation at λ = 235 nm. The most common photoreaction was observed: ring-opening through C–C bond cleavage leading to MMAA as primary photoproduct. Subsequent irradiation at λ = 290 nm led

to the observation of new bands with decrease of bands assigned to conformer **I** of MMAA. The most intense of these bands correlate well with the spectra of methyl formate and acetonitrile, which are then tentatively assigned as minor products of photochemical decomposition of MMAA **I**. In addition, bands assigned to carbon monoxide and carbon dioxide have been identified occurrence of decarbonylation and decarboxylation as secondary photoreactions. Other products still remain unidentified, which shall be a result of C–N bond cleavage of the aziridine ring of MA2C.

Supporting Information Available: Figures S1-S2, High energy conformers of MA2C and of the four most stable conformers of methyl 2-(methyleneamino)-acetate (MMIA) optimized at the DFT(B3LYP)/6-311++G(d,p) level of theory; Figure S3. DFT(B3LYP)/6-311++G(d,p) potential energy map of M3IP; Figures S4-S7. DFT(B3LYP)/6-311++G(d,p) optimized structures of the most stable conformers of methyl 3-iminopropanoate (M3IP) with the HN=CH fragment in *cis* position, methyl 3-aminoacrylate (M3AA), methyl 2-iminopropanoate (M2IP) and methyl 2-aminoacrylate (M2AA); Table S1 – DFT(B3LYP)/6-311++G(d,p) calculated bond lengths and angles of the eight conformers of MA2C; Table S2 – Definition of symmetry coordinates used in the normal mode analysis of the conformations of MA2C; Tables S3-S4 – Calculated [scaled, DFT(B3LYP)/6-311++G(d,p)] wavenumbers, IR intensities and Potential Energy Distributions (PED) for the two most stable conformers of MA2C; Table S5-S6 – DFT(B3LYP)/6-311++G(d,p) calculated relative energies and calculated values for the main conformational dihedral angles of possible photoproducts resulting from different ring-opening reactions of MA2C; Table S7 – Definition of symmetry coordinates used in the normal mode analysis of the conformations of methyl (methyleneamino) acetate (MMAA); Tables S8-S9 – Calculated [scaled, DFT(B3LYP)/6-311++G(d,p)] wavenumbers, IR intensities and Potential Energy Distributions (PED) for the two most stable conformers of MMAA. This material is available free of charge *via* the Internet at …

Acknowledgements

These studies were partially funded by the Portuguese Science Foundation (Project No. FCOMP-01-0124-FEDER-007458, cofunded by QREN-COMPETE-UE. S.L. acknowledges FCT for Grant No. SFRH/BD/29698/2006.

References:

[1] A. Padwa, *Comprehensive Heterocyclic Chemistry III*, 2008, Chapter 1.01 - *Aziridines and Azirines: Monocyclic*, pages 1-104.

[2] A. K. Yudin (Ed.), *Aziridines and Epoxides in Organic Chemistry*, WILEY-VCH Verlag GmbH & Co. KGaA, Weinheim, **2006**.

[3] J.B. Patrick, R.P. Williams, W.E. Meyer, W. Fulmor, D.B. Cosulich, R.W. Broschard, and J.S. Webb, *J. Am. Chem. Soc.*, **86** (1964) 1889.

[4] R.S. Coleman, J.-S. Kong, and T.E. Richardson**,** *J. Am. Chem. Soc.*,**121** (1999) 9088.

[5] E. Vedejs, B. N. Naidu, A. Klapars, D. L. Warner, V.-S. Li, Y. Na, and H. Kohn, *J. Am. Chem. Soc.*,**125** (2003) 15796.

[6] M. Hashimoto, M. Matsumoto, K. Yamada, and S. Terashima, *Tetrahedron*, **59** (2003) 3089.

[7] P. T. Trapentsier, I. Ya. Kalvin'sh, E. E. Liepin'sh, and E. Ya. Lukevits, *Chem. Heter. Comp.*, **19** (1983) 391.

[8] H. M. I. Osborn and J. Sweeney, *Tetrahedron: Asymmetry*, **8** (1987) 1693.

[9] W. McCoull and F. A. Davis, Synthesis, **10** (2000) 1347.

[10] K. J. M. Beresford, N. J. Church, and D. W. Young, *Org. Biomol. Chem.*, **4** (2006) 2888.

[11] J. L. Vicario, D. Badía, and L. Carrillo, *J. Org. Chem.*, **66** (2001) 5801.

[12] J.-Y. Wang, Y. Hu, De-X. Wang, J. Pan, Z.-T.Huang, and M.-X. Wang, *Chem. Commun.*, (2009) 422.

[13] J. M. Concellón, P. L. Bernad, and J. R. Suárez, *J. Org. Chem.*, **70** (2005) 9411.

[14] S. Stanković, M. D'hooghe, and N. De Kimpe, *Org. Biomol. Chem.*, **8** (2010) 4266.

[15] Z.-Q. Liu, Y. Fan, R. Li, B. Zhou, and L.-M. Wu, *Tetrahedron Lett.*, **46** (2005) 1023.

[16] V.C. Vederas, *Can. J. Chem.*, **84** (2006) 1197.

[17] V.H. Dahanukar and L.A. Zavialov, *Curr. Opin. Dug Discov. Devel.*, **5** (2002) 918.

[18] X. E. Hu, *Tetrahedron*, **60** (2004) 2701.

[19] G. Cardillo, L. Gentilucci and A. Tolomelli, *Aldrichim. Acta*, **36** (2003) 39.

[20] B. Zwanenburg and P. ten Holte, *Top. Curr. Chem.*, **216** (2001) 93.

[21] Robert H. Dodd, *Molecules*, **5** (2000) 293.

[22] B. Shtrumfs, J. Hermane, I. Kalvinsh, and P. Trapencieris, *Chem. Heterocycl. Compd.*, **43** (2007) 169.

[23] N. J. Church and D. W: Young, *Tetrahedron Lett.*, **36** (1995) 151.

[24] J. E. Baldwin, R. M. Adlington, I. A. O'Neil, C. Schofield, A. C. Spivey, and J. B. Sweeney, *J. Chem. Soc., Chem. Comm.*, (1989) 1852.

[25] D. Cremer and E. Kraka, *J. Am. Chem. Soc.*,**107** (1985) 3800.

[26] J. B. Sweeney, *Chem. Soc. Rev.*, **31** (2002) 247.

[27] R. Huisgen, W. Scheer, and H. Huber, *J. Am. Chem. Soc.*, **89** (1967) 1753.

[28] A. M. Trozzolo, T. M. Leslie, A. S. Sarpotdar, R. D. Small, G. J. Ferraudi, T. DoMinh and R. L. Hartless, *Pure and Appl. Chem.*, **51** (1979) 261.

[29] P. Deshong, D. A. Kell, D. R. Sidler, *J. Org. Chem.*, **50** (1985) 2309.

[30] B. R. Henke, A. J. Kouklis, C. H. Heathcock, *J. Org. Chem.*, **57** (1992) 7056.

[31] C. Nájera and J. M. Sansano, *Curr. Org. Chem.*, **7** (2003) 1105.

[32] H. Pellissier, *Tetrahedron*, **63** (2007) 3235.

[33] C. Gaebert, J. Mattay, M. Toubartz, S. Steenken, B. Müllen, and T. Bally, *Chem. Eur. J.*, **11** (2005) 1294.

[34] I. M. B. Nielsen, *J. Phys. Chem. A*, **102** (1998) 3193.

[35] H. D. Banks, *J. Org. Chem.*, **73** (2008) 2510.

[36] A. Paasche, M. Arnone, R. F. Flink, T. Schirmeister, and B. Engels, *J. Org. Chem.*, **74** (2009) 5244.

[37] M. J. Frisch, G. W. Trucks, H. B. Schlegel, G. E. Scuseria, M. A. Robb, J. R. Cheeseman, J. A. Montgomery, Jr., T. Vreven, K. N. Kudin, J. C. Burant, J. M. Millam, S. S. Iyengar, J. Tomasi, V. Barone, B. Mennucci, M. Cossi, G. Scalmani, N. Rega, G. A. Petersson, H. Nakatsuji, M. Hada, M. Ehara, K. Toyota, R. Fukuda, J. Hasegawa, M. Ishida, T. Nakajima, Y. Honda, O. Kitao, H. Nakai, M. Klene, X. Li, J. E. Knox, H. P. Hratchian, J. B. Cross, V. Bakken, C. Adamo, J. Jaramillo, R. Gomperts, R. E. Stratmann, O. Yazyev, A. J. Austin, R. Cammi, C. Pomelli, J. W. Ochterski, P. Y. Ayala, K. Morokuma,

G. A. Voth, P. Salvador, J. J. Dannenberg, V. G. Zakrzewski, S. Dapprich, A. D. Daniels, M. C. Strain, O. Farkas, D. K. Malick, A. D. Rabuck, K. Raghavachari, J. B. Foresman, J. V. Ortiz, Q. Cui, A. G. Baboul, S. Clifford, J. Cioslowski, B. B. Stefanov, G. Liu, A. Liashenko, P. Piskorz, I. Komaromi, R. L. Martin, D. J. Fox, T. Keith, M. A. Al-Laham, C. Y. Peng, A. Nanayakkara, M. Challacombe, P. M. W. Gill, B. Johnson, W. Chen, M. W. Wong, C. Gonzalez, J. A. Pople, Gaussian 03, Revision C.02 ed., Gaussian, Inc., Wallingford, CT, 2004.

[38] M. Frisch, M. Head-Gordon, Pople, *J. Chem. Phys. Lett.*, **166** (1990) 281.

[39] A. D. Becke, *Phys. Rev. A.,* **38** (1988) 3098.

[40] C. T. Lee, W. T. Yang and R. G. Parr, *Phys. Review B,* **37** (1988) 785.

[41] C. Peng and H. B. Schlegel, *Isr. J. Chem.*, **33** (1994) 449.

[42] J. H. Schachtschneider and F. S. Mortimer, Vibrational Analysis of Polyatomic Molecules. VI. FORTRAN IV Programs for Solving the Vibrational Secular Equation and for the Least-Squares Refinement of Force Constants. Report Nº. 31450. Structural Interpretation of Spectra, Technical Report nº 57-650, Shell Development Co. Emeryville, CA, 1969.

[43] P. Pulay, G. Fogarasi, F. Pang, J. E. Boggs, *J. Am. Chem. Soc.*, **110** (1979) 2550.

[44] I. Reva, A. J. Lopes Jesus, M. T. S. Rosado, R. Fausto, M. E. Eusébio, and J. S. Redinha, *Phys. Chem. Chem. Phys.*, 8 (2006) 5339.

[45] I. D. Reva, S. G. Stepanian, L. Adamowicz, and R. Fausto, *Chem. Phys. Lett.*, **374** (2003) 631.

[46] A. Borba, A. Gómez-Zavaglia, P. N. N. L. Simões, and R. Fausto, *J. Phys. Chem. A*, **109** (2005) 3578.

[47] S. Braslavsky and J. Heicklen, *Chem. Rev.*, **77** (1977) 473.

[48] B. Bigot, A. Devaquet, and A. Sevin, *J. Org. Chem.*, **45** (1980) 97.

[49] C. E. Blom and Hs. H. Günthard, *Chem. Phys. Lett.*, **84** (1981) 267.

[50] H. Hollenstein and Hs. H. Günthard, *J. Mol. Spectrosc.*, **84** (1980) 457.

[51] H. Dubost, *Chem. Phys.*, **12** (1976) 139.

[52] H. Abe and K. M. T. Yamada, *Struct. Chem.*, **14** (2003) 211.

J. Photochem. Photobiol. A: Chemistry, **2008**, *200*, 169-180.

Low Temperature IR Spectroscopy and Photochemistry of Matrix-Isolated α-Pyridil

Susy Lopes,[a] Andrea Gómez-Zavaglia[a,b] and Rui Fausto[a]

[a]*Department of Chemistry,University of Coimbra, P-3004-535 Coimbra, Portugal*
[b]*Faculdad de Farmacia y Bioquímica, Universidad de Buenos Aires, Junín 956, 1113 Buenos Aires, Argentina*

ABSTRACT

α-Pyridil [$(C_6H_4NO)_2$] has been isolated in low temperature argon and xenon matrices and studied by FTIR spectroscopy, supported by DFT(B3LYP)/6-311++G(d,p) calculations. Calculations predicted the existence of three different conformers exhibiting skewed conformations around the intercarbonyl bond and the two C_5H_4N-C(=O) fragments nearly planar. The two higher energy forms, ***TCG*** and ***CCSk*** were estimated theoretically to be respectively 21.0 and 35.1 kJ mol^{-1} higher in energy than the most stable form, ***TTG***. In consonance with the relatively high energies predicted by the calculations for the two less stable conformers of α-pyridil, only the most stable conformer was found spectroscopically to be present in the studied matrices. Infrared spectra obtained for the neat low temperature amorphous and crystalline states reveals that the ***TTG*** conformer is also the sole conformer present in these phases. UV irradiation (λ > 235 nm) of matrix-isolated α-pyridil led to its isomerization to unusual molecular species bearing Hückel-type pyridine (aza-benzvalene) rings.

Introduction

In general, simple α–dicarbonyl compounds show interesting structural, spectroscopic and photophysical properties, including photorotamerism, due to conformational changes associated with the internal rotation around the flexible O=C-C=O intercarbonyl torsional coordinate in the ground or excited electronic states.[1-8] Because of that, these compounds have received particular attention concerning their potential use for the development of molecular devices.[9-14] These compounds have also received application in other fields. For example, derivatives of α–pyridil [C_6NH_4-C(=O)-C(=O)-C_6NH_4], which is a typical representative of aromatic heterocyclic α-dicarbonyls are main components of many pesticides, herbicides and fungicides[15-17] and have been used as reagents in the production of several compounds with pharmaceutical interest.[18-21] α-Pyridils have also found important applications in the preparation of transition metal complexes[22-24] and as organic inhibitors for mild steel corrosion in hydrochloric acid.[25]

The crystal structure of α–pyridil has already been determined by X-ray crystallography.[26,27] It crystallizes in the monoclinic system, space group $P2_1/n$, with four molecules per unit cell. In the crystal, the molecule is known to adopt a structure in which two nearly planar fragments, each of which including a pyridine ring, a carbonyl group and its adjacent carbon atom, are *skewed* to each other, the angle between the two pyridyl fragments being *ca.* 83º. The predominant forces gathering the molecules in the crystal were found to be plane-to-plane interactions between approximately parallel pyridine rings.[26,27]

α–Pyridil was also studied in the past by FT-IR, Raman, NMR and UV spectroscopies in the solid state and in solution either in the ground or in excited states.[28-40] Some of these studies addressed the question of the conformational preferences of this molecule.[28,33-40]

As in other α-dicarbonyl compounds, the geometry of α–pyridil is the result of a balance between steric and resonance effects and seem to be different in different electronic states. The conjugation of the carbonyl groups with the pyridyl rings would favor the planar molecular configurations in order to achieve maximum π overlap, but the steric repulsions between the carbonyl oxygens, between these atoms and the nearest hydrogen atoms of the pyridyl rings and between the two pyridyl substituents

preferably twist the whole molecule, making *skewed* structures to be more stable than the planar ones in the electronic ground state. Investigations carried out for the compound in different solutions[28,33,40] indicated that in these media the compound exists in a single conformation similar to that observed in the crystal, with the intercarbonyl angle decreasing with the increase in polarity of the solvent.[33] On the other hand, according to time-resolved transient absorption spectra measurements, the lowest energy triplet state of α–pyridil seems to be planar in non-polar solvents.[41]

To the best of our knowledge, no structural or vibrational studies have been performed on gaseous α–pyridil as well as for the compound isolated in a low temperature inert matrix hitherto. In addition, its photochemistry has also been addressed only for the compound in solution,[36,37,41] where the media was found to play an active role, such as, for example, as source for hydrogen atoms in the photochemical reduction of α–pyridil into the enediol, 1,2-di(2-pyridyl)-1,2-ethenediol.

In the present work, the conformational study of the molecule of α–pyridil was undertaken using low-temperature matrix-isolation FTIR spectroscopy combined with theoretical calculations preformed at the DFT(B3LYP)/6-311++G(d,p) level of theory. These studies allowed for the identification and vibrational characterization of the most stable conformer of α–pyridil. Irradiation of matrix-isolated α–pyridil with UV light ($\lambda > 235$ nm) was also carried out in order to study its unimolecular photochemistry. As it will be described in detail below, under these experimental conditions α–pyridil isomerizes to molecular species bearing Hückel-type pyridyl (aza-benzvalene) substituents. Finally, low temperature infrared spectra of neat α–pyridil in the amorphous and crystalline states were also obtained and interpreted.

Materials and Methods

Infrared spectroscopy

The sample of α-pyridil (97 % purity) was obtained from Aldrich and used without any further purification.

The IR spectra were recorded with 0.5 cm^{-1} spectral resolution in a Mattson (Infinity 60AR Series) Fourier Transform infrared spectrometer, equipped with a

deuterated triglycine sulphate (DTGS) detector and a Ge/KBr beam splitter. Necessary modifications of the sample compartment of the spectrometer were done in order to accommodate the cryostat head and allow purging of the instrument by a stream of dry nitrogen, to remove water vapors and CO_2. The solid sample of α-pyridil was placed in a specially designed thermoelectrically heatable mini-furnace assembled within the cryostat chamber. The temperatures of sublimation of the compound under these conditions varied within the 80-125 ºC range. Matrices were prepared by co-deposition of α-pyridil vapors coming out of the mini-furnace and large excess of the matrix gas (argon N60 or xenon N48, both obtained from Air Liquide) onto the CsI substrate of the cryostat (APD Cryogenics, model DE-202A), cooled to 10 K (for argon matrices) or 20 K (for xenon matrices).

Irradiation of the matrices was carried out with unfiltered light from a 500 W Hg(Xe) lamp (Newport, Oriel Instruments), with output power set to 200 W, through the outer KBr windows of the cryostat ($\lambda > 235$ nm).

The low temperature solid amorphous layer of α–pyridil was prepared in the same way as matrices but with the flux of matrix gas cut off. The layer was then allowed to anneal at slowly increasing temperature up to 300 K. After the temperature exceeded 250 K the crystallization of the amorphous layer occurred. Subsequently, the sample was cooled back to 10 K and the spectrum of the crystalline phase was collected.

Computational methodology

The quantum chemical calculations were performed with Gaussian 03 (Revision C.02)[42] at the DFT level of theory, using the split valence triple-ζ 6-311++G(d,p) basis set and the three-parameter B3LYP density functional, which includes Becke's gradient exchange correction[43] and the Lee, Yang and Parr correlation functional.[44]

Geometrical parameters of the considered conformations were optimized using the Geometry Direct Inversion of the Invariant Subspace (GDIIS) method.[45] In order to assist the analysis of the experimental spectra, vibrational frequencies and IR intensities were also calculated at the same level of approximation. The computed harmonic frequencies were scaled down by a single factor (0.978) to correct them for

the effects of basis set limitations, neglected part of electron correlation and anharmonicity effects. Normal coordinate calculations were undertaken in the internal coordinate space, as described by Schachtschneider,[46] using the program BALGA and the optimized geometries and harmonic force constants resulting from the DFT calculations.

Results and Discussion

Geometries and energies

The DFT(B3LYP)/6-311++G(d,p) calculations performed in this study predicted the existence of three non-symmetrically-equivalent minima on the potential energy surface of α-pyridil. These structures are displayed in Figure 1 and exhibit a *skewed* conformation around the intercarbonyl bond and the two C_5H_4N-C(=O) fragments nearly planar. The names here adopted to designate the different conformers are based on the values of the O=C-C-N and O=C-C=O dihedral angles, where ***T***, ***C***, ***G*** and ***Sk*** refer to values of these angles of *ca.* 180º (*trans*), 0º (*cis*), 90º (*gauche*) and 120º (*skew*). The two most stable forms have the O=C-C=O moiety in the *gauche* configuration: ***TTG***, with C_2 symmetry and the O=C-C=O intercarbonyl dihedral angle equal to 82.3º, and ***TCG***, with C_1 symmetry and the intercarbonyl dihedral angle equal to 102.1º. In the less stable form, ***CCSk*** (C_2 symmetry), the O=C-C=O dihedral angle is 118.3º (*skew*). The three conformers differ in the orientation of the pyridyl rings relatively to the carbonyl groups. In the most stable conformer (***TTG***) both pyridyl rings adopt the *trans* orientation relatively to the nearest carbonyl group, the CH···O distance in the two H-C=C-C=O five-membered rings being 259.2 pm. The second most stable conformer (***TCG***) has one pyridyl ring orientated that way, while the other is rotated by *ca.* 180º, resulting in an energetically less favorable H24-C16=C6-C3-C1=O2 six-membered ring. In this conformer, the calculated CH···O distances are 268.5 and 261.2 pm, for the six and five-membered ring, respectively. Finally, in the third conformer both pyridyl rings are in the *cis* orientation with respect to the carbonyl groups, forming two H-C=C-C-C=O six-membered rings where the CH···O distance is 244.2 pm. The theoretical calculations predicted the two higher

energy forms to be respectively 21.0 and 35.1 kJ mol^{-1} higher in energy than the ***TTG*** form.

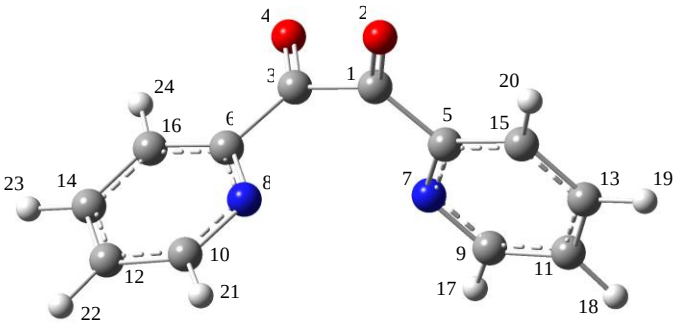

TTG (C_2)
E= 0.0 kJ mol^{-1}; μ = 4.94 D
(180.0, 180.0, 82.3º)

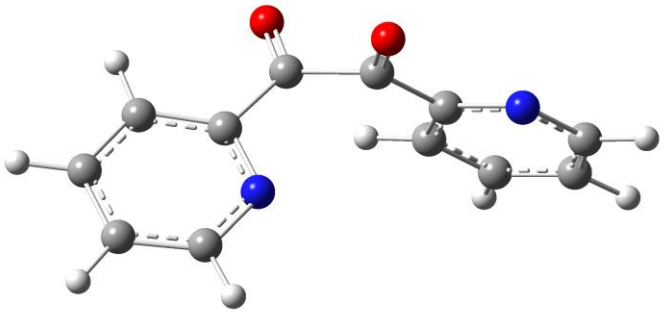

TCG (C_1)
ΔE= 21.0 kJ mol^{-1}; μ = 5.56 D
(164.7, 6.0, 102.1º)

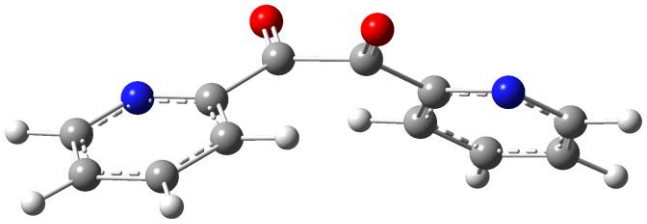

CCSk (C_2)
ΔE= 35.1 kJ mol^{-1}; μ = 4.90 D
(5.2, 5.2, 118.3º)

Figure 1. Conformers of α-pyridil with atom numbering. Calculated relative energies and dipole moments of the conformers are also provided, as well as the values of their defining dihedral angles (O_4=C_3-C_6-N_8, O_2=C_1-C_5-N_7, O_2=C_1-C_3=O_4).

The calculated geometries for all three conformers of α–pyridil are given in Table S1 (Supplementary Material), together with the geometry of the molecular unit in the crystal of the compound previously obtained by X-ray diffraction, which corresponds to a conformation similar to the ***TTG*** conformer, but slightly distorted from the C_2 symmetry.[27] The experimental parameters obtained by X-ray diffraction and those calculated for the isolated ***TTG*** conformer show a fairly good agreement, indicating that the crystal packing forces do not introduce substantial geometrical constraints. This is also in agreement with the almost perfect match found between the calculated value for the most flexible molecular coordinate (the intercarbonyl dihedral angle) in the isolated α–pyridil molecule (82.3º) and that observed in the crystalline state (82º).[27]

A few remarks can be made by comparing the values of the geometrical parameters obtained theoretically for the different conformers of α-pyridil. In addition, some insights regarding the prevalent intramolecular interactions in the different conformers can also be obtained by comparing the geometries of α-pyridil and some analogous compounds, like diacetyl,[1] benzil[2] and α-furil:[4]

(a) The intercarbonyl dihedral angle in the three conformers decreases in the order ***CCSk*** > ***TCG*** > ***TTG***. This is essentially a consequence of three factors: *(i)* steric repulsion between the lone-electron pairs of the carbonyl oxygen atoms, *(ii)* steric repulsion between the pyridyl rings, which correlate with the number of hydrogen atoms in the *ortho* position located in the inner side of the molecule (2, 1 and 0, respectively in ***CCSk***, ***TCG*** and ***TTG***) and *(iii)* the CH…O interactions stabilizing the H-C=C-C-C=O six-membered rings, which tend to be favored by a more planar arrangement of the molecule – there are two of such interactions in conformer ***CCSk***, only one in ***TCG*** and none in ***TTG*** [the similar interaction stabilizing the H-C=C-C=O five-membered rings present in conformers ***TCG*** (one five-membered ring) and ***TTG*** (two five-membered rings) involves only atoms from the same half of the molecule and are not important in determining the geometry around the intercarbonyl bond; they are, however, important in determining the trend to the planarity exhibited by the C_5H_4N-C(=O) fragments]. Factor *(i)* dominates in the ***TTG*** conformer, while factor *(ii)* and specially *(iii)* dominate in forms ***TCG*** and ***CCSk***.

(b) In agreement with (a), a comparison of the value of the intercarbonyl dihedral angle calculated at DFT(B3LYP)/6-311++G(d,p) level for α-pyridil (O=C-C=O: 82.3º ***TTG***; 118.3º ***CCSk***) with those found in other α-dicarbonyl molecules previously studied in our laboratory, such as diacetyl (CH_3-C(=O)-C(=O)-CH_3, O=C-C=O: 180º, ref. 1), benzil (C_6H_6-C(=O)-C(=O)-C_6H_6, O=C-C=O: 116.6º, ref. 2) and α-furil (C_4OH_3-C(=O)-C(=O)-C_4OH_3, O=C-C=O: 106º ***TTG***; 153º ***CCSk***, ref. 4[1]) shows that the value of the intercarbonyl dihedral angle depends strongly of the structure of the substituent connected to the carbonyl groups. In acetyl, the substituents are small and the prevalent interaction is the repulsion between the lone electron pairs of the oxygen atoms, leading to a most stable *trans* configuration around the central bond.[1] The interactions described in (a) are similar in benzil and in the ***CCSk*** conformer of α-pyridil, and the intercarbonyl dihedral angle is similar in these two molecules. On the other hand, when compared to the analogous conformers of α-furil, the α-pyridil conformers have smaller intercarbonyl dihedral angles. Both in the case of ***CCSk*** and ***TTG*** conformers, this result is in consonance with the calculated more negative charges on the carbonyl oxygen atoms in α-furil (–0.234 and –0.224 *e*, for ***TTG*** and ***CCSk*** forms, respectively) than in α-pyridyl (–0.190 and –0.166 *e*), which make more important the above mentioned factors in α-furil (factor *(i)* and *(iii)* in the ***TTG*** and ***CCSk*** forms, respectively).

(c) The length of the C-C intercarbonyl bond in α-pyridil conformers varies in the range 154.7-154.4 pm. This range of values is typical for a non-conjugated C-C single bond and follows the trend previously observed for other α-dicarbonyls, like diacetyl, benzil, 1-phenyl-1,2-propanedione and α-furil (155.7, 154.4, 155.0 and *ca.* 154.7 pm, respectively).[1-4] As discussed in detail elsewhere,[4] the long intercarbonyl bond length in α-dicarbonyls results essentially from the balance between the relatively weak π-electron delocalization within the O=C–C=O fragment and the more important σ-electron system repulsion due to the interaction between the positively charged carbonyl carbon atoms. This result is in consonance with the well-

[1] In ref. 4 the α-furil conformers here mentioned, ***TTG*** and ***CCSk***, were designated as III and I, respectively.

known large conformational flexibility around the C-C central bond in α-dicarbonyls[1-4] and also with the previously reported photochemistry of this type of compounds, where the intercarbonyl bond cleavage appears as a prevalent pathway.[3,47]

(d) The C_1-C_5 and C_3-C_6 bonds, connecting the O=C-C=O group to the pyridyl rings (149.5-150.7 pm) are longer than in the previous α-dicarbonyl compounds studied in our laboratory, in particular, benzil, 1-phenyl-1,2-propanedione and α-furil (148.7, 148.6 and 145.6-145.8 pm, respectively).[2-4] This result indicates that the conjugation between the pyridyl substituents and the dicarbonyl moiety is less important in α-pyridil than between this group and the phenyl or furanyl substituents in the remaining molecules.

(e) In agreement with the reduced delocalization between the pyridyl rings and the dicarbonyl group indicated by the calculated lengths of the C_1-C_5 and C_3-C_6 bonds, the carbon-carbon and carbon-nitrogen bond lengths within the pyridyl rings were estimated to be similar to those found in benzene (139.7 pm[48]) and pyridine (139.3 and 133.8 pm, average value for CC and CN bond lengths, respectively[49]) in all conformers of α-pyridil: the carbon-carbon bond lengths vary within the range 138.9-139.9 pm, and the nitrogen-carbon bond lengths within the range 132.8-134.2 pm.

(f) The O_2=C_1-C_3 and C_1-C_3=O_4 angles in α-pyridil correspond to the valence angles that differ more among the various conformers. As expected, in the most stable ***TTG*** conformer, where the steric repulsion between the lone-electron pairs of the carbonyl oxygen atoms dominates, the sum of these angles attain its maximum value (238.6º), while in the ***TCG*** and ***CCSk*** conformers it is 235.9º and 235.6º, respectively.

An important result coming out from the calculations in relation with the experimental study described in this work concerns the relatively high energies predicted for the two less stable conformers of α-pyridil. In fact, using the Boltzmann distribution and the calculated relative energies of the conformers, the estimated joint population of these two forms in the gaseous phase in the range of temperatures used to sublimate the compound (80-125 ºC) is less than 0.2%. In practical terms, this result shows the impossibility of trapping the higher energy forms of α-pyridil in the

cryogenic matrices in a detectable amount. Indeed, as described in detail below, only the most stable conformer could be observed experimentally in the present investigation.

Infrared spectroscopy: analysis of the matrix isolation spectra and UV-irradiation experiments

The α-pyridil molecule has 66 fundamental vibrations (of 34*A* and 32*B* symmetry, for the C_2 conformers), all of them active in the infrared. The definition of the internal coordinates adopted in the vibrational analysis undertaken in this study is provided in Table S2 (Supplementary Material). The calculated frequencies, infrared intensities and potential energy distributions resulting from normal mode analysis, carried out for the experimentally relevant ***TTG*** conformer, are presented in Table S3 (Supplementary Material). The infrared spectra of α-pyridil isolated in both solid argon and xenon (as-deposited matrices; sublimation and CsI substrate temperatures: Ar, 85 ºC and 10 K; Xe, 125 ºC and 20 K) together with the calculated spectrum of the ***TTG*** conformer are presented in Figure 2. Table 1 presents the assignments for the fundamental bands, which were strongly aided by the good agreement between the experimental and the calculated data.

According to the calculations, the 4 most intense bands in the spectrum of α-pyridil correspond to the stretching vibrations of the C=O groups (observed in argon at *ca.* 1727 and 1702 cm^{-1}), the asymmetric stretching of the C-C bonds connecting the carbonyl groups to the pyridyl rings (νC-C_α as.; 1227 cm^{-1}) and a skeletal deformational mode observed at *ca.* 654 cm^{-1}, which has a significant contribution from the in-plane asymmetric bending mode of the carbonyl groups. All these bands show extensive matrix-site splitting as it could be expected considering the high flexibility of the molecule around the intercarbonyl C-C bond (the calculated frequency for the intercarbonyl C-C torsion is as low as 24 cm^{-1}; see Table 1), and were fairly well predicted by the calculations both regarding frequencies and relative intensities (see Table 1 and Figure 2). The general agreement between the calculated and experimental data for the less intense bands is also good, as shown in Figure 2, so that the proposed assignments (Table 1) could be made with high degree of confidence.

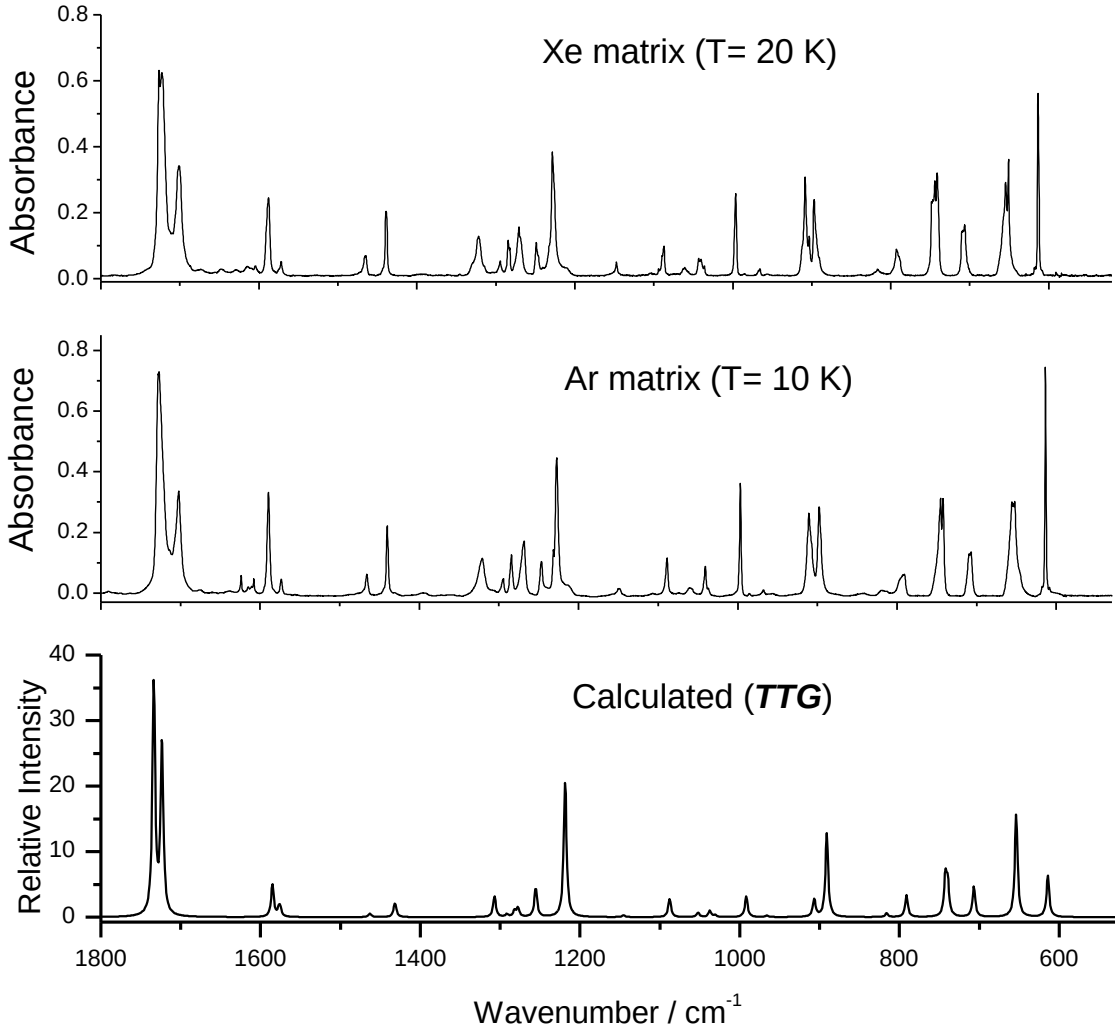

Figure 2. Infrared spectra of α-pyridil isolated in solid argon (sublimation and substrate temperatures: 85 ºC and 10 K, respectively) and solid xenon (125 ºC; 20 K) and DFT(B3LYP)/ 6-311++G(d,p) calculated spectrum for the ***TTG*** conformer.

Table 1 – Experimental (matrix-isolation) and calculated (***TTG*** form) vibrational data for α-pyridil and vibrational assignments based on the results of normal coordinate analysis.[a]

		Calculated		Experimental			
Approximate description		ν	I	Ar (10 K)	I[b]	Xe (20 K)	I[b]
ν(C-H 2) s		3134.9	0.9	3147.5	w	3145.5	w
ν(C-H 2) as	*B*	3134.8	6.4	3147.5	w	3145.5	w
ν(C-H 3) as	*A*	3123.2	8.5	3073.7/3070.4	w	3070.0	w
ν(C-H 3) as	*B*	3123.1	16.0	3073.7/3069.5	w	3070.0	w
ν(C-H 4) as	*B*	3106.0	12.6	3064.6/3060.4	w	3058.4/3053.7	w
ν(C-H 4) s	*A*	3106.0	2.4	3064.6/3060.4	w	3051.8/3050.6	w
ν(C-H 1) s	*A*	3087.1	11.3	3017.2	w	3015.5/3009.7	w
ν(C-H 1) as	*B*	3087.0	14.6	3017.2	w	3015.5/3009.7	w
ν(C=O) s	*A*	1733.8	225.8	1728.2/1726.8/1713.4	S/S/sh	1727.7/1726.4/1723.0/1721.6/ 1712.4/1709.6	sh/S/S/sh
ν(C=O) as	*B*	1723.5	169.5	1703.6/1702.2	sh/S	1702.5/1701.2	sh/S
ν(ring 3) as	*B*	1585.2	9.2	1594.7/1589.5	sh/m	1591.0/1589.2/1587.7	sh/sh/S
ν(ring 3) s	*A*	1585.2	22.3	1594.7/1589.5	sh/m	1591.1/1587.8	sh
ν(ring 4) s	*A*	1577.1	5.3	1573.4	w	1591.1/1574.7	sh
ν(ring 4) as	*B*	1575.6	7.1	1573.4	w	1571.9	w
ν(ring 6) s; δ(C-H 4) s	*A*	1463.6	2.0	1467.7	sh	1466.3	sh
δ(C-H 4) as; ν(ring 6) as	*B*	1462.6	1.6	1466.1	w	1465.4/1464.5	w/w
δ(C-H 3) s	*A*	1434.3	0.7	1444.7	sh	1443.2/1444.7	sh/sh
δ(C-H 3) as	*B*	1431.7	13.2	1440.5/1431.4	S/sh	1439.1	m
ν(ring 5) s	*A*	1307.1	19.7	1321.3/1317.2	m/sh	1330.1/1323.3/1322.0/1314.6	sh/sh/m/sh
ν(ring 5) as	*B*	1291.6	2.4	1294.4	w	1294.5	w
δ(C-H 4) s	*A*	1282.1	6.1	1284.3/1282.6	m/sh	1284.5/1282.3	m/m
ν(ring 2) as	*B*	1277.8	8.7	1273.2/1268.3	sh/m	1270.8/1269.2	m/sh
ν(ring 2) s; ν(ring 5) s; ν(C-C_α) s	*A*	1255.5	28.4	1246.3	m	1248.9/1246.4/1240.4	m/sh/w
ν(C-C_α) as	*B*	1218.7	131.2	1231.7/1227.4/1213.5	w/S/w	1232.7/1228.5/1210.2	sh/S/sh
δ(C-H 2) s	*A*	1145.7	1.0	1149.5	w	1147.4	w
δ(C-H 2) as	*B*	1145.2	0.9	1149.5	w	1147.4	w
ν(ring 2) s; δ(C-H 3) s; δ(C-H 1) s	*A*	1088.6	1.3	1088.8	m	1094.2/1089.5/1087.3	sh/sh/m
ν(ring 2) as;δ(C-H 3) as;δ(C-H 1) as	*B*	1087.8	16.3	1088.8	m	1094.2/1089.5/1087.3	sh/sh/m
ν(ring 6) s; ν(C-C)	*A*	1052.3	4.4	1060.3	w	1063.3/1061.1	w
ν(ring 6) as	*B*	1037.6	6.3	1040.8	w	1043.2/1040.2	w/w
ν(ring 6) s, ν(ring 1) s	*A*	1030.8	2.0	1037.1	w	1036.0	w
γ(C-H 3) as	*B*	996.6	0.1	996.8	S	998.0	sh
γ(C-H 3) s	*A*	996.1	<0.1	996.8	S	998.0	sh
ν(ring 1) s; δ(ring 2) s	*A*	992.2	0.1	996.8/985.5	S/w	996.3/985.4	S/w
δ(ring 2) as; ν(ring 1) as	*B*	991.9	19.9	996.8/985.5	S/w	996.3/985.4	S/w
γ(C-H 4) as	*B*	966.1	1.2	970.0/967.8/955.3	sh/w/w	968.3/967.4/965.7/957.2	sh/w/w/w
γ(C-H 4) s	*A*	965.8	0.2	970.0/967.8/955.3	sh/w/w	968.3/967.4/965.7/957.2	sh/w/w/w
γ(C-H 2) as	*B*	906.8	16.5	910.7	m	912.0/908.6	sh/m
γ(C-H 2) s	*A*	904.8	0.2	907.5	sh	903.3	w
Skeletal	*B*	891.0	80.3	897.8/895.6	m/sh	897.0/894.6/890.5	m/sh/sh
τ(ring 1) s; γ(C=O) s	*A*	816.2	3.5	819.7/812.7	w/w	816.7	w
τ(ring 1) as; γ(C=O) as	*B*	791.2	21.3	790.6	w	792.9/791.5/789.3/788.1	w/sh/sh/sh
γ(C-H 1) s	*A*	742.5	36.9	746.8	sh	748.4/747.0/744.3	m/m/m
γ(C-H 1) as; τ(ring 3) as	*B*	739.6	28.8	745.2/742.2	m/m	741.4	m
δ(ring 1) s	*A*	732.4	0.4	745.2/742.2	m/m	740.2	sh
δ(ring 1) as	*B*	707.2	11.7	709.5	m	710.2/708.5	m/m
τ(ring 3) s; γ(C=O) s	*A*	706.7	18.2	707.0	m	706.5	m
Skeletal	*B*	653.9	98.6	655.9/654.3/652.1/645.6	m/m/m/sh	657.1/654.7/650.9/646.6	sh/m/m/sh
δ(ring 3) s	*A*	617.9	0.2	613.5	S	613.7/613.1/612.1	S/sh/sh
δ(ring 3) as	*B*	614.2	39.9	613.5	S	613.7/613.1/612.1	S/sh/sh
Skeletal	*A*	474.8	4.4	479.7	w	483.4/478.0	w/w
τ(ring 4) as	*B*	472.0	11.3	476.3/469.6	w/sh	473.6	w
τ(ring 2) s; τ(ring 4) s	*A*	422.5	1.9	424.2	sh	423.9	w
τ(ring 2) as	*B*	422.1	9.2	422.2/420.5/417.8	w/sh/w	422.4/421.4/419.6	sh/w/w
τ(ring 4) s; τ(ring 2) s	*A*	399.4	1.5				
τ(ring 4) as; τ(ring 2) as	*B*	395.4	0.9				
δ(C=O) s	*A*	325.9	4.7				
δ(C=O) as; w(ring) as	*B*	263.8	27.4				
w(ring) s	*A*	258.6	3.2				
τ(ring 1) s	*A*	148.5	0.1				
τ(ring 1) as	*B*	145.8	1.7	n.i.		n.i.	
δ(CCC$_\alpha$) as	*B*	120.8	0.0				
δ(CCC$_\alpha$) s	*A*	111.3	0.1				
τ(C-C$_\alpha$) s	*A*	52.4	0.4				
τ(C-C$_\alpha$) as	*B*	41.6	4.1				
τ(C-C)	*A*	24.0	3.5				

[a] Frequencies (cm^{-1}, scaled by 0.978), calculated intensities in km mol^{-1}. ν, bond stretching; δ, bending; w, wagging; γ, rocking; τ, torsion; s, symmetric; as, asymmetric; n.i., not investigated. See Table S2 for definition of symmetry coordinates. Only bands assigned to fundamental modes are presented in the Table. [b] Experimental intensities are presented in qualitative terms: S= strong, m= medium, w= weak, sh= shoulder.

UV irradiation ($\lambda > 235$ nm) of matrix-isolated α-pyridil resulted in a decrease of intensity of the bands of the initial spectrum and appearance of new bands due to photoproducts. The intensity of the bands due to the reactant decrease only by *ca.* 20%, indicating that the observed photoprocesses have a relatively low efficiency. In argon matrix, the process is even less efficient, what points to a photochemical mechanism involving an $n \rightarrow \pi^*$ excitation and a triplet state.

In order to identify the chemical species formed by irradiation of the matrix, a series of theoretical calculations of the spectroscopic signatures of possible photoproducts was carried out. The following putative general types of photoprocesses could *a priori* be considered: *(i)* intercarbonyl bond cleavage, leading to formation of 2-pyridylcarbonyl radicals, that can then loose carbon monoxide followed by recombination to form either di-(2-pyridyl) ketone or 2,2'-bipyridine (pathway A in Scheme 1); *(ii)* isomerization of the pyridine rings to the valence Dewar or Hückel (aza-benzvalene) isomers (B and C in Scheme 1).

The first type of reaction was observed for 1-phenyl-1,2-propandione isolated in cryogenic inert matrices,[3] leading to single decarbonylation and production of acetophenone. In turn, efficient isomerization of Kekulé ring structures to their Dewar analogues have been found to take place in matrices for related compounds, like α-pyrones and α-thiopyranones,[50-53] while some Dewar pyridines, including the unsubstituted one, could also be observed experimentally as result of photochemical transformation of their most stable Kekulé isomers.[54-62] On the other hand, to the best of our knowledge, experimental observation of Hückel pyridine isomers was only reported once, in a study where the ultrafast dynamics of isomerization of pyridine (and a few other analogue compounds) was investigated by femtosecond-resolved mass spectrometry complemented by DFT/ab initio calculations.[62] Nevertheless, some Hückel isomers of pyridine have been consistently predicted by theoretical methods to be most stable than the Dewar forms,[62-65] so that the possibility of their photochemical formation under the present experimental conditions could not be excluded. Moreover, according to Zong *et al.*,[62] conical intersections appear to be fundamental in driving the valence photoisomerization reactions of pyridine, which then take place partially in the ground-state potential energy surface. This fact enabled us to exclude *a priori* other valence isomerization reactions within the pyridine rings (*e.g.*, to the prismane

and bicyclopropyl-2,2'-diene like species), since the energies required for these processes to take place are too much high to make them possible under the present experimental conditions (the maximum energy available in our experiment is *ca.* 500 kJ mol^{-1} and those required for those isomerization processes are over 630 kJ mol^{-1}, ref. 62).

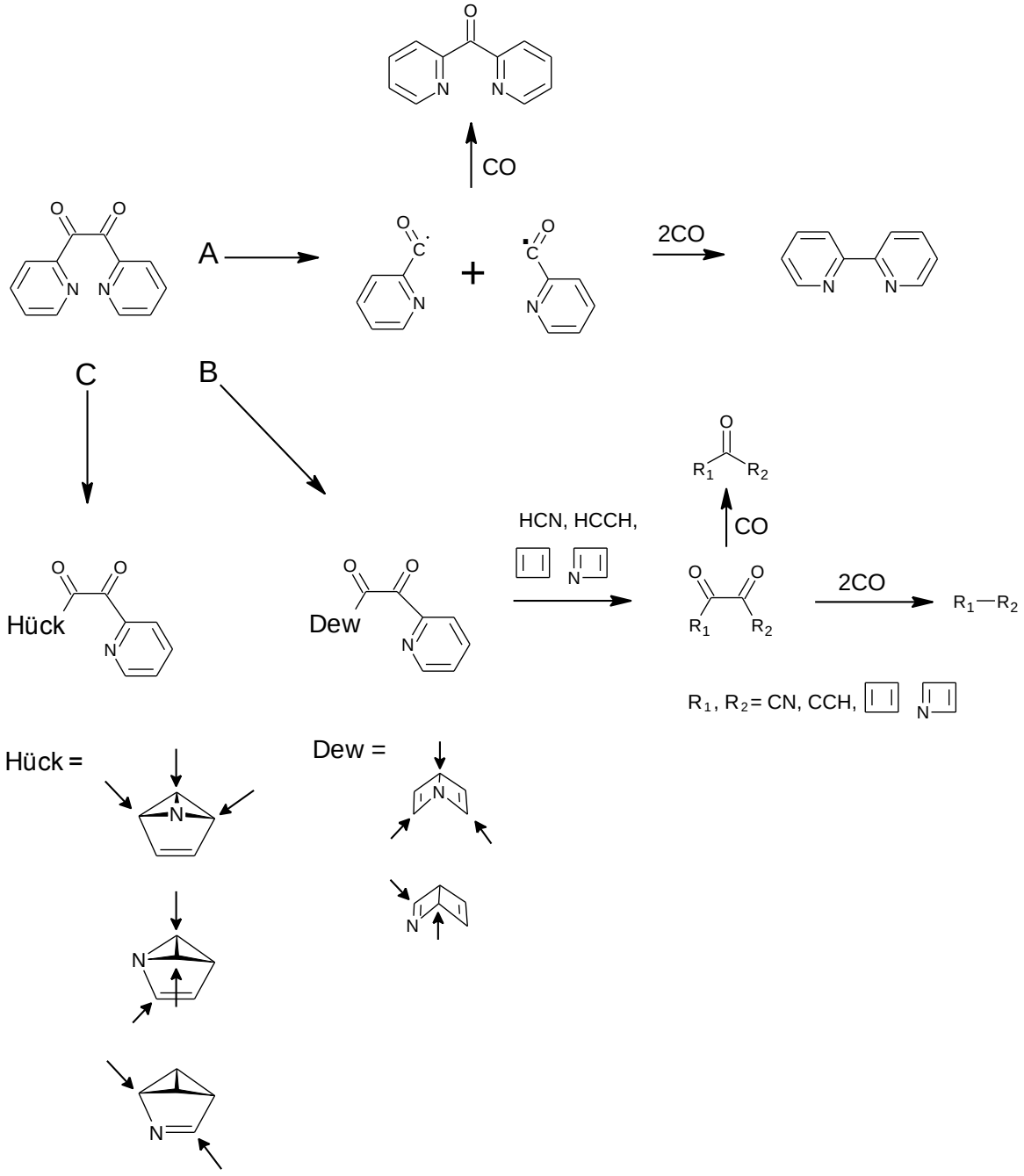

Scheme 1. *A priori* possible photochemical pathways for α-pyridil. The arrows in the Dewar (Dew) and Hückel (Hück) type pyridine structures show the possible places for the bonding of these groups to the dicarbonyl moiety in α-pyridil. Pathways A and B were not observed experimentally.

In the specific case of isomerization of the pyridyl groups of α-pyridil to their Dewar forms, subsequent photochemical processes could be expected to take place, in a similar form to what has been observed for α-pyrones and α-thiopyranones,[50-53] resulting in the production of cyclobutadiene (or aza-cyclobutadiene, or a mixture of these compounds, depending on the specific pyridine Dewar isomer initially formed) and cyano- or ethyne-substituted ethanediones (see Scheme 1). In turn, if they were formed, these ethanediones could also undergo single or double decarbonylation to form the corresponding ketones or dicyano (or diethyne, or cyano-ethyne) derivatives. Other *a priori* possible secondary photochemical reactions starting from Dewar pyridines would be the release of HCN or ethyne and formation of cyclobutadien- or aza-cyclobutadien-ethanediones (see Scheme 1), in consonance with the known photochemistry of Dewar pyridine.[62] However, the spectroscopic results doubtlessly show that the photochemistry of matrix isolated α-pyridil is considerably simpler than it could be expected. In fact, none of the characteristic bands of carbon monoxide {at 2138 (Ar) or 2133 (Xe) cm^{-1}, see ref. 66,67}, HCN {3306, 2098, 721 (Ar) cm^{-1}; *ca.* 3280, 2090, 718 (Xe) cm^{-1}, see ref. 68}, ethyne {3303/3289 (Fermi resonance doublet) and 737 (Ar) cm^{-1}, see ref. 69} and cyclobutadiene {1241, 575 (Ar); 1239, 574 (Xe) cm^{-1}, see ref. 51,70} were observed in the spectra of the photolysed matrix, implying that all putative reaction steps implying the production of these species did not take place and could be promptly discarded. This significantly reduces the number of possible photoproducts and, in particular, excludes the intercarbonyl bond cleavage reaction path and all reactions putatively occurring after formation of the pyridine valence isomers' based products.

In addition, comparison of the experimental spectra of the photolysed matrix with those of Dewar pyridine containing species also showed unambiguously that the isomerization of the pyridine rings of α-pyridil to Dewar forms did not take place. On the other hand, the results are in consonance with the presence in the photolysed matrix of Hückel pyridine containing compounds.

It is worth to note that the number of possible *a priori* chemical species derived from α-pyridil containing the Hückel pyridine moiety is still very large. Unsubstituted Hückel pyridine may exist in three different structures: 1-aza-benzvalene, 2-aza-benzvalene and 3-aza-benzvalene (see Scheme 1). Upon single substitution in a position vicinal to the nitrogen atom (a requirement for a derivative of α-pyridil),

there are three possible different isomeric forms derived from 1-and 2-aza-benzvalene and 2 different isomeric forms derived from 3-aza-benzvalene. Considering then that the isomerization reactions might occur in one or in both of the pyridine rings of α-pyridil, and taking into account the conformational degrees of rotation around both the intercarbonyl bond and the two C-C bonds linking the dicarbonyl moiety to the pyridine rings, the possible structures quickly grow up to a non-manageable number. However, though the identification of the precise Hückel-type pyridine containing species obtained in the described photolysis experiments appeared *a priori* an impossible task, the type of Hückel structures produced under the present experimental conditions could still be guessed. First of all, extensive molecular rearrangements in a matrix are not favoured due to the geometric constraints imposed by the matrix cage. This means that the formed Hückel pyridine containing species shall be directly related with the initially trapped ***TTG*** conformer of α-pyridil. In addition, the dominant stabilizing interactions existent in this conformer shall be kept in the photoproducts, in particular, the nearly *syn*-periplanar arrangement of the H-C-C-C=O fragment. Finally, we can expect that singly substituted species (*i.e.*, species containing just one Hückel type pyridine ring) are prevalent. Under these three structure constraints, the number of relevant species reduces to 2 (!): forms 2C and 3A in Figure 3.

In Figure 4 (A and B), we compare the spectroscopic changes resulting from irradiation of the xenon matrix during 5 h with the calculated spectra for the Hückel pyridine containing forms 2C and 3A. There is a good general agreement between these spectra, allowing to conclude that, as predicted, 2C and 3A are the main (if not the sole) photoproducts of α-pyridil under the used experimental conditions. The proposed assignments for the bands given rise by the two observed photoproducts are provided in Table 2. Table S4 gives the optimized geometries and full set of calculated frequencies and infrared intensities for these species. For 2C, 26 out of the 35 infrared bands predicted with intensities greater than 5 km mol^{-1} in the 500-1800 cm^{-1} region were observed experimentally (23 out of 34, in the case of 3A); see Tables 2 and S4.

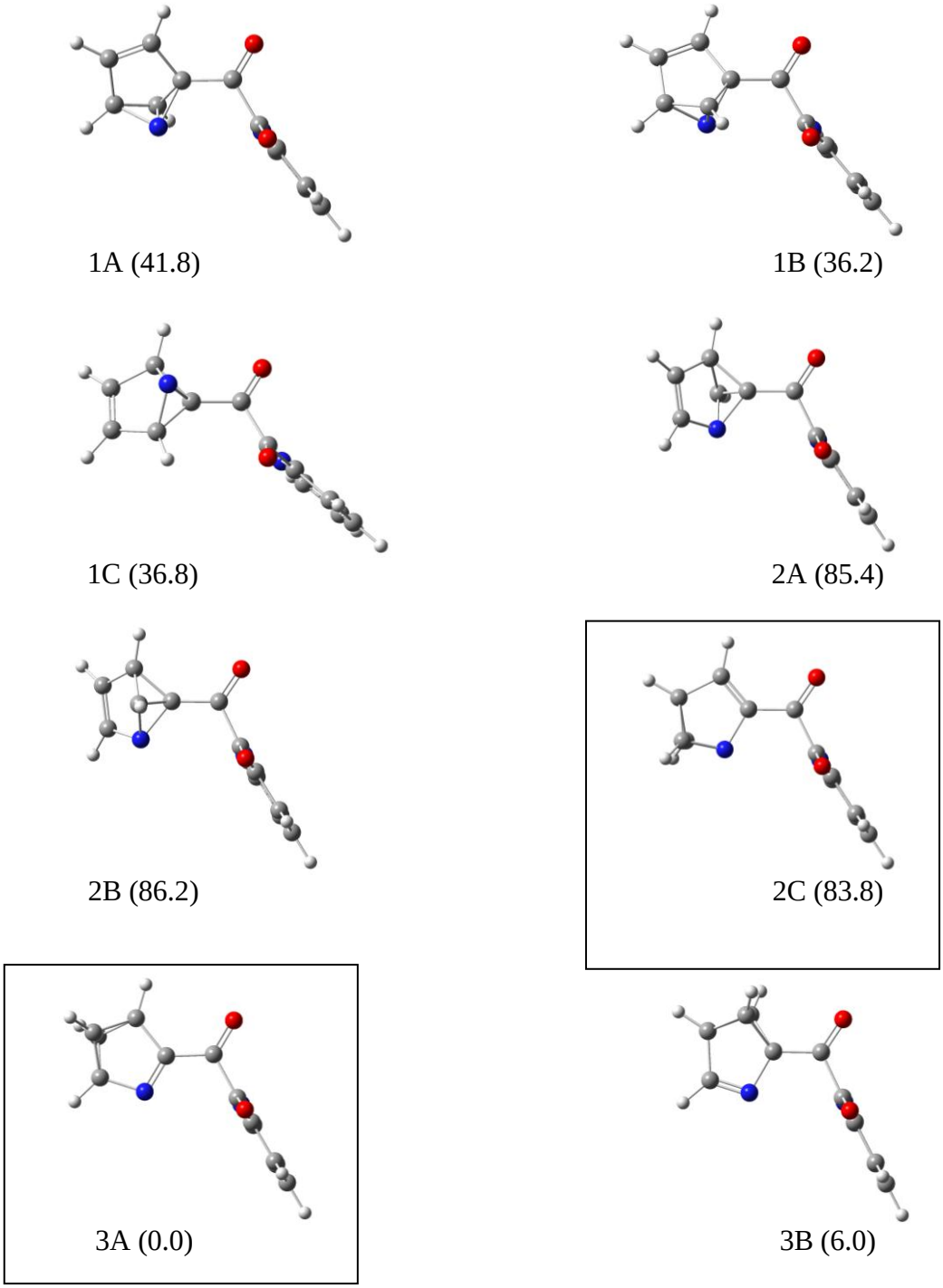

Figure 3. Calculated structures of the *a priori* possible mono-substituded Hückel pyridine containing α-pyridil isomers derived from the ***TTG*** conformer of α-pyridil. The two forms that keep the *syn*-periplanar arrangement of the H-C-C-C=O fragment are included in boxes and are those observed experimentally. Numbers in parentheses are relative energies (with zero point corrections) in kJ mol^{-1}. The pyridine ring is, in all cases, perpendicular to the plane of the sheet. Note that form 1C is a special case where the structure directly related with ***TTG*** conformer of α-pyridil is not stable; the structure presented corresponds to that matching as closer as possible the remaining forms shown in the figure.

An interesting observation is the apparently similar amount of the two photoproducts obtained (see Figure 4), in spite of the considerably higher relative energy of 2C compared to 3A. This result can, however, be promptly rationalized taking into account the findings of Zong *et al.*[62] that conical intersections are fundamental in driving the valence photoisomerization reactions of pyridine rings, which then take place partially in the ground-state potential energy surface. Indeed, the predicted energy barriers for conversion of pyridine into all its possible Hückel-type isomers, in the ground electronic state, were found to be similar, ranging from *ca.* 385 to about 420 kJ mol^{-1} (311-284 nm).[62]

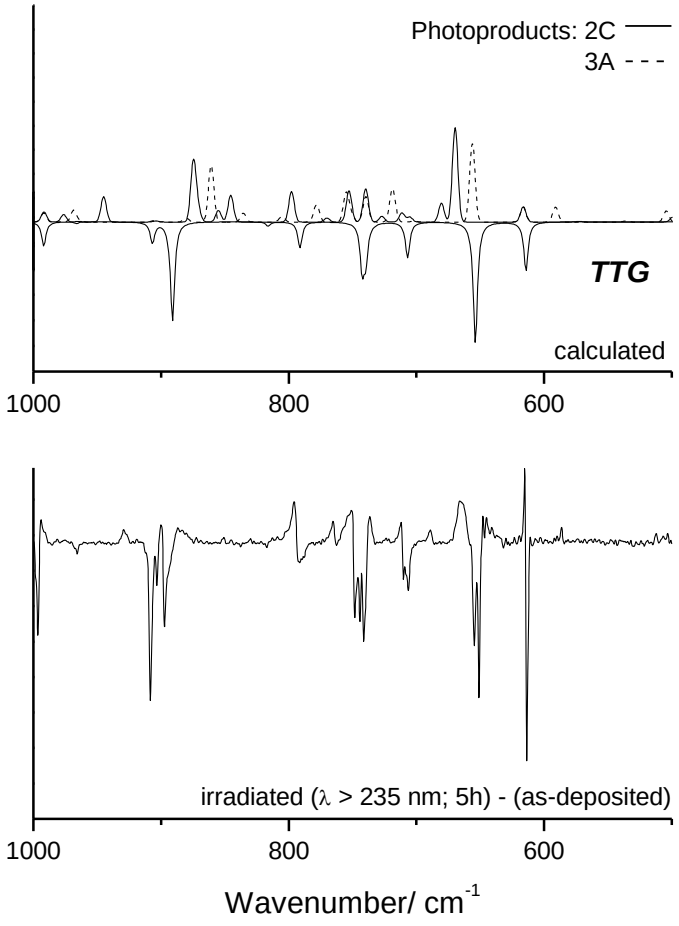

Figure 4 (A: 1000-500 cm^{-1} spectral range**)** – Bottom: experimental difference spectrum for α-pyridil isolated in xenon matrix [(irradiated sample after 5 h of irradiation with UV light, λ> 235 nm) *minus* (as-deposited sample)]. Top: Calculated spectra for the ***TTG*** conformer of α-pyridil (bands pointing down) and for photoproducts 2C and 3A (bands pointing up). The calculated intensities of the bands due to the photoproducts assume a 1:1 ratio of these species; those of the reactant bands were arbitrarily chosen in order to reproduce approximately the experimental difference spectrum shown in the figure.

On the other hand, it can easily be assumed that the isomerization reactions of the pyridine rings of α-pyridil leading to formation of 2C and 3A do also have similar energy barriers [in particular because the valence isomerization rearrangement is localized in the side of the pyridine ring that is more distant from the substituent (see Figure 3)], thus justifying the nearly equal amount of 2C and 3A formed in the photolysis experiments.

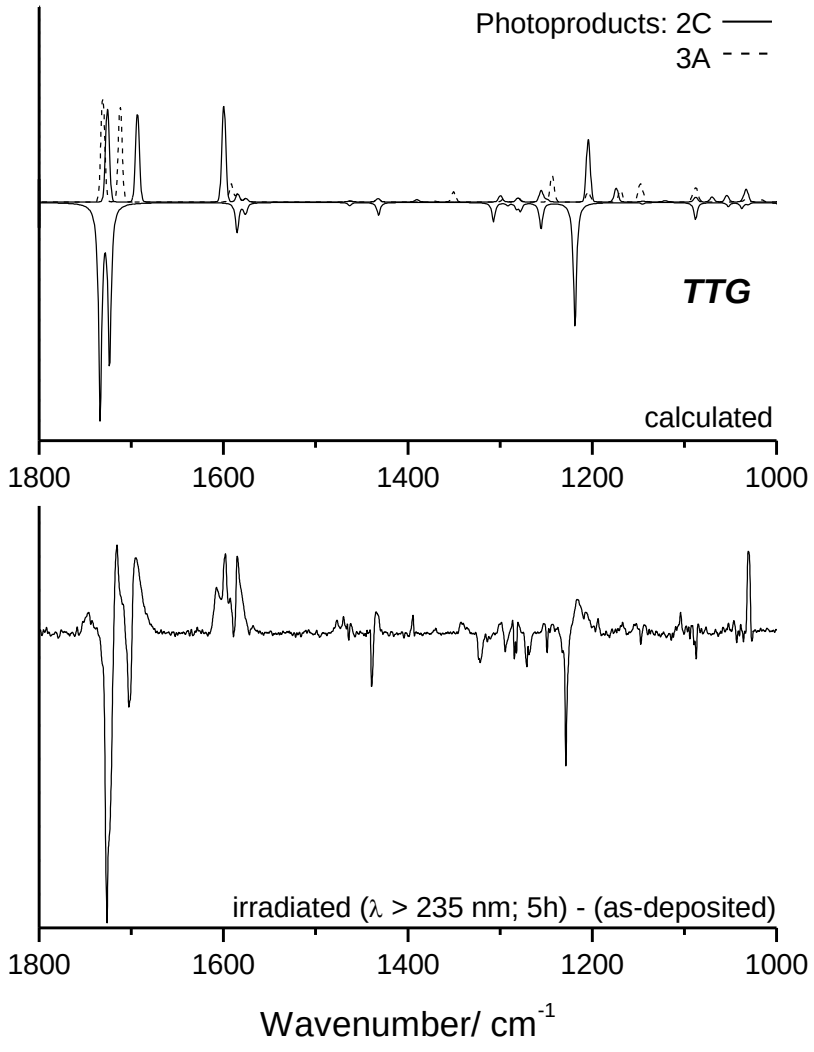

Figure 4 (B: 1800-1000 cm^{-1} spectral range**)** – Bottom: experimental difference spectrum for α-pyridil isolated in xenon matrix [(irradiated sample after 5 h of irradiation with UV light, λ> 235 nm) *minus* (as-deposited sample)]. Top: Calculated spectra for the ***TTG*** conformer of α-pyridil (bands pointing down) and for photoproducts 2C and 3A (bands pointing up). The calculated intensities of the bands due to the photoproducts assume a 1:1 ratio of these species; those of the reactant bands were arbitrarily chosen in order to reproduce approximately the experimental difference spectrum shown in the figure.

Table 2 – Assignment of the observed infrared bands of the photoproducts 2C and 3A.[a]

Approximate	Obs.	Calculated	
Description[b]	Xe matrix	2C	3A
νC=O p	1716	1725	1731
νC=O h	1695	1693	1712
νC=C h	1608/1599	1599	
νC=N h	1592		1592
ν ring p	1584	1584	1584
δC-H/ν ring p	1478/1470	1463	1462
δC-H p	1443	1432	1432
δC-H h	1370		1372
νC-C_α h	1341		1350
ν ring/δC-H p	1299	1299	
δC-H/ν ring p	1280	1280	1280
νC-C_α sym	1252	1255	
νC-C_α p	1243		1243
δC-H h	1215/1206	1204	1204
νC-N h	1168	1174	
ν ring h	1168		1169
δC-H h	1153		1148
δC-H p	1143		1144
ν ring/δC-H h	1104	1121	
γC-H h	1077	1070	
νC-C intercarbonyl	1046	1053	
δ ring p	1030	1035	
γC-H h	1030	1032	1032
δ ring p	994	992	
δ ring h	930	945	
δ ring h	887	874	
γC=O p	883		861
γC=O p	795	798	
δ skeletal	765		778
γC=O h	753	752	755
γC-H p	736	740	739
γC-H h	~723	727	
τ ring h	712		719
τ ring h	689	680	
δ skeletal	665	669	
δ ring p	615	616	616
γC=N h	586		591
τ ring p	512		504

[a] Wavenumbers (scaled by 0.978) in cm^{-1}. [b] The approximate descriptions of the vibrations were made by examining the composition of the modes in terms of internal coordinates through their animation using a graphical interface. ν, stretching; δ, bending; γ, rocking; τ, torsion; sym, symmetric; p, pyridine ring; h, Hückel-pyridine (aza-benzvalene) ring. See Table S4 for complete calculated spectra.

Infrared spectroscopy: α-pyridil low temperature crystalline and glassy states

Figure 5 presents the infrared spectra of α-pyridil in the neat low temperature amorphous phase and crystalline state, together with the calculated spectrum of the ***TTG*** conformer. The assignment of the recorded spectra is provided in Table 3.

As described in the *Materials and Methods* section, the amorphous phase of the compound was prepared by deposition of its vapors directly onto the cold (20 K) CsI substrate of the cryostat. As expected, the spectrum of the amorphous phase is constituted by relatively wide bands, with maximum frequency values fitting nicely those calculated for the ***TTG*** conformer (in vacuum), which is the conformer present in the vapor prior to deposition of the solid layer. The crystal was obtained after heating the amorphous layer up to 250 K. Subsequently, the CsI substrate was cooled down to 10 K and a new spectrum of the crystalline phase was collected. Compared with the spectrum of the amorphous phase, the bands in the spectrum of the crystal are much narrower. However, the positions of the bands do not differ significantly in both spectra. Indeed, the spectrum of the crystal fits very well those obtained for the matrix-isolated compound and also that calculated for the ***TTG*** form. All these observations indicate that the intermolecular interactions in the solid state are rather weak in α-pyridil, in consonance with its low melting point 154-156 ºC in comparison with isomeric compounds like, for example, (2,2')bipyridinyl-4,4'-dicarbaldehyde (188 ºC), 3-nitrocarbazole (212-214 ºC), 4,7-dihydroxy-1,10-phenanthroline (> 300 ºC) or 4-amino-1,8-naphthalimide (360 ºC).[71]

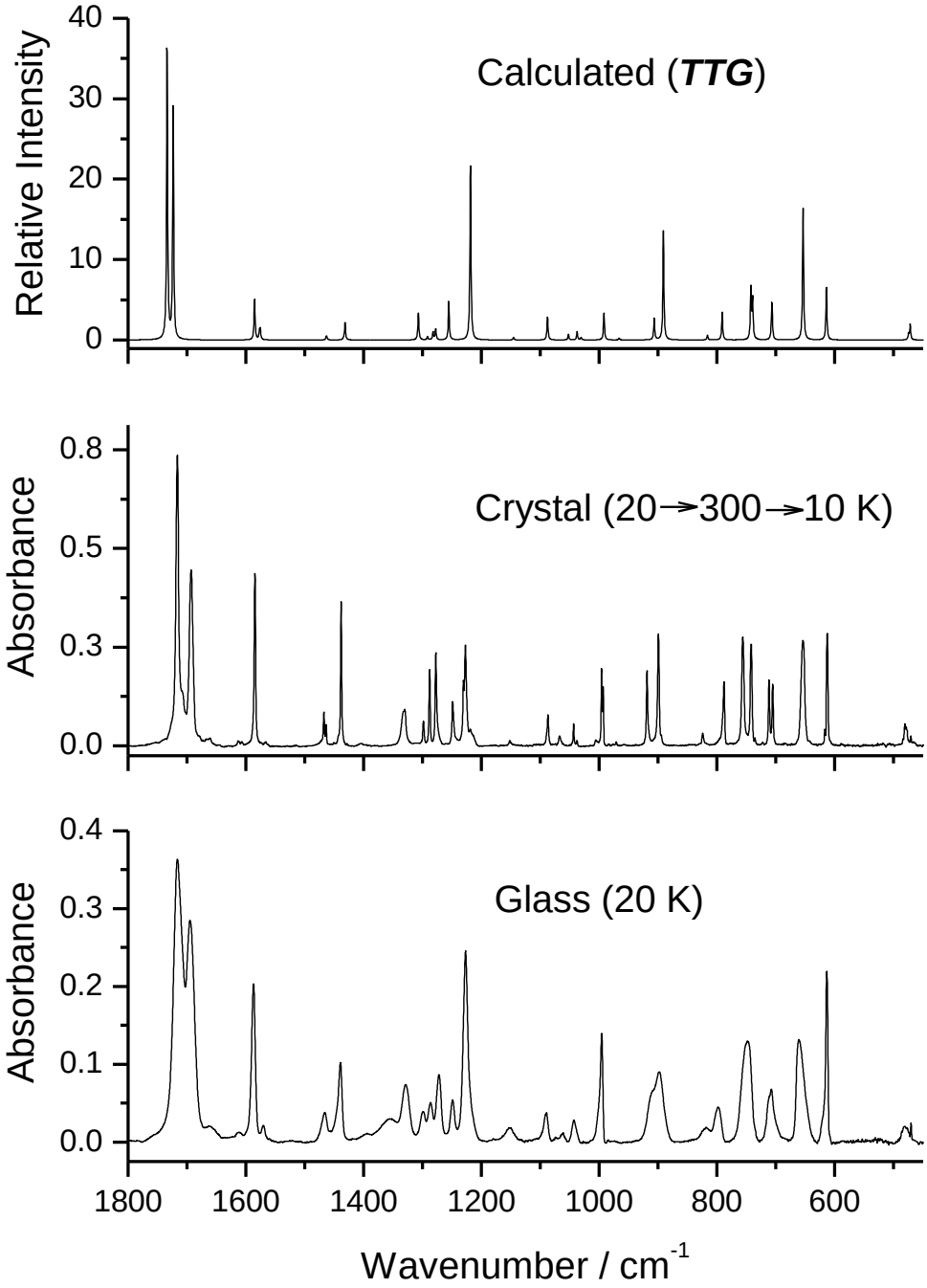

Figure 5. Infrared spectra of α-pyridil in the low temperature crystalline and glassy states (see the *Materials and Methods* section to detailed description of the experimental conditions) and the spectrum of the ***TTG*** conformer calculated at the DFT(B3LYP)/ 6-311++G(d,p) level of theory.

Table 3 – Observed frequencies of α-pyridil in the low temperature crystalline and glassy states.[a]

		Calculated		Experimental [b]			
Approximate Description		ν	Intensity	Glass (20 K)		Crystal (10 K)	
ν(C-H 2) s		3134.9	0.9	3112.8	w	3094.5/3083.0	w
ν(C-H 2) as	*B*	3134.8	6.4				
ν(C-H 3) as	*A*	3123.2	8.5	3061.1	w	3060.4/3048.6	w
ν(C-H 3) as	*B*	3123.1	16.0				
ν(C-H 4) as	*B*	3106.0	12.6	3056.6	w	3045.4	sh
ν(C-H 4) s	*A*	3106.0	2.4				
ν(C-H 1) s	*A*	3087.1	11.3	3013.9	w	3013.6	w
ν(C-H 1) as	*B*	3087.0	14.6				
ν(C=O) s	*A*	1733.8	225.8	1716.2	S	1716.4/1708.2	S/sh
ν(C=O) as	*B*	1723.5	169.5	1694.7	S	1693.0	S
ν(ring 3) as	*B*	1585.2	9.2	1587.0	m	1584.5	S
ν(ring 3) s	*A*	1585.2	22.3				
ν(ring 4) s	*A*	1577.1	5.3	1570.6	w	1565.9	w
ν(ring 4) as	*B*	1575.6	7.1				
ν(ring 6) s; δ(C-H 4) s	*A*	1463.6	2.0	1465.7	m	1467.6/1463.8	m/m
δ(C-H 4) as; ν(ring 6) as	*B*	1462.6	1.6				
δ(C-H 3) s	*A*	1434.3	0.7	1439.5	m	1443.4/1438.3	m/S
δ(C-H 3) as	*B*	1431.7	13.2				
ν(ring 5) s	*A*	1307.1	19.7	1328.5	m	1333.4/1330.3	sh/m
ν(ring 5) as	*B*	1291.6	2.4	1299.3	w	1298.5	w
δ(C-H 4) s	*A*	1282.1	6.1	1286.2	m	1288.0	m
ν(ring 2) as	*B*	1277.8	8.7	1272.1	m	1277.6	m
ν(ring 2) s; ν(ring 5) s;ν(C-C_α) s	*A*	1255.5	28.4	1248.9	w	1248.7	w
ν(C-C_α) as	*B*	1218.7	131.2	1227.0	m	1230.2/1227.4/1218.8	m/m/w
δ(C-H 2) s	*A*	1145.7	1.0	1152.4	w	1151.7	w
δ(C-H 2) as	*B*	1145.2	0.9				
ν(ring 2) s; δ(C-H 3) s; δ(C-H 1) s	*A*	1088.6	1.3	1089.8	m	1093.5	sh
ν(ring 2) as;δ(C-H 3) as;δ(C-H 1) as	*B*	1087.8	16.3			1087.0	m
ν(ring 6) s; ν(C-C)	*A*	1052.3	4.4	1061.3	w	1067.7	w
ν(ring 6) as	*B*	1037.6	6.3	1043.4	w	1043.6	w
ν(ring 6) s; ν(ring 1) s	*A*	1030.8	2.0			1037.8	w
γ(C-H 3) as	*B*	996.6	0.1	996.0	m	1006.7/1002.7	w/w
γ(C-H 3) s	*A*	996.1	<0.1				
ν(ring 1) s; δ(ring 2) s	*A*	992.2	0.1			996.1/993.4	m/m
δ(ring 2) as; ν(ring 1) as	*B*	991.9	19.9				
γ(C-H 4) as	*B*	966.1	1.2	975.4	m	984.2/976.6/971.1	w/w/w
γ(C-H 4) s	*A*	965.8	0.2				
γ(C-H 2) as	*B*	906.8	16.5	909.0	sh	918.8	m
γ(C-H 2) s	*A*	904.8	0.2				
Skeletal	*B*	891.0	80.3	897.8	m	899.5/894.8	S/m
τ(ring 1) s; γ(C=O) s	*A*	816.2	3.5	798.6	w	788.1	m
τ(ring 1) as; γ(C=O) as	*B*	791.2	21.3	748.6	m	756.2	S
τ(ring 1) as; γ(C=O) as	*A*	742.5	36.9			748.3	sh
γ(C-H 1) s; γ(C-H 1) as; τ(ring 3) as	*B*	739.6	28.8	710.8	sh	741.9/735.8	S/w
δ(ring 1) s	*A*	732.4	0.4			722.3	w
δ(ring 1) as	*B*	707.2	11.7	707.9	m	711.8	m
τ(ring 3) s; γ(C=O) s	*A*	706.7	18.2			705.5	m
Skeletal	*B*	653.9	98.6	661.0	m	654.1	S
δ(ring 3) s	*A*	617.9	0.2	613.4	w	617.0	w
δ(ring 3) as	*B*	614.2	39.9			612.8	S
Skeletal	*A*	474.8	4.4	470.3	w	470.8	w
τ(ring 4) as	*B*	472.0	11.3	480.3	m	483.8/480.9/478.7/477.4	w/w/w/sh
τ(ring 2) s; τ(ring 4) s	*A*	422.5	1.9			422.0	w
τ(ring 2) as	*B*	422.1	9.2				
τ(ring 4) s; τ(ring 2) s	*A*	399.4	1.5	408.5	w	408.5	w
τ(ring 4) as; τ(ring 2) as	*B*	395.4	0.9	404.2	w	404.2	w

[a] Frequencies in cm^{-1}, calculated intensities in km mol^{-1}. ν, bond stretching, δ, bending, γ rocking, τ torsion, w, wagging, s, symmetric, as, asymmetric, n.o., not observed. See Table S2 for definition of internal symmetry coordinates. [b] Experimental intensities are presented in qualitative terms: S= strong, m= medium, w= weak, sh= shoulder.

Conclusion

α-Pyridil was, for the first time, isolated in low temperature noble gases (argon, xenon) matrices, and its molecular structure and vibrational signature probed by FTIR spectroscopy, supported by DFT(B3LYP)/6-311++G(d,p) calculations. Calculations predicted the existence of three different conformers (***TTG***, ***TCG*** and ***CCSk***), all of them exhibiting skewed conformations around the intercarbonyl bond and the two C_5H_4N-C(=O) fragments nearly planar, and differing in the orientation of the pyridine rings relatively to the carbonyl groups. The ***TTG*** form was predicted to be the most stable conformer, accounting for more than 99 % of the total population at 125 ºC, whereas the two higher energy forms, ***TCG*** and ***CCSk*** were estimated theoretically to be respectively 21.0 and 35.1 kJ mol^{-1} higher in energy than the most stable form. Accordingly to these results, the ***TTG*** conformer was found to be the sole form of α-pyridil present in the studied low temperature Ar and Xe matrices.

The ***TTG*** form was also found to be the unique conformer of α-pyridil present in both the neat amorphous and crystalline phases of the compound. The IR spectra of the low temperature neat solid samples were found to match very closely those obtained for the matrix-isolated compound (and also with the calculated data for ***TTG***), indicating that the intermolecular interactions in the solid state are rather weak in α-pyridil.

Irradiation of matrix-isolated compound with UV light (λ > 235 nm) led to its isomerization to unusual molecular species bearing a Hückel-type pyridine (aza-benzvalene) ring (forms 2C and 3A), which are directly structurally correlated with the ***TTG*** conformer of α-pyridil, in particular where the *syn*-periplanar arrangement of the H-C-C-C=O fragment is kept in order to preserve the stabilizing CH…O intramolecular H-bond type interaction prevalent in the reactant species.

Appendix A. Supplementary data: Table S1 – Experimental and calculated [DFT(B3LYP)/6-311++G(d,p)] bond lengths and angles for the three conformers of α-pyridil; Table S2 – Definition of internal symmetry coordinates used in the normal mode analysis of α-pyridil; Table S3 – Calculated [scaled, DFT(B3LYP)/6-311++G(d,p)] wavenumbers, IR intensities and Potential Energy Distributions (PED)

for the most stable conformer of α-pyridil; Table S4 – Calculated geometries and infrared spectra (non-scaled) for observed Hückel pyridine containing photoproducts (2C and 3A forms). Supplementary data associated with this article can be found in the online version, at doi:10.1016/j.jphotochem.20 08.07.0 05.

Acknowledgements

This work was funded by Fundação para a Ciência e a Tecnologia (FCT), Portugal (POCTI/QUI/59019/2004 and POCTI/QUI/58937/2004), We also thank FCT(GRICES)/MinCyT for the award of a Collaborative Bilateral Research Grant. SL acknowledges FCT for the grant SFRH/BD/29698/2006. AGZ thanks ANPCyT (Project PICT/2006/0068).

References:

[1] A. Gómez-Zavaglia and R. Fausto, *J. Mol. Struct.,* **661-662** (2003) 195.

[2] S. Lopes, A. Gómez-Zavaglia, L. Lapinski, N. Chattopadhayay and R. Fausto, *J. Phys. Chem. A,* **108** (2004) 8256.

[3] S. Lopes, A. Gómez-Zavaglia, L. Lapinski and R. Fausto, *J. Phys. Chem. A*, **109** (2005) 5560.

[4] S. Lopes, A. Gómez-Zavaglia and R. Fausto, *Phys. Chem. Chem. Phys.*, **8** (2006) 1794.

[5] A. K. Sing, D. K. Palit and J. Mittal, *Chem. Phys. Lett.*, **360** (2002) 443.

[6] A. K. Singh and D.K. Palit, *Chem. Phys. Lett.*, **357** (2002) 173.

[7] A. Sarkar and S. Chakravorti, *J. Lumin.*, **69** (1996) 161.

[8] M. Mizuno, K. Iwata and H. Takahashi, *J. Mol. Struct.*, **661-662** (2003) 3.

[9] M. Pawlikowski, M. Zgierski and G. Orlandi, *Chem. Phys. Lett.*, **105** (1984) 612.

[10] S. Bera, R. Mukherjee and M. Choudhury, *J. Chem. Phys.*, **51** (1969) 754.

[11] D. S. Roy, K. Bhattacharyya, *Chem. Phys. Lett.*, **69** (1980) 134.

[12] J. Arnett and S. McGlynn, *J. Phys. Chem.,* **79** (1975) 626.

[13] J. Arnett, G. Newkome, W. Mattice and S. McGlynn, *J. Am. Chem. Soc.*, **96** (1974) 4385.

[14] D. J. Morantz and A. J. C. Wright, *J. Chem. Phys.*, **54** (1971) 692.

[15] A. M. Garcia, F. G. Benavides, T. Fletcher and E. Orts, *Scand. J. Environ. Health*, **24(6)** (1998) 445.

[16] C. W. Ellwood, A. Ya. Tikhonov, Rhone Poulenc Agriculture (GB) and Novosib of Organic Chemistry (RU), Patent WO9803479 (1998).

[17] M. J. Robson, P. A. Worthington, ICI PLC (GB), Patent WO9208714, (1992).

[18] M. A. Brodney, Pfizer Prod Inc. (US), Patent WO2006106416, (2006).

[19] R. A. Schnettler, W. D. Jones Jr., G. P. Claxton, Merrell Dow Pharma (US), Patent KR900000369B, (1990).

[20] J. Fevig, J. Cacciola, C. G. Clark, Y.-S. L. Patrick, J. P. P. Donald, J. R. Pruitt, K. A. Rossi, Qi. Han, M. Quan, DU PONT Pharm CO (US), Patent EA4515, (2004).

[21] D. Cheshire, D. Cladingboel, D. Hardern, M. Stocks, Astra Pharma Prod (GB), Patent HU9900143, (1999).

[22] J. W. Slater, D. M. D'Alessandro, F. R. Keene and P. J. Steel, *Dalton Trans.*, (2006) 1954.

[23] R. López, D. Boys, B. Loeb and F. Zuloaga, *J. Chem. Perkin Trans. 2* (1998) 877.

[24] D. F. Colton and W. J. Geary, *J. Chem. Soc. Dalton Trans.*, **4** (1972) 547.

[25] B. I. Ita and O. E. Offiong, *Mat. Chem. Phys*., **51** (1997) 203.

[26] S. Hirokawa and T. Ashida, *Acta Crystallogr.*, **14** (1961) 774.

[27] T. Ashida and S. Hirokawa, *Acta Crystallogr.*, **B26** (1970) 454.

[28] R. W. Le Fèvre and P. J. Stiles, *J. Chem. Soc. B*, (1966) 420.

[29] I. Bernal, *Nature*, **200** (1963) 1318.

[30] H. Sterk, *Monatsh. Chem.*, **99** (1968) 999.

[31] T. Kolev, *J. Mol. Struct.*, **349** (1995**)** 381.

[32] T. Kolev and P. Bleckmann, *Spectrosc. Lett.*, **23** (1990) 1331.

[33] P. Migchels, G. Maes, Th. Zeegers-Huyskens and M. Rospenk, *J. Mol. Struct.*, **193** (1989) 223.

[34] V. Háda, A. Tungler and L. Szepesy, *J. Catal.*, **209** (2002) 472.

[35] H. Inoue and K. Nagaya, *J. Chem. Soc. Perkin Trans. 2*, **10** (1983) 1581.

[36] H. Inoue, T. Sakurai, T. Hoshi and J. Okubo, *J. Photochem. Photobiol. A: Chem*, **72** (1993) 41.

[37] H. Inoue, T. Sakurai, T. Hoshi and J. Okubo, *J. Photochem. Photobiol. A: Chem*, **60** (1991) 121.

[38] S. Bera, R. Mukherjee, D. Mukherjee and M. Choudhury, *J. Chem. Phys.*, **55** (1971) 5826.

[39] T. R. Evans and P. A. Leermakers, *J. Am. Chem. Soc.*, **89** (1967) 4380.

[40] J. Barassin, *Ann. Chim.*, **8** (1963) 637.

[41] N. Yamada, M. Hasegawa, K. Kumagai, S. Enomoto, H. Horiuchi, T. Yoshinaga, H. Hiratsuka, M. Kobayashi and T. Hoshi, *Bull. Chem. Soc. Jpn.*, **78** (2005) 1018.

[42] M. J. Frisch, G. W. Trucks, H. B. Schlegel, G. E. Scuseria, M. A. Robb, J. R. Cheeseman, J. Montgomery, J. A., T. Vreven, K. N. Kudin, J. C. Burant, J. M. Millam, S. S. Iyengar, J. Tomasi, V. Barone, B. Mennucci, M. Cossi, G. Scalmani, N. Rega, G. A. Petersson, H. Nakatsuji, M. Hada, M. Ehara, K. Toyota, R. Fukuda, J. Hasegawa, M. Ishida, T. Nakajima, Y. Honda, O. Kitao, H. Nakai, M. Klene, X. Li, J. E. Knox, H. P. Hratchian, J. B. Cross, V. Bakken, C. Adamo, J. Jaramillo, R. Gomperts, R. E. Stratmann, O. Yazyev, A. J. Austin, R. Cammi, C. Pomelli, J. W. Ochterski, P. Y. Ayala, K. Morokuma, G. A. Voth, P. Salvador, J. J. Dannenberg, V. G. Zakrzewski, S. Dapprich, A. D. Daniels, M. C. Strain, O. Farkas, D. K. Malick, A. D. Rabuck, K. Raghavachari, J. B. Foresman, J. V. Ortiz, Q. Cui, A. G. Baboul, S. Clifford, J. Cioslowski, B. B. Stefanov, G. Liu, A. Liashenko, P. Piskorz, I. Komaromi, R. L. Martin, D. J. Fox, T. Keith, M. A. Al-Laham, C. Y. Peng, A. Nanayakkara, M. Challacombe, P. M. W. Gill, B. Johnson, W. Chen, M. W. Wong, C. Gonzalez and J. A. Pople. *Gaussian 03*, Revision C.02, Gaussian, Inc.: Wallingford CT, 2004.]

[43] A. D. Becke, *Phys. Rev. A.*, **38** (1988) 3098.

[44] C. T. Lee, W. T. Yang and R.G. Parr, *Phys. Review B*, **37** (1988) 785.

[45] P. Csaszar and P. Pulay, *J. Mol. Struct. (Theochem.)*, **114** (1984) 31.

[46] J. H. Schachtschneider, *Technical Report*, Shell Development Co. Emeryville, CA, 1969.

[47] N.J.Turro, *Modern Molecular Photochemistry*, (Ed.: The Benjamin/Cummings Publishing Co., Inc.), 1978.

[48] B. P. Stoicheff, *Can. J. Phys.*, **32** (1954) 339.

[49] F. Mata, M. J. Quintana and G. O. Sørensen, *J. Mol. Struct.*, **42** (1977) 1.

[50] S. Breda, L. Lapinski, I. Reva and R. Fausto, *J. Photochem. Photobiol. A*, **162** (2004) 139.

[51] S. Breda, I. D. Reva, L. Lapinski and R. Fausto, *Phys. Chem. Chem. Phys.*, **6** (2004) 929.

[52] S. Breda, I. D. Reva, L. Lapinski, L. Frija, M. L. Cristiano and R. Fausto, *J. Phys. Chem. A*, **110** (2006) 6415.

[53] I. D. Reva, M. J. Nowak, L. Lapinski and R. Fausto, *Chem. Phys. Lett*, **452** (2008) 20.

[54] O. L. Chapman, C.L. McIntosh, J. Pacansky, *J. Am. Chem. Soc.*, **95** (1993) 614.

[55] D. E. Johnstone and J. R. Sodeau, *J. Phys. Chem.*, **95** (1991) 165.

[56] S. Kudoh, M. Takayanagi and M. Nakata, *J. Photochem. Photobiol. A*, **123** (199) 25.

[57] U. Hees, U.-J. Vogelbacher, G. Michela and M. Regitz, *Tetrahedron*, **45** (1989) 3115.

[58] S. Kudoh, M. Takayanagi and M. Nakata, *Chem. Phys. Lett.*, **322** (2000) 363.

[59] M. G. Barlow, R. Barlow, R. N. Haszeldine and J. G. Dingwall, *J. Chem. Soc. Perkin Trans. I*, (1973) 1542.

[60] R. D. Chambers, R. Middleton and R. P. Corbally, *J. Chem. Soc. Chem. Commun.*, (1975) 731; *ibidim* (1977) 154.

[61] K. E. Wilzbach and D. J. Raush, *J. Am. Chem. Soc.*, **92** (1970) 2178.

[62] D. Zhong, E. W.-G. Diau, T. M. Bernhardt, S. De Feyter, J. D. Roberts and A. H. Zewail, *Chem. Phys. Lett.*, **298** (1998) 129.

[63] I. Yavari, S. Moradi, H. K. Fard, F. Mourmohammadian and D. Tahmassebi, *Theochem.*, **578** (2002) 249.

[64] U. D. Priyakumar, T. C. Dinadayalane and G. N. Sastry, *Chem. Phys. Lett.*, **337** (2001) 361.

[65] R. Lium X. Zhou and P. Pulay, *J. Phys. Chem.*, **96** (1992) 3669.

[67] H. Abe and K. M. T. Yamada, *Struct. Chem.*, **14** (2003) 211.

[68] H. Dubost, *Chem. Phys.*, **12** (1976) 139.

[69] A. D. Abbate and C. B. Moore, *J. Chem. Phys.*, **82** (1985) 1255.

[70] E. Sánchez-García, A. Mardyukov, A. Tekin, R. Crespo-Otero, L. A. Montero, W. Sander and G. Jansen, *Chem. Phys.*, **343** (2008) 168.

[71] R. G. S. Pong, B. S. Huang, J. Laureni and A. Krantz, *J. Am. Chem. Soc.*, **99** (1977) 4153.

[72] Sigma-Aldrich online Catalog 2008, http://www.sigmaaldrich.com.

4 Case Studies

In this Chapter, the studies performed on monomers and dimers of formic and acetic acids are presented:

Formic and Acetic Acids in a Nitrogen Matrix: Enhanced Stability of the Higher Energy Conformer, S. Lopes, A. Domanskaya, R. Fausto, M. Räsänen and L. Khriachtchev, J. Chem. Phys., **2010**, *133*, 144507-7.

Acetic Acid Dimers in Solid Nitrogen Matrix, S. Lopes, A. Domanskaya, R. Fausto, M. Räsänen and L. Khriachtchev (*to be submitted*)

J. Chem. Phys., **2010**, *133*, 144507-7.

Formic and Acetic Acids in a Nitrogen Matrix: Enhanced Stability of the Higher Energy Conformer

Susy Lopes,[1] Alexandra V. Domanskaya,[2] Rui Fausto,[1] Markku Räsänen,[2] and Leonid Khriachtchev[2]

[1]*Department of Chemistry, University of Coimbra, Rua Larga, P-3004-535 Coimbra, Portugal*
[2]*Department of Chemistry, University of Helsinki, P.O. Box 55, FIN-00014 Helsinki, Finland*

ABSTRACT

Formic acid (HCOOH, FA) and acetic acid (CH_3COOH, AA) are studied in a nitrogen matrix. The infrared (IR) spectra of *cis* and *trans* conformers of these carboxylic acids (and also of the HCOOD isotopologue of FA) are reported and analyzed. The higher-energy *cis* conformer of these molecules is produced by narrowband near-IR excitation of the more stable *trans* conformer, and the *cis*-to-*trans* tunneling decay is evaluated spectroscopically. The tunneling process in both molecules is found to be substantially slower in a nitrogen matrix than in rare-gas matrices, the *cis*-form decay constants being ca. 55 and 600 times smaller in a nitrogen matrix than in an argon matrix, for FA and AA respectively. The stabilization of the higher-energy *cis* conformer is discussed in terms of specific interactions with nitrogen molecule binding with the OH group of the carboxylic acid. This model is in agreement with the observed differences in the IR spectra in nitrogen and argon matrices, in particular, the relative frequencies of the νOH and τCOH modes and the relative intensities of the νOH and νC=O bands.

1. Introduction

Formic acid (HCOOH, FA) and acetic acid (CH_3COOH, AA) are simple carboxylic acids both identified in the interstellar medium.[1,2] Carboxylic acids have biological value and provide an insight into prebiotic organic chemistry in the protoplanetary nebula.[3] Acetic acid is of particular importance due to its structural proximity to glycine, the simplest amino acid. Formation of acetic acid was detected upon irradiation of binary mixtures of methane (CH_4) and carbon dioxide (CO_2) ices by energetic electrons at 12 K.[4] Electron bombardment mimics the energy transfer processes that occur in the track of the trajectories of MeV cosmic-ray particles.

Organic acids in the gas phase can partition into aerosol particles[5] with the aid of foreign nuclei, such as alkaline mineral particles and elemental carbon, and by condensation and co-condensation with NH_3. It is hypothesized that organic acids are at least one of the primary sources of CCN in the atmosphere, especially over the continental forested areas, due to their ubiquitous presence in the troposphere.[6]

FA and AA have two conformers (*cis* and *trans)*, which differ by the orientation of the OH group (Figure 1). They are good model systems for fundamental studies of conformational changes and intramolecular energy redistribution. The *cis* form is higher in energy than the *trans* form by ca. 1365 cm^{-1} for FA (gas-phase experimental data),[7] and ca. 1880 cm^{-1} for AA (theoretical value).[8] The calculated *trans*-to-*cis* conversion barriers are 44 kJ mol^{-1} (3921 cm^{-1})[9] and 49 kJ mol^{-1} (4400 cm^{-1})[8] for FA and AA, respectively. Detailed infrared (IR) spectroscopic data for *trans* and *cis* conformers of these acids and their isotopomers have been reported in rare-gas matrices.[10-14]

The *cis* form of carboxylic acids can be obtained by vibrational excitation of the *trans* form.[10,13,15] Once obtained, the higher-energy *cis* conformer converts back to the ground-state *trans* form. At low temperatures, quantum tunneling dominates the over–barrier reactions. Hydrogen tunneling in FA and AA has been the subject of several studies.[9,15-19]

cis-CH_3COOH has a shorter lifetime in rare-gas matrices than *cis*-HCOOH (approximately 50 s[18] *versus* 8 min[16] in solid argon at 8 K). Deuteration of the OH group influences greatly the tunneling process, slowing it down by about four orders of magnitude. The conversion process of *cis*-CH_3COOD and *cis*-HCOOD to the *trans* forms in an argon matrix at 8 K takes about 15 days.[18,19] On the other hand, the

tunneling rates in formic[16] and acetic acids[18] increase upon deuteration of CH or CH_3 groups. This secondary isotopic effect is very interesting but lacks an explanation.

The tunneling rates in these species are strongly dependent on the matrix material. The *cis*-HCOOH decay rates increase with the matrix polarizability as $k_{Xe} < k_{Kr} < k_{Ar} < k_{Ne}$.[15,16] However, the decay of *cis*-HCOOD follows almost the opposite trend: $k_{Xe} \approx k_{Kr} > k_{Ar} \approx k_{Ne}$.[19] With respect to the reaction barrier height, which increases in more polarizable hosts, the order of the rate constants in HCOOD is anomalous.[15,16] Similar "anomalous" behavior was also reported for AA ($k_{Xe} \geq k_{Ar} > k_{Kr}$).[18] Clearly, in addition to the barrier change upon solvation in polarizable media, other factors can also influence the *cis*-to-*trans* conversion.[15,16,19]

trans *cis*

Figure 1 – *Trans* (most stable) and *cis* (higher energy) conformers of formic acid (R= H) and acetic acid (R= CH_3).

Some experimental results suggest that the *cis* conformers might be stabilized in media resembling interstellar and atmospheric environments. An experimental study of AA and FA aerosol nanoparticles generated at 78 K and investigated using *in situ* rapid-scan FTIR spectroscopy shows that the spectra of the particles have the same characteristic splitting of the ν(C=O), δ(CH), and ν(C–O) bands as the crystalline bulk.[20] One possible explanation for the observed splitting is the coexistence of the *trans* and *cis* conformations in the chains, which would presumably destroy the planarity of the chains; however, the polymorphism of molecular chains made from *trans* subunits cannot be excluded. Crystalline acetic acid shows similar spectral splitting which might also be attributed to the inclusion of *cis*-oriented subunits.[21]

The tentative observation of the *cis* conformation in hydrogen-bonded systems agrees well with the general idea that complexation, dimerization, or solvation of higher-energy conformers can significantly decelerate or even stop the tunneling decay process.[15] For example, the *cis*-HCOOH···H_2O complex is stable at 9 K on a day

scale. The lifetime of *cis*-FA in this complex might be practically infinite at low temperatures, *i.e.*, tunneling to the *trans* conformer is efficiently suppressed.[15] Studies of the interaction of carboxylic acids with nitrogen might lead to a better understanding of the role of conformational isomerism in dark interstellar clouds[23] and the Earth's atmosphere.

In the present work, we report new results on spectroscopy of formic and acetic acids in a nitrogen matrix and on the stabilization of higher-energy *cis* conformers in this medium. The stabilization effect is discussed in terms of specific interactions between the matrix and embedded molecules.

2. Computational details and results

The quantum chemical calculations were performed using Gamess, version R1 (24-Mar-2007)[24] at the MP2 level of theory[25] using the 6-311++G(2d,2p) basis set.[26,27] This basis set has been shown to reproduce the experimental structural and vibrational properties of FA with an acceptable accuracy.[11,28,29] The optimization criteria parameter OPTTOL was set to 0.00001 hartree/bohr. This parameter corresponds to the maximum value allowed to the energy gradient and also controls the maximum allowed value of the root mean square gradient, which is given by 1/3 of OPTTOL. The optimized structures of all FA$^{\cdots}$N$_2$ and AA$^{\cdots}$N$_2$ complexes were confirmed to correspond to the true energy minima on the potential energy surfaces by inspection of the Hessian matrices. The vibrational spectra were computed at the same level of theory. The calculated MP2/6-311++G(2d,2p) vibrational frequencies and intensities of the fundamental modes for the *cis* and *trans* forms of HCOOH, HCOOD and CH_3COOH are listed together with the assignments of the observed fundamental transitions (Tables I and II). The calculated spectra of FA and AA are shown in Figures 2 and 3 (lower traces).

The most stable complex has the N_2 molecule interacting with the OH bond of the carboxylic acid (Figure 4). This result is in agreement with the previous study on the *trans*-FA$^{\cdots}$N$_2$ system.[28] All optimized complexes are presented in Figures S1-S4.[29] Most of the *trans*-FA$^{\cdots}$N$_2$ structures (Figure S2) were not detected previously by Lundell *et al*.[28]

Table I. Assignment of the spectra of the *trans* and *cis* forms of HCOOH and HCOOD isolated in argon and nitrogen matrices. The calculated fundamental frequencies (in cm^{-1}) and intensities (in km mol^{-1}, in parenthesis) for *trans* and *cis* conformers of HCOOH and HCOOD were obtained at the MP2/6-311++G(2d,2p) level of theory. Frequencies in *italic* indicate tentative assignments.

	N_2 matrix		Ar matrix[a]		Calculated	
Assignment	*trans*	*cis*	*trans*	*cis*	*trans*	*cis*
HCOOH						
νOH	3528.2	3598.1	3549	3617	3777.9 (81.8)	3844.5 (81.6)
νCH	2967.5	2900.6	2955	2898	3127.2 (33.6)	3039.4 (64.8)
νC=O	1762.2	1803.0	1768	1808	1784.2 (334.3)	1824.4 (268.3)
γCH	*1342* w	*1391*w	1383	1392	1424.4 (1.5)	1439.3 (0.1)
CO–COH def.	*1265* w	1275.9	1215	1246	1314.3 (9.0)	1285.5 (294.4)
COH–CO def.	1119.4	*~1120*	1103	1106	1119.9 (284.2)	1109.4 (81.6)
wCH	1040.5	1047.0	1038	–	1060.8 (3.8)	1038.8 (0.2)
τCOH	672.3	536.2	635	504	674.7 (143.5)	535.2 (88.1)
δOCO	637.0	667.8	629	662	629.9 (39.1)	659.1 (11.7)
HCOOD						
νOD	2602.5	2657.4	2619.5	2668.7	3127.7 (30.0)	3039.3 (63.1)
νCH	2973.7	2899.4	2961.2	2895.3	1777.5 (317.7)	1816.8 (297.1)
νC=O	1749.6	1790.6	1767.2	1799.3	1415.5 (1.4)	1437.9 (0.6)
γCH	–	–	1374.3	1395.4	1191.7 (179.6)	1172.6 (303.2)
νC–O	1187.9	1176.8	1181.7	1164.0	1058.2 (1.3)	1038.8 (0.1)
wCH	1038.2	–	1036.4	1041.0	1000.1 (85.0)	925.7 (2.9)
δCOD	989.8	929.5	971.0	910.5	564.6 (40.1)	631.9 (12.1)
OCO–COD def.	571.3	*641.2*	559.7	633.6	530.2 (88.7)	402.5 (33.1)
τCOD	528.9	–	506.7	–	3127.7 (30.0)	3039.3 (63.1)

[a] From refs. 11,19 (averaged value of two sites).

Table II. Assignment of the spectra of the *trans* and *cis* forms of CH_3COOH isolated in argon and nitrogen matrices. The calculated fundamental frequencies (in cm^{-1}) and intensities (in km mol^{-1}, in parenthesis) for *trans* and *cis* conformers of CH_3COOH were obtained at the MP2/6-311++G(2d,2p) level of theory.

Assignment	CH_3COOH (N_2)			CH_3COOH (Ar)[14]		Calculated	
	trans		*cis*	*trans*	*cis*	*trans*	*cis*
	Site I	Site II					
νOH	3544.1	3551.9	3610.7	3563.8	3622.6	3787.3 (77.5)	3852.9 (63.3)
νHCH_2 s	3035.8	3035.8	-	3051	-	3228.7 (2.6)	3221.6 (1.9)
νHCH_2 a	3002.4	2995.6	2990.0	2996	-	3187.8 (1.8)	3169.8 (3.8)
νCH_3	2965.4	2954.0 2947.4	2942.3	2944	-	3107.6 (1.2)	3091.7 (3.5)
νC=O	1775.1	1777.6	1797.2	1779.0	1807.4	1801.0 (290.3)	1828.1 (247.4)
δHCH_2 a	1445.5	1441.0	1445.7	1438.8	1448.3	1505.4 (8.4)	1513.2 (7.8)
δHCH_2 s	1435.7	1435.7	1438.8 (?)	1433.6	1444.5	1500.3 (16.2)	1500.5 (7.4)
δCH_3	1387.6	1385.7	1371.9 1370.2	1379.4 1324.4	1368.3	1432.7 (48.9)	1420.4 (44.3)
CO-COH def.	1275.9	1280.5	1234.0 1210.4 (?)	1259.4	1192.9	1350.3 (39.0)	1215.0 (7.6)
COH-CO def.	1205.9 1183.9	1196.5 1177.4	1301.7 1290.5 } [a]	1179.8	1285.4 1271.9 } [a]	1208.1 (212.8)	1306.3 (373.5)
γCH_3 a	1048.1	-	1044.1	1047.2	1042.4	1082.7 (5.1)	1076.8 (3.3)
γCH_3 s	990.9	-	-	985.5	982.2	1009.4 (82.4)	1000.4 (11.9)
νC-C	856.3	-	857.4	-	848.6	867.8 (7.9)	860.6 (40.5)
τCOH	663.2	656.1	489.3	637.8	458.0	661.0 (90.3)	465.1 (101.3)
δOCO	588.3	585.7	600.6	580.4	-	584.6 (36.3)	602.3 (1.4)
γC=O	554.2 546.4	556.0 549.4	-	534.2	-	550.7 (30.9)	598.6 (7.4)
δCC=O	430.2 (?)	-	-	428	-	425.4 (4.1)	434.4 (3.7)
τCH_3	-	-	-	-	-	75.4 (0.2)	92.2 (1.2)

[a] Fermi resonance with νC-C+τC-O.

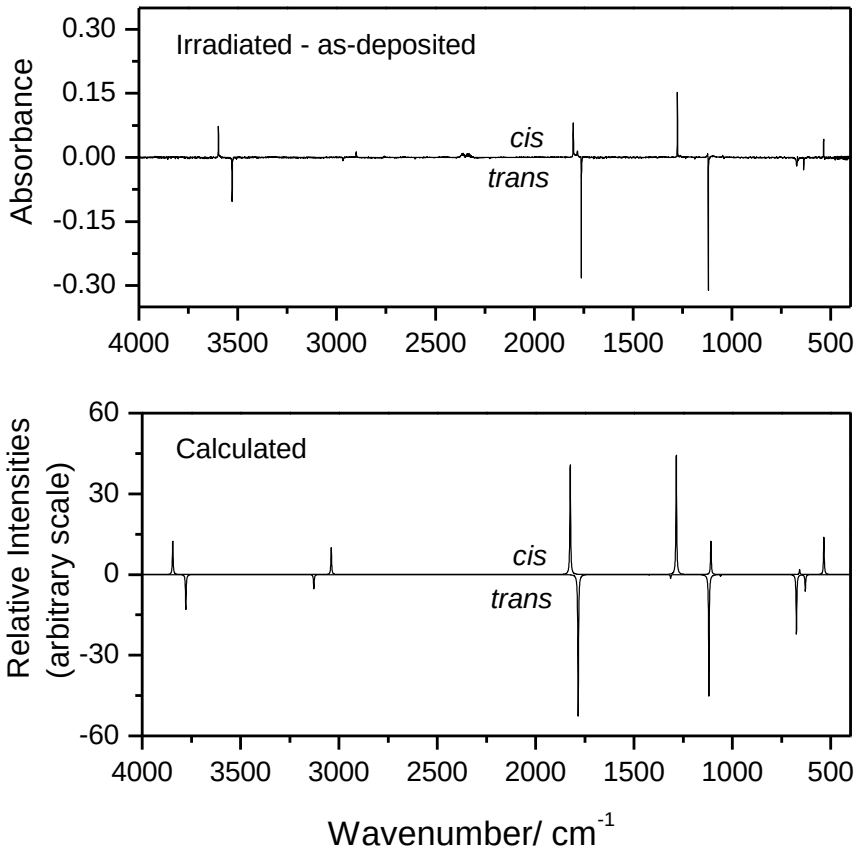

Figure 2. ***Top:*** FTIR difference spectrum of FA in solid N_2. Result of irradiation at 5288 cm^{-1}, showing conversion of *trans*-FA into *cis*-FA. ***Bottom:*** MP2/6-311++G(2d,2p) calculated infrared spectra of *trans*-FA (downward peaks) and *cis*-FA (upward peaks). In the calculated spectra, bands were represented by Lorentzian functions centered at the calculated wavenumbers and with FWHM (full width at half maximum) equal to 4 cm^{-1}.

The interaction energies of the FA···N_2 and AA···N_2 complexes were evaluated (see Figure 4). For the *trans* species, the interaction energy of approximately –4.0 kJ mol^{-1} (zero point and basis set superposition error corrected energy) was obtained for both FA and AA. This value agrees fairly with the interaction energy reported by Lundell *et al.*[28] for the *trans*-FA···N_2 complex (–5.3 to –6.2 kJ mol^{-1} depending on the basis set). The interaction is slightly stronger in the complexes of the *cis* conformers. The calculations reveal a stronger stabilization for AA than for FA (–5.1 kJ mol^{-1} in AA *vs.* –4.4 kJ mol^{-1} in FA; Figure 4).

The calculated characteristic vibrational frequencies and intensities for the strongest complexes are compared with the data for the monomers in Table III. According to the calculations, the OH stretching frequency decreases by *ca.* 20 to 30 cm^{-1} and substantially intensifies (three to four times) for both acids in both

conformational states. The OH torsional mode shows blue shifts (approximately 60 to 80 cm^{-1}) and its intensity slightly decreases upon complexation except for *trans* $AA^{\cdots}N_2$ complexes. The νC=O mode red shifts by *ca.* 5 cm^{-1} and slightly gains intensity for the *cis* conformers, whereas the intensity slightly decreases for the *trans* forms. The changes of both frequency and intensity upon complexation of FA and AA are in agreement with the expectations for an H-bond type interaction.[31-34] The spectral data for other complexes are presented in Table S-I.[35]

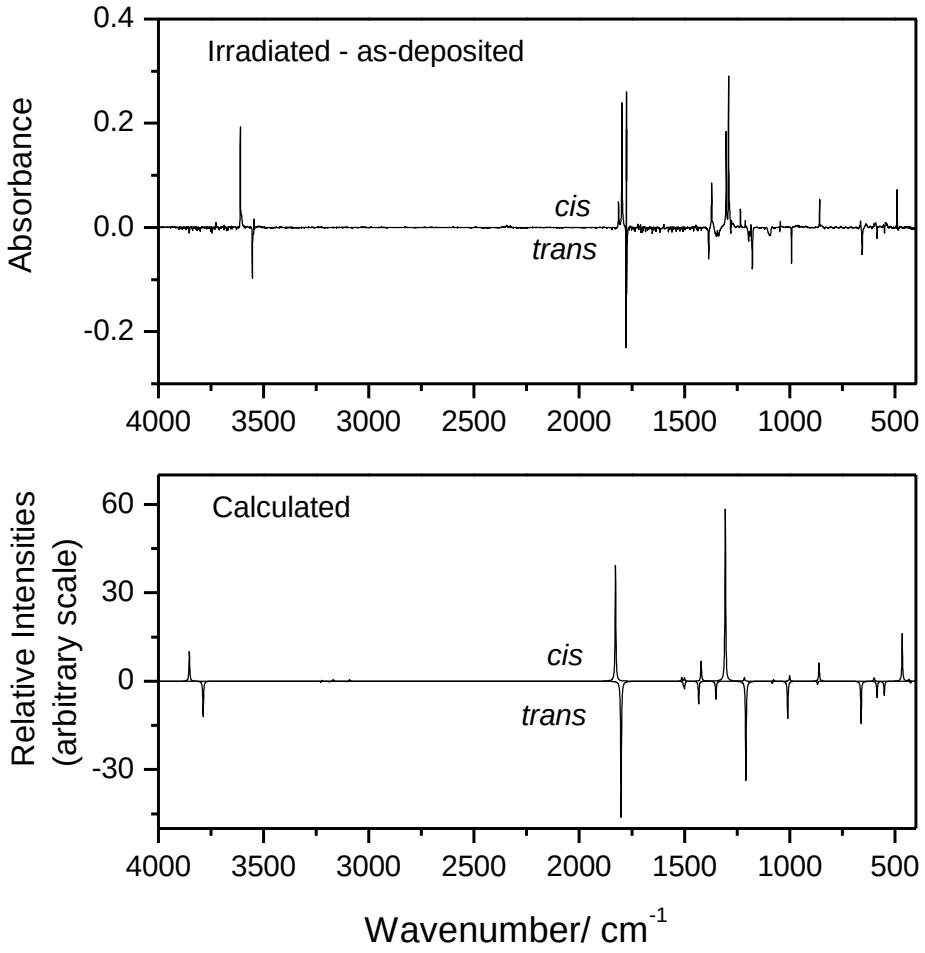

Figure 3. ***Top:*** FTIR difference spectrum of AA in solid N_2. Result of irradiation at 4724.5 cm^{-1}, showing conversion of *trans*-AA into *cis*-AA. ***Bottom:*** MP2/6-311++G(2d,2p) calculated infrared spectra of *trans*-AA (downward peaks) and *cis*-AA (upward peaks). In the calculated spectra, bands were represented by Lorentzian functions centered at the calculated wavenumbers and with FWHM (full width at half maximum) equal to 4 cm^{-1}.

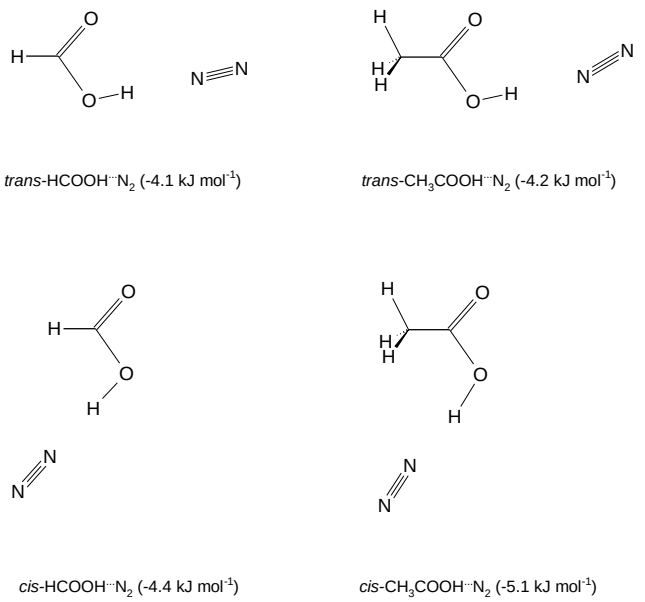

Figure 4. Schematic structures of the strongest complexes of formic and acetic acids in *cis* and *trans* forms with molecular nitrogen at the MP2/6-311++G(2d,2p) level of theory. The interaction energies of the complexes are given in parenthesis and correspond to zero point and basis set superposition error (BSSE) corrected values. The calculated BSSE for *cis* and *trans* complexes amount to –2.6 and –2.3 kJ mol^{-1}, respectively. Optimized structures for the complexes are provided in Figures S1-S4 (Supplementary Material). Calculated N···H distances are 2.199, 2.209, 2.218 and 2.223 Å, for *trans*-HCOOH···N_2, *cis*-HCOOH···N_2, *trans*-CH_3COOH···N_2 and *cis*-CH_3COOH···N_2, respectively.

Table III. Calculated νOH, νC=O and τCOH wavenumbers (ν in cm^{-1}) and infrared intensities (I_{IR} in km mol^{-1}) for monomeric *cis* and *trans* forms of FA and AA and their most stable complexes with N_2.[a]

	νOH		νC=O		τCOH		νOH		νC=O		τCOH	
	ν	I_{IR}	ν	I_{IR}	ν	I_{IR}	ν	I_{IR}	ν	I_{IR}	ν	I_{IR}
	cis-HCOOH						*trans*-HCOOH					
Monomer	3844.5	81.6	1824.4	268.3	535.2	88.1	3777.9	81.8	1784.2	334.3	674.7	143.5
Complex	3820.3	292.3	1820.6	297.9	620.9	79.0	3747.6	282.1	1779.1	321.0	747.7	118.5
[b]	-24.2	3.6	-3.8	1.1	85.7	0.9	-30.3	3.4	-5.1	0.96	73.0	0.8
	cis-CH_3COOH						*trans*-CH_3COOH					
Monomer	3852.9	63.3	1828.1	247.4	465.1	101.3	3787.3	77.5	1801.0	290.3	661.0	90.3
Complex	3833.6	233.1	1824.6	270.0	537.5	72.3	3762.6	266.8	1795.2	277.1	718.6	96.9
[b]	-19.3	3.7	-3.5	1.1	72.4	0.7	-24.7	3.4	-5.8	0.95	57.6	1.1

[a] See Figures 1-4. [b] The values presented in this row correspond to frequency shifts ($\nu_{complex}-\nu_{monomer}$) or intensity ratios ($I_{complex}/I_{monomer}$)

Experimental details and results

Gaseous mixtures of FA (HCOOH, KEBO LAB, 99%) and AA (CH_3COOH, KEBO LAB, 99%) with nitrogen (AGA/Linde 6.0) were prepared with a typical ratio of 1:1200. The acids were purified by a few freezing-pumping cycles. Nitrogen was used as supplied. The mixtures were deposited onto a CsI window at 8.5 K in a close–cycle helium cryostat (APD, DE 202A). The spectra were recorded with a Nicolet 60SX FTIR instrument by co–adding 200 interferograms with 1 cm^{-1} spectral resolution. HCOOD molecules were produced by an H/D exchange with deuterated surfaces in the deposition line. The obtained deuteration degree (~15%) was sufficient to observe and assign the main fundamental frequencies.

The *trans*–to–*cis* conversion was promoted by selective vibrational excitation by using an optical parametric oscillator with IR extension (Sunlite Continuum, FWHM ~ 0.1 cm^{-1}). *cis*-AA was produced by exciting the νOH+δCOH combination mode of *trans*-AA at 4724.5 cm^{-1}. *cis*-FA was prepared by exciting the νOH+νC=O combination mode of *trans*-FA at 5288 cm^{-1}. The *cis*-HCOOD was produced by the IR light source of the spectrometer (Globar).

In the kinetic measurements, the *cis*-conformer decay was monitored by measuring the intensity of the CO–COH def. fundamental band of *cis*-HCOOH (1275.9 cm^{-1}) as a function of time. In the case of *cis*-CH_3COOH, the split COH–CO def. band (1301.7 and 1290.5 cm^{-1}) and the δCH_3 band (1370.5 cm^{-1}) were used. A long–pass optical filter (>1500 cm^{-1}) was inserted between the sample and the Globar source in order to suppress high frequency light components which could accelerate the *cis*–to–*trans* conversion process. The Globar light was blocked between the measurements. The OD form of the *cis*-FA is very stable over time due to the well-known mass effect on the tunneling rate[12,15-19] and its decay was not studied here.

The spectra of FA and AA in a nitrogen matrix at ca. 8.5 K are presented in Figures 2 and 3. The results of vibrational excitation (at 5288 cm^{-1} for FA and at 4724.5 cm^{-1} for AA) are shown. The assignments of the observed fundamental transitions are given in Tables I and II, together with the calculated MP2/6-311++G(2d,2p) vibrational frequencies and intensities of the fundamental modes for the *cis* and *trans* forms of HCOOH, HCOOD and CH_3COOH.

The *cis*–to–*trans* decay curves for FA and AA are shown in Figures 5 and 6. The decay rates obtained in a nitrogen matrix at different temperatures are compared with the rates previously measured in an argon matrix[16,18] in Figure 7.

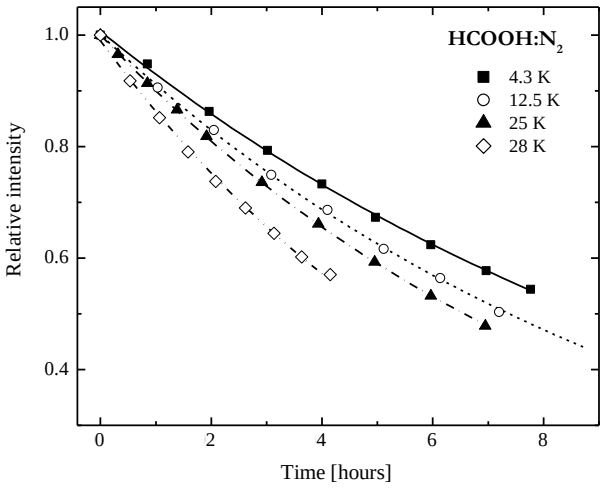

Figure 5 – Decay of *cis*-HCOOH in a nitrogen matrix at different temperatures.

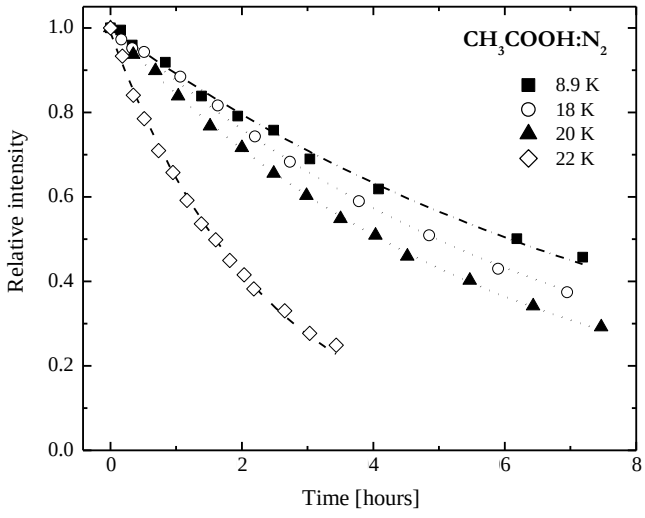

Figure 6 – Decay of *cis*-CH_3COOH in a nitrogen matrix at different temperatures.

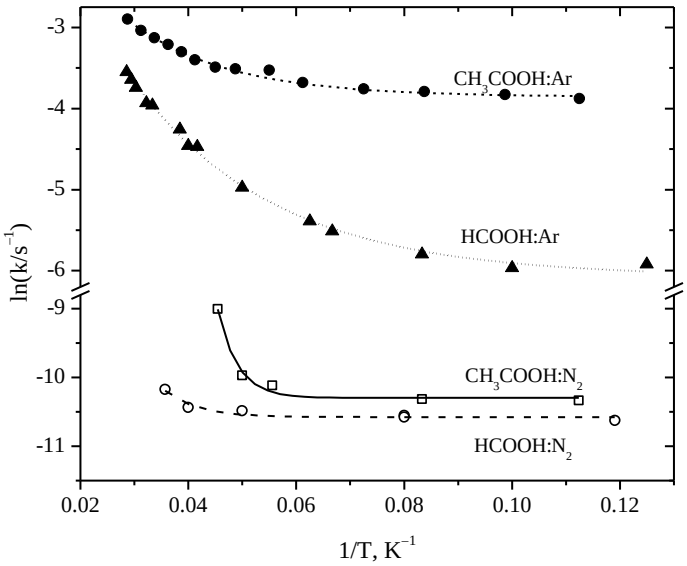

Figure 7 – Tunneling rate constants for *cis*-HCOOH and *cis*-CH_3COOH in nitrogen (this work) and argon (data from Refs. 16,18) matrices.

4. Discussion

A. Spectral assignment

For both acids, the experimental IR spectra are reproduced well by theory, which allows a straightforward identification of the bands (Figures 2 and 3). The assignments of the observed fundamental transitions are given in Tables I and II, where they are compared with the experimental data obtained in an argon matrix.[11,14,19]

The assignments for *trans*-HCOOH are doubtless except for the low intensity CO-COH def. and γCH modes, which are tentatively assigned to the weak bands at 1265 and 1342 cm^{-1} in a nitrogen matrix (1215 and 1383 cm^{-1} in an Ar matrix).[11] For *cis*-HCOOH, γCH is also predicted to have low intensity (see Table I), and it is tentatively ascribed to the band observed at 1391 cm^{-1}, appearing at almost the same frequency as in Ar matrix (1392 cm^{-1}).[11] The assignment of the COH-CO def. mode of *cis*-HCOOH is complicated by a fact that this vibration almost coincides with the analogous vibration of the *trans* conformer. The band of the *cis* form is hidden by the wing of the *trans*-FA band and even in the difference spectrum is not easy to be noticed. Nevertheless, the theory predicts this band to be intense (see Table I), so that there is no other possibility for assignment.

In the case of HCOOD, the very weak γCH and wCH modes (see Table I) could not be observed experimentally. The assignment of the OCO–COD def. mode of the *cis* form is uncertain also due to its low intensity.

The results for *trans*-AA indicate trapping into two main matrix sites (named I and II) in a nitrogen matrix. In our experiments, only molecules in site II were vibrationally excited by IR radiation and consequently converted to the *cis* form.

B. Interaction with nitrogen

The potential energy surfaces (PES) of the FA···N_2 and AA···N_2 systems reveal that the 1:1 hydrogen-bonded complexes feature the most important interaction in a nitrogen matrix. If a specific interaction dominates one can consider the 1:1 complex surrounded by a matrix. For an Ar matrix, this approach is validated by calculations of FA···Ar complexes by Wawrzyniak *et al.*[35,36] They found that the FA···Ar structures with an Ar atom bonded to the OH group of FA have substantially smaller interaction energies (–1.5 to –2.0 kJ mol^{-1}) than in the present case of similar nitrogen complexes. Thus, the substitution of the Ar atom by a nitrogen molecule is energetically favorable. If the OH···N_2 interaction is dominant, the result of complexation will be accordingly reflected in the vibrational spectra. Adding additional N_2 molecules to the 1:1 complexes to describe the matrix effect is computationally difficult and, in the present case, does not seem to be strictly required.

The data obtained in solid nitrogen can be compared with less perturbing hosts such as neon and argon matrices.[11,14,22] The experimental observations in a nitrogen matrix agree with the spectral predictions for the strongest 1:1 complexes. The νOH frequency of FA decreases by 19 and 21 cm^{-1} for *cis* and *trans* forms, respectively, from values in an argon matrix (Table IV) and by 39 and 41 cm^{-1} compared to a neon matrix. The τCOH frequency increases by 32 (*cis*) and 37 cm^{-1} (*trans*) from values in an argon matrix and by 39 and 34 cm^{-1} compared to a Ne matrix. For AA, νOH shows red shifts by 12 cm^{-1} (*cis*), 20 cm^{-1} (*trans*, site I) and –12 cm^{-1} (*trans*, site II), and τCOH shifts by +31 (*cis*), +25 cm^{-1} (*trans*, site I) and 12 cm^{-1} (*trans*, site II) compared to an Ar matrix. These trends are in agreement with the calculations for the

strongest complexes (Table III). The 1:1 interaction with nitrogen produces larger red shifts compared to interaction with argon, as calculated for FA.[35,36]

Analysis of the experimental intensities leads to similar conclusions. We assume that the νOH/νC=O intensity ratio is a fingerprint of the OH···N_2 interaction in a nitrogen matrix because the C=O stretching intensity does not change much upon complexation. For FA, this ratio in a nitrogen matrix increases by a factor of *ca.* 2 compared to an argon matrix (see Table IV). It should also be remembered that the relative band intensities are already changed in an argon matrix. Wawrzyniak *et al.*[35,36] reported a two-fold increase of the OH stretching intensity for the hydrogen bonded FA···Ar complex. Combining these data, one may estimate that complexation with nitrogen leads to a 4-fold increase of the OH-stretching intensity, which is in reasonable agreement with our theoretical value for the strongest complexes (*ca.* 3.5). The results for AA follow the same general trends. However, for this compound the uncertainties in the determined experimental intensities are considerably larger due to band overlapping in the carbonyl stretching region making impossible the quantitative analysis. It is also probable that the rest of the matrix (in addition to the specific interaction) somewhat affects the vibrational intensities. Perhaps this leads to the large effect observed for the torsional intensities, which is not so well predicted by the model of specific interactions.

Table IV. Experimental relative intensities of FA and AA in nitrogen and argon[14] matrices and the corresponding matrix shift (cm^{-1}).

	N_2 matrix	Ar matrix	Shift	N_2 matrix	Ar matrix	Shift
	cis-FA			*trans*-FA		
νOH	0.83	0.45	–19	0.57	0.32	–21
νC=O	1	1	–5	1	1	–6
τCOH	0.45	0.28	+32	0.21	0.50	+37
	cis-AA			*trans*-AA[a]		
νOH	0.73	0.09	–12	0.53	0.47	–12 (–20)
νC=O	1	1	–10	1	1	–1 (–4)
τCOH	0.21	1.02	+31	0.63	0.82	+18 (+25)

[a] Data for site II; shifts for site I in parenthesis.

C. Tunneling rates

At the lowest temperatures, the *cis*-HCOOH decay rate in a nitrogen matrix is smaller by ~55 and 10000 times compared to argon and neon matrices, respectively.[16,22] For CH_3COOH, the *cis*–to–*trans* conversion in a nitrogen matrix is slower by a factor of ~600 than in an argon matrix. At *ca.* 8.5 K, the *cis*-HCOOH decay in a nitrogen matrix is about 5 times slower than the decay in a xenon matrix[16] and *ca.* 30 times slower than in a krypton matrix. For CH_3COOH, the tunneling rate is very similar in argon and krypton matrices, but it is 5 times faster in a xenon matrix.[18] The tunneling rate of AA in a Xe matrix is *ca.* 3000 times greater than in a nitrogen matrix. *Cis*–to–*trans* conversion accelerates at elevated temperatures (Figure 7), which suggests the influence of the matrix phonons to the tunneling process.[16] The observed temperature dependence in a nitrogen matrix has a plateau for both acids where the tunneling rate remains practically constant. Such behavior demonstrates that up to a certain temperature (*ca.* 15 K in our case) the conversion process goes solely by tunneling.

We emphasize three experimental observations: (i) faster decay of *cis*-AA compared to *cis*-FA in all matrices; (ii) slower decay of the *cis* conformers in solid nitrogen than in rare-gas matrices; and (iii) closer decay rates of *cis*-AA and *cis*-FA in a nitrogen compared to argon matrix.

The faster decay of of *cis*-AA compared to *cis*-FA can be explained by the lower *cis*–to–*trans* barrier for AA. The calculated *cis*–to–*trans* barriers are 4400 and 3921 cm^{-1} for AA and FA, respectively.[8,9] Indeed, the barrier height is the most important factor controlling the tunneling rate. The different barriers also explain why the decay slows down in solid nitrogen compared to an Ar matrix. As discussed above, the spectroscopic data indicate the importance of the specific interaction between the hydrogen atom of the OH group and a nitrogen molecule. This interaction lowers the total energy of the system. On the other hand, this interaction is not efficient in the transition state for the case of a short tunneling time when the coordinates of the atoms are fixed (except the tunneling hydrogen). It follows that the *cis*–to–*trans* barrier becomes higher within the model of specific interactions approximately by the value of the dissociation energy of the corresponding hydrogen-bonded complex. This interaction is substantially weaker for an argon atom than for a nitrogen molecule. In agreement with the model of specific interactions, Marushkevich *et al*. have found

recently that the *cis*-FA···N_2 complex in an argon matrix has a lifetime of 48 min, *i.e.*, 6.5 times longer compared to the *cis*-FA monomer.[37] The same discussion is relevant to the third experimental observation that the decays of *cis*-AA and *cis*-FA in solid nitrogen become closer compared to an Ar matrix. Indeed, the hydrogen bonding to nitrogen is stronger for AA than for FA (by 0.7 kJ mol^{-1}); hence the *cis*–to–*trans* barriers become similar for these molecules. It should be mentioned that additional factors exist which influence the tunneling rates.[15,16,18,19]

Conclusion

Formic and acetic acids have been studied in nitrogen matrices. The IR spectra of the *cis* and *trans* conformers of these species are assigned (Tables I and II). The higher energy *cis* conformer of these molecules is produced by vibrational excitation of the more stable *trans* conformer. The decay of the *cis* forms is observed and explained by tunneling of hydrogen through the *cis*–to–*trans* torsional barrier, similarly to these species in rare-gas matrices.[16,18] On the other hand, the tunneling for both molecules is considerably slower in a nitrogen matrix than in rare-gas matrices, for example, the *cis*–to–*trans* conversion of HCOOH slows down in a nitrogen matrix by four orders of magnitude compared to a neon matrix.

Both spectroscopic and tunneling data indicate that the OH···N_2 specific interactions are important for both acids in a nitrogen matrix. Within the model of specific interactions, the tunneling barrier height should be higher in a nitrogen matrix than in an argon matrix. This conclusion is in agreement with the experimental observations on tunneling decay of AA and FA in a nitrogen matrix.

Acknowledgments

These studies were partially funded by the Portuguese Science Foundation (Project FCOMP-01-0124-FEDER-007458, co-funded by QREN-COMPETE-UE and Grant #SFRH/BD/29698/2006) and by the Academy of Finland through the Finnish Centre of Excellence in Computational Molecular Science. R.F. and S.L. acknowledge Milipeia Computer Centre (University of Coimbra), research project "Computação

Avançada em Espectroscopia Molecular". A.D. acknowledges a postdoctoral grant from the Faculty of Science, University of Helsinki (project No 7500101).

References:

1. B. Zuckerman, J. A. Ball, C. A. Gottlieb, Astrophys. J. **163**, L41 (1971).
2. D. M. Mehringer, L. E. Snyder, Y. Miao, F. J. Lovas, Astrophys. J. **480**, L71-L74 (1997).
3. P. Ehrenfreund, S. B. Charnley, Ann. Rev. Astron. Astrophys. **38**, 427 (2000).
4. C. J. Bennett, R. I. Kaiser, Astrophys. J. **660**, 1289 (2007).
5. Z. Y. Meng, J. H. Seinfeld, P. Saxena, **23**, 561 (1995).
6. S. Yu, Atmosph. Res. **53**, 185 (2000).
7. W. H. Hocking, Z. Naturforsch. A **31**, 1113 (1976).
8. M. L. Senent, Mol. Phys. **99**, 1311 (2001).
9. M. Pettersson, E. M. S. Maçôas, L. Khriachtchev, R. Fausto, M. Räsänen, J. Am. Chem. Soc. **125**, 4058 (2003).
10. M. Pettersson, J. Lundell, L. Khriachtchev, M. Räsänen, J. Am. Chem. Soc. **119**, 11715 (1997).
11. E. M. S. Maçôas, J. Lundell, M. Pettersson, L. Khriachtchev, R. Fausto, M. Räsänen, J. Mol. Spectrosc. **219**, 70 (2003).
12. K. Marushkevich, L. Khriachtchev, J. Lundell, A. V. Domanskaya, M. Räsänen, J. Mol. Spectrosc. **259**, 105 (2009).
13. E. M. S. Maçôas, L. Khriachtchev, M. Pettersson, R. Fausto, M. Räsänen, J. Am. Chem. Soc. **125**, 16188 (2003).
14. E. M. S. Maçôas, L. Khriachtchev, R. Fausto, M. Räsänen, J. Phys. Chem. A **108**, 3380 (2004).
15. L. Khriachtchev, J. Mol. Struct. **880**, 14 (2008).
16. M. Pettersson, E. M. S. Maçôas, L. Khriachtchev, J. Lundell, R. Fausto, M. Räsänen, J. Chem. Phys. **117**, 9095 (2002).
17. E. M. S. Maçôas, L. Khriachtchev, M. Pettersson, R. Fausto, M. Räsänen, Phys. Chem. Chem. Phys. **7**, 743 (2005).
18. E. M. S. Maçôas, L. Khriachtchev, M. Pettersson, R. Fausto, M. Räsänen, J. Chem. Phys. **121**, 1331 (2004).

19. A. Domanskaya, K. Marushkevich, L. Khriachtchev, M. Räsänen, J. Chem. Phys. **130**, 154509 (2009).
20. M. Gadermann, D. Vollmar, R. Signorell, Phys. Chem. Chem. Phys. **9**, 4535 (2007).
21. P. Teragni, G. Masetti, G. Zerbi, Chem. Phys. **28**, 55 (1978).
22. K. Marushkevich, L. Khriachtchev, M. Räsänen, J. Chem. Phys. **126**, 241102 (2007).
23. T. P. Snow, Nature **429**, 615 (2004).
24. GAMESS, version R1 (24-Mar-2007), M. Schmidt, K. Baldridge, J. Boatz, S. Elbert, M. Gordon, J. Jensen, S. Koseki, N. Matsunaga, K. Nguyen, S. Su, T. Windus, M. Dupuis, J. Montgomery, J. Comput. Chem. **14**, 1347 (1993).
25. C. Moller, M. S. Plesset, Phys. Rev. **46**, 618 (1934).
26. A. D. McLean, G. S. Chandler, J. Chem. Phys. **72**, 5639 (1980).
27. M. J. Frisch, J. A. Pople, J. S. Binkley, J. Chem. Phys. **80**, 3265 (1984).
28. J. Lundell, M. Räsänen, Z. Latajka, Chem. Phys. **189**, 245 (1994).
29. J. Lundell, Chem. Phys. Lett. **266**, 1 (1997).
30. See Supplementary Material at http://dx.doi.org/10.1063/1.3484943 for Figures S1-S4, showing the calculated structures of the N_2 complexes of *cis* and *trans* FA and AA and for Table S-I, showing the calculated νOH, νC=O and τCOH frequencies and IR intensities for monomeric *cis* and *trans* forms of FA and AA and their complexes with N_2.
31. R. Fausto, L. A. E. Batista de Carvalho, J. J. C. Teixeira-Dias, M. N. Ramos, J. Chem. Soc. Faraday Trans. II **85**, 1945 (1989).
32. M. Rozenberg, G. Shoham, I.D. Reva, R. Fausto, Phys. Chem. Chem. Phys. 7, 2376 (2005).
33. M. Rozenberg, G. Shoham, I. D. Reva, R. Fausto, Spectrochim. Acta A **60**, 463 (2004).
34. R. Fausto, J. Mol. Struct. (Theochem.) **315**, 123 (1994).
35. P. K. Wawrzyniak, J. Panek, J. Lundell, Z. Latajka, J. Mol. Model. **11**, 351 (2005).
36. P. K. Wawrzyniak, J. Panek, Z. Latajka, J. Lundell, J. Mol. Struct. **704**, 297 (2004).
37. K. Marushkevich, M. Räsänen, and L. Khriachtchev, J. Phys. Chem. A **114**, 10584 (2010)

Acetic Acid Dimers in a Solid Nitrogen Matrix

Susy Lopes,[1] Alexandra V. Domanskaya,[2] Markku Räsänen,[2]

Leonid Khriachtchev[2] and Rui Fausto[1]

[1]*Department of Chemistry, University of Coimbra, Rua Larga, P-3004-535 Coimbra, Portugal*

[2]*Department of Chemistry, University of Helsinki, P.O. Box 55, FIN-00014 Helsinki, Finland*

ABSTRACT

Acetic acid (CH_3COOH; AA) dimers were studied in a nitrogen matrix. The infrared spectra of three *trans-trans* and two *trans-cis* acetic acid dimers are reported and analyzed. Among these, one *trans-trans* and both *trans-cis* forms have been observed for the first time. One of the *trans-cis* AA dimers (D2'_TC), bearing an eight-membered ring with one C-H$^{\cdots}$O= and one OH$^{\cdots}$O= intermolecular H-bond, was produced by selective vibrational excitation (at 6896 cm^{-1}) of the structurally related *trans-trans* dimer. The second one (D2_TC), with a single OH$^{\cdots}$O= intermolecular hydrogen bond and the two monomeric units in a nearly perpendicular position, was obtained by thermal mobilization of a mixture of *trans* and *cis* monomers of AA, the latter being produced from the first by excitation of the νOH +δCOH combination mode at 4724.5 cm^{-1}. Interpretation of the experimental data was helped by an extensive theoretical study of the various possible structures of acetic acid dimers (*trans-trans* and *trans-cis*), carried out at the MP2/6-311++G(2d,2p) level of approximation. The tunneling decay rate at 8.5 K of the D2'_TC *trans-cis* dimer was estimated as ~7.5 h.

1. Introduction

Hydrogen bonds are among the most well-known intermolecular interactions, which are of essential importance in many fields of chemistry and molecular biology.[1,2] Nowadays, the term "hydrogen bonding" portrays a much vaster significance due to the ubiquitous occurrence of hydrogen bonds in nature, as it includes interactions in the gas, liquid and solid states. Understanding the nature of this interaction is fundamental in determining molecular conformation and crystal packing,[3] in molecular recognition[4] and self-assembly of nanomaterials,[5] and in the activity of biological molecules.[6] Therefore, the properties of hydrogen bonding interaction have been studied both theoretically and experimentally.[7-9] For instance, hydrogen bonds such as N-H···O play a crucial role in the structure and properties of double hydrogen bonded systems such as proteins or nucleic acid base pairs.[10-12]

Dimers of carboxylic acids such as formic (HCOOH, FA) or acetic (CH_3COOH, AA) acids represent interesting model systems where C-H···O and O-H···O hydrogen bonds are present in cyclic and open dimers. In particular, in cyclic centrosymmetric dimers of carboxylic acids the two intermolecular O-H···O=C hydrogen bonds are coupled and strengthened.[13-15] In the gas phase, acetic acid exists in a mixture of two species, monomeric acetic acid and the cyclic dimer (with C_{2h} symmetry) as determined by electron diffraction[16] and other methods,[17-19] while X-ray diffraction studies indicate that in the crystalline state acetic acid crystallizes in long polymer chains that involve C-H···O=C as well O-H···O=C hydrogen bonds.[20] The structure of acetic acid in the liquid phase still seems to be a controversial issue, some studies suggesting that besides the presence of the cyclic dimer, linear chains are also present.[21,22] However, Monte Carlo simulations have suggested that liquid acetic acid consists mainly of hydrogen-bonded chains, not the cyclic dimer.[23] The nature of hydrogen bonding between acetic acid and water and in different environments as well as complexes formed between acetic acid and other polar molecules have also been the subject to many theoretical and experimental studies.[24-28]

Acetic acid has only two conformers (*trans* and *cis*) which can interconvert in one another through internal rotation around the C–O bond (Scheme 1). The *cis* form is higher in energy than the *trans* form by *ca.* 1880 cm^{-1} (theoretical value) and the *trans*-to-*cis* conversion barrier was predicted to be *ca.* 49 kJ mol^{-1} (4400 cm^{-1}).[29]

The infrared spectra of matrix-isolated monomeric forms of acetic acid (*trans*-AA and *cis*-AA) have been reported previously in different cryogenic matrices.[30-33] The higher energy conformer, *cis*-AA, was obtained by selective vibrational excitation of the lower energy *trans* form using narrowband tunable infrared radiation. The *cis* form subsequently converts to the lower energy conformer via dissipative proton tunneling through the torsional barrier, which limits their lifetime. The tunneling process is a strongly anharmonic motion. The *cis* to *trans* decay rate depends on the noble gas being used, isotopic substitution and working temperature.[31] In addition to AA, the higher energy *cis* forms of formic, propionic and other carboxylic acids derivatives have also been investigated in noble gas matrices.[34-38]

Previous theoretical studies of AA dimers carried out using semi-empirical and *ab initio* quantum chemical calculations undertaken at different levels of theory (from Hartree-Fock to MP2) and different basis sets have focused mainly on the most stable cyclic dimer, however, higher energy dimers have been considered.[15,22,24-26,39-44] Xu and Yang[41] reported eight *trans-trans* acetic acid dimers optimized by the PM6 method, while in an earlier publication by Chocholousová *et al.*[24] only six minima were calculated at the DFT and MP2 levels. Furthermore, the possibility of a linear open dimer formed by keeping one AA monomer in *trans* orientation and another monomer positioned in *cis*, with one O-H···O=C hydrogen bond has also been addressed.[15]

The matrix isolation infrared spectra of the two most stable dimeric forms of acetic acid, the centrosymmetric cyclic dimer (C_{2h} symmetry) and the C_s symmetry dimer bearing one O-H···O=C and one C-H···O=C intermolecular bonds were first assigned by Grenie *et al.*[45] in an argon matrix, following the work by Redington and Lin,[46] which reported only the cyclic dimer. The gas phase infrared spectrum of the AA cyclic dimer provided a useful basis in the assignment of the matrix-isolated cyclic dimer.[17-19] In a more recent work,[42] the presence of the two previously[45] identified AA *trans-trans* dimers was confirmed, and a much more complete assignment of the main vibrations was produced for these species in an argon matrix. Interestingly, these two dimeric forms of acetic acid were also detected in interstellar ice analogs,[47] upon irradiation of binary mixtures of methane (CH_4) and carbon dioxide (CO_2). Using matrix isolation together with supersonic jet expansion, and replacing one acetic acid unit by its methyl ester, Emmeluth and Suhm[44] suggested the

possibility of observation of three *trans-trans* dimers. The additional dimer would be formed by one O-H···O-H and one O-H···O=C intermolecular bonds.

The Raman spectra of monomeric acetic acid and of their most stable dimers isolated in solid argon have also been studied by Olbert-Majkut *et al.*[44] Besides the most stable cyclic dimer, two less stable dimers were also identified. One of these latter is characterized by O-H···O and C-H···O intermolecular interactions, while the other has an O-H···O-H intermolecular hydrogen bond.

In contrast to formic acid,[36,48,49] where *trans-trans* and *trans-cis* dimers could be experimentally identified in noble gas matrices, the number of the hitherto observed dimers of acetic acid is, as described above, still very reduced. In particular, no *trans-cis* acetic acid dimers have been observed hitherto.

In the present work, an extensive theoretical study of the various possible structures of acetic acid dimers (*trans-trans* and *trans-cis*) was carried out using quantum chemical calculations (at the MP2 level). These data were used to help interpretation of the experimental results obtained for the compound in nitrogen matrix. We report the first assignment of 3 *trans-trans* and 2 *trans-cis* acetic acid dimers in this matrix media. Among these, one *trans-trans* and both *trans-cis* forms have been observed for the first time. The tunneling decay rate of one of the observed *trans-cis* dimer into its *trans-trans* counterpart was also estimated.

trans *cis*

Scheme 1 – *Trans* (most stable) and *cis* (higher energy) conformers of acetic acid.

2. Computational details and results

The quantum chemical calculations were performed using Gamess, version R2 (24-Mar-2010)[50] at the MP2 level of theory[51] using the 6-311++G(2d,2p) basis set.[52,53]

This basis set has been shown to reproduce the experimental structural and vibrational properties of FA with an acceptable accuracy.[54-56] The optimization criteria parameter OPTTOL was set to 0.0001 hartree/bohr. This parameter corresponds to the maximum value allowed to the energy gradient and also controls the maximum allowed value of the root mean square gradient, which is given by 1/3 of OPTTOL. The optimized structures of all reported *trans-trans* and *trans-cis* dimers were confirmed to correspond to true energy minima by inspection of the corresponding Hessian matrix. The calculated structures were not constrained to planarity. The vibrational spectra were computed at the same level of theory. The calculated MP2/6-311++G(2d,2p) vibrational frequencies and intensities of the fundamental modes for the *trans-trans* and *trans-cis* forms of CH_3COOH are listed in the Supplementary Material (Tables S1-S2).

Figures 1 and 2 shows the optimized structures for the *trans-trans* and *trans-cis* dimers of acetic acid. The basis set superposition error (BSSE) was calculated as described by the counterpoise method proposed by Boys and Bernardi.[57] The computed interaction energies for each dimer and calculated hydrogen bond and angle lengths are listed in Tables 1-3.

Trans-trans **dimers**

Besides the well-known centrosymmetric cyclic (C_{2h}) dimer with two strong O-H···O= hydrogen bonds, which corresponds to the global minimum, the potential energy surface of acetic acid dimer shows that other open or cyclic dimers of the compound with higher energies can be formed with either a strong O-H···O= or weaker C-H···O= and O-H···O-H hydrogen bonds. AA *trans-trans* dimers can then be classified in four families (Figure 1): ***a)*** centrosymmetric cyclic dimer, with two OH···O= hydrogen bonds; ***b)*** dimers bearing one strong OH···O= hydrogen bond; ***c)*** dimer without any OH···O= bond, but possessing one OH···OH bond; ***d)*** dimers without any OH···O= or OH···OH bonds. On the whole, 9 different AA *trans-trans* dimers were predicted to exist.

Group *a)*

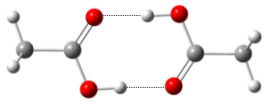

D1_TT (C_{2h})

Group *b)*

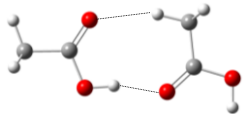

D2_TT (C_s)

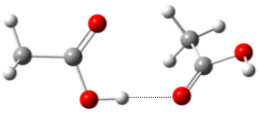

D2'_TT (C_1)

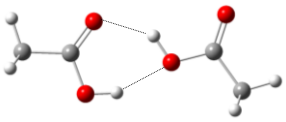

D2''_TT (C_s)

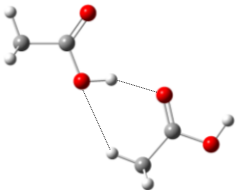

D2'''_TT (C_s)

Group *c)*

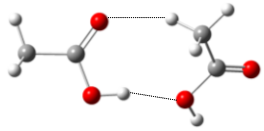

D3_TT (C_1)

Group *d)*

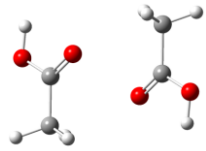

D4_TT (C_i)

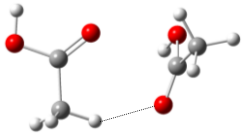

D4'_TT (C_1)

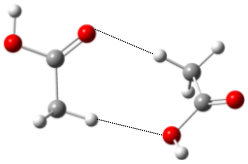

D4''_TT (C_1)

Figure 1. Calculated structures for AA dimers (*trans-trans*), and their classification in groups: ***a)*** cyclic centrosymmetric dimer, with two OH···O= hydrogen bonds; ***b)*** dimers bearing one OH···O= hydrogen bond; ***c)*** dimer without any OH···O= bond, but possessing one OH···OH bond; ***d)*** dimers without any OH···O= or OH···OH bonds.

The most stable cyclic dimer (D1_TT, in Figure 1) has a centrosymmetric eight-membered ring structure with two symmetrical O-H···O= bonds (1.677 Å long). This is the predominant dimer in the gas phase,[16-19] with a calculated interaction energy of –60.2 kJ mol^{-1} (Table 1). Members of family ***b)*** have a single OH···O= bond

and can be converted to each other essentially by rotation about this hydrogen bond. Their close energies and structural similarity point to low energy barriers separating these forms from each other. Dimer D2_TT is the most stable member of this family, with an interaction energy of −33.0 kJ mol^{-1}. In this dimer, which belong to the C_s symmetry point group, besides the strong O-H···O= hydrogen bond (1.796 Å), one weak C-H···O= hydrogen bond exists (2.295 Å). By moving one monomer unit to a nearly perpendicular orientation in relation to the other, the two equivalent-by-symmetry D2'_TT forms (C_1 point group) can be obtained from dimer D2_TT, with an interaction energy of −32.5 kJ mol^{-1}. Dimers D2''_TT and D2'''_TT (both having a planar heavy atom skeleton) possess, in addition to the strong O-H···O= hydrogen bond weaker O-H···O-H (1.940 Å) or C-H···O-H (2.587 Å) hydrogen bonds, respectively. These dimers have calculated interaction energies of −29.2 and −24.5 kJ mol^{-1}. Dimer D3_TT (with C_1 symmetry; interaction energy: −23.7 kJ mol^{-1}) is the only form belonging to group ***c)***. It exhibits a hydrogen bond between the two hydroxyl groups (1.893 Å) and an additional one between the methyl group and the carbonyl group (2.347 Å). Three dimers were found that belong to group ***d)***. Dimer D4_TT (with C_i symmetry), being the most stable form within this group (interaction energy: −16.6 kJ mol^{-1}), shows a stacked structure where dispersion forces are the main stabilizing factor. Dimer D4'_TT (C_1 symmetry) contains a weak C-H···O hydrogen bond (2.375 Å) between the two monomers, and the two units are located nearly perpendicularly to each other (interaction energy: −16.6 kJ mol^{-1}). The third dimer belonging to group ***d)*** (D4''_TT) has one C-H···O=C (2.350 Å) and one C-H···O-H (2.492 Å) bond and has an interaction energy of −11.3 kJ mol^{-1}. On the other hand, the calculations showed that *trans-trans* dimeric structures having all heavy atoms in a single plane and exhibiting only C-H···O or/and dispersion interactions are not minima.

The six AA *trans-trans* dimers previously predicted (at the DFT and MP2 levels) by Chocholousová *et al.*[24] and by Xu and Yang[41] (PM6) correspond to dimers D1_TT, D2_TT, D2''_TT, D2'''_TT, D3_TT and D4_TT calculated in present study, while those reported by Olbert-Majkut *et al.*[44] [B3LYP/6-311++G(2d,2p) calculations] have correspondence in D1_TT, D2_TT, D2''_TT, D3_TT and a dimer closely related to D4_TT but exhibiting a planar heavy atom skeleton. Two of the structures obtained by the PM6 method by Xu and Yang[41] (C and D, of C_{2h} and C_i symmetry, with two

C-H···O-H hydrogen bonds and two O-H···O-H interactions, respectively) were found not to correspond to minima at the MP2 level.

Table 1 – Interaction energies (IE/ kJ mol^{-1}) including zero-point energy and basis set superposition error corrections for *trans-trans* dimers, obtained in the present study, and previously reported interaction energy values

Dimer *trans-trans*[a]	IE			
	This study	Ref. 24[b]	Ref.41[c]	Ref.44[d]
D1_TT	–60.2	–66.3	–43.2	–59.2
D2_TT	–33.0	–36.6	–32.5	–29.0
D2'_TT	–32.5	-	-	-
D2''_TT	–29.2	–32.2	–28.7	–23.8
D2'''_TT	–24.5	–26.0	–20.8	-
D3_TT	–23.7	–21.7	–25.3	–16.5
D4_TT	–16.6	–17.2	–24.4	–8.6
D4'_TT	–15.8	-	-	-
D4''_TT	–11.3	-	-	-

[a] See Figure1 for structures of the dimers.
[b] BSSE corrected RI MP2/augTZVPP calculations.
[c] PM6 calculations.
[d] BSSE and zero point energy corrected B3LYP/6-311++G(2d,2p) calculations.

Trans-cis dimers

Twelve different AA *trans-cis* dimers were predicted by the MP2/6-311++G(2d,2p) calculations in the present study (Figure 2). Like in the case of the *trans-trans* dimers, one can classify the *trans-cis* dimers in four main families: ***a)*** dimers with one O-H···O= and one O-H…O-H hydrogen bond; ***b)*** dimers bearing a single O-H···O= bond; ***c)*** dimer without any O-H···O= bond, but possessing one O-H···O-H bond; ***d)*** dimers without any O-H···O= or O-H···O-H bonds.

Group *a)*

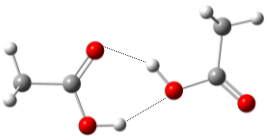

D1_TC (C_s)

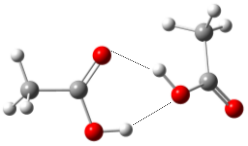

D1'_TC (C_1)

Group *b)*

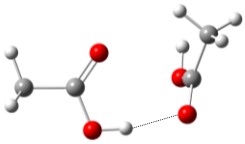

D2_TC (C_1)

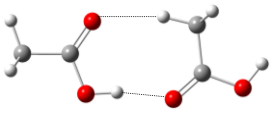

D2'_TC (C_s)

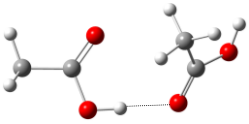

D2''_TC (C_1)

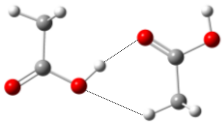

D2'''_TC (C_s)

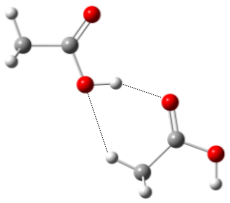

D2''''_TC (C_s)

Group *c)*

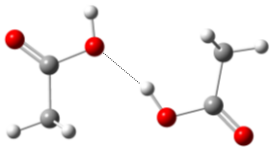

D3_TC (C_1)

Group *d)*

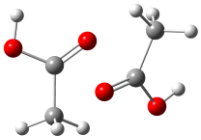

D4_TC (C_1)

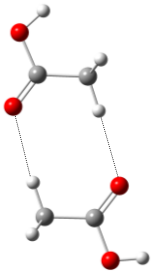

D4'_TC (C_s)

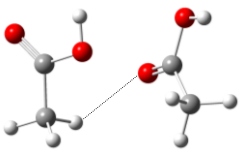

D4''_TC (C_1)

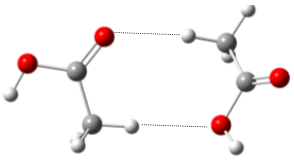

D4'''_TC (C_1)

Figure 2. Calculated structures for AA dimers (*trans-cis*), and their classification in groups: ***a)*** dimers with one OH···O= and one OH···OH hydrogen bond; ***b)*** dimers bearing a single OH···O= hydrogen bond; ***c)*** dimer without any OH···O= bond, but possessing one OH···OH bond; ***d)*** dimers without any OH···O= or OH···OH bonds.

The most stable *trans-cis* dimers belong to type ***a)***, having simultaneously one O-H···O= and one O-H···O-H hydrogen bond, forming a six-membered ring. Dimer D1_TC (with C_s symmetry) is the most stable form (interaction energy: –40.4 kJ mol^{-1}). In this form, the O-H···O= and O-H···O-H hydrogen bonds are predicted to be 1.807 and 1.930 Å long, respectively. Dimer D1'_TC is structurally similar to D1_TC, but has the monomeric units in a nearly perpendicular orientation; it has also similar interaction energy (–40.2 kJ mol^{-1}) and hydrogen bond lengths (1.813 and 1.930 Å) to those of D1_TT. With the exception of D2'''_TC, all members of family ***b)*** have the *trans* monomeric unit as donor in the O-H···O= bond. These forms can be converted to each other essentially by rotation about this hydrogen bond. In turn, the OH group of the *cis* unit does not take part in any hydrogen bond. On the other hand, dimer D2'''_TC has the *cis* unit involved as donor in the O-H···O= bond and the OH group of the *trans* unit free. The interaction energies of group ***b)*** dimers are the second largest ones, ranging from –24.6 to –35.9 kJ mol^{-1} (see Table 2). Weak C-H···O= or C-H···O-H interactions can be devised to take place in type ***b)*** dimers (see Figure 2 and Table 3) which shall also partially account to determine their relative energies.

Table 2 – Interaction energies (IE/ kJ mol^{-1}) including zero-point energy and basis set superposition error corrections for *trans-cis* dimers.

Dimer *trans-cis*	IE
D1_TC	–40.4
D1'_TC	–40.2
D2_TC	–35.9
D2'_TC	–35.6
D2''_TC	–34.7
D2'''_TC	–34.7
D2''''_TC	–24.6
D3_TC	–22.5
D4_TC	–23.7
D4'_TC	–16.0
D4''_TC	–15.4
D4'''_TC	–12.2

[a] See Figure 2 for structures of the dimers.

Dimer D3_TC is the only member of family ***c)***, with the *cis* unit acting as donor in its O-H···O-H hydrogen bond. The calculated interaction energy of this dimer is –22.5 kJ mol^{-1}. In members of family ***d)***, the dominant interactions are of dispersive type and weak C-H···O hydrogen bond like interactions. In none of these dimers the OH groups are involved in H-bonds as donors, and only in D4'''_TC one of the OH groups acts as H-bond acceptor. Furthermore, with exception of D4'_TC, all ***d)*** type acetic acid *trans-cis* dimers have the heavy atom skeleton of the two monomeric units in different planes. Their calculated interaction energies range from –12.2 to –23.7 kJ mol^{-1}.

Table 3 – Calculated hydrogen bond lengths (Å) and angles (degrees) of the *trans-trans* and *trans-cis* acetic acid dimers.

Dimer[a]		Bond length		Bond angle	
		O–H···O	C–H···O	O–H···O	C–H···O
D1_TT		1.677	–	178.5	–
D2_TT		1.796	2.295	169.8	161.8
D2'_TT		1.776	–	176.8	–
D2''_TT	(O=)	1.918	–	137.7	–
	(OH)	1.940	–	153.1	–
D2'''_TT		1.831	2.587	161.0	134.2
D3_TT		1.893	2.347	171.1	153.2
D4_TT		–	–	–	–
D4'_TT		–	2.375	–	146.5
D4''_TT	(=O)	–	2.350	–	169.6
	(OH	–	2.492	–	168.0
D1_TC	(O=)	1.807	–	145.0	–
	(OH)	1.930	–	149.8	–
D1'_TC	(O=)	1.813	–	146.6	–
	(OH)	1.930	–	150.7	–
D2_TC		1.845	–	169.5	–
D2'_TC		1.785	2.245	170.7	163.0
D2''_TC		1.777	–	174.7	–
D2'''_TC		1.795	2.555	168.9	133.9
D2''''_TC		1.842	2.492	158.0	135.9
D3_TC		1.900	–	162.5	–
D4_TC		–	–	–	–
D4'_TC	[b]	–	2.326	–	177.7
	[c]	–	2.349	–	176.1
D4''_TC		–	2.484	–	134.9
D4'''_TC	(O=)	–	2.334	–	169.0
	(OH)	–	2.458	–	170.8

[a] See Figures 1 and 2 for structures of dimers.
[b] Acceptor atom: carbonyl oxygen of the *trans* unit.
[c] Acceptor atom: carbonyl oxygen of the *cis* unit.

3. Experimental details and results

Gaseous mixtures of acetic acid (KEBO LAB, 99%) with nitrogen (AGA/Linde 6.0) were prepared with a typical ratio of 1:1500. The acid was purified by a few freezing-pumping cycles. Nitrogen was used as supplied. The mixtures were deposited onto a cooled CsI window at 8.5 K in a close–cycle helium cryostat (APD, DE 202A). The spectra were recorded with a Nicolet 60SX FTIR instrument, by co–adding 200 interferograms with 1 cm^{-1} spectral resolution.

The *trans*–to–*cis* conversion was promoted by selective vibrational excitation by using an optical parametric oscillator with infrared extension (Sunlite Continuum, FWHM ~0.1 cm^{-1}). The *trans-cis* acetic acid dimer D2'_TC was produced by excitation of the 1st overtone of the νOH free OH group of the *trans-trans* dimer D2_TT at 6896 cm^{-1}. D2_TC was produced by thermal mobilization of a mixture of *trans* and *cis* monomers of AA, the latter being produced from the first by excitation of the νOH +δCOH combination mode at 4724.5 cm^{-1}.

In the kinetic measurements, the *trans-cis* dimer (D2'_TC) decay was monitored by measuring the intensity of the COH-CO def fundamental band at 1306.8 cm^{-1} as a function of time. A long–pass optical filter (> 1500 cm^{-1}) was inserted between the sample and the Globar source in order to suppress high-frequency light components which could accelerate the *cis*–to–*trans* conversion process. The Globar light was blocked between the measurements.

Trans-trans dimers present in the as-deposited matrices and after annealing of the matrices to 28 K (D1_TT and D2_TT): spectral assignments

Figure 3 shows a selected region (2000-1550 cm^{-1}) of the spectra of two samples of acetic acid in N_2 matrix with two different concentrations. Spectrum *a)* corresponds to a highly diluted matrix (<1:2000) and shows essentially bands due to the *trans*-AA monomer,[33] while spectrum *b)* is of a more concentrated sample, where bands due to a minor amount of dimers could be easily identified. Comparison of the experimental spectra with those calculated for the different dimers obtained from the MP2/6-311++G(2d,2p) calculations indicates that the dominant dimers in the matrix are D1_TT and D2_TT (see Figure 1), *i.e.*, the two most stable AA *trans-trans* dimers. The characteristic bands that can be used as fingerprint of these two dimers (in the

shown spectral region) are marked in the Figure. The infrared active C=O stretching mode of D1_TT is predicted by the calculations to be shifted in relation to the monomer by –40 cm^{-1}, and is observed at 1720.9 cm^{-1} in N_2 matrix, *i.e.*, red-shifted in relation to the average position of the absorptions due to *trans*-AA monomer in the two main matrix sites[33] by *ca.* –55 cm^{-1}. On the other hand, the two νC=O bands of D2_TT were observed at 1762.6 and 1733.4 cm^{-1}, shifted by *ca.* –14 and –43 cm^{-1} relatively to the average position of the bands of the monomer. The predicted shifts for these vibrations are –17 and –38 cm^{-1}, respectively.

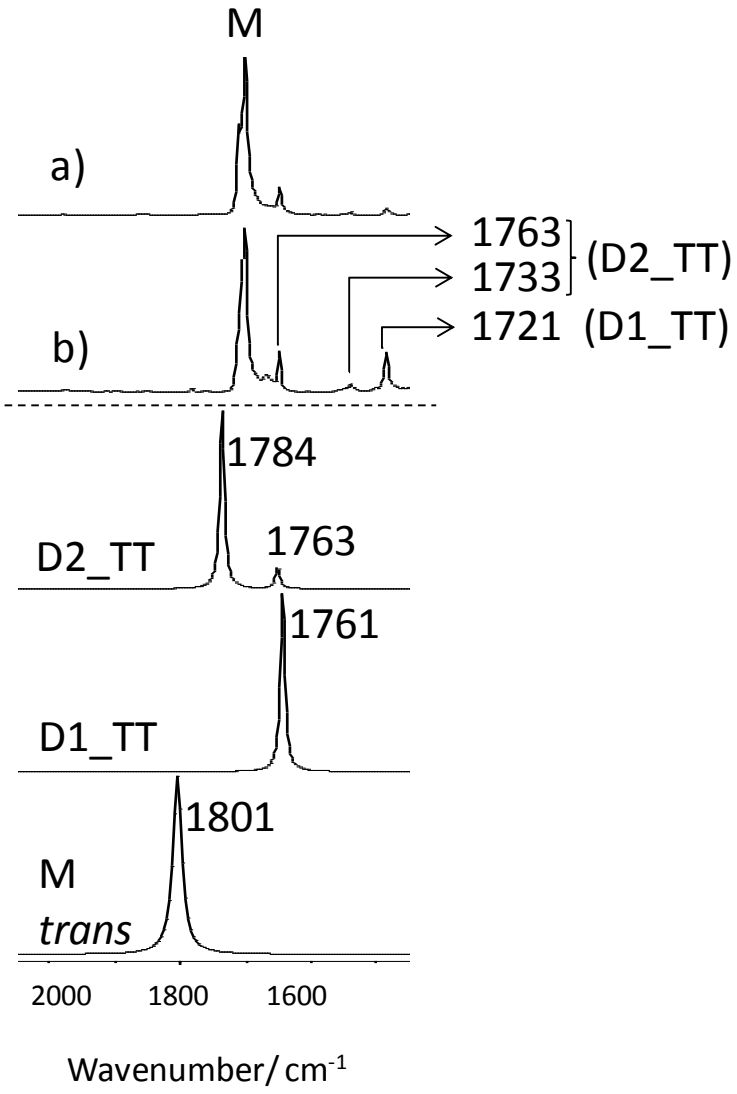

Figure 3. 2000-1550 cm^{-1} spectral range of AA in N_2 matrix (as-deposited; two different experiments: a) M:S ratio <1:2000; b) M:S ratio ~1:1500) and MP2/6-311++G(2d,2p) calculated spectra for *trans* monomer (M), D1_TT and D2_TT in the same spectral region. The dotted line separates the experimental from the calculated spectra.

The spectrum of the most stable dimer (D1_TT) is much simplified because of the C_{2h} symmetry of this dimer, which reduces the number of IR active vibrational modes to half. On the other hand, dimer D2_TT is of C_s symmetry, so that all modes are expected to be IR active. The complete lists of assignments made for D1_TT and D2_TT in N_2 matrix are given in Table 4 and Table 5. A few illustrative examples are discussed below. These assignments took also into account the annealing and irradiation experiments described later in this paper and improve upon the assignments previously proposed by Sander and Gantenberg,[42] Redington and Lin[46] and Grenie *et al.*[45] (in argon matrix), and Emmeluth and Suhm[43] (in supersonic jet expansion).

Table 4. MP2/6-311++G(2d,2p) calculated infrared spectra for dimer D1_TT (C_{2h}), wavenumber shifts in relation to the monomer and observed wavenumbers and shifts in N_2 matrix. [a]

Calculated			N_2 matrix			
ν	I^{IR}	Δν	ν	Δν[b]	Assignment[c]	Symmetry
3303.4	2979.0	−483.9			νO-H	B_u
3228.2	12.8	−0.5			νHCH_2 s	B_u
3187.1	2.9	−0.7			νHCH_2 a	A_u
3107.0	1.9	−0.6			νCH_3	B_u
1760.9	716.0	−40.1	1720.9	−55.4	νC=O	B_u
1504.8	17.0	−0.6	1434.0	−9.2	δHCH_2 a	A_u
1499.7	59.5	−0.6	1434.0	−1.7	δHCH_2 s	B_u
1479.0	123.4	+270.9	1422.2	+231.3	COH-CO def	B_u
1416.0	43.8	−16.7	1362.4	−24.2	δCH_3	B_u
1336.2	392.2	−14.1	1303.8	+25.6	CO-COH def	B_u
1087.6	6.5	+4.9	1052.3	+4.2	γCH_3 a	A_u
1042.3	41.1	+32.9	1018.6	+27.7	γCH_3 s	B_u
1033.4	169.7	+372.4	972.2	+312.5	τC-O	A_u
			967.2	+307.5		
909.9	7.2	+42.1			νC-C	B_u
635.3	44.0	+50.7	632.8	+45.8	δOCO	B_u
604.2	0.5	+53.5			γC=O	A_u
483.6	45.9	+58.2	484.6	+54.4	δCC=O	B_u

[a] Wavenumbers (ν) and shifts in wavenumbers (Δν) relatively to the monomer in cm^{-1}; Infrared intensities (I^{IR}) in km mol^{-1}. [b] Average wavenumber shifts in relation to the position of the observed bands of the *trans*-AA monomer[33] in the two matrix sites. [c] ν, stretching; δ, bending; γ, rocking; τ, torsion; a, antisymmetric; s, symmetric.

Table 5. MP2/6-311++G(2d,2p) calculated infrared spectra for dimer D2_TT (C_s), wavenumber shifts in relation to the monomer and observed wavenumbers and shifts in N_2 matrix. [a]

Calculated			N_2 matrix			
ν	I^{IR}	Δν	ν	Δν[b]	Assignment[c]	Symmetry
3780.0	83.7	–7.3	3532.5	–15.5	νO-H (2)	A´
3515.7	1016.7	–271.6			νO-H (1)	A´
3224.7	5.6	–4.0			νHCH_2 s (1)	A´
3223.6	15.0	–5.1			νHCH_2 s (2)	A´
3185.1	2.9	–2.7			νHCH_2 a (1)	A´´
3183.4	1.1	–4.4			νHCH_2 a (2)	A´´
3105.2	2.1	–2.4			νCH_3 (1)	A´
3100.9	13.3	–6.7			νCH_3 (2)	A´
1784.0	620.0	–17.0	1762.6	–13.8	νC=O a	A´
1762.8	76.2	–38.2	1733.4	–42.9	νC=O s	A´
1518.4	7.9	+13.0	1442.8	–0.45	δHCH_2 a (2)	A´´
1505.4	7.7	0.0			δHCH_2 a (1)	A´´
1500.8	27.7	+0.5			δHCH_2 s (1)	A´
1499.4	0.5	–0.9			δHCH_2 s (2)	A´
1448.8	38.7	+16.1	1400.2	+13.5	δCH_3 (1)	A´
1442.7	63.2	–10.0	1392.4	+5.7	δCH_3 (2)	A´
1398.7	16.6	+190.6	1342.7	+151.7	COH-CO def (1)	A´
1368.3	92.2	+160.2	1318.0	+127.0	COH-CO def (2)	A´
1271.0	268.2	–79.3	1246.0	–32.2	CO-COH def (1)	A´
			1243.6	–34.6		
1227.5	219.4	–122.8	1202.7	–75.5	CO-COH def (2)	A´
1093.7	5.9	+11.0	1056.3	+8.2	γCH_3 a (2)	A´´
1083.1	4.4	+0.4	1049.0	+0.9	γCH_3 a (1)	A´´
1029.9	53.5	+20.5	1014.6	+23.7	γCH_3 s (2)	A´
			1012.6	+21.7		
1028.1	69.4	+18.7	1003.2	+12.3	γCH_3 s (1)	A´
903.7	85.0	+242.7	860.3	+200.6	τC-O (1)	A´´
890.6	4.2	+22.8	855.5	–0.8	νC-C (1)	A´
882.2	6.3	+14.4	843.7	–12.6	νC-C (2)	A´
			836.6(?)	–19.7		
673.8	92.9	+12.8	676.8	+17.1	τC-O (2)	A´´
609.9	32.7	+25.3	606.4	+19.4	δOCO (1)	A´
600.5	38.8	+53.9	604.4	+17.4	δOCO (2)	A´
599.4	0.5	+48.7			γC=O (1)	A´´
558.7	26.5	+8.0	550.9	–0.6	γC=O (2)	A´´
447.9	16.5	+22.5	440.5(?)	+10.3	δCC=O (1)	A´
434.1	3.1	+8.7			δCC=O (2)	A´

[a] Wavenumbers (ν) and shifts in wavenumbers (Δν) relatively to the monomer in cm^{-1}; Infrared intensities (I^{IR}) in km mol^{-1}. [b] Average wavenumber shifts in relation to the position of the observed bands of the *trans*-AA monomer[33] in the two matrix sites. [c] ν, stretching; δ, bending; γ, rocking; τ, torsion; a, antisymmetric; s, symmetric; (1), molecule 1 in the dimer (OH···O bond donor molecule); (2), molecule 2 in the dimer (CH···O bond donor molecule).

The calculations predict a very large red-shift (−484 cm^{-1}) for the IR active OH stretching vibration of D1_TT in relation to the monomer. This band is predicted to be very intense (2979 km mol^{-1}) and could be anticipated to be very broad. Indeed, experiment demonstrates that it extends for a so wide range of frequencies that it is not possible to distinguish it from the spectral baseline. The same happens to the OH stretching band of the H-bonded OH group in D2_TT, which is predicted to be shifted by –272 cm^{-1} in relation to the monomer. On the other hand, the νOH vibration of the unbounded OH group of D2_TT is predicted by the calculations to be shifted by –7 cm^{-1} in relation to the monomer, and could be easily assigned to the experimental band at 3532.5 cm^{-1} (average shift: –15 cm^{-1}).

The frequencies of the COH-CO def modes undergo significant blue-shifts in the dimers: +271 cm^{-1} for D1_TT, and +191 and +160 cm^{-1} for D2_TT. The band observed at 1422.2 cm^{-1} and the two bands at 1342.7 and 1318.0 cm^{-1} were then ascribed to the COH-CO def modes in D1_TT and D2_TT, respectively, with average shifts of +231, +152 and +127 cm^{-1}, in good consonance with the theoretical predictions.

In the case of the CO-COH def modes, the calculations predict red-shifted frequencies for the dimers (–14 cm^{-1} for D1_TT, and –79 and –123 cm^{-1} for D2_TT), the experimental bands being observed at 1303.8 cm^{-1} (D1_TT) and at 1246.0/1243.6 and 1202.7 cm^{-1} (D2_TT), *i.e.*, exhibiting shifts of +26, –33 and –75 cm^{-1}, respectively.

The pair of bands at 972.2/967.2 cm^{-1} can be assigned to the τC-O torsion of D1_TT which shows, as it could be anticipated, a large blue-shift in relation to the monomer (+310 cm^{-1}; predicted: +372 cm^{-1}). For D2_TT, the τC-O torsional vibrations are observed at 860.3 and 676.8 cm^{-1}, with blue-shifts of +201 and 17 cm^{-1}, which compare well with the theoretical predictions (+243 and +13 cm^{-1}, respectively).

Annealing of the matrices to 28 K (see Figure 4) after deposition led to an increase of the population of the two dimers, D1_TT and D2_TT, at expenses of the monomer. This means that annealing of the matrix to this temperature is enough to lead to the thermodynamically more stable dimers, overpassing any putative kinetically favored higher-energy dimer.

Production of the *trans-cis* dimer D2'_TC from selective vibrational excitation of D2_TT ($\tilde{\nu}$= 6896.0 cm^{-1}) and assignment of its IR spectrum

Irradiation of a matrix containing monomeric *trans*-AA as well as D1_TT and D2_TT dimers at $\tilde{\nu}$= 6896.0 cm^{-1} was found to lead to conversion of dimer D2_TT into the analogous *trans-cis* dimer (D2'_TC; see Figure 2), by rotation of the non-hydrogen bonded OH group of D2_TT. Irradiation was performed at the wavenumber corresponding to the 1st overtone of the O-H stretching mode of the "free" OH group of the D2_TT dimer, exciting selectively this species, while both the D1_TT dimer and the *trans*-AA monomer were stable upon irradiation at this wavenumber. This corresponds to the first experimental observation of a *trans-cis* dimer of acetic acid.

Figure 4 shows an illustrative region of the spectra obtained by subtracting the spectrum of a AA matrix annealed to 28 K to that of the same matrix after irradiation at $\tilde{\nu}$= 6896.0 cm^{-1} (30 min.). In the Figure, the calculated spectra for D2_TT and D2'_TC, as well as that of *trans*-AA monomer, are also shown for comparison. The bands ascribed to D2'_TC in this spectral region are due to its νC=O vibrations and appear at 1775.8 and 1742.2 cm^{-1}, shifted by –21 and +34 cm^{-1}, respectively, in relation to the corresponding bands in *cis*- and *trans*-AA monomers. The observed shifts agree very well with those predicted by the calculations (–21 and +35 cm^{-1}). Table 6 shows the proposed assignments for the D2'_TC dimer in N_2 matrix. The dimer is of C_s symmetry, so that all the modes are IR active. The bands originated in the OH stretching vibrations of the D2'_TC dimer are observed at 3598.2 cm^{-1} and 3174.0 cm^{-1} (for the *cis* and *trans* monomeric units). These bands show shifts of –12 and –374 cm^{-1}, respectively, in relation to the corresponding bands in the AA monomers, in good agreement with the theoretical predictions: –6 and –285 cm^{-1}. The bands observed at 1306.8 cm^{-1} (COH-CO def (*cis*)) and 1247.0 cm^{-1} (CO-COH def (*trans*)) have shifts of +11 and –29 cm^{-1}, which can be compared with the theoretically predicted shifts of +18 and –76 cm^{-1}. The COH-CO def (*trans*) and CO-COH def (*cis*) vibrations are predicted to have a low intensity and could not be observed experimentally. The τC-O torsion of the H-bonded *trans* unit in D2'_TC (observed at 862.4 cm^{-1}) is blue-shifted in relation to *trans*-AA by +267 cm^{-1} (calculated shift; +248 cm^{-1}), while in the *cis* unit the observed blue-shift amounts to +12 cm^{-1}, which can be compared with the theoretical predicted value of +34 cm^{-1}. Globally, the

predicted spectrum for this dimer shows a quite good agreement with the experimental bands formed upon irradiation at $\tilde{\nu}$= 6896.0 cm^{-1} at expenses of those belonging to D2_TT, thus making doubtless the identification of the *in situ* produced *trans-cis* dimer.

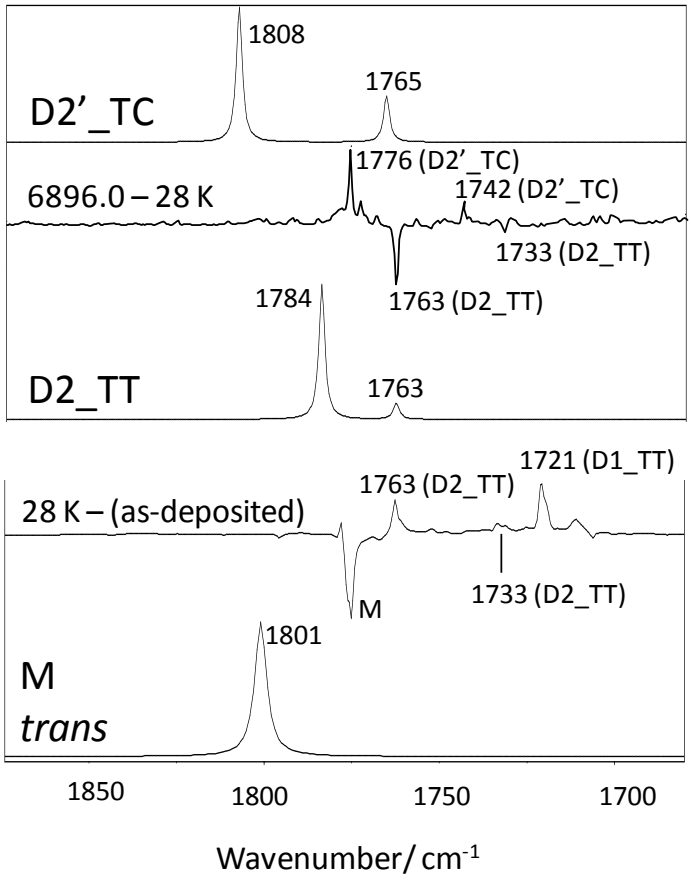

Figure 4. *Bottom to top:* calculated spectrum (1900-1675 cm^{-1} spectral range) of AA monomer (*trans* form; M), spectrum of the compound isolated in N_2 matrix and annealed to 28 K *minus* spectrum of the as-deposited matrix, calculated spectrum of D2_TT dimer, spectrum of the irradiated matrix at 6896.0 cm^{-1} *minus* spectrum of the matrix annealed to 28 K, and calculated spectrum of D2'_TC (*trans-cis* dimer).

Table.6. MP2/6-311++G(2d,2p) calculated infrared spectra for dimer D2'_TC (C_s), wavenumber shifts in relation to the monomer and observed wavenumbers and shifts in N_2 matrix. [a]

Calculated			N_2 matrix			
ν	I^{IR}	Δν	ν	Δν[b]	Assignment[c]	Symmetry
3846.9	77.2	−6.0	3598.2	−12.4	νO-H (c)	A´
3502.4	1055.8	−284.9	~3174.0	−374.0	νO-H (t)	A´
3224.8	5.1	−3.9			νHCH_2 s (t)	A´
3209.6	24.5	−12.0			νHCH_2 s (c)	A´
3185.1	2.8	−2.7			νHCH_2 a (t)	A´´
3165.3	2.7	−4.5			νHCH_2 a (c)	A´´
3105.2	2.1	−2.4			νCH_3 (t)	A´
3084.0	25.1	−7.7			νCH_3 (c)	A´
1807.6	471.7	−20.5	1775.8	−21.4	νC=O (c)	A´
1765.6	160.7	−35.4	1742.2	−34.1	νC=O (t)	A´
1527.1	6.9	+13.9			δHCH_2 a (c)	A´´
1505.3	7.7	−0.1			δHCH_2 a (t)	A´´
1500.9	20.6	0.6			δHCH_2 s (t)	A´
1499.4	1.1	−1.1			δHCH_2 s (c)	A´
1450.1	53.3	+17.4	1379.0	−7.6	δCH_3 (t)	A´
1432.0	36.9	+11.6	1350.3	−20.7	δCH_3 (c)	A´
1398.7	12.7	+190.6			COH-CO def (t)	A´
1324.4	506.2	+18.1	1306.8	+10.7	COH-CO def (c)	A´
1274.5	238.6	−75.8	1247.0	−28.9	CO-COH def (t)	A´
1239.8	2.8	+24.8			CO-COH def (c)	A´
1089.6	4.0	+12.8			γCH_3 a (c)	A´´
1083.4	4.4	+0.7			γCH_3 a (t)	A´´
1029.6	37.6	+20.2	1005.9	+15.0	γCH_3 s (t)	A´
1023.5	12.8	+23.1	990.1		γCH_3 s (c)	A´
909.0	87.5	+248.0	862.4	+266.6	τC-O (t)	A´´
892.3	2.3	+24.5			νC-C (t)	A´
879.8	36.8	+19.2	872.2	+14.8	νC-C (c)	A´
613.6	10.2	+11.3			δOCO (c)	A´
610.9	2.8	+12.3			γC=O (c)	A´´
610.2	20.7	+25.6	608.8	+21.8	δOCO (t)	A´
600.5	0.2	+49.8			γC=O (t)	A´´
499.2	95.9	+34.1	501.7(?)	+12.4	τC-O (c)	A´´

[a] Wavenumbers (ν) and shifts in wavenumbers (Δν) relatively to the monomer in cm^{-1}; Infrared intensities (I^{IR}) in km mol^{-1}. [b] Average wavenumber shifts in relation to the position of the observed bands of the *trans*-AA monomer in its two matrix sites or *cis*-AA monomer.[33] [c] ν, stretching; δ, bending; γ, rocking; τ, torsion; a, antisymmetric; s, symmetric; (t), *trans* molecule in the dimer; (c), *cis* molecule in the dimer.

Production of the *trans-cis* D2_TC dimer from thermal mobilization of *trans*- and *cis*-AA monomers and of D2'_TT from decay of D2_TC, and assignment of their IR spectra

A different experiment was undertaken, involving thermal mobilization of *trans*- and *cis*-AA monomers (this latter previously produced by vibrational excitation of the N_2 matrix isolated *trans*-AA monomer by *in situ* irradiation at $\tilde{\nu}$= 4724.5 cm^{-1}), and resulting in the observation and positive identification of two hitherto unobserved AA dimers: D2'_TT and D2_TC (see Figures 1 and 2 for structures).

In these experiments, AA was isolated in N_2 matrix at 8.5 K. This matrix contained the low-energy *trans*-AA monomeric form (together with traces of D1_TT and D2_TT dimers). The matrix was subsequently irradiated at $\tilde{\nu}$= 4724.5 cm^{-1}, *i.e.*, at the νOH +δCOH combination mode wavenumber of *trans*-AA, to partially convert this species into the *cis* monomer. These results are illustrated in Figure 5, where a representative spectral region is depicted. In this Figure (trace b), the positive peaks correspond to the emerging bands of *cis*-AA and the negative peaks to the decreasing bands of *trans*-AA.[33] From the band intensities, the relative amount of *cis* and *trans*-AA in the matrix after irradiation could be roughly estimated as being in a ~1:1 proportion. Subsequent annealing of the matrix to 28 K led to decrease of the bands due to both *trans* and *cis* monomers, which indicates the consumption of these forms, and to the appearance of new bands belonging to a new species, which could be identified as being the D2_TC dimer. Formation of this species implies the thermal mobilization of the monomers upon increase of the temperature of the matrix.

D2_TC dimer is the most stable *trans-cis* dimer possessing the strong O-H···O= hydrogen bond formed with the *trans*-AA unit as H-bond donor, and has the calculated interaction energy of −36 kJ mol^{-1}. This interaction energy results mainly from the establishment of the H-bond, since no other energetically relevant interactions are present in this dimer. Dimers D1_TC and D1'_TC have larger interaction energies than D2_TC. However, the preferential formation of D2_TC over both D1_TC and D1'_TC can be easily explained considering that upon annealing, molecular diffusion lead to the preferential initial formation of the strongest possible single hydrogen bond, which is present in D2_TC ($O\text{-}H_{(trans)}\cdots O=$) but absent in both D1_TC and D1'_TC. Both these two forms have interaction energies of ~40 kJ mol^{-1},

but this energy results from the establishment of two H-bonds (O-H$_{(cis)}$···O= and O-H$_{(trans)}$···O-H), which must then be individually considerably weaker than that present in D2_TC. Once the strongest O-H$_{(trans)}$···O= bond is established, access to D1_TC and D1'_TC is blocked, so that among the accessible forms the most stable one is formed (D2_TC).

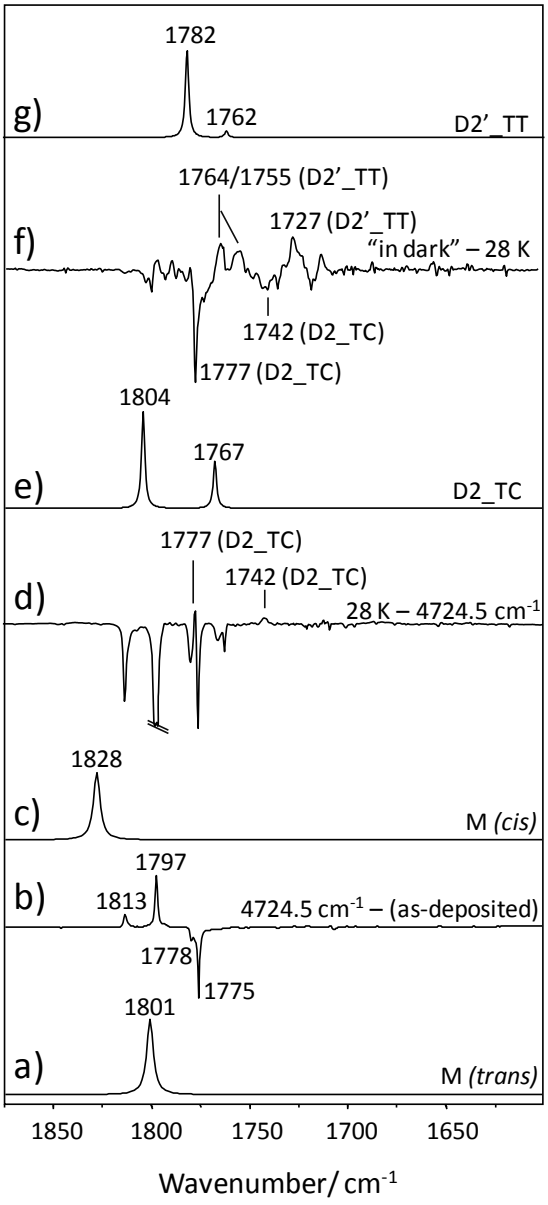

Figure 5. 1875-1600 cm^{-1} spectral range of the: a) calculated spectrum of AA-*trans* monomer, b) spectrum of the compound isolated in N_2 matrix and irradiated at 4724.5 cm^{-1} *minus* spectrum of the as-deposited matrix (T= 8.5 K), c) calculated spectrum of AA-*cis* monomer, d) spectrum after annealing to 28 K the irradiated (4724.5 cm^{-1}) matrix *minus* spectrum of the irradiated matrix (T= 8.5 K), e) calculated spectrum of D2_TC dimer, f) spectrum of the annealed to 28 K irradiated sample let in the dark (T=8.5 K) for 7 h. *minus* spectrum of the annealed to 28 K irradiated matrix, and g) calculated spectrum of D2'_TT dimer. Note that the intensity scales of the experimental spectra (b, d, f) were successively expanded by a factor of ~10.

Table 7. MP2/6-311++G(2d,2p) calculated infrared spectra for dimer D2_TC (C_1) wavenumber shifts in relation to the monomer and observed wavenumbers and shifts in N_2 matrix. [a]

Calculated			N_2 matrix			
ν	I^{IR}	Δν	ν	Δν[b]	Assignment[c]	Symmetry
3847.3	76.9	−5.6	3587.1	−23.6	νO-H (c)	A
3563.9	619.3	−223.4	3385.1	−162.9	νO-H (t)	A
			3377.5	−173.5		
3224.4	4.2	−4.3			νHCH_2 s (t)	A
3221.8	1.7	+0.2			νHCH_2 s (c)	A
3185.4	2.4	−2.4			νHCH_2 a (t)	A
3176.1	2.3	+6.3			νHCH_2 a (c)	A
3105.2	1.9	−2.4			νCH_3 (t)	A
3093.2	4.4	+1.5			νCH_3 (c)	A
1804.0	378.0	−24.1	1777.3	−19.9	νC=O (c)	A
1767.5	182.7	−33.5	1741.5	−34.8	νC=O (t)	A
1513.5	5.1	+0.3			δHCH_2 a (c)	A
1505.3	8.0	−0.1			δHCH_2 a (t)	A
1500.1	19.9	−0.2			δHCH_2 s (t)	A
1497.9	13.1	−2.6			δHCH_2 s (c)	A
1443.2	73.5	+10.5	1379.3	−7.3	δCH_3 (t)	A
1419.0	72.8	−1.4	1351.9	−19.5	δCH_3 (c)	A
1389.0	4.4	+180.9			COH-CO def (t)	A
1324.6	342.6	+18.3	1310.1	+14.0	COH-CO def (c)	A
1266.8	205.5	−83.5	1239.0	−39.2	CO-COH def (t)	A
1237.3	4.1	+22.3			CO-COH def (c)	A
1083.0	3.7	+0.3			γCH_3 a (t)	A
1078.4	10.2	+1.6	1055.0	+9.2	γCH_3 a (c)	A
			1051.6	+5.8		
1027.6	40.2	+18.2			γCH_3 s (t)	A
1016.1	9.0	+15.7			γCH_3 s (c)	A
888.1	4.3	+20.3			νC-C (t)	A
879.6	26.5	+19.0	871.0	+13.6	νC-C (c)	A
			862.8	+5.4		
818.0	63.7	+157.0	802.7	+143.0	τC-O (t)	A
615.8	7.6	+13.5			δOCO (c)	A
608.7	19.6	+24.1	611.3	+24.3	δOCO (t)	A
595.4	0.7	+44.7			γC=O (t)	A
589.8	4.7	+0.2			γC=O (c)	A
472.2	113.3	+7.1	539.6	+50.3	τC-O (c)	A

[a] Wavenumbers (ν) and shifts in wavenumbers (Δν) relatively to the monomer in cm^{-1}; Infrared intensities (I^{IR}) in km mol^{-1}. [b] Average wavenumber shifts in relation to the position of the observed bands of the *trans*-AA monomer[33] in the two matrix sites and of the *cis*-AA monomer. [c] ν, stretching; δ, bending; γ, rocking; τ, torsion; a, antisymmetric; s, symmetric; (t), *trans* molecule in the dimer; (c), *cis* molecule in the dimer.

The proposed assignments for observed bands of D2_TC are given in Table 7. In the selected spectral region shown in Figure 5, the bands due to D2_TC are observed at 1777.3 and 1741.5 cm^{-1}, corresponding to the two C=O stretching modes (see traces d and e). The observed shifts of these bands are −20 and −35 cm^{-1}, in very good agreement with the predicted shifts of −24 and −33 cm^{-1}.

The agreement between the experimental and calculated spectra for D2_TC in other spectral regions is also fairly good. For example, in the OH stretching region the bands at 3587.1 cm^{-1} and the doublet at 3377.5/3385.1 cm^{-1}, with experimental shifts of −24 and −163/−173, are easily ascribed to the vibrations of the unbound OH group of the *cis*-AA unit in the dimer and the H-bonded *trans*-AA unit, respectively, which have predicted shifts of −6 and −223 cm^{-1}. Additional bands due to the produced species were observed at 1379.3 (δCH_3 (*trans*)), ~1352 (δCH_3 (*cis*)), 1310.1 (COH-CO def (*cis*)), 1239.0 (CO-COH def (*trans*)), 1055.0/1051.6 (γCH_3 (*cis*)), 871.0/862.8 (νC-C (*cis*)), 611.3 (δOCO (trans)) and 539.6 (τC-O (cis)) cm^{-1} and correspond well to the bands with the highest calculated intensities for D2_TC.

Another piece of information supporting the dominant formation of D2_TC in the experiment described above resulted from the analysis of the product of the decay of the formed dimer when the sample is kept in the dark. D2_TC has a free OH *cis* fragment and can then decay to a *trans-trans* dimer, in particular for D2'_TT, whose formation from D2_TC requires the smallest structural rearrangement among all *trans-trans* dimers (see Figures 1 and 2). Indeed, the product resulting from decay of the initially formed *trans-cis* dimer has a spectral signature that fits well that of D2'_TT (see traces f and g in Figure 5), and is here tentatively assigned to this species. In the shown spectral region, for D2'_TT gives rise to the bands 1763.5/1755.7 cm^{-1} and 1726.8 cm^{-1}, assigned to the νC=O vibrations. The observed (−13/−21 and −49 cm^{-1}) and predicted (−19, −39 cm^{-1}) shifts for these bands are in good agreement.

Though the low intensity of the experimental bands made the analysis of the spectrum of D2'_TT difficult, still the experimental and calculated spectra for this dimer show a general good agreement also in other spectral regions, as shown in Table 8, where the band assignments for this dimer are provided. For example, the "free" OH stretching mode of D2'_TT is tentatively attributed to the band at 3556.7 cm^{-1} (shifts: +9 experimental; −11 cm^{-1} calculated). Other observed bands

corresponding to intense predicted bands appear at 1389.1, 1373.7, 1341.5, 1252.1/1250.4, 1241.2/1230.0, 1053.4, 1005.1, 1001.1, 869.0/865.0, 658.7, 614.9, 601.5 and 557.3 cm^{-1} (see Table 8 for details). Note also that as for D1_TT and D2_TT, the stretching vibration of the H-bonded OH group of D2'_TT is not observable.

Table 8. MP2/6-311++G(2d,2p) calculated infrared spectra for dimer D2'_TT (C_1) wavenumber shifts in relation to the monomer and observed wavenumbers and shifts in N_2 matrix. [a]

Calculated			N_2 matrix			
ν	I^{IR}	Δν	ν	Δν[b]	Assignment[c]	Symmetry
3776.5	85.1	–10.8	3556.7	+8.7	νO-H (2)	A
3489.7	956.0	–297.6			νO-H (1)	A
3224.5	4.7	+36.7			νHCH_2 s (1)	A
3223.3	4.0	+35.5			νHCH_2 a (2)	A
3195.5	3.3	+7.7			νHCH_2 s (2)	A
3185.1	2.9	–2.7			νHCH_2 a (1)	A
3108.2	4.3	+0.6			νCH_3 (2)	A
3105.1	2.1	–2.5			νCH_3 (1)	A
1781.7	604.7	–19.3	1763.5	–12.8	νC=O a	A
			1755.7	–20.6		
1761.6	43.8	–39.4	1726.8	–49.5	νC=O s	A
1511.8	11.7	+6.4			δHCH_2 a (2)	A
1505.8	7.9	+0.4			δHCH_2 a (1)	A
1500.2	18.1	–0.1			δHCH_2 s (1)	A
1493.7	21.5	–6.6			δHCH_2 s (2)	A
1448.4	40.1	+15.7	1389.1	+2.4	δCH_3 (1)	A
1434.5	88.8	+1.8	1373.7	–12.9	δCH_3 (2)	A
1399.2	6.9	+191.1			COH-CO def (1)	A
1369.0	73.0	+160.9	1341.5	+150.5	COH-CO def (2)	A
1273.6	248.9	–76.7	1252.1	–26.1	CO-COH def (1)	A
			1250.4	–27.8		
1223.2	241.7	–127.1	1241.2	–40.3	CO-COH def (2)	A
			1230.0	–44.9		
1087.1	8.2	+4.4			γCH_3 a (2)	A
1082.8	4.2	+0.1	1053.4	+5.3	γCH_3 a (1)	A
1032.7	55.7	+23.3	1005.1	+14.2	γCH_3 s (2)	A
1027.3	43.5	+17.9	1001.1	+10.2	γCH_3 s (1)	A
910.4	80.8	+249.4	869.0	+203.8	τC-O (1)	A
			865.0	+210.9		
887.7	5.5	+19.9			νC-C (1)	A
881.5	4.6	+13.7			νC-C (2)	A
692.7	95.9	+31.7	658.7	–0.8	τC-O (2)	A
610.8	11.8	+26.2			δOCO (1)	A
602.0	26.1	+17.4	614.9	+27.4	δOCO (2)	A
597.0	31.8	+46.3	601.5	+50.0	γC=O (1)	A
550.4	22.4	–0.3	557.3	+5.8	γC=O (2)	A
445.4	12.7	+20.0			δCC=O (1)	A
435.7	0.7	+10.3			δCC=O (2)	A

[a] Wavenumbers (ν) and shifts in wavenumbers (Δν) relatively to the monomer in cm^{-1}; Infrared intensities (I^{IR}) in km mol^{-1}. [b] Average wavenumber shifts in relation to the position of the observed bands of the *trans*-AA monomer[33] in the two matrix sites. [c] ν, stretching; δ, bending; γ, rocking; τ, torsion; a, antisymmetric; s, symmetric; (1), molecule 1 in the dimer (OH···O bond donor molecule); (2), molecule 2 in the dimer (CH···O bond donor molecule).

Tunneling decay rate of the D2'_TC *trans-cis* dimer at 8.5 K

As already mentioned, the two observed *trans-cis* dimers (D2'_TC and D2_TC) were found to decay in the dark to the structurally closely related D2_TT and D2'_TT, respectively, by tunneling. The tunneling decay rate of D2'_TC into D2_TT was evaluated at 8.5 K (Figure 6). According to the performed relaxation studies, D2'_TC has a slow tunneling decay constant (~7.5 h, at 8.5 K).

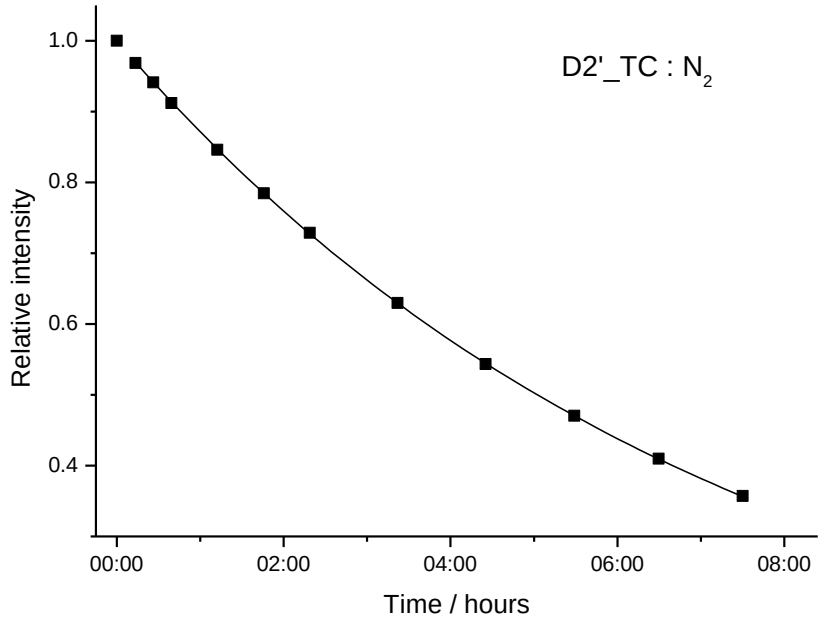

Figure 6. Decay of the band at 1306.8 cm^{-1} assigned to the COH-CO def (c) mode of D2'_TC in N_2 matrix at 8.5 K.

The *cis*–to–*trans* conversion in a nitrogen matrix has been previously studied for monomeric formic and acetic acids.[33] At *ca.* 8.9 K, the *cis*-AA lifetime is ~8 hours, whereas the *cis*-HCOOH lifetime is ~11.4 hours, in a nitrogen matrix. The faster decay of monomeric *cis*-AA compared to *cis*-HCOOH was explained by the lower *cis*–to–*trans* barrier for AA.[33] The D2'_TC lifetime, being approximately 7.5 h, is then identical to that of monomeric *cis*-AA, indicating similar stabilization of the cis arrangement in the monomer and in the dimer.

The measurement of the tunneling decay rate of D2_TC was also attempted, but the small amount of this form produced and the consequent low signal-to-noise

spectroscopic ratio precluded made our efforts unsuccessful. However, considering both the similarity of D2_TC and D2'_TC dimers and the analogous values found for the decay rates of this latter dimer and the monomer, we can expect that the tunneling decay rate of D2_TC in a nitrogen matrix shall also be close to 7-8 h.

4. Conclusion

In this study, dimers of acetic acid were investigated in a solid nitrogen matrix. Three *trans-trans* (D1_TT, D2_TT, D2'_TT) and two *trans-cis* (D2_TC and D2'_TC) AA dimers were observed experimentally, the D2'_TT, D2_TC and D2'_TC forms being reported for the first time. D2'_TC, was produced by selective vibrational excitation (at at 6896 cm^{-1}) of the structurally related D2_TT *trans-trans* AA dimer. D2_TC was obtained by thermal mobilization of a mixture of *trans* and *cis* monomers of AA, the latter being produced from the first one by vibrational excitation at 4724.5 cm^{-1}. The D2'_TT dimer was tentatively identified as resulting from tunneling decay of D2_TC. Interpretation of the experimental data was helped by an extensive theoretical study of the various possible structures of acetic acid dimers (*trans-trans* and *trans-cis*), carried out at the MP2/6-311++G(2d,2p) level of approximation. The tunneling decay rate at 8.5 K of D2'_TC into D2_TT was estimated as being ~7.5 h, a value close to that found previously for the decay of *cis*-AA monomer into the trans form in the same matrix.

Supplementary Material: Tables S1 and S2 with calculated infrared spectra for AA dimers. This material can be obtained at http://dx.doi.org/...

Acknowledgements

These studies were partially funded by the Portuguese Science Foundation (Projects PTDC/QUI/71203/2006 - No. FCOMP-01-0124-FEDER-007458 and PTDC/QUI-QUI/111879/2009, co-funded by QREN-COMPETE-UE, and Grant No. SFRH/BD/29698/2006) and by the Academy of Finland through the Finnish Centre of

Excellence in Computational Molecular Science. R.F. and S.L. acknowledge Milipeia Computer Centre (University of Coimbra), research project “Computação Avançada em Espectroscopia Molecular”. A.D. acknowledges a postdoctoral grant from the Faculty of Science, University of Helsinki (Project No. 7500101).

References:

1 S. Scheiner, *Hydrogen Bonding: A Theoretical Perspective*, Oxford University Press, New York, 1997.

2 S. J. Grabowski (ed.), *Hydrogen Bonding – New Insights*, Springer, Dortrecht, Netherlands, 2006.

3 E. T. J. Nibbering and T. Elsaesser, *Chem. Rev.*, 2004, **104**, 1887-1914.

4 N. J. Singh, H. M. Lee, I.-C. Hwang and K. S. Kim, *Supramol. Chem.*, 2007, **19**, 321-332.

5 B. H. Hong, J. Y. Lee, C.-W. Lee, J. C. Kim, S. C. Bae, and K. S. Kim, *J. Am. Chem. Soc.*, 2001, **123**, 10748-10749.

6 R. A. Musah, G. M: Jensen, R. J. Rosenfeld, D. E. McRee, *J. Am. Chem. Soc.*, 1997, **119**, 9083-9084.

7 P. Raveendran and S. L. Wallen, *J. Am. Chem. Soc.*, 2002, **124**, 12590-12599.

8 H. Myoung, A. Kumar, M. Kolaski, D. Y. Kim, E. C. Lee, S. K. Min, M. Park, Y. C. Choi and K. S. Kim, *Phys. Chem. Chem. Phys.*, 2010, **2**, 6278-6287.

9 T. Steiner, *Angew. Chem. Int. Ed.*, 2002, **41**, 48-76.

10 S. Scheiner, T. Kar and Y. Gu, *J. Biol. Chem.*, 2001, **13**, 9832-9837.

11 A. Bende, *Theor. Chem. Acc.*, 2010, **125**, 253-268.

12 H. E. Herbert, M. D. Halls, H. P. Hratchian and K. Raghavachari, *J. Chem. Phys. B*, 2006, **110**, 3336-3343.

13 L. Turi, *J. Chem. Phys.*, 1996, **100**, 11285-11291.

14 J. Chocholousova, J. Vacek and P. Hobza, *Phys. Chem. Chem. Phys.*, 2002, **4**, 2119-2122.

15 L. Turi and J. J. Dannenberg, *J. Phys. Chem.*, 1993, **97**, 12197-12204.

16 J. L. Derissen, *J. Mol. Struct.*, 1971, **7**, 67-80.

17 W. Weltner, Jr., *J. Am. Chem. Soc.*, 1955, **77**, 3941-3950.

18 M. Haurie and A. Novak, *J. Chim. Phys.*, 1965, **62**, 146-157.

19 Y. Maréchal, *J. Chem. Phys.*, 1987, **87**, 6344-6353.

20 R. E. Jones and D. E. Templeton, *Acta Crystallogr.*, 1958, **11**, 484-487.

21 F. Génin, F. Quiles and A. Burneau, *Phys. Chem. Chem. Phys.*, 2001, **3**, 932-942.

22 T. Nakabayashi, K. Kosugi and N. Nishi, *J. Phys. Chem. A*, 1999, **103**, 8595-8603.

23 J. M. Briggs, T. Nakabayachi and N. Nishi, *J. Phys. Chem.*, 1994, **95**, 3315-3322.

24 J. Chocholousova, J. Vacek and P. Hobza, *J. Phys. Chem. A*, 2003, **107**, 3086-3092.

25 M. Tjahjono, A. D. Allian and M. Garland, *Phys. Chem. B*, 2008, **112**, 6448-6459.

26 H. Pasalic, A. J. A. Aquino, D. Tunega, G. Haberhauer, M. H. Grezabek, H. G. Georg, T. F. Moraes, K. Coutinho, S. Canuto and H. Lischka, *J. Comput. Chem.*, 2010, **31**, 2046-2055.

27 K. Heyne, N. Huse, J. Dreyer, E. T. J. Nibbering and T. Elsaesser, *J. Chem. Phys.*, 2004, **121**, 903-913.

28 A. J. A. Aquino, D. Tunega, G. Haberhauer, M. H. Grezabek and H. Lischka, *J. Phys. Chem. A*, 2002, **106**, 1862-1871.

29 M. L. Senent, *Mol. Phys.*, 2001, 99, 1311-1321.

30 E. M. S. Maçôas, L. Khriachtchev, R. Fausto and M. Räsänen, *J. Phys. Chem. A*, 2004, **108**, 3380-3389.

31 E. M. S. Maçôas, L. Khriachtchev, M. Pettersson, R. Fausto and M. Räsänen, *J. Chem. Phys.*, 2004, **121**, 1331-1338.

32 E. M. S. Maçôas, L. Khriachtchev, M. Pettersson, R. Fausto and M. Räsänen, *J. Am. Chem. Soc.*, 2003, **125**, 16188-1338.

33 S. Lopes, A. V. Domanskaya, R. Fausto, M. Räsänen, L. Khriachtchev, *J. Chem. Phys.*, 2010, **133**, 144507-144577.

34 K. Maruskevich, L. Khriachtchev and M. Räsänen, *Phys. Chem. Chem. Phys.*, 2007, **9**, 5748-5751.

35 K. Maruskevich, L. Khriachtchev and M. Räsänen, *J. Chem. Phys.*, 2007, **126**, 241102-241104.

36 E. Maçôas, L. Khriachtchev, M. Pettersson, R. Fausto and M. Räsänen, *J. Phys. Chem.*, 2005, **109**, 3617-3624.

37 E. Maçôas, L. Khriachtchev, M. Pettersson, J. Lundell, R. Fausto and M. Räsänen, *Vib. Spectrosc.*, 2004, **34**, 73-84.

38 S. Amiri, H. P. Reisenauer and P. R. Schreiner, *J. Am. Chem. Soc.*, 2010, **132**, 15902-15904.

39 T. Nakabayashi, H. Sato, F. Hirata and N. Nishi, *J. Phys.Chem. A*, 2001, **105**, 245-250.

40 A. Burneau, F. Génin and F. Quilès, *Phys. Chem. Chem. Phys.*, 2000, **2**, 5020-5029.

41 W. Xu and J. Yang, *J. Phys.Chem. A*, 2010, **114**, 5377-5388.

42 W. Sander and M. Gantenberg, *Spectrochim. Acta A*, 2005, **62**, 902-909.

43 C. Emmeluth and M. A. Suhm, *Phys. Chem. Chem. Phys.*, 2003, **5**, 3094-6099.

44 A. Olbert-Majkut, J. Ahokas, J. Lundell and M. Pettersson, *J. Raman Spectrosc.*, 2011,

45 Y. Grenie, J.-C. Cornut and J.-C. Lassegues, *J. Chem. Phys.*, 1971, **55**, 5844-5846.

46 R. L. Redington and K. C. Lin, *J. Chem. Phys.*, 1971, **54**, 4111-4119.

47 C. J. Bennet and R. I. Kaiser, *Astrophys. J.*, 2007, **660**, 1289-1295.

48 K. Maruskevich, L. Khriachtchev, J. Lundell and M. Räsänen, *J. Am. Chem. Soc.*, 2006, **128**, 12060-12061.

49 K. Maruskevich, L. Khriachtchev, J. Lundell, A. Domanskaya and M. Räsänen, *J. Phys. Chem. A*, 2010, **114**, 3495-3502.

50 GAMESS, version R2 (25-Mar-2010), M. Schmidt, K. Baldridge, J. Boatz, S. T. Elbert, M. S. Gordon, J. H. Jensen, S. Koseki, N. Matsunaga, K. A. Nguyen, S. J. Su, T. L. Windus, M. Dupuis, J. Montgomery, *J. Comput. Chem.*, 1993, **14**, 1347-1363.

51 C. Moller and M. S. Plesset, *Phys. Rev.*,1934, **46**, 618-622.

52 A. D. McLean and G. S. Chandler, *J. Chem. Phys.*, 1980, **72**, 5639-5648.

53 M. J. Frisch, J. A. Pople and J. S. Binkley, *J. Chem. Phys.*, 1984, **80**, 3265-3269.

54 E. M. S. Maçôas, J. Lundell, M. Pettersson, L. Khriachtchev, R. Fausto, M. Räsänen, *J. Mol. Spectrosc.*, 2003, **219**, 70-80.

55 J. Lundell, M. Räsänen, Z. Latajka, *Chem. Phys.*, 1994, **189**, 245-260.

56 J. Lundell, *Chem. Phys. Lett.*, 1997, **266**, 1-6.

57 S. F. Boys and F. Bernardi, *Mol. Phys.*, 1970, **19**, 553-566.

5 Conclusion and Perspectives

In the first part of this work, a matrix-isolation infrared spectroscopy and quantum chemical calculations were used in a combined way as main techniques to investigate a series of criteriously selected examples of nitrogen containing heterocycles.

Theoretical calculations carried out at contemporary levels of theory revealed the low energy minima and the transition states associated with the preferred conformational interconversion pathways for each molecule studied. This allowed making predictions about the species which should be present in the cryogenic matrices of the compounds. For all compounds studied, the precise structural and spectroscopic characterization of the conformers present in the initially deposited matrices could be performed, in most of the cases taking into account results of temperature variation studies.

The identification and assignment of the spectra of the photoproducts of the different systems investigated was also carried out in argon and xenon matrices. For methyl 4-chloro-5-phenylisoxazole-3-carboxylate (**MCPIC**) and methyl (Z)-2-azido-3-chloro-3-benzoylpropenoate (**MACBP**), the photochemical transformations resulting from broadband *in situ* irradiation of the matrices with ultraviolet light (λ > 235 nm) yielded the corresponding azirine (methyl 2-benzoyl-2-chloro-2*H*-azirine-3-carboxylate, MBCAC), which subsequently undergoes ring expansion to the oxazole (**MCPOC**) as final photoproduct; other photoproducts were also observed resulting from cleavage of both C−C and C−N bonds. In particular, in the case of MACBP this primary reaction is accompanied by a second one leading to formation of the ketenimine *C*-chloro-*C*-benzoyl-*N*-methoxycarbonylketenimine (CBMK). In the case of the oxazole heteroclycle no photoreactions were observed. This work demonstrated that methyl 2-benzoyl-2-halo-2*H*-azirine-3-carboxylates undergo thermal ring expansion to give 4-halo-5-phenyl-1,3-oxazole-2-carboxylates and not the isomeric isoxazoles. The performed studies gave some important clues regarding the importance of the vinyl nitrene intermediate in azirine reactions. For the compounds studied, there are indications that this putative intermediate is not involved in the ring opening reactions. Of course it must be noticed that the studied molecules bear

voluminous electron attractor substituents and the reactions took place for the compounds under the volume constrains imposed by the matrices. Nevertheless, the results now obtained open interesting perspectives for the examination of the role of the vinyl nitrene intermediate in the general type of reactions investigated.

For methyl aziridine-2-carboxylate (**MA2C**), narrowband tunable laser light irradiation (λ = 235 nm) let to the preferred photochemical breakage of the C−C bond. The primary photoproduct, methyl 2-(methyleneamino)-acetate (MMAA), was positively identified and found to undergo further bond-breaking reactions to other photoproducts (methyl formate; acetonitrile). Photoproducts resulting from the C−N cleavage of the aziridine ring have also been observed. One interesting result was the conformational dependence of the photochemistry of MMAA. Conformationally dependent photochemical processes are nowadays an active area of research in Coimbra, and the observed conformational photo-selectivity can be explored in more detail in the future.

In the case of **α–pyridil**, the compound was found to prefer to isomerize into unusual molecular species bearing Hückel-type pyridine (aza-benzvalene) rings. The study of this type of substances is simultaneously a challenge and a very interesting subject. It appears to be important to look to the behavior of other molecules similar to α-pyridil, bearing, for instance, diazine or triazine rings.

In the second part of this study, **formic** and **acetic acids** were investigated. These simple carboxylic acids are interesting systems capable of forming hydrogen bonds with themselves or with other small molecules. The higher-energy *cis* conformers of the monomeric forms of these molecules were produced by vibrational excitation of the more stable *trans* conformers. The decay of the *cis* forms is observed and explained by tunneling of hydrogen atom through the *cis*–to–*trans* torsional barrier, similarly to these species in rare-gas matrices.

For acetic acid, three *trans-trans* dimers and two *trans-cis* dimers were observed experimentally in a solid nitrogen matrix, three of them being novel species observed experimentally for the first time here.

The continuation of these studies is planned for the next few years. Other simple carboxylic acids, like propionic, propiolic and oxalic acids, are planned to be studied.

Supporting Information

J. Phys. Chem. A, **2010**, *114*, 9074-9082.

Supporting Information

for

Conformational Space and Vibrational Spectra of Methyl 4-Chloro-5-phenyl-1,3-oxazole-2-carboxylate

Susy Lopes,[a] Cláudio M. Nunes,[a] Andrea Gómez-Zavaglia,[a,b]

Teresa M.V.D. Pinho e Melo[a] and Rui Fausto[a]

[a] *Department of Chemistry, University of Coimbra, P-3004-535 Coimbra, Portugal*
[b] *Centro de Investigación y Desarrollo en Criotecnología de Alimentos (Conicet La Plata, UNLP) RA-1900, La Plata, Argentina*

Contents

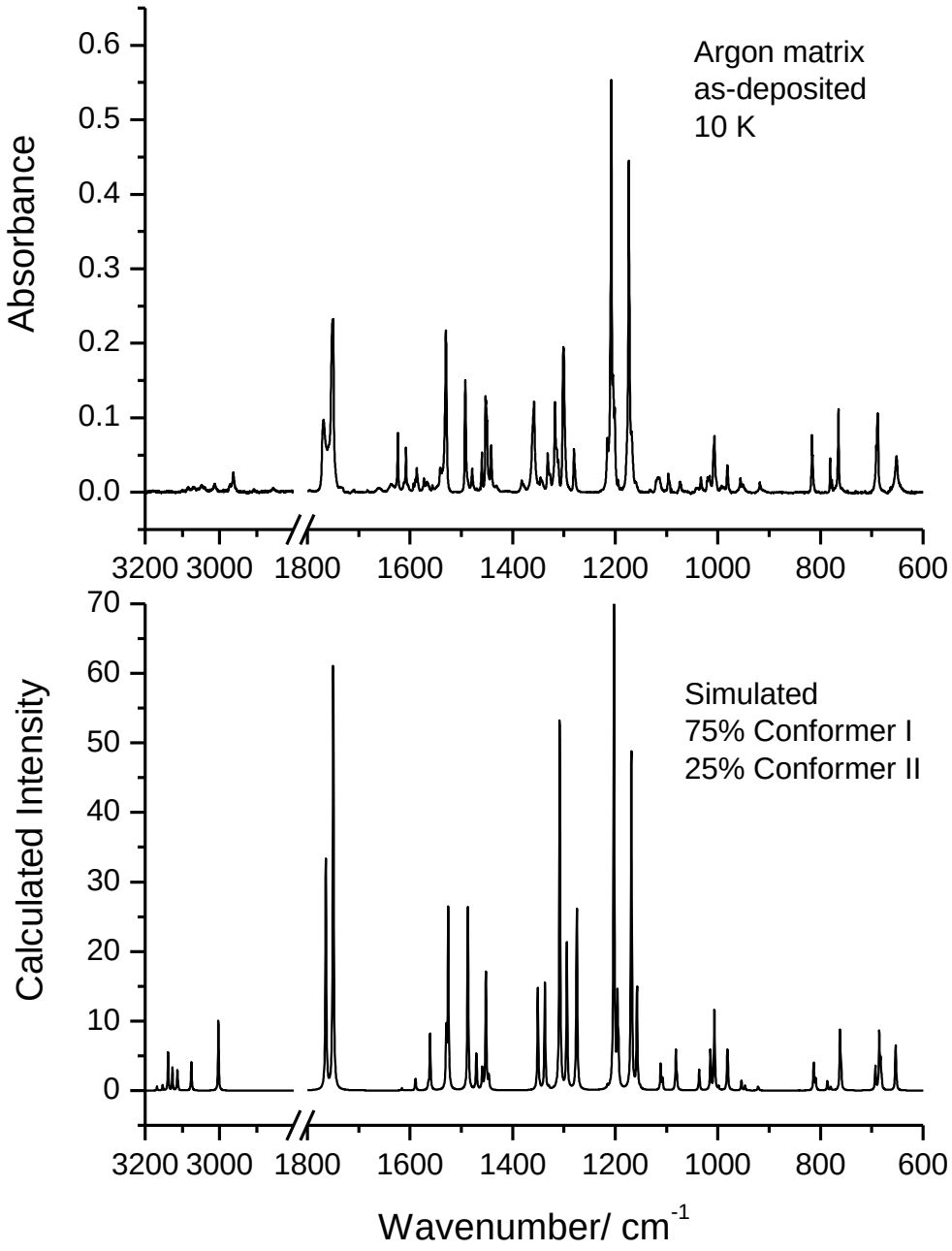

Figure S1. ***Top:*** Infrared spectrum of MCPOC isolated in solid argon (as-deposited matrix; temperature of the vapor, 323 K; substrate temperature 10 K). In the 1650-1550 cm^{-1} region, in addition to the bands of the compound there are bands due to traces of monomeric water impurity present in the matrix. ***Bottom:*** Simulated spectrum obtained by summing the DFT(B3LYP)/6-311++G(d,p) predicted spectra of the experimentally relevant conformers **I** and **II**, weighted by their expected populations (0.75 : 0.25). In the simulated spectrum, bands were represented by Lorentzian functions centered at the calculated wavenumbers scaled by 0.9835 and with fwhm (full width at half maximum) equal to 2 cm^{-1}.

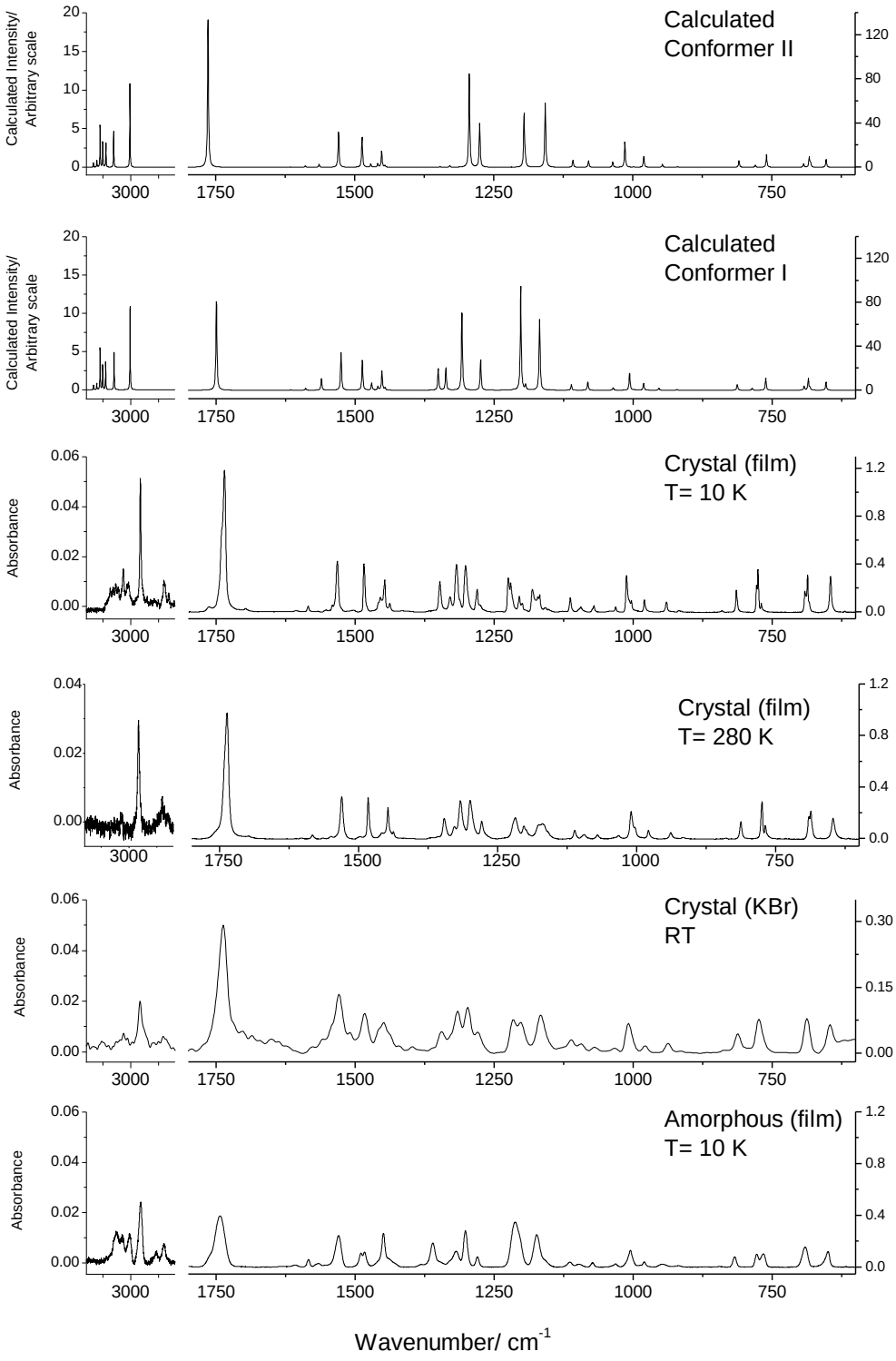

Figure S2. ***From bottom to top:*** Infrared spectrum (3200-600 cm^{-1}) of MCPOC *(i)* in the amorphous layer resulting from fast deposition of the vapor of the compound at 343 K onto the cold substrate (10 K) of the cryostat; *(ii)* in the room temperature crystalline phase, as a KBr pellet; *(iii)* in the crystalline phase resulting from warming the amorphous layer at 280 K; *(iv)* in the crystalline phase resulting from warming the amorphous layer to 280 K, subsequently cooled down to 10 K; *(v)* and *(vi)* DFT(B3LYP)/6-311++G(d,p) calculated infrared spectra of conformers **I** and **II**, respectively. In the calculated spectra, bands were represented by Lorentzian functions centered at the calculated wavenumbers scaled by 0.9835 and with fwhm (full width at half maximum) equal to 2 cm^{-1}.

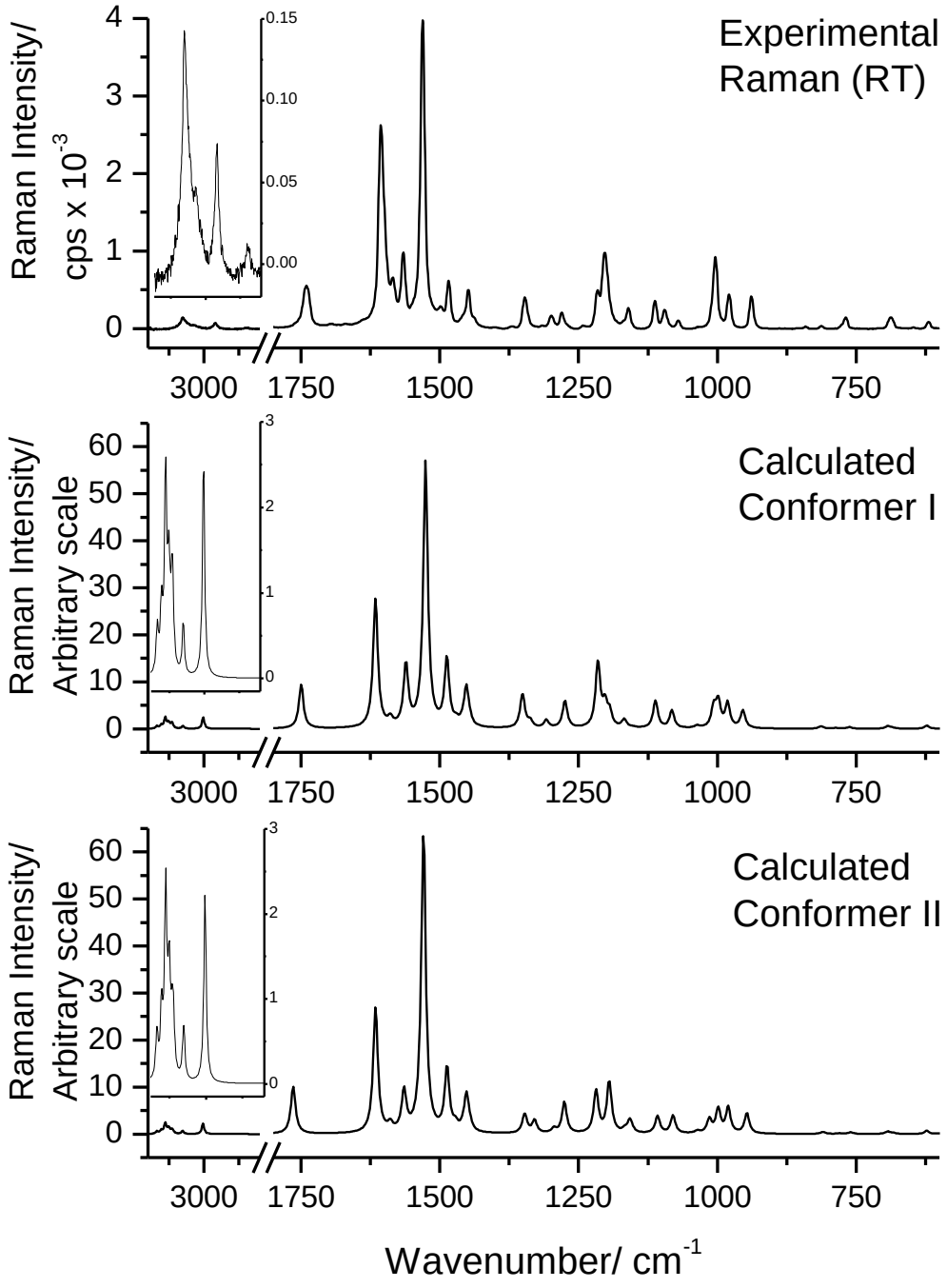

Figure S3. ***Top:*** Raman spectrum of MCPOC room temperature crystalline phase. ***Middle and bottom:*** DFT(B3LYP)/6-311++G(d,p) calculated Raman spectra of conformers **I** and **II**. In the calculated spectra, bands were represented by Lorentzian functions centered at the calculated wavenumbers scaled by 0.9835 and with fwhm (full width at half maximum) equal to 10 cm^{-1}. Theoretical Raman intensities were obtained from the calculated Raman scattering activities as described in the text.

Table S1 (Supporting Information) - DFT(B3LYP)/6-311++G(d,p) calculated bond lengths (pm) and angles (º) for the two most stable conformers of MCPOC.[a]

	Conformer **I**	Conformer **II**		Conformer **I**	Conformer **II**
Bond lengths /pm					
$C_1=C_2$	137.9	137.9	$C_{21}–H_{24}$	109.1	109.1
$C_1–C_3$	136.9	137.0	$C_5–C_6$	140.5	140.5
$C_1–C_5$	145.5	145.6	$C_5–C_{10}$	140.7	140.7
$C_2–Cl_4$	172.6	172.5	$C_6–C_7$	139.1	139.1
$C_2–N_{16}$	136.3	136.2	$C_6–H_{11}$	108.1	108.1
$O_3–C_{17}$	135.4	135.7	$C_7–C_8$	139.4	139.4
$N_{16}=C_{17}$	129.9	129.8	$C_7–H_{12}$	108.4	108.4
$C_{17}–C_{18}$	148.2	148.3	$C_8–C_9$	139.5	139.5
$C_{18}=O_{19}$	120.7	120.4	$C_8–H_{13}$	108.4	108.4
$C_{18}–O_{20}$	133.7	134.4	$C_9–C_{10}$	138.9	138.9
$O_{20}–C_{21}$	144.1	144.2	$C_9–H_{14}$	108.4	108.4
$C_{21}–H_{22}$	109.1	109.1	$C_{10}–H_{15}$	108.2	108.2
$C_{21}–H_{23}$	108.7	108.7			
Angles / º					
$C_2=C_1–O_3$	105.2	105.1	$C_8–C_7–H_{12}$	120.1	120.1
$C_2=C_1–C_5$	137.5	137.5	$C_7–C_8–C_9$	119.6	119.6
$O_3–C_1–C_5$	117.3	117.4	$C_7–C_8–H_{13}$	120.2	120.2
$C_1=C_2–Cl_4$	129.0	129.0	$C_9–C_8–H_{13}$	120.2	120.2
$C_1=C_2–N_{16}$	110.7	110.8	$C_9–C_{10}–H_{15}$	120.0	120.0
$Cl_4–C_2–N_{16}$	120.2	120.2	$C_8–C_9–C_{10}$	120.4	120.4
$C_1–O_3–C_{17}$	106.0	106.0	$C_8–C_9–H_{14}$	120.1	120.1
$C_1–C_5–C_6$	121.7	121.7	$C_{10}–C_9–H_{14}$	119.5	119.5
$C_1–C_5–C_{10}$	119.4	119.5	$N_{16}=C_{17}–C_{18}$	129.8	126.6
$C_2–N_{16}=C_{17}$	104.4	104.5	$C_{17}–C_{18}=O_{19}$	123.4	123.6
$O_3–C_{17}–N_{16}$	113.7	113.6	$C_{17}–C_{18}–O_{20}$	111.1	111.2
$O_3–C_{17}–C_{18}$	116.6	119.8	$O_{19}=C_{18}–O_{20}$	125.5	125.3
$C_6–C_5–C_{10}$	118.9	118.8	$C_{18}–O_{20}–C_{21}$	115.6	115.5
$C_5–C_6–C_7$	120.3	120.3	$O_{20}–C_{21}–H_{22}$	110.3	110.3
$C_5–C_6–H_{11}$	120.2	120.2	$O_{20}–C_{21}–H_{23}$	105.2	105.3
$C_5–C_{10}–C_9$	120.4	120.5	$O_{20}–C_{21}–H_{24}$	110.3	110.3
$C_5–C_{10}–H_{15}$	119.6	119.5	$H_{22}–C_{21}–H_{23}$	110.8	110.8
$C_7–C_6–H_{11}$	119.5	119.6	$H_{22}–C_{21}–H_{24}$	109.4	109.4
$C_6–C_7–C_8$	120.5	120.5	$H_{23}–C_{21}–H_{24}$	110.8	110.8
$C_6–C_7–H_{12}$	119.4	119.4			
Dihedrals / º					
$C_{18}–O_{20}$-$C_{21}–H_{22}$	–60.5	–60.5	$C_{18}–O_{20}–C_{21}–H_{24}$	60.5	60.5
$C_{18}–O_{20}–C_{21}–H_{23}$	180.0	180.0			

[a] See Figure 1 for atom numbering.

Table S2 (Supporting Information) – Optimized geometries of the MCPOC minimum energy conformations in Cartesian coordinates (Å).

Atom	Coordinates		
	X	Y	Z
Conformer **I**			
C1	0.000000	0.544650	0.000000
C2	1.366375	0.357952	0.000000
O3	-0.533861	-0.715795	0.000000
Cl4	2.624522	1.539194	0.000000
C5	-0.930456	1.663776	0.000000
C6	-0.483523	2.995902	0.000000
C7	-1.399546	4.042438	0.000000
C8	-2.769183	3.784248	0.000000
C9	-3.220873	2.464752	0.000000
C10	-2.314470	1.411858	0.000000
H11	0.574771	3.214497	0.000000
H12	-1.038995	5.064666	0.000000
H13	-3.478607	4.603770	0.000000
H14	-4.284066	2.253613	0.000000
H15	-2.671571	0.390217	0.000000
N16	1.672535	-0.970562	0.000000
C17	0.518345	-1.567595	0.000000
C18	0.200019	-3.014983	0.000000
O19	-0.927362	-3.446723	0.000000
O20	1.314524	-3.753497	0.000000
C21	1.116627	-5.181199	0.000000
H22	0.565455	-5.487212	0.890015
H23	2.116637	-5.607372	0.000000
H24	0.565455	-5.487212	-0.890015
Conformer **II**			
C1	0.000000	0.543343	0.000000
C2	-1.342606	0.858111	0.000000
O3	0.046704	-0.825920	0.000000
Cl4	-2.093879	2.411273	0.000000
C5	1.268591	1.256780	0.000000
C6	1.325440	2.660844	0.000000
C7	2.553854	3.312983	0.000000
C8	3.742147	2.584775	0.000000
C9	3.694686	1.190928	0.000000
C10	2.472796	0.529612	0.000000
H11	0.414472	3.242050	0.000000
H12	2.580309	4.396595	0.000000
H13	4.696680	3.098313	0.000000
H14	4.613327	0.615449	0.000000
H15	2.443134	-0.552201	0.000000
N16	-2.104696	-0.271167	0.000000

C17	-1.244127	-1.243382	0.000000
C18	-1.549202	-2.694588	0.000000
O19	-2.667509	-3.139681	0.000000
O20	-0.422519	-3.427188	0.000000
C21	-0.611605	-4.856502	0.000000
H22	-1.161406	-5.165283	0.889771
H23	0.390459	-5.278218	0.000000
H24	-1.161406	-5.165283	-0.889771
Conformer **III** [a]			
C1	-0.428980	0.106042	-0.014933
C2	0.336232	1.251512	-0.050384
O3	0.467880	-0.925554	-0.004281
Cl4	-0.167248	2.901297	-0.088368
C5	-1.842947	-0.238125	0.011765
C6	-2.842161	0.748414	0.060993
C7	-4.184378	0.385023	0.084406
C8	-4.553455	-0.958756	0.060862
C9	-3.567268	-1.943841	0.013338
C10	-2.223463	-1.592125	-0.010978
H11	-2.574270	1.795203	0.081727
H12	-4.944135	1.157116	0.122301
H13	-5.601007	-1.236583	0.079346
H14	-3.844976	-2.991383	-0.005314
H15	-1.462654	-2.360955	-0.048688
N16	1.664039	0.939118	-0.057168
C17	1.699639	-0.362377	-0.029573
C18	2.841673	-1.322275	-0.054621
O19	2.632881	-2.503724	-0.156249
O20	4.098626	-0.861601	0.025397
C21	4.474783	0.516033	0.240530
H22	4.191407	1.136459	-0.607879
H23	5.557366	0.484562	0.344604
H24	4.020061	0.909602	1.148978
Conformer **IV** [a]			
C1	0.306297	0.292749	-0.048653
C2	-0.246045	1.549482	0.035790
O3	-0.765535	-0.562525	-0.162836
Cl4	0.548593	3.071190	0.192051
C5	1.639317	-0.291320	-0.072514
C6	1.807595	-1.630204	-0.468013
C7	3.073424	-2.202867	-0.496062
C8	4.192859	-1.455621	-0.131305
C9	4.034964	-0.128220	0.263190
C10	2.772124	0.453548	0.295912
H11	0.945114	-2.214448	-0.761930
H12	3.186349	-3.234963	-0.807506

H13	5.179347	-1.903903	-0.155424
H14	4.898771	0.459425	0.551872
H15	2.667040	1.482098	0.611084
N16	-1.608894	1.489594	-0.040135
C17	-1.873924	0.226057	-0.151351
C18	-3.223999	-0.389285	-0.351304
O19	-4.065502	0.173525	-0.993524
O20	-3.456231	-1.607618	0.177161
C21	-2.672949	-2.150437	1.259470
H22	-1.787049	-2.657376	0.878673
H23	-3.328329	-2.865547	1.752552
H24	-2.384895	-1.373019	1.969392

[a] The geometry provided corresponds to that of one of the symmetry equivalent minimum energy structures (see text for discussion).

Table S3 (Supporting Information) – Definition of symmetry coordinates used in the normal coordinate analysis of MCPOC (conformers **I** and **II**).

Nº	Definition [a]	Approximate description	Symmetry
S_1	$\nu(C_{17}–C_{18})$	$\nu(C–C_\alpha)$	A´
S_2	$\nu(C_{18}=O_{19})$	$\nu(C=O)$	A´
S_3	$\nu(C_{18}–O_{20})$	$\nu(C–O)$	A´
S_4	$\nu(O_{20}–C_{21})$	$\nu(O–CH_3)$	A´
S_5	$\nu(C_{21}–H_{23})+\nu(C_{21}–H_{24})+\nu(C_{21}–H_{22})$	νCH_3 s	A´
S_6	$2\nu(C_{21}–H_{23})–\nu(C_{21}–H_{24})–\nu(C_{21}–H_{22})$	νCH_3 as´	A´
S_7	$\nu(C_{21}–H_{24})–\nu(C_{21}–H_{22})$	νCH_3 as´´	A´´
S_8	$\nu(C_2–Cl_4)$	$\nu(C–Cl)$	A´
S_9	$\nu(C_1–C_5)$	$\nu(C–C_{IR})$	A´
S_{10}	$\delta(H_{22}–C_{21}–H_{24})+\delta(H_{23}–C_{21}–H_{24})+\delta(H_{23}–C_{21}–H_{22})–\delta(H_{23}–C_{21}–O_{20})–$ $–\delta(H_{24}–C_{21}–O_{20})–\delta(H_{22}–C_{21}–O_{20})$	δCH_3 s	A´
S_{11}	$2\delta(H_{22}–C_{21}–H_{24})–\delta(H_{23}–C_{21}–H_{24})–\delta(H_{23}–C_{21}–H_{22})$	δCH_3 as´	A´
S_{12}	$\delta(H_{23}–C_{21}–H_{24})–\delta(H_{23}–C_{21}–H_{22})$	δCH_3 as´´	A´´
S_{13}	$2\delta(H_{23}–C_{21}–O_{20})–\delta(H_{24}–C_{21}–O_{20})–\delta(H_{22}–C_{21}–O_{20})$	γCH_3´	A´
S_{14}	$\delta(H_{24}–C_{21}–O_{20})–\delta(H_{22}–C_{21}–O_{20})$	γCH_3´´	A´´
S_{15}	$\tau(H_{23}–C_{21}–O_{20}–C_{18})+\tau(H_{22}–C_{21}–O_{20}–C_{18})+\tau(H_{24}–C_{21}–O_{20}–C_{18})$	τCH_3	A´´
S_{16}	$\tau(C_2–C_1–C_5–C_{10})+\tau(O_3–C_1–C_5–H_6)+\tau(C_2–C_1–C_5–C_6)+\tau(O_3–C_1–C_5–H_{10})$	$\tau(C–C_{IR})$	A´´
S_{17}	$\tau(O_3–C_{17}–C_{18}–O_{20})+\tau(N_{16}=C_{17}–C_{18}=O_{19})+\tau(O_3–C_{17}–C_{18}=O_{19})+$ $+\tau(N_{16}=C_{17}–C_{18}–O_{20})$	$\tau(C–C_\alpha)$	A´´
S_{18}	$\tau(O_{19}=C_{18}–O_{20}–C_{21})+\tau(C_{17}–C_{18}–O_{20}–C_{21})$	$\tau(C–O)$	A´´
S_{19}	$2\delta(O_{19}=C_{18}–O_{20})–\delta(O_{19}=C_{18}–C_{17})–\delta(C_{17}–C_{18}–O_{20})$	$\delta(OCO)$	A´
S_{20}	$\delta(O_{19}=C_{18}–C_{17})–\delta(C_{17}–C_{18}–O_{20})$	$\delta(CC=O)$	A´
S_{21}	$\gamma(O_{19}=O_{20}–O_{18}–C_{17})$	$\gamma(C=O)$	A´´
S_{22}	$\nu(C_1=C_2)+\nu(C_2–N_{16})+\nu(N_{16}=C_{17})+\nu(C_{17}–O_3)+\nu(O_3–C_1)$	$\nu Ox1$	A´
S_{23}	$3\nu(C_1=C_2)+3\nu(C_2–N_{16})–2\nu(N_{16}=C_{17})–2\nu(C_{17}–O_3)–2\nu(O_3–C_1)$	$\nu Ox2$	A´
S_{24}	$\nu(C_1=C_2)–\nu(N_{16}=C_{17})$	$\nu Ox3$	A´
S_{25}	$2\nu(C_2–N_{16})–\nu(O_3–C_1)–\nu(C_{17}–O_3)$	$\nu Ox4$	A´
S_{26}	$\nu(O_3–C_1)–\nu(C_{17}–O_3)$	$\nu Ox5$	A´
S_{27}	$\delta(N_{16}=C_{17}–C_{18})–\delta(O_3–C_{17}–C_{18})$	w(Ox–E)	A´
S_{28}	$\delta(C_2=C_1–C_5)–\delta(O_3–C_1–C_5)$	w(Ox–Ph)	A´
S_{29}	$\delta(C_{17}–O_3–C_1)–0.809\delta(N_{16}=C_{17}–O_3)–0.809\delta(O_3–C_1=C_2)+$ $+0.309\delta(C_2–N_{16}=C_{17})+0.309\delta(C_1=C_2–N_{16})$	$\delta Ox1$	A´
S_{30}	$–1.118\delta(N_{16}=C_{17}–O_3)+1.118\delta(O_3–C_1=C_2)+1.809\delta(C_2–N_{16}=C_{17})–$ $–1.809\delta(C_1=C_2–C_{16})$	$\delta Ox2$	A´
S_{31}	$\tau(C_1=C_2–N_{16}=C_{17})–0.809\tau(O_3–C_1=C_2–N_{16})–0.809\tau(C_2–N_{16}=C_{17}–O_3)+$ $+0.309\tau(C_{17}–O_3–C_1=C_2)+$ $+0.309\tau(N_{16}=C_{17}–O_3–C_1)$	$\tau Ox1$	A´´
S_{32}	$1.118\tau(O_3–C_1=C_2–N_{16})–1.118\tau(N_{16}–C_2=C_1–O_3)–1.809\tau(C_1–O_3–C_{17}=N_{16})+$ $+1.809\tau(C_2=C_1–O_3–C_{17})$	$\tau Ox2$	A´´
S_{33}	$\nu(C_5–C_6)+\nu(C_6–C_7)+\nu(C_7–C_8)+\nu(C_8–C_9)+\nu(C_9–C_{10})+\nu(C_{10}–C_5)$	$\nu Ph1$	A´
S_{34}	$\nu(C_5–C_6)+\nu(C_7–C_8)–\nu(C_8–C_9)–\nu(C_{10}–C_5)$	$\nu Ph2$	A´
S_{35}	$–\nu(C_5–C_6)+2\nu(C_6–C_7)–\nu(C_7–C_8)–\nu(C_8–C_9)+2\nu(C_9–C_{10})–\nu(C_{10}–C_5)$	$\nu Ph3$	A´
S_{36}	$\nu(C_5–C_6)–\nu(C_7–C_8)+\nu(C_8–C_9)–\nu(C_{10}–C_5)$	$\nu Ph4$	A´
S_{37}	$\nu(C_5–C_6)–\nu(C_7–C_8)–\nu(C_8–C_9)+\nu(C_{10}–C_5)$	$\nu Ph5$	A´
S_{38}	$\nu(C_6–C_7)–\nu(C_9–C_{10})$	$\nu Ph6$	A´
S_{39}	$\nu(C_6–H_{11})$	$\nu(C–H1)$	A´
S_{40}	$\nu(C_8–H_{13})+\nu(C_7–H_{12})+\nu(C_9–H_{14})$	$\nu(C–H2)$	A´
S_{41}	$\nu(C_7–H_{12})–\nu(C_9–H_{14})$	$\nu(C–H3)$	A´
S_{42}	$2\nu(C_8–H_{13})–\nu(C_7–H_{12})–\nu(C_9–H_{14})$	$\nu(C–H4)$	A´
S_{43}	$\nu(C_{10}–H_{15})$	$\nu(C–H5)$	A´
S_{44}	$\delta(C_6–C_5–C_{10})–\delta(C_5–C_{10}–C_9)+\delta(C_{10}–C_9–C_8)–\delta(C_9–C_8–C_7)+$ $+\delta(C_8–C_7–C_6)–\delta(C_7–C_6–C_5)$	$\delta Ph1$	A´
S_{45}	$\delta(C_5–C_{10}–C_9)–\delta(C_{10}–C_9–C_8)+\delta(C_8–C_7–C_6)–\delta(C_7–C_6–C_5)$	$\delta Ph2$	A´
S_{46}	$2\delta(C_6–C_5–C_{10})–\delta(C_5–C_{10}–C_9)–\delta(C_{10}–C_9–C_8)+2\delta(C_9–C_8–C_7)–$ $–\delta(C_8–C_7–C_6)–\delta(C_7–C_6–C_5)$	$\delta Ph3$	A´
S_{47}	$\tau(C_6–C_5–C_{10}–C_9)+\tau(C_6–C_5–C_{10}–H_{15})+\tau(C_1–C_5–C_{10}–C_9)+\tau(C_1–C_5–C_{10}–H_{15})–$ $–\tau(C_1–C_5–C_{10}–H_{15})–\tau(C_5–C_{10}–C_9–C_8)–\tau(C_5–C_{10}–C_9–H_{14})–\tau(H_{15}–C_{10}–C_9–C_8)–$	$\tau Ph1$	A´´

	$-\tau(H_{15}-C_{10}-C_9-H_{14})+\tau(C_{10}-C_9-C_8-C_7)+\tau(C_{10}-C_9-C_8-H_{13})+\tau(H_{14}-C_9-C_8-C_7)+$ $+\tau(H_{14}-C_9-C_8-H_{13})-\tau(C_9-C_8-C_7-C_6)-\tau(C_9-C_8-C_7-H_{12})-\tau(H_{13}-C_8-C_7-C_6)-$ $-\tau(H_{13}-C_8-C_7-H_{12})+\tau(C_8-C_7-C_6-C_5)+\tau(C_8-C_7-C_6-H_{11})+\tau(H_{12}-C_7-C_6-C_5)+$ $+\tau(H_{12}-C_7-C_6-H_{11})-\tau(C_7-C_6-C_5-C_{10})-\tau(C_7-C_6-C_5-C_1)-\tau(H_{11}-C_6-C_5-C_{10})-$ $-\tau(H_{11}-C_6-C_5-C_1)$		
S_{48}	$\tau(C_6-C_5-C_{10}-C_9)+\tau(C_6-C_5-C_{10}-H_{15})+\tau(C_1-C_5-C_{10}-C_9)+\tau(C_1-C_5-C_{10}-H_{15})-$ $-\tau(C_{10}-C_9-C_8-C_7)-\tau(C_{10}-C_9-C_8-H_{13})-\tau(H_{14}-C_9-C_8-C_7)-\tau(H_{14}-C_9-C_8-H_{13})+$ $+\tau(C_9-C_8-C_7-C_6)+\tau(C_9-C_8-C_7-H_{12})+\tau(H_{13}-C_8-C_7-C_6)+\tau(H_{13}-C_8-C_7-H_{12})-$ $-\tau(C_7-C_6-C_5-C_{10})-\tau(C_7-C_6-C_5-C_1)-\tau(H_{11}-C_6-C_5-C_{10})-\tau(H_{11}-C_6-C_5-C_1)$	τPh2	A´´
S_{49}	$-\tau(C_6-C_5-C_{10}-C_9)-\tau(C_6-C_5-C_{10}-H_{15})-\tau(C_1-C_5-C_{10}-C_9)-\tau(C_1-C_5-C_{10}-H_{15})+$ $+2\tau(C_5-C_{10}-C_9-C_8)+2\tau(C_5-C_{10}-C_9-H_{14})+2\tau(H_{15}-C_{10}-C_9-C_8)+2\tau(H_{15}-C_{10}-C_9-H_{14})-$ $-\tau(C_{10}-C_9-C_8-C_7)-\tau(C_{10}-C_9-C_8-H_{13})-\tau(H_{14}-C_9-C_8-C_7)-\tau(H_{14}-C_9-C_8-H_{13})-$ $-\tau(C_9-C_8-C_7-C_6)-\tau(C_9-C_8-C_7-H_{12})-\tau(H_{13}-C_8-C_7-C_6)-\tau(H_{13}-C_8-C_7-H_{12})+$ $+2\tau(C_8-C_7-C_6-C_5)+2\tau(C_8-C_7-C_6-H_{11})+2\tau(H_{12}-C_7-C_6-C_5)+2\tau(H_{12}-C_7-C_6-H_{11})-$ $-\tau(C_7-C_6-C_5-C_{10})-\tau(C_7-C_6-C_5-C_1)-\tau(H_{11}-C_6-C_5-C_{10})-\tau(H_{11}-C_6-C_5-C_1)$	τPh3	A´´
S_{50}	$\delta(C_{10}-C_5-C_1)-\delta(C_6-C_5-C_1)$	w(Ph–Ox)	A´
S_{51}	$\gamma(C_1-C_6-C_5-C_{10})$	γ(Ph–Ox)	A´´
S_{52}	$\delta(H_{11}-C_6-C_5)-\delta(H_{11}-C_6-C_7)+\delta(H_{12}-C_7-C_6)-\delta(H_{12}-C_7-C_8)+\delta(H_{13}-C_8-C_7)-$ $-\delta(H_{13}-C_8-C_9)+\delta(H_{14}-C_9-C_8)-\delta(H_{14}-C_9-C_{10})+\delta(H_{15}-C_{10}-C_9)-\delta(H_{15}-C_{10}-C_5)$	δ(C–H1)	A´
S_{53}	$\delta(H_{11}-C_6-C_5)-\delta(H_{11}-C_6-C_7)+\delta(H_{12}-C_7-C_6)-\delta(H_{12}-C_7-C_8)-\delta(H_{14}-C_9-C_8)+$ $+\delta(H_{14}-C_9-C_{10})+\delta(H_{15}-C_{10}-C_9)+\delta(H_{15}-C_{10}-C_5)$	δ(C–H2)	A´
S_{54}	$\delta(H_{11}-C_6-C_5)-\delta(H_{11}-C_6-C_7)-2\delta(H_{13}-C_8-C_7)+2\delta(H_{13}-C_8-C_9)+\delta(H_{15}-C_{10}-C_9)-$ $-\delta(H_{15}-C_{10}-C_5)$	δ(C–H3)	A´
S_{55}	$\delta(H_{11}-C_6-C_5)-\delta(H_{11}-C_6-C_7)-\delta(H_{12}-C_7-C_6)+\delta(H_{12}-C_7-C_8)+\delta(H_{14}-C_9-C_8)-$ $-\delta(H_{14}-C_9-C_{10})+-\delta(H_{15}-C_{10}-C_9)+\delta(H_{15}-C_{10}-C_5)$	δ(C–H4)	A´
S_{56}	$2\delta(H_{11}-C_6-C_5)-2\delta(H_{11}-C_6-C_7)-3\delta(H_{12}-C_7-C_6)+3\delta(H_{12}-C_7-C_8)+2\delta(H_{13}-C_8-C_7)-$ $-2\delta(H_{13}-C_8-C_9)-3\delta(H_{14}-C_9-C_8)+3\delta(H_{14}-C_9-C_{10})+2\delta(H_{15}-C_{10}-C_9)-2\delta(H_{15}-C_{10}-C_5)$	δ(C–H5)	A´
S_{57}	$\gamma(H_{11}-C_5-C_6-C_7)+\gamma(H_{12}-C_6-C_7-C_8)+\gamma(H_{13}-C_7-C_8-C_9)+\gamma(H_{14}-C_8-C_9-C_{10})+$ $+\gamma(H_{15}-C_9-C_{10}-C_5)$	γ(C–H1)	A´´
S_{58}	$\gamma(H_{11}-C_5-C_6-C_7)+\gamma(H_{12}-C_6-C_7-C_8)-\gamma(H_{14}-C_8-C_9-C_{10})-\gamma(H_{15}-C_9-C_{10}-C_5)$	γ(C–H2)	A´´
S_{59}	$\gamma(H_{11}-C_5-C_6-C_7)-2\gamma(H_{13}-C_7-C_8-C_9)+\gamma(H_{15}-C_9-C_{10}-C_5)$	γ(C–H3)	A´´
S_{60}	$\gamma(H_{11}-C_5-C_6-C_7)-\gamma(H_{12}-C_6-C_7-C_8)+\gamma(H_{14}-C_8-C_9-C_{10})-\gamma(H_{15}-C_9-C_{10}-C_5)$	γ(C–H4)	A´´
S_{61}	$2\gamma(H_{11}-C_5-C_6-C_7)-3\gamma(H_{12}-C_6-C_7-C_8)+2\gamma(H_{13}-C_7-C_8-C_9)-3\gamma(H_{14}-C_8-C_9-C_{10})$ $+2\gamma(H_{15}-C_9-C_{10}-C_5)$	γ(C–H5)	A´´
S_{62}	$\gamma(Cl_4-C_1=C_2-N_{16})$	γ(C–Cl)	A´´
S_{63}	$\gamma(C_5-C_2=C_1-O_3)$	γ(Ox–Ph)	A´´
S_{64}	$\gamma(C_{18}-N_{16}=C_{17}-O_3)$	γ(Ox–E)	A´´
S_{65}	$\delta(Cl_4-C_2-N_{16})-\delta(C_1=C_2-Cl_4)$	w(C–Cl)	A´
S_{66}	$\delta(C_{21}-O_{20}-C_{18})$	$\delta(C-O-CH_3)$	A´

[a] Normalization factors not shown. ν, bond stretching; δ, bending; γ, rocking; w, wagging; τ, torsion; IR, inter–ring; Ox, oxazole ring; Ph, phenyl ring; E, ester group. See Figure 1 for atom numbering.

Table S4 (Supporting Information): Calculated [scaled, DFT(B3LYP)/6–311++G(d,p)] wavenumbers, IR and Raman intensities and Potential Energy Distributions (PED) for conformer **I** of MCPOC. [a]

Approximate description	Symmetry	Wavenumber [b]	Infrared Intensity	Raman Intensity	PED [c]
ν(C–H1)	A´	3168	1.9	8.2	$S_{39}(96)$
ν(C–H5)	A´	3153	2.5	11.6	$S_{43}(88)$
ν(C–H2)	A´	3138	17.5	35.5	$S_{40}(91)$
ν(C–H3)	A´	3127	10.8	18.4	$S_{41}(95)$
ν(C–H4)	A´	3117	0.2	7.4	$S_{42}(98)$
νCH_3 as´	A´	3113	11.5	12.9	$S_6(97)$
νCH_3 as´´	A´´	3075	16.3	9.3	$S_7(100)$
νCH_3 s	A´	3003	35.9	38.6	$S_5(97)$
ν(C=O)	A´	1750	265.1	147.0	$S_2(86)$
νPh3	A´	1616	1.1	430.1	$S_{35}(65)$, $S_{55}(22)$, $S_{46}(10)$
νPh4	A´	1589	5.7	24.4	$S_{36}(65)$, $S_{54}(16)$
νOx3	A´	1561	33.9	205.7	$S_{24}(65)$, $S_9(13)$
νOx1	A´	1526	112.5	890.2	$S_{22}(21)$, $S_{23}(17)$, $S_{53}(14)$, $S_9(11)$
δ(C–H2)	A´	1487	87.0	224.6	$S_{53}(43)$, $S_{37}(18)$
δCH_3 as´	A´	1471	20.5	16.3	$S_{11}(81)$, $S_{13}(10)$
δCH_3 as´´	A´´	1459	10.4	9.2	$S_{12}(93)$
δ(C–H3)	A´	1452	57.5	128.4	$S_{38}(21)$, $S_{54}(22)$, $S_{52}(13)$
δCH_3 s	A´	1447	6.7	14.8	$S_{10}(77)$
δ(C–H1)	A´	1351	61.4	114.3	$S_{52}(50)$, $S_{25}(10)$
νPh2	A´	1337	65.8	20.7	$S_{52}(24)$, $S_{38}(16)$, $S_{34}(15)$
νOx2; $\nu(C–C_\alpha)$	A´	1308	233.8	26.3	$S_{34}(29)$, $S_1(10)$, $S_{23}(10)$
νOx4	A´	1275	88.5	91.1	$S_{34}(18)$, $S_{25}(17)$, $S_{30}(13)$
$\nu C\text{-}C_{IR}$	A´	1215	1.9	219.5	$S_{25}(43)$, $S_{23}(16)$, $S_9(11)$
ν(C–O), γCH3´	A´	1203	299.6	73.4	$S_{13}(38)$, $S_3(26)$
δ(C–H4)	A´	1194	15.1	48.6	$S_{55}(73)$, $S_{35}(23)$
γCH_3´, ν(C–O)	A´	1169	209.0	12.0	$S_{13}(35)$, $S_3(14)$
δ(C–H5)	A´	1167	8.8	15.5	$S_{56}(68)$, $S_{54}(11)$
γCH_3´´	A´´	1151	0.8	2.7	$S_{14}(92)$
νOx5	A´	1112	15.6	92.4	$S_{26}(34)$, $S_{54}(14)$, $S_{38}(12)$
νPh6	A´	1082	23.8	58.7	$S_{26}(20)$, $S_{38}(25)$, $S_{54}(19)$, $S_{34}(11)$
νPh5	A´	1036	7.6	8.4	$S_{37}(54)$, $S_{53}(22)$, $S_{33}(14)$
δOx1	A´	1007	50.8	66.9	$S_{29}(29)$, $S_4(23)$, $S_{22}(12)$
δPh1	A´	999	1.6	86.1	$S_{44}(71)$, $S_{33}(25)$
γ(C–H5)	A´´	984	0.1	0.6	$S_{61}(61)$, $S_{47}(28)$
νPh1	A´	982	19.6	83.1	$S_{33}(35)$, $S_{30}(23)$
γ(C–H4)	A´´	973	0.1	0.0	$S_{60}(69)$, $S_{49}(26)$
$\nu(O–CH_3)$	A´	954	5.9	59.2	$S_4(51)$, $S_{29}(15)$, $S_{30}(13)$
γ(C–H3)	A´´	922	2.3	0.0	$S_{59}(75)$, $S_{48}(13)$
γ(C–H2)	A´´	842	0.1	0.1	$S_{58}(99)$
δ(OCO)	A´	813	17.1	8.6	$S_{19}(33)$, $S_3(19)$, $S_{66}(13)$
γ(C=O)	A´´	786	5.5	2.3	$S_{21}(62)$, $S_{64}(21)$, $S_{32}(10)$
γ(C–H1)	A´´	762	34.7	6.1	$S_{57}(54)$, $S_{51}(23)$
δPh3	A´	693	11.1	8.4	$S_{46}(52)$, $S_9(11)$
τOx1	A´´	685	34.6	2.6	$S_{57}(29)$, $S_{31}(23)$, $S_{47}(11)$, $S_{63}(13)$
τPh1	A´´	682	7.1	0.9	$S_{47}(36)$, $S_{31}(27)$, $S_{62}(17)$
τOx2	A´´	654	23.4	0.1	$S_{32}(50)$, $S_{21}(22)$, $S_{31}(15)$
δPh2	A´	623	<0.1	10.6	$S_{45}(86)$
w(Ox–Ph)	A´	588	0.7	1.0	$S_{28}(24)$, $S_{27}(23)$, $S_{65}(17)$, $S_{20}(11)$
ν(C–Cl)	A´	556	2.4	5.1	$S_8(36)$, $S_1(12)$, $S_{29}(11)$
γ(Ph–Ox)	A´´	495	3.4	1.7	$S_{51}(39)$, $S_{48}(18)$
δ(CC=O)	A´	429	2.0	2.1	$S_{46}(18)$, $S_{20}(21)$, $S_9(11)$
τPh3	A´´	399	<0.1	0.1	$S_{49}(72)$, $S_{60}(28)$
δOx2	A´	366	3.5	13.4	$S_8(27)$, $S_{30}(18)$, $S_1(12)$, $S_{19}(11)$
γ(C–Cl)	A´´	339	1.3	5.9	$S_{62}(32)$, $S_{64}(20)$, $S_{48}(18)$, $S_{63}(16)$
$\delta(C–O–CH_3)$	A´	309	18.3	6.8	$S_{66}(55)$

$\nu(C–C_\alpha)$, w(Ph–Ox)	A´	267	0.3	8.5	$S_{50}(26)$, $S_1(12)$
w(C–Cl)	A´	230	3.3	11.4	$S_{65}(35)$, $S_{20}(12)$
τPh2	A´´	230	1.8	8.9	$S_{48}(23)$, $S_{62}(17)$, $S_{32}(16)$, $S_{31}(12)$, $S_{63}(11)$
τ(C–O)	A´´	186	1.8	0.2	$S_{18}(44)$, $S_{62}(21)$
w(Ph–Ox)	A´	141	0.6	18.5	$S_{28}(27)$, $S_{65}(23)$, $S_{27}(13)$, $S_{50}(13)$, $S_{20}(12)$
τCH_3	A´´	127	0.1	4.0	$S_{15}(73)$
γ(Ox–Ph)	A´´	114	1.5	13.0	$S_{18}(29)$, $S_{15}(18)$, $S_{63}(14)$, $S_{48}(12)$
w(Ox–E)	A´	80	1.7	32.5	$S_{27}(36)$, $S_{28}(28)$, $S_{50}(13)$, $S_{20}(12)$
γ(Ox–E)	A´´	69	<0.1	12.7	$S_{64}(36)$, $S_{63}(13)$, $S_{17}(13)$, $S_{18}(12)$
$\tau(C–C_\alpha)$	A´´	41	2.7	5.6	$S_{17}(75)$, $S_{63}(12)$
$\tau(C–C_{IR})$	A´´	21	<0.1	193.8	$S_{16}(99)$

[a] Wavenumbers in cm^{-1}; infrared intensities in km mol^{-1}; Raman intensities were calculated from the Raman activities produced by Gaussian as described in the text and then normalized to the most intense band among those of conformers **I** and **II**: νOx1 in form **II** (1529 cm^{-1}; see Table S5); ν, bond stretching; δ, bending; γ, rocking; w, wagging; τ, torsion; s, symmetric; as, asymmetric; IR, inter–ring; Ox, oxazole ring; Ph, phenyl ring; E, ester. See Table S3 for definition of internal coordinates and Figure 1 for atom numbering. [b] Scaled (0.9835). [c] Only PED values greater than 10 % are given.

Table S5 (Supporting Information): Calculated [scaled, DFT(B3LYP)/6–311++G(d,p)] wavenumbers, IR and Raman intensities and Potential Energy Distributions (PED) for conformer **II** of MCPOC. [a]

Approximate description	Symmetry	Wavenumber [b]	Infrared Intensity	Raman Intensity	PED [c]
ν(C–H1)	A´	3169	1.8	8.2	S_{39}(96)
ν(C–H5)	A´	3153	2.9	11.9	S_{43}(88)
ν(C–H2)	A´	3138	17.5	35.0	S_{40}(91)
ν(C–H3)	A´	3126	10.6	18.4	S_{41}(94)
ν(C–H4)	A´	3116	0.4	7.5	S_{42}(98)
νCH_3 as´	A´	3112	10.0	9.0	S_6(97)
νCH_3 as´´	A´´	3077	15.2	10.1	S_7(100)
νCH_3 s	A´	3004	34.0	34.9	S_5(97)
ν(C=O)	A´	1764	430.3	157.5	S_2(88)
νPh3	A´	1616	1.1	417.7	S_{35}(65), S_{55}(22), S_{46}(10)
νPh4	A´	1589	4.4	24.4	S_{36}(65), S_{54}(16)
νOx3	A´	1564	8.9	133.7	S_{24}(68)
νOx1	A´	1529	101.3	1000.0	S_{22}(21), S_{23}(16), S_{53}(14), S_9(13)
δ(C–H2)	A´	1487	86.7	213.6	S_{53}(44), S_{37}(19)
δCH_3 as´	A´	1472	9.3	22.6	S_{11}(81), S_{13}(10)
δCH_3 as´´	A´´	1459	10.2	8.0	S_{12}(93)
δ(C–H3)	A´	1452	46.3	123.0	S_{54}(23), S_{38}(22), S_{52}(14)
δCH_3 s	A´	1446	4.8	14.6	S_{10}(82)
δ(C–H1)	A´	1347	2.0	64.9	S_{52}(70)
νPh2	A´	1329	4.4	42.5	S_{34}(30), S_{38}(19)
νOx2, ν(C–C_α)	A´	1294	271.4	14.8	S_{23}(27), S_{34}(15), S_1(17), S_3(11)
νOx4	A´	1276	127.3	103.9	S_{25}(19), S_{34}(18), S_{30}(12)
ν(C–C_{IR})	A´	1219	0.5	142.6	S_{25}(37), S_9(11)
γCH_3´, ν(C–O)	A´	1196	156.9	107.5	S_{13}(45), S_3(18)
δ(C–H4)	A´	1193	14.7	71.5	S_{55}(68), S_{35}(22)
δ(C–H5)	A´	1167	0.1	10.5	S_{56}(70), S_{54}(10)
ν(C–O), γCH_3´	A´	1158	189.1	44.5	S_{13}(22), S_3(20), S_{22}(11), S_{19}(11)
γCH_3´´	A´´	1152	0.9	2.6	S_{14}(92)
νOx5	A´	1108	20.7	57.6	S_{26}(33), S_{54}(16), S_{38}(14)
νPh6	A´	1080	18.6	60.2	S_{38}(22), S_{26}(25), S_{54}(17), S_{34}(10)
νPh5	A´	1036	15.3	8.2	S_{37}(53), S_{53}(22), S_{33}(14)
δOx1	A´	1014	72.4	46.4	S_4(39), S_{29}(20), S_{22}(10)
δPh1	A´	999	1.4	81.8	S_{44}(71), S_{33}(25)
γ(C–H5)	A´´	981	<0.1	0.5	S_{61}(63), S_{47}(29)
νPh1	A´	981	31.6	86.9	S_{33}(35), S_{30}(26)
γ(C–H4)	A´´	972	0.2	0.0	S_{60}(72), S_{49}(28)
ν(O–CH_3)	A´	947	9.1	68.1	S_4(41), S_{29}(23)
γ(C–H3)	A´´	920	2.2	0.0	S_{59}(76), S_{48}(13)
γ(C–H2)	A´´	841	<0.1	0.1	S_{58}(100)
δ(OCO)	A´	809	19.9	7.1	S_{19}(32), S_3(21), S_{66}(13)
γ(C=O)	A´´	780	5.9	2.3	S_{21}(63), S_{64}(20)
γ(C–H1)	A´´	760	36.9	6.0	S_{57}(56), S_{51}(23)
δPh3	A´	693	9.6	8.4	S_{46}(51), S_9(11)
τOx1	A´´	683	28.0	2.9	S_{31}(29), S_{57}(26), S_{63}(17)
τPh1	A´´	681	11.9	0.3	S_{47}(43), S_{61}(21), S_{31}(17)
τOx2	A´´	653	22.3	0.1	S_{32}(48), S_{21}(23), S_{31}(18)
δPh2	A´	623	<0.1	10.8	S_{45}(84)
w(Ox–Ph)	A´	592	2.5	4.3	S_{28}(24), S_{27}(18), S_{65}(12)
ν(C–Cl)	A´	537	0.4	2.7	S_8(35)
γ(Ph–Ox)	A´´	496	3.7	1.7	S_{51}(39), S_{48}(17)
δ(CC=O)	A´	450	2.5	3.7	S_{20}(22), S_{46}(14), S_{30}(11)
τPh3	A´´	398	<0.1	0.1	S_{49}(72), S_{60}(28)

δOx2	A´	347	10.4	14.5	S_{66}(24), S_{8}(18), S_{30}(12), S_{20}(12)
γ(C–Cl)	A´´	336	1.1	5.1	S_{48}(18), S_{62}(32), S_{64}(20), S_{63}(16)
δ(C–O–CH_3)	A´	303	3.0	5.6	S_{66}(17), S_{19}(22)
ν(C–$C_α$), δ(C–O–CH_3)	A´	286	4.5	4.1	S_{66}(22), S_{9}(13), S_{1}(12), S_{50}(11)
τPh2	A´´	229	1.7	10.0	S_{48}(23), S_{32}(16), S_{62}(16), S_{31}(12), S_{63}(11)
w(C–Cl)	A´	225	1.7	22.0	S_{65}(41), S_{20}(12), S_{50}(17)
τ(C–O)	A´´	187	2.0	0.3	S_{18}(49), S_{62}(21)
w(Ph–Ox)	A´	146	0.4	9.6	S_{28}(26), S_{65}(23), S_{27}(15), S_{50}(14), S_{20}(11)
τCH_3	A´´	132	0.1	4.0	S_{15}(62)
γ(Ox–Ph)	A´´	112	0.8	9.9	S_{15}(31), S_{18}(25), S_{63}(11)
w(Ox–E)	A´	77	0.6	43.6	S_{27}(36), S_{28}(29), S_{20}(13), S_{50}(12)
γ(Ox–E)	A´´	68	0.1	10.1	S_{64}(33), S_{63}(23), S_{18}(10)
τ(C–$C_α$)	A´´	41	1.9	8.2	S_{17}(87)
τ(C–C_{IR})	A´´	10	0.1	425.7	S_{16}(100)

[a] Wavenumbers in cm^{-1}; infrared intensities in km mol^{-1}; Raman intensities were calculated from the Raman activities produced by Gaussian as described in the text and then normalized to the most intense band among those of conformers **I** and **II**: νOx1 in form **II** (1529 cm^{-1}); ν, bond stretching; δ, bending; γ, rocking; w, wagging; τ, torsion; s, symmetric; as, asymmetric; IR, inter-ring; Ox, oxazole ring; Ph, phenyl ring; E, ester. See Table S3 for definition of internal coordinates and Figure 1 for atom numbering. [b] Scaled (0.9835). [c] Only PED values greater than 10 % are given.

J. Phys. Chem. A, **2011**, *115*, 1199-1209.

Supporting Information

for

Photochemistry and Vibrational Spectra of Matrix-Isolated Methyl 4-Chloro-5-phenylisoxazole-3-carboxylate

Susy Lopes,[a] Cláudio M. Nunes,[a] Andrea Gómez-Zavaglia,[a,b]

Teresa M.V.D. Pinho e Melo[a] and Rui Fausto[a]

[a] *Department of Chemistry, University of Coimbra, P-3004-535 Coimbra, Portugal*
[b] *Centro de Investigación y Desarrollo en Criotecnología de Alimentos (Conicet La Plata, UNLP) RA-1900, Argentina*

Contents

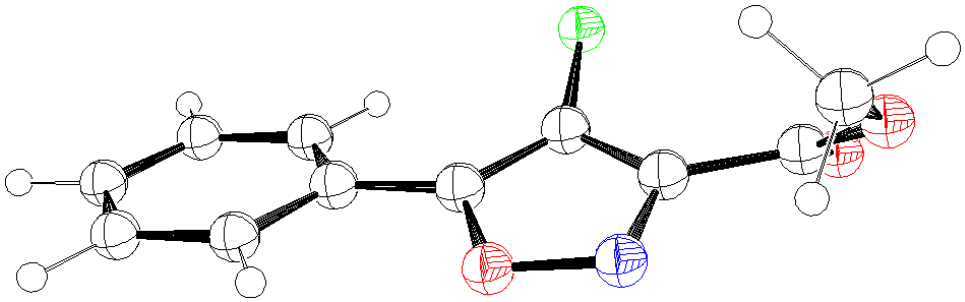

IV (29.3)

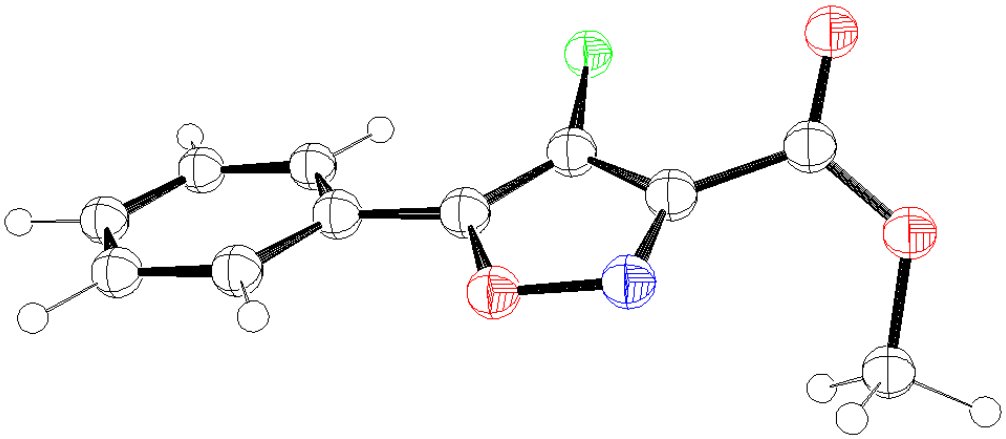

V (29.8)

Figure S1. High energy conformers of MCPIC, optimized at the DFT(B3LYP)/6-311++G(d,p) level of theory. Relative energies (to the most stable conformer, **I**), including zero point corrections (ΔE^o/ kJ mol^{-1}) are given in parenthesis. The values of dipole moments (□) for these conformers are: 5.07 and 5.12 D (1 D= 3.33564 x 10^{-30} C m), respectively. The picture was made using the Ortep-3 for Windows program (Farrugia, L. J. *J. Appl. Cryst*. 1997, **30**, 565). Atoms color code: carbon, hydrogen: black; nitrogen: blue; chlorine: green; oxygen: red.

Table S1 - Calculated bond lengths (pm) and angles (º) for the three most stable conformers of MCPIC.[a]

Parameter	I	II	III	Parameter	I	II	III
Bond lengths				*Bond angles*			
C_1C_2	137.3	137.3	137.3	$C_{17}C_{18}C_{19}$	120.4	120.4	120.5
C_1O_5	135.7	135.6	135.7	$C_{17}C_{18}H_{23}$	120.1	120.1	120.1
C_1C_{14}	146.1	146.1	146.1	$C_{19}C_{18}H_{23}$	119.5	119.5	119.4
C_2C_3	142.8	142.8	142.9	$C_{14}C_{19}C_{18}$	120.2	120.2	120.2
C_2Cl_{13}	172.3	172.6	172.6	$C_{14}C_{19}H_{24}$	120.2	120.2	120.2
C_3N_4	131.3	131.2	131.3	$C_{18}C_{19}H_{24}$	119.6	119.6	119.5
C_3C_6	149.3	149.7	149.7	*Dihedrals*			
N_4O_5	138.0	138.0	137.9	$O_5C_1C_2C_3$	-0.2	-0.5	0.4
C_6O_7	120.6	120.2	120.2	$O_5C_1C_2Cl_{13}$	-177.6	-176.7	-179.6
C_6O_8	133.7	134.2	134.2	$C_{14}C_1C_2C_3$	178.5	178.1	179.4
O_8C_9	144.2	144.2	144.2	$C_{14}C_1C_2Cl_{13}$	1.2	2.0	-0.6
C_9H_{10}	109.1	109.1	109.0	$C_2C_1O_5N_4$	0.3	0.7	-0.5
C_9H_{11}	109.1	109.0	109.1	$C_{14}C_1O_5N_4$	-178.7	-178.3	-179.8
C_9H_{12}	108.7	108.7	108.7	$C_2C_1C_{14}C_{15}$	-160.2	-159.5	-163.0
$C_{14}C_{15}$	140.5	140.5	140.6	$C_2C_1C_{14}C_{19}$	20.3	21.1	17.5
$C_{14}C_{19}$	140.4	140.3	140.4	$O_5C_1C_{14}C_{15}$	18.5	19.0	16.0
$C_{15}C_{16}$	139.0	139.0	138.9	$O_5C_1C_{14}C_{19}$	-161.0	-160.4	-163.5
$C_{15}H_{20}$	108.2	108.2	108.2	$C_1C_2C_3N_4$	0.1	0.2	-0.2
$C_{16}C_{17}$	139.5	139.5	139.5	$C_1C_2C_3C_6$	179.1	-179.3	179.7
$C_{16}H_{21}$	108.4	108.4	108.4	$Cl_{13}C_2C_3N_4$	177.5	176.4	179.8
$C_{17}C_{18}$	139.4	139.4	139.3	$Cl_{13}C_2C_3C_6$	-3.5	-3.2	-0.3
$C_{17}H_{22}$	108.4	108.4	108.4	$C_2C_3N_4O_5$	0.1	0.2	-0.1
$C_{18}C_{19}$	139.1	139.1	139.1	$C_6C_3N_4O_5$	-179.0	179.8	180.0
$C_{18}H_{23}$	108.4	108.4	108.4	$C_2C_3C_6O_7$	-10.8	153.7	-156.1
$C_{19}H_{24}$	108.1	108.1	108.1	$C_2C_3C_6O_8$	169.3	-26.9	24.5
Bond angles				$N_4C_3C_6O_7$	168.1	-25.8	23.8
$C_2C_1O_5$	107.5	107.5	107.4	$N_4C_3C_6O_8$	-11.7	153.6	-155.7
$C_2C_1C_{14}$	136.0	136.0	136.3	$C_3N_4O_5C_1$	-0.3	-0.5	0.4
$O_5C_1C_{14}$	116.5	116.5	116.3	$C_3C_6O_8C_9$	178.6	179.8	-179.9
$C_1C_2C_3$	104.9	104.9	104.9	$O_7C_6O_8C_9$	-1.2	-0.8	0.6
$C_1C_2Cl_{13}$	128.0	127.6	127.7	$C_6O_8C_9H_{10}$	-60.5	-59.7	-61.0
$C_3C_2Cl_{13}$	127.1	127.4	127.4	$C_6O_8C_9H_{11}$	60.4	61.1	59.8
$C_2C_3N_4$	111.1	111.0	110.9	$C_6O_8C_9H_{12}$	180.0	-179.3	179.4
$C_2C_3C_6$	127.8	131.2	131.5	$C_1C_{14}C_{15}H_{16}$	-179.8	-179.7	-179.8
$N_4C_3C_6$	121.1	117.8	117.6	$C_1C_{14}C_{15}H_{20}$	0.4	0.5	0.3
$C_3N_4O_5$	105.8	105.9	105.9	$C_{19}C_{14}C_{15}C_{16}$	-0.3	-0.3	-0.3
$C_1O_5N_4$	110.8	110.8	110.9	$C_{19}C_{14}C_{15}H_{20}$	179.9	179.9	179.8
$C_3C_6O_7$	123.3	124.3	124.2	$C_{19}C_{14}C_1O_5$	-161.0	-160.4	-163.5
$C_3C_6O_8$	111.8	110.7	110.9	$C_1C_{14}C_{19}C_{18}$	179.8	179.7	179.7
$O_7C_6O_8$	124.9	124.9	124.9	$C_1C_{14}C_{19}H_{24}$	0.4	0.3	0.3
$C_6O_8C_9$	115.8	115.8	115.8	$C_{15}C_{14}C_{19}C_{18}$	0.3	0.3	0.2
$O_8C_9H_{10}$	110.3	110.2	110.2	$C_{15}C_{14}C_{19}H_{24}$	-179.1	-179.0	-179.2
$O_8C_9H_{11}$	110.3	110.2	110.3	$C_{15}C_{14}C_1O_5$	18.5	19.0	15.6
$O_8C_9H_{12}$	105.2	105.3	105.3	$C_{14}C_{15}C_{16}C_{17}$	0.1	0.1	0.1
$H_{10}C_9H_{11}$	109.4	109.4	109.4	$C_{14}C_{15}C_{16}H_{21}$	-179.8	-179.8	-179.8
$H_{10}C_9H_{12}$	110.8	110.8	110.8	$H_{20}C_{15}C_{16}C_{17}$	179.9	179.9	-180.0
$H_{11}C_9H_{12}$	110.8	110.8	110.8	$H_{20}C_{15}C_{16}H_{21}$	0.0	0.0	0.1
$C_1C_{14}C_{15}$	119.4	119.3	119.2	$C_{15}C_{16}C_{17}C_{18}$	0.2	0.2	0.1
$C_1C_{14}C_{19}$	121.6	121.6	121.8	$C_{15}C_{16}C_{17}H_{22}$	-180.0	-180.0	-180.0
$C_{15}C_{14}C_{19}$	119.1	119.1	119.0	$H_{21}C_{16}C_{17}C_{18}$	-179.9	-180.0	-179.9
$C_{14}C_{15}C_{16}$	120.3	120.3	120.4	$H_{21}C_{16}C_{17}H_{22}$	-0.1	-0.1	-0.1
$C_{14}C_{15}H_{20}$	119.6	119.6	119.6	$C_{16}C_{17}C_{18}C_{19}$	-0.2	-0.2	-0.2
$C_{16}C_{15}H_{20}$	120.1	120.1	120.0	$C_{16}C_{17}C_{18}H_{23}$	179.6	179.5	179.6
$C_{15}C_{16}C_{17}$	120.3	120.3	120.3	$H_{22}C_{17}C_{18}C_{19}$	179.9	179.9	179.9
$C_{15}C_{16}H_{21}$	119.6	119.6	119.6	$H_{22}C_{17}C_{18}H_{23}$	-0.3	-0.3	-0.3
$C_{17}C_{16}H_{21}$	120.1	120.1	120.1	$C_{17}C_{18}C_{19}C_{14}$	-0.1	-0.1	0.0
$C_{16}C_{17}C_{18}$	119.7	119.7	119.7	$C_{17}C_{18}C_{19}H_{24}$	179.3	179.3	179.4
$C_{16}C_{17}H_{22}$	120.2	120.1	120.2	$H_{23}C_{18}C_{19}C_{14}$	-179.8	-179.8	-179.8
$C_{18}C_{17}H_{22}$	120.1	120.1	120.2	$H_{23}C_{18}C_{19}H_{24}$	-0.4	-0.4	-0.4

[a] See Figure 1 for atom numbering and Figure 2 for examining the position of the different minima corresponding to each conformer in the PES. The dihedral angles provided in this table correspond to those of the minima located in the 1st quadrant of Figure 2 for conformers **I** and **III** and in the 4th quadrant for conformer **II** (i.e., central valley, top right side; $C_{15}C_{14}C_1O_5$ ca. 20º).

Table S2 – Definition of internal coordinates used in the normal coordinate analysis of MCPIC.

Nº	Definition [a]	Approximate description
S_1	$\nu(C_3–C_6)$	$\nu(C–C_\alpha)$
S_2	$\nu(C_6=O_7)$	$\nu(C=O)$
S_3	$\nu(C_6–O_8)$	$\nu(C–O)$
S_4	$\nu(O_8–C_9)$	$\nu(O–CH_3)$
S_5	$\nu(C_2–Cl_{13})$	$\nu(C–Cl)$
S_6	$\nu(C_1–C_{14})$	$\nu(C–C_{IR})$
S_7	$\nu(C_9–H_{12})+\nu(C_9–H_{10})+\nu(C_9–H_{11})$	νCH_3 s
S_8	$2\nu(C_9–H_{12})–\nu(C_9–H_{10})–\nu(C_9–H_{11})$	νCH_3 as´
S_9	$\nu(C_9–H_{10})–\nu(C_9–H_{11})$	νCH_3 as´´
S_{10}	$\delta(H_{10}–C_9–H_{11})+\delta(H_{12}–C_9–H_{10})+\delta(H_{12}–C_9–H_{11})–\delta(H_{12}–C_9–O_8)–\delta(H_{10}–C_9–O_8)–$ $–\delta(H_{11}–C_9–O_8)$	δCH_3 s
S_{11}	$2\delta(H_{10}–C_9–H_{11})–\delta(H_{12}–C_9–H_{10})–\delta(H_{12}–C_9–H_{11})$	δCH_3 as´
S_{12}	$\delta(H_{12}–C_9–H_{10})–\delta(H_{12}–C_9–H_{11})$	δCH_3 as´´
S_{13}	$2\delta(H_{12}–C_9–O_8)–\delta(H_{10}–C_9–O_8)–\delta(H_{11}–C_9–O_8)$	$\gamma CH_3´$
S_{14}	$\delta(H_{10}–C_9–O_8)–\delta(H_{11}–C_9–O_8)$	$\gamma CH_3´´$
S_{15}	$\tau(H_{12}–C_9–O_8–C_6)+\tau(H_{10}–C_9–O_8–C_6)+\tau(H_{11}–C_9–O_8–C_6)$	τCH_3
S_{16}	$\tau(N_4=C_3–C_6=O_7)+\tau(C_2–C_3–C_6=O_7)+\tau(N_4=C_3–C_6–O_8)+\tau(C_2–C_3–C_6–O_8)$	$\tau(C–C_\alpha)$
S_{17}	$\tau(O_7=C_6–O_8–C_9)+\tau(C_3–C_6–O_8–C_9)$	$\tau(C–O)$
S_{18}	$\tau(C_2=C_1–C_{14}–C_{19})+\tau(O_5–C_1–C_{14}–C_{19})+\tau(C_2=C_1–C_{14}–C_{15})+\tau(O_5–C_1–C_{14}–C_{15})$	$\tau(C–C_{IR})$
S_{19}	$2\delta(O_8–C_6=O_7)–\delta(O_8–C_6–C_3)–\delta(O_7=C_6–C_3)$	$\delta(OCO)$
S_{20}	$\delta(O_8–C_6–C_3)–\delta(O_7=C_6–C_3)$	$\delta(CC=O)$
S_{21}	$\gamma(O_7=O_8–O_6–C_3)$	$\gamma(C=O)$
S_{22}	$\nu(C_1=C_2)+\nu(C_2–C_3)+\nu(C_3=N_4)+\nu(N_4–O_5)+\nu(O_5–C_1)$	νIsox1
S_{23}	$3\nu(C_1=C_2)+3\nu(C_3=N_4)–2\nu(C_2–C_3)–2\nu(N_4–O_5)–2\nu(O_5–C_1)$	νIsox2
S_{24}	$\nu(C_1=C_2)–\nu(C_3=N_4)$	νIsox3
S_{25}	$2\nu(C_2–C_3)–\nu(N_4–O_5)–\nu(O_5–C_1)$	νIsox4
S_{26}	$\nu(N_4–O_5)–\nu(O_5–C_1)$	νIsox5
	S_{27} $\delta(N_4–O_5–C_1)–0.809\delta(C_3=N_4–O_5)–0.809\delta(O_5–C_1=C_2)+0.309\delta(C_2–C_3=N_4)+$ $+0.309\delta(C_1=C_2–C_3)$	δIsox1
S_{28}	$–1.118\delta(C_3=N_4–O_5)+1.118\delta(O_5–C_1=C_2)+1.809\delta(C_2–C_3=N_4)–1.809\delta(C_1=C_2–C_3)$	δIsox2
S_{29}	$\tau(C_3–C_2=C_1–O_5)–0.809\tau(N_4=C_3–C_2=C_1)–0.809\tau(C_2=C_1–O_5–N_4)+$ $+0.309\tau(O_5–N_4=C_3–C_2)+0.309\tau(C_1–O_5–N_4=C_3)$	τIsox1
S_{30}	$1.118\tau(C_2=C_1–O_5–N_4)–1.118\tau(N_4=C_3–C_2=C_1)–1.809\tau(C_1–O_5–N_4=C_3)+$ $+1.809\tau(O_5–N_4=C_3–C_2)$	τIsox2
S_{31}	$\nu(C_{14}–C_{15})+\nu(C_{15}–C_{16})+\nu(C_{16}–C_{17})+\nu(C_{17}–C_{18})+\nu(C_{18}–C_{19})+\nu(C_{19}–C_{14})$	νPh1
S_{32}	$\nu(C_{14}–C_{15})+\nu(C_{16}–C_{17})–\nu(C_{17}–C_{18})–\nu(C_{19}–C_{14})$	νPh2
S_{33}	$–\nu(C_{14}–C_{15})+2\nu(C_{15}–C_{16})–\nu(C_{16}–C_{17})–\nu(C_{17}–C_{18})+2\nu(C_{18}–C_{19})–\nu(C_{19}–C_{14})$	νPh3
S_{34}	$\nu(C_{14}–C_{15})–\nu(C_{16}–C_{17})+\nu(C_{17}–C_{18})–\nu(C_{19}–C_{14})$	νPh4
S_{35}	$\nu(C_{14}–C_{15})–\nu(C_{16}–C_{17})–\nu(C_{17}–C_{18})+\nu(C_{19}–C_{14})$	νPh5
S_{36}	$\nu(C_{15}–C_{16})–\nu(C_{18}–C_{19})$	νPh6
S_{37}	$\nu(C_{15}–H_{20})$	$\nu(C–H1)$
S_{38}	$\nu(C_{16}–H_{21})+\nu(C_{17}–H_{22})+\nu(C_{18}–H_{23})$	$\nu(C–H2)$
S_{39}	$\nu(C_{16}–H_{21})–\nu(C_{18}–H_{23})$	$\nu(C–H3)$
S_{40}	$2\nu(C_{17}–H_{22})–\nu(C_{16}–H_{21})–\nu(C_{18}–H_{23})$	$\nu(C–H4)$
S_{41}	$\nu(C_{19}–H_{24})$	$\nu(C–H5)$
S_{42}	$\delta(C_{15}–C_{14}–C_{19})–\delta(C_{14}–C_{19}–C_{18})+\delta(C_{19}–C_{18}–C_{18})–\delta(C_{18}–C_{17}–C_{16})+$ $+\delta(C_{17}–C_{16}–C_{15})–\delta(C_{16}–C_{15}–C_{14})$	δPh1
S_{43}	$\delta(C_{15}–C_{14}–C_{19})–\delta(C_{19}–C_{18}–C_{18})+\delta(C_{17}–C_{16}–C_{15})–\delta(C_{16}–C_{15}–C_{14})$	δPh2
S_{44}	$2\delta(C_{15}–C_{14}–C_{19})–\delta(C_{14}–C_{19}–C_{18})–\delta(C_{19}–C_{18}–C_{18})+2\delta(C_{18}–C_{17}–C_{16})–$ $–\delta(C_{17}–C_{16}–C_{15})–\delta(C_{16}–C_{15}–C_{14})$	δPh3
S_{45}	$\tau(C_{15}–C_{14}–C_{19}–C_{18})+\tau(C_{15}–C_{14}–C_{19}–H_{24})+\tau(C_1–C_{14}–C_{19}–C_{18})+\tau(C_1–C_{14}–C_{19}–H_{24})–$ $–\tau(C_{14}–C_{19}–C_{18}–C_{17})–\tau(C_{14}–C_{19}–C_{18}–H_{23})–\tau(H_{24}–C_{19}–C_{18}–C_{17})–\tau(H_{24}–C_{19}–C_{18}–H_{23})+$ $+\tau(C_{19}–C_{18}–C_{17}–C_{16})+\tau(C_{19}–C_{18}–C_{17}–H_{22})+\tau(H_{23}–C_{18}–C_{17}–C_{16})+\tau(H_{23}–C_{18}–C_{17}–H_{22})–$ $–\tau(C_{18}–C_{17}–C_{16}–C_{15})–\tau(C_{18}–C_{17}–C_{16}–H_{21})–\tau(H_{22}–C_{17}–C_{16}–C_{15})–\tau(H_{22}–C_{17}–C_{16}–H_{21})+$ $+\tau(C_{17}–C_{16}–C_{15}–C_{14})+\tau(C_{17}–C_{16}–C_{15}–H_{20})+\tau(H_{21}–C_{16}–C_{15}–C_{14})+\tau(H_{21}–C_{16}–C_{15}–H_{20})–$ $–\tau(C_{16}–C_{15}–C_{14}–C_{19})–\tau(C_{16}–C_{15}–C_{14}–C_1)–\tau(H_{20}–C_{15}–C_{14}–C_{19})–\tau(H_{20}–C_{15}–C_{14}–C_1)$	τPh1

S_{46}	$\tau(C_{15}–C_{14}–C_{19}–C_{18})+\tau(C_{15}–C_{14}–C_{19}–H_{24})+\tau(C_1–C_{14}–C_{19}–C_{18})+\tau(C_1–C_{14}–C_{19}–H_{24})–$ $–\tau(C_{19}–C_{18}–C_{17}–C_{16})–\tau(C_{19}–C_{18}–C_{17}–H_{22})–\tau(H_{23}–C_{18}–C_{17}–C_{16})–\tau(H_{23}–C_{18}–C_{17}–H_{22})+$ $+\tau(C_{18}–C_{17}–C_{16}–C_{15})+\tau(C_{18}–C_{17}–C_{16}–H_{21})+\tau(H_{22}–C_{17}–C_{16}–C_{15})+\tau(H_{22}–C_{17}–C_{16}–H_{21})–$ $–\tau(C_{16}–C_{15}–C_{14}–C_{19})–\tau(C_{16}–C_{15}–C_{14}–C_1)–\tau(H_{20}–C_{15}–C_{14}–C_{19})–\tau(H_{20}–C_{15}–C_{14}–C_1)$	τPh2
S_{47}	$–\tau(C_{15}–C_{14}–C_{19}–C_{18})–\tau(C_{15}–C_{14}–C_{19}–H_{24})–\tau(C_1–C_{14}–C_{19}–C_{18})–\tau(C_1–C_{14}–C_{19}–H_{24})+$ $+2\tau(C_{14}–C_{19}–C_{18}–C_{17})+2\tau(C_{14}–C_{19}–C_{18}–H_{23})+2\tau(H_{24}–C_{19}–C_{18}–C_{17})+2\tau(H_{24}–C_{19}–C_{18}–H_{23})+$ $–\tau(C_{19}–C_{18}–C_{17}–C_{16})–\tau(C_{19}–C_{18}–C_{17}–H_{22})–\tau(H_{23}–C_{18}–C_{17}–C_{16})–\tau(H_{23}–C_{18}–C_{17}–H_{22})–$ $–\tau(C_{18}–C_{17}–C_{16}–C_{15})–\tau(C_{18}–C_{17}–C_{16}–H_{21})–\tau(H_{22}–C_{17}–C_{16}–C_{15})–\tau(H_{22}–C_{17}–C_{16}–H_{21})+$ $+2\tau(C_{17}–C_{16}–C_{15}–C_{14})+2\tau(C_{17}–C_{16}–C_{15}–H_{20})+2\tau(H_{21}–C_{16}–C_{15}–C_{14})+2\tau(H_{21}–C_{16}–C_{15}–H_{20})–$ $–\tau(C_{16}–C_{15}–C_{14}–C_{19})–\tau(C_{16}–C_{15}–C_{14}–C_1)–\tau(H_{20}–C_{15}–C_{14}–C_{19})–\tau(H_{20}–C_{15}–C_{14}–C_1)$	τPh3
S_{48}	$\delta(C_{15}–C_{14}–C_1)–\delta(C_{19}–C_{14}–C_1)$	w(Ph–Isox)
S_{49}	$\delta(H_{20}–C_{15}–C_{14})–\delta(H_{20}–C_{15}–C_{16})+\delta(H_{21}–C_{16}–C_{15})–\delta(H_{21}–C_{16}–C_{17})+\delta(H_{22}–C_{17}–C_{16})–$ $–\delta(H_{22}–C_{17}–C_{18})+\delta(H_{23}–C_{18}–C_{17})–\delta(H_{23}–C_{18}–C_{19})+\delta(H_{24}–C_{19}–C_{14})–\delta(H_{24}–C_{19}–C_{18})$	δ(C–H1)
S_{50}	$\delta(H_{20}–C_{15}–C_{14})–\delta(H_{20}–C_{15}–C_{16})+\delta(H_{21}–C_{16}–C_{15})–\delta(H_{21}–C_{16}–C_{17})$ $+\delta(H_{23}–C_{18}–C_{17})–\delta(H_{23}–C_{18}–C_{19})+\delta(H_{24}–C_{19}–C_{14})–\delta(H_{24}–C_{19}–C_{18})$	δ(C–H2)
S_{51}	$\delta(H_{20}–C_{15}–C_{14})–\delta(H_{20}–C_{15}–C_{16})–2\delta(H_{22}–C_{17}–C_{16})+2\delta(H_{22}–C_{17}–C_{18})+$ $+\delta(H_{24}–C_{19}–C_{14})–\delta(H_{24}–C_{19}–C_{18})$	δ(C–H3)
S_{52}	$\delta(H_{20}–C_{15}–C_{14})–\delta(H_{20}–C_{15}–C_{16})–\delta(H_{21}–C_{16}–C_{15})+\delta(H_{21}–C_{16}–C_{17})+$ $+\delta(H_{23}–C_{18}–C_{17})–\delta(H_{23}–C_{18}–C_{19})–\delta(H_{24}–C_{19}–C_{14})+\delta(H_{24}–C_{19}–C_{18})$	δ(C–H4)
S_{53}	$2\delta(H_{20}–C_{15}–C_{14})–2\delta(H_{20}–C_{15}–C_{16})–3\delta(H_{21}–C_{16}–C_{15})+3\delta(H_{21}–C_{16}–C_{17})+2\delta(H_{22}–C_{17}–C_{16})–$ $–2\delta(H_{22}–C_{17}–C_{18})–3\delta(H_{23}–C_{18}–C_{17})+3\delta(H_{23}–C_{18}–C_{19})+2\delta(H_{24}–C_{19}–C_{14})–2\delta(H_{24}–C_{19}–C_{18})$	δ(C–H5)
S_{54}	$\gamma(H_{20}–C_{14}–C_{15}–C_{16})+\gamma(H_{21}–C_{15}–C_{16}–C_{17})+\gamma(H_{22}–C_{16}–C_{17}–C_{18})+\gamma(H_{23}–C_{17}–C_{18}–C_{19})+$ $+\gamma(H_{24}–C_{18}–C_{19}–C_{14})$	γ(C–H1)
S_{55}	$\gamma(H_{20}–C_{14}–C_{15}–C_{16})+\gamma(H_{21}–C_{15}–C_{16}–C_{17})–\gamma(H_{23}–C_{17}–C_{18}–C_{19})–\gamma(H_{24}–C_{18}–C_{19}–C_{14})$	γ(C–H2)
S_{56}	$\gamma(H_{20}–C_{14}–C_{15}–C_{16})–2\gamma(H_{22}–C_{16}–C_{17}–C_{18})+\gamma(H_{24}–C_{18}–C_{19}–C_{14})$	γ(C–H3)
S_{57}	$\gamma(H_{20}–C_{14}–C_{15}–C_{16})–\gamma(H_{21}–C_{15}–C_{16}–C_{17})+\gamma(H_{23}–C_{17}–C_{18}–C_{19})–\gamma(H_{24}–C_{18}–C_{19}–C_{14})$	γ(C–H4)
S_{58}	$2\gamma(H_{20}–C_{14}–C_{15}–C_{16})–3\gamma(H_{21}–C_{15}–C_{16}–C_{17})+2\gamma(H_{22}–C_{16}–C_{17}–C_{18})–3\gamma(H_{23}–C_{17}–C_{18}–C_{19})+$ $+2\gamma(H_{24}–C_{18}–C_{19}–C_{14})$	γ(C–H5)
S_{59}	$\gamma(Cl_{13}–C_1=C_2–C_3)$	γ(C–Cl)
S_{60}	$\gamma(C_6–C_2–C_3=N_4)$	γ(Isox–E)
S_{61}	$\gamma(C_{14}–C_2=C_1–O_5)$	γ(Isox–Ph)
S_{62}	$\gamma(C_1–C_{15}–C_{14}–C_{19})$	γ(Ph–Isox)
S_{63}	$\delta(C_6–O_8–C_9)$	$\delta(C–O–CH_3)$
S_{64}	$\delta(Cl_{13}–C_2–C_3)–\delta(Cl_{13}–C_2=C_1)$	w(C–Cl)
S_{65}	$\delta(C_2–C_3–C_6)–\delta(N_4=C_3–C_6)$	w(Isox–E)
S_{66}	$\delta(C_2=C_1–C_{14})–\delta(O_5–C_1–C_{14})$	w(Isox–Ph)

[a] Normalization factors not shown. ν, bond stretching, δ, bending, γ, rocking, w, wagging, τ, torsion, IR, inter–ring; Isox, isoxazole ring; Ph, phenyl ring; E, ester. See Figure 1 for atom numbering. The molecule belongs to the C_1 symmetry point group (all coordinates belong to the A symmetry species).

Table S3 - Calculated [scaled, DFT(B3LYP)/6-311++G(d,p)] wavenumbers, IR intensities and Potential Energy Distributions (PED) for conformer **I** of MCPIC.[a]

Approximate description	Wavenumber	Intensity	PED[b]
ν(C-H1)	3159	1.7	S_{37}(95)
ν(C-H5)	3146	3.0	S_{41}(86)
ν(C-H2)	3132	16.9	S_{38}(84)
ν(C-H3)	3121	9.9	S_{39}(93)
ν(C-H4)	3111	0.1	S_{40} (94)
νCH_3 as´	3107	11.0	S_8(97)
νCH_3 as´´	3070	16.3	S_9(100)
νCH_3 s	2998	34.3	S_7(97)
ν(C=O)	1753	237.5	S_2(87)
νPh3	1614	1.0	S_{33}(63), S_{44}(10)
νPh4	1591	4.8	S_{34}(55), S_{22}(11)
νIsox3	1570	13.1	S_{24}(44), S_6(13), S_{34}(12)
δ(C-H4)	1499	1.8	S_{35}(26), S_{49}(14), S_{24}(12), S_{52}(16), S_{50}(11)
δCH_3 as´	1469	5.2	S_{11}(73), S_{10}(13)
δ(C-H1), νIsox1	1459	83.7	S_{10}(12), S_{49}(11), S_{22}(11), S_{11}(11), S_1(10)
δCH_3 as´´	1457	11.6	S_{12}(90)
δCH_3 s	1448	29.7	S_{10}(35), S_{36}(14), S_{49}(12), S_{51}(12)
νIsox2	1446	53.1	S_{23}24), S_{10}(14), S_{22}(12)
νIsox4	1416	25.5	S_{25}(29), S_{10}(24), S_1(15)
δ(C-H2)	1339	5.6	S_{50}(31), S_{52}(28), S_{49}(16)
νPh2	1312	12.1	S_{32}(51), S_{36}(16)
νIsox2,ν(C-C_{IR})	1258	94.7	S_{23}(16), S_6(13), S_{28}(10), S_{32}(10)
ν(C-O)	1215	465.5	S_3(38), S_{13}(11)
δ(C-H3)	1190	5.8	S_{33}(24), S_{50}(19), S_{52}(18), S_{49}(15), S_{51}(12), S_{53}(12)
γCH_3´	1182	34.2	S_{13}(65)
δ(C-H5)	1165	0.5	S_{53}(48), S_{51}(24)
γCH_3´´	1149	0.9	S_{14}(92)
νIsox1	1121	19.6	S_{26}(22), S_{22}(17)
νPh6	1084	14.7	S_{36}(29), S_{32}(13), S_{49}(12), S_{52}(10)
δIsox2	1060	111.5	S_{28}(25), S_4(15), S_5(12)
νPh5	1031	0.5	S_{35}(45), S_{31}(20)
δPh1, νPh1	997	0.6	S_{42}(61), S_{31}(38)
γ(C-H2)	989	0.1	S_{45}(26), S_{56}(23), S_{57}(21), S_{55}(16)
νIsox5	978	53.5	S_{26}(32), S_{25}(17), S_4(14)
γ(C-H4)	973	1.0	S_{47}(26), S_{53}(21), S_{58}(17), S_{57}(17), S_{54}(16)
ν(O-CH_3)	953	5.5	S_4(48), S_{26}(18)
δIsox1	932	8.1	S_{27}(44), S_{23}(12)
γ(C-H5)	924	2.6	S_{56}(28), S_{54}(28), S_{58}(26), S_{46}(12)
γ(C-H1)	840	0.4	S_{54}(28); S_{58}(26), S_{57}(24), S_{55}(22)
δ(OCO)	809	31.9	S_{19}(36), S_3(17), S_{63}(14)
γ(C=O)	791	9.5	S_{21}(62), S_{60}(22)
γ(C-H3)	769	23.2	S_{56}(29), S_{62}(24.1)
δPh3	696	6.1	S_{44}(46), S_6(11), S_{27}(10)
τPh1	691	44.0	S_{45}(41), S_{57}(23), S_{55}(23)
τIsox1	680	23.4	S_{29}(35), S_{61}(25)
τIsox2	632	4.3	S_{30}(72), S_{21}(10)
δPh2	621	0.1	S_{43}(86)
w(Isox-E),w(Isox-Ph),w(C-Cl)	573	1.1	S_{66}(16), S_{65}(16), S_{64}(16), S_{20}(11)
ν(C-Cl)	540	2.7	S_5(39), S_{20}(10), S_{22}(12)
γ(Ph-Isox)	485	2.7	S_{62}(34), S_{46}(19), S_{29}(11)
ν(C-C_α)	447	0.02	S_1(22), S_{44}(16), S_{19}(10)
τPh3	401	0.05	S_{47}(72)
δ(CC=O)	362	10.3	S_{20}(22), S_{63}(18), S_5(13), S_{48}(11)
γ(Isox-E)	326	4.2	S_{46}(19), S_{61}(16), S_{60}(13)
δ(C-O-CH_3)	302	13.7	S_{63}(38), S_{60}(10), S_{19}(10)
γ(C-Cl)	278	3.0	S_{59}(51), S_{60}(10)
ν(C-Cα),ν(C-C_{IR})	250	0.4	S_6(19), S_1(14), S_{44}(12), S_{28}(12)
w(C-Cl)	215	1.1	S_{64}(47), S_{20}(15), S_{48}(11)
τIsox1, γ(C-Cl)	178	0.8	S_{17}(26), S_{29}(16), S_{59}(15), S_{46}(13)
w(C-Cl),w(Ph-Isox)	150	1.1	S_{64}(18), S_{65}(17), S_{66}(15), S_{48}(12), S_{20}(10)
τCH_3	135	0.1	S_{15}(75)
τ(C-O)	116	1.1	S_{17}(42), S_{15}(16)
w(Isox-Ph)	85	1.8	S_{66}(29), S_{65}(28), S_{48}(13, S_{20}(10)
γ(Isox-E), γ(Isox-Ph)	45	0.5	S_{60}(28), S_{61}(27), S_{29}(20)
τ(C-C_{IR})	29	0.1	S_{18}(95)
τ(C-C_α)	20	2.6	S_{16}(100)

[a] Wavenumbers (cm^{-1}, scaled by 0.9817), ν, bond stretching, δ, bending, γ, rocking, w, wagging, τ, torsion, s, symmetric, as, anti-symmetric, IR, inter–ring; Isox, isoxazole ring; Ph, phenyl ring; E, ester. See Table S2 for definition of internal coordinates. [b] Only PED values greater than 10% are given.

Table S4 - Calculated [scaled, DFT(B3LYP)/6-311++G(d,p)] wavenumbers, IR intensities and Potential Energy Distributions (PED) for conformer **II** of MCPIC.[a]

Approximate description	Wavenumber	Intensity	PED[b]
ν(C-H1)	3159	1.7	S_{37}(95)
ν(C-H5)	3146	3.2	S_{41}(84), S_{40}(10)
ν(C-H2)	3132	16.5	S_{38}(83)
ν(C-H3)	3122	9.7	S_{39}(93)
ν(C-H4)	3111	0.1	S_{40}(94)
νCH_3 as´	3107	9.6	S_8(97)
νCH_3 as´´	3073	14.4	S_9(100)
νCH_3 s	2999	32.1	S_7(97)
ν(C=O)	1769	316.2	S_2(88)
νPh3	1614	0.8	S_{33}(63), S_{44}(10)
νPh4	1591	4.5	S_{34}(54), S_{22}(13)
νIsox3	1572	6.8	S_{24}(44), S_{34}(13), S_6(12)
νPh5	1500	0.7	S_{35}(25), S_{52}(15), S_{24}(11), S_{49}(12), S_{50}(11)
δCH_3 as´	1469	9.0	S_{11}(73), S_{10}(11)
νIsox1	1461	102.1	S_{22}(16), S_{23}(15), S_{49}(13)
δCH_3 as´´	1456	10.1	S_{12}(90)
δ(C-H3)	1448	45.8	S_{51}(20), S_{36}(19), S_{49}(12)
δCH_3 s	1442	7.7	S_{10}(70)
νIsox4	1392	18.7	S_{25}(42), S_1(14)
δ(C-H2), δ(C-H4)	1339	0.7	S_{50}(30), S_{52}(28), S_{49}(15)
νPh2	1310	11.8	S_{32}(51), S_{36}(16)
νIsox2	1259	129.4	S_{23}(20), S_6(12), S_3(10)
ν(C-O)	1213	356.0	S_3(36), S_{13}(14)
δ(C-H4)	1190	4.4	S_{33}(24), S_{50}(19), S_{52}(18), S_{49}(15), S_{51}(12), S_{53}(12)
γCH_3´	1180	45.9	S_{13}(63)
δ(C-H5)	1165	0.1	S_{53}(48), S_{51}(24)
γCH_3´´	1150	0.9	S_{14}(91)
νIsox5,νIsox1	1123	14.0	S_{26}(21), S_{22}(18)
νPh6	1084	14.9	S_{36}(31), S_{32}(13), S_{49}(12), S_{52}(10)
δIsox2	1055	48.0	S_{28}(28), S_4(15), S_5(12)
νPh1	1031	0.7	S_{35}(44), S_{31}(20), S_{42}(10)
δPh1	997	0.9	S_{42}(61), S_{31}(38)
νIsox5	992	70.8	S_4(27), S_{26}(24), S_{25}(11)
γ(C-H5)	987	0.3	S_{58}(55), S_{45}(26), S_{56}(14)
γ(C-H4)	972	0.2	S_{57}(76), S_{47}(26)
ν(O-CH_3)	940	4.1	S_4(43), S_{25}(25), S_3(10)
δIsox1	936	0.5	S_{27}(43), S_{23}(15), S_{25}(13)
γ(C-H3)	923	2.3	S_{56}(55), S_{58}(16), S_{54}(13), S_{46}(12)
γ(C-H2)	840	0.4	S_{55}(98)
δ(OCO)	808	41.0	S_{19}(34), S_3(18), S_{63}(14)
γ(C=O)	786	9.7	S_{21}(61), S_{60}(20)
γ(C-H1)	768	23.6	S_{54}(34), S_{62}(24), S_{56}(19)
δPh3	699	2.8	S_{44}(41), S_6(11), S_{27}(10)
τPh1	689	50.1	S_{45}(37), S_{54}(31), S_{58}(17), S_{62}(10)
τIsox1	683	18.5	S_{29}(35), S_{61}(23), S_{45}(12)
τIsox2	641	4.4	S_{30}(58)
δPh2	620	0.1	S_{43}(87)
w(Isox-Ph), w(C-Cl)	572	3.2	S_{66}(15), S_{64}(14), S_{30}(11)
ν(C-Cl)	526	2.8	S_5(32), S_{20}(10)
γ(Ph-Isox)	482	2.2	S_{62}(32), S_{46}(18), S_{29}(11)
ν(C-C_α)	429	0.5	S_1(22), S_{44}(14)
τPh3	401	0.03	S_{47}(73), S_{57}(27)
δ(CC=O)	375	8.2	S_{20}(26), S_5(12), S_{63}(10)
τPh2	327	2.8	S_{46}(19), S_{61}(16), S_{60}(13)
δ(C-O-CH_3)	302	8.0	S_{63}(44), S_{19}(16), S_{59}(14)
γ(C-Cl)	269	1.1	S_{59}(22), S_{28}(11)
ν(C-C_α), ν(C-C_{IR})	264	1.7	S_{59}(21), S_6(13), S_1(10)
w(C-Cl)	211	0.6	S_{64}(49)
τIsox1, γ(C-Cl)	182	1.0	S_{17}(32), S_{29}(16), S_{59}(16), S_{46}(12)
w(Ph-Isox),w(Isox-E),w(Isox-Ph)	149	0.4	S_{48}(16), S_{66}(16), S_{65}(16), S_{20}(14)
τCH_3	128	0.03	S_{15}(66)
τ(C-O)	114	0.7	S_{17}(32), S_{15}(27)
w(Isox-E)	81	1.0	S_{65}(30), S_{66}(25), S_{48}(11), S_{20}(10)
γ(Isox-E)	47	0.3	S_{61}(28), S_{60}(24), S_{29}(22)
ν(C-C_{IR})	28	0.2	S_{18}(53), S_{16}(36)
τ(C-C_α)	21	1.6	S_{16}(57), S_{18}(41)

[a] Wavenumbers (cm^{-1}, scaled by 0.9817), ν, bond stretching, δ, bending, γ, rocking, w, wagging, τ, torsion, s, symmetric, as, anti-symmetric, IR, inter–ring; Isox, isoxazole ring; Ph, phenyl ring; E, ester. See Table S2 for definition of internal coordinates.
[b] Only PED values greater than 10% are given.

Tetrahedron – Submitted (**2011**)

Supporting Information

for

3-Azido-Acrylophonones as Photochemical Precursors of Oxazoles: A Matrix Isolation Infrared Spectroscopy Study

Susy Lopes,[†] Cláudio M. Nunes,[†] Andrea Gómez-Zavaglia,[†,‡]

Teresa M.V.D. Pinho e Melo[†] and Rui Fausto[†]

[†] *Department of Chemistry, University of Coimbra, P-3004-535 Coimbra, Portugal*
[‡] *Centro de Investigación y Desarrollo en Criotecnología de Alimentos (Conicet La Plata, UNLP) RA-1900, Argentina*

Contents

Table S5. Cartesian coordinates and absolute energies for conformers **I**, **II**, and **III** of MACBP, and for the global minima of MBCAC, CBMK and MCPOC.

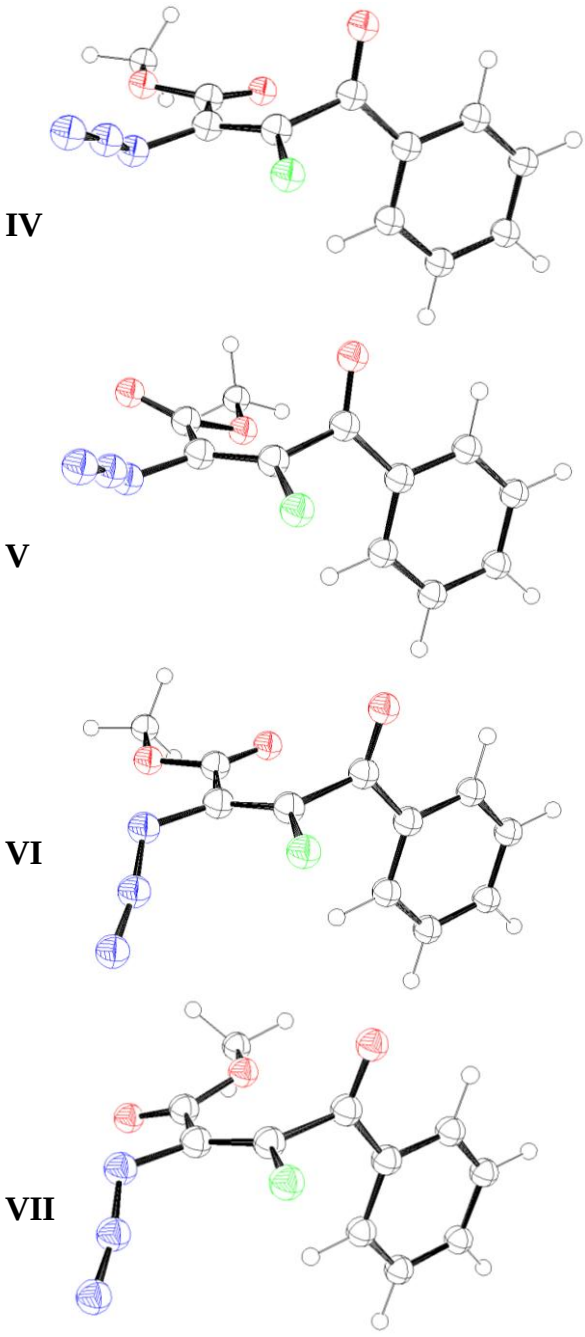

Figure S1. High energy conformers of MACBP, optimized at the DFT(B3LYP)/6-311++G(d,p) level of theory. The picture was made using the Ortep-3 for Windows program (Farrugia, L. J. *J. Appl. Cryst.* **1997**, *30*, 565). Atoms color code: carbon, hydrogen: black; nitrogen: blue; chlorine: green; oxygen, red.

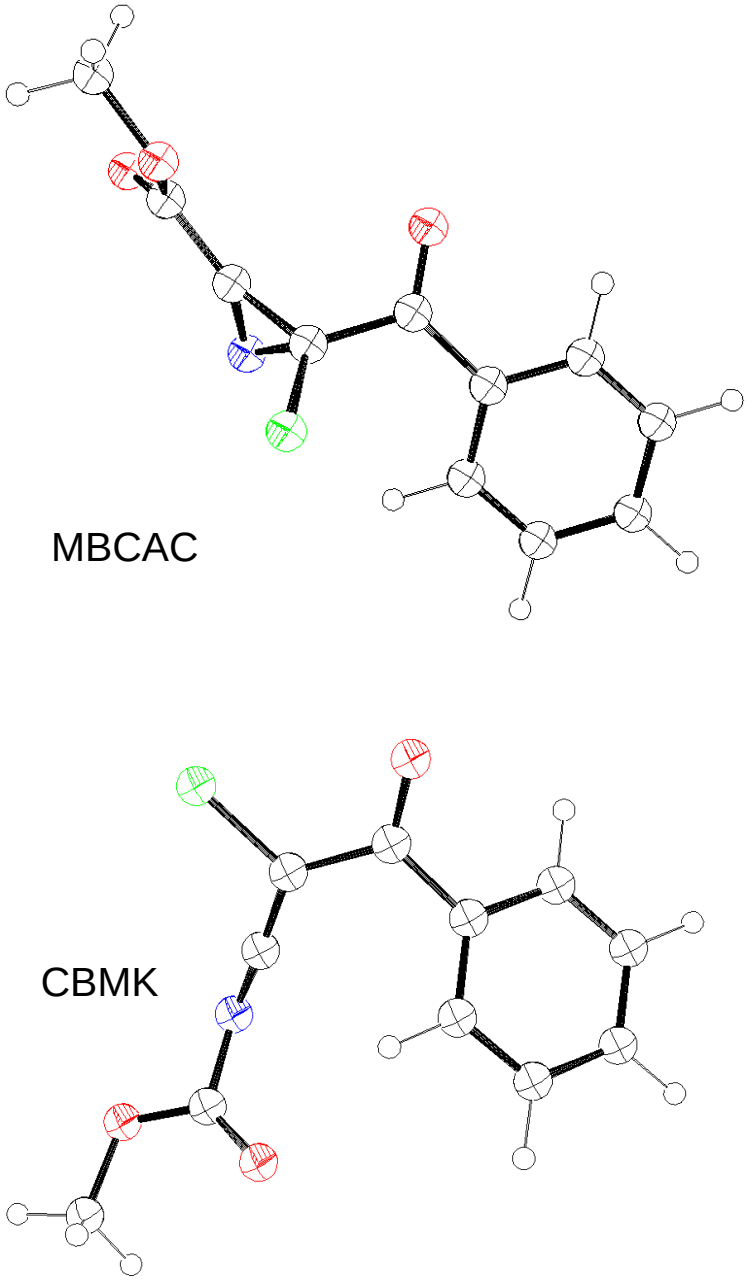

Figure S2. Lowest energy conformers of MBCAC and CBMK, optimized at the DFT(B3LYP)/6-311++G(d,p) level of theory. The picture was made using the Ortep-3 for Windows program (Farrugia, L. J. *J. Appl. Cryst.* **1997**, *30*, 565). Atoms color code: carbon, hydrogen: black; nitrogen: blue; chlorine: green; oxygen, red.

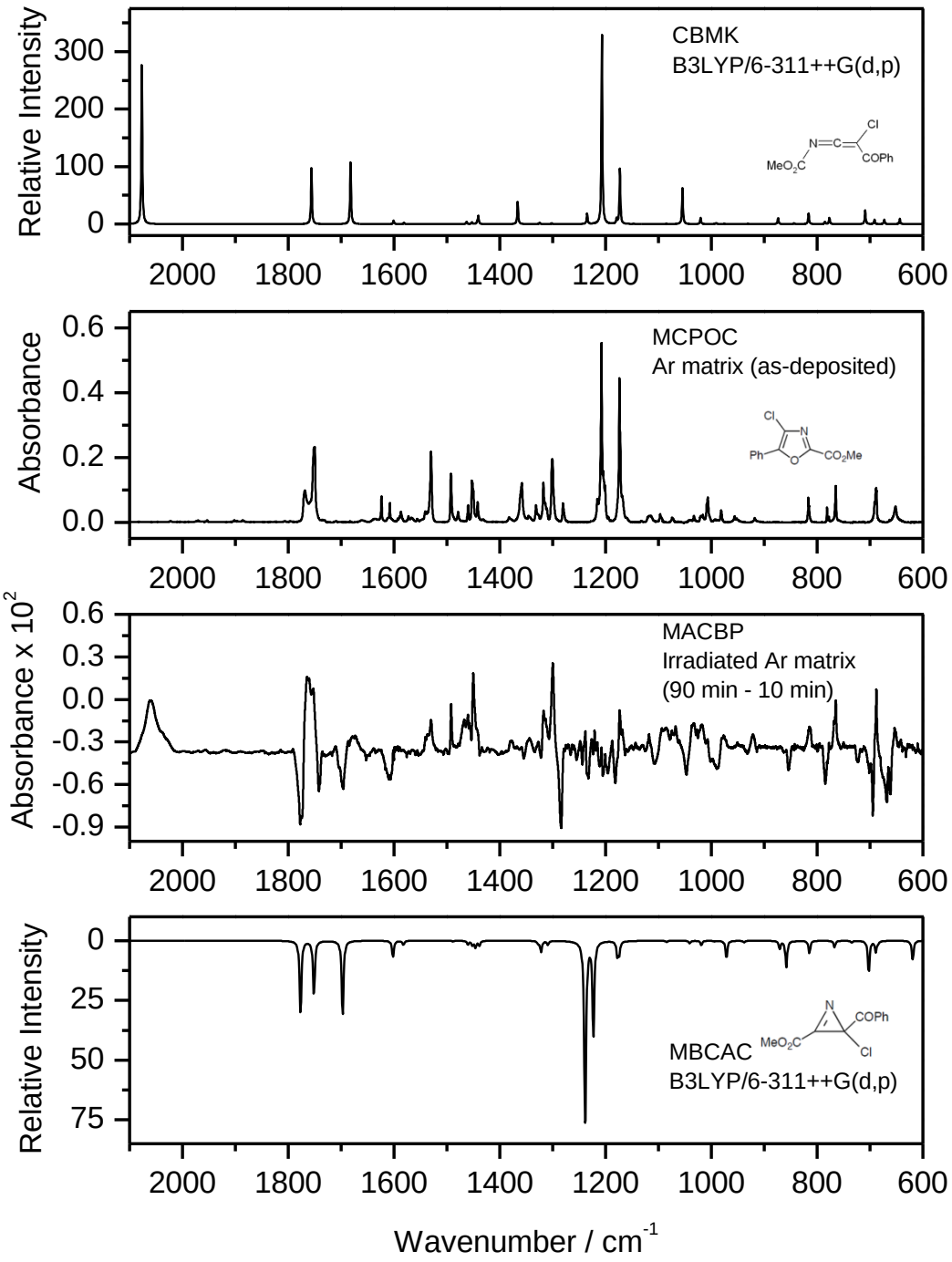

Figure S3. ***Top*****:** Simulated IR spectrum of CBMK (most stable conformer); ***Middle top:*** IR spectrum of MCPOC in argon matrix (as deposited; 10 K); ***Middle bottom*****:** IR difference spectrum of irradiated Ar matrix of MACBP (λ> 235 nm irradiated matrix during 90 min *minus* λ> 235 nm irradiated matrix during 10 min; before subtraction, residual bands due MACBP were subtracted from the spectra of the irradiated matrix); ***Bottom:*** simulated IR spectrum of MBCAC (most stable conformer). In the simulated spectra, bands were represented by Lorenztian functions centered at the DFT(B3LYP)/6-311++G(d,p) calculated wavenumbers (scaled by 0.978) and with fwhm (full width at half maximum) equal to 2 cm^{-1} (in case of MBCAC, the spectrum was multiplied by –1).

Table S1. Calculated Bond Lengths (Pm) and Angles (º) for the Three Most Stable Conformers of MACBP.[A]

Parameter	I	II	III	Parameter	I	II	III
Bond lengths				*Bond angles*			
$C_1=C_2$	134.9	134.9	135.0	$C_{18}–C_{19}–H_{24}$	119.9	119.9	120.0
$C_1–Cl_6$	174.3	173.8	173.5	$C_{20}–C_{19}–H_{24}$	119.9	119.9	119.9
$C_1–C_{14}$	152.1	152.5	152.6	$C_{19}–C_{20}–C_{21}$	120.0	119.9	119.9
$C_2–N_3$	139.9	140.5	140.7	$C_{19}–C_{20}–H_{25}$	120.0	120.1	120.1
$C_2–C_7$	150.0	149.9	149.7	$C_{21}–C_{20}–H_{25}$	120.0	119.9	119.9
$N_3=N_4$	123.9	123.4	123.4	$C_{16}–C_{21}–C_{20}$	120.2	120.2	120.2
$N_4=N_5$	112.9	113.1	113.0	$C_{16}–C_{21}–H_{26}$	118.7	120.0	120.1
$C_7=O_8$	120.8	120.6	120.7	$C_{20}–C_{21}–H_{26}$	121.1	119.8	119.7
$C_7–O_9$	133.7	134.2	134.2				
$O_9–C_{10}$	144.5	144.5	144.4	*Dihedrals*			
$C_{10}–H_{11}$	109.0	109.0	109.0				
$C_{10}–H_{12}$	108.7	108.7	108.7	$Cl_6–C_1=C_2=N_3$	2.4	3.8	–3.4
$C_{10}–H_{13}$	109.0	109.0	109.0	$Cl_6–C_1=C_2–C_7$	178.7	–179.7	–178.8
$C_{14}=O_{15}$	121.3	121.2	121.1	$C_{14}–C_1=C_2–N_3$	–169.6	–168.7	–179.2
$C_{14}–C_{16}$	148.8	148.6	148.7	$C_{14}–C_1=C_2–C_7$	6.8	7.8	5.4
$C_{16}–C_{17}$	140.0	140.2	140.2	$C_2=C_1–C_{14}=O_{15}$	69.3	78.1	94.3
$C_{16}–C_{21}$	140.2	140.0	140.0	$C_2=C_1–C_{14}–C_{16}$	–114.1	–106.6	–91.0
$C_{17}–C_{18}$	139.2	138.9	138.9	$Cl_6–C_1–C_{14}=O_{15}$	–103.2	–95.0	–81.8
$C_{17}–H_{22}$	108.4	108.3	108.3	$Cl_6–C_1–C_{14}–C_{16}$	73.4	80.4	92.9
$C_{18}–C_{19}$	139.4	139.7	139.7	$C_1=C_2–N_3=N_4$	–171.0	–160.1	154.9
$C_{18}–H_{23}$	108.4	108.4	108.4	$C_7–C_2–N_3=N_4$	12.5	23.6	–29.9
$C_{19}–C_{20}$	139.7	139.4	139.4	$C_1=C_2–C_7=O_8$	–155.8	19.6	–2.8
$C_{19}–H_{24}$	108.4	108.4	108.4	$C_1=C_2–C_7–O_9$	25.5	–160.4	176.8
$C_{20}–C_{21}$	138.9	139.2	139.2	$N_3–C_2–C_7=O_8$	20.6	–164.0	–178.0
$C_{20}–H_{25}$	108.4	108.4	108.4	$N_3–C_2–C_7–O_9$	–158.1	15.9	1.6
$C_{21}–H_{26}$	108.3	108.4	108.4	$C_2–N_3=N_4=N_5$	178.0	–179.6	–179.7
				$C_2–C_7–O_9–C_{10}$	–174.3	179.7	179.5
Bond angles				$O_8=C_7–O_9–C_{10}$	7.0	–0.3	–0.9
				$C_7–O_9–C_{10}–H_{11}$	61.3	59.5	61.9
$C_2=C_1–Cl_6$	120.5	120.9	120.8	$C_7–O_9–C_{10}–H_{12}$	–179.4	179.2	–178.6
$C_2=C_1–C_{14}$	126.5	126.1	126.7	$C_7–O_9–C_{10}–H_{13}$	–59.8	–61.3	–59.0
$Cl_6–C_1–C_{14}$	112.5	112.6	112.3	$C_1–C_{14}–C_{16}–C_{17}$	14.0	–171.1	–180.0
$C_1=C_2–N_3$	119.1	119.1	118.8	$C_1–C_{14}–C_{16}–C_{21}$	–167.5	9.6	–0.6
$C_1=C_2–C_7$	122.2	118.3	118.3	$O_{15}=C_{14}–C_{16}–C_{17}$	–169.6	4.0	–5.6
$N_3–C_2–C_7$	118.6	122.5	122.7	$O_{15}=C_{14}–C_{16}–C_{21}$	8.9	–175.3	173.8
$C_2–N_3=N_4$	121.1	121.5	122.2	$C_{14}–C_{16}–C_{17}–C_{18}$	178.4	–179.5	179.7
$N_3=N_4=N_5$	169.0	170.3	170.0	$C_{14}–C_{16}–C_{17}–H_{22}$	–1.2	0.4	–0.6
$C_2–C_7=O_8$	122.8	124.1	124.1	$C_{21}–C_{16}–C_{17}–C_{18}$	0.0	–0.2	0.2
$C_2–C_7–O_9$	112.5	111.5	111.7	$C_{21}–C_{16}–C_{17}–H_{22}$	–179.7	179.7	180.0
$O_8=C_7–O_9$	124.8	124.5	124.2	$C_{14}–C_{16}–C_{21}–C_{20}$	–178.8	179.4	–179.4
$C_7–O_9–C_{10}$	116.2	116.1	116.2	$C_{14}–C_{16}–C_{21}–H_{26}$	1.3	–0.3	0.2
$O_9–C_{10}–H_{11}$	110.0	110.2	110.0	$C_{17}–C_{16}–C_{21}–C_{20}$	–0.3	0.1	0.0
$O_9–C_{10}–H_{12}$	105.2	105.2	105.2	$C_{17}–C_{16}–C_{21}–H_{26}$	179.9	–179.6	179.6
$O_9–C_{10}–H_{13}$	110.1	109.9	110.1	$C_{16}–C_{17}–C_{18}–C_{19}$	0.3	0.1	–0.3
$H_{11}–C_{10}–H_{12}$	110.8	110.9	110.9	$C_{16}–C_{17}–C_{18}–H_{23}$	–179.8	–179.9	179.7
$H_{11}–C_{10}–H_{13}$	109.7	109.6	109.5	$H_{22}–C_{17}–C_{18}–C_{19}$	179.9	–179.8	180.0
$H_{12}–C_{10}–H_{13}$	111.0	110.9	111.0	$H_{22}–C_{17}–C_{18}–H_{23}$	–0.2	0.2	0.0
$C_1–C_{14}=O_{15}$	118.7	117.9	117.9	$C_{17}–C_{18}–C_{19}–C_{20}$	–0.2	0.1	0.1
$C_1–C_{14}–C_{16}$	118.3	118.4	118.4	$C_{17}–C_{18}–C_{19}–H_{24}$	179.7	180.0	–179.9
$O_{15}=C_{14}–C_{16}$	122.9	123.5	123.5	$H_{23}–C_{18}–C_{19}–C_{20}$	179.9	–179.9	–179.9
$C_{14}–C_{16}–C_{17}$	122.0	118.4	118.3	$H_{23}–C_{18}–C_{19}–H_{24}$	–0.2	0.0	0.1
$C_{14}–C_{16}–C_{21}$	118.4	122.0	122.1	$C_{18}–C_{19}–C_{20}–C_{21}$	–0.1	–0.2	0.2
$C_{17}–C_{16}–C_{21}$	119.6	119.6	119.6	$C_{18}–C_{19}–C_{20}–H_{25}$	179.8	179.8	–179.8
$C_{16}–C_{17}–C_{18}$	120.2	120.1	120.1	$H_{24}–C_{19}–C_{20}–C_{21}$	180.0	179.9	–179.9
$C_{16}–C_{17}–H_{22}$	120.0	118.7	118.7	$H_{24}–C_{19}–C_{20}–H_{25}$	–0.1	–0.1	0.2
$C_{18}–C_{17}–H_{22}$	119.8	121.2	121.2	$C_{19}–C_{20}–C_{21}–C_{16}$	0.3	0.1	–0.2
$C_{17}–C_{18}–C_{19}$	120.0	120.0	120.0	$C_{19}–C_{20}–C_{21}–H_{26}$	–179.8	179.8	–179.8
$C_{17}–C_{18}–H_{23}$	119.9	120.0	119.9	$H_{25}–C_{20}–C_{21}–C_{16}$	–179.6	–179.9	179.7
$C_{19}–C_{18}–H_{23}$	120.1	120.0	120.0	$H_{25}–C_{20}–C_{21}–H_{26}$	0.3	–0.2	0.1
$C_{18}–C_{19}–C_{20}$	120.1	120.1	120.1				

[a] See Figure 1 for atom numbering.

Table S2. Definition of Internal Coordinates Used in the Normal Coordinate Analysis of MACBP.

Nº	Definition [a]	Approximate description
S_1	$\nu(C_1=C_2)$	ν(C=C)
S_2	$\nu(C_2-N_3)$	ν(C-N)
S_3	$\nu(N_3=N_4)+\nu(N_4=N_5)$	ν(N=N) s
S_4	$\nu(N_3=N_4)-\nu(N_4=N_5)$	ν(N=N) as
S_5	$\nu(C_2-C_7)$	$\nu(C-C_\alpha)$ E
S_6	$\nu(C_7=O_8)$	ν(C=O) E
S_7	$\nu(C_7-O_9)$	ν(C-O)
S_8	$\nu(O_9-C_{10})$	$\nu(O-CH_3)$
S_9	$\nu(C_{10}-H_{12})+\nu(C_{10}-H_{11})+\nu(C_{10}-H_{13})$	νCH_3 s
S_{10}	$2\nu(C_{10}-H_{12})-\nu(C_{10}-H_{11})-\nu(C_{10}-H_{13})$	νCH_3 as´
S_{11}	$\nu(C_{10}-H_{11})-\nu(C_{10}-H_{13})$	νCH_3 as´´
S_{12}	$\nu(C_1-Cl_6)$	ν(C-Cl)
S_{13}	$\nu(C_1-C_{14})$	ν(C-C)
S_{14}	$\nu(C_{14}=O_{15})$	ν(C=O) Ph
S_{15}	$\nu(C_{14}-C_{16})$	$\nu(C-C_{Ph})$
S_{16}	$\nu(C_{16}-C_{17})+\nu(C_{17}-C_{18})+\nu(C_{18}-C_{19})+\nu(C_{19}-C_{20})+\nu(C_{20}-C_{21})+\nu(C_{21}-C_{16})$	νPh1
S_{17}	$\nu(C_{16}-C_{17})+\nu(C_{18}-C_{19})-\nu(C_{19}-C_{20})-\nu(C_{21}-C_{16})$	νPh2
S_{18}	$-\nu(C_{16}-C_{17})+2\nu(C_{17}-C_{18})-\nu(C_{18}-C_{19})-\nu(C_{19}-C_{20})+2\nu(C_{20}-C_{21})-\nu(C_{21}-C_{16})$	νPh3
S_{19}	$\nu(C_{16}-C_{17})-\nu(C_{18}-C_{19})+\nu(C_{19}-C_{20})-\nu(C_{21}-C_{16})$	νPh4
S_{20}	$\nu(C_{16}-C_{17})-\nu(C_{18}-C_{19})-\nu(C_{19}-C_{20})+\nu(C_{21}-C_{16})$	νPh5
S_{21}	$\nu(C_{17}-C_{18})-\nu(C_{19}-C_{20})$	νPh6
S_{22}	$\nu(C_{17}-H_{22})$	ν(C-H1)
S_{23}	$\nu(C_{18}-H_{23})+\nu(C_{20}-H_{25})$	ν(C-H2)
S_{24}	$2\nu(C_{19}-H_{24})-\nu(C_{18}-H_{23})-\nu(C_{20}-H_{25})$	ν(C-H3)
S_{25}	$\nu(C_{18}-H_{23})+\nu(C_{19}-H_{24})+\nu(C_{20}-H_{25})$	ν(C-H4)
S_{26}	$\nu(C_{21}-H_{26})$	ν(C-H5)
S_{27}	$\delta(H_{12}-C_{10}-H_{13})+\delta(H_{12}-C_{10}-H_{11})+\delta(H_{13}-C_{10}-H_{11})-\delta(H_{13}-C_{10}-O_9)-\delta(H_{11}-C_{10}-O_9)-\delta(H_{12}-C_{10}-O_9)$	δCH_3 s
S_{28}	$2\delta(H_{13}-C_{10}-H_{12})-\delta(H_{12}-C_{10}-H_{13})-\delta(H_{12}-C_{10}-H_{11})$	δCH_3 as´
S_{29}	$\delta(H_{12}-C_{10}-H_{11})-\delta(H_{12}-C_{10}-H_{13})$	δCH_3 as´´
S_{30}	$2\delta(H_{12}-C_{10}-O_9)-\delta(H_{13}-C_{10}-O_9)-\delta(H_{11}-C_{10}-O_9)$	γCH_3´
S_{31}	$\delta(H_{11}-C_{10}-O_9)-\delta(H_{13}-C_{10}-O_9)$	γCH_3´´
S_{32}	$\tau(H_{11}-C_{10}-O_9-C_7)+\tau(H_{13}-C_{10}-O_9-C_7)+\tau(H_{12}-C_{10}-O_9-C_7)$	τCH_3
S_{33}	$\delta(C_{17}-C_{16}-C_{21})-\delta(C_{16}-C_{21}-C_{20})+\delta(C_{21}-C_{20}-C_{19})-\delta(C_{20}-C_{19}-C_{18})+\delta(C_{19}-C_{18}-C_{17})-\delta(C_{18}-C_{17}-C_{16})$	δPh1
S_{34}	$\delta(C_{17}-C_{16}-C_{21})-\delta(C_{21}-C_{20}-C_{19})+\delta(C_{20}-C_{19}-C_{18})-\delta(C_{18}-C_{17}-C_{16})$	δPh2
S_{35}	$2\delta(C_{17}-C_{16}-C_{21})-\delta(C_{16}-C_{21}-C_{20})-\delta(C_{21}-C_{20}-C_{19})+2\delta(C_{20}-C_{19}-C_{18})-\delta(C_{19}-C_{18}-C_{17})-\delta(C_{18}-C_{17}-C_{16})$	δPh3
S_{36}	$\tau(C_{17}-C_{16}-C_{21}-C_{20})+\tau(C_{17}-C_{16}-C_{21}-H_{26})+\tau(C_{14}-C_{16}-C_{21}-C_{20})+\tau(C_{14}-C_{16}-C_{21}-H_{26})-\tau(C_{16}-C_{21}-C_{20}-C_{19})-\tau(C_{16}-C_{21}-C_{20}-H_{25})-\tau(H_{26}-C_{21}-C_{20}-C_{19})-\tau(H_{26}-C_{21}-C_{20}-H_{25})+\tau(C_{21}-C_{20}-C_{19}-C_{18})+\tau(C_{21}-C_{20}-C_{19}-H_{24})+\tau(H_{25}-C_{20}-C_{19}-C_{18})+\tau(H_{25}-C_{20}-C_{19}-H_{24})-\tau(C_{20}-C_{19}-C_{18}-C_{17})-\tau(C_{20}-C_{19}-C_{18}-H_{23})-\tau(H_{24}-C_{19}-C_{18}-C_{17})-\tau(H_{24}-C_{19}-C_{168}-H_{23})+\tau(C_{19}-C_{18}-C_{17}-C_{16})+\tau(C_{19}-C_{18}-C_{17}-H_{22})+\tau(H_{23}-C_{18}-C_{17}-C_{16})+\tau(H_{23}-C_{18}-C_{17}-H_{22})-\tau(C_{18}-C_{17}-C_{16}-C_{21})-\tau(C_{18}-C_{17}-C_{16}-C_{14})-\tau(H_{22}-C_{17}-C_{16}-C_{21})-\tau(H_{22}-C_{17}-C_{16}-C_{14})$	τPh1
S_{37}	$\tau(C_{17}-C_{16}-C_{21}-C_{20})+\tau(C_{17}-C_{16}-C_{21}-H_{26})+\tau(C_{14}-C_{16}-C_{21}-C_{20})+\tau(C_{14}-C_{16}-C_{21}-H_{26})-\tau(C_{21}-C_{20}-C_{19}-C_{18})-\tau(C_{21}-C_{20}-C_{19}-H_{24})-\tau(H_{25}-C_{20}-C_{19}-C_{18})-\tau(H_{25}-C_{20}-C_{19}-H_{24})+\tau(C_{20}-C_{19}-C_{18}-C_{17})+\tau(C_{20}-C_{19}-C_{18}-H_{23})+\tau(H_{24}-C_{19}-C_{18}-C_{17})+\tau(H_{24}-C_{19}-C_{168}-H_{23})-\tau(C_{18}-C_{17}-C_{16}-C_{21})-\tau(C_{18}-C_{17}-C_{16}-C_{14})-\tau(H_{22}-C_{17}-C_{16}-C_{21})-\tau(H_{22}-C_{17}-C_{16}-C_{14})$	τPh2
S_{38}	$-\tau(C_{17}-C_{16}-C_{21}-C_{20})-\tau(C_{17}-C_{16}-C_{21}-H_{26})-\tau(C_{14}-C_{16}-C_{21}-C_{20})-\tau(C_{14}-C_{16}-C_{21}-H_{26})+2\tau(C_{16}-C_{21}-C_{20}-C_{19})+2\tau(C_{16}-C_{21}-C_{20}-H_{25})+2\tau(H_{26}-C_{21}-C_{20}-C_{19})+2\tau(H_{26}-C_{21}-C_{20}-H_{25})-\tau(C_{21}-C_{20}-C_{19}-C_{18})-\tau(C_{21}-C_{20}-C_{19}-H_{24})-\tau(H_{25}-C_{20}-C_{19}-C_{18})-\tau(H_{25}-C_{20}-C_{19}-H_{24})-\tau(C_{20}-C_{19}-C_{18}-C_{17})-\tau(C_{20}-C_{19}-C_{18}-H_{23})-\tau(H_{24}-C_{19}-C_{18}-C_{17})-\tau(H_{24}-C_{19}-C_{168}-H_{23})+2\tau(C_{19}-C_{18}-C_{17}-C_{16})+2\tau(C_{19}-C_{18}-C_{17}-H_{22})+2\tau(H_{23}-C_{18}-C_{17}-C_{16})+2\tau(H_{23}-C_{18}-C_{17}-H_{22})-\tau(C_{18}-C_{17}-C_{16}-C_{21})-\tau(C_{18}-C_{17}-C_{16}-C_{14})-\tau(H_{22}-C_{17}-C_{16}-C_{21})-\tau(H_{22}-C_{17}-C_{16}-C_{14})$	τPh3
S_{39}	$\delta(H_{22}-C_{17}-C_{16})-\delta(H_{22}-C_{17}-C_{18})+\delta(H_{23}-C_{18}-C_{17})-\delta(H_{23}-C_{18}-C_{19})+\delta(H_{24}-C_{19}-C_{18})-\delta(H_{24}-C_{19}-C_{20})+\delta(H_{25}-C_{20}-C_{19})-\delta(H_{25}-C_{20}-C_{21})+\delta(H_{26}-C_{21}-C_{20})-\delta(H_{26}-C_{21}-C_{16})$	δ(C-H1)
S_{40}	$\delta(H_{22}-C_{17}-C_{16})-\delta(H_{22}-C_{17}-C_{18})+\delta(H_{23}-C_{18}-C_{17})-\delta(H_{23}-C_{18}-C_{19})-\delta(H_{25}-C_{20}-C_{19})+\delta(H_{25}-C_{20}-C_{21})-\delta(H_{26}-C_{21}-C_{20})+\delta(H_{26}-C_{21}-C_{16})$	δ(C-H2)
S_{41}	$\delta(H_{22}-C_{17}-C_{16})-\delta(H_{22}-C_{17}-C_{18})-2\delta(H_{24}-C_{19}-C_{18})+2\delta(H_{24}-C_{19}-C_{20})+\delta(H_{26}-C_{21}-C_{20})-\delta(H_{26}-C_{21}-C_{16})$	δ(C-H3)

S_{42}	$\delta(H_{22}\text{-}C_{17}\text{-}C_{16})\text{-}\delta(H_{22}\text{-}C_{17}\text{-}C_{18})\text{-}\delta(H_{23}\text{-}C_{18}\text{-}C_{17})+\delta(H_{23}\text{-}C_{18}\text{-}C_{19})+$ $+\delta(H_{25}\text{-}C_{20}\text{-}C_{19})\text{-}\delta(H_{25}\text{-}C_{20}\text{-}C_{21})\text{-}\delta(H_{26}\text{-}C_{21}\text{-}C_{20})+\delta(H_{26}\text{-}C_{21}\text{-}C_{16})$	δ(C-H4)
S_{43}	$2\delta(H_{22}\text{-}C_{17}\text{-}C_{16})\text{-}2\delta(H_{22}\text{-}C_{17}\text{-}C_{18})\text{-}3\delta(H_{23}\text{-}C_{18}\text{-}C_{17})+3\delta(H_{23}\text{-}C_{18}\text{-}C_{19})+2\delta(H_{24}\text{-}C_{19}\text{-}C_{18})\text{-}$ $\text{-}2\delta(H_{24}\text{-}C_{19}\text{-}C_{20})\text{-}3\delta(H_{25}\text{-}C_{20}\text{-}C_{19})+3\delta(H_{25}\text{-}C_{20}\text{-}C_{21})+2\delta(H_{26}\text{-}C_{21}\text{-}C_{20})\text{-}2\delta(H_{26}\text{-}C_{21}\text{-}C_{16})$	δ(C-H5)
S_{44}	$\gamma(H_{22}\text{-}C_{18}\text{-}C_{17}\text{-}C_{16})+\gamma(H_{23}\text{-}C_{19}\text{-}C_{18}\text{-}C_{17})+\gamma(H_{24}\text{-}C_{20}\text{-}C_{19}\text{-}C_{18})+\gamma(H_{25}\text{-}C_{21}\text{-}C_{20}\text{-}C_{19})+$ $+\gamma(H_{26}\text{-}C_{16}\text{-}C_{21}\text{-}C_{20})$	γ(C-H1)
S_{45}	$\gamma(H_{22}\text{-}C_{18}\text{-}C_{17}\text{-}C_{16})+\gamma(H_{23}\text{-}C_{19}\text{-}C_{18}\text{-}C_{17})\text{-}\gamma(H_{25}\text{-}C_{21}\text{-}C_{20}\text{-}C_{19})\text{-}\gamma(H_{26}\text{-}C_{16}\text{-}C_{21}\text{-}C_{20})$	γ(C-H2)
S_{46}	$\gamma(H_{22}\text{-}C_{18}\text{-}C_{17}\text{-}C_{16})\text{-}2\gamma(H_{24}\text{-}C_{20}\text{-}C_{19}\text{-}C_{18})+\gamma(H_{26}\text{-}C_{16}\text{-}C_{21}\text{-}C_{20})$	γ(C-H3)
S_{47}	$\gamma(H_{22}\text{-}C_{18}\text{-}C_{17}\text{-}C_{16})\text{-}\gamma(H_{23}\text{-}C_{19}\text{-}C_{18}\text{-}C_{17})+\gamma(H_{25}\text{-}C_{21}\text{-}C_{20}\text{-}C_{19})\text{-}\gamma(H_{26}\text{-}C_{16}\text{-}C_{21}\text{-}C_{20})$	γ(C-H4)
S_{48}	$2\gamma(H_{22}\text{-}C_{18}\text{-}C_{17}\text{-}C_{16})\text{-}3\gamma(H_{23}\text{-}C_{19}\text{-}C_{18}\text{-}C_{17})+2\gamma(H_{24}\text{-}C_{20}\text{-}C_{19}\text{-}C_{18})\text{-}3\gamma(H_{25}\text{-}C_{21}\text{-}C_{20}\text{-}C_{19})+$ $+2\gamma(H_{26}\text{-}C_{16}\text{-}C_{21}\text{-}C_{20})$	γ(C-H5)
S_{49}	$\tau(N_3\text{-}C_2\text{=}C_1\text{-}C_{14})+\tau(N_3\text{-}C_2\text{=}C_1\text{-}Cl_6)+\tau(C_7\text{-}C_2\text{=}C_1\text{-}C_{14})+\tau(C_7\text{-}C_2\text{=}C_1\text{-}Cl_6)$	τ(C=C)
S_{50}	$\tau(C_1\text{=}C_2\text{-}N_3\text{=}N_4)+\tau(C_7\text{-}C_2\text{-}N_3\text{=}N_4)$	τ(C-N)
S_{51}	$\tau(C_1\text{=}C_2\text{-}C_7\text{=}O_8)+\tau(C_1\text{=}C_2\text{-}C_7\text{-}O_9)+\tau(N_3\text{-}C_2\text{-}C_7\text{=}O_8)+\tau(N_3\text{-}C_2\text{-}C_7\text{-}O_9)$	$\tau(C\text{-}C_\alpha)$ E
S_{52}	$\tau(C_2\text{-}C_7\text{-}O_9\text{-}C_{10})+\tau(O_8\text{=}C_7\text{-}O_9\text{-}C_{10})$	τ(C-O)
S_{53}	$\tau(C_2\text{=}C_1\text{-}C_{14}\text{=}O_{15})+\tau(C_2\text{=}C_1\text{-}C_{14}\text{-}C_{16})+\tau(Cl_6\text{-}C_1\text{-}C_{14}\text{=}O_{15})+\tau(Cl_6\text{-}C_1\text{-}C_{14}\text{-}C_{16})$	$\tau(C\text{-}C_\alpha)$ Ph
S_{54}	$\tau(C_1\text{-}C_{14}\text{-}C_{16}\text{-}C_{17})+\tau(C_1\text{-}C_{14}\text{-}C_{16}\text{-}C_{21})+\tau(O_{15}\text{=}C_{14}\text{-}C_{16}\text{-}C_{17})+\tau(O_{15}\text{=}C_{14}\text{-}C_{16}\text{-}C_{21})$	τ(C-C) Ph
S_{55}	$2\delta(O_8\text{=}C_7\text{-}O_9)\text{-}\delta(O_8\text{=}C_7\text{-}C_2)\text{-}\delta(O_9\text{-}C_7\text{-}C_2)$	δ(OCO)
S_{56}	$\delta(O_8\text{=}C_7\text{-}C_2)\text{-}\delta(O_9\text{-}C_7\text{-}C_2)$	δ(CC=O)
S_{57}	$\delta(C_{10}\text{-}O_9\text{-}C_7)$	$\delta(C\text{-}O\text{-}CH_3)$
S_{58}	$\gamma(O_8\text{=}O_9\text{-}O_7\text{-}C_2)$	γ(C=O) E
S_{59}	$\gamma(N_5\text{=}N_3\text{=}N_4)$	γ(NNN)
S_{60}	$2\delta(C_1\text{-}C_{14}\text{-}C_{16})\text{-}\delta(O_{15}\text{=}C_{14}\text{-}C_{16})\text{-}\delta(O_{15}\text{=}C_{14}\text{-}C_1)$	$\delta(CCC_{Ph})$
S_{61}	$\delta(O_{15}\text{=}C_{14}\text{-}C_{16})\text{-}\delta(O_{15}\text{=}C_{14}\text{-}C_1)$	δ(C=O)
S_{62}	$\gamma(O_7\text{=}C_{16}\text{-}C_{14}\text{-}C_1)$	γ(C=O)
S_{63}	$\delta(C_{17}\text{-}C_{16}\text{-}C_{14})\text{-}\delta(C_{21}\text{-}C_{16}\text{-}C_{14})$	w(Ph)
S_{64}	$\gamma(C_{14}\text{-}C_{17}\text{-}C_{16}\text{-}C_{21})$	γ(Ph)
S_{65}	$2\delta(C_2\text{=}C_1\text{-}C_{14})\text{-}\delta(C_2\text{=}C_1\text{-}Cl_6)\text{-}\delta(C_{14}\text{-}C_1\text{-}Cl_6)$	δ(C-Cl)
S_{66}	$\delta(Cl_6\text{-}C_1\text{-}C_{14})\text{-}\delta(C_2\text{=}C_1\text{-}C_{14})$	δ(CCC)
S_{67}	$\gamma(Cl_6\text{-}C_{14}\text{-}C_1\text{=}C_2)$	γ(C-Cl)
S_{68}	$2\delta(C_1\text{=}C_2\text{-}C_7)\text{-}\delta(N_3\text{-}C_2\text{=}C_1)\text{-}\delta(N_3\text{-}C_2\text{-}C_7)$	δ(CC2C)
S_{69}	$\delta(N_3\text{-}C_2\text{=}C_1)\text{-}\delta(N_3\text{-}C_2\text{-}C_7)$	δ(Azide)
S_{70}	$\delta(C_2\text{-}N_3\text{=}N_4)$	δ(CNN)
S_{71}	$\delta(N_5\text{=}N_3\text{=}N_4)$	δ(NNN)
S_{72}	$\gamma(N_3\text{-}C_7\text{-}C_2\text{=}C_1)$	γ(Azide)

[a] Normalization factors not shown. ν, bond stretching, δ, bending, γ, rocking, w, wagging, τ, torsion, Ph, phenyl ring; E, ester. See Figure 1 for atom numbering. The molecule belongs to the C_1 symmetry point group (all coordinates belong to the A symmetry species).

Table S3. Calculated [Scaled, DFT(B3LYP)/6-311++G(D,P)] Wavenumbers, IR Intensities and Potential Energy Distributions (PED) for Conformer I of MACBP.[A]

Approximate description	Wavenumber	Intensity	PED[b]
ν(C-H5)	3129	7.8	S_{26}(83), S_{25}(22)
ν(C-H1)	3124	7.4	S_{22}(80), S_{25}(34)
ν(C-H4)	3115	15.5	S_{25}(41), S_{24}(28), S_{26}(27)
ν(C-H2)	3107	5.6	S_{23}(100)
νCH_3 as´	3100	6.9	S_{10}(98)
ν(C-H3)	3097	0.1	S_{24}(66), S_{22}(26)
νCH_3 as´´	3067	10.0	S_{11}(100)
νCH_3 s	2991	24.1	S_9(98)
ν(N=N) as	2213	981.5	S_4(91)
ν(C=O) E	1734	274.2	S_6(89)
ν(C=O) Ph	1696	215.0	S_{14}(90)
νPh3	1603	81.2	S_{18}(56), S_{42}(18), S_1(12), S_{35}(10)
ν(C=C)	1596	140.2	S_1(66), S_{18}(11)
νPh4	1583	16.5	S_{19}(62), S_{41}(16), S_{34}(10)
δ(C-H2)	1486	0.8	S_{40}(62), S_{20}(33)
δCH_3 as´	1461	10.6	S_{28}(83), S_{30}(10)
δCH_3 as´´	1451	7.5	S_{29}(92)
νPh6, δ(C-H3)	1447	18.3	S_{21}(30), S_{41}(29), S_{39}(18)
δCH_3 s	1437	25.2	S_{27}(87)
ν(N=N) s	1370	194.6	S_3(48), S_2(34)
δ(C-H1)	1323	3.5	S_{39}(48), S_{17}(32), S_{43}(10)
νPh2	1309	17.1	S_{17}(55), S_{39}(30)
ν(C-O), ν(C-C_α) E	1251	323.7	S_7(36), S_5(24), S_{55}(11)
ν(C-C_{Ph})	1231	413.1	S_{15}(37), S_{13}(11)
γCH_3´	1185	8.5	S_{30}(70), S_{28}(10)
δ(C-H4)	1171	55.2	S_{42}(72), S_{18}(18)
δ(C-H5)	1159	1.5	S_{43}(65), S_{41}(14), S_{17}(12), S_{19}(11)
γCH_3´´	1144	1.7	S_{31}(91)
ν(C-O), ν(O-CH_3)	1119	72.5	S_7(15), S_8(11), S_2(10)
νPh6	1082	6.7	S_{21}(59), S_{41}(31), S_{43}(10)
νPh5, ν(C-C)	1041	53.8	S_{20}(28), S_{13}(25), S_{40}(12)
νPh1	1019	29.2	S_{20}(30), S_{16}(22), S_{33}(18), S_{40}(14)
δPh1	994	1.1	S_{33}(54), S_{16}(45)
γ(C-H5)	992	0.1	S_{48}(62), S_{36}(24)
γ(C-H4)	977	0.6	S_{47}(65), S_{38}(24)
ν(O-CH_3)	958	26.1	S_8(68), S_2(10)
γ(C-H3)	935	1.3	S_{46}(64), S_{37}(11)
ν(C-Cl)	889	16.5	S_{12}(23), S_5(10)
γ(C-H2)	843	0.8	S_{45}(98)
δ(C=O), ν(C-N)	834	40.1	S_{61}(13), S_2(12)
γ(C=O)	795	33.1	S_{62}(19), S_{44}(15), S_{64}(14), S_{55}(10)
γ(C=O) E	775	15.4	S_{58}(49), S_{72}(11)
γ(C=O) E, δ(OCO)	742	17.4	S_{44}(21), S_{58}(15), S_{55}(11)
γ(C-H1)	690	91.9	S_{44}(44), S_{36}(16), S_{62}(10)
τPh1	677	11.9	S_{36}(36), S_{62}(16), S_{48}(16)
δPh3	665	46.3	S_{35}(38), S_{60}(14)
δ(NNN)	643	33.7	S_{71}(39), S_{70}(21)
δPh2	617	0.4	S_{34}(78), S_{19}(10)
γ(C-Cl)	614	5.0	S_{60}(27), S_{67}(22), S_{34}(14)
γ(NNN)	516	4.0	S_{59}(65), S_{72}(10)
γ(NNN)	485	8.3	S_{59}(40), S_{72}(16)
γ(Ph), τPh2	438	0.3	S_{64}(28), S_{37}(28)
δ(CC=O)	425	0.2	S_{56}(15), S_{35}(10)
τPh3	403	0.1	S_{38}(72), S_{47}(26)
δ(C=O)	399	5.6	S_{61}(18), S_{71}(11), S_5(10)
δ(OCO), γ(Azide)	354	7.1	S_{55}(15), S_{69}(12), S_{72}(12), S_{56}(10), S_5(10)
δ(C-O-CH_3), δ(CC2C)	310	12.5	S_{57}(37), S_{68}(17), S_{12}(11)
δ(CNN)	285	2.5	S_{70}(18), S_{13}(12), S_{57}(11), S_{69}(10)
w(Ph)	255	7.5	S_{63}(43), S_{67}(13)
δ(C-Cl)	214	0.3	S_{66}(20), S_{65}(15)
δ(CCC)	193	0.8	S_{66}(40), S_{65}(15), S_{37}(11)
τ(C=C)	180	0.4	S_{52}(31), S_{49}(20)
τPh2	141	0.2	S_{37}(21), S_{64}(17), S_{62}(11), S_{69}(10), S_{70}(10)
δ(CNN), δ(Azide)	138	1.8	S_{69}(19), S_{70}(18), S_{51}(16)
τCH_3	108	1.1	S_{32}(64)
δ(CCC_{Ph})	106	0.4	S_{60}(21), S_{67}(19), S_{68}(11)
τ(C-O)	96	2.4	S_{52}(25), S_{50}(19), S_{51}(15), S_{32}(12)

τ(C=C)	78	0.7	S_{49}(33), S_{50}(25), S_{52}(19)
τ(C-C_α) E	50	1.6	S_{51}(38), S_{54}(29), S_{50}(19)
τ(C-C) Ph	42	0.3	S_{54}(47), S_{50}(12), S_{51}(10)
τ(C-N)	37	0.3	S_{50}(30), S_{49}(21)
τ(C-C_α) Ph	18	0.3	S_{53}(79), S_{51}(16)

[a] Wavenumbers (cm^{-1}, scaled by 0.978), calculated intensities (km mol^{-1}), ν, bond stretching, δ bending, γ rocking, w, wagging, τ, torsion, s, symmetric, as, asymmetric, Ph, phenyl ring, E, ester. See Table S2 for definition of internal coordinates. [b] Only PED values greater than 10 % are given.

Table S4. Calculated [scaled, DFT(B3LYP)/6-311++G(d,p)] wavenumbers, IR intensities and Potential Energy Distributions (PED) for conformer II of MACBP.[a]

Approximate description	Wavenumber	Intensity	PED[b]
ν(C-H1)	3131	7.2	$S_{22}(77)$, $S_{25}(15)$
ν(C-H4)	3123	8.6	$S_{25}(43)$, $S_{22}(29)$, $S_{26}(26)$
ν(C-H5)	3115	18.2	$S_{26}(50)$, $S_{25}(38)$, $S_{23}(20)$, $S_{24}(16)$
ν(C-H2)	3107	5.5	$S_{23}(82)$, $S_{26}(15)$
νCH_3 as´	3100	8.5	$S_{10}(98)$
ν(C-H3)	3097	0.2	$S_{24}(77)$, $S_{22}(13)$
νCH_3 as´´	3067	11.3	$S_{11}(100)$
νCH_3 s	2991	25.2	$S_9(98)$
ν(N=N) as	2212	972.7	$S_4(92)$
ν(C=O) E	1739	156.0	$S_6(85)$
ν(C=O) Ph	1699	252.4	$S_{14}(88)$
νPh3	1603	71.2	$S_{18}(59)$, $S_{42}(19)$
ν(C=C)	1595	162.4	$S_1(71)$
νPh4	1584	14.7	$S_{19}(62)$, $S_{41}(16)$
δ(C-H2)	1487	0.9	$S_{40}(62)$, $S_{20}(33)$
δCH_3 as´	1463	8.7	$S_{28}(81)$, $S_{30}(10)$
δCH_3 as´´	1451	10.8	$S_{29}(92)$
δ(C-H3)	1447	16.8	$S_{41}(29)$, $S_{21}(28)$, $S_{39}(18)$
δCH_3 s	1439	21.5	$S_{27}(87)$
ν(N=N) s	1372	265.6	$S_3(54)$, $S_2(31)$
δ(C-H1)	1323	3.8	$S_{39}(46)$, $S_{17}(34)$, $S_{43}(10)$
νPh2	1310	16.3	$S_{17}(53)$, $S_{39}(32)$
ν(C-O), $\nu(C\text{-}C_\alpha)$ E	1238	595.2	$S_7(24)$, $S_5(22)$, $S_{15}(10)$
$\nu(C\text{-}C_{Ph})$	1230	141.9	$S_{15}(28)$, $S_7(17)$
γCH_3´	1186	18.9	$S_{30}(71)$, $S_{10}(28)$
δ(C-H4)	1172	52.4	$S_{42}(73)$, $S_{18}(25)$
δ(C-H5)	1158	1.0	$S_{43}(65)$, $S_{41}(14)$, $S_{17}(12)$, $S_{19}(11)$
γCH_3´´	1147	0.9	$S_{31}(91)$
ν(C-O), $\nu(O\text{-}CH_3)$	1115	33.5	$S_7(12)$, $S_8(12)$, $S_2(10)$
νPh6	1082	5.5	$S_{21}(56)$, $S_{41}(32)$, $S_{43}(10)$
νPh5, ν(C-C)	1036	50.5	$S_{20}(24)$, $S_{13}(21)$, $S_{40}(15)$
νPh1	1018	40.6	$S_{20}(29)$, $S_{16}(22)$, $S_{33}(20)$, $S_{40}(11)$
δPh1	994	1.1	$S_{33}(54)$, $S_{16}(45)$
γ(C-H5)	990	8.6	$S_{48}(54)$, $S_{36}(21)$
$\nu(O\text{-}CH_3)$	986	57.4	$S_8(61)$
γ(C-H4)	975	0.2	$S_{47}(64)$, $S_{38}(23)$
γ(C-H3)	933	0.2	$S_{46}(68)$, $S_{37}(11)$
ν(C-Cl)	865	12.1	$S_{12}(19)$, $S_7(16)$
γ(C-H2)	841	0.5	$S_{45}(99)$
ν(C-N)	829	67.7	$S_2(14)$, $S_7(12)$, $S_{55}(11)$
γ(C=O)	792	20.7	$S_{62}(19)$, $S_{44}(17)$, $S_{64}(15)$
γ(C=O) E	771	17.6	$S_{58}(52)$, $S_{72}(13)$
γ(C=O) E, ν(C-Cl)	737	8.5	$S_{44}(21)$, $S_{58}(14)$, $S_{12}(12)$
γ(C-H1)	686	74.4	$S_{44}(39)$, $S_{36}(26)$, $S_{48}(12)$
τPh1	674	20.6	$S_{36}(22)$, $S_{35}(19)$, $S_{62}(13)$, $S_{48}(10)$
δ(NNN), δ(OCO)	664	25.4	$S_{71}(14)$, $S_{55}(14)$, $S_{12}(12)$
δPh3	655	68.6	$S_{71}(23)$, $S_{70}(14)$, $S_{35}(13)$
$\delta(CCC_{Ph})$, γ(C-Cl)	622	8.0	$S_{60}(25)$, $S_{67}(25)$
δPh2	616	2.4	$S_{34}(79)$
γ(NNN)	522	7.5	$S_{59}(90)$
γ(Azide)	489	6.2	$S_{72}(18)$, $S_{56}(15)$, $S_{59}(14)$
δ(NNN)	452	5.0	$S_{71}(18)$, $S_{72}(11)$
γ(Ph), γ(C-H4)	435	0.2	$S_{64}(37)$, $S_{37}(37)$
τPh3	403	0.0	$S_{38}(72)$, $S_{47}(25)$
δ(C=O)	397	4.3	$S_{61}(23)$, $S_{35}(16)$, $S_{15}(13)$, $S_{72}(11)$
$\delta(C\text{-}O\text{-}CH_3)$	337	21.6	$S_{57}(42)$, $S_{56}(13)$, $S_{69}(10)$
δ(OCO)	305	4.3	$S_{12}(19)$, $S_{68}(14)$, $S_{55}(12)$, $S_5(10)$
δ(Azide), δ(CNN)	279	5.5	$S_{69}(14)$, $S_{70}(14)$, $S_{13}(13)$
w(Ph)	253	9.3	$S_{63}(45)$, $S_{67}(13)$
δ(CC=O)	230	0.8	$S_{66}(15)$, $S_{56}(13)$, $S_{65}(12)$, $S_{57}(10)$
δ(CCC)	191	0.8	$S_{66}(44)$, $S_{65}(12)$
τ(C-O)	179	0.9	$S_{52}(38)$, $S_{49}(11)$
τPh2	146	0.4	$S_{37}(26)$, $S_{64}(20)$, $S_{62}(12)$
$\tau(C\text{-}C_\alpha)$ E, δ(C-Cl)	133	0.6	$S_{51}(14)$, $S_{65}(13)$, $S_{49}(12)$, $S_{32}(10)$
τCH_3	121	0.4	$S_{32}(61)$, $S_{70}(11)$, $S_{69}(10)$
δ(CC2C)	109	0.3	$S_{68}(25)$, $S_{32}(15)$, $S_{52}(15)$, $S_{65}(11)$, $S_{56}(10)$

γ(C-Cl),	δ(CCC_{Ph}),			S_{67}(17), S_{60}(16), S_{56}(16), S_{72}(12)
δ(CC=O)		101	0.9	
τ(C=C)		81	0.5	S_{50}(54), S_{49}(40)
τ(C-C_{α}) E		58	0.7	S_{51}(45), S_{54}(21), S_{53}(15)
τ(C-C) Ph		41	0.3	S_{54}(67), S_{51}(11)
τ(C-N)		37	0.6	S_{50}(49), S_{49}(24)
τ(C-C_{α}) Ph		21	1.7	S_{53}(75), S_{51}(20)

[a] Wavenumbers (cm^{-1}, scaled by 0.978), calculated intensities (km mol^{-1}), ν, bond stretching, δ bending, γ rocking, w, wagging, τ, torsion, s, symmetric, as, asymmetric, Ph, phenyl ring, E, ester. See Table S2 for definition of internal coordinates. [b] Only PED values greater than 10 % are given.

Table S5. Optimized Geometries of Conformers I, II and III of MACBP and of the Global Minima of MBCAC, CBMK and MCPOC in Cartesian Coordinates (Å) and Their Absolute Energies (A.U.).

Atom	Coordinates		
	X	Y	Z
*Conformer **I** (E = -1274.2737893 a.u.; E(+ZPE) = -1274.095012 a.u.)*			
C1	0.450876	-0.856122	-0.478543
C2	1.627216	-0.317439	-0.095126
N3	2.702603	-1.164202	0.192490
N4	3.743600	-0.727104	0.703182
N5	4.756017	-0.536225	1.164832
Cl6	0.251920	-2.586454	-0.555601
C7	1.846834	1.164966	-0.042590
O8	2.942185	1.666400	-0.124667
O9	0.708066	1.844429	0.130248
C10	0.807671	3.284237	0.065920
H11	1.165961	3.588855	-0.917647
H12	-0.202048	3.647768	0.237950
H13	1.489190	3.647788	0.834950
C14	-0.747878	-0.107503	-1.039224
O15	-0.662396	0.382179	-2.146041
C16	-1.999942	-0.076644	-0.235299
C17	-2.024542	-0.451739	1.113204
C18	-3.210157	-0.377785	1.838387
C19	-4.378465	0.064953	1.219621
C20	-4.360722	0.439427	-0.125745
C21	-3.177155	0.372796	-0.849704
H22	-1.117578	-0.794862	1.596641
H23	-3.223609	-0.666451	2.882976
H24	-5.302820	0.117650	1.783996
H25	-5.270562	0.780970	-0.605892
H26	-3.141971	0.661781	-1.893024
*Conformer **II** (E = -1274.2723887 a.u.; E(+ZPE) = -1274.093509 a.u.)*			
C1	-0.235867	0.933089	-0.498263
C2	-1.425040	0.419963	-0.122765
N3	-2.483056	1.295226	0.175455
N4	-3.448608	0.932946	0.853492
N5	-4.398097	0.779662	1.447612
Cl6	0.028420	2.650387	-0.521845
C7	-1.586082	-1.070302	-0.118577
O8	-0.665392	-1.849372	-0.094275
O9	-2.880019	-1.424514	-0.144573
C10	-3.151001	-2.843493	-0.150228
H11	-2.729753	-3.310097	0.740416
H12	-4.234621	-2.927387	-0.156922
H13	-2.719594	-3.300664	-1.040730
C14	0.934719	0.151247	-1.085604
O15	0.877322	-0.163586	-2.254835
C16	2.123700	-0.090954	-0.228173
C17	3.271093	-0.639300	-0.817433
C18	4.398942	-0.889265	-0.046587
C19	4.390721	-0.596790	1.319061
C20	3.251411	-0.054773	1.912070

C21	2.120937	0.198537	1.141067
H22	3.255835	-0.862238	-1.877193
H23	5.285453	-1.311757	-0.505480
H24	5.271904	-0.792648	1.919857
H25	3.244207	0.169245	2.972470
H26	1.235268	0.616150	1.605093
*Conformer **III** (E = -1274.271764 a.u.; E(+ZPE) = - 1274.092954 a.u.)*			
C1	-0.307078	-1.115149	0.279929
C2	-1.397259	-0.372623	-0.006789
N3	-2.467706	-0.977469	-0.690535
N4	-3.625295	-0.560217	-0.599504
N5	-4.730333	-0.326419	-0.638850
Cl6	-0.257153	-2.806629	-0.104620
C7	-1.369851	1.087025	0.324812
O8	-0.450248	1.637662	0.879601
O9	-2.489031	1.708768	-0.078264
C10	-2.569144	3.122903	0.204690
H11	-1.767398	3.652943	-0.309749
H12	-3.541609	3.433999	-0.168100
H13	-2.489901	3.294885	1.278085
C14	0.942320	-0.652427	1.024461
O15	0.994012	-0.847157	2.218856
C16	2.073819	-0.099761	0.232827
C17	3.220320	0.323914	0.918517
C18	4.301740	0.839354	0.216355
C19	4.251587	0.930990	-1.176588
C20	3.116173	0.507218	-1.864948
C21	2.028457	-0.004657	-1.162799
H22	3.239046	0.243763	1.998367
H23	5.185293	1.170329	0.750046
H24	5.097683	1.331807	-1.723619
H25	3.078538	0.574437	-2.946089
H26	1.148906	-0.335652	-1.702509
MBCAC (E = -1164.752016 au.; E(+ZPE) = -1164.583098 a.u.)			
C1	-1.727897	0.294156	0.628145
C2	-0.429893	0.504132	0.058603
N3	-0.940385	0.866532	1.431269
C4	0.543176	-0.666375	-0.080371
O5	0.060162	-1.773754	-0.204531
C6	2.006659	-0.428080	-0.012714
C7	2.543878	0.741044	0.542333
C8	3.923379	0.891125	0.647782
C9	4.772648	-0.113324	0.186043
C10	4.242899	-1.279796	-0.369771
C11	2.866753	-1.441790	-0.459897
H12	1.890389	1.523887	0.905407
H13	4.334982	1.791727	1.088169
H14	5.847240	0.010581	0.261052
H15	4.904560	-2.060534	-0.726793
H16	2.436897	-2.345740	-0.873701
Cl17	-0.172961	1.849869	-1.103664
C18	-3.144266	-0.165803	0.589574
O19	-3.790626	-0.385732	1.578305
O20	-3.552004	-0.287618	-0.673110
C21	-4.916428	-0.728193	-0.858223

H22	-5.046406	-1.722653	-0.430750
H23	-5.604218	-0.030327	-0.380062
H24	-5.066122	-0.746184	-1.934232
CBMK (E = -1164.781548 a.u.; E(+ZPE) = - 1164.612234 a.u.)			
C1	-0.066305	1.617132	0.024486
C2	0.854185	0.757504	0.418609
N3	1.709157	0.035343	0.884834
Cl4	0.468518	3.270811	-0.210964
C5	2.555870	-0.862857	0.179299
O6	2.159176	-1.769938	-0.500834
O7	3.820581	-0.570616	0.459847
C8	4.811396	-1.427414	-0.153345
H9	4.733624	-1.375876	-1.239409
H10	5.768011	-1.037913	0.184268
H11	4.671507	-2.456221	0.178283
C12	-1.524212	1.336575	-0.132101
O13	-2.300407	2.263063	-0.252120
C14	-1.997958	-0.081396	-0.082977
C15	-3.268228	-0.314195	0.464866
C16	-3.779205	-1.604179	0.525223
C17	-3.036990	-2.674846	0.021820
C18	-1.784594	-2.448426	-0.543154
C19	-1.263184	-1.156989	-0.595753
H20	-3.837470	0.528087	0.838349
H21	-4.756150	-1.777666	0.961837
H22	-3.438833	-3.681006	0.064836
H23	-1.209799	-3.272343	-0.949328
H24	-0.299241	-1.003776	-1.063265
MCPOC (E = -1164.817323 a.u.; E(+ZPE) = - 1164.645452 a.u.)			
C1	0.000000	0.544650	0.000000
C2	1.366375	0.357952	0.000000
O3	-0.533861	-0.715795	0.000000
Cl4	2.624522	1.539194	0.000000
C5	-0.930456	1.663776	0.000000
C6	-0.483523	2.995902	0.000000
C7	-1.399546	4.042438	0.000000
C8	-2.769183	3.784248	0.000000
C9	-3.220873	2.464752	0.000000
C10	-2.314470	1.411858	0.000000
H11	0.574771	3.214497	0.000000
H12	-1.038995	5.064666	0.000000
H13	-3.478607	4.603770	0.000000
H14	-4.284066	2.253613	0.000000
H15	-2.671571	0.390217	0.000000
N16	1.672535	-0.970562	0.000000
C17	0.518345	-1.567595	0.000000
C18	0.200019	-3.014983	0.000000
O19	-0.927362	-3.446723	0.000000
O20	1.314524	-3.753497	0.000000
C21	1.116627	-5.181199	0.000000
H22	0.565455	-5.487212	0.890015
H23	2.116637	-5.607372	0.000000
H24	0.565455	-5.487212	-0.890015

(*to be submitted*)

Supporting Information

for

UV-Induced Photochemistry of Methyl Aziridine-2-Carboxylate Isolated in Low Temperature Inert Matrices

Susy Lopes, Igor Reva, and Rui Fausto

Department of Chemistry, University of Coimbra, P-3004-535 Coimbra, Portugal

Contents

Table S3 – Calculated [scaled, DFT(B3LYP)/6-311++G(d,p)] wavenumbers, IR intensities and Potential Energy Distributions (PED) for conformer **I** of MA2C.

Table S4 – Calculated [scaled, DFT(B3LYP)/6-311++G(d,p)] wavenumbers, IR intensities and Potential Energy Distributions (PED) for conformer **II** of MA2C.

Table S5 – DFT(B3LYP)/6-311++G(d,p) calculated relative energies (ΔE/ kJ mol^{-1}) including zero-point vibrational contributions for relevant structures of possible photoproducts resulting from different ring-opening reactions of MA2C (see Figure 5).

Table S6 – DFT(B3LYP)/6-311++G(d,p) calculated values for the main conformational dihedral angles (º) for relevant structures of possible photoproducts resulting from different ring-opening reactions of MA2C (see Figure 5).

Table S7 – Definition of symmetry coordinates used in the normal mode analysis of the conformations of methyl (methyleneamino) acetate (MMAA).

Table S8 – Calculated [scaled, DFT(B3LYP)/6-311++G(d,p)] wavenumbers, IR intensities and Potential Energy Distributions (PED) for conformer **I** of MMAA.

Table S9 – Calculated [scaled, DFT(B3LYP)/6-311++G(d,p)] wavenumbers, IR intensities and Potential Energy Distributions (PED) for conformer **II** of MMAA.

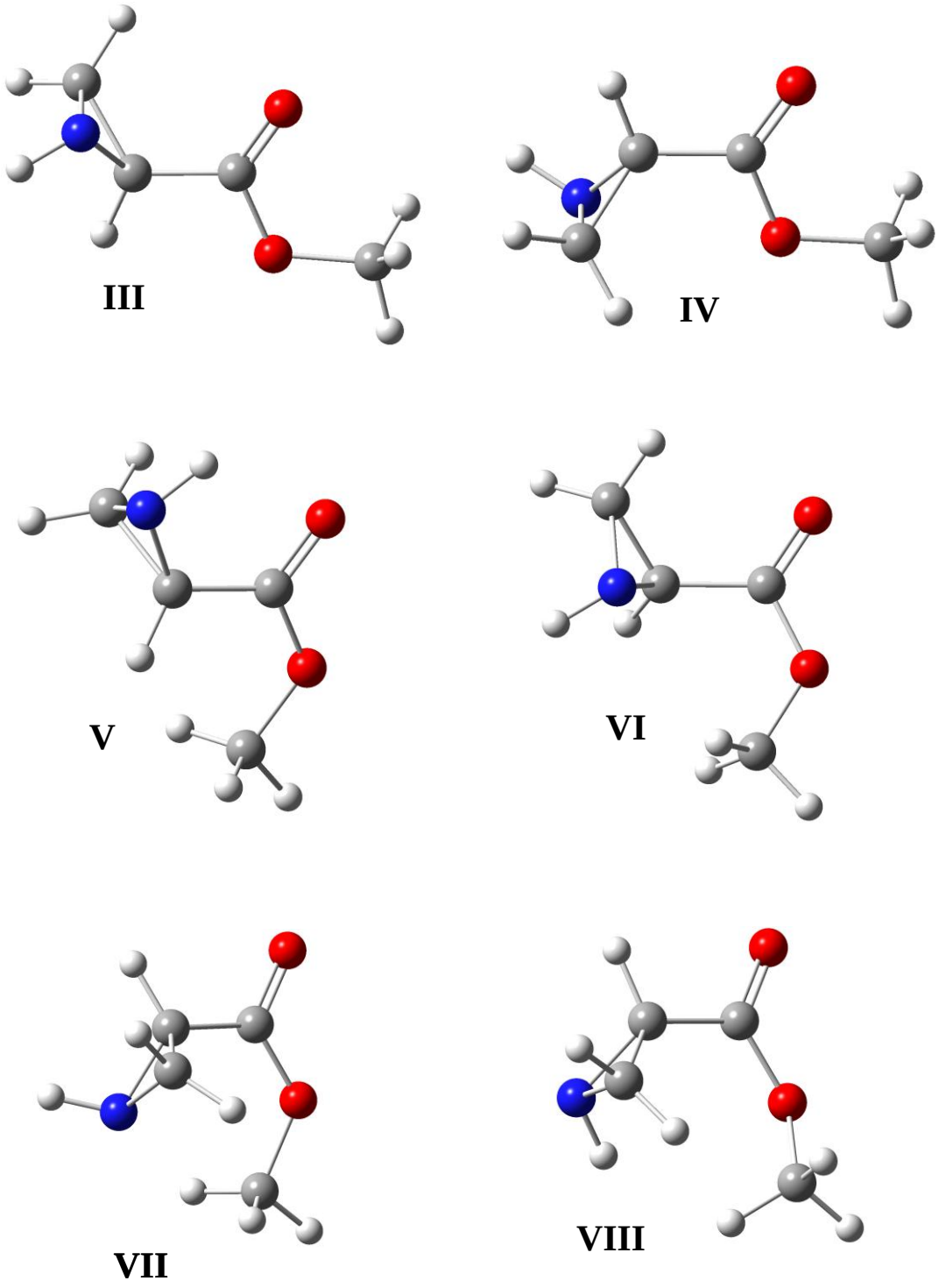

Figure S1. High energy conformers of MA2C, optimized at the DFT(B3LYP)/6-311++G(d,p) level of theory. Color codes: carbon – grey, hydrogen – white, oxygen – red, nitrogen – blue.

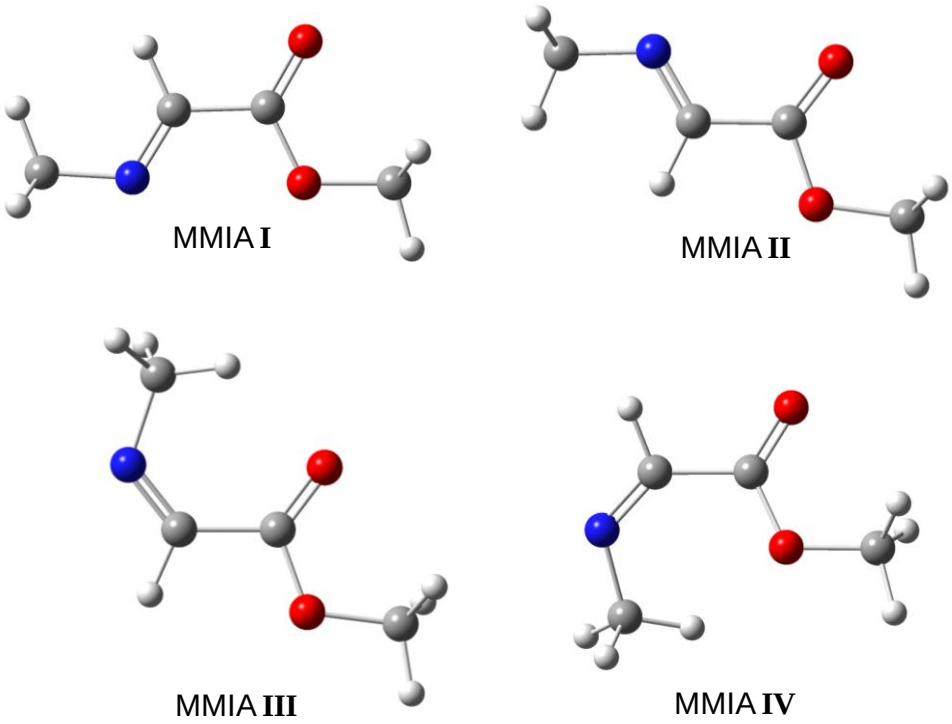

Figure S2. DFT(B3LYP)/6-311++G(d,p) optimized structures of the four most stable conformers of methyl 2-(methyleneamino)-acetate (MMIA). Color codes: carbon – grey, hydrogen – white, oxygen – red, nitrogen – blue.

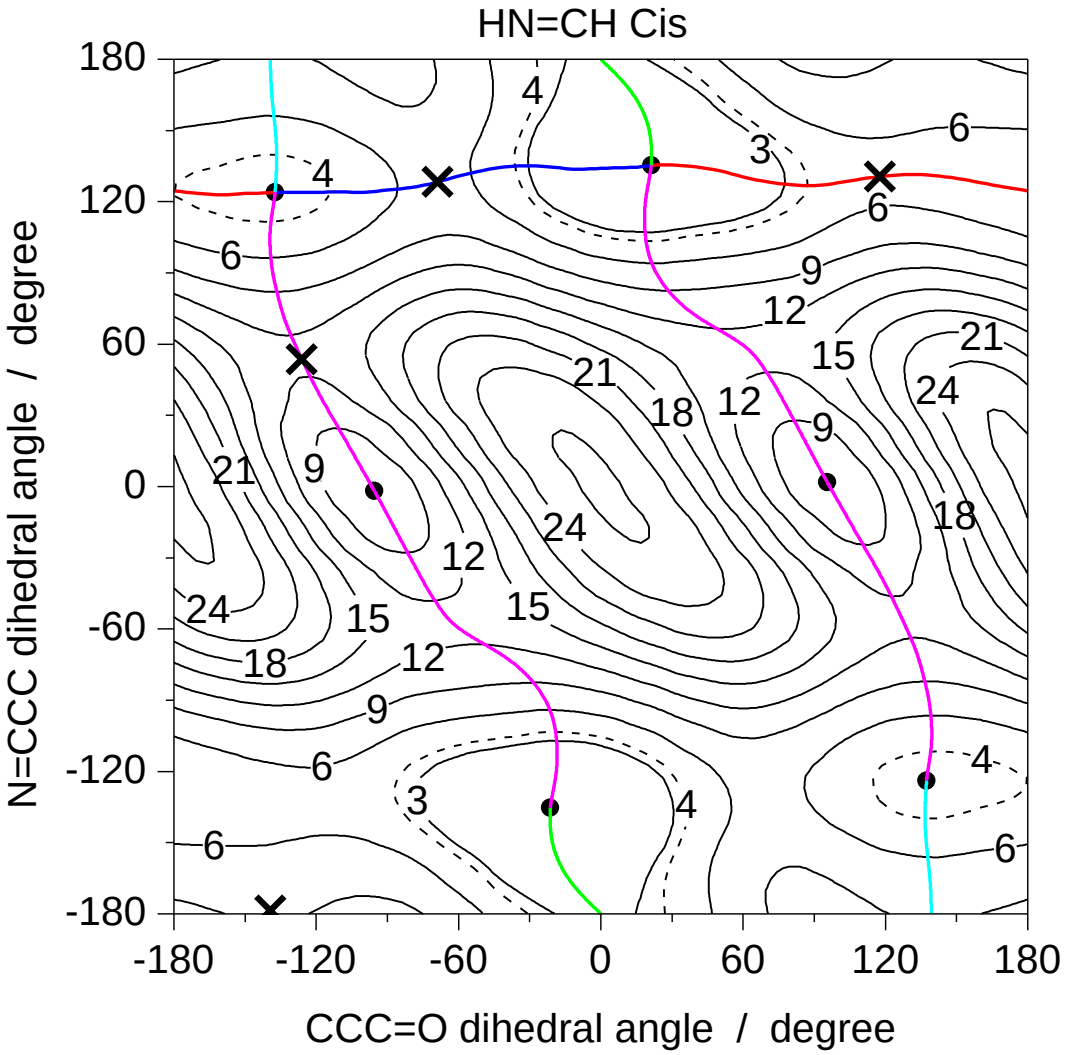

Figure S3. Potential energy map showing the position of the three low energy conformers of M3IP as a function of N=CCC and CCC=O dihedral angles. Calculations were carried out at the DFT/B3LYP/6-311++G(d,p) level. These dihedral angles were incremented in steps of 20º and all remaining internal coordinates were optimized at each point. Each conformer correspond to equivalent-by-symmetry minima and are represented by black circles (●) corresponding to conformer **I** (135.3 and 21.2º), **II** (123.9 and –137.4º) and **III** (–1.9 and –95.5º). Their respective mirror-like counterparts are also represented. 1st order transition states interconnecting the conformers are represented by crosses (**x**). Energies are relative to the most stable conformer (**I**) and do not include zero-point vibrational corrections. The corresponding one-dimensional potential energy profiles are shown in different colors (**II→I**, dark blue); (**II→I'** and **I→II'**, pink); (**I→I'**, green) and (**II→II'**, blue). Isoenergy levels are spaced by 2 kJ mol^{-1}. See Figure S5 for conformer structures.

HN=CH *Cis*

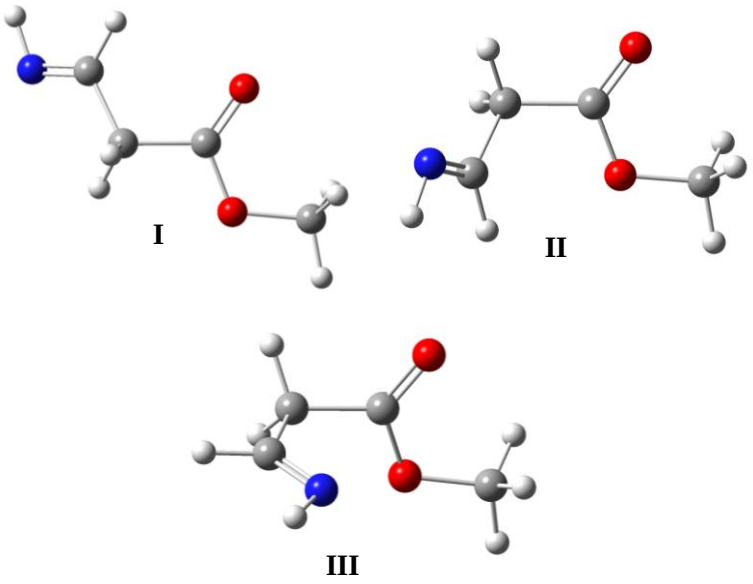

Figure S4. DFT(B3LYP)/6-311++G(d,p) optimized structures of the three most stable conformers of methyl 3-iminopropanoate (M3IP) with the HN=CH fragment in *cis* position. Color codes: carbon – grey, hydrogen – white, oxygen – red, nitrogen – blue.

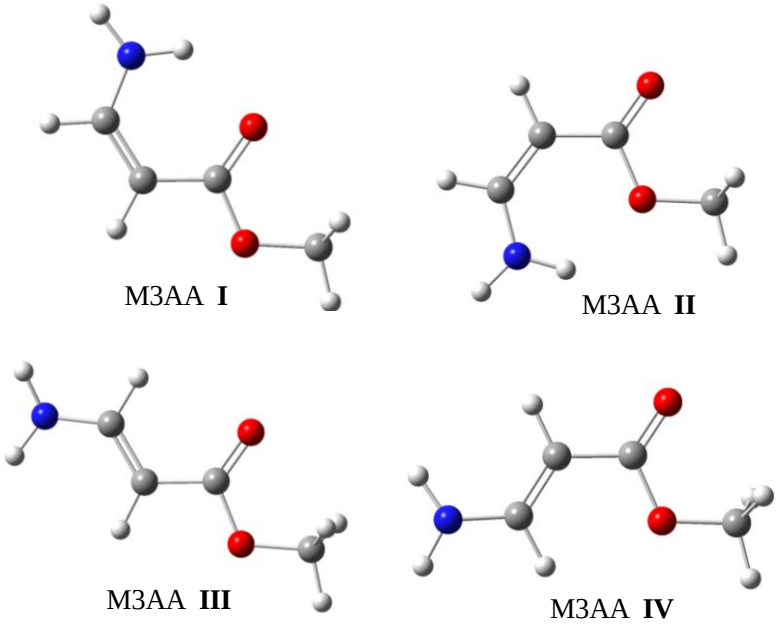

Figure S5. DFT(B3LYP)/6-311++G(d,p) optimized structures of the four most stable conformers of methyl 3-aminoacrylate (M3AA). Color codes: carbon – grey, hydrogen – white, oxygen – red, nitrogen – blue.

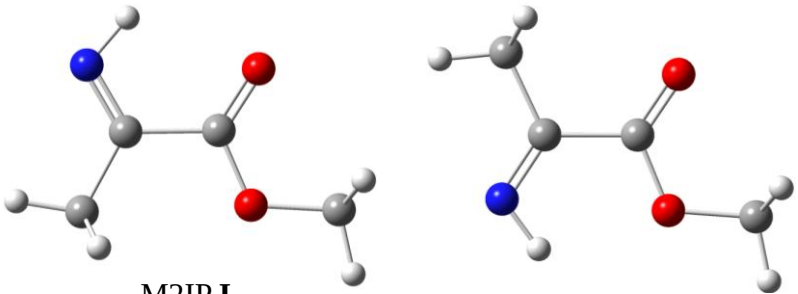

Figure S6. DFT(B3LYP)/6-311++G(d,p) optimized structures of the two most stable conformers of methyl 2-iminopropanoate (M2IP). Color codes: carbon – grey, hydrogen – white, oxygen – red, nitrogen – blue.

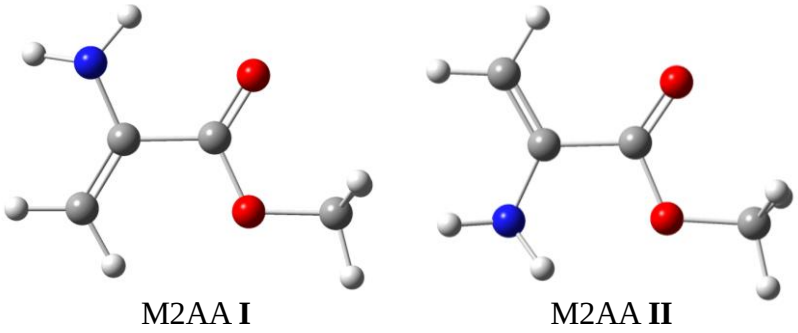

Figure S7. DFT(B3LYP)/6-311++G(d,p) optimized structures of the two most stable conformers of methyl 2-aminoacrylate (M2AA). Color codes: carbon – grey, hydrogen – white, oxygen – red, nitrogen – blue.

Table S1 - DFT(B3LYP)/6-311++G(d,p) calculated bond lengths (Å) and angles (º) of the eight conformers of MA2C.[a]

	I	II	III	IV	V	VI	VII	VIII
Bond lengths /Å								
C_1=O_2	1.211	1.207	1.205	1.215	1.206	1.202	1.203	1.203
C_1–C_3	1.491	1.491	1.497	1.492	1.501	1.513	1.505	1.505
C_1–O_{10}	1.344	1.355	1.352	1.344	1.351	1.354	1.367	1.367
C_3–N_4	1.470	1.472	1.480	1.482	1.466	1.479	1.476	1.476
C_3–C_5	1.498	1.498	1.492	1.492	1.502	1.477	1.497	1.497
C_3–H_8	1.083	1.083	1.084	1.085	1.082	1.087	1.083	1.083
N_4–C_5	1.458	1.459	1.461	1.470	1.457	1.476	1.461	1.461
N_4–H_9	1.019	1.017	1.017	1.019	1.020	1.017	1.016	1.016
C_5–H_6	1.084	1.084	1.086	1.086	1.085	1.085	1.084	1.084
C_5–H_7	1.085	1.085	1.084	1.083	1.085	1.083	1.082	1.082
O_{10}-C_{11}	1.442	1.441	1.440	1.436	1.436	1.437	1.432	1.432
C_{11}–H_{12}	1.091	1.090	1.091	1.091	1.093	1.091	1.092	1.092
C_{11}–H_{13}	1.087	1.088	1.088	1.088	1.088	1.088	1.089	1.089
C_{11}–H_{14}	1.091	1.091	1.091	1.091	1.092	1.093	1.093	1.093
Angles / º								
O_2=C_1–C_3	124.5	124.2	125.7	123.5	122.0	123.2	119.4	119.4
O_2=C_1–O_{10}	124.0	123.6	123.9	124.3	119.3	119.5	117.9	117.9
C_3–C_1–O_{10}	111.5	112.2	110.4	112.2	118.7	117.3	122.3	122.3
C_1–C_3–N_4	117.4	121.6	115.5	117.2	116.7	115.8	123.9	123.9
C_1–C_3–C_5	116.7	119.3	119.3	121.8	116.1	119.7	126.8	126.8
C_1–C_3–H_8	115.9	112.5	114.9	112.6	118.2	114.7	108.8	108.8
N_4–C_3–H_8	116.1	115.6	118.3	118.2	114.6	118.0	113.4	113.4
C_5–C_3–H_8	119.8	119.2	118.4	117.9	118.7	118.0	117.0	117.0
C_3–N_4–H_9	108.1	109.0	108.9	107.8	107.7	110.1	110.8	110.8
C_5–N_4–H_9	109.3	109.7	110.8	109.5	109.4	110.7	111.5	111.5
C_3–C_5–H_6	118.3	118.2	117.2	116.8	118.6	117.8	117.3	117.3
C_3–C_5–H_7	117.1	117.5	118.0	118.4	116.9	118.6	119.7	119.7
N_4–C_5–H_6	115.6	115.5	119.5	118.8	115.7	118.5	114.8	114.8
N_4–C_5–H_7	118.6	118.8	114.3	114.0	118.6	114.9	119.8	119.8
H_6–C_5–H_7	116.0	115.7	116.1	116.7	115.9	115.6	114.6	114.6
C_1–O_{10}–C_{11}	116.1	116.1	115.8	114.2	121.6	121.0	125.3	125.3
O_{10}–C_{11}–H_{12}	110.4	110.3	110.4	110.3	111.3	110.9	111.1	111.1
O_{10}–C_{11}–H_{13}	105.4	105.5	105.5	105.3	105.2	105.2	105.1	105.1
O_{10}–C_{11}–H_{14}	110.3	110.3	110.3	110.5	111.5	111.4	112.9	112.9
H_{12}–C_{11}–H_{13}	110.7	110.7	110.7	110.7	109.2	109.9	108.9	108.9
Dihedrals / º								
O_2=C_1–C_3–N_4	-21.2	158.3	-42.3	141.6	-12.5	-100.6	140.9	140.9
O_2=C_1–C_3–C_5	45.8	-132.3	24.8	-149.4	53.9	-32.1	-145.0	-145.0
O_2=C_1–C_3–H_8	-164.6	14.7	174.4	-0.6	-155.6	116.7	3.6	3.6
O_{10}–C_1–C_3–N_4	158.6	-21.7	138.5	-39.1	167.5	80.9	-32.5	-32.5
O_{10}–C_1–C_3–O_5	-134.4	47.8	-154.3	30.0	-126.1	149.4	41.5	41.5
O_{10}–C_1–C_3–H_8	15.2	-165.2	-4.7	178.8	24.4	-61.8	-169.8	-169.8
O_2=C_1–O_{10}–C_{11}	-0.7	1.4	0.2	-2.6	-175.3	173.9	147.8	147.8
C_3–C_1–O_{10}–C_{11}	179.5	-178.7	179.3	178.0	4.7	-7.6	-38.7	-38.7
C_1–C_3–N_4–H_9	3.6	4.8	-145.9	-144.7	2.8	-146.3	12.1	12.1
H_8–C_3–N_4–H_9	146.9	147.3	-4.0	-4.7	147.1	-4.9	147.7	147.7
C_1–C_3–C_5–H_6	148.0	144.1	146.2	145.6	148.6	147.0	144.5	144.5
C_1–C_3–C_5–H_7	1.4	-2.4	-0.3	-2.1	2.1	-0.5	-2.0	-2.0
H_8–C_3–C_5–H_6	-0.4	-0.7	-2.3	-1.6	-1.7	-0.8	-2.0	-2.0
H_8–C_3–C_5–H_7	-146.9	-147.2	-148.9	-149.3	-148.2	-148.3	-148.4	-148.4

H_9–N_4–C_5–H_6	-150.1	-149.3	5.7	6.1	-150.4	5.5	-148.9	-148.9
H_9–N_4–C_5–H_6	-5.7	-5.3	149.7	149.8	-5.8	148.1	-6.5	-6.5
C_1–O_{10}–C_{11}–H_{12}	-61.2	-59.9	-60.1	-59.9	-70.6	-57.7	-52.1	-52.1
C_1–O_{10}–C_{11}–H_{13}	179.2	-179.5	-179.7	-179.3	171.3	-176.5	-169.7	-169.7
C_1–O_{10}–C_{11}–H_{14}	59.7	60.9	60.7	61.0	53.0	65.6	72.3	72.3

[a] See Figure 1 for atom numbering.

Table S2 – Definition of symmetry coordinates used in the normal mode analysis of the conformations of methyl aziridine-2-carboxylate (MA2C)[a].

$S_1 = r_{1,2}$	ν(C=O)
$S_2 = r_{1,3}$	ν(C1C3)
$S_3 = r_{3,4}$	ν(CN)
$S_4 = r_{4,5}$	ν(NC)
$S_5 = r_{3,5}$	ν(C3C5)
$S_6 = 2^{-1/2} (r_{5,6} + r_{5,7})$	$\nu_s(CH_2)$
$S_7 = 2^{-1/2} (r_{5,6} - r_{5,7})$	$\nu_a(CH_2)$
$S_8 = r_{3,8}$	ν(CH)
$S_9 = r_{4,9}$	ν(NH)
$S_{10} = r_{1,10}$	ν(CO)
$S_{11} = r_{10,11}$	ν(O-CH_3)
$S_{12} = 3^{-1/2} (r_{11,13} + r_{11,14} + r_{11,12})$	$\nu_s(CH_3)$
$S_{13} = 6^{-1/2} (2r_{11,13} - r_{11,14} - r_{11,12})$	$\nu_a(CH_3)'$
$S_{14} = 2^{-1/2} (r_{11,14} - r_{11,12})$	$\nu_a(CH_3)''$
$S_{15} = 6^{-1/2} (\beta_{12,14,11}+\beta_{13,14,11}+\beta_{13,12,11}-\beta_{13,10,11}-\beta_{14,10,11}-\beta_{12,10,11})$	$\delta_1(CH_3)$
$S_{16} = 6^{-1/2} (2\beta_{12,14,11}-\beta_{13,14,11}-\beta_{13,12,11})$	$\delta_2(CH_3)$
$S_{17} = 2^{-1/2} (\beta_{13,14,11}-\beta_{13,12,11})$	$\delta_3(CH_3)$
$S_{18} = 6^{-1/2} (2\beta_{13,10,11}-\beta_{14,10,11}-\beta_{12,10,11})$	$\delta_4(CH_3)$
$S_{19} = 2^{-1/2} (\beta_{14,10,11}-\beta_{12,10,11})$	$\delta_5(CH_3)$
$S_{20} = 3^{-1/2} (\tau_{13,11,10,1}+\tau_{12,11,10,1}+\tau_{14,11,10,1})$	τCH_3
$S_{21} = 6^{-1/2} (2\beta_{3,10,1}-\beta_{2,3,1}-\beta_{2,10,1})$	δ(OCC)
$S_{22} = 2^{-1/2} (\beta_{2,3,1}-\beta_{2,10,1})$	δ(CC=O)
$S_{23} = \gamma_{2,10,1,3}$	γ(C=O)
$S_{24} = \beta_{1,11,10}$	δ(C-O-CH_3)
$S_{25} = 2^{-1/2} (\beta_{8,4,3}+\beta_{8,5,3})$	γ(CH8)
$S_{26} = 2^{-1/2} (\beta_{8,4,3}-\beta_{8,5,3})$	δ(CH8)
$S_{27} = 2^{-1/2} (\beta_{1,4,3}+\beta_{1,5,3})$	γ(C1C3)
$S_{28} = 2^{-1/2} (\beta_{1,4,3}-\beta_{1,5,3})$	δ(C1C3)
$S_{29} = 2^{-1/2} (\beta_{3,9,4}+\beta_{5,9,4})$	γ(NH)
$S_{30} = 2^{-1/2} (\beta_{3,9,4}-\beta_{5,9,4})$	δ(NH)
$S_{31} = 20^{-1/2} (4\beta_{6,7,5}-\beta_{6,4,5}-\beta_{7,4,5}-\beta_{6,3,5}-\beta_{7,3,5})$	$\delta(CH_2)$
$S_{32} = 1/2(\beta_{6,4,5}+\beta_{7,4,5}-\beta_{6,3,5}-\beta_{7,3,5})$	wag(CH_2)
$S_{33} = 1/2(\beta_{6,4,5}-\beta_{7,4,5}-\beta_{6,3,5}+\beta_{7,3,5})$	twist(CH_2)
$S_{34} = 1/2(\beta_{6,4,5}-\beta_{7,4,5}+\beta_{6,3,5}-\beta_{7,3,5})$	rock(CH_2)
$S_{35} = 2^{-1/2} (\tau_{3,1,10,11}+\tau_{2,1,10,1})$	τ(CO)
$S_{36} = 6^{-1/2} (\tau_{5,3,1,10}+\tau_{5,3,1,2}+\tau_{4,3,1,10}+\tau_{4,3,1,2}+\tau_{8,3,1,10}+\tau_{8,3,1,2})$	τ(CC)

[a] See Figure 1 for atom numbering. $r_{m,n}$ is the distance between atoms A_m and A_n; $\beta_{m,n,l}$ is the angle between vectors A_lA_m and A_lA_n; $\gamma_{m,n,l,o}$ is the angle between the vector A_lA_m and the plane defined by atoms A_n, A_l, A_o; $\tau_{m,n,l,o}$ is the dihedral angle between the plane defined by A_m, A_n, A_l and the plane defined by A_n, A_l, A_o atoms; s = symmetric; a = antisymmetric; ν = stretching; δ = in-plane bending; γ = out-of-plane bending; τ = torsion; rock = rocking; wag = wagging; twist = twisting. The molecule belongs to the C_1 symmetry point group (all coordinates belong to the A symmetry species).

Table S3 - Calculated [scaled, DFT(B3LYP)/6-311++G(d,p)] wavenumbers, IR intensities and Potential Energy Distributions (PED) for conformer **I** of MA2C.[a]

Approximate description	ν	I_{IR}	PED[b]
ν(NH)	3402.3	11.4	ν(NH) (100)
$\nu_a(CH_2)$	3129.8	9.6	$\nu_a(CH_2)$ (97)
ν(CH)	3107.7	4.2	ν(CH) (97)
$\nu_a(CH_3)'$	3091.4	12.6	$\nu_a(CH_3)'$ (97)
$\nu_a(CH_3)''$	3058.4	17.7	$\nu_a(CH_3)''$ (100)
$\nu_s(CH_2)$	3039.6	17.8	$\nu_s(CH_2)$ (100)
$\nu_s(CH_3)$	2986.0	29.6	$\nu_s(CH_3)$ (98)
ν(C=O)	1733.3	220.1	ν(C=O) (86)
$\delta(CH_2)$	1467.7	5.7	$\delta(CH_2)$ (90)
$\delta_2(CH_3)$	1464.2	8.8	$\delta_2(CH_3)$ (80), $\delta_4(CH_3)$ (10)
$\delta_3(CH_3)$	1451.5	10.0	$\delta_3(CH_3)$ (92)
$\delta_1(CH_3)$	1440.9	30.4	$\delta_1(CH_3)$ (81)
γ(CH8)	1378.6	83.8	γ(CH8) (44), ν(C1C3) (14)
γ(NH)	1274.3	2.4	γ(NH) (35), twist(CH_2) (12), ν(NC) (12), ν(CN) (11)
δ(NH)	1251.3	52.8	δ(NH) (60), rock(CH_2) (13)
ν(CO)	1203.3	399.3	ν(CO) (42), $\delta_4(CH_3)$ (18)
$\delta_4(CH_3)$	1177.1	66.0	$\delta_4(CH_3)$ (58)
γ(CH8), γ(NH)	1149.3	7.6	γ(CH8) (27), γ(NH) (22), δ(NH) (11), ν(C3C5) (11), wag(CH_2)(10)
$\delta_5(CH_3)$	1145.2	1.9	$\delta_5(CH_3)$ (89)
δ(CH8)	1108.4	14.4	δ(CH8) (54), twist(CH_2) (17), rock(CH_2) (12)
wag(CH_2)	1088.6	13.4	wag(CH_2) (80)
ν(O-CH_3)	1003.0	19.0	ν(O-CH_3) (31), ν(C1C3) (14), $\nu_s(CH_3)$ (12), twist(CH_2) (10)
ν(O-CH_3), twist(CH_2)	978.9	6.5	ν(O-CH_3) (33), twist(CH_2) (31), γ(NH) (11)
rock(CH_2)	948.4	6.9	rock(CH_2) (47), δ(NH) (12), δ(CH8) (11), ν(O-CH_3) (11)
ν(NC)	878.8	38.9	ν(NC) (34), ν(CO) (14), ν(C1C3) (12), ν(O-CH_3) (12)
ν(CN)	846.6	1.2	ν(CN) (46), ν(NC) (18)
ν(C3C5)	802.2	56.8	ν(C3C5) (34), ν(CN) (15), ν(NC) (11)
γ(C=O)	750.5	8.8	γ(C=O) (70)
δ(CC=O), ν(C1C3)	665.5	9.5	δ(CC=O) (43), ν(C1C3) (16), γ(C1C3) (15)
δ(OCC)	412.2	2.4	δ(OCC) (31), ν(C1C3) (15), δ(C-O-CH_3) (14)
δ(C-O-CH_3)	319.9	25.7	δ(C-O-CH_3) (41), δ(OCC) (26), γ(C1C3) (20)
δ(C1C3)	293.6	13.2	δ(C1C3) (60), τ(CO) (20)
γ(C1C3)	200.0	0.6	δ(OCC) (43), **γ(C1C3) (31)**, δ(C-O-CH_3) (22)
τ(CO)	159.3	1.2	τ(CO) (45), τCH_3 (21), τ(CC) (14), δ(C1C3) (11)
τCH_3	123.8	0.4	τCH_3 (77), τ(CO) (19)
τ(CC)	75.7	2.8	τ(CC) (83), τ(CO) (10)

[a] Wavenumbers (cm^{-1}, scaled by 0.978), calculated intensities (km mol^{-1}), s = symmetric; a = antisymmetric; ν = stretching; δ = in-plane bending; γ = out-of-plane bending; τ = torsion; rock = rocking; wag = wagging; twist = twisting. See Table S2 for definition of symmetry coordinates. [b] Only PED values greater than 10 % are given.

Table S4 - Calculated [scaled, DFT(B3LYP)/6-311++G(d,p)] wavenumbers, IR intensities and Potential Energy Distributions (PED) for conformer **II** of MA2C.[a]

Approximate description	ν	I_{IR}	PED[b]
ν(NH)	3434.6	10.9	ν(NH) (100)
$\nu_a(CH_2)$	3129.2	11.1	$\nu_a(CH_2)$ (96)
ν(CH)	3108.0	3.6	ν(CH) (96)
$\nu_a(CH_3)'$	3089.1	11.8	$\nu_a(CH_3)'$ (98)
$\nu_a(CH_3)''$	3058.3	17.1	$\nu_a(CH_3)''$ (100)
$\nu_s(CH_2)$	3041.0	17.9	$\nu_s(CH_2)$ (100)
$\nu_s(CH_3)$	2985.6	30.8	$\nu_s(CH_3)$ (98)
ν(C=O)	1751.7	333.4	ν(C=O) (87)
$\delta(CH_2)$	1470.9	0.4	$\delta(CH_2)$ (94)
$\delta_2(CH_3)$	1465.7	9.4	$\delta_2(CH_3)$ (80), $\delta_4(CH_3)$ (10), $\delta_1(CH_3)$ (10)
$\delta_3(CH_3)$	1450.0	9.6	$\delta_3(CH_3)$ (93)
$\delta_1(CH_3)$	1438.7	15.6	$\delta_1(CH_3)$ (86)
γ(CH8)	1354.0	17.1	γ(CH8) (51), ν(C3C5) (11)
γ(NH)	1268.6	39.4	γ(NH) (29), γ(CH8) (19), ν(NC) (12), ν(CN) (11)
ν(CO), ν(C1C3)	1252.9	222.1	ν(CO) (25), ν(C1C3) (20), γ(C1C3) (11), δ(OCC) (11)
δ(NH)	1241.1	23.5	δ(NH) (53), $rock(CH_2)$ (16), ν(C3C5) (10)
$\delta_4(CH_3)$	1179.2	10.6	$\delta_4(CH_3)$ (78), $\delta_2(CH_3)$ (11)
$\delta_5(CH_3)$	1146.9	11.0	$\delta_5(CH_3)$ (72)
$\delta_5(CH_3)$, $wag(CH_2)$	1143.7	39.8	$\delta_5(CH_3)$ (20), $wag(CH_2)$ (20), γ(NH) (15)
δ(CH8)	1108.3	37.0	δ(CH8) (54), $twist(CH_2)$ (17), $rock(CH_2)$ (12)
$wag(CH_2)$	1080.9	73.5	$wag(CH_2)$ (69)
$\nu(O\text{-}CH_3)$	1023.3	55.6	$\nu(O\text{-}CH_3)$ (52), γ(NH) (11)
$rock(CH_2)$	955.8	9.1	$rock(CH_2)$ (34), $twist(CH_2)$ (22), δ(NH) (15), γ(NH) (13)
$twist(CH_2)$	946.0	9.0	$twist(CH_2)$ (25), $rock(CH_2)$ (18), $\nu(O\text{-}CH_3)$ (17)
ν(NC)	883.6	28.6	ν(NC) (48), ν(CN) (13)
ν(CN)	814.4	55.9	ν(CN) (43), ν(CO) (17), ν(C3C5) (12)
ν(C3C5)	797.3	21.2	ν(C3C5) (26), ν(NC) (16), ν(CO) (14), β(CC=O) (10)
γ(C=O)	743.5	7.5	γ(C=O) (70)
γ(C1C3), ν(C1C3)	615.3	9.2	δ(OCC) (21), γ(C1C3) (19), ν(C1C3) (18), δ(CC=O)(11), $\nu(O\text{-}CH_3)$(10)
δ(CC=O)	466.8	7.6	δ(CC=O) (35), ν(C1C3) (18), γ(C1C3)(13), δ(OCC)(11), ν(CN)(10)
$\delta(C\text{-}O\text{-}CH_3)$	317.4	18.6	$\delta(C\text{-}O\text{-}CH_3)$ (58), δ(CC=O) (17), γ(C1C3) (16)
δ(C1C3)	291.7	11.3	δ(C1C3) (64), τ(CO) (18)
δ(OCC)	195.3	0.2	δ(OCC) (47), γ(C1C3) (31), $\delta(C\text{-}O\text{-}CH_3)$ (16)
τ(CO)	142.5	1.0	τ(CO) (50), τCH_3 (29)
τCH_3	119.6	1.0	τCH_3 (64), τ(CO) (25)
τ(CC)	85.7	1.1	τ(CC) (92)

[a] Wavenumbers (cm^{-1}, scaled by 0.978), calculated intensities (km mol^{-1}), s = symmetric; a = antisymmetric; ν = stretching; δ = in-plane bending; γ = out-of-plane bending; τ = torsion; rock = rocking; wag = wagging; twist = twisting. See Table S2 for definition of symmetry coordinates. [b] Only PED values greater than 10 % are given.

Table S5 – DFT(B3LYP)/6-311++G(d,p) calculated relative energies (ΔE/ kJ mol^{-1}) including zero-point vibrational contributions for relevant structures of possible photoproducts resulting from different ring-opening reactions of MA2C (see Figure 5).

MMAA[a]	ΔE_{DFT}	Symmetry
I	0.0	C1
II	1.3	C1
III	6.0	C1
MMIA[b]		
I	0.0	C_s
II	2.1	C_s
III	11.3	C_s
IV	17.5	C_s
M3IP (HN=CH cis)[c]		
I	0.0	C1
II	3.4	C1
III	6.9	C1
M3IP (HN=CH trans)[d]		
I	0.0	C1
II	0.1	C1
III	0.4	C1
IV	3.9	C1
M3AA[e]		
I	0.0	C_s
II	12.4	C_s
III	14.7	C1
IV	19.1	C1
M2IP[f]		
I	0.0	C_s
II	1.6	C_s
M2AA[g]		
I	0.0	C1
II	4.8	C1

[a] See Figure 6 for structures of the conformers. [b] See Figure S2 for structures of conformers. [c] See Figure S4 for structures of the conformers. [d] See Figure 11 for structures of the conformers. [e] See Figure S5 for structures of the conformers. [f] See Figure S6 for structures of the conformers. [g] See Figure S7 for structures of the conformers.

Table S6 - DFT(B3LYP)/6-311++G(d,p) calculated values for the main conformational dihedral angles (º) for relevant structures of possible photoproducts resulting from different ring-opening reactions of MA2C (see Figure 5).

	MMAA **I**	MMAA **II**	MMAA **III**	
Dihedral angles / º				
O_2=C_1–C_3–N_4	–35.2/(35.2)	138.3/(–138.3)	46.8/(–46.8)	
C_1–C_3–N_4=C_5	111.5/(–111.5)	122.4/(–122.4)	–0.9/(0.9)	
	MMIA **I**	MMIA **II**	MMIA **III**	MMIA **IV**
O_2=C_1–C_3=N_4	180	0	0	180
C_5–N_4=C_3–C_1	180	180	0	0
	M3IP **I** (HN=CH cis)	M3IP **II**	M3IP **III**	
N_4=C_5–C_3–C_1	135.3	123.9	–1.9	
C_5–C_3–C_1=O_2	21.2	–137.4	–95.5	
	M3IP **I** (HN=CH trans)	M3IP **II**	M3IP **III**	M3IP **IV**
N_4=C_5–C_3–C_1	16.0	134.6	120.4	23.4
C_5–C_3–C_1=O_2	–41.2	48.2	–119.4	–60.9
	M3AA **I**	M3AA **II**	M3AA **III**	M3AA **IV**
N_4=C_5–C_3–C_1	0.0	0.0	180.0	180.0
C_5–C_3–C_1=O_2	0.0	180.0	0.0	180.0
	M2IP **I**	M2IP **II**		
H_9=N_4–C_3–C_1	0.0	0.0		
N_4=C_3–C_1=O_2	0.0	180.0		
	M2AA **I**	MAA **II**		
H_9=N_4–C_3–C_1	19.001	24.289		
N_4=C_3–C_1=O_2	-9.440	–9.107		

[a] See Figure 6 for atom numbering. [b] See Figure S2 for structures of conformers. [c] See Figure S5 for structures of the conformers. [d] See Figure 11 for structures of the conformers. [e] See Figure S5 for structures of the conformers. [f] See Figure S6 for structures of the conformers. [g] See Figure S7 for structures of the conformers.

Table S7 – Definition of symmetry coordinates used in the normal mode analysis of the conformations of methyl (methyleneamino) acetate (MMAA)[a].

$S_1 = r_{1,2}$	ν(C=O)
$S_2 = r_{1,3}$	ν(CC)
$S_3 = r_{3,4}$	ν(CN)
$S_4 = r_{4,5}$	ν(N=C)
$S_5 = r_{5,6}$	ν(CH6)
$S_6 = r_{5,7}$	ν(CH7)
$S_7 = r_{3,8}$	ν(CH8)
$S_8 = r_{4,9}$	ν(CH9)
$S_9 = r_{1,10}$	ν(CO)
$S_{10} = r_{10,11}$	ν(O-CH_3)
$S_{11} = 3^{-1/2} (r_{11,13} + r_{11,14} + r_{11,12})$	$\nu_s(CH_3)$
$S_{12} = 6^{-1/2} (2r_{11,13} - r_{11,14} - r_{11,12})$	$\nu_a(CH_3)'$
$S_{13} = 2^{-1/2} (r_{11,14} - r_{11,12})$	$\nu_a(CH_3)''$
$S_{14} = 6^{-1/2} (\beta_{12,14,11}+\beta_{13,14,11}+\beta_{13,12,11}-\beta_{13,10,11}-\beta_{14,10,11}-\beta_{12,10,11})$	$\delta_1(CH_3)$
$S_{15} = 6^{-1/2} (2\beta_{12,14,11}-\beta_{13,14,11}-\beta_{13,12,11})$	$\delta_2(CH_3)$
$S_{16} = 2^{-1/2} (\beta_{13,14,11}-\beta_{13,12,11})$	$\delta_3(CH_3)$
$S_{17} = 6^{-1/2} (2\beta_{13,10,11}-\beta_{14,10,11}-\beta_{12,10,11})$	$\delta_4(CH_3)$
$S_{18} = 2^{-1/2} (\beta_{14,10,11}-\beta_{12,10,11})$	$\delta_5(CH_3)$
$S_{19} = 3^{-1/2} (\tau_{13,11,10,1}+\tau_{12,11,10,1}+\tau_{14,11,10,1})$	τCH_3
$S_{20} = 6^{-1/2} (2\beta_{3,10,1}-\beta_{2,3,1}-\beta_{2,10,1})$	δ(OCC)
$S_{21} = 2^{-1/2} (\beta_{2,3,1}-\beta_{2,10,1})$	δ(CC=O)
$S_{22} = \gamma_{2,10,1,3}$	γ(C=O)
$S_{23} = \beta_{1,11,10}$	δ(C-O-CH_3)
$S_{24} = 6^{-1/2} (2\beta_{6,7,5}-\beta_{6,4,5}-\beta_{7,4,5})$	$\delta(C5H_2)$
$S_{25} = 2^{-1/2} (\beta_{6,4,5}-\beta_{7,4,5})$	wag($C5H_2$)
$S_{26} = \beta_{3,5,4}$	δ(CN=C)
$S_{27} = \gamma_{6,4,5,7}$	γ(CH)
$S_{28} = 20^{-1/2} (4\beta_{8,9,3}-\beta_{8,9,1}-\beta_{9,1,3}-\beta_{8,4,3}-\beta_{9,4,3})$	$\delta(CH_2)$
$S_{29} = 1/2(\beta_{8,9,1}+\beta_{9,1,3}-\beta_{8,4,3}-\beta_{9,4,3})$	wag(CH_2)
$S_{30} = 1/2(\beta_{8,9,1}-\beta_{9,1,3}-\beta_{8,4,3}+\beta_{9,4,3})$	twist(CH_2)
$S_{31} = 1/2(\beta_{8,9,1}-\beta_{9,1,3}+\beta_{8,4,3}-\beta_{9,4,3})$	rock(CH_2)
$S_{32} = \beta_{1,4,3}$	δ(CCN)
$S_{33} = 2^{-1/2} (\tau_{3,1,10,11}+\tau_{2,1,10,1})$	τ(CO)
$S_{34} = 6^{-1/2} (\tau_{4,3,1,10}+\tau_{4,3,1,2}+\tau_{8,3,1,10}+\tau_{8,3,1,2}+\tau_{9,3,1,10}+\tau_{9,3,1,2})$	τ(CC)
$S_{35} = 3^{-1/2} (\tau_{1,3,4,5}+\tau_{8,3,4,5}+\tau_{9,3,4,5})$	τ(CN)
$S_{36} = 2^{-1/2} (\tau_{3,4,5,6}+\tau_{3,4,5,7})$	τ(N=C)

[a] See Figure 6 for atom numbering. $r_{m,n}$ is the distance between atoms A_m and A_n; $\beta_{m,n,l}$ is the angle between vectors A_lA_m and A_lA_n; $\gamma_{m,n,l,o}$ is the angle between the vector A_lA_m and the plane defined by atoms A_n, A_l, A_o; $\tau_{m,n,l,o}$ is the dihedral angle between the plane defined by A_m, A_n, A_l and the plane defined by A_n, A_l, A_o atoms; s = symmetric; a = antisymmetric; ν = stretching; δ = in-plane bending; γ = out-of-plane bending; τ = torsion; rock = rocking; wag = wagging; twist = twisting. The molecule belongs to the C_1 symmetry point group (all coordinates belong to the A symmetry species).

Table S8 - Calculated [scaled, DFT(B3LYP)/6-311++G(d,p)] wavenumbers, IR intensities and Potential Energy Distributions (PED) for conformer **I** of MMAA.[a]

Approximate description	ν	I_{IR}	PED[b]
$\nu_a(CH_3)'$	3089.9	13.2	$\nu_a(CH_3)'$ (97)
ν(CH7)	3067.2	24.1	ν(CH7) (92)
$\nu_a(CH_3)''$	3057.1	17.9	$\nu_a(CH_3)''$ (100)
ν(CH9)	3028.0	5.4	ν(CH9) (98)
$\nu_s(CH_3)$	2985.0	29.9	$\nu_s(CH_3)$ (98)
ν(CH6)	2922.5	59.4	ν(CH6) (92)
ν(CH8)	2884.6	38.0	ν(CH8) (98)
ν(C=O)	1767.4	235.9	ν(C=O) (87)
ν(N=C)	1699.7	27.5	ν(N=C) (85), $\delta(C5H_2)$ (11)
$\delta_2(CH_3)$	1464.3	8.4	$\delta_2(CH_3)$ (79), $\delta_4(CH_3)$ (10)
$\delta(C5H_2)$	1463.8	18.4	$\delta(C5H_2)$ (78)
$\delta_3(CH_3)$	1450.8	10.2	$\delta_3(CH_3)$ (93)
$\delta(CH_2)$	1439.3	2.9	$\delta(CH_2)$ (66), $\delta_1(CH_3)$ (22)
$\delta_1(CH_3)$	1436.8	19.8	$\delta_1(CH_3)$ (66), $\delta(CH_2)$ (23)
$wag(CH_2)$	1345.3	40.4	$wag(CH_2)$ (74)
$twist(CH_2)$	1241.2	54.5	$twist(CH_2)$ (67), $wag(C5H_2)$ (17)
$wag(C5H_2)$	1196.2	248.8	ν(CO) (28), $wag(C5H_2)$ (27), $\beta_4(CH_3)$ (15)
$\delta_4(CH_3)$	1180.7	2.4	$\delta_4(CH_3)$ (52), $wag(C5H_2)$ (22)
$wag(C5H_2)$,$twist(CH_2)$	1161.1	170.5	$wag(C5H_2)$ (21), ν(CO) (17), $twist(CH_2)$ (17), $\delta_4(CH_3)$ (11)
$\delta_5(CH_3)$	1145.5	2.6	$\delta_5(CH_3)$ (91)
γ(CH)	1049.0	18.3	γ(CH) (100)
$\nu(O\text{-}CH_3)$	1023.8	26.0	$\nu(O\text{-}CH_3)$ (39), ν(CN) (28)
$rock(CH_2)$	1000.9	1.2	$rock(CH_2)$ (51), ν(CN) (18), γ(C=O) (14)
ν(CN)	950.7	16.5	$\nu(O\text{-}CH_3)$ (35), ν(CN) (28), ν(CC) (13)
ν(CO)	893.3	7.1	ν(CO) (19), ν(CC) (17), $\nu(O\text{-}CH_3)$ (14)
τ(N=C)	765.6	19.3	τ(N=C) (34), β(CC=O) (19), ν(CO) (16)
γ(C=O)	639.0	7.0	τ(N=C) (36), γ(C=O) (35)
δ(CC=O)	589.3	10.9	γ(C=O) (23) ν(CC) (20) β(CC=O) (18) β(CN=C) (12)
δ(CN=C)	458.2	2.3	δ(CN=C) (55), $rock(CH_2)$ (13), δ(OCC) (10), δ(CC=O)(10)
$\delta(C\text{-}O\text{-}CH_3)$	380.7	4.5	δ(OCC) (22), δ(CN=C) (18), $\delta(C\text{-}O\text{-}CH_3)$ (18), ν(CC) (10)
δ(CCN)	312.9	10.9	δ(CCN) (35), $\delta(C\text{-}O\text{-}CH_3)$ (30), δ(CC=O) (21)
δ(OCC)	230.9	6.1	δ(OCC) (37), $\delta(C\text{-}O\text{-}CH_3)$ (25), δ(CCN) (16), τ(CO) (13)
τ(CO)	166.8	5.3	τ(CO) (62), τCH_3 (10)
τCH_3	121.6	0.6	τCH_3 (89), τ(CO) (10)
τ(CN)	68.2	9.7	τ(CN) (86)
τ(CC)	36.7	3.2	τ(CC) (90)

[a] Wavenumbers (cm^{-1}, scaled by 0.978), calculated intensities (km mol^{-1}), s = symmetric; a = antisymmetric; ν = stretching; δ = in-plane bending; γ = out-of-plane bending; τ = torsion; rock = rocking; wag = wagging; twist = twisting. See Table S7 for definition of internal coordinates. [b] Only PED values greater than 10 % are given.

Table S9 - Calculated [scaled, DFT(B3LYP)/6-311++G(d,p)] wavenumbers, IR intensities and Potential Energy Distributions (PED) for conformer **II** of MMAA.[a]

Approximate description	ν	I_{IR}	PED[b]
$\nu_a(CH_3)'$	3089.9	12.4	$\nu_a(CH_3)'$ (98)
ν(CH7)	3065.4	24.4	ν(CH7) (92)
$\nu_a(CH_3)''$	3057.4	17.5	$\nu_a(CH_3)''$ (100)
ν(CH9)	3031.5	3.7	ν(CH9) (98)
$\nu_s(CH_3)$	2985.3	30.4	$\nu_s(CH_3)$ (98)
ν(CH6)	2921.4	59.4	ν(CH6) (92)
ν(CH8)	2886.0	38.0	ν(CH8) (98)
ν(C=O)	1755.0	339.5	ν(C=O) (87)
ν(N=C)	1694.9	7.0	ν(N=C) (84), $\delta(C5H_2)$ (11)
$\delta_2(CH_3)$	1463.7	8.6	$\delta_2(CH_3)$ (80), $\delta_4(CH_3)$ (10)
$\delta(C5H_2)$	1462.3	13.4	$\delta(C5H_2)$ (80)
$\delta_3(CH_3)$	1451.1	10.0	$\delta_3(CH_3)$ (93)
$\delta(CH_2)$	1440.4	3.7	$\delta(CH_2)$ (60), $\delta_1(CH_3)$ (28)
$\delta_1(CH_3)$	1435.6	14.0	$\delta_1(CH_3)$ (65), $\delta(CH_2)$ (28)
$wag(CH_2)$	1330.3	14.7	$wag(CH_2)$ (84)
$twist(CH_2)$	1273.4	166.3	$twist(CH_2)$ (40), ν(CO) (23), δ(CC=O) (10)
$wag(C5H_2)$,$twist(CH_2)$	1209.0	171.7	$wag(C5H_2)$ (24), $twist(CH_2)$ (23), ν(CO) (21)
$\delta_4(CH_3)$	1180.6	4.2	$\delta_4(CH_3)$ (64), $wag(C5H_2)$ (13)
$wag(C5H_2)$	1178.5	21.4	$wag(C5H_2)$ (45), $twist(CH_2)$ (26), $\delta_4(CH_3)$ (11)
$\delta_5(CH_3)$	1145.2	0.9	$\delta_5(CH_3)$ (92)
γ(CH)	1046.3	10.9	γ(CH) (99)
$\nu(O\text{-}CH_3)$	1027.7	76.4	$\nu(O\text{-}CH_3)$ (52), $rock(CH_2)$ (25)
ν(CN)	988.4	9.3	ν(CN) (64)
$rock(CH_2)$	977.9	6.3	$rock(CH_2)$ (37), $\nu(O\text{-}CH_3)$ (18), ν(CC) (15)
ν(CO)	843.7	22.0	ν(CO) (40), $\nu(O\text{-}CH_3)$ (15), ν(CC) (10)
τ(N=C)	769.3	16.9	τ(N=C) (37), β(CC=O) (14), γ(C=O) (10)
γ(C=O)	648.2	6.7	γ(C=O) (41), τ(N=C) (34), $rock(CH_2)$ (10)
ν(CC)	596.2	10.0	ν(CC) (25), β(CC=O) (21), β(CN=C) (14), γ(C=O) (11), τ(N=C) (10)
δ(CN=C)	438.1	3.8	δ(CN=C) (40), δ(OCC) (20), $rock(CH_2)$ (10)
δ(CC=O)	414.3	2.7	δ(CN=C) (31), δ(CC=O) (25), ν(CC) (11)
$\delta(C\text{-}O\text{-}CH_3)$	309.1	19.6	$\delta(C\text{-}O\text{-}CH_3)$ (49), δ(CCN) (27)
δ(OCC)	232.4	3.4	δ(OCC) (35), $\delta(C\text{-}O\text{-}CH_3)$ (19), τ(CO) (16), δ(CCN) (16), τ(CN) (11)
τ(CO)	152.3	7.0	τ(CO) (54), τCH_3 (19), γ(C=O) (10)
τCH_3	124.5	1.4	τCH_3 (79), τ(CO) (18)
τ(CN)	81.2	5.4	τ(CN) (84)
τ(CC)	39.9	3.1	τ(CC) (95)

[a] Wavenumbers (cm^{-1}, scaled by 0.978), calculated intensities (km mol^{-1}), s = symmetric; a = antisymmetric; ν = stretching; δ = in-plane bending; γ = out-of-plane bending; τ = torsion; rock = rocking; wag = wagging; twist = twisting. See Table S7 for definition of internal coordinates. [b] Only PED values greater than 10 % are given.

J. Photochem. Photobiol. A: Chemistry, **2008**, *200*, 169-180.

Supporting Information

for

Low Temperature IR Spectroscopy and Photochemistry of Matrix-Isolated α-Pyridil

Susy Lopes,[a] Andrea Gómez-Zavaglia[a,b] and Rui Fausto[a]

[a]*Department of Chemistry,University of Coimbra, P-3004-535 Coimbra, Portugal*
[b]*Faculdad de Farmacia y Bioquímica, Universidad de Buenos Aires, Junín 956, 1113 Buenos Aires, Argentina*

Contents

Table S1 – Experimental and calculated [DFT(B3LYP)/6-311++G(d,p)] bond lengths and angles for the three conformers of α-pyridil.[a]

	Experimental X-ray [27][b]	Caculated [DFT(B3LYP)/6-311++G(d,p)]		
		TTG	***TCG***	***CCSk***
ΔE / kJ mol^{-1}		0.0	21.0	35.1
Bond length / pm				
C_1-C_3	152.1 (4)	154.7	154.5	154.4
C_1=O_2 / C_3=O_4	121.8 (4) / 121.6 (4)	121.0	120.7 / 121.3	121.1
C_1-C_5 / C_3-C_6	147.8 (4) / 149.4 (4)	149.5	150.2 / 149.6	150.7
C_5-N_7 / C_6-N_8	135.3 (4) / 134.7 (4)	133.9	134.0 / 133.9	134.2
C_5=C_{15} / C_6=C_{16}	137.9 (5) / 137.7 (4)	139.6	139.8 / 139.6	139.9
N_7=C_9 / N_8=C_{10}	134.6 (5) / 133.8 (4)	133.3	132.9 / 133.2	132.8
C_9-C_{11} / C_{10}-C_{12}	136.2 (6) / 137.7 (5)	139.6	139.9 / 139.6	139.9
C_9-H_{17} / C_{10}-H_{21}	100.0 (4) / 103.0 (3)	108.6	108.7 / 108.6	108.7
C_{11}=C_{13} / C_{12}=C_{14}	137.3 (6) / 138.5 (5)	139.3	138.9 / 139.3	138.9
C_{11}-H_{18} / C_{12}-H_{22}	99.0 (4) / 99.0 (3)	108.4	108.4 / 108.4	108.4
C_{13}-C_{15} / C_{14}-C_{16}	140.2 (6) / 139.5 (5)	139.0	139.3 / 139.0	139.3
C_{13}-H_{19} / C_{14}-H_{23}	96.0 (4) / 100.0 (3)	108.4	108.4 / 108.4	108.4
C_{15}-H_{20} / C_{16}-H_{24}	105.0 (3) / 102.0 (3)	108.3	108.2 / 108.3	108.1
Bond angle /º				
O_2=C_1-C_3 / C_1-C_3=O_4	118.7 (3) / 118.8 (3)	119.3	116.2 / 119.7	117.8
O_2=C_1-C_5 / O_4=C_3-C_6	124.0 (3) / 123.6 (3)	123.6	124.3 / 123.1	123.2
C_3-C_1-C_5 / C_1-C_3-C_6	117.1 (3) / 117.4 (3)	117.0	119.4 / 117.0	118.9
C_1-C_5-N_7 / C_3-C_6-N_8	114.5 (3) / 114.7 (3)	115.8	116.1 / 115.7	115.2
C_1-C_5=C_{15} / C_3-C_6=C_{16}	120.9 (3) / 120.5 (3)	120.5	123.0 / 120.5	122.0
N_7-C_5=C_{15} / N_8-C_6=C_{16}	124.6 (3) / 124.7 (3)	123.7	123.0 / 123.7	122.8
C_5-N_7=C_9 / C_6-N_8=C_{10}	116.3 (3) / 117.0 (3)	117.7	117.8 / 117.6	118.0
N_7=C_9-C_{11} / N_8=C_{10}-C_{12}	123.7 (3) / 122.4 (3)	123.1	123.5 / 123.1	123.5
N_7=C_9-H_{17} / N_8=C_{10}-H_{21}	112.0 (2) / 114.0 (2)	116.3	116.2 / 116.3	116.2
C_{11}-C_9-H_{17} / C_{12}-C_{10}-H_{21}	124.0 (2)	120.6	120.3 / 120.6	120.4
C_9-C_{11}=C_{13} / C_{10}-C_{12}=C_{14}	119.1 (4) / 120.1 (3)	118.8	118.4 / 118.8	118.4
C_9-C_{11}-H_{18} / C_{10}-C_{12}-H_{22}	120.0 (2) / 122.0 (2)	120.1	120.2 / 120.1	120.2
C_{13}=C_{11}-H_{18} / C_{14}=C_{12}-H_{22}	120.0 (2) / 117.0 (2)	121.2	121.3 / 121.2	121.4
C_{11}=C_{13}-C_{15} / C_{12}=C_{14}-C_{16}	119.8 (4) / 118.5 (3)	118.7	118.6 / 118.7	118.8
C_{11}=C_{13}-H_{19} / C_{12}=C_{14}-H_{23}	125.0 (2) / 126.0 (2)	120.7	120.9 / 120.7	120.9
C_{15}-C_{13}-H_{19} / C_{16}-C_{14}-H_{23}	115.0 (2)	120.7	120.5 / 120.6	120.3
C_5=C_{15}-C_{13} / C_6=C_{16}-C_{14}	116.6 (3) / 117.4 (3)	118.1	118.6 / 118.1	118.5
C_5=C_{15}-H_{20} / C_6=C_{16}-H_{24}	119.0 (2) / 123.0 (2)	119.4	120.8 / 119.6	120.8
C_{13}-C_{15}-H_{20} / C_{14}-C_{16}-H_{24}	124.0 (2) / 119.0 (2)	122.5	120.6 / 122.4	120.6
Dihedral angle /º				
O_2=C_1-C_3=O_4	82.0	82.3	102.1	118.3
O_2=C_1-C_3-C_6 / C_5-C_1-C_3=O_4	-97.6 / -97.4	-93.6	-73.1 / -73.4	-58.2
C_5-C_1-C_3-C_6	86.5	90.5	111.4	125.2
O_2=C_1-C_5-N_7 / O_4=C_3-C_6-N_8	-179.0 / -179.1	180.0	6.0 / 164.7	5.2
O_2=C_1-C_5=C_{15} / O_4=C_3-C_6=C_{16}	1.3 / 1.5	0.2	-174.9 / -13.6	-176.5
C_3-C_1-C_5-N_7 / C_1-C_3-C_6-N_8	-3.3 / -3.1	-4.3	-178.9 / -20.3	-178.5
C_3-C_1-C_5=C_{15} / C_1-C_3-C_6=C_{16}	176.9 / 177.5	176.0	0.3 / 161.5	-0.2
C_1-C_5-N_7=C_9 / C_3-C_6-N_8=C_{10}	-178.6 / -179.4	-179.8	179.1 / -178.4	178.7
C_{15}=C_5-N_7=C_9 / C_{16}=C_6-N_8=C_{10}	1.1 / <0.1	-0.1	-0.1 / -0.2	0.3
C_1-C_5=C_{15}-C_{13} / C_3-C_6=C_{16}-C_{14}	179.0 / 179.5	179.8	-179.2 / 179.0	-178.6
C_1-C_5=C_{15}-H_{20} / C_3-C_6=C_{16}-H_{24}	-0.2 / 4.1	-0.2	1.8 / -1.2	2.8
N_7-C_5=C_{15}-C_{13} / N_8-C_6=C_{16}-C_{14}	-0.7 / 0.1	0.1	-0.1 / 0.9	-0.4
N_7-C_5=C_{15}-H_{20} / N_8-C_6=C_{16}-H_{24}	-179.9 / -175.3	180.0	-179.1 /-179.3	-179.0

C_5-N_7=C_9-C_{11} / C_6-N_8=C_{10}-C_{12}	-0.5 / <0.1	0.0	0.1 / -0.6	-0.1
C_5-N_7=C_9-H_{17} / C_6-N_8=C_{10}-H_{21}	-174.3 / -175.7	-179.9	-179.8 / 179.7	180.0
N_7=C_9-C_{11}=C_{13} / N_8=C_{10}-C_{12}=C_{14}	-0.5 / -0.4	0.0	0.0 / 0.7	-0.1
N_7=C_9-C_{11}-H_{18} / N_8=C_{10}-C_{12}-H_{22}	-178.7 / 179.3	-180.0	179.9 / -179.2	179.9
H_{17}-C_9-C_{11}=C_{13} / H_{21}-C_{10}-C_{12}=C_{14}	172.5 / 174.9	180.0	179.9 / -179.6	179.8
H_{17}-C_9-C_{11}-H_{18} / H_{21}-C_{10}-C_{12}-H_{22}	-5.7 / -5.4	0.0	-0.1 / 0.5	-0.2
C_9-C_{11}=C_{13}-C_{15} / C_{10}-C_{12}=C_{14}-C_{16}	1.0 / 0.6	0.0	-0.1 / 0.0	0.0
C_9-C_{11}=C_{13}-H_{19} / C_{10}-C_{12}=C_{14}-H_{23}	-179.5 / -179.3	-180.0	179.7 / 180.0	179.8
H_{18}-C_{11}=C_{13}-C_{15} / H_{22}-C_{12}=C_{14}-C_{16}	179.2 / -179.1	179.9	179.9 / 180.0	-180.0
H_{18}-C_{11}=C_{13}-H_{19} / H_{22}-C_{12}-C_{14}-H_{23}	-1.3 / 1.0	0.0	-0.2 / 0.0	-0.2
C_{11}=C_{13}-C_{15}=C_5 / C_{12}=C_{14}-C_{16}=C_6	-0.5 / -0.5	0.0	0.2 / -0.8	0.2
C_{11}=C_{13}-C_{15}-H_{20} / C_{12}=C_{14}-C_{16}-H_{24}	178.7 / 175.2	-180.0	179.2 / 179.5	178.8
H_{19}-C_{13}-C_{15}=C_5 / H_{23}-C_{14}-C_{16}=C_6	-180.0 / 179.5	180.0	-179.7 / 179.2	-179.6
H_{19}-C_{13}-C_{15}-H_{20} / H_{23}-C_{14}-C_{16}-H_{24}	-0.8 / -4.9	0.0	-0.7 / -0.5	-1.0

[a] See Figure 1 for atom numbering. [b] In the crystalline state, the molecules adopt a conformation similar to that of the ***TTG*** conformer (in particular in what concerns the O=C-C=O dihedral angle and relative arrangements of the pyridyl and carbonyl groups), but with the C_2 symmetry broken.[27]

Table S2 – Definition of internal symmetry coordinates used in the normal mode analysis of α-pyridil.

	Definition[a]	Symmetry[b]	Approximate description
S_1	$\nu(C_1\text{-}C_3)$	*A*	ν(C-C)
S_2	$\nu(C_1\text{=}O_2)+\nu(C_3\text{=}O_4)$	*A*	ν(C=O) s
S_3	$\nu(C_1\text{=}O_2)-\nu(C_3\text{=}O_4)$	*B*	ν(C=O) as
S_4	$\nu(C_1\text{-}C_5)+\nu(C_3\text{-}C_6)$	*A*	$\nu(C\text{-}C_\alpha)$ s
S_5	$\nu(C_1\text{-}C_5)-\nu(C_3\text{-}C_6)$	*B*	$\nu(C\text{-}C_\alpha)$ as
S_6	$\nu(C_{15}\text{-}C_{13})+\nu(C_{13}\text{-}C_{11})+\nu(C_5\text{-}C_{15})+\nu(C_9\text{-}N_7)+\nu(N_7\text{-}C_5)+\nu(C_{11}\text{-}C_9)+$ $+\nu(C_{16}\text{-}C_{14})+\nu(C_{14}\text{-}C_{12})+\nu(C_6\text{-}C_{16})+\nu(C_{10}\text{-}N_8)+\nu(N_8\text{-}C_6)+\nu(C_{12}\text{-}C_{10})$	*A*	ν(ring 1) s
S_7	$\nu(C_{15}\text{-}C_{13})+\nu(C_{13}\text{-}C_{11})+\nu(C_5\text{-}C_{15})+\nu(C_9\text{-}N_7)+\nu(N_7\text{-}C_5)+\nu(C_{11}\text{-}C_9)-$ $-\nu(C_{16}\text{-}C_{14})-\nu(C_{14}\text{-}C_{12})-\nu(C_6\text{-}C_{16})-\nu(C_{10}\text{-}N_8)-\nu(N_8\text{-}C_6)-\nu(C_{12}\text{-}C_{10})$	*B*	ν(ring 1) as
S_8	$\nu(C_{15}\text{-}C_{13})-\nu(C_{13}\text{-}C_{11})+\nu(C_5\text{-}C_{15})-\nu(C_9\text{-}N_7)+\nu(N_7\text{-}C_5)-\nu(C_{11}\text{-}C_9)+$ $+\nu(C_{16}\text{-}C_{14})-\nu(C_{14}\text{-}C_{12})+\nu(C_6\text{-}C_{16})-\nu(C_{10}\text{-}N_8)+\nu(N_8\text{-}C_6)-\nu(C_{12}\text{-}C_{10})$	*A*	ν(ring 2) s
S_9	$\nu(C_{15}\text{-}C_{13})-\nu(C_{13}\text{-}C_{11})+\nu(C_5\text{-}C_{15})-\nu(C_9\text{-}N_7)+\nu(N_7\text{-}C_5)-\nu(C_{11}\text{-}C_9)-$ $-\nu(C_{16}\text{-}C_{14})+\nu(C_{14}\text{-}C_{12})-\nu(C_6\text{-}C_{16})+\nu(C_{10}\text{-}N_8)-\nu(N_8\text{-}C_6)+\nu(C_{12}\text{-}C_{10})$	*B*	ν(ring 2) as
S_{10}	$2\nu(C_{15}\text{-}C_{13})-\nu(C_{13}\text{-}C_{11})-\nu(C_5\text{-}C_{15})+2\nu(C_9\text{-}N_7)-\nu(N_7\text{-}C_5)-\nu(C_{11}\text{-}C_9)+$ $+2\nu(C_{16}\text{-}C_{14})-\nu(C_{14}\text{-}C_{12})-\nu(C_6\text{-}C_{16})+2\nu(C_{10}\text{-}N_8)-\nu(N_8\text{-}C_6)-\nu(C_{12}\text{-}C_{10})$	*A*	ν(ring 3) s
S_{11}	$2\nu(C_{15}\text{-}C_{13})-\nu(C_{13}\text{-}C_{11})-\nu(C_5\text{-}C_{15})+2\nu(C_9\text{-}N_7)-\nu(N_7\text{-}C_5)-\nu(C_{11}\text{-}C_9)-$ $-2\nu(C_{16}\text{-}C_{14})+\nu(C_{14}\text{-}C_{12})+\nu(C_6\text{-}C_{16})-2\nu(C_{10}\text{-}N_8)+\nu(N_8\text{-}C_6)+\nu(C_{12}\text{-}C_{10})$	*B*	ν(ring 3) as
S_{12}	$\nu(C_{13}\text{-}C_{11})-\nu(C_5\text{-}C_{15})+\nu(N_7\text{-}C_5)+\nu(C_{11}\text{-}C_9)+\nu(C_{14}\text{-}C_{12})-\nu(C_6\text{-}C_{16})+$ $+\nu(N_8\text{-}C_6)-\nu(C_{12}\text{-}C_{10})$	*A*	ν(ring 4) s
S_{13}	$\nu(C_{13}\text{-}C_{11})-\nu(C_5\text{-}C_{15})+\nu(N_7\text{-}C_5)+\nu(C_{11}\text{-}C_9)-\nu(C_{14}\text{-}C_{12})+\nu(C_6\text{-}C_{16})-$ $-\nu(N_8\text{-}C_6)+\nu(C_{12}\text{-}C_{10})$	*B*	ν(ring 4) as
S_{14}	$\nu(C_{13}\text{-}C_{11})+\nu(C_5\text{-}C_{15})-\nu(N_7\text{-}C_5)-\nu(C_{11}\text{-}C_9)+\nu(C_{14}\text{-}C_{12})+\nu(C_6\text{-}C_{16})-$ $-\nu(N_8\text{-}C_6)-\nu(C_{12}\text{-}C_{10})$	*A*	ν(ring 5) s
S_{15}	$\nu(C_{13}\text{-}C_{11})+\nu(C_5\text{-}C_{15})-\nu(N_7\text{-}C_5)-\nu(C_{11}\text{-}C_9)-\nu(C_{14}\text{-}C_{12})-\nu(C_6\text{-}C_{16})+$ $+\nu(N_8\text{-}C_6)+\nu(C_{12}\text{-}C_{10})$	*B*	ν(ring 5) as
S_{16}	$\nu(C_{13}\text{-}C_{11})-\nu(C_5\text{-}C_{15})-\nu(N_7\text{-}C_5)+\nu(C_{11}\text{-}C_9)+\nu(C_{14}\text{-}C_{12})-\nu(C_6\text{-}C_{16})-$ $-\nu(N_8\text{-}C_6)+\nu(C_{12}\text{-}C_{10})$	*A*	ν(ring 6) s
S_{17}	$\nu(C_{13}\text{-}C_{11})-\nu(C_5\text{-}C_{15})-\nu(N_7\text{-}C_5)+\nu(C_{11}\text{-}C_9)-\nu(C_{14}\text{-}C_{12})+\nu(C_6\text{-}C_{16})+$ $+\nu(N_8\text{-}C_6)-\nu(C_{12}\text{-}C_{10})$	*B*	ν(ring 6) as
S_{18}	$\nu(C_9\text{-}H_{17})+\nu(C_{10}\text{-}H_{21})$	*A*	ν(C-H 1) s
S_{19}	$\nu(C_9\text{-}H_{17})-\nu(C_{10}\text{-}H_{21})$	*B*	ν(C-H 1) as
S_{20}	$\nu(C_{15}\text{-}H_{20})+\nu(C_{16}\text{-}H_{24})$	*A*	ν(C-H 2) s
S_{21}	$\nu(C_{15}\text{-}H_{20})-\nu(C_{16}\text{-}H_{24})$	*B*	ν(C-H 2) as
S_{22}	$\nu(C_{11}\text{-}H_{18})+\nu(C_{13}\text{-}H_{19})+\nu(C_{12}\text{-}H_{22})+\nu(C_{14}\text{-}H_{23})$	*A*	ν(C-H 3) s
S_{23}	$\nu(C_{11}\text{-}H_{18})+\nu(C_{13}\text{-}H_{19})-\nu(C_{12}\text{-}H_{22})-\nu(C_{14}\text{-}H_{23})$	*B*	ν(C-H 3) as
S_{24}	$\nu(C_{11}\text{-}H_{18})-\nu(C_{13}\text{-}H_{19})+\nu(C_{12}\text{-}H_{22})-\nu(C_{14}\text{-}H_{23})$	*A*	ν(C-H 4) s
S_{25}	$\nu(C_{11}\text{-}H_{18})-\nu(C_{13}\text{-}H_{19})-\nu(C_{12}\text{-}H_{22})+\nu(C_{14}\text{-}H_{23})$	*B*	ν(C-H 4) as
S_{26}	$\delta(C_5\text{-}C_1\text{=}O_2)-\delta(C_3\text{-}C_1\text{=}O_2)+\delta(C_6\text{-}C_3\text{=}O_4)-\delta(C_1\text{-}C_3\text{=}O_4)$	*A*	δ(C=O) s
S_{27}	$\delta(C_5\text{-}C_1\text{=}O_2)-\delta(C_3\text{-}C_1\text{=}O_2)-\delta(C_6\text{-}C_3\text{=}O_4)+\delta(C_1\text{-}C_3\text{=}O_4)$	*B*	δ(C=O) as
S_{28}	$2\delta(C_5\text{-}C_1\text{-}C_3)-\delta(C_5\text{-}C_1\text{-}C_2)-\delta(C_3\text{-}C_1\text{-}C_2)+$ $+2\delta(C_6\text{-}C_3\text{-}C_1)-\delta(C_6\text{-}C_3\text{-}C_4)-\delta(C_1\text{-}C_3\text{-}C_4)$	*A*	$\delta(CCC_\alpha)$ s
S_{29}	$2\delta(C_5\text{-}C_1\text{-}C_3)-\delta(C_5\text{-}C_1\text{-}C_2)-\delta(C_3\text{-}C_1\text{-}C_2)-$ $-2\delta(C_6\text{-}C_3\text{-}C_1)+\delta(C_6\text{-}C_3\text{-}C_4)+\delta(C_1\text{-}C_3\text{-}C_4)$	*B*	$\delta(CCC_\alpha)$ as

S_{30}	$\delta(C_{15}\text{-}C_5\text{-}C_1)\text{-}\delta(N_7\text{-}C_5\text{-}C_1)+\delta(C_{16}\text{-}C_6\text{-}C_3)\text{-}\delta(N_8\text{-}C_6\text{-}C_3)$	*A*	w(ring) s
S_{31}	$\delta(C_{15}\text{-}C_5\text{-}C_1)\text{-}\delta(N_7\text{-}C_5\text{-}C_1)\text{-}\delta(C_{16}\text{-}C_6\text{-}C_3)+\delta(N_8\text{-}C_6\text{-}C_3)$	*B*	w(ring) as
S_{32}	$4\delta(C_{15}\text{-}C_5\text{-}N_7)\text{-}2\delta(C_{15}\text{-}C_5\text{-}C_1)\text{-}2\delta(N_7\text{-}C_5\text{-}C_1)\text{-}2\delta(C_{13}\text{-}C_{15}\text{-}C_5)+\delta(C_{13}\text{-}C_{15}\text{-}H_{20})+$ $+\delta(C_5\text{-}C_{15}\text{-}H_{20})\text{-}2\delta(C_{11}\text{-}C_{13}\text{-}C_{15})+\delta(C_{11}\text{-}C_{13}\text{-}H_{19})+\delta(C_{15}\text{-}C_{13}\text{-}H_{19})+4\delta(C_9\text{-}C_{11}\text{-}C_{13})\text{-}$ $\text{-}2\delta(C_9\text{-}C_{11}\text{-}H_{18})\text{-}2\delta(C_{13}\text{-}C_{11}\text{-}H_{18})\text{-}2\delta(N_7\text{-}C_9\text{-}C_{11})+\delta(N_7\text{-}C_9\text{-}H_{17})+\delta(C_{11}\text{-}C_9\text{-}H_{17})-$ $\text{-}2\delta(C_5\text{-}N_7\text{-}C_9)+4\delta(C_{16}\text{-}C_6\text{-}N_8)\text{-}2\delta(C_{16}\text{-}C_6\text{-}C_3)\text{-}2\delta(N_8\text{-}C_6\text{-}C_3)\text{-}2\delta(C_{14}\text{-}C_{16}\text{-}C_6)+$ $+\delta(C_{14}\text{-}C_{16}\text{-}H_{24})+\delta(C_6\text{-}C_{16}\text{-}H_{24})\text{-}2\delta(C_{12}\text{-}C_{14}\text{-}C_{16})+\delta(C_{12}\text{-}C_{14}\text{-}H_{23})+\delta(C_{16}\text{-}C_{14}\text{-}H_{23})+$ $+4\delta(C_{10}\text{-}C_{12}\text{-}C_{14})\text{-}2\delta(C_{10}\text{-}C_{12}\text{-}H_{22})\text{-}2\delta(C_{14}\text{-}C_{12}\text{-}H_{22})\text{-}2\delta(N_8\text{-}C_{10}\text{-}C_{12})+\delta(N_8\text{-}C_{10}\text{-}H_{21})+$ $+\delta(C_{12}\text{-}C_{10}\text{-}H_{21})\text{-}2\delta(C_6\text{-}N_8\text{-}C_{10})$	*A*	δ(ring 1) s
S_{33}	$4\delta(C_{15}\text{-}C_5\text{-}N_7)\text{-}2\delta(C_{15}\text{-}C_5\text{-}C_1)\text{-}2\delta(N_7\text{-}C_5\text{-}C_1)\text{-}2\delta(C_{13}\text{-}C_{15}\text{-}C_5)+\delta(C_{13}\text{-}C_{15}\text{-}H_{20})+$ $+\delta(C_5\text{-}C_{15}\text{-}H_{20})\text{-}2\delta(C_{11}\text{-}C_{13}\text{-}C_{15})+\delta(C_{11}\text{-}C_{13}\text{-}H_{19})+\delta(C_{15}\text{-}C_{13}\text{-}H_{19})+4\delta(C_9\text{-}C_{11}\text{-}C_{13})\text{-}$ $\text{-}2\delta(C_9\text{-}C_{11}\text{-}H_{18})\text{-}2\delta(C_{13}\text{-}C_{11}\text{-}H_{18})\text{-}2\delta(N_7\text{-}C_9\text{-}C_{11})+\delta(N_7\text{-}C_9\text{-}H_{17})+\delta(C_{11}\text{-}C_9\text{-}H_{17})-$ $\text{-}2\delta(C_5\text{-}N_7\text{-}C_9)\text{-}4\delta(C_{16}\text{-}C_6\text{-}N_8)+2\delta(C_{16}\text{-}C_6\text{-}C_3)+2\delta(N_8\text{-}C_6\text{-}C_3)+2\delta(C_{14}\text{-}C_{16}\text{-}C_6)\text{-}$ $\text{-}\delta(C_{14}\text{-}C_{16}\text{-}H_{24})\text{-}\delta(C_6\text{-}C_{16}\text{-}H_{24})+2\delta(C_{12}\text{-}C_{14}\text{-}C_{16})\text{-}\delta(C_{12}\text{-}C_{14}\text{-}H_{23})\text{-}\delta(C_{16}\text{-}C_{14}\text{-}H_{23})\text{-}$ $\text{-}4\delta(C_{10}\text{-}C_{12}\text{-}C_{14})+2\delta(C_{10}\text{-}C_{12}\text{-}H_{22})+2\delta(C_{14}\text{-}C_{12}\text{-}H_{22})+2\delta(N_8\text{-}C_{10}\text{-}C_{12})\text{-}\delta(N_8\text{-}C_{10}\text{-}H_{21})\text{-}$ $\text{-}\delta(C_{12}\text{-}C_{10}\text{-}H_{21})+2\delta(C_6\text{-}N_8\text{-}C_{10})$	*B*	δ(ring 1) as
S_{34}	$2\delta(C_{15}\text{-}C_5\text{-}N_7)\text{-}\delta(C_{15}\text{-}C_5\text{-}C_1)\text{-}\delta(N_7\text{-}C_5\text{-}C_1)\text{-}2\delta(C_{13}\text{-}C_{15}\text{-}C_5)+\delta(C_{13}\text{-}C_{15}\text{-}H_{20})+$ $+\delta(C_5\text{-}C_{15}\text{-}H_{20})+2\delta(C_{11}\text{-}C_{13}\text{-}C_{15})\text{-}\delta(C_{11}\text{-}C_{13}\text{-}H_{19})\text{-}\delta(C_{15}\text{-}C_{13}\text{-}H_{19})\text{-}2\delta(C_9\text{-}C_{11}\text{-}C_{13})+$ $+\delta(C_9\text{-}C_{11}\text{-}H_{18})+\delta(C_{13}\text{-}C_{11}\text{-}H_{18})+2\delta(N_7\text{-}C_9\text{-}C_{11})\text{-}\delta(N_7\text{-}C_9\text{-}H_{17})\text{-}\delta(C_{11}\text{-}C_9\text{-}H_{17})-$ $\text{-}2\delta(C_5\text{-}N_7\text{-}C_9)+2\delta(C_{16}\text{-}C_6\text{-}N_8)\text{-}\delta(C_{16}\text{-}C_6\text{-}C_3)\text{-}\delta(N_8\text{-}C_6\text{-}C_3)\text{-}2\delta(C_{14}\text{-}C_{16}\text{-}C_6)+$ $+\delta(C_{14}\text{-}C_{16}\text{-}H_{24})+\delta(C_6\text{-}C_{16}\text{-}H_{24})+2\delta(C_{12}\text{-}C_{14}\text{-}C_{16})\text{-}\delta(C_{12}\text{-}C_{14}\text{-}H_{23})\text{-}\delta(C_{16}\text{-}C_{14}\text{-}H_{23})\text{-}$ $\text{-}2\delta(C_{10}\text{-}C_{12}\text{-}C_{14})+\delta(C_{10}\text{-}C_{12}\text{-}H_{22})+\delta(C_{14}\text{-}C_{12}\text{-}H_{22})+2\delta(N_8\text{-}C_{10}\text{-}C_{12})\text{-}\delta(N_8\text{-}C_{10}\text{-}H_{21})\text{-}$ $\text{-}\delta(C_{12}\text{-}C_{10}\text{-}H_{21})\text{-}2\delta(C_6\text{-}N_8\text{-}C_{10})$	*A*	δ(ring 2) s
S_{35}	$2\delta(C_{15}\text{-}C_5\text{-}N_7)\text{-}\delta(C_{15}\text{-}C_5\text{-}C_1)\text{-}\delta(N_7\text{-}C_5\text{-}C_1)\text{-}2\delta(C_{13}\text{-}C_{15}\text{-}C_5)+\delta(C_{13}\text{-}C_{15}\text{-}H_{20})+$ $+\delta(C_5\text{-}C_{15}\text{-}H_{20})+2\delta(C_{11}\text{-}C_{13}\text{-}C_{15})\text{-}\delta(C_{11}\text{-}C_{13}\text{-}H_{19})\text{-}\delta(C_{15}\text{-}C_{13}\text{-}H_{19})\text{-}2\delta(C_9\text{-}C_{11}\text{-}C_{13})+$ $+\delta(C_9\text{-}C_{11}\text{-}H_{18})+\delta(C_{13}\text{-}C_{11}\text{-}H_{18})+2\delta(N_7\text{-}C_9\text{-}C_{11})\text{-}\delta(N_7\text{-}C_9\text{-}H_{17})\text{-}\delta(C_{11}\text{-}C_9\text{-}H_{17})-$ $\text{-}2\delta(C_5\text{-}N_7\text{-}C_9)\text{-}2\delta(C_{16}\text{-}C_6\text{-}N_8)+\delta(C_{16}\text{-}C_6\text{-}C_3)+\delta(N_8\text{-}C_6\text{-}C_3)+2\delta(C_{14}\text{-}C_{16}\text{-}C_6)\text{-}$ $\text{-}\delta(C_{14}\text{-}C_{16}\text{-}H_{24})\text{-}\delta(C_6\text{-}C_{16}\text{-}H_{24})\text{-}2\delta(C_{12}\text{-}C_{14}\text{-}C_{16})+\delta(C_{12}\text{-}C_{14}\text{-}H_{23})+\delta(C_{16}\text{-}C_{14}\text{-}H_{23})+$ $+2\delta(C_{10}\text{-}C_{12}\text{-}C_{14})\text{-}\delta(C_{10}\text{-}C_{12}\text{-}H_{22})\text{-}\delta(C_{14}\text{-}C_{12}\text{-}H_{22})\text{-}2\delta(N_8\text{-}C_{10}\text{-}C_{12})+\delta(N_8\text{-}C_{10}\text{-}H_{21})+$ $+\delta(C_{12}\text{-}C_{10}\text{-}H_{21})+2\delta(C_6\text{-}N_8\text{-}C_{10})$	*B*	δ(ring 2) as
S_{36}	$2\delta(C_{13}\text{-}C_{15}\text{-}C_5)\text{-}\delta(C_{13}\text{-}C_{15}\text{-}H_{20})\text{-}\delta(C_5\text{-}C_{15}\text{-}H_{20})\text{-}2\delta(C_{11}\text{-}C_{13}\text{-}C_{15})+\delta(C_{11}\text{-}C_{13}\text{-}H_{19})+$ $+\delta(C_{15}\text{-}C_{13}\text{-}H_{19})+2\delta(N_7\text{-}C_9\text{-}C_{11})\text{-}\delta(N_7\text{-}C_9\text{-}H_{17})\text{-}\delta(C_{11}\text{-}C_9\text{-}H_{17})-2\delta(C_5\text{-}N_7\text{-}C_9)+$ $+2\delta(C_{14}\text{-}C_{16}\text{-}C_6)\text{-}\delta(C_{14}\text{-}C_{16}\text{-}H_{24})\text{-}\delta(C_6\text{-}C_{16}\text{-}H_{24})\text{-}2\delta(C_{12}\text{-}C_{14}\text{-}C_{16})+\delta(C_{12}\text{-}C_{14}\text{-}H_{23})+$ $+\delta(C_{16}\text{-}C_{14}\text{-}H_{23})+2\delta(N_8\text{-}C_{10}\text{-}C_{12})\text{-}\delta(N_8\text{-}C_{10}\text{-}H_{21})\text{-}\delta(C_{12}\text{-}C_{10}\text{-}H_{21})\text{-}2\delta(C_6\text{-}N_8\text{-}C_{10})$	*A*	δ(ring 3) s
S_{37}	$2\delta(C_{13}\text{-}C_{15}\text{-}C_5)\text{-}\delta(C_{13}\text{-}C_{15}\text{-}H_{20})\text{-}\delta(C_5\text{-}C_{15}\text{-}H_{20})\text{-}2\delta(C_{11}\text{-}C_{13}\text{-}C_{15})+\delta(C_{11}\text{-}C_{13}\text{-}H_{19})+$ $+\delta(C_{15}\text{-}C_{13}\text{-}H_{19})+2\delta(N_7\text{-}C_9\text{-}C_{11})\text{-}\delta(N_7\text{-}C_9\text{-}H_{17})\text{-}\delta(C_{11}\text{-}C_9\text{-}H_{17})-2\delta(C_5\text{-}N_7\text{-}C_9)\text{-}$ $\text{-}2\delta(C_{14}\text{-}C_{16}\text{-}C_6)+\delta(C_{14}\text{-}C_{16}\text{-}H_{24})+\delta(C_6\text{-}C_{16}\text{-}H_{24})+2\delta(C_{12}\text{-}C_{14}\text{-}C_{16})\text{-}\delta(C_{12}\text{-}C_{14}\text{-}H_{23})\text{-}$ $\text{-}\delta(C_{16}\text{-}C_{14}\text{-}H_{23})\text{-}2\delta(N_8\text{-}C_{10}\text{-}C_{12})+\delta(N_8\text{-}C_{10}\text{-}H_{21})+\delta(C_{12}\text{-}C_{10}\text{-}H_{21})+2\delta(C_6\text{-}N_8\text{-}C_{10})$	*B*	δ(ring 3) as
S_{38}	$\delta(C_5\text{-}C_{15}\text{-}H_{20})\text{-}\delta(C_{13}\text{-}C_{15}\text{-}H_{20})+\delta(C_6\text{-}C_{16}\text{-}H_{24})\text{-}\delta(C_{14}\text{-}C_{16}\text{-}H_{24})$	*A*	δ(C-H 1) s
S_{39}	$\delta(C_5\text{-}C_{15}\text{-}H_{20})\text{-}\delta(C_{13}\text{-}C_{15}\text{-}H_{20})\text{-}\delta(C_6\text{-}C_{16}\text{-}H_{24})+\delta(C_{14}\text{-}C_{16}\text{-}H_{24})$	*B*	δ(C-H 1) as
S_{40}	$\delta(C_{15}\text{-}C_{13}\text{-}H_{19})\text{-}\delta(C_{11}\text{-}C_{13}\text{-}H_{19})\text{-}\delta(C_{13}\text{-}C_{11}\text{-}H_{18})+\delta(C_9\text{-}C_{11}\text{-}H_{18})+$ $+\delta(C_{16}\text{-}C_{14}\text{-}H_{23})\text{-}\delta(C_{12}\text{-}C_{14}\text{-}H_{23})\text{-}\delta(C_{14}\text{-}C_{12}\text{-}H_{22})+\delta(C_{10}\text{-}C_{12}\text{-}H_{22})$	*A*	δ(C-H 2) s
S_{41}	$\delta(C_{15}\text{-}C_{13}\text{-}H_{19})\text{-}\delta(C_{11}\text{-}C_{13}\text{-}H_{19})\text{-}\delta(C_{13}\text{-}C_{11}\text{-}H_{18})+\delta(C_9\text{-}C_{11}\text{-}H_{18})\text{-}$ $\text{-}\delta(C_{16}\text{-}C_{14}\text{-}H_{23})+\delta(C_{12}\text{-}C_{14}\text{-}H_{23})+\delta(C_{14}\text{-}C_{12}\text{-}H_{22})\text{-}\delta(C_{10}\text{-}C_{12}\text{-}H_{22})$	*B*	δ(C-H 2) as
S_{42}	$\delta(C_{15}\text{-}C_{13}\text{-}H_{19})\text{-}\delta(C_{11}\text{-}C_{13}\text{-}H_{19})+\delta(C_{13}\text{-}C_{11}\text{-}H_{18})\text{-}\delta(C_9\text{-}C_{11}\text{-}H_{18})+$ $+\delta(C_{16}\text{-}C_{14}\text{-}H_{23})\text{-}\delta(C_{12}\text{-}C_{14}\text{-}H_{23})+\delta(C_{14}\text{-}C_{12}\text{-}H_{22})\text{-}\delta(C_{10}\text{-}C_{12}\text{-}H_{22})$	*A*	δ(C-H 3) s
S_{43}	$\delta(C_{15}\text{-}C_{13}\text{-}H_{19})\text{-}\delta(C_{11}\text{-}C_{13}\text{-}H_{19})+\delta(C_{13}\text{-}C_{11}\text{-}H_{18})\text{-}\delta(C_9\text{-}C_{11}\text{-}H_{18})\text{-}$ $\text{-}\delta(C_{16}\text{-}C_{14}\text{-}H_{23})+\delta(C_{12}\text{-}C_{14}\text{-}H_{23})\text{-}\delta(C_{14}\text{-}C_{12}\text{-}H_{22})+\delta(C_{10}\text{-}C_{12}\text{-}H_{22})$	*B*	δ(C-H 3) as
S_{44}	$\delta(C_{11}\text{-}C_9\text{-}H_{17})\text{-}\delta(N_7\text{-}C_9\text{-}H_{17})+\delta(C_{12}\text{-}C_{10}\text{-}H_{21})\text{-}\delta(N_8\text{-}C_{10}\text{-}H_{21})$	*A*	δ(C-H 4) s
S_{45}	$\delta(C_{11}\text{-}C_9\text{-}H_{17})\text{-}\delta(N_7\text{-}C_9\text{-}H_{17})\text{-}\delta(C_{12}\text{-}C_{10}\text{-}H_{21})+\delta(N_8\text{-}C_{10}\text{-}H_{21})$	*B*	δ(C-H 4) as
S_{46}	$\tau(C_1\text{-}C_5\text{-}C_{15}\text{-}C_{13})+\tau(C_1\text{-}C_5\text{-}C_{15}\text{-}H_{20})+\tau(N_7\text{-}C_5\text{-}C_{15}\text{-}C_{13})+\tau(N_7\text{-}C_5\text{-}C_{15}\text{-}H_{20})+$ $+\tau(C_5\text{-}C_{15}\text{-}C_{13}\text{-}C_{11})+\tau(C_5\text{-}C_{15}\text{-}C_{13}\text{-}H_{19})+\tau(H_{20}\text{-}C_{15}\text{-}C_{13}\text{-}C_{11})+\tau(H_{20}\text{-}C_{15}\text{-}C_{13}\text{-}H_{19})+$ $+\tau(C_{15}\text{-}C_{13}\text{-}C_{11}\text{-}C_9)+\tau(C_{15}\text{-}C_{13}\text{-}C_{11}\text{-}H_{18})+\tau(H_{19}\text{-}C_{13}\text{-}C_{11}\text{-}C_9)+\tau(H_{19}\text{-}C_{13}\text{-}C_{11}\text{-}H_{18})+$ $+\tau(C_{13}\text{-}C_{11}\text{-}C_9\text{-}N_7)+\tau(C_{13}\text{-}C_{11}\text{-}C_9\text{-}H_{17})+\tau(H_{18}\text{-}C_{11}\text{-}C_9\text{-}N_7)+\tau(H_{18}\text{-}C_{11}\text{-}C_9\text{-}H_{17})+$ $+\tau(C_3\text{-}C_6\text{-}C_{16}\text{-}C_{14})+\tau(C_3\text{-}C_6\text{-}C_{16}\text{-}H_{24})+\tau(N_8\text{-}C_6\text{-}C_{16}\text{-}C_{14})+\tau(N_8\text{-}C_6\text{-}C_{16}\text{-}H_{24})+$	*A*	τ(ring 1) s

+τ(C_6-C_{16}-C_{14}-C_{12})+τ(C_6-C_{16}-C_{14}-H_{23})+τ(H_{24}-C_{16}-C_{14}-C_{12})+τ(H_{24}-C_{16}-C_{14}-H_{23})+
+τ(C_{16}-C_{14}-C_{12}-C_{10}) +τ(C_{16}-C_{14}-C_{12}-H_{22})+τ(H_{23}-C_{14}-C_{12}-C_{10})+τ(H_{23}-C_{14}-C_{12}-H_{22})+
+τ(C_{14}-C_{12}-C_{10}-N_8)+τ(C_{14}-C_{12}-C_{10}-H_{21})+τ(H_{22}-C_{12}-C_{10}-N_8)+τ(H_{22}-C_{12}-C_{10}-H_{21})

S_{47}	τ(C_1-C_5-C_{15}-C_{13})+τ(C_1-C_5-C_{15}-H_{20})+τ(N_7-C_5-C_{15}-C_{13})+τ(N_7-C_5-C_{15}-H_{20})+ +τ(C_5-C_{15}-C_{13}-C_{11})+τ(C_5-C_{15}-C_{13}-H_{19})+τ(H_{20}-C_{15}-C_{13}-C_{11})+τ(H_{20}-C_{15}-C_{13}-H_{19})+ +τ(C_{15}-C_{13}-C_{11}-C_9)+τ(C_{15}-C_{13}-C_{11}-H_{18})+τ(H_{19}-C_{13}-C_{11}-C_9)+τ(H_{19}-C_{13}-C_{11}-H_{18})+ +τ(C_{13}-C_{11}-C_9-N_7)+τ(C_{13}-C_{11}-C_9-H_{17})+τ(H_{18}-C_{11}-C_9-N_7)+τ(H_{18}-C_{11}-C_9-H_{17})- -τ(C_3-C_6-C_{16}-C_{14})-τ(C_3-C_6-C_{16}-H_{24})-τ(N_8-C_6-C_{16}-C_{14})-τ(N_8-C_6-C_{16}-H_{24})- -τ(C_6-C_{16}-C_{14}-C_{12})-τ(C_6-C_{16}-C_{14}-H_{23})-τ(H_{24}-C_{16}-C_{14}-C_{12})-τ(H_{24}-C_{16}-C_{14}-H_{23})- -τ(C_{16}-C_{14}-C_{12}-C_{10}) -τ(C_{16}-C_{14}-C_{12}-H_{22})-τ(H_{23}-C_{14}-C_{12}-C_{10})-τ(H_{23}-C_{14}-C_{12}-H_{22})- -τ(C_{14}-C_{12}-C_{10}-N_8)-τ(C_{14}-C_{12}-C_{10}-H_{21})-τ(H_{22}-C_{12}-C_{10}-N_8)-τ(H_{22}-C_{12}-C_{10}-H_{21})	*B*	τ(ring 1) as
S_{48}	τ(C_1-C_5-C_{15}-C_{13})+τ(C_1-C_5-C_{15}-H_{20})+τ(N_7-C_5-C_{15}-C_{13})+τ(N_7-C_5-C_{15}-H_{20})+ +τ(C_5-C_{15}-C_{13}-C_{11})+τ(C_5-C_{15}-C_{13}-H_{19})+τ(H_{20}-C_{15}-C_{13}-C_{11})+τ(H_{20}-C_{15}-C_{13}-H_{19})- -τ(C_{15}-C_{13}-C_{11}-C_9)-τ(C_{15}-C_{13}-C_{11}-H_{18})-τ(H_{19}-C_{13}-C_{11}-C_9)-τ(H_{19}-C_{13}-C_{11}-H_{18})- -τ(C_{13}-C_{11}-C_9-N_7)-τ(C_{13}-C_{11}-C_9-H_{17})-τ(H_{18}-C_{11}-C_9-N_7)-τ(H_{18}-C_{11}-C_9-H_{17})+ +τ(C_3-C_6-C_{16}-C_{14})+τ(C_3-C_6-C_{16}-H_{24})+τ(N_8-C_6-C_{16}-C_{14})+τ(N_8-C_6-C_{16}-H_{24})+ +τ(C_6-C_{16}-C_{14}-C_{12})+τ(C_6-C_{16}-C_{14}-H_{23})+τ(H_{24}-C_{16}-C_{14}-C_{12})+τ(H_{24}-C_{16}-C_{14}-H_{23})- -τ(C_{16}-C_{14}-C_{12}-C_{10}) -τ(C_{16}-C_{14}-C_{12}-H_{22})-τ(H_{23}-C_{14}-C_{12}-C_{10})-τ(H_{23}-C_{14}-C_{12}-H_{22})- -τ(C_{14}-C_{12}-C_{10}-N_8)-τ(C_{14}-C_{12}-C_{10}-H_{21})-τ(H_{22}-C_{12}-C_{10}-N_8)-τ(H_{22}-C_{12}-C_{10}-H_{21})	*A*	τ(ring 2) s
S_{49}	τ(C_1-C_5-C_{15}-C_{13})+τ(C_1-C_5-C_{15}-H_{20})+τ(N_7-C_5-C_{15}-C_{13})+τ(N_7-C_5-C_{15}-H_{20})+ +τ(C_5-C_{15}-C_{13}-C_{11})+τ(C_5-C_{15}-C_{13}-H_{19})+τ(H_{20}-C_{15}-C_{13}-C_{11})+τ(H_{20}-C_{15}-C_{13}-H_{19})- -τ(C_{15}-C_{13}-C_{11}-C_9)-τ(C_{15}-C_{13}-C_{11}-H_{18})-τ(H_{19}-C_{13}-C_{11}-C_9)-τ(H_{19}-C_{13}-C_{11}-H_{18})- -τ(C_{13}-C_{11}-C_9-N_7)-τ(C_{13}-C_{11}-C_9-H_{17})-τ(H_{18}-C_{11}-C_9-N_7)-τ(H_{18}-C_{11}-C_9-H_{17})- -τ(C_3-C_6-C_{16}-C_{14})-τ(C_3-C_6-C_{16}-H_{24})-τ(N_8-C_6-C_{16}-C_{14})-τ(N_8-C_6-C_{16}-H_{24})- -τ(C_6-C_{16}-C_{14}-C_{12})-τ(C_6-C_{16}-C_{14}-H_{23})-τ(H_{24}-C_{16}-C_{14}-C_{12})-τ(H_{24}-C_{16}-C_{14}-H_{23})+ +τ(C_{16}-C_{14}-C_{12}-C_{10}) +τ(C_{16}-C_{14}-C_{12}-H_{22})+τ(H_{23}-C_{14}-C_{12}-C_{10})+τ(H_{23}-C_{14}-C_{12}-H_{22})+ +τ(C_{14}-C_{12}-C_{10}-N_8)+τ(C_{14}-C_{12}-C_{10}-H_{21})+τ(H_{22}-C_{12}-C_{10}-N_8)+τ(H_{22}-C_{12}-C_{10}-H_{21})	*B*	τ(ring 2) as
S_{50}	τ(C_1-C_5-C_{15}-C_{13})+τ(C_1-C_5-C_{15}-H_{20})+τ(N_7-C_5-C_{15}-C_{13})+τ(N_7-C_5-C_{15}-H_{20})- -τ(C_5-C_{15}-C_{13}-C_{11})-τ(C_5-C_{15}-C_{13}-H_{19})-τ(H_{20}-C_{15}-C_{13}-C_{11})-τ(H_{20}-C_{15}-C_{13}-H_{19})+ +τ(C_{15}-C_{13}-C_{11}-C_9)+τ(C_{15}-C_{13}-C_{11}-H_{18})+τ(H_{19}-C_{13}-C_{11}-C_9)+τ(H_{19}-C_{13}-C_{11}-H_{18})- -τ(C_{13}-C_{11}-C_9-N_7)-τ(C_{13}-C_{11}-C_9-H_{17})-τ(H_{18}-C_{11}-C_9-N_7)-τ(H_{18}-C_{11}-C_9-H_{17})+ +τ(C_3-C_6-C_{16}-C_{14})+τ(C_3-C_6-C_{16}-H_{24})+τ(N_8-C_6-C_{16}-C_{14})+τ(N_8-C_6-C_{16}-H_{24})- -τ(C_6-C_{16}-C_{14}-C_{12})-τ(C_6-C_{16}-C_{14}-H_{23})-τ(H_{24}-C_{16}-C_{14}-C_{12})-τ(H_{24}-C_{16}-C_{14}-H_{23})+ +τ(C_{16}-C_{14}-C_{12}-C_{10})+τ(C_{16}-C_{14}-C_{12}-H_{22})+τ(H_{23}-C_{14}-C_{12}-C_{10})+τ(H_{23}-C_{14}-C_{12}-H_{22})- -τ(C_{14}-C_{12}-C_{10}-N_8)-τ(C_{14}-C_{12}-C_{10}-H_{21})-τ(H_{22}-C_{12}-C_{10}-N_8)-τ(H_{22}-C_{12}-C_{10}-H_{21})	*A*	τ(ring 3) s
S_{51}	τ(C_1-C_5-C_{15}-C_{13})+τ(C_1-C_5-C_{15}-H_{20})+τ(N_7-C_5-C_{15}-C_{13})+τ(N_7-C_5-C_{15}-H_{20})- -τ(C_5-C_{15}-C_{13}-C_{11})-τ(C_5-C_{15}-C_{13}-H_{19})-τ(H_{20}-C_{15}-C_{13}-C_{11})-τ(H_{20}-C_{15}-C_{13}-H_{19})+ +τ(C_{15}-C_{13}-C_{11}-C_9)+τ(C_{15}-C_{13}-C_{11}-H_{18})+τ(H_{19}-C_{13}-C_{11}-C_9)+τ(H_{19}-C_{13}-C_{11}-H_{18})- -τ(C_{13}-C_{11}-C_9-N_7)-τ(C_{13}-C_{11}-C_9-H_{17})-τ(H_{18}-C_{11}-C_9-N_7)-τ(H_{18}-C_{11}-C_9-H_{17})- -τ(C_3-C_6-C_{16}-C_{14})-τ(C_3-C_6-C_{16}-H_{24})-τ(N_8-C_6-C_{16}-C_{14})-τ(N_8-C_6-C_{16}-H_{24})+ +τ(C_6-C_{16}-C_{14}-C_{12})+τ(C_6-C_{16}-C_{14}-H_{23})+τ(H_{24}-C_{16}-C_{14}-C_{12})+τ(H_{24}-C_{16}-C_{14}-H_{23})- -τ(C_{16}-C_{14}-C_{12}-C_{10})-τ(C_{16}-C_{14}-C_{12}-H_{22})-τ(H_{23}-C_{14}-C_{12}-C_{10})-τ(H_{23}-C_{14}-C_{12}-H_{22})+ +τ(C_{14}-C_{12}-C_{10}-N_8)+τ(C_{14}-C_{12}-C_{10}-H_{21})+τ(H_{22}-C_{12}-C_{10}-N_8)+τ(H_{22}-C_{12}-C_{10}-H_{21})	*B*	τ(ring 3) as
S_{52}	τ(C_1-C_5-C_{15}-C_{13})+τ(C_1-C_5-C_{15}-H_{20})+τ(N_7-C_5-C_{15}-C_{13})+τ(N_7-C_5-C_{15}-H_{20})- -τ(C_5-C_{15}-C_{13}-C_{11})-τ(C_5-C_{15}-C_{13}-H_{19})-τ(H_{20}-C_{15}-C_{13}-C_{11})-τ(H_{20}-C_{15}-C_{13}-H_{19})- -τ(C_{15}-C_{13}-C_{11}-C_9)-τ(C_{15}-C_{13}-C_{11}-H_{18})-τ(H_{19}-C_{13}-C_{11}-C_9)-τ(H_{19}-C_{13}-C_{11}-H_{18})+ +τ(C_{13}-C_{11}-C_9-N_7)+τ(C_{13}-C_{11}-C_9-H_{17})+τ(H_{18}-C_{11}-C_9-N_7)+τ(H_{18}-C_{11}-C_9-H_{17})+ +τ(C_3-C_6-C_{16}-C_{14})+τ(C_3-C_6-C_{16}-H_{24})+τ(N_8-C_6-C_{16}-C_{14})+τ(N_8-C_6-C_{16}-H_{24})- -τ(C_6-C_{16}-C_{14}-C_{12})-τ(C_6-C_{16}-C_{14}-H_{23})-τ(H_{24}-C_{16}-C_{14}-C_{12})-τ(H_{24}-C_{16}-C_{14}-H_{23})- -τ(C_{16}-C_{14}-C_{12}-C_{10})-τ(C_{16}-C_{14}-C_{12}-H_{22})-τ(H_{23}-C_{14}-C_{12}-C_{10})-τ(H_{23}-C_{14}-C_{12}-H_{22})+ +τ(C_{14}-C_{12}-C_{10}-N_8)+τ(C_{14}-C_{12}-C_{10}-H_{21})+τ(H_{22}-C_{12}-C_{10}-N_8)+τ(H_{22}-C_{12}-C_{10}-H_{21})	*A*	τ(ring 4) s
S_{53}	τ(C_1-C_5-C_{15}-C_{13})+τ(C_1-C_5-C_{15}-H_{20})+τ(N_7-C_5-C_{15}-C_{13})+τ(N_7-C_5-C_{15}-H_{20})- -τ(C_5-C_{15}-C_{13}-C_{11})-τ(C_5-C_{15}-C_{13}-H_{19})-τ(H_{20}-C_{15}-C_{13}-C_{11})-τ(H_{20}-C_{15}-C_{13}-H_{19})- -τ(C_{15}-C_{13}-C_{11}-C_9)-τ(C_{15}-C_{13}-C_{11}-H_{18})-τ(H_{19}-C_{13}-C_{11}-C_9)-τ(H_{19}-C_{13}-C_{11}-H_{18})+ +τ(C_{13}-C_{11}-C_9-N_7)+τ(C_{13}-C_{11}-C_9-H_{17})+τ(H_{18}-C_{11}-C_9-N_7)+τ(H_{18}-C_{11}-C_9-H_{17})- -τ(C_3-C_6-C_{16}-C_{14})-τ(C_3-C_6-C_{16}-H_{24})-τ(N_8-C_6-C_{16}-C_{14})-τ(N_8-C_6-C_{16}-H_{24})+ +τ(C_6-C_{16}-C_{14}-C_{12})+τ(C_6-C_{16}-C_{14}-H_{23})+τ(H_{24}-C_{16}-C_{14}-C_{12})+τ(H_{24}-C_{16}-C_{14}-H_{23})+ +τ(C_{16}-C_{14}-C_{12}-C_{10})+τ(C_{16}-C_{14}-C_{12}-H_{22})+τ(H_{23}-C_{14}-C_{12}-C_{10})+τ(H_{23}-C_{14}-C_{12}-H_{22})- -τ(C_{14}-C_{12}-C_{10}-N_8)-τ(C_{14}-C_{12}-C_{10}-H_{21})-τ(H_{22}-C_{12}-C_{10}-N_8)-τ(H_{22}-C_{12}-C_{10}-H_{21})	*B*	τ(ring 4) as

S_{54}	$\tau(O_2=C_1-C_3=O_4)+\tau(O_2=C_1-C_3-C_6)+\tau(C_5-C_1-C_3-C_6)+\tau(C_5-C_1-C_3=O_4)$	*A*	τ(C-C)
S_{55}	$\tau(N_7-C_5-C_1-C_3)+\tau(C_{15}-C_5-C_1-C_3)+\tau(N_8-C_6-C_3-C_1)+\tau(C_{16}-C_6-C_3-C_1)+$ $+\tau(N_7-C_5-C_1=O_2)+\tau(C_{15}-C_5-C_1=O_2)+\tau(N_8-C_6-C_3=O_4)+\tau(C_{16}-C_6-C_3=O_4)$	*A*	$\tau(C-C_\alpha)$ s
S_{56}	$\tau(N_7-C_5-C_1-C_3)+\tau(C_{15}-C_5-C_1-C_3)-\tau(N_8-C_6-C_3-C_1)-\tau(C_{16}-C_6-C_3-C_1)+$ $+\tau(N_7-C_5-C_1=O_2)+\tau(C_{15}-C_5-C_1=O_2)-\tau(N_8-C_6-C_3=O_4)-\tau(C_{16}-C_6-C_3=O_4)$	*B*	$\tau(C-C_\alpha)$ as
S_{57}	$\tau(O_2=C_3-C_1-C_5)+\tau(O_4=C_1-C_3-C_6)$	*A*	γ(C=O) s
S_{58}	$\tau(O_2=C_3-C_1-C_5)-\tau(O_4=C_1-C_3-C_6)$	*B*	γ(C=O) as
S_{59}	$\gamma(H_{17}-N_7-C_9-C_{11})+\gamma(H_{18}-C_9-C_{11}-C_{13})+\gamma(H_{19}-C_{11}-C_{13}-C_{15})+\gamma(H_{20}-C_{13}-C_{15}-C_5)+$ $+\gamma(H_{21}-N_8-C_{10}-C_{12})+\gamma(H_{22}-C_{10}-C_{12}-C_{14})+\gamma(H_{23}-C_{12}-C_{14}-C_{16})+\gamma(H_{24}-C_{14}-C_{16}-C_6)$	*A*	γ(C-H 1) s
S_{60}	$\gamma(H_{17}-N_7-C_9-C_{11})+\gamma(H_{18}-C_9-C_{11}-C_{13})+\gamma(H_{19}-C_{11}-C_{13}-C_{15})+\gamma(H_{20}-C_{13}-C_{15}-C_5)-$ $-\gamma(H_{21}-N_8-C_{10}-C_{12})-\gamma(H_{22}-C_{10}-C_{12}-C_{14})-\gamma(H_{23}-C_{12}-C_{14}-C_{16})-\gamma(H_{24}-C_{14}-C_{16}-C_6)$	*B*	γ(C-H 1) as
S_{61}	$\gamma(H_{17}-N_7-C_9-C_{11})+\gamma(H_{18}-C_9-C_{11}-C_{13})-\gamma(H_{19}-C_{11}-C_{13}-C_{15})-\gamma(H_{20}-C_{13}-C_{15}-C_5)+$ $+\gamma(H_{21}-N_8-C_{10}-C_{12})+\gamma(H_{22}-C_{10}-C_{12}-C_{14})-\gamma(H_{23}-C_{12}-C_{14}-C_{16})-\gamma(H_{24}-C_{14}-C_{16}-C_6)$	*A*	γ(C-H 2) s
S_{62}	$\gamma(H_{17}-N_7-C_9-C_{11})+\gamma(H_{18}-C_9-C_{11}-C_{13})-\gamma(H_{19}-C_{11}-C_{13}-C_{15})-\gamma(H_{20}-C_{13}-C_{15}-C_5)-$ $-\gamma(H_{21}-N_8-C_{10}-C_{12})-\gamma(H_{22}-C_{10}-C_{12}-C_{14})+\gamma(H_{23}-C_{12}-C_{14}-C_{16})+\gamma(H_{24}-C_{14}-C_{16}-C_6)$	*B*	γ(C-H 2) as
S_{63}	$\gamma(H_{17}-N_7-C_9-C_{11})-\gamma(H_{18}-C_9-C_{11}-C_{13})+\gamma(H_{19}-C_{11}-C_{13}-C_{15})-\gamma(H_{20}-C_{13}-C_{15}-C_5)+$ $+\gamma(H_{21}-N_8-C_{10}-C_{12})-\gamma(H_{22}-C_{10}-C_{12}-C_{14})+\gamma(H_{23}-C_{12}-C_{14}-C_{16})-\gamma(H_{24}-C_{14}-C_{16}-C_6)$	*A*	γ(C-H 3) s
S_{64}	$\gamma(H_{17}-N_7-C_9-C_{11})-\gamma(H_{18}-C_9-C_{11}-C_{13})+\gamma(H_{19}-C_{11}-C_{13}-C_{15})-\gamma(H_{20}-C_{13}-C_{15}-C_5)-$ $-\gamma(H_{21}-N_8-C_{10}-C_{12})+\gamma(H_{22}-C_{10}-C_{12}-C_{14})-\gamma(H_{23}-C_{12}-C_{14}-C_{16})+\gamma(H_{24}-C_{14}-C_{16}-C_6)$	*B*	γ(C-H 3) as
S_{65}	$\gamma(H_{17}-N_7-C_9-C_{11})-\gamma(H_{18}-C_9-C_{11}-C_{13})-\gamma(H_{19}-C_{11}-C_{13}-C_{15})+\gamma(H_{20}-C_{13}-C_{15}-C_5)+$ $+\gamma(H_{21}-N_8-C_{10}-C_{12})-\gamma(H_{22}-C_{10}-C_{12}-C_{14})-\gamma(H_{23}-C_{12}-C_{14}-C_{16})+\gamma(H_{24}-C_{14}-C_{16}-C_6)$	*A*	γ(C-H 4) s
S_{66}	$\gamma(H_{17}-N_7-C_9-C_{11})-\gamma(H_{18}-C_9-C_{11}-C_{13})-\gamma(H_{19}-C_{11}-C_{13}-C_{15})+\gamma(H_{20}-C_{13}-C_{15}-C_5)-$ $-\gamma(H_{21}-N_8-C_{10}-C_{12})+\gamma(H_{22}-C_{10}-C_{12}-C_{14})+\gamma(H_{23}-C_{12}-C_{14}-C_{16})-\gamma(H_{24}-C_{14}-C_{16}-C_6)$	*B*	γ(C-H 4) as

[a] Normalization factors not shown. ν, bond stretching, δ, bending, γ, rocking, w, wagging, τ, torsion, s, symmetric, as, asymmetric. See Figure 1 for atom numbering. [b] C_2 symmetry point group.

Table S3 - Calculated [scaled, DFT(B3LYP)/6-311++G(d,p)] wavenumbers, IR intensities and Potential Energy Distributions (PED) for the most stable conformer of α-pyridil.[a]

Approximate Description[b]	Sym	Wavenumber	Intensity	PED[c]
ν(C-H 2) s	*A*	3134.9	0.9	$S_{20}(88)$, $S_{22}(10)$
ν(C-H 2) as	*B*	3134.8	6.4	$S_{21}(89)$
ν(C-H 3) s	*A*	3123.2	8.5	$S_{22}(78)$
ν(C-H 3) as	*B*	3123.1	16.0	$S_{23}(78)$
ν(C-H 4) as	*B*	3106.0	12.6	$S_{25}(81)$, $S_{23}(10)$
ν(C-H 4) s	*A*	3106.0	2.4	$S_{24}(81)$, $S_{22}(10)$
ν(C-H 1) s	*A*	3087.1	11.3	$S_{18}(92)$
ν(C-H 1) as	*B*	3087.0	14.6	$S_{19}(92)$
ν(C=O) s	*A*	1733.8	225.8	$S_{2}(92)$
ν(C=O) as	*B*	1723.5	169.5	$S_{3}(93)$
ν(ring 3) as	*B*	1585.2	9.2	$S_{11}(40)$, $S_{13}(26)$
ν(ring 3) s	*A*	1585.2	22.3	$S_{10}(37)$, $S_{12}(28)$
ν(ring 4) s	*A*	1577.1	5.3	$S_{12}(41)$, $S_{10}(32)$, $S_{40}(10)$
ν(ring 4) as	*B*	1575.6	7.1	$S_{13}(44)$, $S_{11}(29)$, $S_{41}(11)$
ν(ring 6) s; δ(C-H 4) s	*A*	1463.6	2.0	$S_{16}(40)$, $S_{44}(35)$, $S_{38}(17)$
δ(C-H 4) as; ν(ring 6) as	*B*	1462.6	1.6	$S_{45}(44)$, $S_{17}(40)$, $S_{39}(17)$
δ(C-H 3) s	*A*	1434.3	0.7	$S_{42}(51)$, $S_{8}(26)$, $S_{14}(15)$
δ(C-H 3) as	*B*	1431.7	13.2	$S_{43}(54)$, $S_{9}(27)$, $S_{15}(14)$
ν(ring 5) s	*A*	1307.1	19.7	$S_{14}(26)$, $S_{4}(14)$
ν(ring 5) as	*B*	1291.6	2.4	$S_{15}(39)$, $S_{45}(26)$
δ(C-H 4) s	*A*	1282.1	6.1	$S_{44}(37)$, $S_{8}(15)$, $S_{10}(12)$, $S_{38}(10)$
ν(ring 2) as	*B*	1277.8	8.7	$S_{9}(35)$, $S_{45}(17)$, $S_{11}(13)$, $S_{15}(11)$
ν(ring 2) s; ν(ring 5) s; ν(C-$C_α$) s	*A*	1255.5	28.4	$S_{8}(31)$, $S_{14}(27)$, $S_{4}(16)$
ν(C-$C_α$) as	*B*	1218.7	131.2	$S_{5}(31)$, $S_{9}(19)$, $S_{35}(15)$, $S_{7}(12)$
δ(C-H 2) s	*A*	1145.7	1.0	$S_{40}(62)$, $S_{38}(13)$
δ(C-H 2) as	*B*	1145.2	0.9	$S_{41}(61)$, $S_{39}(15)$, $S_{15}(10)$
ν(ring 2) s; δ(C-H 3) s; δ(C-H 1) s	*A*	1088.6	1.3	$S_{8}(33)$, $S_{42}(28)$,$S_{38}(18)$, $S_{14}(12)$
ν(ring 2) as; δ(C-H 3) as; δ(C-H 1) as	*B*	1087.8	16.3	$S_{9}(30)$, $S_{43}(26)$, $S_{39}(18)$, $S_{15}(11)$
ν(ring 6) s; ν(C-C)	*A*	1052.3	4.4	$S_{16}(37)$, $S_{1}(18)$, $S_{38}(14)$, $S_{26}(11)$
ν(ring 6) as	*B*	1037.6	6.3	$S_{17}(65)$, $S_{7}(16)$, $S_{39}(12)$
ν(ring 6) s; ν(ring 1) s	*A*	1030.8	2.0	$S_{16}(31)$, $S_{6}(29)$, $S_{34}(23)$
γ(C-H 3) as	*B*	996.6	0.1	$S_{64}(56)$, $S_{51}(28)$
γ(C-H 3) s	*A*	996.1	<0.1	$S_{63}(56)$, $S_{50}(29)$
ν(ring 1) s; δ(ring 2) s	*A*	992.2	0.1	$S_{6}(49)$, $S_{34}(48)$
δ(ring 2) as; ν(ring 1) as	*B*	991.9	19.9	$S_{35}(52)$, $S_{7}(45)$
γ(C-H 4) as	*B*	966.1	1.2	$S_{66}(68)$, $S_{47}(14)$
γ(C-H 4) s	*A*	965.8	0.2	$S_{65}(68)$, $S_{46}(12)$
γ(C-H 2) as	*B*	906.8	16.5	$S_{62}(79)$
γ(C-H 2) s	*A*	904.8	0.2	$S_{61}(82)$
Skeletal	*B*	891.0	80.3	$S_{27}(23)$, $S_{53}(13)$, $S_{7}(12)$, $S_{58}(12)$, $S_{47}(12)$, $S_{5}(10)$
τ(ring 1) s; γ(C=O) s	*A*	816.2	3.5	$S_{46}(37)$, $S_{57}(27)$, $S_{52}(17)$, $S_{59}(10)$
τ(ring 1) as; γ(C=O) as	*B*	791.2	21.3	$S_{47}(33)$, $S_{60}(22)$, $S_{53}(11)$
γ(C-H 1) s	*A*	742.5	36.9	$S_{59}(63)$, $S_{50}(20)$
γ(C-H 1) as; τ(ring 3) as	*B*	739.6	28.8	$S_{60}(50)$, $S_{51}(29)$, $S_{64}(11)$, $S_{49}(10)$
δ(ring 1) s	*A*	732.4	0.4	$S_{32}(43)$, $S_{4}(13)$
δ(ring 1) as	*B*	707.2	11.7	$S_{33}(22)$, $S_{51}(17)$, $S_{58}(16)$, $S_{64}(12)$
τ(ring 3) s; γ(C=O) s	*A*	706.7	18.2	$S_{50}(26)$, $S_{57}(22)$, $S_{63}(17)$, $S_{59}(10)$
Skeletal	*B*	653.9	98.6	$S_{27}(17)$, $S_{33}(15)$, $S_{37}(13)$, $S_{29}(12)$, $S_{31}(11)$
δ(ring 3) s	*A*	617.9	0.2	$S_{36}(85)$
δ(ring 3) as	*B*	614.2	39.9	$S_{37}(75)$
Skeletal	*A*	474.8	4.4	$S_{52}(23)$, $S_{32}(20)$, $S_{4}(17)$, $S_{30}(11)$, $S_{28}(11)$, $S_{58}(11)$
τ(ring 4) as	*B*	472.0	11.3	$S_{53}(29)$, $S_{33}(17)$, $S_{5}(15)$, $S_{29}(13)$, $S_{31}(10)$
τ(ring 2) s; τ(ring 4) s	*A*	422.5	1.9	$S_{48}(27)$, $S_{52}(27)$, $S_{61}(23)$, $S_{50}(11)$
τ(ring 2) as	*B*	422.1	9.2	$S_{49}(29)$, $S_{62}(20)$, $S_{53}(19)$, $S_{51}(10)$
τ(ring 4) s; τ(ring 2) s	*A*	399.4	1.5	$S_{52}(36)$, $S_{48}(29)$, $S_{65}(21)$
τ(ring 4) as; τ(ring 2) as	*B*	395.4	0.9	$S_{53}(39)$, $S_{49}(26)$, $S_{66}(21)$
δ(C=O) s	*A*	325.9	4.7	$S_{26}(51)$, $S_{1}(32)$
δ(C=O) as; w(ring) as	*B*	263.8	27.4	$S_{27}(31)$, $S_{31}(29)$, $S_{58}(13)$
w(ring) s	*A*	258.6	3.2	$S_{30}(42)$, $S_{4}(11)$
τ(ring 1) s	*A*	148.5	0.1	$S_{46}(61)$, $S_{48}(16)$, $S_{54}(14)$
τ(ring 1) as	*B*	145.8	1.7	$S_{47}(61)$, $S_{49}(18)$, $S_{31}(11)$
δ(CCC$_α$) as	*B*	120.8	<0.1	$S_{29}(35)$, $S_{31}(24)$, $S_{56}(21)$
δ(CCC$_α$) s	*A*	111.3	0.1	$S_{28}(52)$, $S_{30}(24)$
τ(C-C$_α$) s	*A*	52.4	0.4	$S_{55}(79)$
τ(C-C$_α$) as	*B*	41.6	4.1	$S_{56}(73)$, $S_{29}(12)$
τ(C-C)	*A*	24.0	3.5	$S_{54}(73)$

[a] Frequencies (cm^{-1}, scaled by 0.978), calculated intensities in km mol^{-1}. ν, bond stretching; δ, bending; w, wagging; γ, rocking; τ, torsion; s, symmetric; as, asymmetric. See Table S2 for definition of symmetry coordinates. [b] Skeletal approximate descriptions corresponds to vibrations with more than three PED values identical within 15 units. [c] Only PED values greater than 10 % are given.

Table S4 – Calculated geometries and infrared spectra (non-scaled) for observed Hückel pyridine containing photoproducts (2C and 3A forms)

2C

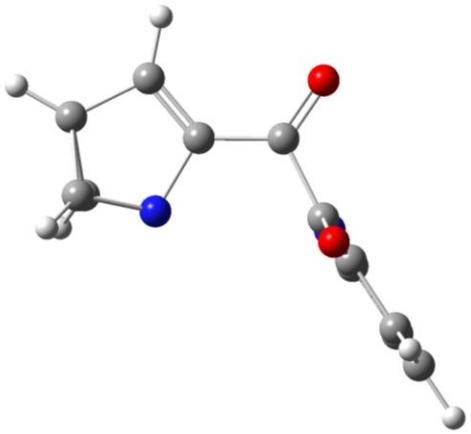

Optimized Geometry (Angstroms)

	X	Y	Z
C	-0.344783	-0.631278	1.211377
O	-0.466592	-0.406100	2.395152
C	1.063569	-0.889445	0.631516
O	1.504919	-2.021785	0.667788
C	1.817136	0.270597	0.158600
C	3.080974	0.371448	-0.275958
C	2.277918	2.594299	0.304747
H	2.311245	3.439999	0.975452
H	3.824629	-0.405607	-0.365198
C	3.231443	1.820333	-0.612440
H	4.140433	2.267811	-0.998281
N	1.186152	1.594266	0.101452
C	1.844707	2.329009	-1.020431
H	1.392642	2.878004	-1.833067
C	-1.505267	-0.753113	0.275428
C	-2.813987	-0.688762	0.758308
C	-3.855827	-0.798472	-0.154639
H	-2.982764	-0.557558	1.819763
C	-2.206637	-1.007320	-1.885466
H	-4.887413	-0.758301	0.176296
H	-1.933566	-1.131945	-2.929248
C	-3.548266	-0.961048	-1.503742
N	-1.198874	-0.907873	-1.019014
H	-4.328640	-1.051563	-2.250093

IR Spectrum (cm^{-1}; km mol^{-1})

Frequency	Intensity
22.0	3.86
45.1	3.51
56.6	1.52
106.9	0.50
121.5	0.03
147.8	0.31
152.6	0.38
265.4	25.66
275.1	3.36
337.2	4.82
405.9	1.60
430.0	2.42
458.6	9.65
470.9	1.55
510.5	5.41
585.3	0.69
630.2	16.77
684.7	104.62
695.7	20.81
721.1	5.54
727.4	10.13
743.4	6.27
756.3	36.82
769.7	34.47
787.4	4.38
815.8	33.65
864.4	29.56
874.3	12.75
890.5	12.95
894.3	66.48
924.2	1.22
966.2	27.96
971.7	0.13
986.4	0.81
998.3	8.24
1014.0	11.17
1017.0	0.10
1055.8	23.24
1058.8	5.56
1077.6	12.99
1094.1	9.85
1112.1	9.32
1146.1	2.45
1170.6	1.23
1200.4	28.00
1231.4	128.01
1277.5	5.39
1283.6	23.40
1309.3	7.88
1328.7	12.64
1421.5	4.48
1464.6	6.84
1495.6	1.80
1611.4	6.99
1620.2	15.51
1635.6	196.29
1731.4	179.27
1764.7	189.55
3155.3	13.48
3175.4	7.70
3176.1	18.07
3193.1	12.51
3204.8	3.85
3210.0	2.96
3229.7	5.79
3250.1	0.08

3A

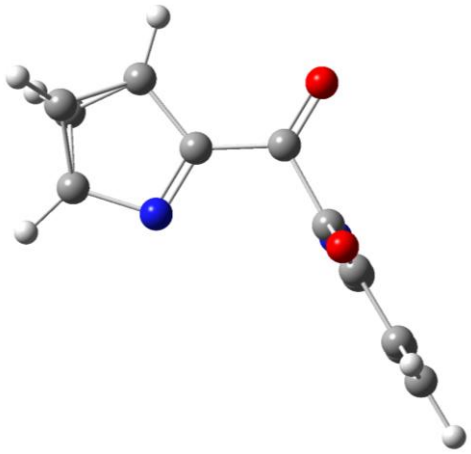

Optimized Geometry (Angstroms)

	X	Y	Z
C	3.959311	-0.296172	-0.441812
C	-0.642976	1.333131	-0.175415
O	-0.691422	2.334095	-0.853323
C	0.605979	1.067614	0.695425
O	0.706414	1.591529	1.783823
C	2.991201	-0.121503	0.727182
H	3.317346	0.191984	1.708376
C	1.676287	0.239756	0.102398
H	4.964982	0.033563	-0.655158
C	3.359740	-1.480633	0.135941
C	2.848950	-0.994822	-1.214211
N	1.583290	-0.284076	-1.066834
H	3.727413	-2.412729	0.538029
H	3.035380	-1.535261	-2.131335
C	-1.762934	0.349169	-0.069450
C	-2.943925	0.538146	-0.789923
C	-3.950501	-0.410912	-0.656943
H	-3.045480	1.407820	-1.426854
C	-2.518910	-1.596916	0.861425
H	-4.884159	-0.305635	-1.197639
H	-2.321095	-2.433293	1.525229
C	-3.736025	-1.499787	0.185025
N	-1.545837	-0.694643	0.740936
H	-4.493681	-2.262840	0.318789

IR Spectrum (cm^{-1}; km mol^{-1})

Frequency	Intensity
25.1	3.82
43.7	4.90
55.4	0.68
109.8	0.48
122.4	0.25
148.4	2.59
149.0	0.32
240.9	14.65
271.0	16.51
336.1	3.82
409.6	1.80
435.8	2.92
456.2	10.07
515.7	12.42
548.6	0.92
604.3	16.42
630.1	16.76
670.9	86.99
717.3	1.16
733.3	7.57
735.2	31.71
756.2	28.41
768.2	8.69
772.1	31.87
795.7	19.49
823.4	6.49
854.4	9.74
880.1	62.95
900.1	4.39
921.7	0.26
926.0	1.33
987.6	1.31
990.4	12.60
1003.2	0.22
1014.2	10.08
1018.6	0.16
1039.0	4.24
1055.6	7.80
1064.3	2.00
1111.1	17.01
1112.6	9.50
1115.0	10.02
1170.7	12.71
1174.1	32.63
1195.7	24.73
1231.4	22.19
1271.4	54.00
1308.7	8.11
1324.9	7.25
1380.9	20.69
1402.2	1.55
1464.7	8.11
1495.8	1.69
1611.9	5.53
1620.1	17.23
1627.4	36.87
1750.5	193.46
1769.9	211.81
3157.1	12.42
3176.6	7.47
3193.0	11.98
3205.7	3.46
3212.3	2.90
3215.3	1.09
3221.4	1.09
3232.6	1.11

J. Chem. Phys., **2010**, *133*, 144507-7.

Supporting Information

for

Formic and Acetic Acids in a Nitrogen Matrix: Enhanced Stability of the Higher Energy Conformer

Susy Lopes,[1] Alexandra V. Domanskaya,[2] Rui Fausto,[1] Markku Räsänen,[2] and Leonid Khriachtchev[2]

[1]*Department of Chemistry, University of Coimbra, Rua Larga, P-3004-535 Coimbra, Portugal*
[2]*Department of Chemistry, University of Helsinki, P.O. Box 55, FIN-00014 Helsinki, Finland*

Contents

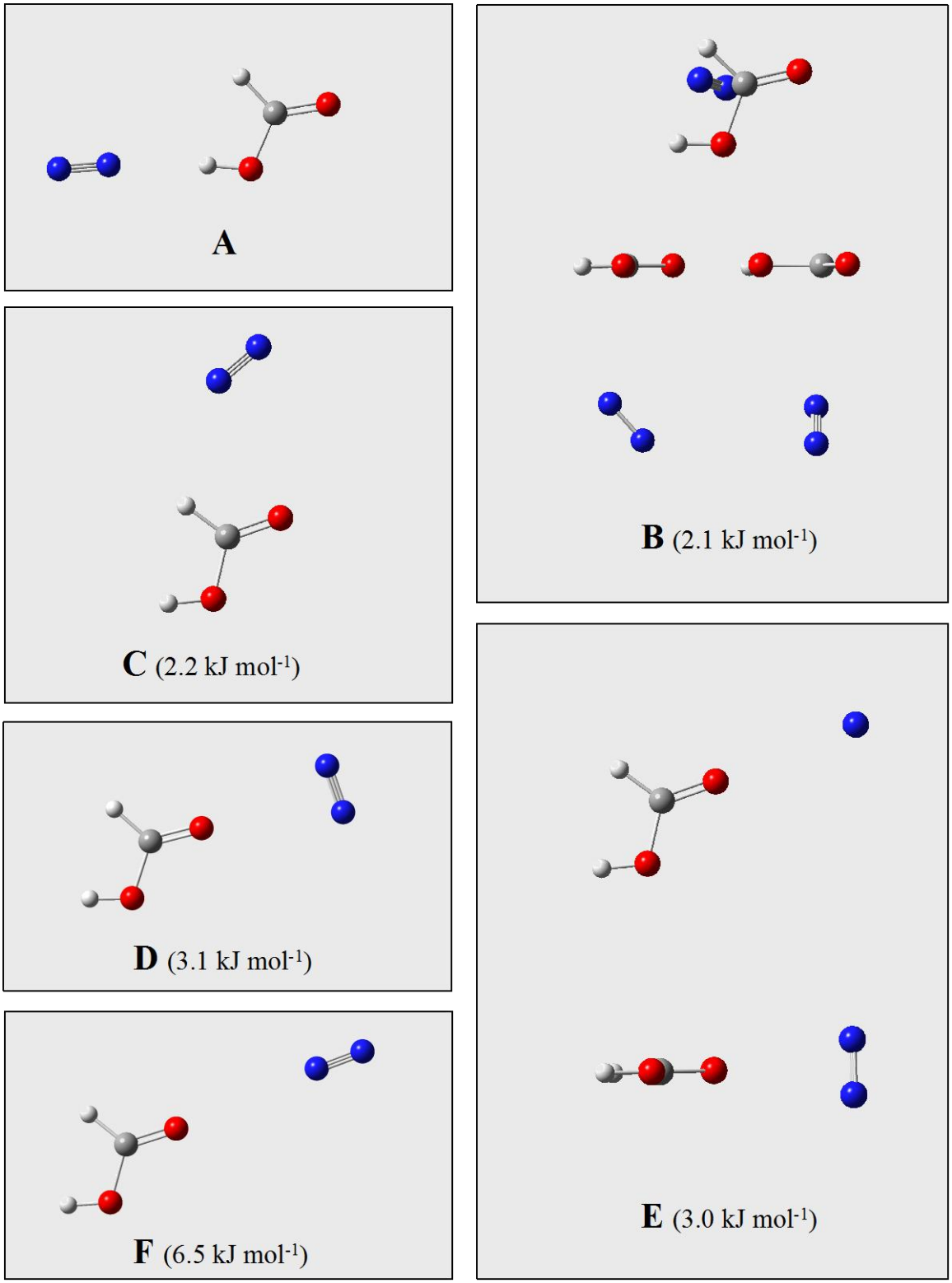

Figure S1 – Optimized structures of the *cis*-HCOOH···N_2 complexes calculated at the MP2/6-311++G(2d,2p) level of theory. Complexes A, C, D and F are planar. Complexes B and E are non-planar forms. For these two latter cases, different views are shown for better perception of the relative position of the HCOOH and N_2 molecules. Numbers in parenthesis are relative energies (with zero point and BSSE corrections).

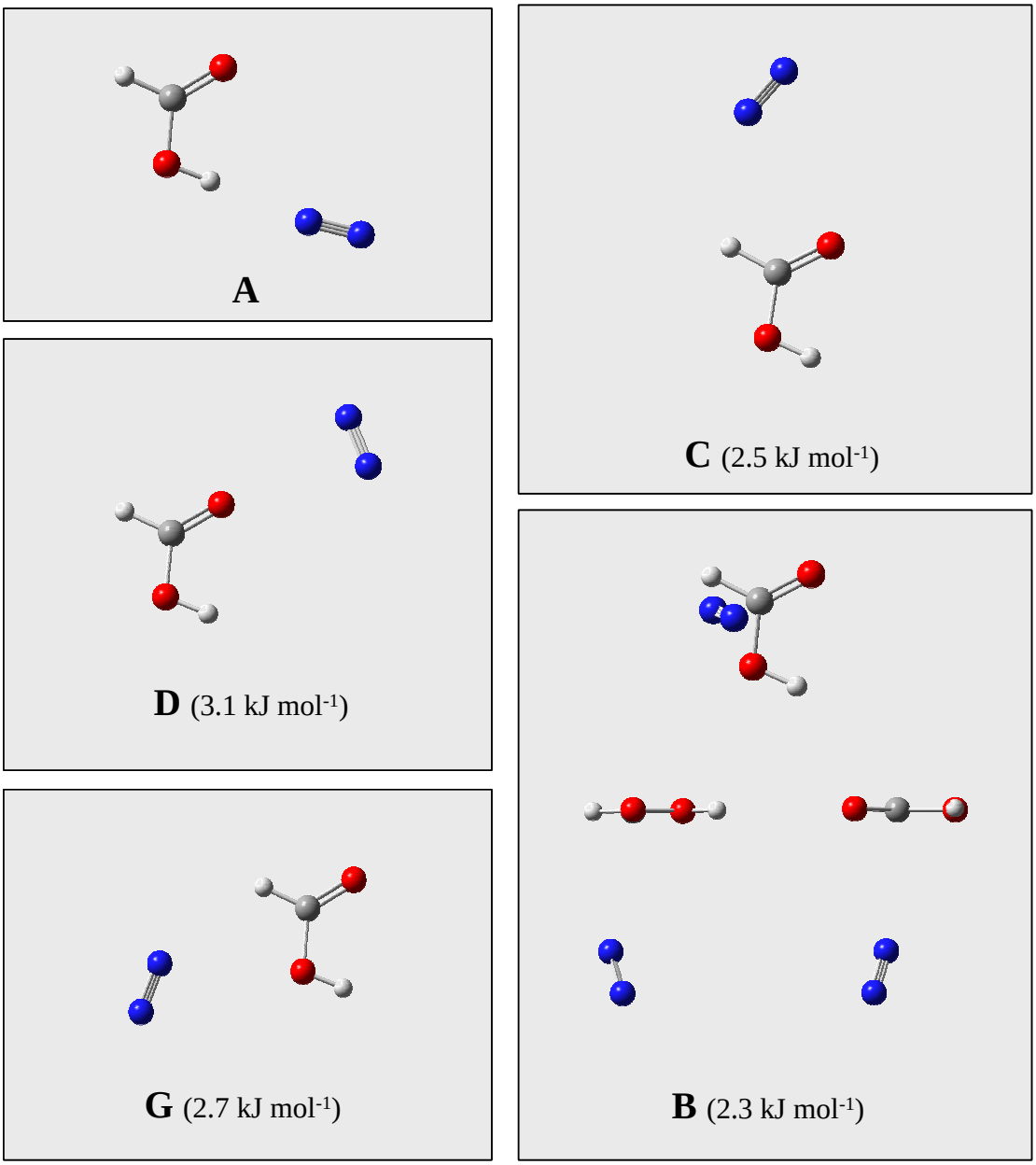

Figure S2 – Optimized structures of the *trans*-HCOOH···N_2 complexes calculated at the MP2/6-311++G(2d,2p) level of theory. Complexes A, C, D and G are planar. Complex B is non-planar. For this latter case, different views are shown for better perception of the relative position of the HCOOH and N_2 molecules. Numbers in parenthesis are relative energies (with zero point and BSSE corrections).

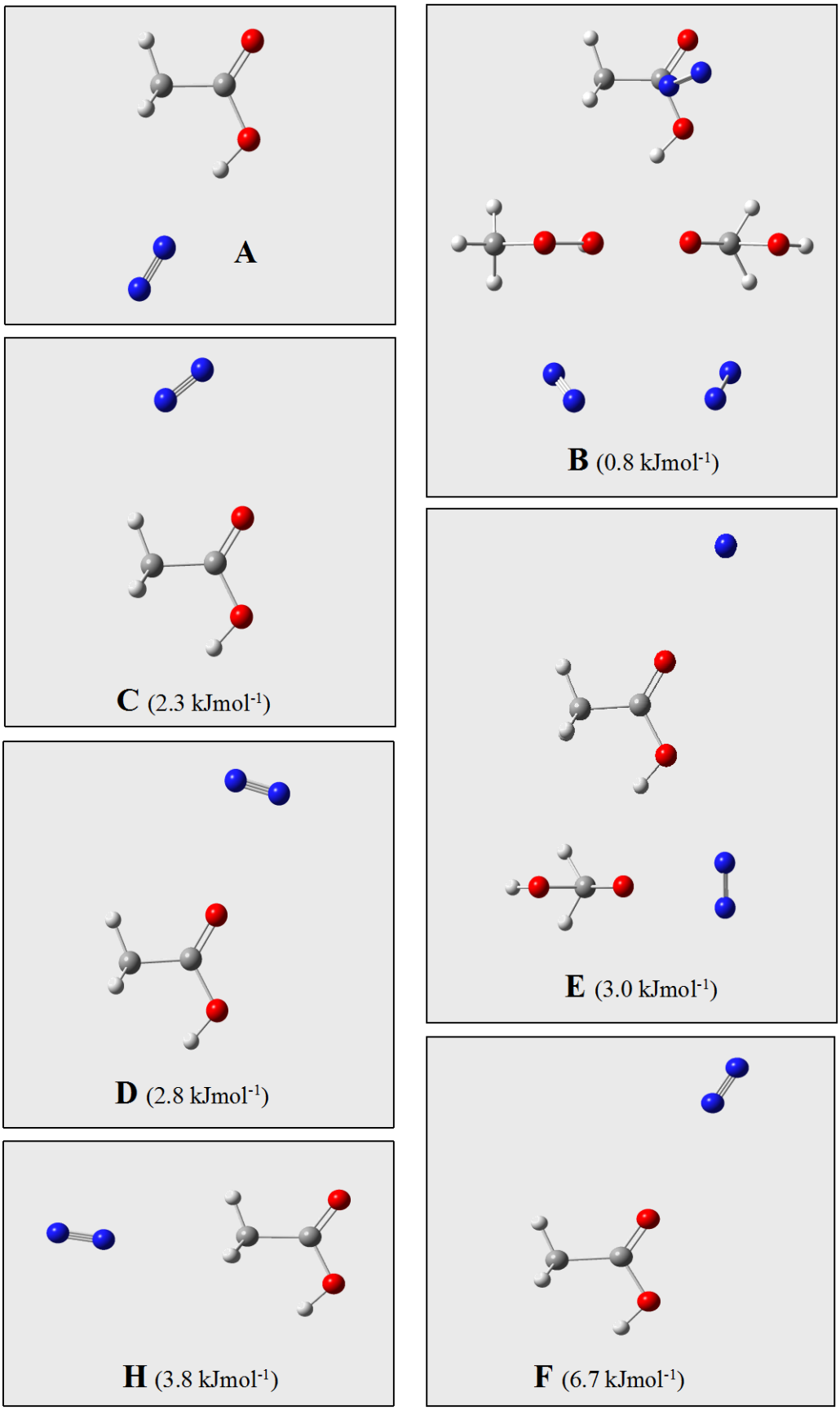

Figure S3 – Optimized structures of the *cis*-$CH_3COOH^{\cdots}N_2$ complexes calculated at the MP2/6-311++G(2d,2p) level of theory. Complexes A, C, D, F and H have the heavy atoms in the same plane. For complexes B and E, which have a non-planar heavy atoms skeleton, different views are shown for better perception of the relative position of the CH_3COOH and N_2 molecules. Numbers in parenthesis are relative energies (with zero point and BSSE corrections).

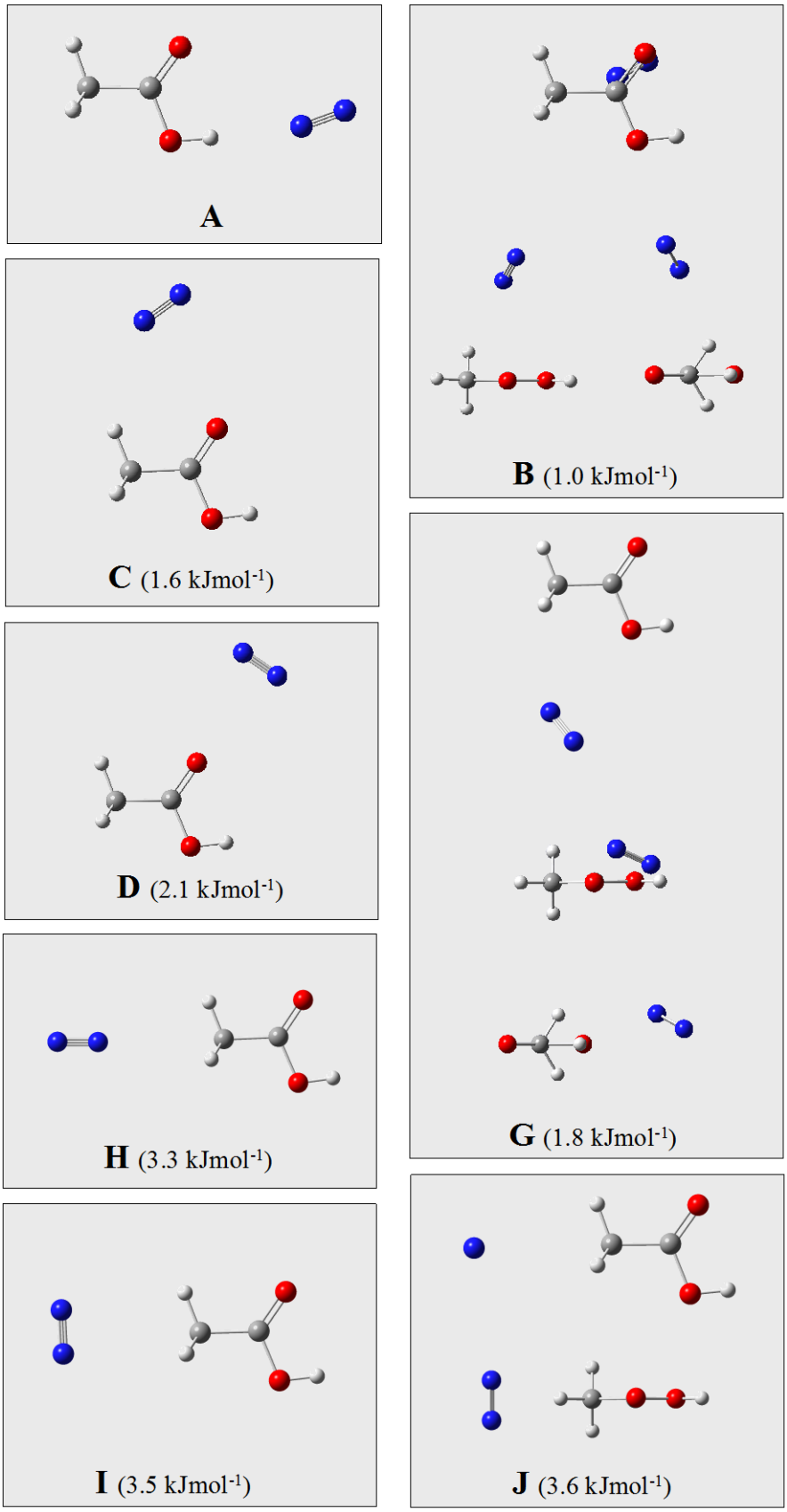

Figure S4 – Optimized structures of the *trans*-$CH_3COOH^{\cdots}N_2$ complexes calculated at the MP2/6-311++G(2d,2p) level of theory. Complexes A, C, D, H and I have the heavy atoms in the same plane. For complexes B, G and J, which have a non-planar heavy atoms skeleton, different views are shown for better perception of the relative position of the CH_3COOH and N_2 molecules. Numbers in parenthesis are relative energies (with zero point and BSSE corrections).

Table S-I. Calculated νOH, νC=O and τCOH wavenumbers (ν in cm^{-1}) and infrared intensities (I_{IR} in km mol^{-1}) for monomeric *cis* and *trans* forms of FA and AA and their complexes with N_2.[a]

	νOH		νC=O		τCOH		νOH		νC=O		τCOH	
	ν	I_{IR}	ν	I_{IR}	ν	I_{IR}	ν	I_{IR}	ν	I_{IR}	ν	I_{IR}
	cis-HCOOH						*trans*-HCOOH					
Monomer	3844.5	81.6	1824.4	268.3	535.2	88.1	3777.9	81.8	1784.2	334.3	674.7	143.5
A	3820.3	292.3	1820.6	297.9	620.9	79.0	3747.6	282.1	1779.1	321.0	747.7	118.5
B	3843.4	80.3	1822.9	253.9	533.3	96.3	3775.5	81.2	1782.1	342.1	674.5	138.8
C	3844.0	83.9	1821.4	257.8	537.7	87.3	3777.5	83.6	1781.1	326.8	675.9	140.3
D	3843.8	85.2	1823.4	289.3	537.5	87.2	3775.5	78.9	1783.1	357.3	676.3	140.0
E	3843.7	85.2	1823.4	288.8	537.5	87.4						
F	3843.8	85.2	1823.4	289.3	537.5	87.2						
G							3777.7	79.4	1783.6	320.0	676.1	150.9
	cis-CH_3COOH						*trans*-CH_3COOH					
Monomer	3852.9	63.3	1828.1	247.4	465.1	101.3	3787.3	77.5	1801.0	290.3	661.0	90.3
A	3833.6	233.1	1824.6	270.0	537.5	72.3	3762.6	266.8	1795.2	277.1	718.6	96.9
B	3851.1	63.5	1826.7	231.0	463.6	109.9	3787.0	73.7	1799.9	275.2	660.8	97.5
C	3851.7	65.0	1826.7	254.7	468.2	100.2	3786.7	78.2	1799.2	301.2	661.4	89.4
D	3851.8	65.7	1827.1	170.9	468.4	100.0	3785.6	75.0	1799.6	316.9	662.3	88.0
E	3851.8	65.9	1827.0	269.8	469.6	99.7						
H	3852.1	61.3	1827.3	251.2	465.5	100.4						
F	3852.5	64.2	1828.9	263.8	465.7	100.1						
G							3784.1	76.7	1801.4	302.0	664.2	90.1
H							3787.0	77.5	1800.0	292.9	662.0	89.6
I							3786.7	78.7	1801.1	292.3	662.1	88.2
J							3786.6	78.6	1801.1	293.2	662.7	87.8

[a] See Figures S1-S4 for structures of the complexes.

(*to be submitted*)

Supporting Information

for

Acetic Acid Dimers in a Solid Nitrogen Matrix

Susy Lopes,[1] Alexandra V. Domanskaya,[2] Rui Fausto,[1] Markku Räsänen,[2]
and Leonid Khriachtchev[2]

[1]*Department of Chemistry, University of Coimbra, Rua Larga, P-3004-535 Coimbra, Portugal*
[2]*Department of Chemistry, University of Helsinki, P.O. Box 55, FIN-00014 Helsinki, Finland*

Contents

Table S1 (Supporting Information) – MP2/6-311++G(2d,2p) calculated IR spectra (wavenumbers, ν in cm^{-1}; infrared intensities, I^{IR} in km mol^{-1}) for AA dimers (*trans-trans*).

D1_TT (C_{2h})		D2_TT (C_s)		D2'_TT (C_1)	
ν	I^{IR}	ν	I^{IR}	ν	I^{IR}
3303.4	2979.0	3780.0	83.7	3776.5	85.1
3229.0	0.0	3515.7	1016.7	3489.7	956.0
3228.2	12.8	3224.7	5.6	3224.5	4.7
3204.7	0.0	3223.6	15.0	3223.3	4.0
3187.1	2.9	3185.1	2.9	3195.5	3.3
3187.1	0.0	3183.4	1.1	3185.1	2.9
3107.0	1.9	3105.2	2.1	3108.2	4.3
3107.0	0.0	3100.9	13.3	3105.1	2.1
1760.9	716.0	1784.0	620.0	1781.7	604.7
1720.1	0.0	1762.8	76.2	1761.6	43.8
1510.9	0.0	1518.4	7.9	1511.8	11.7
1504.8	0.0	1505.4	7.7	1505.8	7.9
1504.8	17.0	1500.8	27.7	1500.2	18.1
1499.7	59.5	1499.4	0.5	1493.7	21.5
1486.0	0.0	1448.8	38.7	1448.4	40.1
1479.0	123.4	1442.7	63.2	1434.5	88.8
1420.9	0.0	1398.7	16.6	1399.2	6.9
1416.0	43.8	1368.3	92.2	1369.0	73.0
1336.2	392.2	1271.0	268.2	1273.6	248.9
1317.8	0.0	1227.5	219.4	1223.2	241.7
1087.6	6.5	1093.7	5.9	1087.1	8.2
1086.6	0.0	1083.1	4.4	1082.8	4.2
1042.3	41.1	1029.9	53.5	1032.7	55.7
1038.7	0.0	1028.1	69.4	1027.3	43.5
1033.4	169.7	903.7	85.0	910.4	80.8
993.4	0.0	890.6	4.2	887.7	5.5
910.9	0.0	882.2	6.3	881.5	4.6
909.9	7.2	673.8	92.9	692.7	95.9
635.3	44.0	609.9	32.7	610.8	11.8
627.2	0.0	600.5	38.8	602.0	26.1
609.5	0.0	599.4	0.5	597.0	31.8
604.2	0.5	558.7	26.5	550.4	22.4
483.6	45.9	447.9	16.5	445.4	12.7
444.0	0.0	434.1	3.1	435.7	0.7
179.8	0.0	145.8	12.9	164.2	17.9
177.6	29.6	110.6	0.1	125.2	1.6
155.7	0.0	108.0	0.3	118.9	0.3
123.1	0.0	99.2	4.0	85.9	1.4
73.9	0.2	94.2	0.4	65.1	0.3
58.6	1.6	62.9	0.01	49.5	0.9
45.0	0.0	35.0	3.5	28.6	3.0

D2’’_TT(C_s)		D2’’’_TT(C_s)		D3_TT (C_1)	
ν	I^{IR}	ν	I^{IR}	ν	I^{IR}
3672.0	637.4	3778.2	88.5	3776.0	81.9
3561.2	330.8	3539.5	868.3	3627.9	634.7
3229.3	2.2	3227.2	0.4	3227.7	2.3
3226.5	3.9	3223.9	5.4	3226.5	3.2
3187.6	1.3	3187.9	0.7	3185.7	2.2
3184.6	2.4	3183.8	3.7	3179.8	11.2
3107.3	0.8	3106.6	1.4	3105.9	1.6
3104.7	1.5	3104.1	2.7	3098.9	11.1
1804.4	151.2	1792.2	125.3	1817.6	312.9
1770.7	475.6	1774.1	571.3	1781.1	282.6
1506.4	8.7	1506.8	2.9	1509.2	24.5
1504.7	8.6	1506.1	13.1	1505.6	8.0
1500.2	21.6	1501.3	24.4	1503.1	9.0
1499.2	13.1	1500.4	9.4	1499.9	22.2
1445.5	44.7	1442.6	70.9	1442.3	59.0
1430.1	40.9	1437.1	30.4	1436.1	36.0
1396.5	11.8	1387.5	0.5	1388.9	3.1
1349.2	11.5	1368.4	43.4	1328.9	24.0
1270.7	384.5	1250.4	269.2	1262.4	270.1
1204.7	471.0	1219.0	463.5	1199.7	207.1
1085.6	5.4	1087.7	6.4	1089.5	5.4
1081.6	3.8	1081.3	4.2	1083.5	4.6
1027.6	55.8	1025.5	57.7	1025.7	56.5
1015.1	134.0	1021.3	109.2	1005.4	82.1
887.6	4.6	882.0	7.4	883.5	11.2
869.9	2.5	877.4	4.9	851.0	33.1
851.5	168.3	876.6	80.0	825.7	91.4
742.2	12.7	672.7	94.0	646.5	66.7
620.3	56.6	611.9	7.5	605.5	34.7
603.3	17.6	597.8	87.5	594.5	2.5
592.1	0.8	595.6	0.6	585.8	19.4
589.0	1.2	557.1	26.6	543.1	38.6
453.4	4.2	442.4	0.6	441.5	7.7
436.2	13.2	434.3	6.1	428.6	1.6
186.1	22.1	164.4	16.9	143.6	0.7
116.1	0.2	95.3	0.5	131.8	8.1
102.6	0.04	82.2	0.1	111.6	3.2
86.1	0.04	71.2	0.1	94.4	3.6
63.7	0.01	64.7	0.6	76.7	0.2
53.7	2.1	42.9	0.7	65.0	1.4
53.2	1.7	31.2	1.4	21.9	1.2
32.6	0.1	17.3	0.2	21.3	0.5

D4_TT (C_i)		D4'_TT (C_1)		D4''_TT(C_1)	
ν	I^{IR}	ν	I^{IR}	ν	I^{IR}
3789.5	0.0	3790.7	68.0	3784.8	79.3
3789.1	134.9	3784.2	75.1	3781.3	74.9
3223.7	0.0	3229.5	3.2	3226.5	2.8
3223.7	8.2	3227.3	3.4	3224.8	3.1
3193.9	0.0	3194.9	2.2	3183.6	1.7
3193.6	3.0	3186.2	2.3	3180.6	13.6
3108.2	0.0	3107.9	3.3	3103.0	5.9
3108.1	4.9	3103.4	6.2	3098.5	14.8
1797.6	555.0	1796.6	507.0	1802.9	263.9
1790.1	0.0	1790.5	102.8	1792.1	372.2
1506.2	0.0	1515.0	8.5	1516.4	21.8
1506.0	18.1	1504.2	9.5	1511.3	4.2
1496.7	0.0	1498.6	7.2	1504.4	7.2
1496.0	49.1	1495.3	19.3	1500.8	16.1
1432.8	101.8	1435.1	28.2	1438.6	27.9
1430.9	0.0	1432.3	72.0	1436.7	54.5
1352.5	76.8	1354.5	53.7	1355.1	53.8
1350.7	0.0	1351.5	41.0	1343.9	36.0
1212.4	0.0	1214.8	265.4	1213.3	245.5
1208.7	415.5	1209.5	169.9	1207.2	174.3
1084.5	0.0	1087.7	4.7	1089.7	6.7
1084.0	18.7	1083.8	14.3	1086.4	3.5
1014.8	152.8	1019.7	83.6	1018.0	76.7
1014.3	0.0	1013.8	72.6	1010.3	98.2
872.8	10.5	873.3	7.4	871.5	8.1
871.1	0.0	870.2	5.9	863.2	14.7
660.4	190.1	671.4	76.5	666.0	99.6
659.6	0.0	658.0	112.3	660.9	74.1
586.8	71.8	588.4	48.2	588.6	48.9
586.3	0.0	586.4	21.5	585.0	21.6
547.9	0.0	550.2	22.7	552.7	37.9
545.0	59.6	545.2	36.0	551.5	24.6
428.0	8.1	432.4	7.7	431.6	7.8
427.9	0.0	428.3	3.5	428.1	2.3
121.7	0.0	117.5	1.2	141.9	0.4
114.7	9.5	109.2	5.2	104.3	1.0
78.7	0.0	86.7	0.2	95.6	3.4
71.2	0.2	80.7	0.6	69.7	1.0
63.7	0.0	56.2	0.1	46.1	1.2
35.7	0.0	48.9	1.6	28.3	1.4
29.6	1.7	19.0	1.9	15.1	0.2
15.6	1.5	14.2	0.1	8.8	0.2

See Figure 1 for structures of the dimers.

Table S2 (Supporting Information) - MP2/6-311++G(2d,2p) calculated IR spectra (wavenumbers, ν in cm^{-1}; infrared intensities, I^{IR} in km mol^{-1}) for AA dimers (*trans-cis*).

D1_TC (C_s)		D1'_TC (C_1)		D2_TC (C_1)	
ν	I^{IR}	ν	I^{IR}	ν	I^{IR}
3646.4	736.8	3620.5	818.9	3847.3	76.9
3533.4	418.2	3519.8	305.7	3563.9	619.3
3229.7	2.2	3229.9	2.1	3224.4	4.2
3221.7	3.8	3221.3	3.6	3221.8	1.7
3188.4	0.9	3187.9	0.9	3185.4	2.4
3172.2	2.7	3171.8	2.5	3176.1	2.3
3107.9	0.4	3107.8	0.4	3105.2	1.9
3094.1	1.8	3093.8	1.5	3093.2	4.4
1822.8	253.5	1824.1	260.5	1804.0	378.0
1762.5	294.1	1759.1	303.6	1767.5	182.7
1511.1	8.0	1511.1	7.3	1513.5	5.1
1504.3	8.8	1504.3	9.0	1505.3	8.0
1500.0	4.2	1500.1	4.4	1500.1	19.9
1498.2	14.5	1498.0	17.0	1497.9	13.1
1452.0	46.5	1452.7	48.2	1443.2	73.5
1422.5	95.6	1423.3	111.3	1419.0	72.8
1409.8	144.4	1412.0	134.2	1389.0	4.4
1339.4	701.4	1357.8	467.6	1324.6	342.6
1262.7	326.5	1270.9	187.3	1266.8	205.5
1240.9	23.5	1242.2	123.1	1237.3	4.1
1086.6	5.1	1086.5	4.9	1083.0	3.7
1079.5	2.3	1078.8	3.0	1078.4	10.2
1031.6	39.2	1032.0	37.0	1027.6	40.2
1014.9	7.5	1014.4	14.6	1016.1	9.0
894.6	4.6	895.1	6.8	888.1	4.3
878.2	49.8	874.4	75.4	879.6	26.5
839.5	154.5	831.7	181.6	818.0	63.7
728.4	8.7	760.6	54.3	615.8	7.6
624.6	7.8	624.0	23.6	608.7	19.6
622.6	30.6	614.1	15.1	595.4	0.7
596.5	0.7	598.2	1.5	589.8	4.7
583.5	10.5	583.5	17.8	472.2	113.3
462.5	1.5	456.3	7.9	447.4	13.7
441.1	17.9	440.7	12.0	437.5	2.0
206.9	9.3	198.1	14.2	162.5	26.2
123.5	0.4	155.1	0.7	129.4	3.4
114.4	1.4	110.7	1.0	101.2	5.1
86.5	0.1	90.8	2.3	96.4	2.9
60.5	3.0	65.0	8.2	83.0	12.7
56.8	17.3	57.3	2.2	71.4	0.7
55.2	0.4	53.9	8.9	62.4	0.8
28.2	1.7	19.0	0.4	37.1	5.2

D2'_TC (C_s)		D2''_TC(C_1)		D2'''_TC(C_s)	
ν	I^{IR}	ν	I^{IR}	ν	I^{IR}
3846.9	77.2	3847.1	78.1	3778.7	86.6
3502.4	1055.8	3497.7	892.1	3583.1	877.1
3224.8	5.1	3224.1	5.3	3226.3	0.5
3209.6	24.5	3224.0	2.7	3219.4	5.8
3185.1	2.8	3185.1	2.7	3187.9	0.3
3165.3	2.7	3179.9	2.1	3172.3	4.2
3105.2	2.1	3105.0	2.0	3106.4	1.2
3084.0	25.1	3095.2	5.7	3094.5	2.8
1807.6	471.7	1806.1	433.7	1815.6	243.8
1765.6	160.7	1768.9	142.7	1770.0	440.9
1527.1	6.9	1509.0	8.9	1510.7	7.1
1505.3	7.7	1505.7	7.8	1505.7	9.4
1500.9	20.6	1500.2	21.0	1504.1	44.1
1499.4	1.1	1489.6	16.1	1495.8	13.0
1450.1	53.3	1447.3	56.2	1445.9	67.9
1432.0	36.9	1427.2	63.0	1423.6	175.0
1398.7	12.7	1398.2	5.2	1409.7	127.8
1324.4	506.2	1325.1	453.8	1365.3	259.3
1274.5	238.6	1274.7	228.0	1264.7	143.1
1239.8	2.8	1237.5	1.2	1225.6	256.8
1089.6	4.0	1083.1	3.0	1088.9	6.1
1083.4	4.4	1081.3	6.6	1078.7	3.5
1029.6	37.6	1028.2	38.8	1029.4	69.6
1023.5	12.8	1016.4	10.0	1017.1	19.3
909.0	87.5	896.1	71.1	883.9	8.7
892.3	2.3	888.2	3.7	877.7	23.4
879.8	36.8	879.6	39.6	803.1	54.2
613.6	10.2	613.5	3.5	673.7	94.4
610.9	2.8	609.8	11.2	620.7	7.3
610.2	20.7	608.3	12.2	600.6	52.9
600.5	0.2	598.8	0.7	588.6	12.6
499.2	95.9	496.5	95.2	558.5	26.8
452.8	5.9	447.4	4.8	449.6	1.1
440.4	5.7	439.5	10.2	438.4	6.6
148.2	22.9	170.9	35.4	177.6	5.2
130.6	1.0	131.6	3.9	109.3	1.4
111.0	8.3	124.8	1.1	91.6	0.7
103.5	2.6	103.1	1.1	71.6	0.5
96.1	0.2	82.0	3.7	59.5	0.4
61.4	0.1	67.4	0.5	48.6	7.5
36.4	8.1	31.9	5.9	34.6	0.7
18.1	3.8	23.7	2.3	25.5	4.5

D2’’’’_TC(C_s)		D3_TC (C_s)		D4_TC (C_1)	
ν	I^{IR}	ν	I^{IR}	ν	I^{IR}
3847.8	78.0	3779.2	77.0	3846.4	67.7
3540.8	819.1	3721.9	510.3	3786.3	71.1
3224.2	5.3	3230.7	2.0	3230.2	2.9
3220.1	0.9	3219.2	4.0	3219.0	2.3
3183.7	3.9	3186.3	0.2	3190.1	2.5
3169.7	2.0	3168.2	4.5	3177.1	1.4
3104.1	2.9	3107.4	0.02	3104.8	4.1
3090.9	6.3	3090.1	4.6	3093.9	4.2
1810.8	140.4	1822.5	11.4	1819.0	282.8
1786.5	488.6	1818.8	561.4	1782.6	210.9
1515.9	6.7	1511.6	9.2	1515.5	6.5
1506.3	8.6	1505.4	9.9	1503.8	9.1
1502.1	8.7	1500.3	8.1	1498.8	1.8
1500.5	13.5	1494.5	5.4	1498.2	32.5
1435.1	41.9	1435.2	17.3	1432.6	62.7
1429.6	46.9	1418.4	80.2	1417.7	47.1
1381.2	0.2	1377.0	356.4	1356.7	58.4
1325.3	290.7	1317.9	224.2	1312.5	314.8
1243.5	446.8	1255.0	66.4	1225.7	14.4
1228.8	226.6	1201.0	216.6	1212.6	196.3
1082.9	4.1	1082.1	5.9	1085.0	8.1
1081.0	4.5	1079.1	3.1	1078.8	11.9
1020.7	104.7	1012.3	2.4	1021.4	71.2
1018.5	3.8	1002.5	104.1	1007.5	8.4
880.0	10.3	873.4	31.3	874.2	8.9
873.3	31.2	847.7	44.8	866.5	27.2
870.3	83.9	709.0	46.6	671.0	89.2
617.2	6.0	646.4	79.7	603.6	4.6
607.9	2.6	612.5	3.0	598.1	3.3
603.8	46.0	586.9	30.2	588.9	35.6
595.1	0.4	579.4	20.3	545.3	30.0
486.8	96.7	538.4	36.4	459.5	125.7
445.6	4.3	445.5	2.0	436.4	4.7
441.4	0.03	431.0	0.5	432.2	3.7
164.9	29.6	148.8	2.2	128.5	5.8
97.5	0.3	105.4	0.3	114.4	8.7
87.4	0.2	103.6	0.2	99.6	0.7
85.4	0.3	84.5	0.2	89.6	4.9
70.5	0.01	70.5	0.5	87.3	5.1
48.9	4.2	40.4	9.2	53.9	3.7
32.2	2.0	27.6	5.3	35.9	5.1
19.0	1.3	19.0	4.5	26.5	5.1

D4'_TC (C_s)		D4''_TC(C_1)		D4'''_TC(C_1)	
ν	I^{IR}	ν	I^{IR}	ν	I^{IR}
3850.3	67.7	3849.7	65.8	3851.5	69.9
3786.0	76.7	3777.4	68.5	3780.2	70.2
3223.7	17.3	3223.5	2.5	3225.5	3.8
3211.8	17.4	3216.6	2.6	3217.8	4.9
3181.7	2.0	3185.7	2.8	3179.8	15.0
3163.2	4.2	3173.4	3.0	3164.6	3.5
3100.9	12.6	3101.2	4.4	3098.5	17.7
3084.0	20.8	3091.9	3.6	3086.5	10.4
1820.8	348.7	1824.7	246.9	1820.8	253.3
1788.8	234.7	1807.6	271.9	1803.9	326.1
1526.3	8.4	1515.5	3.8	1521.6	10.0
1517.4	4.3	1508.1	11.2	1512.2	12.7
1504.6	1.0	1502.2	15.6	1504.4	10.0
1500.3	17.3	1498.6	6.4	1501.6	7.6
1439.3	37.5	1427.5	51.0	1439.0	33.4
1429.0	40.7	1417.3	51.2	1426.3	42.8
1354.0	42.3	1347.0	16.0	1343.0	27.3
1309.0	432.2	1309.8	376.8	1310.0	434.3
1221.8	2.7	1220.6	25.5	1222.4	5.5
1213.8	247.2	1207.1	154.3	1206.9	194.1
1089.8	5.3	1084.5	9.3	1089.4	6.0
1083.8	1.7	1075.4	8.8	1081.1	2.4
1017.4	83.4	1009.9	70.9	1012.4	48.6
1009.5	32.0	1003.6	7.7	1006.9	51.2
871.9	2.7	863.5	27.5	865.9	45.4
864.9	54.2	861.8	24.6	861.4	14.8
664.7	88.3	655.6	79.9	661.4	85.3
606.4	1.4	602.5	3.5	605.8	2.2
601.6	8.0	596.6	3.7	601.4	7.6
588.3	38.8	587.7	26.5	585.4	27.5
554.3	30.8	535.4	22.6	551.6	34.7
480.8	97.3	462.2	129.9	475.8	97.3
443.0	1.6	436.5	4.0	440.7	2.6
433.0	8.2	426.8	13.2	428.1	4.7
137.0	1.2	132.7	0.6	141.1	0.6
116.1	0.2	105.5	2.5	120.0	0.7
86.7	4.8	99.4	12.1	97.9	7.4
84.2	12.3	82.6	0.2	72.9	4.4
53.9	1.6	72.6	7.5	47.2	5.2
29.1	9.1	62.9	1.8	29.1	3.0
24.4	3.9	29.2	2.1	18.0	3.9
12.5	0.3	21.6	1.0	12.3	0.3

See Figure 2 for structures of the dimers.